UNIVERSITY OF CANTERBURY

LIBRARY

AVAILABILITY OF THESIS

AUTHOR'S NAME Jin Tanaka

TITLE OF THESIS Effect of Lateral Confining Reinforcement on the Ductile Behaviour of Reinforced Concrete Columns

DEGREE Ph.D.

SUBJECT Civil Engineering

YEAR 1990

CONSULTATION OF THIS THESIS IS SUBJECT TO THE FOLLOWING CONDITIONS:

1. The thesis will be used only in the library/institution which has requested it.
2. It will be consulted for the purposes of research or private study only.
3. Without written permission from the author, it will not be used for any commercial purpose and no reproduction will be made from it.
4. Due acknowledgement will be made to the author where appropriate.

* I consent/~~do not consent~~ (cross out whichever is not applicable) to make my thesis available for consultation and photocopying under the above conditions.

* I wish the following conditions to apply to use of my thesis :

* Please specify the time limit of any restrictions placed. These should not normally exceed five years.

Signed A. K. Tanaka Author

Date 20/3/90

EFFECT OF LATERAL CONFINING REINFORCEMENT ON THE DUCTILE BEHAVIOUR OF REINFORCED CONCRETE COLUMNS

A thesis
submitted in partial fulfilment
of the requirements for the Degree
of
Doctor of Philosophy in Civil Engineering
at the
University of Canterbury
by
Hitoshi Tanaka

University of Canterbury,
Christchurch, New Zealand

1990

ABSTRACT

This thesis is concerned with the effects of lateral confining reinforcement on the ductile behaviour of reinforced concrete columns. The contents of the chapters are summarized as follows.

In Chapter one, the general problems in seismic design are discussed and earthquake design methods based on the ductile design approach are described. Japanese, New Zealand and United States design codes are compared. Finally, the scope of this research project is outlined.

In Chapter two, after reviewing previous research on confined concrete, the factors which affect the effectiveness of lateral confinement are discussed. Especially the effects of the yield strength of transverse reinforcement, the compressive strength of plain concrete and the strain gradient in the column section due to bending are discussed based on tests which were conducted by the author et al at Kyoto University and Akashi Technological College, Japan. In the axial compression tests on spirally reinforced concrete cylinders (150 mm in diameter by 300 mm in height), the yield strength of transverse reinforcement and the compressive strength of plain concrete were varied from 161 MPa to 1352 MPa and from 17 MPa to 60 MPa, respectively, as experimental parameters. It is found that, when high strength spirals are used as confining reinforcement, the strength and ductility of the confined core concrete are remarkably enhanced but need to be estimated assuming several failure modes which could occur. These are based on the observations that concrete cylinders with high strength spirals suddenly failed at a concrete compressive strain of 2 to 3.5 % due to explosive crushing of the core concrete between the spiral bars or due to bearing failure of the core concrete immediately beneath the spiral bars, while the concrete cylinders with ordinary strength spirals failed in a gentle manner normally observed. In addition, eccentric loading tests were conducted on concrete columns with 200 mm square section confined by square spirals. It is found that the effectiveness of confining reinforcement is reduced by the presence of the strain gradient along the transverse section of column.

In Chapter three, the effectiveness of transverse reinforcement with various types of anchorage details which simplify the fabrication of

reinforcing cages are investigated. Eight reinforced concrete columns, with either 400 mm or 550 mm square cross sections, were tested subjected to axial compression loading and cyclic lateral loading which simulated a severe earthquake. The transverse reinforcement consisted of arrangements of square perimeter hoops with 135° end hooks, cross ties with 90° and 135° or 180° end hooks, and 'U' and 'J' shaped cross ties and perimeter hoops with tension splices. Conclusions are reached with regard to the effectiveness of the tested anchorage details in the plastic hinge regions of columns designed for earthquake resistance.

In Chapter four, the effectiveness of interlocking spirals as transverse reinforcement is studied. Firstly, the general aspects and the related problems of interlocking spirals to provide adequate ductility in the potential plastic hinge region of columns are discussed, referring to the provisions in the New Zealand code, the CALTRANS (California Transportation Authority) code and other related codes. Secondly, based on those discussions, a design method to securely interlock the spirals is proposed. Thirdly, the effectiveness of interlocking spirals is assessed based on column tests conducted as part of this study. Three columns with interlocking spirals and, for comparison, one rectangular column with rectangular hoops and cross ties, were tested under cyclic horizontal loading which simulated a severe earthquake. The sections of those columns were 400 mm by 600 mm.

In Chapter five, analytical models to investigate the buckling behaviour of longitudinal reinforcement restrained by cross ties with 90° and 135° end hooks and by peripheral hoops are proposed. The analyzed results using the proposed models compare well with the experimental observations described in Chapter three. Using those proposed models, a method to check the effectiveness of cross ties with 90° and 135° end hooks is proposed for practical design purposes.

In Chapter six, a theory for the prediction of the ultimate longitudinal compressive concrete strain at the stage of first hoop fracture referred to as the "Energy Balance Theory", which has been developed by Mander, Priestley and Park at University of Canterbury, is introduced. After discussing the problems in the "Energy Balance Theory", a modified theory for the prediction of the ultimate longitudinal compressive concrete strain

at the stage of first hoop fracture is proposed. The predictions from the modified theory are found to compare well with previous experimental results.

ACKNOWLEDGEMENTS

The research presented in this thesis was carried out in the Department of Civil Engineering, University of Canterbury, under the overall guidance of its head, Professor R. Park.

I wish to sincerely thank Prof. R. Park, the superviser of this project, for his invaluable advice, constructive guidance and constant encouragement. The helpful advice given by Prof. T. Paulay is also gratefully acknowledged.

Thanks are extended to the technical staff of the Department of Civil Engineering, for their assistance and advice in the experimental programme. In particular, thanks are due to Messrs N. W. Prebble (now retired), G. E. Hill, A. M. Bell (now retired), G. H. Clarke, P. F. Coursey and R. N. Allen. Mr. L. Gardner is thanked for the photographic work, and Mrs. V. Grey for her drafting assistance.

I also wish to thank my fellow graduate students, in particular Dr. D. Whittaker, Mr. G. A. MacRae, Dr. R. J. T. Park and Dr. Pam H. J. for fruitful discussions.

Thanks are also due to Prof. H. Muguruma, Assoc. Prof. F. Watanabe and Prof. S. Morita, Kyoto University, Japan, for their invaluable advice and constant encouragement over sixteen years since I was a student of Kyoto University.

Above all, I wish to thank my wife, Itsuko, and my parents for their encouragement, understanding and support during the years.

The financial assistance provided by the National Roads Board of New Zealand, University of Canterbury and Akashi Technological College, Japan, are greatly appreciated.

TABLE OF CONTENTS

page

CHAPTER 4: INTERLOCKING SPIRALS

Notation - Chapter 2

A_{ec} = area of effectively confined concrete at critical section

A_c = area of concrete core of section mesured to outside of peripheral spiral or hoop

A_{co} = concrete core area enclosed by the centre line of peripheral hoop or spiral at the level of the hoop or spiral

A_g = gross area of column section

A_s = area of tension reinforcement

A_{sp} = area of spiral bar or circular hoop bar

A_{sh} = total effective area of hoop bars and supplementary cross ties in direction under consideration within spacing s or s_h

A_{st} = total area of longitudinal reinforcement

A_{sx} = total area of lateral reinforcement parallel to x axis

A_{sy} = total area of lateral reinforcement parallel to y axis

B = centre-to-centre dimension of perimeter tie of rectangular core

b_c = concrete core dimension in the x direction

b_w =web width, or diameter of circular section

C_i = confinement index = $(\rho_s - \rho_{so})\, f_{yh} / f'_c$

C_c = confining coefficient = $\rho_s \frac{\sqrt{f_{yh}}}{f'_c} \left(1 - 0.5 \frac{s}{D'}\right)$

D = full depth of a column section

D = diameter of circular column section

D' = diameter of core section measured to outside of spirals

d = effective depth of column section

d_c = concrete core dimension in the y direction

d_b = diameter of a longitudinal bar

d_{bh} = diameter of a transverse reinforcing bar

E_c = initial tangent modulus of concrete

E'_c = $f'_{cc} / \varepsilon_{cu}$

f_{ave} = average stress from zero to an arbitrary strain in stress-strain curve of concrete

f_c = axial stress in concrete specimen

f'_c = compressive strength of plain concrete or compressive strength of unconfined specimen

f_{cp} = plain concrete strength of column

f'_{co} = peak compressive stress of the stress-strain curve of unconfined concrete

f'_{cc} = axial compressive strength of confined concrete

f'_{cu} = compressive stress of confined concrete at ε_{cu}

f'_{cuo} = compressive strain at ε_{cuo}

F_D = a strain-rate dependent constant in modified Kent and Park stress-strain model for confined concrete with square section

f_l = confining fluid pressure

f'_l = effective lateral confining stress acting on concrete in Mander et al stress-strainmodel for concrete

f'_{l1} = smallest confining stress defined in the Mander et al stress-strain model for confined concrete

f'_{l2} = largest confining stress defined in the Mander et al stress-strain model for confined concrete

f_{sl} = equivalent fluid pressure provided by transverse reinforcement

f_{sp} = stress in circular hoop bar or spiral bar

f'_{sh} = stress in rectangular hoop bar

f_y = yield strength of longitudinal reinforcement

f_u = ultimate strength of longitudinal reinforcement.

f_{yh} = yield strength of spiral, hoop or supplementary cross tie reinforcement

H = maximum horizontal shear force applicable to a column

H = centre-to centre dimension of perimeter tie of rectangular core

h = overall thickness of member

h_1 = D - c - h_2

h_2 = length of the part of crack perpendicular the column axis

h " = dimension of concrete core of section measured perpendicular to the direction of the hoop bars to outside of peripheral hoop

h_x" = dimension of concrete core in x direction

h_y" = dimension of concrete core in y direction

h_d = distance between a diagonal shear crack and outer edge of core concrete in interlocking area

k_e = confinement effectiveness coefficient

k_1 = ratio of average stress of concrete in compression zone to $k_3 f'_c$

k_2 = ratio of distance between extreme compression fibre and the centroid of compressive stress distribution to the neutral axis depth, for concrete section subjected to bending

k_3 = ratio of maximum compressive stress of concrete in flexure to f'_c

l_p = plastic hinge length of column

N_f = number of cycles to failure in fatigue tests of concrete

P_e = design axial load in compression at given eccentricity due to gravity and seismic loading acting on the member during an earthquake

P_{occ} = unconfined compressive strength (load) of concrete core

q = reinforcement index = $\frac{\rho_{tn} f_y}{f'_c}$

r_1 = radius of circular core section surrounded by spirals in column transverse section (mesured to outide of spiral)

r_v =the ratio of the volume of the effectively confined core to the original core volume measured outside of spiral bars,

s_h = centre to centre spacing of hoop sets

s = pitch of spiral reinforcement or circular hoop reinforcement

s' = clear spacing between spiral or hoop bars

T = total tension force in longitudinal bars

T_y = tension yield force of longitudinal bars

V_{ec} = volume of the effectively confined core within one spacing of transverse reinforcement

V_{co} = core volume measured outside of spiral bars within one spacing of transverse reinforcement

w = smallest dimension of concrete core section confined by rectangular hoops

y_m= maximum value of y, midway between the hoop sets in the Sheikh and Uzumeri model

α = constant used in Sheikh and Uzumeri stress-strain model for confined concrete

α_s = coefficient of strength increase due to lateral pressure

ε_c = axial strain in concrete specimen

ε_{co} = strain at the ultimate stress of an unconfined concrete specimen

ε_{cc} = strain at the ultimate stress of a confined specimen

ε_{cu}, ε_{km} = available limit of compressive strain defined as the strain at which the avarage stress in a stress-strain curve of confined concrete reaches the maximum value

ε_{cuo}, ε_{km} = available limit of compressive strain defined as the starin at which the avarage stress in a stress-strain curve of unconfined concrete reaches the maximum value

$\varepsilon_{.85}$ = strain at 0.85 of the ultimate stress of a confined concrete specimen in the descending portion of the stress-strain curve

ε_{sp} = concrete compressive strain at spalling

ϕ = curvature

ρ_{cc} = total area of longitudinal reinforcement divided by A_{cc}

ρ_s = ratio of volume of spiral or circular hoop reinforcement to total volume of concrete core (out-to-out of spirals or hoops)

ρ_{so} = value of ρ_s when the pitch of spiral is equal to the least lateral dimension of the column specimen

ρ_{sh} = ratio of volume of rectangular hoops and cross ties to total volume of concrete core (out-to-out of rectangular hoops)

ρ_t = ratio of total area of longitudinal reinforcement to A_g

ρ_{tn} = ratio of tension reinforcement area to b_w d

ρ_w = A_{st} / b_w d

ρ_x = volumetric confinement ratio in x direction

ρ_y = volumetric confinement ratio in y direction

θ = rotation angle of column

θ = angle between spiral tension force and shear force applied to column

θ = spalling angle of confined core concrete

θ_1 = angle between spiral tension force at intersection point of interlocking spirals and shear force applied to column

θ_i = rotation angle of i-th flexural shear crack assumed in the shear deformation model of column

σ_{cm} = applied maximum stress in cyclic loading test

σ_l = lateral confining pressure provided by spiral or circular hoop reinforcement

σ_{lo} = local lateral pressure provided by the spiralcalculated by taking 's' equals to the spiral bar diameter in Eq. 2.9

σ_{lh} = average unit lateral confining pressure provided by rectangular hoop reinforcement

σ_r = the normal stress component in the radial direction in polar coordinates

σ_θ = the normal component in the circumferential direction in polar coordinates

$\tau_{r\theta}$ = the shearing stress component in polar coordinates

Notation - Chapter 3

A_c = area of concrete core of section mesured to outside of peripheral spiral or hoop

A_{co} = concrete core area enclosed by the centre line of peripheral hoop or spiral

A_g = gross area of column section

A_s = area of tension reinforcement

A_{st} = total area of longitudinal reinforcement

B = column width

c = neutral axis depth of member

D = overall depth of column

D' = diameter of core section measured to outside of spirals

d = effective depth of column section

d_b = diameter of a steel bar

E_c = Young's modulus of concrete

E_s = Young's modulus of steel

E_{sh} = tangent modulus of steel at strain of ε_{sh}

f'_c = compressive strength of concrete determined from control cylinders

f_r = modulus of rupture of concrete

f_s = stress in a steel bar

f_{su} = ultimate strength of a steel bar

f_y = yield strength of a steel bar

f_{yh} = yield strength of spiral, hoop or supplementary cross tie reinforcement

G_c = modulus of rigidity of concrete

h = distance from centre of central stub to horizontal load pins at ends of columnunits

H_u = theoretical ultimate horizontal load of a column calculated by the ACI method

I_g = second moment of gross section area of column

k_1 = coefficient for steel to determine L_p proposed by A.L.L. Baker

k_3 = coefficient for concrete to determine L_p proposed by A.L.L. Baker

L = distance from face of the central stub or the base block to point of zero moment at end of column

L_c = cracked region length of column

L_p = equivalent plastic hinge length

L_{uc} = uncracked region length of column

l_d = development length

l_{db} = basic development length of a straight bar, specified in the NZS 3101 code

M_{ACI} = moment calculated using the ACI code method

M_{cr} = cracking moment of column

M_{max} = measured ultimate moment of column

M_{MKP} = theoretical maximum moment obtained from a section analysis using the modified Kent and Park stress-strain model for concrete

P_e = design axial load in compression at given eccentricity due to gravity and seismic loading acting on the member during an earthquake

p = coefficient to determine the shape of a strain hardened curve of a steel bar

s_h = centre to centre spacing of hoop sets

Z_e = elastic section modulus

z = distance of critical section to the point of contraflexure

Δ = horizontal displacement of a column

Δ_b = $\Delta + \theta h$ or $\Delta - \theta h$ given in Fig. 3.23

Δ_t = $\Delta + \theta h$ or $\Delta - \theta h$ given in Fig. 3.23

Δ_{cf} = column deflection due to flexure in cracked region

Δ_{cs} = column deflection due to shear deformation in cracked region

Δ_{ucf} = column deflection due to flexure in uncracked region

Δ_{ucs} = column deflection due to shear deformation in uncracked region

Δ_y^M = calculated lateral displacement of a column at first yield found assuming elastic cracked section behaviour up to the theoretical ultimate horizontal load, H_u

Δ_y^{MKP} = theoretical lateral displacement of a column at first yield obtained using the modified Kent and Park stress-strain model for concrete

ε_{cc} = compressive strain measured at the surface of core concrete

ε_M = strain in extreme tension fibre of column due to moment alone

ε_{pe} = axial strain of column due to axial load alone

ε_{sp} = concrete compressive strain at spalling

ε_{sm} = strain measured by an ordinary scale with a gauge length of five times bar diameter in between points B and C in Fig.3.50 after fracture of a steel bar

ε_s = strain in a steel bar

ε_{sh} = strain at which strain hardening of steel commences

ε_t = strain in extreme tension fiber of column due to axila load and moment

ϕ = curvature

ϕ = strength reduction factor

ϕ_x = theoretical curvature of column section at distance x from horizontal loading point when the column end moment = M_{ACI}

ϕ_y = curvature at first yield

μ_N = nominal displacement ductility factor = Δ/Δ_y^M

μ_R = real displacement ductility factor = Δ_t/Δ_y^M or Δ_b/Δ_y^M

θ = rotation of central stub due to unsymmetrical plastic hinging

Notation- Chapter 4

A_c = area of concrete core of section mesured to outside of peripheral spiral or hoop

A_g = gross area of column section

A_s = area of tension reinforcement

A_{sp} = area of spiral bar

A_{sh} = total effective area of hoop bars and supplementary cross ties in direction under consideration within spacing s_h

A_{st} = total area of longitudinal reinforcement

A_{shx} = A_{sh} in section

A_{shy} = A_{sh} in section y-y

A_v = total area of shear reinforcement within a distance, s

A_{vf} = area of shear friction reinforcement

b_w =web width, or diameter of circular section

b_w' = diameter of the circular core section surrounded by each single spirals (= $2 r_1$)

c = distance of the rotation centre of column from extreme compression fibre in the shear deformation model

C = axial compression force in a separated column in the combined beam-arch action (= $P_e + T$)

D = full depth of a colomun section

D = diameter of circular column section

D' = diameter of the core section of a circular column with spirals(=$2 r_1$)

d = effective depth of column section

d_b = diameter of a longitudinal bar

d_{bh} = diameter of a transverse reinforcing bar

d_{il} = distance between the centres of the adjacent spirals in the transverse section

f'_c = specified compressive cylinder strength of concrete

f_s = average stress in longitudinal reinforcement in the interlocking area due to column load

f_{s3} = average stress in the longitudinal bars in the interlocking area at extreme compressive fibre strain of concrete of 0.003

f_{sl} = equivalent fluid pressure provided by transverse reinforcement

f_y = yield strength of longitudinal reinforcement

f_u = ultimate strength of longitudinal reinforcement.

f_{yh} = yield strength of spiral, hoop or supplementary cross tie reinforcement

H = maximum horizontal shear force applicable to a column

H_1, H_2 = aggregate interlock force

h = overall thickness of member

h_1 = $D - c - h_2$

h_2 = length of the part of crack perpendicular the column axis

h'' = dimension of concrete core of section measured perpendicular to the direction of the hoop bars to outside of peripheral hoop

h_x'' = dimension of concrete core in x direction

h_y'' = dimension of concrete core in y direction

h_d = distance between a diagonal shear crack and outer edge of core concrete in interlocking area

h_d = side length of a concrete segment in Fig. 4.25

l_1 = length of column minus l_2

l_2 = plastic hinge length of column in the combined beam-arch action

l_c = vertical distance between opening edge of a crack and column top

l_d = development length required by the NZS 3101:1982

l_d = side length of a concrete segment in Fig. 4.25

l_{gi} = gauge length for potentiometers

l_{go} = length of column where potentiometers are not placed

l_i = distance between the measuring point of $\Delta_{mid}{}^{M}$ and the center position of i-th pair of potentiometers

l_i' = distance between the measuring point of $\Delta_{top}{}^{M}$ and the center position of i-th pair of potentiometers

$l_i{}^{r}$ = vertical distance between the measuring point of $\Delta^{M}{}_{mid}$ and i-th rotation centre of column

$l'_i{}^{r}$ = vertical distance between the measuring point of $\Delta^{M}{}_{top}$ and i-th rotation centre of column

l_o = vertical distance between the rotation centre of column and the column top

l_p = plastic hinge length of column

l_w = horizontal length of wall

M_A = moment of the separated column in the combined beam-arch action at section A-A

M_{ACI} = moment calculated using the ACI code method

M_C =ultimate moment of the separated column in the combined beam-arch action at section C-C

M_d = moment applied to a longitudinal bar by dowel action

M_{MKP} = theoretical maximum moment obtained from a section analysis using the modified Kent and Park stress-strain model for concrete

M_{MND} = theoretical maximum moment obtained from a section analysis using the Mander et al stress-strain model for concrete

M_{PL} = theoretical maximum moment obtained from section analysis using the Park and Leslie stress-strain model for concrete

M_u = ultimate moment of columin the combined beam-arch action=M_2+M_C

M_1 = Moment calculated using ordinary section analysis

M_2 = Moment due to axial loads T and C in each separated column in combined beam-arch action

n = ratio of direct shear strength of concrete to compressive strength of f'_c

P_e = design axial load in compression at given eccentricity due to gravity and seismic loading acting on the member during an earthquake

r_1 = radius of circular core section surrounded by spirals in column transverse section (mesured to outide of spiral)

s_h = centre to centre spacing of hoop sets

s = pitch of spiral reinforcement

T = total tension force in longitudinal bars

T_1 ,T_2 = component of spiral tension force in the direction of the applied shear force

T_f = dowel failure force defined in the study by Dulácska [4.14]

T_L = total tension force in longitudinal bars

T_y = tension yield force of longitudinal bars

V_c = shear carried by concrete in column section

V_d = maximum shear force carried by a longitudinal bar subjected to direct shear

V_d = shear force carried by dowel action in reference [4.11]

V_d = shear force applied to a longitudinal bar by dowel action

V_{do} = dowel force in reinforcement required for a splitting failure (in kips) defined the study by Jimenez, White and Gergely [4.12]

V_i = ideal strength of section

V_r = a resultant force from τ_{cl} (due to bond action) and τ_{ch} (provided by spiral shear)

V_s = shear carried by transverse reinforcement in column section

V_n = nominal shear strength

V_u = shear force at the section derived from factored load on the structure

y_c = deflection of dowel which causes horizontal cracking

Δ_d = distance between opening edges of a flexural shear crack

Δ_h = vertical distance between crack opening edges when a horizontal flexural crack is formed and the column rotates through angle θ.

$\Delta_{h'}$ = vertical distance between opening edges of a flexural shear crack

Δ_y^M = measured first yield displacements

Δ_y^A = first yield displacement based on theory (A)

Δ_y^B = first yield displacement based on theory (B)

Δ_{top}^M = measured horizontal displacement at the column top where horizontal load is applied

Δ^M_{mid} = measured horizontal displacement at mid-height of column

Δ^B_{top} = horizontal displacement at the column top which is calculated using measured curvature distribution

Δ^B_{mid} = horizontal displacement at mid-height of column which is calculated usin measured curvature distribution

Δ^S_{top} = horizontal displacement at the column top which is calculated using a flexural-shear deformation model

Δ^S_{mid} = horizontal displacement at mid-height of column which is calculated using a flexural-shear deformation

α = angle between column axis and the inclined part of a flexural shear crack

β = angle between horizontal line and the line connected from rotation centre to the opening edge of a flexural shear crack

ε_c = concrete strain at extreme compression fibre of concrete core

ε_c = extreme compression fibre strain used in the strength design method [4.2, 4.6]

ε_{ef} = concrete strain in the extreme compression fiber for the combined beam-arch action

ϕ = strength reduction factor

ϕ = curvature

ϕ_y = first yield curvature

ϕ_y^M = measured first yield curvature

ϕ_y^A = first yield curvature based on theory (A)

ϕ_y^B = first yield curvature based on theory (B)

ϕ_u = ultimate curvature

μ = coefficient of friction; for normal weight of concrete placed monolithically, μ =1.4

v_b = basic shear stress provided by concrete

v_c = ideal shear stress provided by concrete

ρ_s = ratio of volume of spiral or circular hoop reinforcement to total volume of concrete core (out-to-out of spirals or hoops)

ρ_{se} = local volumetric ratio of interlocking spirals in semicircular end region of column section, that is in the core region ouside the area of interlock.

ρ_{sc} = local volumetric ratio of interlocking spirals in central region of column section, that is, in the area of interlock.

ρ_{sh} = ratio of volume of rectangular hoops and cross ties to total volume of concrete core (out-to-out of rectangular hoops)

ρ_t = ratio of total area of longitudinal reinforcement to A_g

ρ_{tn} = ratio of tension reinforcement area to b_w d

ρ_w = A_{st} / b_w d

θ = rotation angle of column

θ = angle between spiral tension force and shear force applied to column

θ_1 = angle between spiral tension force at intersection point of interlocking spirals and shear force applied to column

θ_i = rotation angle of i-th flexural shear crack assumed in the shear deformation model of column

σ_o = yield strength of material

σ_x = axial stress in material

τ_{cl} = shear stess acting along a side of a concrete segment, provided by bond action of a longitudinal bar

τ_{ch} = shear stress acting along a side of a concrete segment, provided by shear force V_s carried by spiral reinforcement

τ_{xy} = shear stress in material

Notation - Chapter 5

A_g = gross sectional area of the column
A_s = area of steel bar section
a = load acting length factor of triangularly distributed load q
d_b = bar diameter of cross tie
d_b = bar diameter of steel bar
d_{bn} = nominal bar diameter of steel bar
d_{bh} = bar diameter of peripheral hoop
d_{bl} = bar diameter of longitudinal bar
E = Young's modulus of steel
E_t = tangent modulus of elasticity of steel in inelastic range
E_t' = secant modulus of elasticity of steel in inelastic range
E_r = equivalent reduced modulus of elasticity for inelastic buckling of column
$E_p I$ = bending stiffness of steel bar which is subjected to high axial compression
F_1 = outward force applied to 90° hook by longitudinal bar
F_1^e = outward force applied to 90° hook by longitudinal bar at 90° end hook deflection of δ_1^e
F_1^p = outward force applied to 90° hook by longitudinal bar at 90° end hook deflection of δ_1^p
F_2 = outward force applied to the mid-span of the peripheral hoop bar by longitudinal bar
F_2^e = outward force applied to the mid-span of the peripheral hoop bar by longitudinal bar at central deflection of the peripheral hoop of δ_2^e
F_2^p = outward force applied to the mid-span of peripheral hoop bar by longitudinal bar at central deflection of the peripheral hoop of δ_2^p
F_3 = outward force applied to 135° or 180° end hook by longitudinal bar
$f_1(\varepsilon_s)$ = a component to determine $f_t(\varepsilon_j)$
$f_2(\varepsilon_s)$ = a component to determine $f_t(\varepsilon_j)$
f'_c = compressive cylinder strength of plain concrete strength
$f_c(\varepsilon_i)$ = stress in i-th layer above the pseudo-neutral axis in bar section
$f_t(\varepsilon_j)$ = stress in j-th layer below the pseudo-neutral axis in bar section
f_{su} = ultimate strength (maximum stress) of steel
f_{yh} = yield strength of peripheral hoop bar steel
f_{yt} = yield strength of tie bar steel
I_t = moment of inertia of bar section of the cross tie

I_h = moment of inertia of the bar section of the peripheral hoop

k_1 = spring stiffness of 90° end hook

k_1^e = initial stiffness of 90° end hook against lateral deflection of longitudinal bar

k_1^p = stiffness of 90° end hook at lateral deflections of longitudinal bar between δ_1^e and δ_1^p

k_2 = spring stiffness of peripheral hoop

k_2^e = initial stiffness of peripheral hoop against lateral deflection of longitudinal bar

k_2^{eu} = upper bound value of initial stiffness of peripheral hoop against lateral deflection of longitudinal bar

k_2^p = stiffness of peripheral hoop at lateral deflections of longitudinal bar between δ_2^e and δ_2^p

k_2^{pp} = stiffness of peripheral hoop at lateral deflections of longitudinal bar which exceed δ_2^p

k_3^e = initial stiffness of cross tie with 135° or 180° end hook

l_s = spacing between 135° or 180° end hooks

l_b = distance between centroids of tie leg section and longitudinal bar section

l_d = development length required to resist F_1 or F_3

l_h = length of peripheral hoop bar between corner longitudinal bars

M_b = fixed end moment of longitudinal bar at position of 135° or 180° end hook

M_c = moment at mid-span of longitudinal bar between 135° or 180° end hooks

M_e^h = elastic moment of resistance of the peripheral hoop bar

M_e^t = elastic moment of resistance of the bar with 90° end hook

M_p^t = full plastic moment of of resistance of the bar with 90° end hook

M_p = maximum inelastic moment of resistance of longitudinal bar subjected to axial compression

M_y^h = moment of resistance of the peripheral hoop bar at yield hinge which is subjected to axial tension.

P_{ecr} = the Euler load in buckling

P_{cr} = critical axial load of intermediate longitudinal bar against buckling

P_y = yield force of longitudinal bar

P_u = ultimate force of longitudinal bar

q = maximum value of triangularly distributed load per unit length on longitudinal bar

R_e = ratio of k_1^e to k_3^e

r = radius of gyration

T_1 = Reacting force against 'w' at pin support

T_2 = Reacting force against 'q' at pin support

T_w = tension force in leg of cross tie with 135° or 180° end hook due to 'w'

T_y = tensile yield force of cross tie bar leg

T_y^h = tensile yield force of peripheral hoop bar

w = lateral pressure uniformly distributed along the peripheral hoop bar or along the longitudinal bar due to the Poisson's effect of core concrete

W_f = work done by outward force of the longitudinal bar

W_r = work done by rotation of yield hinge

x = coordinate of a point along tie bar leg

Z = elastic section modulus

α = a constant to determine stress-starin relation of steel in the strain hardening region

α_1 = a constant to determine stress-starin relation of steel in the strain hardening region

α_2 = a constant to determine stress-starin relation of steel in reversed loading

β = a constant to determine stress-starin relation of steel in reversed loading

ε_r = compression strain at pseudo-neutral axis in longitudinal bar

ε_s = steel strain

ε_{sh} = steel strain at the commencement of strain-hardening

ε_{su} = strain at the ultimate strength (maximum stress) of bar steel

ε_{suc} = ultimate steel strain in compression

ε^r_{su} = strain at ultimate stress in the reversed loading curve

ε_x = tension strain in cross tie bar leg at point x

ε_y = yield strain of bar steel

ΔF_2 = increment of F_2

Δw = increment of uniform lateral pressure along peripheral hoop from core concrete

$\Delta\delta_2^F$ = increment of central deflection of peripheral hoop bar due to increment of F_2

$\Delta\delta_2^w$ = increment of central deflection of peripheral hoop bar due to increment of w

δ = deflection of longitudinal bar at position of 90° end hook

δ_1 = total displacement of 90° end hook at the contact point with the longitudinal bar as the sum of δ_b and δ_s.

δ_1^e = deflection of 90° end hook at the contact point with the longitudinal bar, where the moment at the bent corner of the 90° hook reaches the elastic moment of resistance of the hook bar, M_e^t

δ_1^p = deflection of 90° end hook at the contact point with the longitudinal bar, where extreme fiber strain at the bent corner of the 90° end hook reaches the strain hardening strain ε_{sh}

δ_2 = central deflection of the peripheral hoop

δ_2^e = central deflection of the peripheral hoop bar when the moment at the corner bend of the peripheral hoop bar has reached the elastic moment of resistance of the hoop bar, M_e^h

δ_2^{eu} = δ_2^e calculated from Eq. 5.19

δ_2^p = central deflection of peripheral hoop at which axial force in peripheral hoop bar has just reached its axial yield tension force

δ_b = deflection of 90° end hook at the contact point with the longitudinal bar due to bending

δ_{cr} = ultimate central deflection of longitudinal to be able to maintain axial load P_{cr}

δ_f = deflection of longitudinal bar due to loads F_1 and F_2

δ_m = deflection of longitudinal bar due to fixed end moment M_b

δ_o = initial deflection of longitudinal bar due to imperfection

δ_o^c = maximum value of δ_o to satisfy a state of stable equilibrium in longitudinal bar

δ_p = deflection of longitudinal bar due to axial load P_{cr}

δ_q = deflection of longitudinal bar due to lateral pressure 'q'

δ_s = displacement of 90° end hook at the contact point with the longitudinal bar due to slippage of tie leg from core concrete

$\delta_{s'}$ = displacement of 135° or 180° end hook at the contact point with the longitudinal bar due to slippage of tie leg from core concrete

δ_{st} = deflection of longitudinal bar in a state of stable equiribrium at Stage (1) , taking into account of δ_o

δ_w = deflection of longitudinal bar due to lateral pressure 'w'

γ = a constant to determine stress-starin relation of steel in reversed loading

μ = displacement ductility factor of column

σ_c^i = compression stress increase of i-th layer of steel bar section due to bending

σ_t^j = compression stress decrease of j-th layer of steel bar section due to bending

σ_r = axial stress at the position of the pseudo-neutral axis of bar section

θ^p = rotation of yield hinge of hoop bar expressed by $2\,(\delta_2^p - \delta_2^e)/\,l_h$

$\phi_1(x)$, $\phi_2(x)$ = assumed curvature distribution along the 90° hook

ϕ_p = curvature in longitudinal bar subjected to combined high axial load and moment M_p

τ_b = bond stress assumed to be uniformly distributed along cross tie bar leg

Notation - Chapter 6

A_{cc} = sectional area of concrete core measured to centre of peripheral spiral or hoop

A_{cov} = sectional area of concrete cover

A_s = sectional area of a longitudinal bar

a = maximum lateral deflection of a longitudinal bar due to buckling

c = neutral axis depth

d = effective depth of member section

d_b = diameter of a hoop bar

d_c = core diameter of a reinforced concrete column

E_b = tangent modulus of a longitudinal bar in the inelastic range

f_{cc} = compressive stress in confined concrete in the column core

f_{ccf} = axial stress component in core concrete due to friction between shear sliding surfaces

f_{co} = compressive stress in unconfined concrete in the column concrete cover

f'_{co} = compressive strength of plain concrete assumed to be 85 % of the control cylinder strength

f_{sh} = tensile stress in hoop reinforcement

f_{sl} = compressive stress in longitudinal reinforcement

f_{su} = ultimate tensile strength of steel

f_{yh} = yield strength of transverse reinforcement

I_b = moment of inertia of longitudinal bar cross section

I^T_{ag} = agreement index of the proposed theory to the experimental value defined by Eq. 6.28

I^M_{ag} = agreement index of the energy balance theory to the experimental value defined by Eq. 6.29

k_{cov} = compressive stiffness of cover concrete

k_{cc} = compressive stiffness of core concrete before complete formation of shear sliding surfaces

k_{ccf} = compressive stiffness of core concrete after complete formation of shear sliding surfaces

k_{sc} = compressive stiffness of compression reinforcement

k_h = stiffness of hoop reinforcement as lateral confinement

l = initial length of a longitudinal bar before loading

l_g = gauge length for strain measurement in core concrete

P_{cc} = axial load on core concrete

P_{cov} = axial load on cover concrete
P_{sl} = axial load on compression reinforcement
P_{total} = total axial load on column
s = hoop spacing
T_h = lateral restraining force due to hoop reinforcement
x = coordinate of a point along a longitudinal bar
y = lateral deflection of a longitudinal bar at point x
U_{cc} = strain energy stored in confined concrete prior to first hoop fracture
U_{ccf} = dissipated energy by friction between shear sliding surfaces in concrete core prior to first hoop fracture
U_{co} = strain energy absorbed in core concrete prior to complete formation of shear sliding surfaces
U_{cov} = strain energy absorbed in cover concrete prior to complete spalling
U_g = external work done on an axially loaded column
U_{sc} = external work done on compression reinforcement
U_{scr} = strain energy absorbed in compression reinforcement by axial yielding
U_{sh} = ultimate strain energy capacity of hoop reinforcement determined by fracture strain of steel
U'_{sh} = strain energy stored in hoop reinforcement at first hoop fracture in case where compression reinforcement has not buckled or has buckled within one hoop spacing
α = reduction factor for U'_{sh} determined from strain distribution in hoops along the column axis
β = ratio of strain energy absorbed in compression reinforcement by axial yielding to external work done on compression reinforcement
γ = constant determined by magnitude of friction between shear sliding surfaces in concrete core
δ = lateral deflection of a longitudinal bar at hoop position
ε_c = longitudinal compressive strain in core and cover concrete
ε_{cu} = ultimate concrete compression strain to predict the rotational capacity of plastic hinges in concrete members (defined in previous research)
ε_{cu} = ultimate longitudinal compressive strain of confined concrete defined as that strain at the stage of first hoop fracture (defined in this study)
ε_{max} = maximum allowable concrete strain in Scott, Park and Priestley model

ε_s = axial strain in compression reinforcement

ε'_s = apparent axial strain in compression reinforcement due to axial shortening bybar buckling

ε_{sh} = tensile strain in hoop reinforcement

ε_{sf} = fracture strain of hoop steel bar

ε_{sp} = longitudinal compressive strain in core concrete at which shear sliding surfaces are assumed to be completely formed, simultaneously with the completion of spalling of cover concrete

ε_s^T = longitudinal compressive strain in a longitudinal bar with hoop spacing of s where bar buckling commences

ε_{su} = strain at the ultimate tensile strength of steel

ρ_{cc} = sectional area ratio of compression reinforcement to concrete core

ρ_s = volumetric ratio of hoop reinforcement to concrete core

CHAPTER ONE

INTRODUCTION

1.1. GENERAL PROBLEMS IN SEISMIC DESIGN

1.1.1 Introduction

In this thesis, the ductile behaviour of reinforced concrete members confined by various types of lateral confining reinforcement is studied through experimental and theoretical works. The ultimate purpose of those works is to contribute to the improvement of ductile design rules for earthquake resistant reinforced concrete structures. Hence, the general problems in current seismic design methods are briefly reviewed in the following paragraphs.

1.1.2 Earthquake Engineering and Cost-Benefit Studies

In the last several decades earthquake engineering has rapidly progressed especially after the advent of a computer and the availability of strong motion accelerographs and thus seismic design codes for structures have been considerably improved. However, the earthquake engineering, which provides foundations for those codes, still contains several uncertainties related to seismology, geotectonics, soil and structural dynamics and so on. Consequently, some provisions in codes are still in the category of the rule of trial and error. For example, the prescription of seismic loads in a code is eventually decided by so-called engineering judgement rather than applying logic strictly following seismological theories or probability studies.

It may be said that our modern technology has already made it possible to make structural materials and members as strong and as ductile as required, if the cost-benefit aspects can be neglected. However, decisions concerning the establishment of seismic design regulations including their scope and safety level need to be based on safety studies that consider economic implications and acceptable failure probabilities, as mentioned in the IAEE (International Association for Earthquake Engineering) document

[1.1]. The document also says that the seismic design intensity must be determined on the basis of cost-benefit studies under tolerable risk restrictions. The cost-benefit studies are defined as those based on optimizing a utility function which is the algebraic sum of initial costs and present values of expected benefits and damage.

To establish such design rules, firstly future earthquakes must be predicted precisely in terms of probability. Secondly, the level of damage of a structure subjected to the predicted earthquakes needs to be well controlled. However, it may be said that earthquake engineers are still struggling with the problems of earthquake prediction and the damage control of structures.

1.1.3 Basic Concepts for Seismic Design

The basic objective of seismic design codes is to provide reliability and quality assurance for structures subjected to earthquakes. Reliability may be defined as the probability of satisfying a system requirement or a performance criterion within a reference interval of time [1.1]. Hence, to establish a seismic design code, basic performance criteria for structures under earthquakes and the corresponding reference interval of time need to be firstly determined.

In the SEAOC Recommendations in California [1.2], as fundamental seismic performance criteria, structures are required to :

1.Resist minor earthquakes without damage.

2.Resist moderate earthquakes without structural damage, but with some nonstructural damage

3.Resist major earthquakes, of the intensity of severity of the strongest experienced in California, without collapse, but with some structural as well as nonstructural damage.

The SEAOC recommendations further state that "in most structures, it is expected that structural damage, even in a major earthquake, could be limited to repairable damage ".

The concept of the above criteria has been used in several current seismic design codes just by replacing the word of California in the item 3 with a district name under consideration. In some cases, the expression of

without structural damage in the item 2 may have been modified as 2', with little or no damage to the structural elements [1.3].

To determine the reference interval of time, there are two basic choices. One is the fixed time apart from the nature of the structure, and the other is the relative time which depends on the nature of the structure.

It is considered that the fixed reference interval of time should be used when determining the level of safeguard against loss of life and other hazards under severe earthquakes, in order to standardize the reliability of the safeguard against such matters. In this case, focusing on the return period of the major destructive earthquakes, a period of 150 years or more may be chosen as in the draft revision of the New Zealand building code [1.4].

When a protection level against structural or nonstructural damage under moderate earthquakes is determined, the design life of each structure may be adopted as the reference time interval, simply from the view point of economy. This is because, for a structure with a short design life, a low probability of meeting earthquakes can be expected. The design life is normally wide-ranging from several decades to one hundred years or more depending on the usage, the scale and the type of structure, the materials used, the maintenance cost consideration, etc. Hence, the design intensities against moderate earthquakes may need to be modified in accordance with the design life of each structure.

In the current New Zealand building code [1.5] and in the Japanese building code [1.6, 1.7, 1.8], moderate earthquakes are expressed as those which can occur several times during the life time of a building. This description gives a basic target for the design intensity against moderate earthquakes according to the design life of each structure. Major earthquakes are expressed as those which could occur once or more than once in the life of a building in the New Zealand building code [1.5], and as those which could occur once or not at all in the Japanese building code [1.6, 1.7, 1.8]. However, for major earthquakes, to secure a certain standardized level of safeguard for life, a fixed reference interval of time such as that based on the return period of earthquakes is recommended. It is notable that moderate and major earthquakes are being defined in terms of

probability of their occurrence in recent years [1.3, 1.4, 1.9], typically in China which has a long history of several thousand years of knowledge of earthquake activity.

1.1.4 Earthquake Design Approaches

The items 1 and 2 or 2' in the SEAOC Recommendations can be achieved by providing a building structure with adequate stiffness and strength. When earthquake engineering was in an early stage of development, it was believed that the item 3 could also easily be achieved by providing adequate strength [1.10]. However, modern earthquake engineering has shown that, if the item 3 is to be achieved by strength alone, it would lead to uneconomically large sections of structural elements, especially in frame structures without any walls or braces. For example, the elastic response of buildings with natural period of less than about 0.4 second can easily reach 1.0 g or so when subjected to the major earthquakes [1.4, 1.7]. It may be imagined how large the sections would be for such a condition of loading by recalling the structural element sizes of pure frame buildings which have normally been designed using the seismic base shear coefficient of only about 0.3 g or less.

In these days, as an economical method, the ductile design approach which aims at dissipating seismic energy mainly by inelastic deformations of the structure, and thus permits use of seismic design loads significantly less than the elastic response spectra loads, has been widely used. As an alternative, the base isolation approach which provides special mechanical devices to minimize the input of earthquake energy into the structure has also been adopted in recent years.

1.1.5 Shortage of Strong Earthquake Records

One of the basic requirements necessary for developments in earthquake engineering is accurate knowledge of the ground motions during destructive earthquakes. Such knowledge can be obtained only by actual measurements in the epicentral regions of strong earthquakes. However, to make those measurements it was necessary to wait the advent of strong motion seismographs, the first of which was developed by the U.S. Coast and Geodetic Survey about 1932 [1.11] and completed as the USCGS

accelerograph in 1936 [1.12]. Thereafter, a network of strong motion accelerographs in the USA was built up mainly in the Pacific Coast states.

In other seismic countries around the Pacific Ocean, the formation of a network of strong motion accelerographs was delayed. For example, in Japan the network was expanded after the completion of the SMAC (Strong Motion Acceleration Committee, Japan) accelerograph in 1952 [1.11]. In New Zealand, MO type accelerographs were designed in 1965 and installed in a network about 1966, while a network of early types of non-time base strong motion accelerographs has operated since 1955 [1.13]. Although seismological observatories with sensitive seismographs had already been distributed throughout the world before the advent of the strong motion seismographs, those seismological observatories were not intended to make measurements in the epicentral regions of strong earthquakes and cannot be adapted to do so effectively.

Due to the short lapse of only several decades since the formation of strong motion accelerograph networks, useful strong motion records are limited to a small number. That is, only a few of records such as those of the El Centro (California) earthquake of 1940, the Taft (California) earthquake of 1952 and the Hachinohe (Tokachi-oki, Japan) earthquake of 1968, are available for dynamic response analyses of structures or to draw up design spectra. In effect, the El Centro 1940 NS spectrum has been used world-wide as a standard design spectrum, including in New Zealand [1.4, 1.5, 1.14], although this spectrum should be adequate only in limited areas where seismological conditions are similar with El Centro. This is simply because of the shortage of available records of strong earthquakes.

In New Zealand, on March 2 1987 an earthquake of magnitude (ML) 6.3 occurred near the town of Edgecumbe and, for the first time in New Zealand, the strong motion accelerographs produced records with response spectra comparable to the design level of a 150 year return period spectra for the more seismic parts of the country (See Fig. 1.1) [1.15].

It cannot be overemphasized that, due to the shortage of the strong ground motion records, there may still be unrevealed aspects of destructive earthquakes. As an important lesson, it should be remembered that before 1954 the instrument records had led to the conclusion that all very deep-

focus earthquakes occurred in the Pacific region. Then on March 29, 1954 a magnitude 7.3 earthquake was located some 650 km under Spain [1.12].

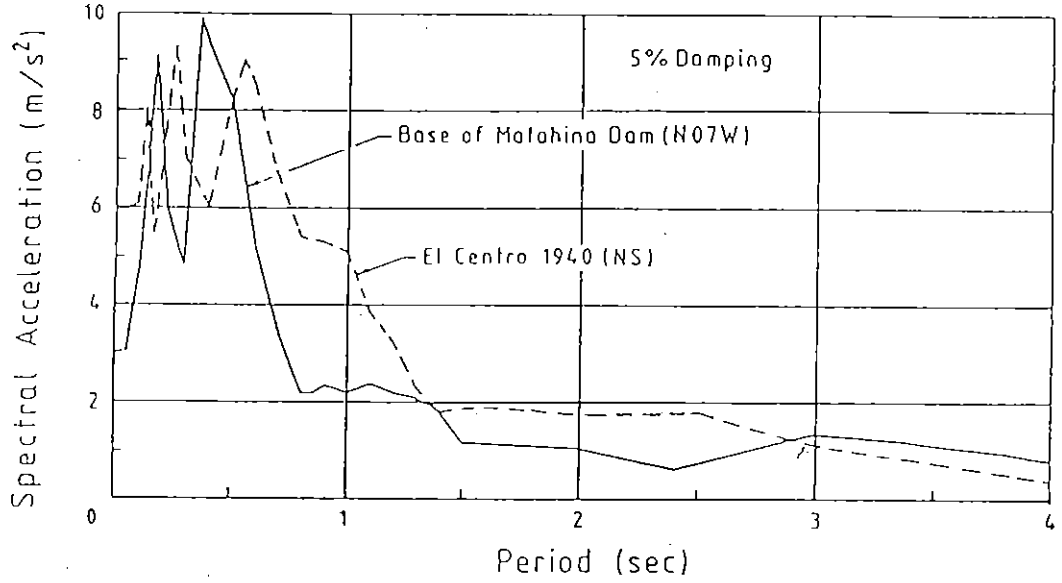

Fig. 1.1 Response Spectrum at The Base of Matahina Dam in Edgecumbe Earthquake of 1987 [1.15]

1.1.6 Design Spectra

The response spectra of past earthquakes provide a basis for the rational design of structures to resist earthquakes. As a matter of course, the ground motion depends on the earthquake source mechanism and extent, the underground geological structures, local soil condition, the distance from the earthquake source and so on. These factors have been more or less taken into account in the design spectra of each country, based on their own measurements of medium magnitude events and of strong ones if available.

In case of the Japanese Building code of 1980 [1.6, 1.7, 1.8], design spectra have been drawn by averaging and normalizing 179 components of ground motion records for three categories of soil conditions [1.16]. However, revisions of those design spectra will sometimes be necessary as the number of strong earthquake records increase. For example, the Mexico earthquake of 1985 showed that the intensities might be much higher than those previously recorded in that area and could have a significant probability of recurring in moderately long time intervals [1.17]. Reference [1.17] also states that the severity and extent of damage are largely a consequence of the discrepancies between the ground motion and the value

implicit in design codes, and of construction practice. In case of New Zealand, the spectra to date, admittedly from medium magnitude events, are quite different in shape from the much broader band El Centro type spectra used in New Zealand design[1.14].

It must be emphasized that the intensity of the design spectrum is eventually determined as an index of target strengths of structures apart from the reality of earthquakes, while its shape represents certain characteristics of ground motions. Unfortunately, most of the design codes do not or cannot clearly describe for what levels of earthquake, and for how long return periods, the design spectra were drawn. Hence, for practitioners it is not easy to recognize the extent of safety or risk of a earthquake design load given by the design spectrum, in practical design work. From this point of view, it is notable that the relations between the risk factor (increase in acceleration ordinates in the elastic response spectra) and the return period of earthquakes are referred to in the draft revision of NZS 4203:1984 [1.4], as shown in Fig. 1.2.

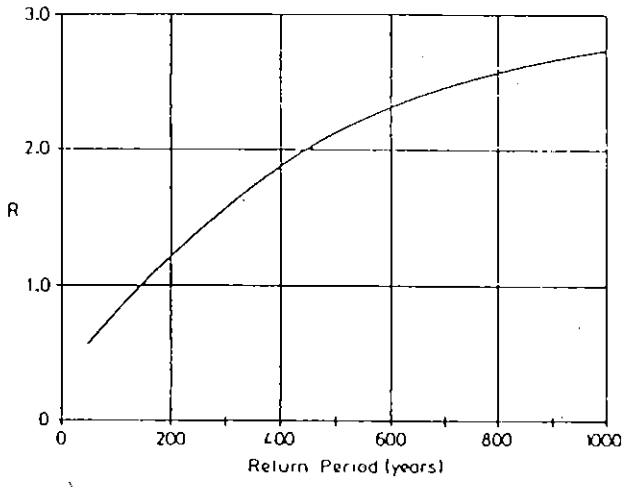

Fig. 1.2 Relationship Between Risk Factor and Return Period [1.4].

1.1.7 Dynamic Response Analyses

Elastic and inelastic dynamic response analyses have been used to check the adequacy of trial or determined values for stiffness, strength and ductility of structures especially for essential buildings or structures. The results of these analyses are significantly affected by the models used for the

structural members, boundary conditions and input ground motions. Hence, the adequacy of those models and input ground motions become keys to making dynamic response analyses reliable and useful. With respect to the accuracy of the modelling techniques of structural members and boundary conditions, it may have already reached the level required for reliable results.

The most important but vexing problem is how to obtain or create a set of suitable input ground motions. The input ground motions need to be those which cover all probable strong earthquake motions at the site during the reference time interval of the structure .

The factors that can influence the surface ground motion are the nature of the source mechanism, the travel path of the seismic wave and local geology [1.12]. The amplitude and duration of surface ground motions can dramatically be changed in the order of 100% by difference in the above factors. This is the reason why the microzoning studies [1.17, 1.18] have been developed in recent years. If it is just required to know the basic behaviour of a structure, typical strong motion records such as 1940 El Centro or 1952 Taft ones may be applied directly to the base of the structure neglecting the above seismological factors. However, for practical design purposes, normally such a method is not applicable, or is meaningless, due to the variety of the seismological factors at each individual site.

An adequate method is to use strong motion records measured at the site if such records exist. However, it can hardly be expected that such records are available because of the shortage of strong motion records as mentioned previously. If there are records of minor or moderate earthquakes measured at the site, those records may be used by simply magnifying the amplitude of acceleration, and sometimes the duration as well, to correspond to major earthquakes. This method was used in the past, when design by dynamic analysis was started, as well as the direct use of the typical strong ground motion records such as the El Centro or Taft ones. However, the validity of this method cannot be assured [1.16], because this method also neglects differences in the seismological factors mentioned above.

A recent method is to modify strong motion records taking account of the local geological condition of the site. As the first step, the soil profiles of both the ground motion recorded site and the site of the structure are investigated, and the bed rock of each is assigned to the seismic wave source. The recorded ground motions are sent back to the bed rock using soil models which represent the soil profile of the recorded site, and the seismic waves at the bed rock are thus calculated. The surface ground motions at the site of the structure are then calculated by sending the obtained bed rock waves up to the ground surface using the soil models for that site. The surface ground motions thus obtained are used as the input motions for the structure.

The above method can be considered to be a great advance. However, it should be noted that, in the method, it is necessary to assume that the seismic waves at the bed rock of the site of the structure are the same as that of the recorded site. Strictly speaking, this method is valid only when the site of structure and the site of the recorded ground motion are sitting on the same bed rock with the same distance from the earthquake source. Moreover, the adequacy of the soil models must also be checked.

A similar method, in which the bed rock motions are assumed to be white noise and are so generated, has also been used. This method is more easy to use, but a significant defect is that the nature of the travelling wave from the earthquake source to the bed rock is not taken into account.

A synthesis method, which takes into account the earthquake source parameters and the wave travel path, has also been developed. This method is to synthesize the ground motions by using the observed seismograms from the small shocks as Green's functions [1.19, 1.20]. However, the method contains many assumptions which need to be proved adequate.

Studies on artificially generated ground motions have led to improvements in the above method, and to several other methods, but each method seems to have some uncertainties. It is notable that in the recent Mexican earthquake of 1985 the peculiarities of accelerograms and spectra at various locations in the valley of Mexico could not be explained in some cases in terms of the uni-dimensional vertically-travelling shear wave

model [1.17]. This may be a good example which indicates that the surface ground motions cannot easily be predicted by a simple model.

Dynamic analysis methods have revealed many unexpected aspects of static analyses. However, it should be remembered that many assumptions which need to be adequate are used in dynamic analyses. Hence, seismic design should not totally rely on the results of dynamic analyses.

1.18 Important Factors for Earthquake Disaster Prevention

A basic measure to prevent earthquake disasters is to use an adequate safety factor according to each extent of uncertainty when estimating the earthquake load, calculating structural member actions and thus designing the structure. From past experiences of earthquake disasters [e.g. 1.21, 1.22], the following basic points are also significant in practice,

1. Adequate member details and careful execution of works. For example, in the case of reinforced concrete structures, adequate reinforcing details and good quality of concrete which is well compacted and cured are essential to obtain satisfactory performance of a structure subjected to severe earthquakes.
2. Selection of the construction site. Landfill, sandy soil and hillsides are especially risky areas. The closer the structure is to a fault line the greater the risk.
3. Regularity of the structure. When planing the structure, the horizontal and vertical regularity of the structure should be kept as far as possible.
4. Flexible structures on stiff ground and stiff structures on flexible ground. This concept is to avoid double resonances.

The above basic points should be considered before starting the design calculations. Even if sophisticated inelastic dynamic response analyses are conducted using real strong motion records or reliable artificial ground motions, the importance of adequate structural detailing and careful execution of works should not be overlooked.

1.2. EARTHQUAKE DESIGN METHODS BASED ON THE DUCTILE DESIGN APPROACH

1.2.1 Methods of Design

If a building structure is designed for elastic response loading, thus providing sufficient strength to satisfy the item 3 of the SEAOC recommendations (See p. 2), then item 2 or 2' will automatically be satisfied. This is simply because only a fraction of the provided strength for the major earthquakes is necessary for moderate earthquakes. However, this method is uneconomical as mentioned previously and hence will normally not be used except for the special structures which require the highest protection against any damage, such as atomic power plants. If for economical reasons the structure is to be designed using the ductile design approach, the following aspects should be considered.

The primary function of a building code is to provide minimum standards to assure public safety. Requirements contained in such codes are intended as a safeguard against major failures or loss of life [1.2]. From this point of view, ductile design methods specified in a design code may be aimed primarily at achieving the structural performance described as in the item 3. As a consequence, lower priority may be given to item 2 or 2', unintentionally or intentionally. This might be acceptable due to the difficulty of determining the design intensity for moderate earthquakes.

For example, it may be assumed that if a structure is designed to possess adequate ductility and sufficient ultimate horizontal load carrying capacity to satisfy item 3, then the item 2 or at least 2' will automatically be satisfied just by ensuring that the inter-storey drift of the structures is restricted. Also by appropriate choice of the level of earthquake loading for item 3, it may be ensured that the structure is undamaged when responding to moderate earthquakes. This type of design approach has been adopted in the Capacity Design method of New Zealand[1.5, 1.23].

As an alternative approach, it may be assumed that if a structure is designed to possess adequate strength for the prescribed moderate earthquake loading, item 3 will be satisfied by providing ductile detailing, reasonable structural regularity and a certain surplus of strength. However, in this case, lower priority might be given to the item 3 instead of the item 2 or 2' in reality. This type of design concept has long been used until inelastic analysis methods were well developed. Design based on this concept is still used, for example, in the SEAOC code [1.2]. In the Japanese Building code [1.6, 1.7, 1.8], design based on this concept is allowed to use as an alternative method for when the height of a building is up to 31m.

As a further alternative, the emphasis placed on the item 2 or 2' may need to be as strong as the emphasis placed on item 3, based on cost benefit studies or from the social and economical importance of a particular type of building or structure. In this case, seismic design should be conducted considering both moderate and major earthquakes. Since "with little or no damage to the structural elements" in item 2 or 2' means that the parts of the structural elements need to remain in the elastic range under moderate earthquakes, this condition must be ensured in addition to the safety of the structure under the major earthquakes. During response to earthquake ground motions, the structural behaviours in the elastic and inelastic ranges are significantly different, due to changes of the natural periods of vibration, mode shapes, damping factors and so on. Hence, the inelastic behaviour of a structure cannot simply be inferred from the analyzed results of the structure under elastic conditions, and vice versa. Design procedures for two intensity levels of earthquakes are thus required if the design concept of the item 2 or 2' of the SEAOC recommendations needs to be strictly observed as well as that of the item 3. In this case, the following design approach can be considered. Firstly, the structure is designed for prescribed moderate earthquake loading using an elastic analysis. Secondly, the safety of the designed structure is examined for the more intensive loads of the major earthquakes using an inelastic analysis. If the safety is not confirmed, the structural elements designed in the first procedure are modified and re-examined. This type of design method is adopted in the Japanese building code [1.6, 1.7, 1.8] and in the seismic design guidelines for essential buildings of the US Army, Navy and Air Force [1.3].

1.2.2 Capacity Design Method of New Zealand

The basic philosophy used in the establishment of the capacity design procedure of New Zealand[1.5, 1.23] may be expressed as making a structure behave in the desirable manner intended or predetermined by designers during a major earthquake. This means that the behaviour of the designed structure during a major earthquake should not be a matter of conjecture based on an elastic analysis or a matter of a prediction based on inelastic dynamic analyses using a limited number of simulated strong ground motions. In the capacity design method, it is assured that the strength and ductility required in the various structural elements and connections for the seismic loads prescribed in a particular code are adequate. The level of seismic design load chosen should also be such that the structure is undamaged during moderate earthquakes.

In the capacity design method, as the first step the most desirable energy dissipating mechanism for the structure during a major earthquake is chosen. In the case of a tall frame building, the most suitable mechanism of inelastic deformation is the beam sidesway (beam hinge) mechanism with the column hinges at the bases represented by Fig. 1.3 .

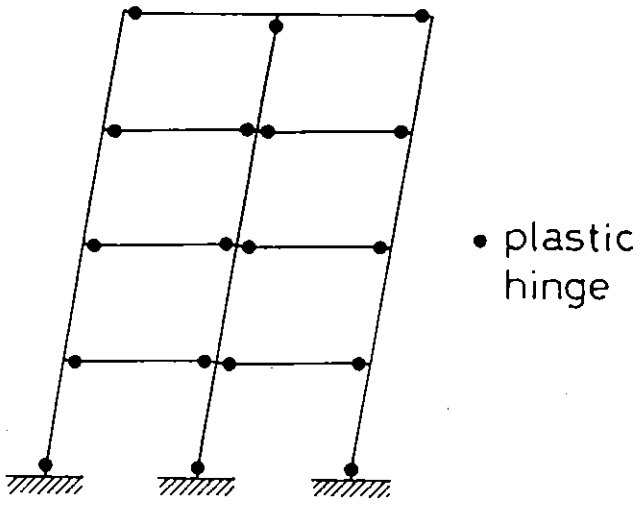

Fig. 1.3 Beam Sidesway (Beam hinge) Mechanism

For tall buildings the formation of column hinge mechanism (see Figs. 1.4 (a) and (b)) must be avoided as far as possible for the following two reasons. Firstly, beams are more easily detailed for ductility than heavily loaded columns. Secondly, in order to reduce the ductility demand at the plastic hinges, the inelastic deformations need to be distributed up the

height of the structure as shown in Figs. 1.3 or 1.4 (a). However, such ideal deformations as in Fig. 1.4 (a) can be hardly achieved, since the actual plastic deformations of the columns will inevitably be concentrated within a particular storey as shown in Fig. 1.4 (b). This is because the storey shear forces induced in each storey by a severe earthquake seldom reach the actual storey shear strength available in all the corresponding storeys. In other words, the formation of column plastic hinges is limited to that storey where the storey shear force first reaches the actual storey shear strength, and thereafter the storey shear forces can hardly increase to generate other column plastic hinges in the rest of storeys.

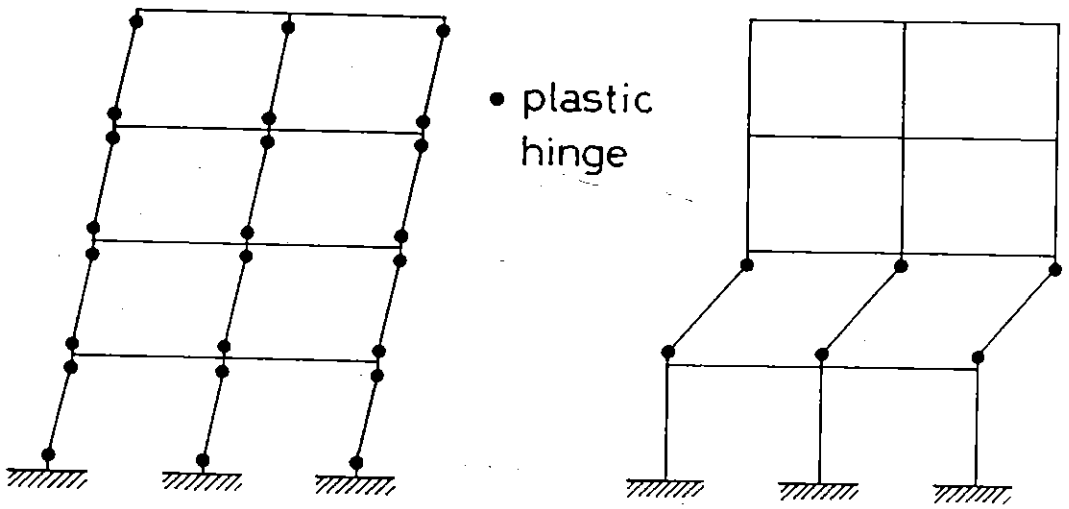

(a) an ideal frame mechanism (b) the most likely mechanism

Fig.1.4 Column Sidesway (Column hinge) Mechanism

A typical design procedure to ensure the formation of a beam sidesway mechanism in a frame building is as follows:

1. Using an elastic frame analysis, the maximum actions in the beams due to the earthquake load and the gravity loads specified in the code are estimated. Redistribution of moments is allowed to be made within the 30% of the absolute maximum moment derived from the elastic analysis. Then, the reinforcement in the beams is designed and detailed.

2. To ensure that the columns have a high degree of protection against flexural yielding, the following factors are evaluated for the determination of the column design moments.

(a)The beam over strength factors, ϕ_0: The beam overstrength factor, ϕ_0, at a column is defined as the ratio of the sum of the flexural

overstrengths developed by the beams as detailed to the sum of the flexural strengths required in the given direction by the Code specified lateral seismic loading alone, both sets of values being taken at the centre line of the relevant column. The flexural overstrength of each beam is estimated, taking into account all possible factors that may contribute to strength such as higher than specified yield strengths of the steel and concrete, strain hardening of steel, and additional steel placed for construction and otherwise uncounted for in calculations.
(b) The dynamic magnification factor, ω: The dynamic magnification factor takes into account the departure of the column bending moment pattern from that which was obtained using the Code specified lateral seismic loading and elastic frame analysis. The departure of the moment pattern is due to dynamic effects, in particular the higher modes of vibration during the response of the structure. Moreover, the concurrent development of plastic hinging in all beams framing into a column due to a possible bi- directional earthquake attack is also taken into account and thus higher dynamic magnification factors are adapted to two-way frame structures than for one-way frame structures.

Each column bending moment at the centre line of a beam, derived using elastic frame analysis for the code specified lateral seismic loading alone without any moment redistribution, is denoted as M_{code}. This M_{code} is now multiplied by the above two factors, $\omega \cdot \phi_0$. Then $M_{code} \cdot \omega \cdot \phi_0$ at the centre line of a beam is reduced assuming that the critical section is at the top or the soffit of the beam, where only 60 % of moment gradient used for the determination of the column shear is considered for the moment reduction. The obtained moment is used as the column design moment. However, a greater reduction is permitted if the design axial load determined in the next step is less than 10 % of $f'_c A_g$ (where f'_c =specified compressive strength of concrete and A_g= gross area of the column section), because column yielding is more acceptable under small axial compression or net tension loads.

3. The design axial load of each column is determined by choosing an adequate combination of dead loads and live loads and an earthquake induced load. Here also, the overstrengths of structural members are

considered when estimating the earthquake induced axial load. A certain reduction is allowed, based on the assumption that, with increasing number of storeys above the specified level, the relative number of beam hinges at which the flexural overstrength may be developed simultaneously is reduced.

4. The design shear force of each column in upper storeys, excluding the first storey, is determined by multiplying the column shear force derived from the elastic analysis by the beam overstrength factor and an additional strength reserve factor. For the shear force in the first storey columns, a more stringent estimate is used because, at the base of the first storey column, hinging with considerable plastic rotations is to be expected.

5. Finally, the columns are designed using the moments, the axial loads and shear forces determined in the above steps.

The ideal values of overstrength factors ϕ_0 shown in the commentary of NZS 3101 code [1.23] are 1.39 using Grade 275 steel and 1.56 using Grade 380 steel, taking into account that the dependable strength is calculated using nominal strengths of materials with a strength reduction factor, ϕ, of 0.9 [1.23]. The commentary of the NZS 3101 code also states that; (a) When gravity load dominates the required beam flexural strength, these values may be greatly exceeded, and (b) When beam moment redistribution is applied the value of ϕ_0 may be locally less than the above values. In the code, for the column at roof level, ϕ_0=1.1 is recommend because the column hinging at this level is acceptable, and the value of ϕ_0 at a column base is specified to be more than 1.4 in order to ensure that the ideal lateral load strength of this storey is comparable with the remainder of the frame.

The values of the dynamic magnification factor, ω, are a function of the computed period of the structure in its first mode of vibration. In case of two-way frame buildings, those values stipulated in the code [1.23] are 1.10 for the ground level floor and the roof, and in the range of 1.50 to 1.90 for from the first floor to the floor immediately below roof level. Hence, the values of products, $\omega \cdot \phi_0$ may result in about 1.2 at the roof, 1.6 at the ground level floor and in the range of about between 2.1 to 3.0 for the rest of floors if the earthquake loading is much more predominant than the gravity loads.

The most prominent aspect of the capacity design method of New Zealand is the significant protection given against premature yielding of columns and hence the assurance of the formation of plastic hinges mainly in beams. As can be seen from the above values of $\omega \cdot \phi_o$, the design flexural strengths of most columns reach to about 2 or more times of the design moments calculated from elastic analysis for the code specified lateral loading for each principal direction.

With regard to the design intensity of earthquake loading prescribed in the New Zealand code [1.5], a base shear coefficient of 0.05 to 0.15 g, depending on the seismic zone and the period of vibration, is adopted for structural steel or reinforced non-prestressed concrete frame buildings with displacement ductility factors of 4 or more, provided that buildings are for normal usage or with normal occupancy. The earthquake loading is increased using risk factors specified in the code depending on the importance of the structure to the community or the likely hazard due to the contents of the structure.

In New Zealand, the earthquake design intensity used for buildings for normal usage or with normal occupancy is that corresponding to the response spectra for the earthquakes of 150 years return period [1.4, 1.25]. The average return period of earthquakes in New Zealand has been assessed by some seismologists [1.24] as:

MM VI every 6 years
MM VII every 21 years
MM VIII every 67 years
MM IX every 220 years

The Modified- Mercalli intensity scale is a subjective measure of the effect of the ground shaking and is not an engineering measure of the ground acceleration. However, the above assessment gives an idea of the seismicity of New Zealand.

The capacity design method is obviously aimed at the prevention of collapse of structures due to the major earthquakes and does not clearly indicate the assurance level of no damage of structures during moderate earthquakes. However, in New Zealand, it is considered that the strengths

of structures implicitly provided by the capacity design procedure will be generally sufficient to prevent damage during moderate earthquakes.

1.2.3 The Japanese Building Code

In the Japanese building code[1.6, 1.7, 1.8], moderate earthquakes in the zones of the highest seismic intensity factor are interpreted as those which generate an elastic response of 0.2 g at the base of low-rise buildings. This value corresponds to the maximum effective horizontal acceleration of 80 to 100 gal on the ground surface. For this load level of earthquake, as the first step elastic structural analysis is conducted using trial member sections and then the details of the member sections are determined based on the derived member actions, using allowable stress design. The allowable compressive and tensile stresses for longitudinal reinforcing steel are the specified yield strength and the allowable compressive stress for concrete is two-third of the specified compressive strength. The inter-storey drifts are checked at this step. The above seismic design load level was determined based on the experience that old buildings, which had been designed using a base shear coefficient of 0.2 g, seldom had structural damage during the moderate earthquakes.

As the second step, the ultimate strength of each structural element designed in the previous step is calculated. Then the ultimate lateral load carrying capacity of each story is calculated by any method including incremental non linear analysis, limit analysis and other simplified methods. Finally, the ultimate lateral load carrying capacity of each story is checked as to whether it is sufficient against each corresponding lateral storey shear due to a major earthquake calculated from the code specifications. If the result of this check was not satisfactory, the designed sections are modified and return to the second step.

A major earthquakes in the zones of the highest seismic intensity factor are interpreted as those which cause the maximum effective horizontal acceleration of 300 to 400 gal on the ground surface, like the great Kanto earthquake of 1923. If a low-rise building with the natural period of vibration of less than about 0.4 second responds elastically to such

earthquakes, a base shear coefficient of 1.0 g or more is required to be used. For ductile frame buildings, 0.25 g for steel structures and 0.3 g for reinforced concrete structures are used as the minimum base shear coefficients. These values may be increased, depending on the ductility level and the vertical and horizontal irregularities of the structure.

These design procedures are compulsory for buildings which are 31 to 60 m in height except when an equivalent or more sophisticated design method, which is approved by the Ministry of Construction, is used. Buildings which are more than 60 m high must be designed by a special study usually incorporating time-history non-linear response analysis and the design method used must be approved by the Ministry of Construction.

In case of buildings up to 31 m in height, the check of the ultimate lateral load carrying capacities of each story can be omitted if the building design against the moderate earthquakes satisfies several restrictions. Those restrictions are related to the horizontal eccentricity of rigidity of each storey, the vertical distribution of storey rigidity, the ductility and the surplus of strength.

The above design methods for two levels of earthquakes may give practitioners a more thorough understanding of structural behaviour under elastic and inelastic conditions during earthquake motions and possibly leads to higher protection of buildings. However, a defect of this design method is that there exists the possibility of the formation of plastic hinges in the columns of one storey if the practitioners' efforts are just directed to meet the inter-storey drift limits and the lateral load carrying capacities required. This may lead to a dangerous situation in a severe earthquake. Because of this point, the Capacity Design method of New Zealand [1.5], which is explicitly aimed at the formation of beam hinge mechanism under major earthquakes, may be said to be more appropriate.

An inconvenience which appears in the design method for two levels of earthquakes is that an iteration of the calculation is required when the result of the second check is not satisfactory. Moreover, the double checking procedures may lose meaning if the following situations occur;

1. For identical types of buildings, the designed sections of structural components are dominated either by the elastic design procedure or by

the inelastic design procedure. In this case one of the procedures can undoubtedly be omitted for the identified type of building.

2. The estimated economical loss under earthquakes due to the neglect of one of the design procedures is not as significant as the additional expenditure and labour due to double checking.

3. The required modifications of the designed sections by the second check are negligible.

4. The designed sections are dominated by the serviceability limit state or wind loading rather than by earthquake loading. In this case, the check for the moderate earthquakes is obviously meaningless. This situation can occur in countries of low seismicity, but it seldom happens in Japan due to its high earthquake design loads.

It should be noted that the effectiveness of the above design methods depends heavily on the setting of each load intensity level against the chosen level of moderate earthquakes and major earthquakes. As a matter of course, each load intensity level must not be selected to intentionally avoid the situations listed above. The two levels of the earthquake design intensities must be determined on the basis of probabilistic studies of earthquakes, such as shown in reference [1.9]. In the reference [1.9], moderate earthquakes are defined using the peak value of the probabilistic density function of seismic intensity.

1.2.4 The Seismic Design Guidelines for Essential Buildings of the US Army, Navy and Air Force

In the seismic design guidelines for essential buildings of the US Army, Navy and Air Force [1.3], the moderate earthquake (designated as the first level of earthquake) is specified as having a 50 % probability of being exceeded in 50 years. The major earthquake (designated as the second level of earthquake) is specified as having a 10 % probability being exceeded in 100 years. The basic design work flow is almost same as the Japanese building code although the checks are more sophisticated as it is specified that spectral modal analysis be used for the first level of earthquake design. The inter-storey drifts are checked for both levels of earthquakes. Another difference from the Japanese building code is that, in the first procedure of the elastic design, some slight flexural yielding of a limited number of

structural components is accepted provided that the overall behaviour of the structure is still substantially linear-elastic.

This United States method is only for essential buildings, where essential buildings are defined as "those which must be functional for emergency post earthquake operations" [1.2].

1.3 SCOPE OF RESEARCH

There are still many aspects of the seismic design of reinforced concrete structures which have not yet been completely determined, as described in the previous sections. However, it is evident that adequate reinforcing details are essential to obtain satisfactory performance of reinforced concrete structures subjected to severe seismic loading. The effective confinement of core concrete by transverse reinforcement is of great importance for that purpose, especially when the ductile design approach is used. The research reported in this thesis is mainly focussed on the effectiveness of various lateral reinforcing details for improving the ductility of reinforced concrete columns.

With regard to the stress-strain behaviour of confined concrete, many studies have been conducted during the past few decades and a number of stress-strain models have been proposed by various researchers. However, the assessment of the strength and ductility enhancement of concrete due to lateral confinement is not always consistent between those researchers. This is because many factors are involved for that assessment, such as the spacing and the configuration of transverse reinforcement, the diameter and yield strength of transverse reinforcing bars, the plain concrete strength, the size and shape of test specimens, the loading and measuring method, etc. In Chapter 2, along with discussion on the effects of those factors, several stress-strain models for confined concrete including the model proposed by the author et al are compared. It is noted that the tests conducted by the author at Kyoto University and Akashi Technological College, Japan, used transverse reinforcement with yield strengths up to 1300 MPa and concrete with compressive strengths up to 60MPa as experimental variables. Most of the previous studies were conducted using the range of strength of materials which are typical of engineering

practice. The improvement of the ductility of high strength concrete by using transverse reinforcement from high strength steel is becoming an important matter since high rise reinforced concrete buildings of more than 20 storeys have recently begun to be constructed even in a severe seismic country like Japan.

When the ductility of the plastic hinge regions of reinforced concrete columns is to be improved, the amount of transverse reinforcement and the anchorage details of transverse reinforcement become important factors. The role of transverse reinforcement is to effectively confine the compressed core concrete, to prevent buckling of longitudinal reinforcement, and to prevent shear failure. In the plastic hinge regions of columns, the transverse reinforcement normally yields due to the tension caused by the lateral expansion of the confined concrete, the outward force from the longitudinal reinforcement, and the opening of inclined flexural shear cracks, when the columns are loaded far into the inelastic range. Hence, transverse reinforcement needs to be securely anchored in order to sustain the yield force of the hoop and cross tie legs until the final deformation condition of the column is reached. For this reason, seismic design codes for concrete structures such as NZS 3101:1982 [1.5], CEB-FIP Model Code:1982 [1.27] and JASS-5:1979 [1.28] specify that hoops and cross ties in the columns shall be anchored by 135° end hooks which turn around longitudinal bars and are embedded in the concrete core or by welding of those tie ends. However, those anchorage details can sometimes result in a complicated reinforcing fixing job, especially on construction sites. In order to ease the difficulty of placing transverse reinforcement several alternative details for cross ties which simplify the fabrication of reinforcing cages have been used in the United States and other countries. One alternative detail involves the use of cross ties with 90° end hook at one end and 135° end hook at the other end. The other alternative detail involves the use of 'J' bars which have a 135° end hook at one end and are inserted from each side of the cage and lapped in the core concrete. A further alternative detail is to use 'U' bars which are inserted from each side of the cage and lapped in the core concrete. However, it is to be noted that those alternative anchorage details for cross ties have not been sufficiently examined to reach a consistent assessment of their effectiveness, although there are several experimental studies with respect to the effectiveness of cross ties with 90° end hook at one end and 135° end hook at the other end. The research

project described in Chapter three was planned to investigate experimentally the effectiveness of those alternative anchorage details.

In Chapter four, an experimental and theoretical study of the effectiveness of interlocking spirals as confining reinforcement is reported. A column section with interlocking spirals has been introduced in the standard specifications for highway bridges adopted by the American Association of State Highway and Transportation Officials with revisions by California Transportation Authority (AASHTO:1977 and by CALTRANS:1983 [1.29]). When a column has a rectangular section, transverse reinforcing details using the interlocking spirals will have the following advantages. Firstly, the amount of transverse reinforcement, required to provide adequate ductility in potential plastic hinge regions of columns, may be considerably reduced by using interlocking spirals instead of overlapping rectangular hoops or rectangular hoops with cross ties. This is because spirals confine the core concrete much more effectively than rectangular hoops. Secondly, the fixing of reinforcement may become easier if interlocking spirals are used instead of overlapping rectangular hoops or rectangular hoops with cross ties, especially when column sectional dimensions are large. This is because, if rectangular perimeter hoops are used for a large rectangular column section, many cross ties and/or overlapping hoops are normally required in order to cross-tie the longitudinal bars which are placed between the corners of the section. Nevertheless the CALTRANS code provisions do not provide all the necessary information or specifications for the use of interlocking spirals, especially on how to securely interlock the spirals in order to prevent shear failure. This is because no past experimental or theoretical study of interlocking spirals has been conducted. The CALTRANS code provisions are based on the studies of circular columns with single spirals or circular hoops. In Chapter four, firstly, the general aspects and related problems of interlocking spirals when used to provide ductility in the potential plastic hinge region of columns are discussed, referring to the provisions in the New Zealand code [1.5], the CALTRANS code [1.29] and other related codes. Secondly, based on those discussions, a design method to securely interlock the spirals is proposed. Thirdly, the effectiveness of interlocking spirals is assessed based on the results of the column test obtained in this current study.

Prevention of premature buckling of longitudinal reinforcement is an important consideration for adequate ductility for reinforced concrete columns. For this reason, in the New Zealand code [1.5] the spacing of hoop sets has been specified to be not greater than 6 times the diameter of the longitudinal bar in the potential plastic hinge region. It is noted that this limit for the spacing of hoop sets has been determined on the premise that the longitudinal bar is strongly restrained by 135° end hooks embedded in the core concrete or the corner of a well anchored hoop. If cross ties with a 90° end hook at one end and a 135° end hook at the other end are accepted to use for seismic resistant members, as admitted in the ACI code, the limit for the spacing of hoop sets specified in the New Zealand code may need to be revised. This is because 90° end hooks can open out after spalling of the cover concrete, leading to the loss of restraint against the buckling of the longitudinal bar. In Chapter five, analytical models to investigate the buckling behaviour of longitudinal reinforcement restrained by cross ties with 90° and 135° end hooks and by peripheral hoops are proposed. Using these models, a method to check the effectiveness of cross ties with 90° and 135° end hooks is proposed for practical design purposes.

When a reinforced concrete column is loaded far into the inelastic range, fracture of the hoop reinforcement sometimes occurs, especially in the case of circular hoops or spirals, and results in a sudden drop in load carrying capacity of the section due to a reduction in confinement of the core concrete and a loss of buckling restraint for the longitudinal bars. This stage of failure signals the destruction of the column. Hence, hoop fracture must be avoided within the expected range of column deformation under any design load condition, especially when the deformations are imposed by a severe earthquake. In order to provide such a restriction to the column deformation, a method for the prediction of the available maximum deformation of the column section limited by the occurrence of hoop fracture is required. Mander et al [1.30] have proposed a theory for the prediction of the ultimate longitudinal compressive concrete strain at the stage of first hoop fracture referred to as the "Energy Balance Theory". In this theory, the relation between the strain energy stored or dissipated in the cover and core concrete, longitudinal reinforcement and hoops was simplified without strictly observing the energy rules and hence the theory does not always give an adequate estimate of the ultimate concrete strain at first hoop fracture. In Chapter 6, after discussing the problems in the

"Energy Balance Theory" proposed by Mander et al, a modified theory for the prediction of the ultimate longitudinal compressive concrete strain at which first hoop fracture occurs is proposed using a simple failure model of a reinforced concrete column under axial compression load. This modified model is assessed by comparison with the results of previous axial compression loading tests on columns and also with the results of the flexural shear tests on the columns with interlocking spirals described in Chapter four.

Finally, the conclusions reached during the course of this research project are summarized in Chapter seven. On the basis of the results obtained in this study, a number of experimental and theoretical topics are recommended for future research work.

CHAPTER TWO

CONFINED CONCRETE

2.1 INTRODUCTION

When ductile design approach is used in seismic design, structural members are required to behave in a ductile manner so as to absorb and dissipate the great energy transmitted from severe earthquakes. Confinement of core concrete is an effective method to provide an adequate ductility for reinforced concrete members, especially when comparatively high axial load is imposed. It is well known that, when the axial load level is not high, the ductility of reinforced concrete members can be secured to some extent by limiting the reinforcement index, $q = \frac{\rho_{tn} f_y}{f'_c}$, to a small magnitude, where ρ_{tn} = ratio of tension reinforcement area to b_w d (where b_w = section width and d= effective depth of section), f_y = yield strength of tension reinforcement and f'_c = compressive strength of concrete. However, such a design method by limiting the magnitude of reinforcement index is normally uneconomical, because a large member section is required due to the small amount of tension reinforcement provided.

It may be said that a great number of studies on confined concrete have been conducted for several decades and much fundamental knowledge about the confined concrete has already been accumulated. However, it must be noted that those studies were mostly conducted in a limited range of strength of materials. That is, the uniaxial compressive strength of concrete and the steel strength of transverse reinforcement used in those studies were mostly up to about 40 MPa and 400 MPa, respectively. In recent years high rise reinforced concrete buildings more than 20 storeys high have begun to be constructed using high strength concrete and transverse reinforcement with high strength steel, for example, in Japan. When columns with high strength concrete are subjected to severe seismic loading combined with high axial load, the ductility demand for columns at yield hinging zones may be satisfied only by providing the core concrete with intensive confinement achieved by using high strength transverse reinforcement. Thus, the importance of profound knowledge about the

characteristics of confined concrete is increasing with increase of material strength used.

In this chapter, after reviewing previous research on the confined concrete, factors which affect effectiveness of lateral confinement are discussed. Especially, the effectiveness of high strength transverse reinforcement with yield strength of more than 800MPa is discussed based on column tests conducted by the author of this thesis at Kyoto University and Akashi Technological College, Japan, under the supervision of Professor H. Muguruma and Associate Professor F. Watanabe, Kyoto Universirty.

2.2 REVIEW OF PREVIOUS RESEARCH AND STRESS-STRAIN MODELS

2.2.1 Active Confinement and Passive Confinement

The strength and ductility of concrete are remarkably enhanced under conditions of triaxial compression. In 1903, Considere had shown the effectiveness of spirally reinforced concrete columns for resisting axial compression and practical details of construction to achieve effective confinement [2.1]. Since then numerous studies on confined concrete have been conducted for application to reinforced and prestressed concrete structures. Those studies can be classified into two basic groups; that is, studies on concrete behaviours obtained from active confinement and those from passive confinement. The studies on active confinement were to investigate the basic behaviour of concrete as a material under triaxial compressive stress condition. Active confinement is normally provided by fluid pressure or mechanical pressure in experimental studies and hence the confining stress level can be freely selected within the limit of pressure devices. On the other hand, passive confinement is normally provided by transverse reinforcement in practice of construction. In this case, at low levels of stress in the concrete, the transverse reinforcement is hardly stressed and hence the concrete is unconfined. The concrete becomes confined when at stresses approaching the uniaxial strength, the transverse strains become very high due to progressive internal cracking and the concrete bears out against the transverse reinforcement, which then applies a confining reaction to the concrete [2.2]. Due to such action, the

confinement by transverse reinforcement is referred to as passive confinement.

With respect to active confinement tests, Richart, Brandzaeg and Brown [2.3] found the following relationship for the strength of concrete cylinders loaded axially to failure while subjected to confining fluid pressure

$$f'_{cc} = f'_c + 4.1\, f_l \qquad \text{.....} \qquad (2.1)$$

where f'_{cc} = axial compressive strength of confined specimen
f'_c = uniaxial compressive strength of unconfined specimen
f_l = confining fluid pressure

Other tests by Balmer [2.4] have given values for the lateral stress coefficient which range between 4.5 to 7.0 with average of 5.6, rather than the 4.1 found by Richart et al. Fig. 2.1 illustrates the axial stress-strain curves obtained by Richart et al [2.3] for triaxial compression tests conducted on concrete cylinders. For each curve the fluid pressure was held constant while the axial compressive stress was increased to failure.

It is notable that the concrete behaviour with active confinement can be closely related to that with passive confinement. For example, Richart et al [2.5] found that the strength increase of concrete with active confinement obtained by fluid pressure was approximately the same as for concrete confined by closely spaced circular spirals causing an equivalent lateral pressure. For this reason, the studies based on active confinement tests have provided the basis of many stress-strain models for concrete confined by transverse reinforcement which were proposed in the past. A typical example is the stress-strain model proposed by Mander et al [2.6], where the stress-strain relationships of confined concrete are modelled using equivalent fluid pressures estimated for various types of transverse reinforcement.

For concrete cylinders with active confinement provided by fluid pressure, a notable fact is that, in all locations of transverse section of a cyclinder, $\sigma_r = \sigma_\theta$ = constant and $\tau_{r\theta} = 0$, where σ_r = the normal stress component in the radial direction, σ_θ = the normal component in the

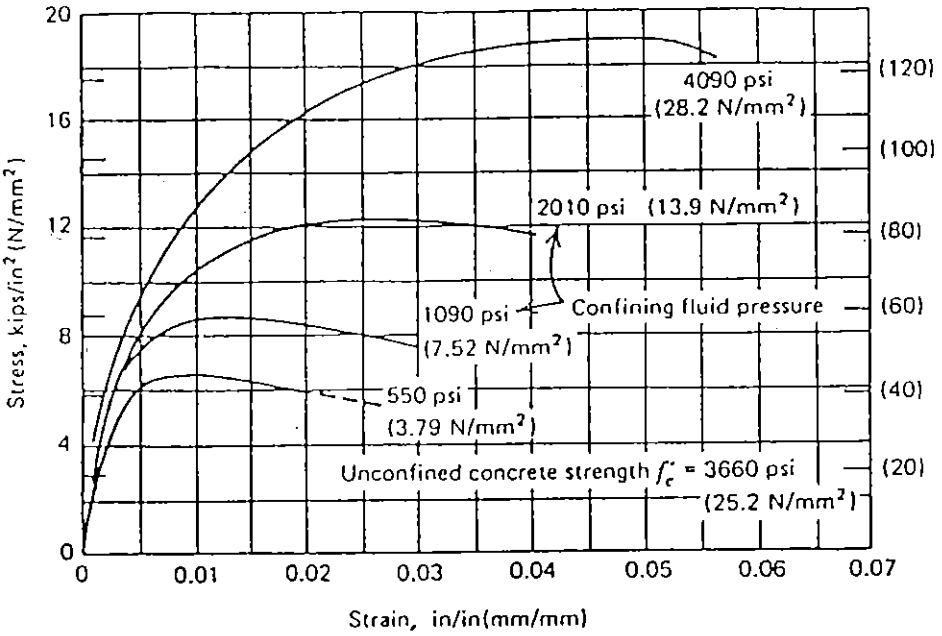

Fig. 2.1 Axial Stress-Strain Curves from Triaxial Compression Tests on Concrete Cylinders [2.3].

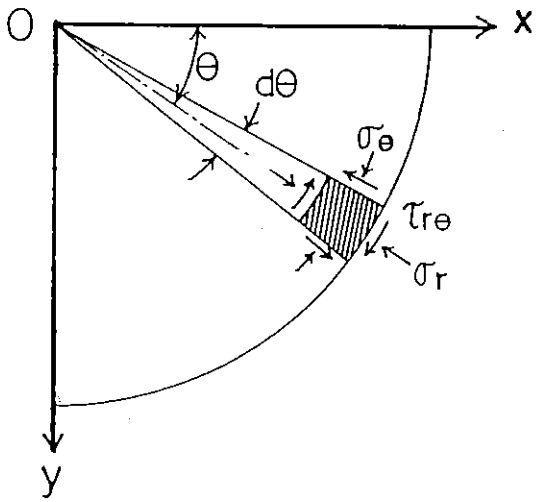

Fig. 2.2 Stress Condition on a Small Element of a Cylinder with Lateral Fluid Pressure Expressed by Polar Coordinates.

circumferential direction and $\tau_{r\theta}$ = the shearing stress component (see Fig. 2.2). This can be proved using polar coordinates as follows [2.7];

Taking a small element shown in Fig. 2.2 and assuming the body force is zero, from equilibrium,

$$\sigma_r = \frac{1}{r}\frac{\partial \phi}{\partial r} + \frac{1}{r^2}\frac{\partial^2 \phi}{\partial \theta^2} \quad \text{.....} \quad (2.2)$$

$$\sigma_\theta = \frac{\partial^2 \phi}{\partial r^2} \quad \text{.....} \quad (2.3)$$

$$\tau_{r\theta} = \frac{1}{r^2}\frac{\partial \phi}{\partial \theta} - \frac{1}{r}\frac{\partial^2 \phi}{\partial r \partial \theta} = -\frac{\partial}{\partial r}\left(\frac{1}{r}\frac{\partial \phi}{\partial \theta}\right) \quad \text{.....} \quad (2.4)$$

where ϕ is the stress function of r and θ.

The equation of compatibility is expressed as

$$\left(\frac{\partial^2}{\partial r^2} + \frac{1}{r}\frac{\partial}{\partial r} + \frac{1}{r^2}\frac{\partial^2}{\partial \theta^2}\right)\left(\frac{\partial^2 \phi}{\partial r^2} + \frac{1}{r}\frac{\partial \phi}{\partial r} + \frac{1}{r^2}\frac{\partial^2 \phi}{\partial \theta^2}\right) = 0$$

As the stress fuction depends on r only for the case under uniform lateral pressure without surface friction, the above compatibility equation becomes

$$\left(\frac{d^2}{dr^2} + \frac{1}{r}\frac{d}{dr}\right)\left(\frac{d^2 \phi}{dr^2} + \frac{1}{r}\frac{d\phi}{dr}\right)$$
$$= \frac{d^4 \phi}{dr^4} + \frac{2}{r}\frac{d^3 \phi}{dr^3} - \frac{1}{r^2}\frac{d^2 \phi}{dr^2} + \frac{1}{r^3}\frac{d\phi}{dr} = 0 \quad \text{.....} \quad (2.5)$$

The general solution of the above equation is

$$\phi = A \log r + B r^2 \log r + C r^2 + D$$

Substituting into Eqs. 2.2 to 2.4,

$$\sigma_r = \frac{1}{r}\frac{\partial \phi}{\partial r} = \frac{A}{r^2} + B(1 + 2\log r) + C \quad \text{.....} \quad (2.6)$$

$$\sigma_\theta = \frac{\partial^2 \phi}{\partial r^2} = -\frac{A}{r^2} + B(3 + 2\log r) + C \quad \text{.....} \quad (2.7)$$

$$\tau_{r\theta} = 0 \quad \text{.....} \quad (2.8)$$

In Eqs. 2.6 and 2.7, constants A and B must be zero since otherwise the stress components expressed by those equarions become infinite when r = 0. Thus, $\sigma_r = \sigma_\theta$ = constant in all locations in the circular section of the cylinder.

Thus, when lateral fluid pressure and axial load are applied to a cylinder, the triaxial stress condition is all the same in all locations inside the cylinder, provided that there is no friction between the end faces of the cylinder and the axial loading plates.

2.2.2 Fundamental Characteristics of Concrete Confined by Transverse Reinforcement

In practice, the core concrete in a member is confined by closely spaced transverse reinforcement in the form of circular spirals or rectangular hoops with or without cross-ties. It has been recognized that confinement by circular hoops or spirals is more effective than by rectangular hoops. Fig. 2.3 [2.8] shows the stress-strain curves obtained from axial compression tests on 150 mm diameter concrete cylinders confined by various contents of spirals. It is obvious that both the strength and ductility can greatly be enhanced by spiral reinforcement. On the other hand, comparatively small effectiveness of confinement by square hoops can be recognized from Fig 2.4 which shows axial load-strain curves for 108 mm square concrete prisms confined by various contents of square ties [2.9].

Circular hoops or spirals, because of their shape, are in axial hoop tension and provide a continuous confining pressure arround the circumference, as illustrated in Fig. 2.5 (a). However, in case of rectangular or square hoops, confining reactions can mostly act near the corners of hoops because the pressure of the core concrete tends to bend the sides outwards as shown in Fig.2.5 (b). This can be explained taking a square hoop with side length, h", as an example;

The area of the square core section is $(h")^2$. In the limit, if the square hoop turns into circular shape due to bending of the hoop side bars, the diameter of circular core section (D') is $4\ h" / \pi$. Hence, the core area A_c is calculated as

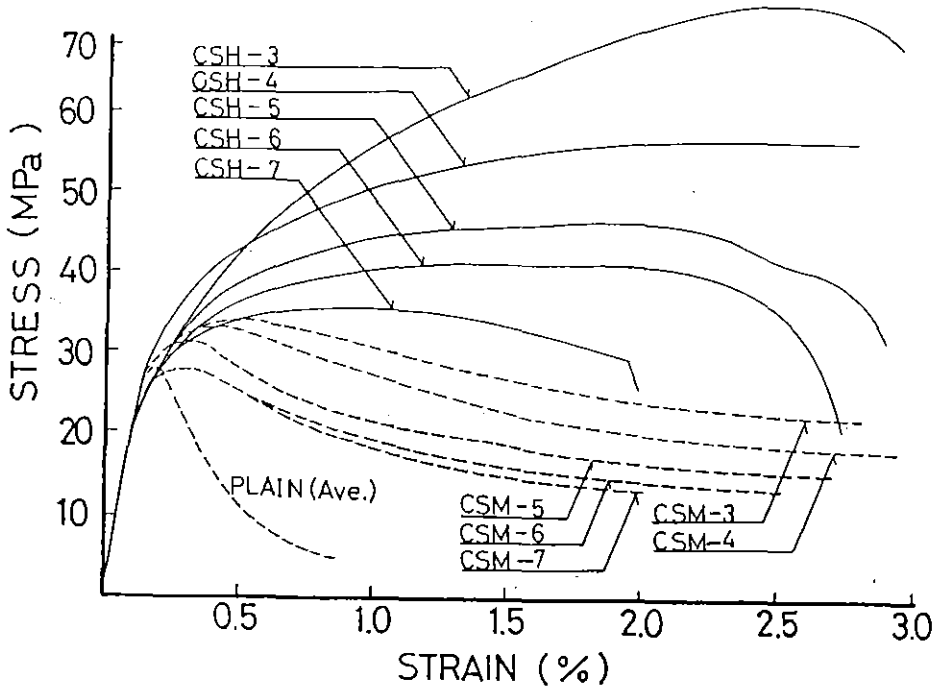

Note; CSM : 5 mm diameter spiral reinforcement with yield strength of 161 MPa
CSH : 6.4 mm diameter spiral reinforcement with yield strength of 1352 MPa
Number following the notation CSM or CSH: pitch of spirals in cm

Fig. 2.3 Stress-Strain Curves for 150 mm diameter Concrete Cylinders with Various Contents of Spirals [2.8].

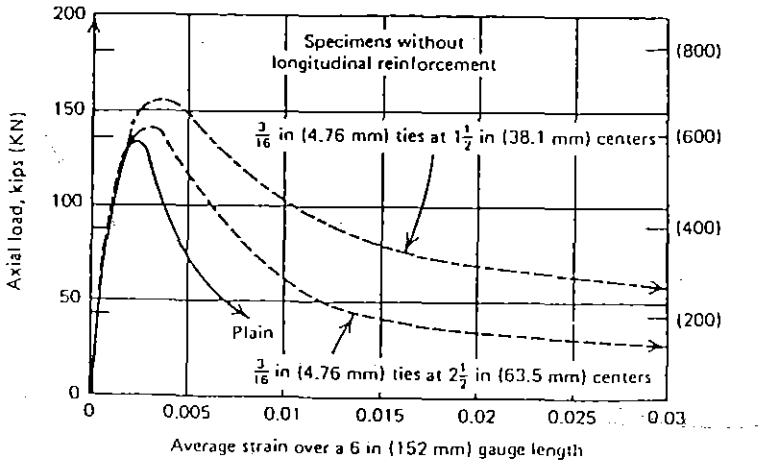

Fig. 2.4 Axial Load - Strain Curves for 108 mm Square Concrete Prisms with Various Contents of Square Ties [2.9].

$$A_c = \frac{\pi (D')^2}{4} = \frac{4 (h'')^2}{\pi} = 1.27 (h'')^2 > (h'')^2$$

This implies that the increase of concrete core area does not necessarily cause hoop tension, if the concrete core section shape gradually changes into a round shape as damage of core concrete progresses. Thus, the square hoop cannot effectively resist the expansion of core concrete unless the core concrete expands without changing the square section shape or the bending stiffness of the hoop bar is significantly large. In reality, the hoop bar diameter is normally much smaller than the support length between corner longitudinal bars and hence the bending stiffness is not dependable. This means that passive confinement by square or rectangular hoops is achieved mainly by expansion of core concrete in the diagonal direction of section.

The relation between the transverse bar stress and the confining pressure is indicated in Fig. 2.6. If the equilibrium of the free body diagram of a column with circular hoops is considered as shown in Fig. 2.6 (a), the confining pressure, σ_l, equivalent to the fluid pressure is

$$\sigma_l = \frac{2 A_{sp} f_{sp}}{s D'} \qquad \text{.....} \qquad (2.9)$$

where A_{sp} = area of circular hoop bar
f_{sp} = stress in circular hoop bar
s = pitch of circular hoop reinforcement

This is because $\sigma_r = \sigma_\theta = \sigma_l$ = constant in all locations in the section plane as has been proved in Section 2.2.1.

The expression for the strength of confined concrete derived from tests with fluid pressure is assumed to be applicable to concrete confined by transverse reinforcement. Hence, from Eqs. 2.1 and 2.9 the strength of confined concrete, f'_{cc}, may be related to the stress in circular hoops or spirals as;

$$f'_{cc} = f'_c + \frac{8.2 A_{sp} f_{sp}}{s D'}$$

Richart et al [2.5] found that this relationship represents the test results of spirally reinforced circular columns when f'_c is replaced by 0.85 f'_c giving

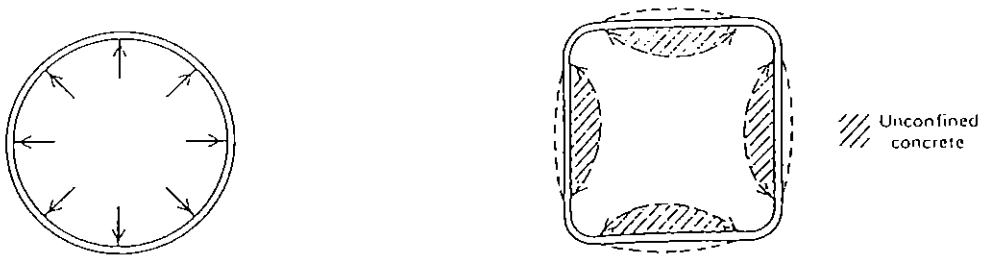

(a) Circular Hoop (b) Square Hoop

Fig. 2.5 Confinement by Square Hoops and Circular Hoops or Spirals [2.2]

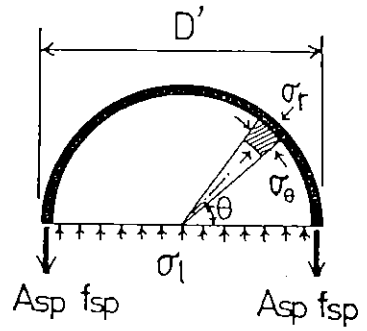

(Section Free-Body Diagram)

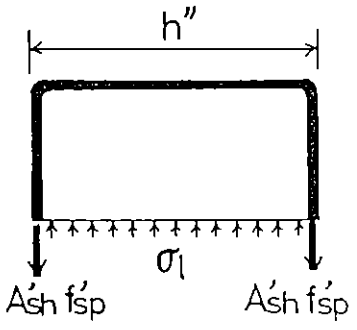

(Section Free-Body Diagram)

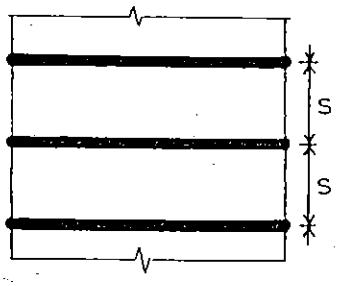

(a) Circular Column With Circular Hoops

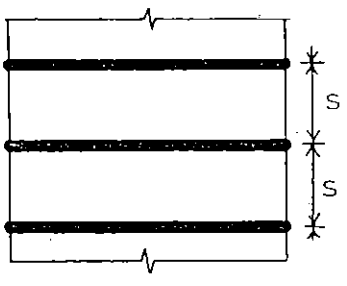

(b) Square Column with Square Hoops

Fig. 2.6 Confinement of Concrete by Transverse Reinforcement.

$$f'_{cc} = 0.85\, f'_c + \frac{8.2\, A_{sp}\, f_{sp}}{s\, D'} \qquad \text{.....} \qquad (2.10)$$

In case of rectangular hoops, if the equilibrium of the free body diagram is considered as shown in Fig. 2.6 (b), the unit lateral confining pressure, σ_{lh}, is

$$\sigma_{lh} = \frac{2\, A'_{sh}\, f'_{sh}}{s_h\, h''} \qquad \text{.....} \qquad (2.11)$$

where A'_{sh} = section area of rectangular hoop bar

f'_{sh} = stress in rectangular hoop bar

s_h = pitch of rectangular hoop reinforcement

However, it must be emphasized that the confining pressure from rectangular hoops cannot be unifom in the transverse section like shown in Fig. 2.5 (b) and hence the efficiency of confinement is significantly reduced compared with the spirals or circular hoop reinforcement. In the reference [2.5], it was recommended to reduce the lateral pressure estimated by Eq. 2.11 by 50 % as expressed by

$$\sigma_{lh} = 0.5\ \frac{2\, A'_{sh}\, f'_{sh}}{s_h\, h''} \qquad \text{.....} \qquad (2.12)$$

and, similar to the core strength of a spirally reinforced circular column expressed by Eq. 2.10, the strength of the core of a rectangular column with closely spaced rectangular hoops was expressed as

$$f'_{cc} = 0.85\, f'_c + \frac{4.1 A'_{sh}\, f'_{sh}}{s_h\, h''} \qquad \text{.....} \qquad (2.13)$$

However, it is notable that the strength enhancement of concrete confined by rectangular hoops has not always been found to be appreciable. For example, Roy and Sozen's tests [2.10] suggested that there was no increase in concrete strength due to confinement by rectangular hoop reinforcement although significant increase in concrete ductility was recognized.

In these days, in order to improve the efficiency of rectangular hoops by reducing the ineffectively confined area, various types of transverse reinforcing details have been contrived combining peripheral hoops with

overlapping hoops and/or supplementary cross ties as shown in Figs. 2.7 and 2.8 [2.11]. These types of transverse reinforcing details may be more effective than expressed by Eq. 2.13. Sheikh and Uzumeri [2.1, 2.13] proposed a method to estimate the effectively confined core area as shown in Fig. 2.9. In the figure, the assumed effectively confined area is surrounded by second degree parbolic curves. This method was used in their stress-strain model for confined concrete [2.13] and agreed well with accompanied test results. Mander, Priestley and Park also used this method for estimating the effectively confined concrete core area when proposing a stress-strain model for confined concrete [2.6].

The ductility enhancement of concrete, due to confinement by transverse reinforcement, is discussed in the following section by reviewing several notable stress-strain models proposed in the past.

2.2.3 Stress-Strain Models of Confined Concrete

For the core concrete confined by various types of transverse reinforcement, a number of stress-strain models have been proposed based on concentric loading tests on concrete specimens or, in some cases, based on eccentric loading tests [eg. 2.8, 2.14] which take into account the effect of concrete strain gradient in the transverse section. Most of those stress-strain models are derived based on the following observations; (1) The lateral confining pressure which increases the strength and ductility of concrete is related to the shape of the arrangements of the transverse reinforcement, the pitch and the yield strength of transverse reinforcement, and the volumetric ratio of transverse reinforcement to concrete core volume, (2) Confinement becomes less effective for concrete with higher uniaxial compressive strength.

In addition to the above factors, the stress-strain relation of the confined concrete is also affected by the reinforcing details of transverse reinforcement combined with longitudinal reinforcement, the scale effect of tested specimens which are used to calibrate the proposed models, the gauge length used to measure the compressive strain of concrete, the rate of loading, etc, as discussed in Section 2.3. However, the stress-strain models proposed for practical use have been simplified by neglecting some of those

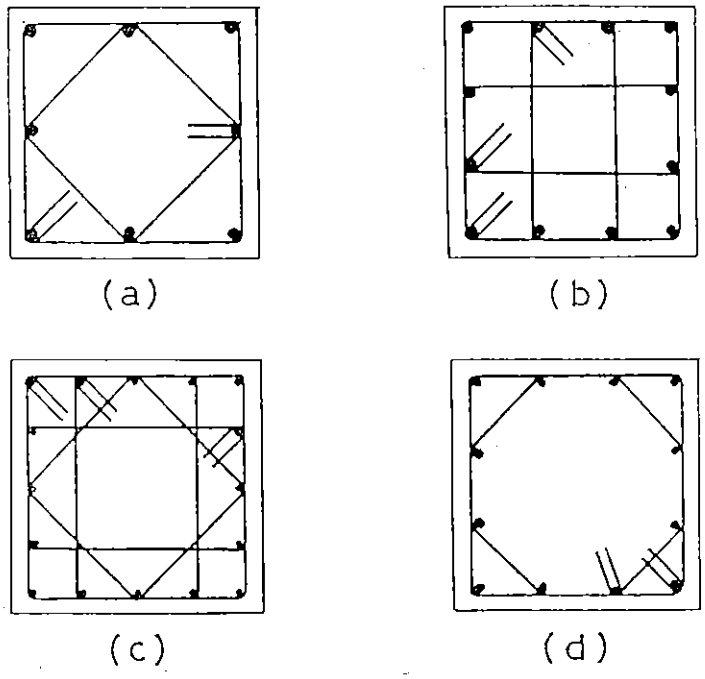

Fig. 2.7 Various Details of Transverse Reinforcement for Square Columns [2.1].

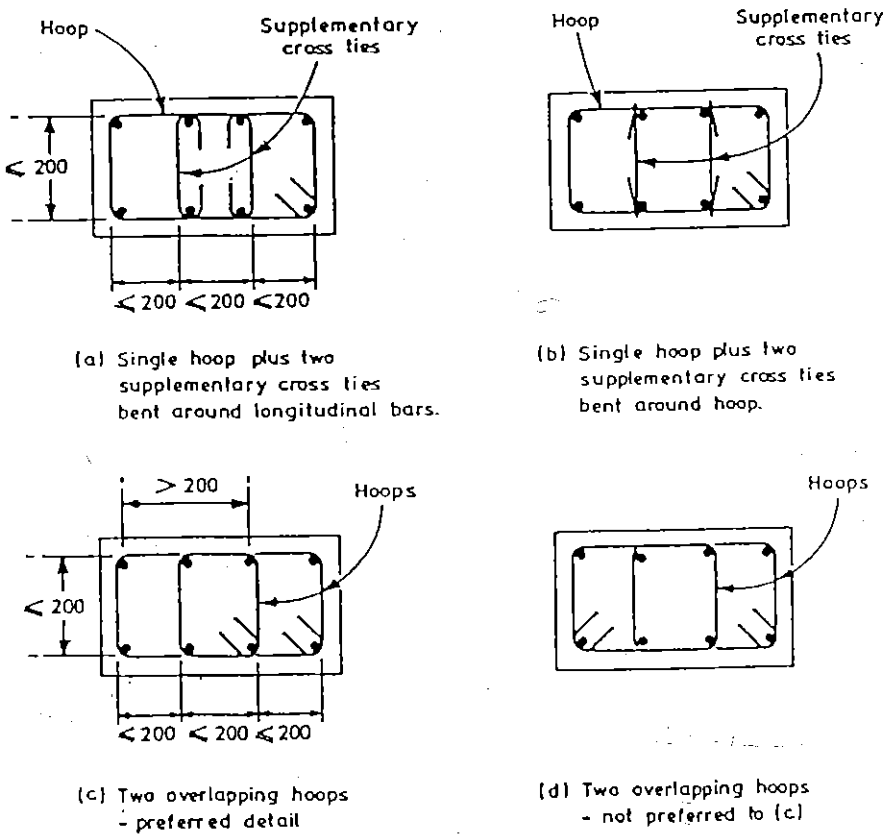

Fig. 2.8 Various Details of Transverse Reinforcement for Rectangular Columns [2.11].

factors and, as a result, sometimes give significantly different predictions for the behaviour of the confined concrete.

In this section, a number of stress-strain models for confined concrete proposed previously, which are good examples to explain the mechanisms of confinement, are selected and reviewed.

2.2.3.1 Stress-Strain Models for Concrete Confined by Circular Spirals

Four stress-strain models proposed by Desayi et al [2.15], Park and Leslie [2.16], Watanabe et al [2.17], and Mander et al [2.6] are introduced here. In the study by Richart et al [2.5], lateral pressure provided by spirals was assumed to be uniformly distributed along the column axis by neglecting the effect of spiral spacing. This assumption may be adequate when very closely spaced spirals are used. However, in practice, the spacings of hoops or spirals are not always small enough to be adequately neglected. The decrease of the effectively confined zone of concrete due to increase of hoop spacing has been taken into account in the following four stress-strain models.

Stress-Strain Model Proposed by Desayi, Iyengar and Reddy (1978)

Iyengar, Desayi and Reddy [2.18] conducted axial loading tests on 150 mm diameter by 300 mm high cylinders with and without spiral reinforcement. The strength of plain concrete was varied from 17.3 MPa to 37.9 MPa. For spirals, two types of steel viz.,(a) 6.2 mm diameter mild steel with yield strength of 299 MPa (b) 4 mm diameter high strength steel with 0.2 % proof stress of 677 MPa were used. The pitch of spirals varied from 3 to 15 cm. The confinement index expressed by Eq. 2.14 was defined to represent the degree of confinement and was used in the stress-strain model proposed [2.15]. The confinement index is expressed as

$$C_i = (\rho_s - \rho_{so})\, f_{yh} / f'_c \qquad \text{.....} \qquad (2.14)$$

where ρ_s = ratio of volume of spiral or circular hoop reinforcement to total volume of concrete core (out-to-out of spirals or hoops)

ρ_{so} = value of ρ_s when the pitch of spiral is equal to the least lateral dimension of the column specimen

f_{yh} = yield strength of circular spiral
f'_c = compressive strength of plain concrete

The first term in the right hand side of Eq. 2.14 was introduced because it was observed that confinement by transverse reinforcement was almost ineffective when the spacing of transverse reinforcement exceeded the least lateral dimension of the column specimen.

By applying a regression analysis to the test data obtained, the increase of strength, increase of strains at peak stress and at 0.85 of the ultimate stress were expressed for the confined concrete using the confinement index as follows;

$$f'_{cc} / f'_c = 1 + 2.3\, C_i \quad \text{.....} \quad (2.15)$$

$$\varepsilon_{cc} / \varepsilon_{co} = 1 + 23.0\, C_i \quad \text{.....} \quad (2.16)$$

$$\varepsilon_{.85} / \varepsilon_{co} = 1.8 + 46.5\, C_i \quad \text{.....} \quad (2.17)$$

where f'_{cc} = compressive strength of a confined concrete specimen
ε_{co} = strain at the compressive strength of a plain concrete specimen
ε_{cc} = strain at the compressive strength of a confined specimen
$\varepsilon_{.85}$ = strain at 0.85 of the compressive strength of a confined concrete specimen in the descending portion of the stress- strain curve

The proposed stress-strain model shown in Fig. 2.10 was expressed in the form of

$$f_c = \frac{A}{1+B\,\varepsilon_c + C\,\varepsilon_c^2 + D\,\varepsilon_c^3} \quad \text{.....} \quad (2.18)$$

where f_c = axial stress in concrete specimen
ε_c = axial strain in concrete specimen
$A = E_c$ = initial tangent modulus = $126580 + 460\, f'_c$ (in kg/cm^2)

$$B = \left\{ \frac{1 - 2k\beta + k\beta^2}{k(1-\beta)^2} \frac{E_c}{E'_c} - \frac{2\beta + 1}{\beta} \right\} \frac{1}{\varepsilon_{cc}}$$

$$C = \left\{ \frac{\beta + 2}{\beta} - \frac{2(1-k)}{k(\beta-1)^2} \frac{E_c}{E'_c} \right\} \frac{1}{\varepsilon_{cc}^2}$$

$$D = \left\{ \frac{1-k}{k(\beta-1)^2} \frac{E_c}{E'_c} - \frac{1}{\beta} \right\} \frac{1}{\varepsilon_{cc}^3}$$

In B, C and D, $k = 0.85$, $E'_c = f'_{cc} / \varepsilon_{cc}$ and $\beta = \dfrac{\varepsilon_{.85}}{\varepsilon_{cc}} = \dfrac{1.8 + 46.5\, C_i}{1 + 23.0\, C_i}$

The coefficients A, B, C and D were determined by complying with the following conditions:

(1) at $\varepsilon_c = 0$, $f_c = 0$ and $\dfrac{df_c}{d\varepsilon_c} = E_c$

(2) at $\varepsilon_c = \varepsilon_{cc}$, $f_c = f'_{cc}$ and $\dfrac{df_c}{d\varepsilon_c} = 0$

(3) at $\varepsilon_c = \beta\, \varepsilon_{cc}$, $f_c = k\, f'_{cc}$

The stress-strain curves expressed by Eq. 2.18 agreed well with the stress-strain curves measured in the accompanied tests. It is notable that the test data obtained in this study and the concept of the confinement index have been used in the following studies by other researchers.

Stress-Strain Model Proposed by Park and Leslie (1977)

Using the tests results obtained by Iyengar, Desayi and Reddy [2.18], Park and Leslie [2.16] also proposed a stress-strain model of concrete confined by spirals. The stress-strain curve was divided into four regions as shown in Fig. 2.11. Each region is described as follows;

Region OA : $0 \le \varepsilon_c \le 0.002$

It is assumed that the passive confining effects is negligible until the axial compressive strain reaches the magnitude of 0.002 and hence the stress-strain curve of this region is identical with that region of plain concrete. This region is expressed by a parabola as

$$f_c = f'_c \left[\frac{2\varepsilon_c}{\varepsilon_{co}} - \left(\frac{\varepsilon_c}{\varepsilon_{co}} \right)^2 \right] \qquad \text{..... (2.19)}$$

where $\varepsilon_{co} = 0.002$

and $0 \le \varepsilon_c \le 0.002$

Region AB : $0.002 \le \varepsilon_c \le \varepsilon_{cc}$

In this region, another parabola is used to express the strength enhancement of core concrete confined by spirals. That is;

$$f_c = f'_c + (f'_{cc} - f'_c) \{ \frac{2 (\varepsilon_c - \varepsilon_{co})}{(\varepsilon_{cc} - \varepsilon_{co})} - [\frac{(\varepsilon_c - \varepsilon_{co})}{(\varepsilon_{cc} - \varepsilon_{co})}]^2 \} \quad \ldots\ldots\ldots\ldots \quad (2.20)$$

where using the confinement index, C_i, expressed by Eq.2.14 and the relation given by Eqs. 2.15 and 2.16,

$$f'_{cc} = f'_c (1 + 2.3\ C_i)$$

$$\varepsilon_{cc} = \varepsilon_{co} (1 + 23.0\ C_i)$$

and $0.002 \le \varepsilon_c \le \varepsilon_{cc}$

Region BC : $\varepsilon_{cc} \le \varepsilon_c \le \varepsilon_{20}$

In this region, a straight line is used to represent the falling branch from the maximum stress to 20% of the maximum stress. That is,

$$f_c = f'_{cc} + z (\varepsilon_c - \varepsilon_{cc}) \quad \ldots\ldots\ldots\ldots \quad (2.21)$$

where $z = \frac{(f'_{cc} - 0.85\ f'_{cc})}{(\varepsilon_{cc} - \varepsilon_{.85})}$

and $\varepsilon_{cc} \le \varepsilon_c \le \varepsilon_{20}$

where ε_{20} = the compressive strain at 0.2 f'_{cc} in the falling branch and $\varepsilon_{.85}$ is given by Eq. 2.17.

Region CD : $\varepsilon_c \ge \varepsilon_{20}$

In this region, it is assumed that the confined concrete can sustain a constant compressive stress of 0.2 f'_{cc} .

This stress-strain model is notable from the point that the following two significant characteristics of stress-strain behaviour of confined concrete were clearly suggested. One is that the passive confinement provided by transverse reinforcement can become effective only after the compressive strain of the concrete reached around the strain at which stress in plain concrete becomes maximum. The other characteristic is that the falling branch of the stress-strain curve eventually reaches to a almost flat curve region keeping a certain magnitude of stress about 20 % of the maximum stress.

Stress-Strain Model Proposed by Watanabe, Muguruma, Tanaka and Katsuda(1980)

The author of this thesis et al [2.8, 2.19, 2.20] conducted axial loading tests on 150 mm diameter by 300 mm high concrete cylinders confined by spirals. The yield strengths of spirals were 161 MPa, 316MPa, 1150 Mpa and 1352MPa. The spiral bar diameter varied from 5 mm to 6.4 mm and the pitch of spirals varied from 3 to 7 cm. The plain concrete strength was varied from 24 MPa to 56 MPa. No longitudinal steel was present.

When regression analysis was conducted on the obtained data plus the data obtained by Iyengar et al [2.18] using the confinement index C_i expressed by Eq. 2.14, the analyzed results were largely scattered. In the analysis, it was found that the increases of the strength and ductility of the confined concrete were proportional to the square root of the yield strength of spirals rather than to the yield strength. It may be said that this tendency did not appear or could not be recognized in the tests by Iyengar et al because only two grades of steel were used for the spirals in their study.

Watanabe et al [2.17] considered that the efficiency of lateral confining reinforcement should be evaluated against the effectively confined core volume. In the analysis, the spirals were replaced by equivalent circular hoops for convenience and it was assumed that effectively confined zone could be separated by straight lines with slope of 30° against vertical line in the longitudinal section as shown in Fig.2.12. The calculated volume of the effectively confined zone separated by the assumed straight lines is almost equal that calculated using the second degree parabola with 45° end slope assumed by Sheikh et al [2.1, 2.13]. For one spacing of the equivalent circular hoops, the ratio of the volume of the effectively confined core (V_{ec}) to the original core volume measured outside of spiral bars (V_{co}) is

$$r_v = V_{ec} / V_{co} = 1 - \frac{\sqrt{3}\, s}{3\, D'} + \frac{s^2}{9D'^2} \approx 1 - 0.5\ \frac{s}{D'} \quad \text{.....} \quad (2.22)$$

where D' = diameter of core section measured to outside of spirals

$$V_{co} = \pi\, D'^2\, s / 4$$

$$V_{ec} = V_{co} - \frac{\sqrt{3}}{12}\pi\, D'\, s^2 + \frac{\pi\, s^3}{36}$$

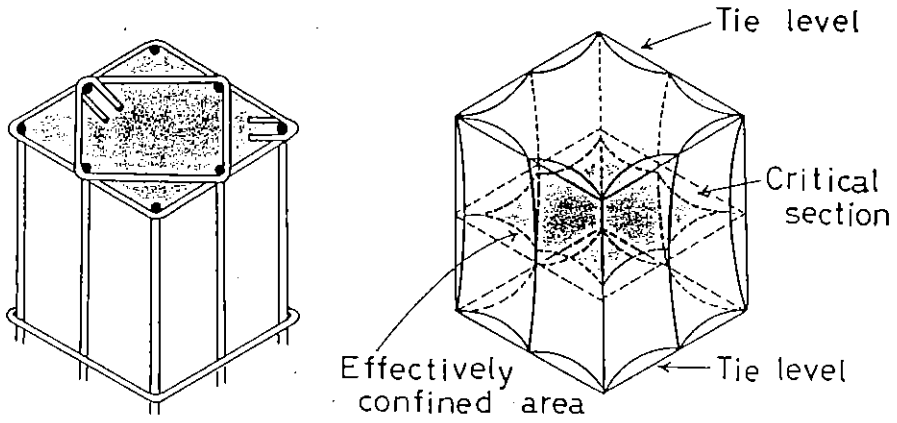

(a) Reinforcing Arrangement (b) Critical Section

Fig. 2.9 A Three Dimensional View of the Critical Section between Hoop Sets [2.1].

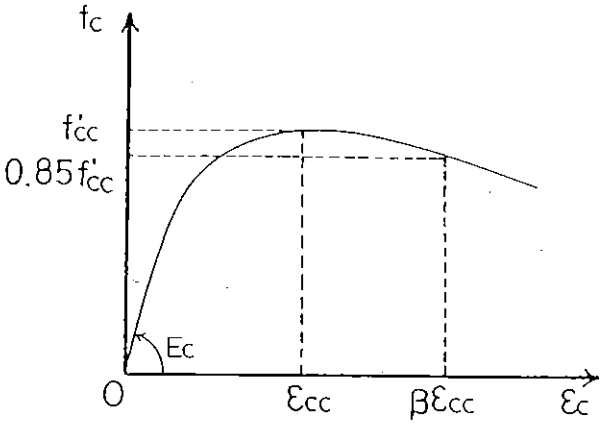

Fig. 2.10 Stress-Strain Model for Spirally Confined Concrete Proposed by Parakash Desayi et al [2.15,2.18]

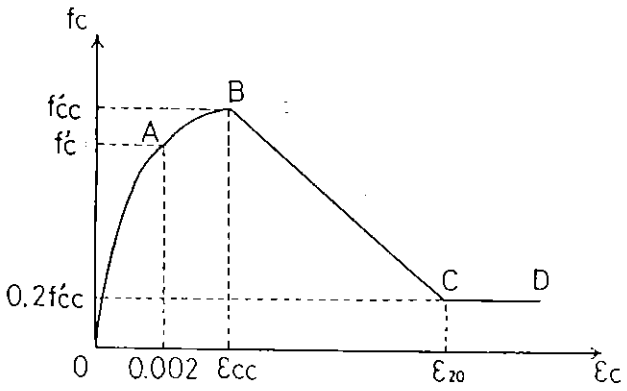

Fig. 2.11 Stress-Strain Model for Spirally Confined Concrete Proposed by Park and Leslie [2.16]

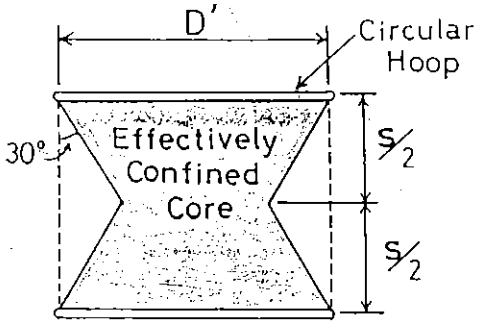

(a) Longitudinal Section

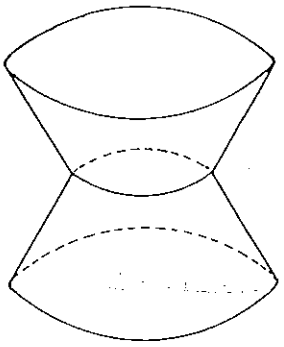

(b) Perspective View

Fig. 2.12 Effectively Confined Core Assumed for a Cylinder with Circular Hoops

Thus, the confining coefficient, C_c, given by the following equation was defined.

$$C_c = \rho_s \frac{\sqrt{f_{yh}}}{f'_c} \left(1 - 0.5 \frac{s}{D'} \right) \quad \text{.....} \quad (2.23)$$

where units of f_{yh} and f'_c are in kg/cm^2

Fig. 2.13 illustrates the proposed stress-strain models for confined and unconfined concrete. In the figure, the points A and D represent the maximum stresses for unconfined and confined concrete, respectively. The points B and E are the assumed available limits of flexural compressive strain for unconfined and confined concrete, respectively. The available limit of flexural compressive strain is defined, in this study, as the strain at which the average stress in the stress-strain curve reaches the maximum value. The curve OA is a second degree parabola, the initial tangent of which is expressed as E_c. The curve for the confined concrete is further extended from A to D using another parabola having the vertex at the point D. For the falling branches AB (for unconfined concrete) and DE (for confined concrete), straight lines are used.

The stress-strain model for the unconfined concrete is expressed as follows;

Region OA : $0 \le \varepsilon_c \le \varepsilon_{co}$

$$f_c = E_c \varepsilon_c + \{ (f'_c - E_c \varepsilon_{co}) / \varepsilon_{co}^2 \} \varepsilon_c^2 \quad \text{.....} \quad (2.24)$$

where ε_{co} = compressive strain at maximum stress of unconfined concrete

Region AB : $\varepsilon_{co} \le \varepsilon_c \le \varepsilon_{cuo}$

$$f_c = \frac{(f'_{cuo} - f'_c)}{(\varepsilon_{cuo} - \varepsilon_{co})} (\varepsilon_c - \varepsilon_{co}) + f'_c \quad \text{.....} \quad (2.25)$$

where ε_{cuo} = available limit of compressive strain defined as the strain at which the average stress in stress-strain curve of unconfined concrete reaches the maximum value

f'_{cuo} = compressive strain at ε_{cuo}

The values of E_c, ε_{co} and ε_{cuo} are given by the following empirical equations obtained from the reference [2.21].

$$E_c = 231000 \sqrt{f'_c / 200} \quad \text{.....} \quad (2.26)$$

$\varepsilon_{co} = 0.0013\,(1 + f'_c/1000)$ ..... (2.27)

$\varepsilon_{cuo} = 0.00413\,(1 - f'_c/2000)$ ..... (2.28)

where the unit of f'_c is kg/cm^2

The value of f'_{cuo} can be determined based on the definition of the available limit of strain ε_{cuo}. That is, from Eqs. 2.24 and 2.25, the average stress f_{ave} from ε_c of 0 to an arbitrary value more than ε_{co} is expressed as

$$f_{ave} = \frac{1}{\varepsilon_c}\left\{ S + \frac{f'_{cuo} - f'_c}{\varepsilon_{cuo} - \varepsilon_{co}} \frac{(\varepsilon_c - \varepsilon_{co})^2}{2} + f'_c\,(\varepsilon_c - \varepsilon_{co}) \right\} \quad \text{.....} \quad (2.29)$$

where S = the area between the curve OA and the strain axis

$$= \int_0^{\varepsilon_{co}} f_c\, d\varepsilon_c$$

From the definition of ε_{cuo}, $\frac{\partial f_{ave}}{\partial \varepsilon_c} = 0$ at $\varepsilon_c = \varepsilon_{cuo}$. Hence,

$$f'_{cuo} = \frac{2\,(S - f'_c\,\varepsilon_{co})}{(\varepsilon_{cuo} + \varepsilon_{co})} + f'_c \quad \text{.....} \quad (2.30)$$

The stress-strain model for the confined concrete is expressed as follows;

Region OA : $0 \le \varepsilon_c \le \varepsilon_{co}$

The same relation for the unconfined concrete expressed by Eq. 2.24 is used.

Region AD : $\varepsilon_{co} \le \varepsilon_c \le \varepsilon_{cc}$

$$f_c = \frac{(f'_c - f'_{cc})}{(\varepsilon_{co} - \varepsilon_{cc})^2}\,(\varepsilon_c - \varepsilon_{cc})^2 + f'_{cc} \quad \text{.....} \quad (2.31)$$

Region DE : $\varepsilon_{cc} \le \varepsilon_c \le \varepsilon_{cu}$

$$f_c = \frac{(f'_{cu} - f'_{cc})}{(\varepsilon_{cu} - \varepsilon_{cc})}\,(\varepsilon_c - \varepsilon_{cc}) + f'_{cc} \quad \text{.....} \quad (2.32)$$

where ε_{cu} = available limit of compressive strain defined as the strain at which the average stress in stress-strain curve of confined concrete reaches the maximum value

f'_{cu} = compressive stress of confined concrete at ε_{cu}

From the regression analyses of the test results obtained in this study [2.8, 2.19, 2.20] plus the data obtained by Iyengar et al [2.18] using the confining coefficient C_c, the following realtions were derived.

$$f'_{cc} = (1 + 150\, C_c)\, f'_c \quad \text{.....} \quad (2.33)$$

$$\varepsilon_{cc} = (1 + 1460\, C_c)\, \varepsilon_{co} \quad \text{.....} \quad (2.34)$$

$$\varepsilon_{cu} = (1 + 990\, C_c)\, \varepsilon_{cuo} \quad \text{.....} \quad (2.35)$$

where the unit of f'_c is kg/cm^2

In Figs. 2.14 to 2.16, the tested data is plotted with the lines given by the Eqs, 2.33 to 2.35. The value of f'_{cu} is determined in the same manner as f'_{cuo} for plain concrete given by Eq. 2.30. That is,

$$f'_{cu} = \frac{2\,(S' - f'_{cc}\,\varepsilon_{cc})}{(\varepsilon_{cc} + \varepsilon_{cu})} + f'_{cc} \quad \text{.....} \quad (2.30')$$

where S' = the area between the curve OAD and the strain axis

$$= \int_0^{\varepsilon cu} f_c\, d\varepsilon_c$$

In Figs. 2.14 to 2.16, the test results obtained from the axial load tests on concrete prisms with square spiral hoops [2.8, 2.19, 2.20] are also plotted for reference. The specimens were concrete prisms having 194 mm square section and 400 mm high. The plain concrete strength used ranged from 31 MPa to 44 MPa. The square spiral hoops were made from round bars of diameter from 7.3 mm to 9.2 mm and the pitch was varied from 25 mm to 320 mm. The steel yield strengths were 235 MPa, 348 MPa, 517 MPa, 497 MPa, 980 MPa and 1397 MPa. From the regression analysis of this data plus the data obtained by Iyengar et al [2.18], the following relations were derived.

$$f'_{cc} = (1 + 50\, C_c)\, f'_c \quad \text{.....} \quad (2.36)$$

$$\varepsilon_{cc} = (1 + 450\, C_c)\, \varepsilon_{co} \quad \text{.....} \quad (2.37)$$

$$\varepsilon_{cu} = (1 + 450\, C_c)\, \varepsilon_{cuo} \quad \text{.....} \quad (2.38)$$

where the unit of f'_c is in kg/cm^2

The stress-strain model expressed by Eqs. 2.24 to 32 is also applicable to square columns with square hoops, by replacing Eqs. 2.33 to 2.35 with the Eqs. 2.36 to 2.38.

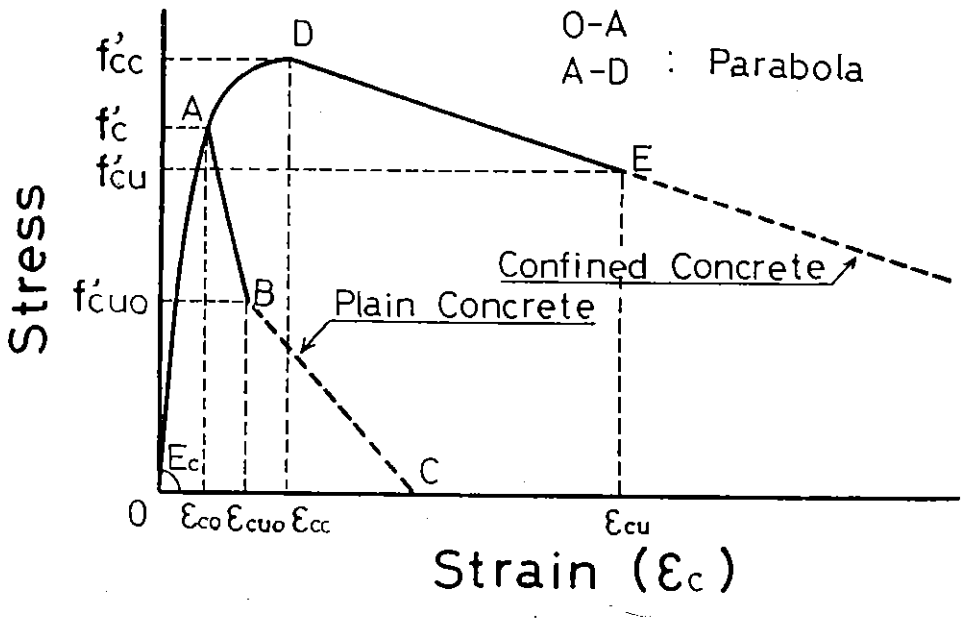

Fig. 2.13 Stress-Strain Models for Confined and Unconfined Concrete Proposed by Watanabe et al [2.17].

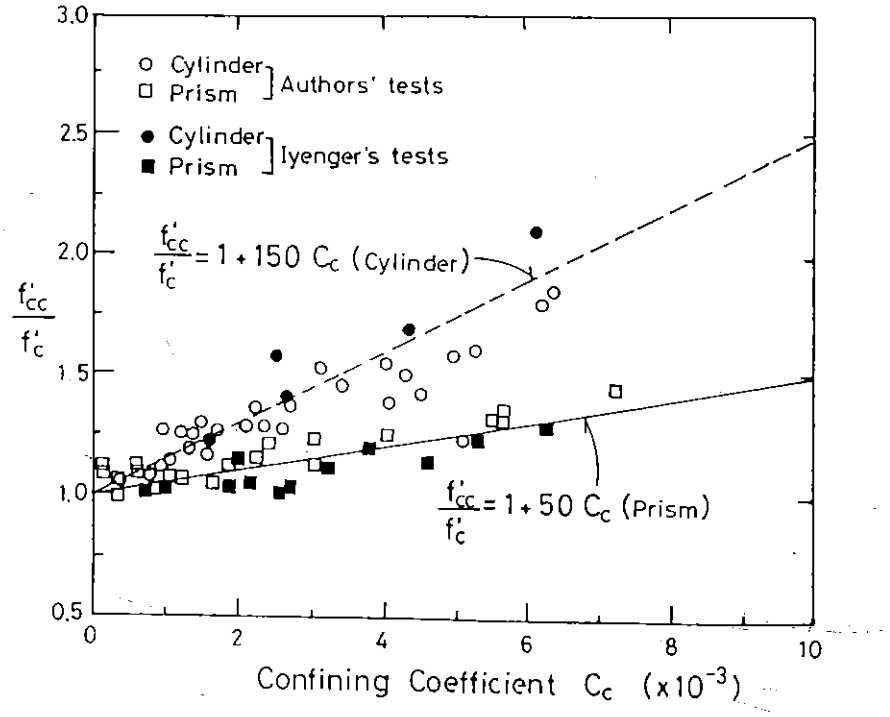

Fig. 2.14 Relations between Compressive Strength and Confining Coefficient C_c [2.17].

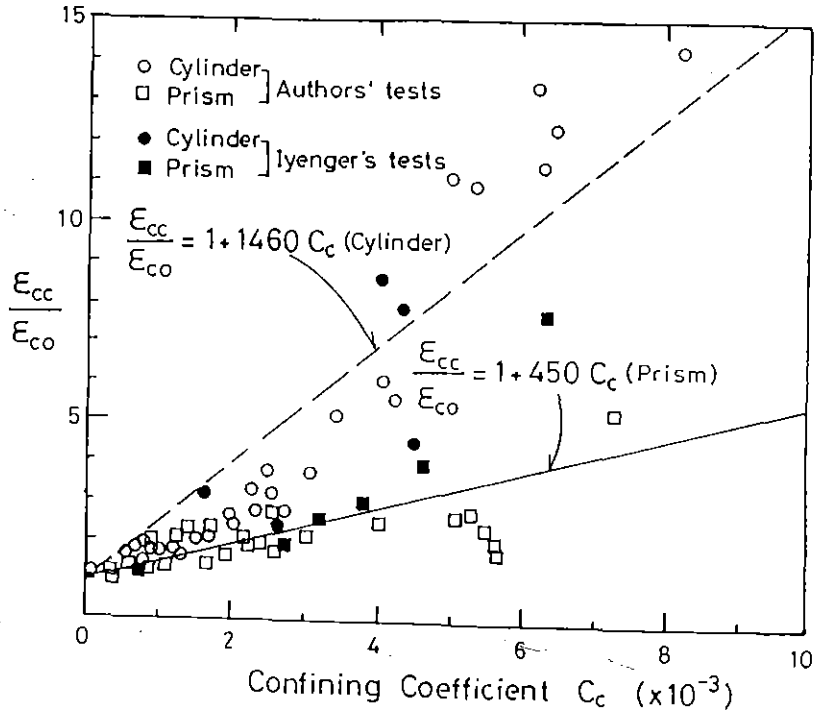

Fig. 2.15 Relations between Compressive Strain at the Compressive Strength and Confining Coefficient C_c [2.17]

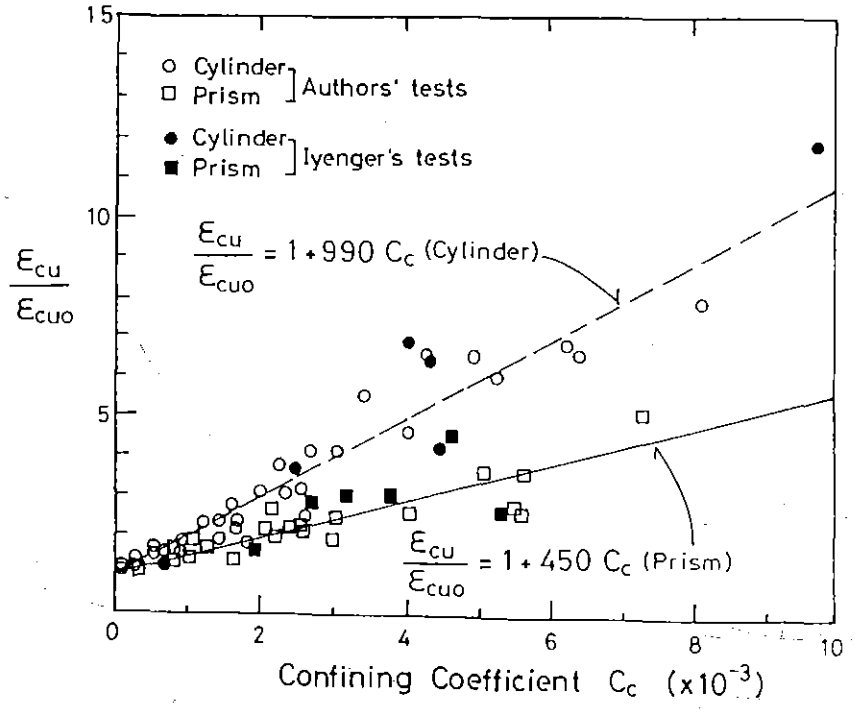

Fig. 2.16 Relations between Available Limit Strain and Confining Coefficient C_c [2.17].

It is notable that this study has proposed the available limit of extreme compressive fibre strain of concrete for the members subjected to bending with or without axial load. For the bending section of a member, the resultant compressive force of concrete is conventionally expressed as $k_1k_3 \times f'_c\, b\, c$ [2.2] (where k_1 = ratio of average stress of concrete in compression zone to $k_3\, f'_c$, k_3 = ratio of maximum compressive stress of concrete in flexure to f'_c, b = width of the member section and c = neutral axis depth). The available limit strain was defined as the strain at which the average stress in the stress-strain curve becomes maximum, namely, as the strain at which the product of the stress block coeffients k_1 and k_3 reaches the maximum value. This is based on the following consideration:

Consider a singly reinforced concrete beam which is subjected to bending and for which the amount of tension reinforcement is small enough for the beam to fail in the mode of tension failure (= under-reinforcement condition). In the initial stage of loading, the neutral axis depth of the beam section becomes shallower as the load increases, and the maximum moment is reached at when the value of $k_2/(k_1k_3)$ becomes a minimum [2.22], where k_2 = ratio of the distance between extreme compression fiber and the centroid of the compressive stress distribution to the neutral axis depth. For further loading, when the strain at the extreme compression fibre of concrete reaches the proposed available limit strain, namely, at the strain where k_1k_3 for the concrete stress block reaches the maximum value, deepening of the neutral axis begins unless the resultant tension force of the reinforcement is reduced. Assuming that the deepening of the neutral axis is indicating a critical condition of the beam, the above available limit strain of the concrete was defined for the beam. It is further assumed that the above defined available limit strain of concrete is also applicable to columns subjected to combined bending and axial load.

If the critical (ultimate limit) deformation of a structural member can be determined from a particular value of the extreme compression fibre strain of concrete, it is quite convenient in design practice due to the relatively simple calculation of the critical deformation. However, the proposed available limit strain normally gives a conservative estimation for the critical point of a moment-curvature curve or a load-deflection curve. For example, Fig. 2.17 shows measured moment-curvature curves for six prestressed rectangular beams and the corresponding theoretical curves

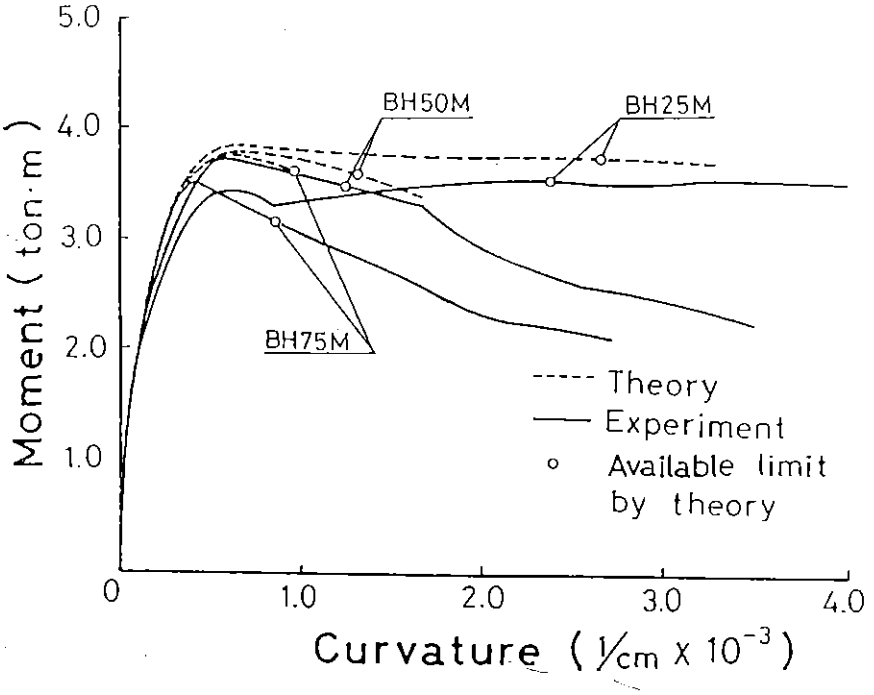

(a) Prestressed Concrete Beams Confined by Rectangular Spirals of High Strength Steel

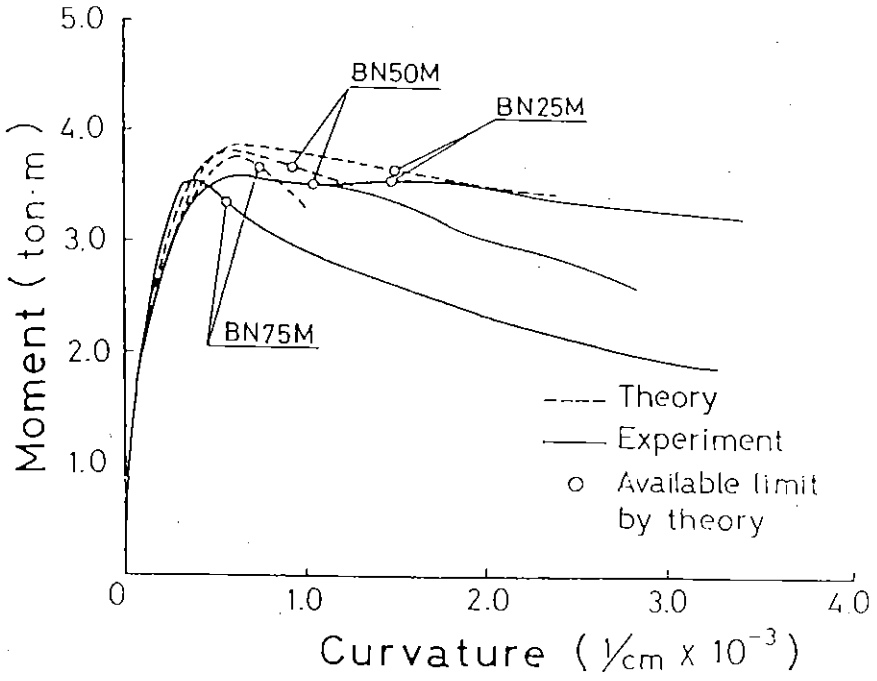

(b) Prestressed Concrete Beams Confined by Rectangular Spirals of Ordinary Strength Steel

Fig. 2.17 Measured and Calculated Moment-Curvature Curves for Prestressed Concrete Beams with Rectangular Spirals [2.17].

calculated using the above stress-strain model [2.17]. For the beams, the prestressing force was 190 KN and the beam section was 16 cm by 21 cm (confined core section = 14 cm by 19 cm). The compressive strength of concrete was 34.7 MPa at the time of the tests. Rectangular spirals having yield strengths of 300 MPa and 1147 MP were provided for the BN and BH series specimens, respectively, with pitch of 25 mm, 50 mm and 75 mm. The beams had total length of 2.8 m and were simply supported with span length of 2.6 m and monotonically loaded so as to provide a region of pure bending region at mid span of length 60 cm. The curvature was measured at the centre of the pure bending region by two pairs of electric linear transformers with gauge length of 50 cm. In the figure, the available limits of the curvatures which were determined from the above defined available limit strain are indicated by open circles. It may be said that the indicated available limit curvatures are too conservative when compared with the standard required in NZS 4203 [2.23] which allows a loss of load carrying capacity of up to 30% of the member strength after four cycles to displacement ductility factor $\mu = \pm 4$.

Stress-Strain Model Proposed by Mander, Priestley and Park (1984)

Mander, Priestley and Park conducted axial loading tests on spirally confined concrete columns with 500 mm diameter and 1500 mm height [2.6, 2.24]. It is notable that those confined columns also contained from 8 to 36 longitudinal bars to make the specimens realistic. The concrete compressive strength measured by 100 mm diameter and 200 mm high was about 30 MPa. For the spirals, 12 to 16 mm diameter round bars of Grade 275 steel were used and the measured yield strength of those bars was about 300 MPa. The spiral spacing was varied from 36 mm to 119 mm. For the longitudinal reinforcement, 16 to 28 mm diameter deformed bars of Grade 275 steel were used except for one specimen in which 16 mm diameter deformed bars of Grade 380 steel were used. Referring to those test results and to an equation suggested by Popovics [2.25], they proposed the stress-strain model illustrated in Fig. 2.18. The proposed model is expressed as

$$f_c = \frac{f'_{cc} \times r}{r - 1 + x^r} \qquad \text{.....} \quad (2.39)$$

$$\text{where } f'_{cc} = f'_{co} \left(2.254 \sqrt{1 + \frac{7.94\, f'_l}{f'_{co}}} - \frac{2\, f'_l}{f'_{co}} - 1.254 \right) \quad \text{... (2.40)}$$

is the peak longitudinal compressive stress of the stress-strain curve for confined concrete.

$$f'_l = \frac{1}{2} k_e \rho_s f_{yh} \quad \text{.....} \quad (2.41)$$

is the effective lateral confining stress and k_e is the confinement effectiveness coefficient explained later.

$$x = \varepsilon_c / \varepsilon_{cc} \quad \text{.....} \quad (2.42)$$

is the ratio of strain to the strain at peak confined stress f'_{cc}.

$$\varepsilon_{cc} = [R (\frac{f'_{cc}}{f'_{co}} - 1) + 1] \varepsilon_{co} \quad \text{.....} \quad (2.43)$$

$$r = \frac{E_c}{E_c - E_{sec}} \quad \text{.....} \quad (2.44)$$

$$E_c = 5000 \sqrt{f'_{co}} \quad \text{.....} \quad (2.45)$$

$$E_{sec} = f'_{cc} / \varepsilon_{cc} \quad \text{.....} \quad (2.46)$$

The value of R in Eq. 2.43 can be determined by experimental calibration. It was recommended to take R as 5.

Equation 2.41, giving the effective lateral confining stress, depends on the confinement effectiveness coefficient k_e which relates the minimum fully confined core area to the full core area. Assuming that the arching between spirals or hoops is parabolic with end slope of 45° as shown in Fig. 2.19, the following expressions were suggested.

$$\text{circular hoops : } k_e = \frac{(1 - 0.5 s' / d_s)^2}{1 - \rho_{cc}} \quad \text{.....} \quad (2.47)$$

$$\text{spirals : } k_e = \frac{(1 - 0.5 s' / d_s)}{1 - \rho_{cc}} \quad \text{.....} \quad (2.48)$$

where ρ_{cc} = the ratio of volume of longitudinal steel to volume of concrete core

s' = the clear spacing between circular hoops or spirals

d_s = the effective core diameter between circular hoop or spiral bar centres

Fig. 2.18 includes the complete stress-strain curve for unconfined concrete, appropriate for the cover concrete of members. For analytical simplicity, the part of the falling branch in region where $\varepsilon_c > 2 \varepsilon_{co}$ was

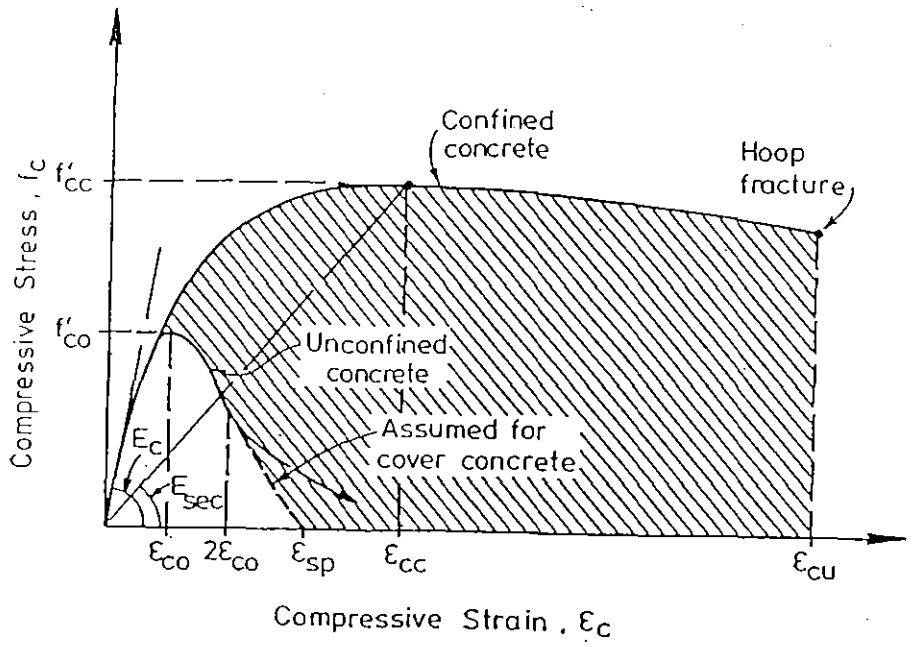

Fig. 2.18 Stress-Strain Models for Confined and Unconfined Concrete Proposed by Mander et al [2.6].

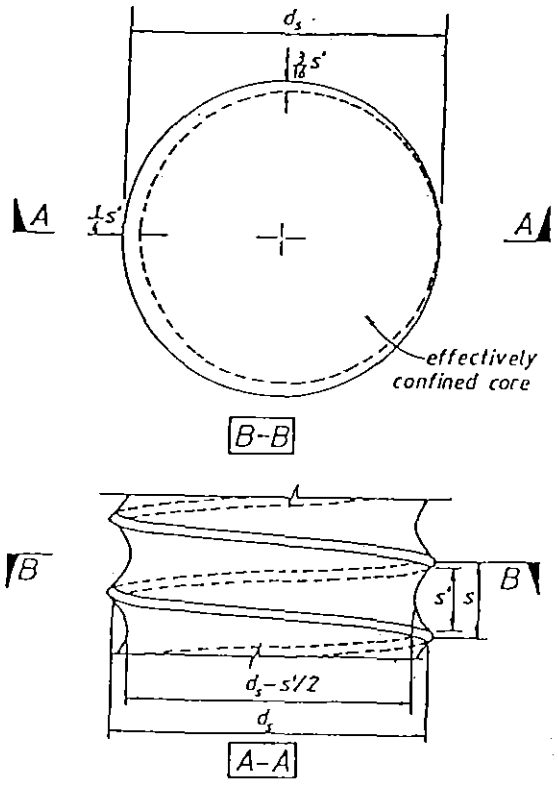

Fig. 2.19 Effectively Confined Core for Spiral Reinforcement [2.6]

assumed to be a straight line which reaches zero stress at the spalling strain, ε_{sp}.

This study is distinguished from the point that the proposed stress-strain model had been calibrated by the loading tests on the realistically sized columns containing longitudinal reinforcement. This stress-strain model is most reliable when circular hoops or spirals of Grade 275 or so steel are used as confining reinforcement. However, when high yield strength steel is used for transverse reinforcement, at least following two points must be re-examined;

(1) For Eq. 2.43 it was recommended to assume R = 5 based on the calibrated values of R varied from 2.8 to 6.1 for the tested range of spirally confined columns by Mander et al [2.6, 2.24]. However, when higher yield strength steel is used for the circular hoops or spirals, different value of R may be required. This can be predicted from the study by Watanabe et al [2.17]. For example, in the study by Watanabe et al, when a value of C_c gives $\frac{f'_{cc}}{f'_c} = 2$ for Eq. 2.33, the corresponding value of $\frac{\varepsilon_{cc}}{\varepsilon_{co}}$ becomes 10.7 from Eq. 2.34. When substituting these values into Eq. 2.43, R= 9.7 is obtained. This may be attributed to the nature of passive confinement by the transverse reinforcement. That is, as the steel strength of the transverse reinforcement becomes higher, larger axial compressive strain of core concrete is required to reach the maximum lateral confining pressure due to yielding of the confining transverse reinforcement and thus larger R will be required to be used.

(2) With respect to the buckling modes of the longitudinal reinforcement, a significant difference may appear in between the columns with ordinary strength circular hoops or spirals and with high strength ones, affecting the stress-strain behaviour of the confined concrete in the falling branch. It can be predicted that as the steel strength of the circular hoops or spirals becomes higher, buckling length of longitudinal reinforcement will become shorter. The reason can be described as follows. When columns confined by circular hoops or spirals with ordinary strength are axially loaded, those transverse bars begin to yield at a comparatively small compressive strain of concrete of about 0.2 % to 0.5 % and thereafter core concrete expands rapidly. This can be seen from the transverse bar strains measured in the Mander et al tests [2.24] as well as in the Muguruma et al tests [2.8, 2.19, 2.20]. Hence, after yielding of those transverse

reinforcement, the longitudinal reinforcement which has already yielded from axial compressive strain of 0.15 % or so will tend to buckle with the buckling length of several hoop spacings (see Fig. 2.20 (a)). On the contrary, when circular hoops or spirals with yield strength of more than 1000 MPa are used, expansion of core concrete is strongly restrained until the compressive concrete strain reaches 1.5 % or more at which those hoop bars are likely to yield [2.8, 2.19, 2.20]. This will lead to a buckling length which can be limited to one hoop spacing up to such large axial compressive strain of concrete, thus reducing the ineffectively confined zone within the region between neighbouring hoop bars (see Fig. 2.20 (b)). Hence, when high strength spirals are used, the difference in the buckling mode of the longitudinal bars may affect the stress-strain relation of core concrete in the falling branch.

Comparison between the Above Stress-Strain Models

It is notable that all the above stress-strain models for concrete confined by circular hoops or spirals indicate considerable increase of both strength and ductility due to the confinement. For comparison of those stress-strain models, the stress-strain relations were calculated assuming that the plain concrete strength f'_c = 30 MPa, the yield strength of spirals f_{yh} = 300 MPa, the spacing of spirals s = 50 mm, the concrete core diameter D' = 500 mm, the spiral bar diameter d_{bh} = 12 mm (and hence the volumetric ratio of spirals to concrete core volume ρ_s = 1.8 %) and no longitudinal reinforcement. The calculated stress-strain curves are shown in Fig. 2.21. The comparison between those stress-strain curves except for Watanabe et al model can also be seen in Section 4.3 and in References [2.6, 2.26], indicating results similar to those shown here.

It can be said that Mander et al model normally gives the largest estimation of the strength enhancement due to confinement in comparison with other researchers' models. This may be attributed to the fact that the Mander et al model was calibrated using the realistically sized test columns with longitudinal reinforcement but the other models were calibrated by comparatively small cylinders without longitudinal reinforcement. That is, the scale effect of tested columns and the effect of longitudinal reinforcement may have led to such a difference between the models. Although in the above comparison shown in Fig. 2. 21 it was attempted to

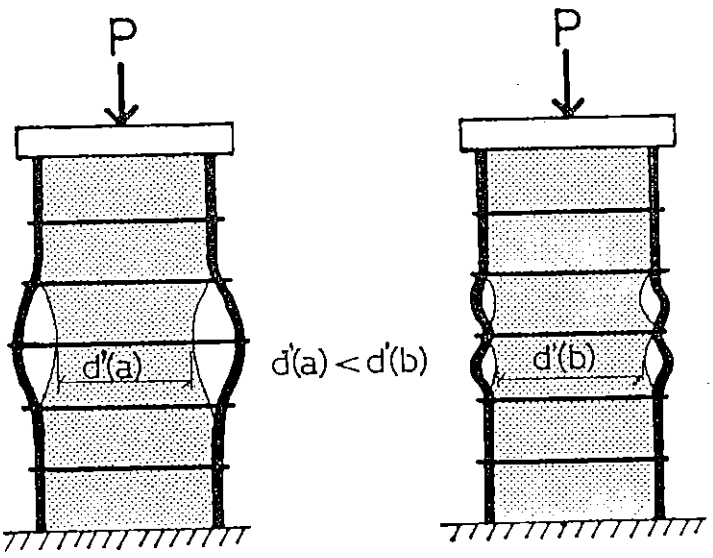

(a) Longitudinal Reinforcement Restrained by Ordinary Strength Circular Hoops

(b) Longitudinal Reinforcement Restrained by High Strength Circular Hoops

Fig. 2.20 Predicted Buckling Models of Longitudinal Reinforcement Restrained by Circular Hoops with Various Strengths

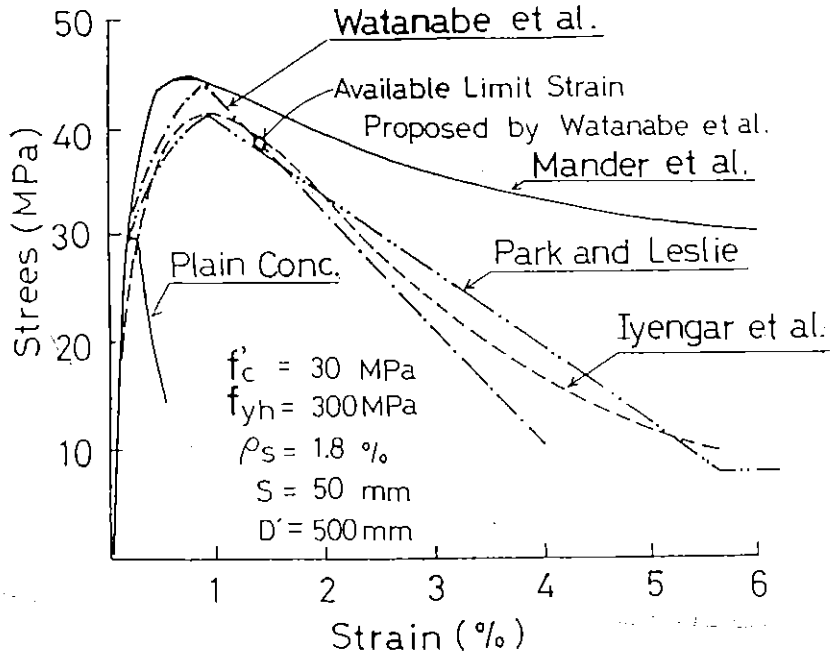

Fig. 2.21 Comparison Between Proposed Stress-Strain Models for Concrete Confined by Circular Spirals.

eliminate the effect of longitudinal reinforcement by taking the volumetric ratio of longitudinal reinforcement ρ_{cc} in Eq. 2.48 as zero for the Mander et al model, the effect of longitudinal reinforcement might be more significant than expressed by Eq. 2.48. The presence of longitudinal reinforcement will yield two effects on the strength increase of the confined concrete. One is that longitudinal reinforcement will also confine the core concrete at least until the longitudinal reinforcement has axially yielded and has lost the flexural stiffness. The other is that lateral pressure from the transeverse reinforcement will disperse wider through longitudinal reinforcement compared with the case when that transverse reinforcement is in direct contact with the core concrete.

The slope of the stress-strain curve in the falling branch is also more gentle in the model proposed by Mander et al. In this case, the reason cannot simply be attributed to the scale effect of the tested columns or the presence of the longitudinal reinforcement in the tests by Mander et al. It must be emphasized that the compressive strain at the peak stress of confined concrete is more than 0.2 %. This means that, when the yield strength of longitudinal reinforcement is less than 400 MPa, the longitudinal bars have axially yielded and the flexural stiffness of those bars is rapidly lost at strains in the region of the falling branch of the stress-strain curve of confined concrete. Hence, the improvement of confining stress distribution which is related to the flexural stiffness of longitudinal reinforcement may be insignificant in the post peak stress region of the confined concrete. Moreover, when the longitudinal reinforcement begins to buckle over several spiral spacings, the confining stress distribution becomes worse than the case without longitudinal reinforcement (see Fig. 2.20). Actually, the experimental study by Mander et al [2.24] indicated that there is no significant decrease of the the falling branch slope when the number of longitudinal bars ranged from 8 to 36. This matter is discussed in detail in Section 2.3.4. On the other hand, it is notable that the magnitude of the compressive concrete strain measured in the post peak stress region significantly depends on the gauge length of the concrete strain measurement as represented by Fig. 2.22 [2.10]. In the Mander et al tests [2.24], the ratio of the gauge length to the concrete core diameter was 1.0, while in the Iyengar et al tests [2.18] and the Muguruma et al tests [2.8, 2.19, 2.20] the corresponding ratios were 1.33 and 1.67, respectively. This may be one of the reasons why the slope of the falling branch is most gentle in the

concrete stress-strain model proposed by Mander et al, as described in the following paragraph.

In the study by Mander et al [2.6, 2.24], it was stated that a diagonal failure plane (shear sliding plane) with an angle θ of about 60° to 70° to the horizontal plane was observed (see Fig. 2.23) and the failure angle θ was not particularly sensitive to the amount of confinement. The axial strain for the falling branch was primarily calculated by dividing the gauge length of 450 mm (= concrete core diameter) into the measured relative displacement between the points A and A' and/or between the points C and C' which cross over the failure plane. The measured realtive displacement such as between the points B and B', which do not cross the failure plane was discarded. It must be emphasized that in the Mander et al study it was assumed that the compressive deformation concentrated in the central region over the length of 450 mm equal to the core diameter, although the diagonal shear sliding would have occurred over the column height of about 780 mm (= $\sqrt{3}$ x 450 mm) if the angle of the failure plane was θ = 60°. Thus, the axial compressive strain for the falling branch becomes larger since the assumed compression failure zone length is less, when it is calculated based on the relative displacement measured between particular points. However, due to lack of theoretical and experimental evidences, at this stage, it is difficult to say what is the most appropriate gauge length to use to estimate the compressive strain of concrete when applying the stress-strain relation of concrete to a member subjected to bending with or without axial load.

It is of interest to compare the estimations of effective lateral pressure from spirals from the above four stress-strain models. The confinement index expressed by Eq. 2.14, which was used by Iyengar et al and Park et al, can be rewritten as

$$C_i = \rho_s \frac{f_{yh}}{f'_c}\left(1 - \frac{s}{D'}\right) \qquad \text{.....} \qquad (2.14')$$

The confining coefficient defined by Watanabe et al was

$$C_c = \rho_s \frac{\sqrt{f_{yh}}}{f'_c}\left(1 - 0.5\,\frac{s}{D'}\right) \qquad \text{.....} \qquad (2.23)$$

Using Eqs. 2.41 and 2.48, Mander et al have expressed the effective lateral stress provided by spirals as

$$f'_l = \frac{1}{2}\, k_e\, \rho_s\, f_{yh} = \frac{1}{2}\,\frac{(1 - 0.5\, s'/\, d_s)}{1 - \rho_{cc}}\,\rho_s\, f_{yh} \qquad \text{.....} \qquad (2.41')$$

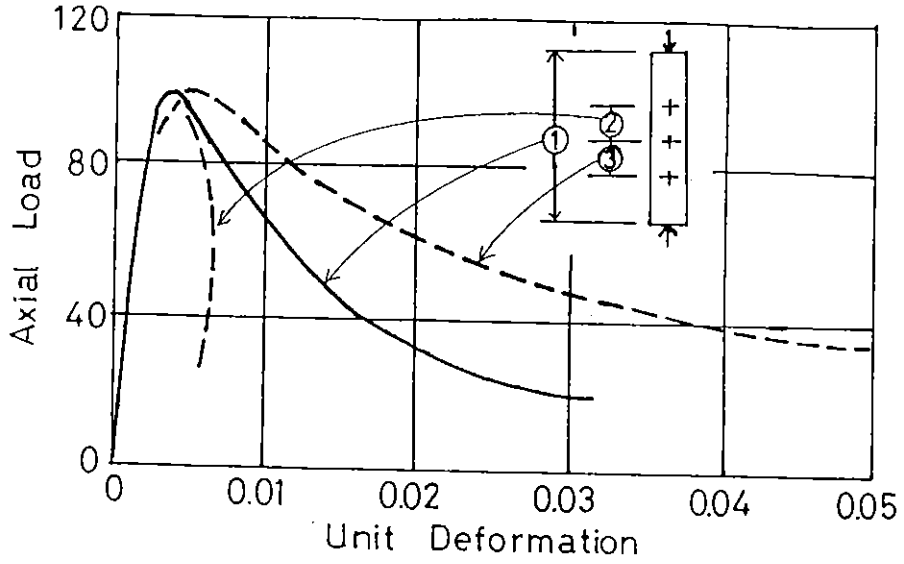

Fig. 2.22 Influence of the Gauge Length and Location of Strain Measurement on the Stress-Strain Relation of Concrete [2.10].

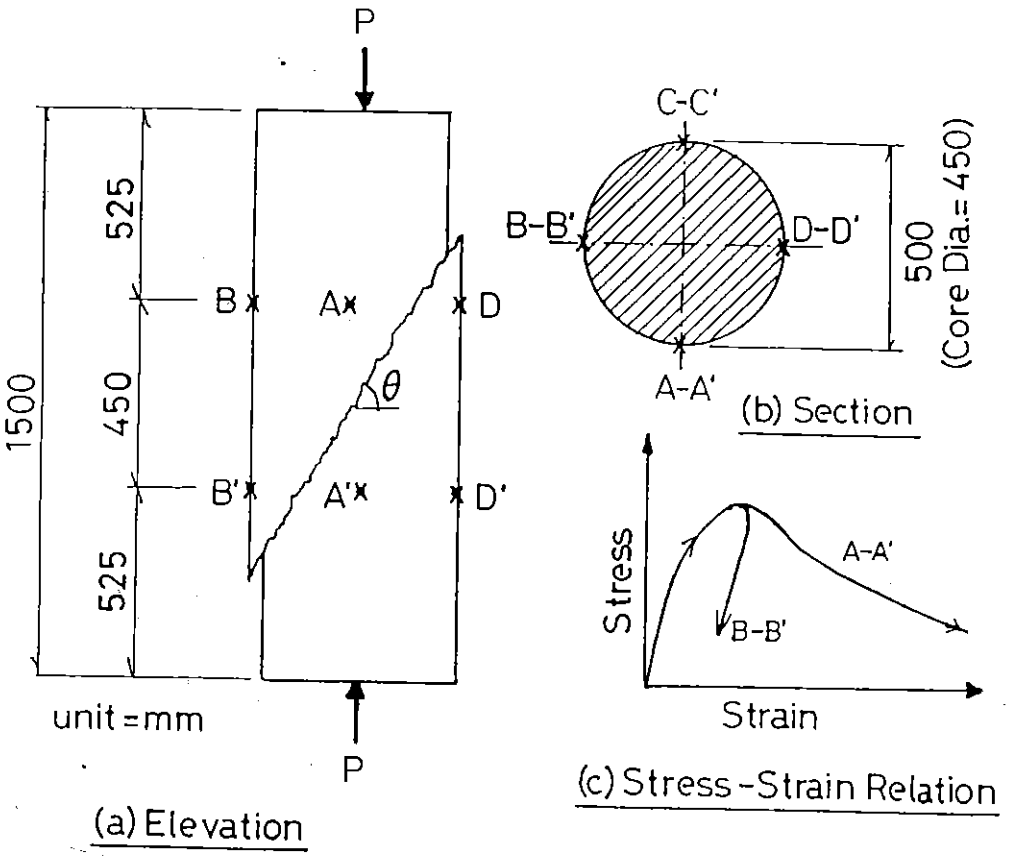

Fig. 2.23 Influence of the Gauge Length and Location of Strain Measurement on the Stress-Strain Relation of Concrete.

As can be seen by comparing Eqs. 2.23 and 2.41', in the Watanabe et al and Mander et al studies the spiral confinement becomes effective when the spiral spacing is less than two times of core diameter, although the derivations of those equations are not exactly the same. This assumption may possibly results in an overestimation of the confining effect when the spiral spacing exceeds the diameter of concrete core, because the study by Iyengar et al suggested that the effectiveness of comfinement cannot be appreciable when spiral spacing exceeds the concrete core diameter as expressed by Eq. 2.14'. Howevere, since the earthquake design codes [eg. 2.11, 2.12, 2.27] do not allow use of such a large spiral spacing more than the concrete core diameter, this will not cause a problem in practice.

The most significant difference between the above equations may be whether the confining effect is proportinal to the yield strength of the spiral steel or the square root of it. As long as the yield strength of transeverse bar steel is within a range of about between 275 MPa to 380 MPa in practical use, it may be said that this difference is insignificant. This is because the difference between the ratios of 380MPa/275MPa = 1.38 and $\sqrt{380MPa/275MPa}$ = 1.18 will have little affect on the modelled stress-strain curves determined including other factors. However, since in recent years high strength transverse reinforcement having a yield strength of more than 800 MPa has been used in Japan for the columns of high rise buildings, due to the high axial design load imposed, this point may need to be thoroughly re-investigated. This matter is discussed in Sections 2.3.3.2 and 2.4 referring to the peculiar failure mode of concrete columns confined by high strength spirals.

2.2.3.2 Stress-Strain Models for Concrete Confined by Rectangular Hoops with Supplementary Cross Ties.

In the past, for rectangular columns, rectangular hoop reinforcement was used without supplementary cross ties and hence a large volume of hoop reinforcement with a small spacing was used in an attempt to confine core concrete. In last two decades, a number of studies [eg. 2.1, 2.28, 2.29, 2.30] have indicated that the confining effects of rectangular hoops can be significantly improved by adding supplementary cross ties or overlapping hoops. Since then, transverse reinforcing details using rectangular hoops and supplementary cross ties or overlapping hoops have been

recommended or required to use in seismic design practice to provide adequate ductility for columns. For example, in NZS 3101[2.11] and ACI 318-89 [2.12] the spacing across the section between the legs of supplementary cross ties or overlapping hoops, in the potential plastic hinge regions of columns subjected to seismic loading, is not permitted to exceed 200 mm and 14 inches (= 360 mm), respectively (see Figs. 2.8 and 2.24). In this section, three stress-strain models for concrete confined by rectangular hoops with supplementary cross ties or overlapping hoops are reviewed.

Modified Kent and Park Stress-Strain Model (1982)

The original Kent and Park stress-strain model [2.31] for concrete confined by rectangular hoops without supplementary cross ties was proposed in 1971, based on the experimental data obtained by Roy and Sozen [2.10], Bertero and Felipa [2.32], and Soliman and Yu [2.33], etc. In this model, the ductility improvement of concrete due to confinement was adequately expressed but the strength enhancement was neglected. This was because no strength enhancement was found in the tests by Roy and Sozen conducted on 45 concrete prisms confined by square hoops when compared with 15 plain concrete prisms, taking also into account the fact that the strength enhancement recognized in other researchers' tests [2.32, 2.33] was small enough to be neglected. However, in the study by Park, Priestley and Gill [2.30] where four full size reinforced concrete columns confined by rectangular hoops with supplementary cross ties were tested under combined axial load and flexure, strength enhancement of core concrete was evident. Consequently, they proposed a modified form of the original Kent and Park model taking into account the strength enhancement and increase of strain at maximum stress of confined core concrete, as illustrated in Fig. 2.25.

In the modified Kent and Park model, it is assumed that the maximum stress, Kf'_c, is reached at a strain of 0.002K, and the stress-strain relation is;

For $\varepsilon_c \leq 0.002K$

$$f_c = K f'_c \left[\frac{2\varepsilon_c}{0.002K} - \left(\frac{\varepsilon_c}{0.002K} \right)^2 \right] \quad \text{.....} \quad (2.49)$$

For $\varepsilon_c > 0.002K$

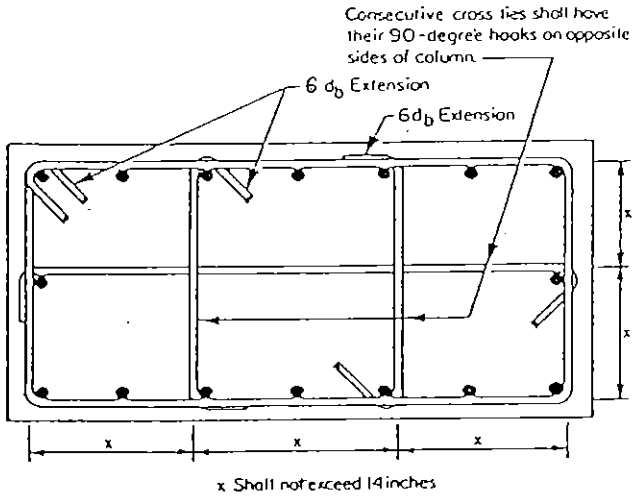

Fig. 2.24 Transverse Reinforcing Details Using a Hoop and Supplementary Cross Ties Suggested in ACI 318R-89 [2.12].

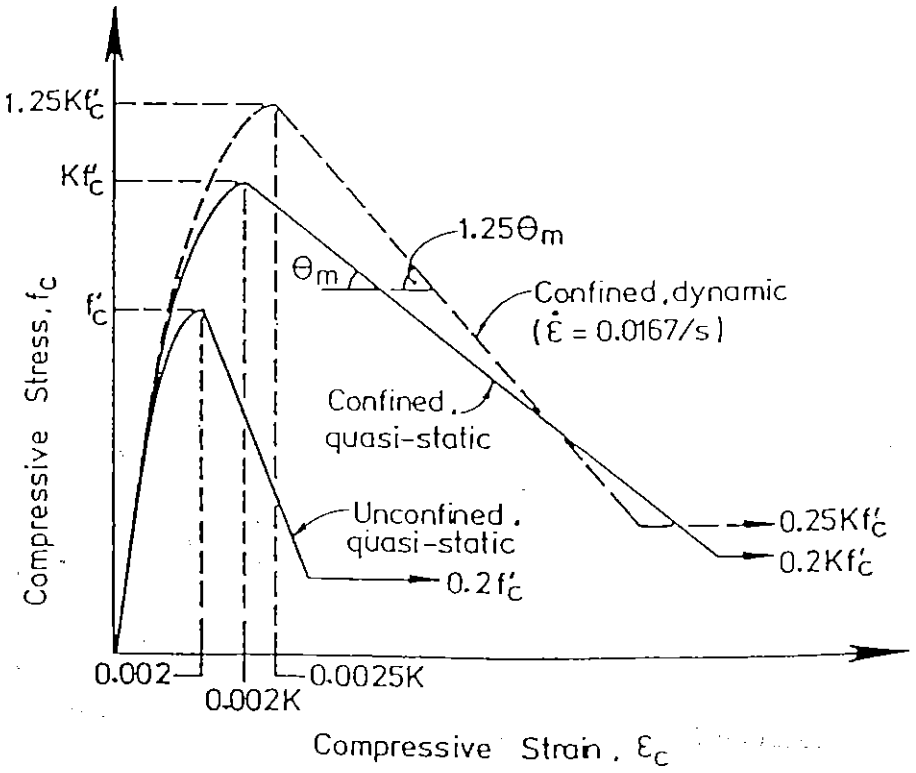

Fig. 2.25 Modified Kent and Park Model for Concrete Confined by Rectangular Hoops with Supplementary Cross Ties, IncludingHigh Strain Rate Allowance [2.29].

$$f_c = K f'_c [1 - Z_m (\varepsilon_c - 0.002 K)] \quad \text{.....} \quad (2.50)$$

but not less than $0.2 K f'_c$

$$\text{where } K = F_D [1 + \rho_s \frac{f_{yh}}{f'_c}] \quad \text{.....} \quad (2.51)$$

and

$$Z_m = \frac{0.5 F_D}{[\frac{3 + 0.29 f'_c}{145 f'_c - 1000}] + \frac{3}{4} \rho_s \sqrt{\frac{h''}{s_h}} - 0.002K} \quad \text{.....} \quad (2.52)$$

where F_D = is a strain-rate dependent constant taken as 1.0 for low rates.

Other variables have the meanings used in previous section.

On the basis of observed stress-strain behaviour from concentric loading tests on concrete prisms with high strain rate of 0.0167/sec, Scott et al [2.29] proposed that the modified Kent and Park stress-strain relation may be adapted for the high strain rate by applying a multiplying factor of 1.25 to the paek stress, and the slope of the falling branch. This is effected in the above equations by setting $F_D = 1.25$ in Eqs. 2.51 and 2.52.

Stress-Strain Model Proposed by Sheikh and Uzumeri (1979)

Sheikh and Uzumeri tested 24 reinforced concrete columns with the various transverse reinforcing details shown in Fig. 2.8 [2.13, 2.34]. The tested columns were 305 mm square x 1960 mm high and loaded monotonically in quasi-static concentric axial compression. From these test results, it was concluded that both the ductility and strength were enhanced by confinement from overlapping rectangular hoops.

The most notable feature of this model is the concept used to define the effectively confined concrete area within the concrete core surrounded by perimeter ties. The area of the effectively confined concrete is determined by the tie spacing, the distribution of longitudinal steel around the core perimeter and the resulting tie configuration (see Fig. 2.9). The ratio of effectively confined concrete core area at the critical section to the concrete core area bounded by the centre line of the perimeter tie, λ^*, was evaluated for various tie configurations as shown in Fig. 2.26. This λ^* was

derived as follows. The area of the effectively confined concrete core at the tie level is expressed as

$$A_{co} - \sum_{i=1}^{n} C_i^2/\alpha = \lambda A_{co} \qquad \text{.....} \qquad (2.53)$$

where A_{co} = the core area enclosed by the centre line of outer tie

C_i = the centre-to-centre distance between adjacent longitudinal bars (see Fig. 2.27 (a))

n = the number of arcs in the transverse section (the arcs represent the boundary lines of effectively confined area, see Fig. 2.9)

α = a constant, the value of which is determined by the exact shape of the arcs (α = 5.5 in this study)

$$\lambda = \left(1 - \frac{1}{\alpha A_{co}} \sum_{i=1}^{n} C_i^2 \right)$$

When the concrete core area, A_{co}, is expressed by B x H (where B and H = the centre-to centre principal dimensions of the perimeter tie of rectangular core), at a section midway between the tie sets the rectangular core area surrounded by arcs shown in Fig. 2.27 (b) is

$$(B - 2y_m) \times (H - 2y_m)$$

where y_m = the maximum value of y, midway between the hoop sets

$= 0.25\, s \tan\theta$

In their study, $\theta = 45°$ was assumed and hence the effectively confined concrete area at the critical section becomes zero when the hoop spacing 's' is two times B (see Fig. 2.26). By combining the above two relations, the resulting area of the effectively confined concrete at the critical section, A_{ec} was expressed by

$$A_{ec} = \lambda (B - 2y_m) \times (H - 2y_m) = \lambda^* A_{co} \qquad \text{.....} \qquad (2.54)$$

The value of λ^* for various hoop configurations and s/B values are shown in Fig. 2.26.

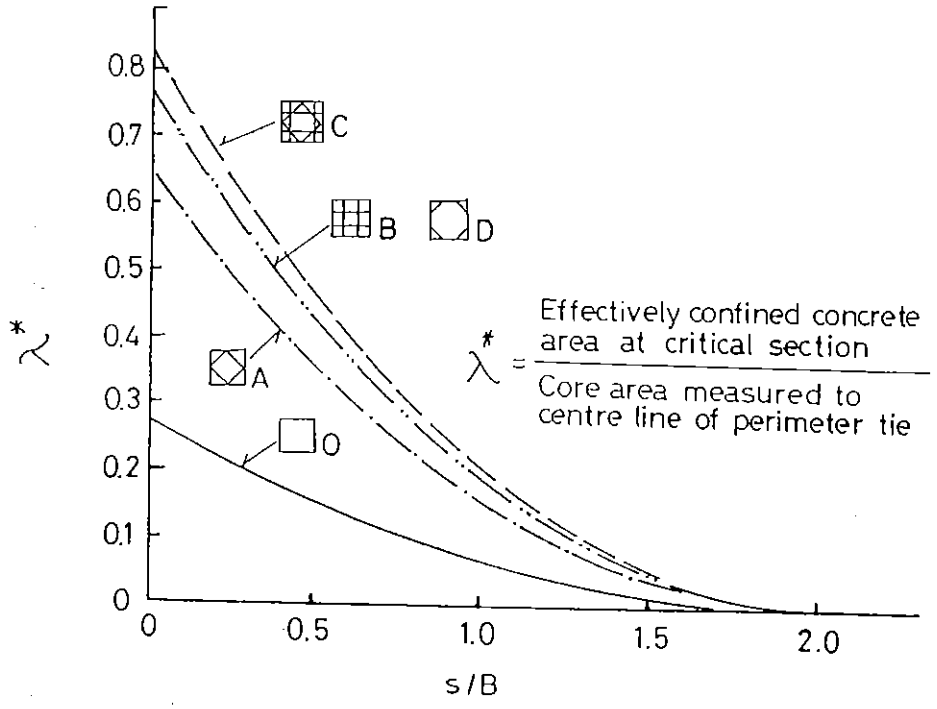

Fig. 2.26 Effectively Confined Concrete Area as a Function of Tie Spacing and Core Size for Various Square Steel Configurations [2.13].

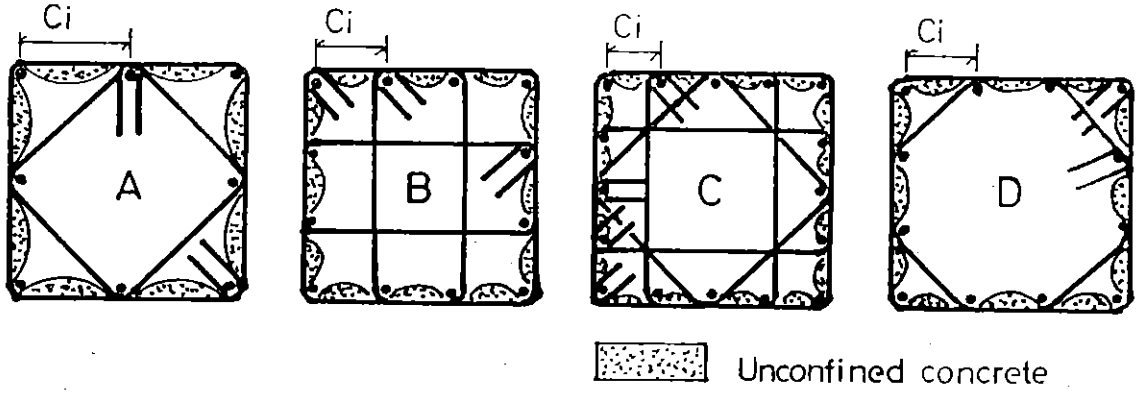

(a) Unconfined Concrete Area at Tie Level

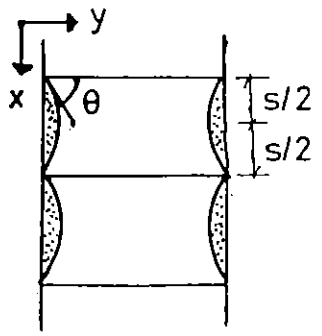

(b) Unconfined Concrete Area between Hoop Sets

Fig. 2.27 Unconfined Concrete Area Assumed in Sheikh and Uzumeri Model [2.13].

Based on the above experimental data and considerations, a stress-strain model illustrated in Fig. 2.28 was proposed. The ascending part OA is a second degree parabola and followed by a horizontal straight line AB. The falling branch is represented by a straight line which continues to decrease down to 30 % of the maximum stress, maintaining this magnitude of stress for further loading. The following equations were derived to determine each point in the stress-strain curves.

The ratio of the confined concrete strength to the unconfined strength, K_s, is expressed by

$$K_s = 1.0 + \frac{1}{140 P_{occ}} \left[\left(1 - \frac{n C^2}{5.5 B^2} \right) \left(1 - \frac{s}{2 B} \right)^2 \right] \sqrt{\rho_s f'_{sh}} \quad \text{.....} \quad (2.55)$$

where ρ_s = the volumetric ratio of the lateral reinforcement to the concrete core volume

f'_{sh} = the stress in the lateral reinforcement at the time of maximum resistance of confined concrete (in MPa)

P_{occ} = the unconfined compressive strength of the concrete core in kilonewtons = $0.85 f'_c (A_{co} - A_s)$, where A_s is the longitudinal steel area

The confined concrete strength f_{cc} is given by

$$f_{cc} = K_s f_{cp} \quad \text{.....} \quad (2.56)$$

where f_{cp} = the plain concrete strength of the column = $0.85 f'_c$

The minimum and maximum strains corresponding to the maximum stress plateau, ε_{s1} and ε_{s2} are given by

$$\varepsilon_{s1} = 80 K_s f'_c \times 10^{-6} \quad \text{.....} \quad (2.57)$$

where f'_c is in MPa

$$\frac{\varepsilon_{s2}}{\varepsilon_{oo}} = 1 + \frac{248}{C} \left[1 - 5.0 \left(\frac{s}{B} \right)^2 \right] \frac{\rho_s f'_{sh}}{\sqrt{f'_c}} \quad \text{.....} \quad (2.58)$$

where ε_{oo} = strain corresponding to the maximum stress in plain concrete = 0.0022 in the case of their study

The strain at 85 % of the maximum stress on the falling branch of the stress-strain curve is given by

$$\varepsilon_{s85} = 0.225\ \rho_s \sqrt{\frac{B}{s}} + \varepsilon_{s2} \qquad \text{.....} \qquad (2.59)$$

Stress-Strain Model Proposed by Mander et al (1984)

Mander et al [2.6] theoretically investigated the behaviour of rectangular sections with unequal confinement in the two principal directions as part of an initial study into the behaviour of confined hollow rectangular columns. The method proposed by Mander et al is basically the same as that for circular columns with circular hoops or spirals described in Section 2.2.3.1. That is, Eqs. 2.39 to 2.46 are equally applied to rectangular and circular sections, except for Eq. 2.40 which gives the confined concrete strength f'_{cc}. That is, the difference for rectangular sections lies in the method for estimating the confined concrete strength, f'_{cc}. This model has been calibrated using several test columns with 450 mm square cross section and 1200 mm high. The transverse reinforcing details were the types A and D shown in Fig. 2.27 (a).

To find f'_{cc} it is first necessary to find the confinement effectiveness coefficient k_e appropriate to the rectangular section, and the lateral confining stresses in the two principal transverse directions. As for circular sections, k_e represents the ratio of the minimum effectively confined core area to the total core area bounded by the centre lines of perimeter hoops. To represent the boundary between effectively confined area and ineffectively confined area, the arcs shown in Fig. 2.29 were assumed for between longitudinal bars in the transverse section and for between hoop sets in the vertical section. In the Sheikh and Uzumeri model, for the transverse section, the ineffectively confined core area at hoop set level bounded by the archs was given by $\sum_{i=1}^{n} C_i^2/\alpha$ in Eq. 2.53 and $\alpha = 5.5$ was selected from a regression analysis for 24 tested columns. In the Mander et al model, these arcs were assumed to be second degree parabolas with initial slope of 45° and hence $\alpha = 6$ was automatically determined from geometry. Also for the arcs in the vertical section shown in Fig. 2.27 (b), second degree

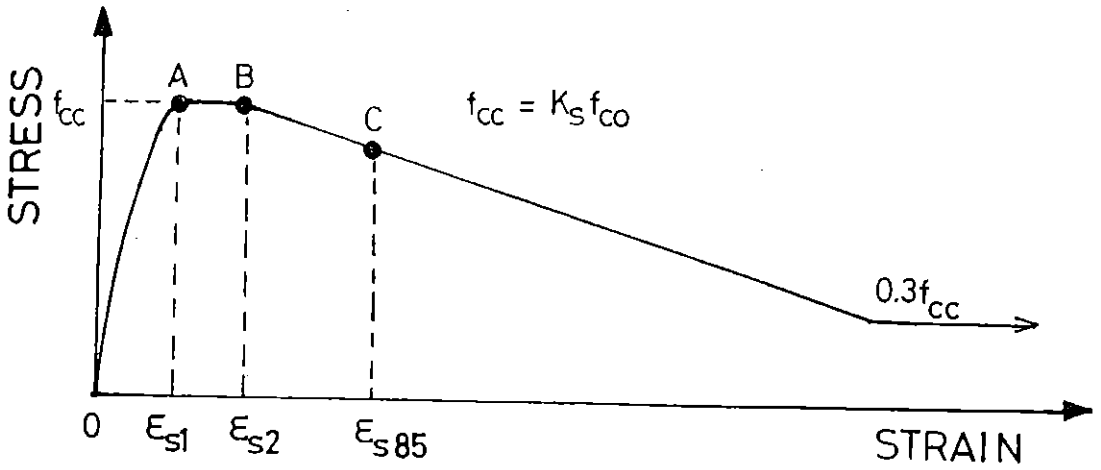

Fig. 2.28 Sheikh and Uzumeri Stress-Strain Model for Concrete Confined by Rectangular Hoops with Supplementary Cross Ties [2.13].

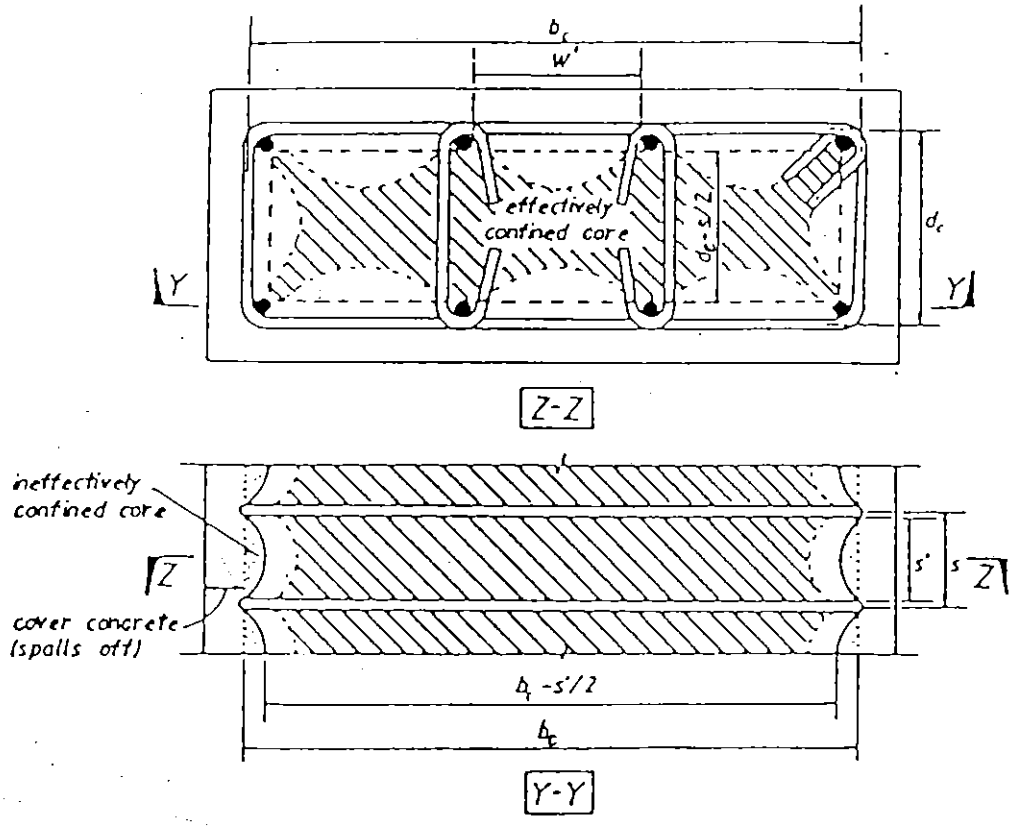

Fig. 2.29 Confined Core of Rectangular Section

parabolas with initial slope of 45° were applied. By incorporating those assumed arcs, the area of effectively confined core area was expressed by

$$A_{ec} = [\, b_c\, d_c - \sum_{i=1}^{n} C_i^2/6\,]\,(1 - 0.5\,\frac{s'}{b_c})(1 - 0.5\,\frac{s'}{d_c}) \quad \text{.....} \quad (2.60)$$

where b_c = concrete core dimension in the x direction

d_c = concrete core dimension in the y direction

s' = clear spacing between spiral or hoop bars

Since the concrete core area enclosed for the section is $A_{co} = b_c \times d_c\,(1 - \rho_{cc})$, the confinement effectiveness coefficient is

$$k_e = \frac{A_{ec}}{A_{co}} = [\,1 - \sum_{i=1}^{n} C_i^2/(6\, b_c\, d_c)\,]\,(1 - 0.5\,\frac{s'}{b_c})(1 - 0.5\,\frac{s'}{d_c})]/\,(1 - \rho_{cc}) \quad \text{.....} \quad (2.61)$$

The effective confining stress in the two principal directions are given by

$$f_{lx} = k_e\, \rho_x\, f_{yh} \quad \text{.....} \quad (2.62)$$

and $$f_{ly} = k_e\, \rho_y\, f_{yh} \quad \text{.....} \quad (2.63)$$

where $$\rho_x = \frac{A_{sx}}{s\, d_c} \quad \text{.....} \quad (2.64)$$

and $$\rho_y = \frac{A_{sy}}{s\, b_c} \quad \text{.....} \quad (2.65)$$

are the volumetric confinement ratios in x and y directions respectively, where the x and y axes are parallel to the long and short sides of the section, respectively, and A_{sx} and A_{sy} are the total areas of lateral reinforcement parallel to the x and y axes, respectively.

For the situation envisaged here, the core concrete is placed in triaxial compression with unequal lateral confining pressures. The ultimate strength surface adopted by Mander et al [2.6] follows the 'five parameter' model of William and Warnke [2.35], and has been plotted for design purposes in the interaction curves of Fig. 2.30. In the figure, f'_{l1} and f'_{l2} were defined as the smallest and the largest confining stresses, respectively, and are corresponding to f_{lx} and f_{ly} or to f_{ly} and f_{lx}. Using Fig. 2.30, the strength enhancement of confined core concrete can be estimated from unequal lateral confining pressures, f_{lx} and f_{ly}. Thus, the stress-strain curves can be derived from Eq 2.39 and Eqs. from 2.42 to 2.46.

Comparison between the Above Stress-Strain Models

In order to compare the above three stress-strain models, example calculations were conducted for the section type A shown in Fig. 2.27 (a). It was assumed that plain concrete strength f'_c = 30 MPa, yield strength of transverse reinforcement f_{yh}= 300 MPa, volumetric ratio of transverse reinforcement to concrete core ρ_s (= $\rho_x + \rho_y$ for the Mander et al stress-strain model) = 2% , section area ratio of longitudinal reinforcement to concrete core ρ_{cc} = 2%, hoop spacing s = 100 mm, core dimensions B H (denoted in the Sheikh et al stress-strain model) = b_c d_c (denoted in the Mander et al stress-strain model) = 500 x 500mm. It can be seen in Fig. 2.31 that the Mander et al model gives the largest strength increase and the most gentle falling branch of the three models introduced here, as well as for the case for concrete confined by circular hoops or spirals mentioned in Section 2.2.3.1.

From Fig. 2.31 it can be seen that the Modified Kent and Park model gives most conservative estimate for the strength increase due to confinement. The strength increase estimated by the Mander et al model is largest but is almost the same as that by the Sheikh and Uzumeri model. With respect to the slope of the falling branch up to 2% strain, the three models gave almost similar estimates.

It should be noted that the stress-strain model by Sheikh et al was calibrated up to a compressive strain of about 2.5 % using the accompanied tests on 24 columns [2.13] and hence this model might be inadequate when it is necessary to predict the behaviour of confined concrete for the strain region of more than 3 %. On the other hand, the stress-strain model by Mander et al [2.6] was calibrated by several column tests where the measured concrete strain reached over 4%. This may be attributed to the fact that the gauge lengths used for the measurement of the concrete compressive strain were different between the tests by Mander et al and by Sheikh and Uzumeri. In the tests by Sheikh and Uzumeri, the gauge length used was 1.33 times the concrete core width(=356mm), except for 6 specimens in which the gauge length was 1.14 times the concrete core width (=305 mm). In the tests by Mander et al, the gauge length and the concrete core width were the same, 400mm. If the difference of the ratio of the gauge length to

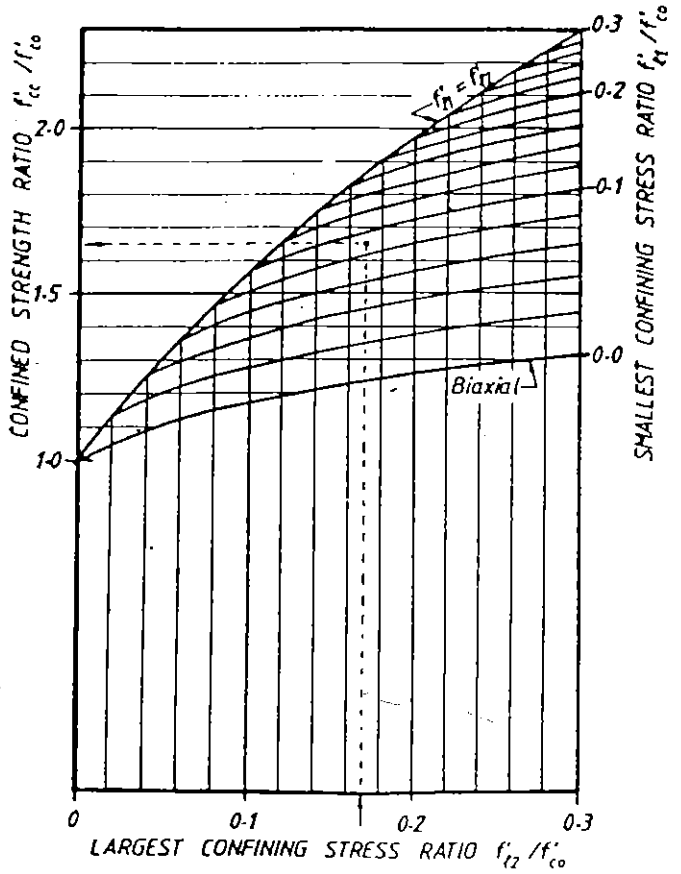

Fig. 2.30 Confined Concrete Strength Determined from Lateral Confining Stresses for Rectangular Section [2.6].

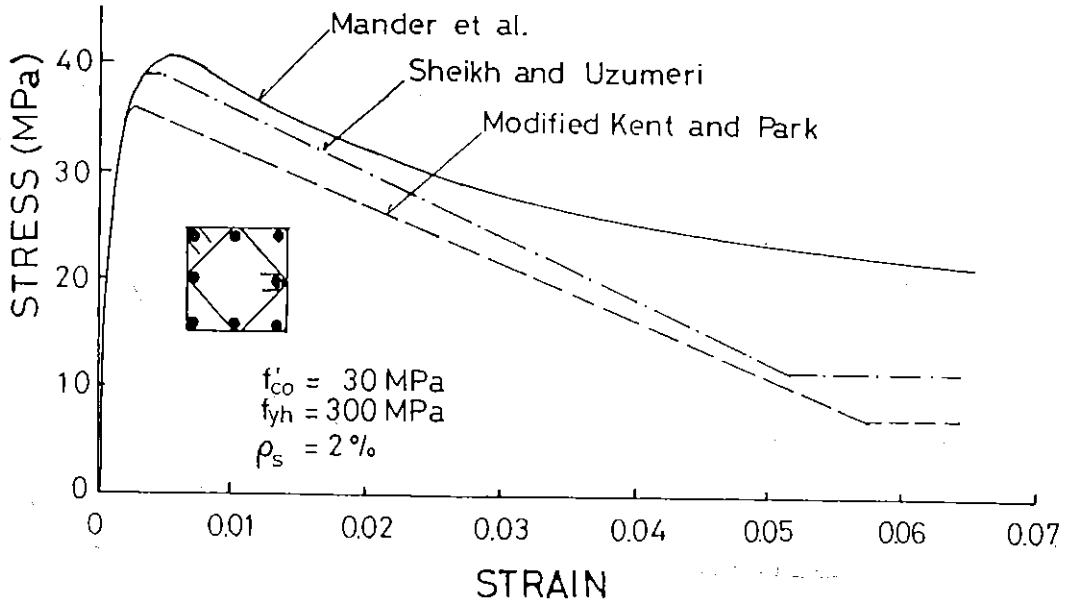

Fig. 2.31 Comparison of the Modified Kent and Park Model, Sheikh and Uzumeri Model, and Mander et al Model.

the core dimension is taken into account, 3% strain in the Sheikh and Uzumeri model may possibly correspond to 4% strain (= 1.33 x 3%) in Mander et al model. This is because; (1) When the diagonal failure plane (see Fig. 2.23) is formed, the column axial deformation is governed partly by the shear sliding between upper and lower parts of column separated by the failure plane, (2) In such a case, the apparent axial strain of concrete in the falling brach, which is calculated by dividing the gauge length into the relative vertical displacement between the shear sliding surfaces, is governed by the gauge length used for the strain calculation.

Thus, similar to the case of circular hoops and spirals mentioned in Section 2.2.3.1, the magnitude of the axial compressive strain of concrete measured in the falling branch will significantly depend on the gauge length used in the particular tests. When a column is subjected to bending and axial load, the length of compression failure zone along the column axis varies mainly depending on the moment gradient and the axial load level imposed. Hence, it cannot be simply said what is the most appropriate gauge length to be adopted in column tests for applying an analysis of columns under combined bending and axial load. As a future study, a method to appropriately modify the strains measured in axial compression tests with a certain gauge length may need to be established for application to flexural members with various axial load levels.

2.3 FACTORS WHICH AFFECT EFFECTIVENESS OF LATERAL CONFINEMENT

2.3.1 General Factors

Major factors which affect the effectiveness of lateral confinement have normally been employed in the stress-strain models for the confined concrete. For the stress-strain models reviewed in Section 2.2.3, the major variables adopted to determine the shape of stress-strain curves of confined concrete were as follows:

1. The ratio of the volume of transverse steel to the volume of the concrete core, because a high transverse steel content will lead to a high lateral confining pressure for the core concrete.

2. The yield strength of the transverse steel which gives an upper limit to the confining pressure.

3.The ratio of the spacing of the transverse reinforcement to the dimensions of the concrete core, because a smaller spacing leads to larger area confined effectively (see Figs. 2.12 and 2.27 (b)).

4. The strength of plain concrete. This is because low-strength concrete is more ductile than high-strength concrete [2.2] and ductility enhancement due to confinement appears smaller as the concrete strength increase [2.36, 2.37].

5. The ratio of the distance between the supported longitudinal bars to the core dimension for the case of rectangular hoops and supplementary cross ties, because a smaller distance between the supported longitudinal bars leads to larger area confined effectively (see Figs. 2.27 (a) and 2.29).

6. The content of longitudinal reinforcement (see Eqs. 2.47 and 2.48), because additional confinement by the longitudinal reinforcement may be expected until the bending stiffness of longitudinal reinforcement becomes zero due to its axial compression yielding.

7. The rate of loading, because the stress-strain characteristics of concrete are time dependant (see Fig. 2.25).

In addtion to the above factors, the following factors also affect the effectiveness of lateral confinement.

1. The ratio of the diameter of the transverse bar to the unsupported length of the transverse bars, in the case of rectangular hoops: This is because the area of the effectively confined concrete becomes larger for the higher bending stiffness of the hoop bar. However, this factor is normally negligible for the practically sized reinforcing details (see an example calculation shown in Section 5.2.).

2. The strain gradient in column section: This is mainly because the lateral expansion of concrete tends to be large at the extreme compression fibre and ideally non-existent at the neutral axis, and hence the lateral confining stresses provided by transverse reinforcement due to the Poisson's effect varies along the depth of member section in accordance with the magnitude of the strain gradient. This matter is further discussed with other reasons in Section 2.3.2.

3. The longitudinal stress gradient of concrete: This is based on the experimental study by Uppal and Kemp [2.38] which demonstrated that the strength of concrete is significantly increased in the presence of

longitudinal stress gradient. The tests were conducted using tapered beams subjected to pure bending and tapered columns subjected to axial compression. From the compression tests, the concrete strength increase due to the longitudinal stress gradient was up to 42% of the strength obtained by the accompanied uniform stress tests. From the tapered beam tests, the increased strength of the concrete compression block was as high as 44 % above the uniform beam value. It must be emphasized that these test results did not involve the strength increase normally attributed to the biaxial stress condition produced in the vicinity of loading points. This factor may be significant when a column with comparatively small aspect ratio is loaded by a horizontal load and hence the moment gradient along the column axis is large.

4. The concrete cover thickness and curing condition of concrete: If the core concrete shrinks excessively due to thin cover concrete with bad curing condition, the appearance of the lateral confining effects will be delayed [2.28]. To ensure that the confining reinforcement resists the early lateral expansion of the core concrete, large shrinkage of core concrete must be prevented by providing adequate thickness for concrete cover and by curing the concrete appropriately. In construction practice, this point will be important to secure the stiffness of the confined concrete members for the early stage of inelastic loading, although this point seems to be often overlooked.

In the following sections, the influences of strain gradient in the column section, plain concrete strength and longitudinal reinforcement on confinement are discussed in more detail, by introducing several tests carried out by the author and by other researchers.

2.3.2 Strain Gradient in Column Section

2.3.2.1 Introduction

The strain gradient in a column section influences the stress-strain behaviour of the confined concrete with respect to the following three aspects. Firstly, since the compression strain imposed in each compression fibre becomes smaller as its location becomes further from the extreme compression fibre, the progress of concrete damage at the extreme compression fibre region will be restrained by the adjacent concrete fibres

with lower strains. Secondly, the lateral expansion of core concrete tends to be large at the extreme compression fibre and ideally non-existent at the neutral axis, resulting in the passive lateral confining stresses provided by transverse reinforcement varying down the depth of the member section in accordance with the magnitude of the strain gradient. Thirdly, the magnitude of hoop tensile strain attained in the extreme compression fibre zone in a column subjected to bending is significantly smaller than that attained in a column subjected to axial compression, for when the extreme compression fibre strain in the bent column is the same as the compression strain in the axially loaded column [2.8]. These aspects are further discussed in the following sections.

2.3.2.2 The Influence of the Strain Gradient on the Progress of Damage in Compressed Concrete

The influence of flexural strain gradient in column sections on the stress-strain relationships of plain concrete has been studied by Hognestad et al [2.39], Sturman et al [2.40], Karsan and Jirsa [2.41], Morita and Adachi [2.42] and others, by carrying out comparative concentric and eccentric compressive loading tests on concrete specimens. The conclusions reached in these studies are not always in agreement. For example, in the study by Hognestad et al [2.39] a striking similarity was found between the stress-strain relations obtained in the presence of a strain gradient and those obtained in concentric compression tests on 6 by 12-inches cylinders, while in the study by Sturman et al [2.40] it was found that the peak of the flexural stress-strain curve was located at a strain about 50 % higher and stress about 20 % larger than the peak of the curve for the concentric loading specimen. In the study by Morita and Adachi [2.42] where the obtained test results were similar to those by Sturman et al [2.40], it was pointed out that the shape of the flexural stress-strain curve was significantly affected by the gauge length used for the strain measurement.

Although the estimated degrees of influence of the flexural strain gradient are not consistent between researchers as mentioned above, it is apparent that the strength and ductility of plain concrete must be increased more or less by the presence of flexural strain gradient in the section for the following reason. Since the compression strain imposed in each

compression fibre becomes smaller as its location becomes further from the extreme compression fibre, the progress of damage in the extreme compression fibre region will be restrained by the adjacent concrete fibres with lower strains. To verify this phenomenon, using x-ray technique Sturman et al [2.40] have shown that micro-cracking, particularly mortar cracking, in the specimens eccentrically loaded is retarded and is reduced compared with cracking at the same strain in the axially loaded specimens. This phenomenon observed for the plain concrete specimens will also appear in confined concrete specimens and improve the stress-strain relationship of the confined concrete, although it has not yet been demonstrated in experiments using confined concrete specimens.

When the ductility of beams or columns is discussed, the influence of the strain gradient will need to be considered mainly for the confined core concrete rather than for the unconfined cover concrete. This is because the unconfined cover concrete spalls off relatively early in the inelastic range of loading and hence the contribution of cover concrete to the ductile behaviour of those members at high concrete compressive strains is normally insignificant.

2.3.2.3 The Influence of the Strain Gradient on the Stress-Strain Relationships of Confined Concrete

Soliman and Yu (1967, [2.14]) have conducted an experimental study on the stress-strain relationships of confined concrete in flexure. Sixteen specimens having two or four longitudinal bars and rectangular hoops were tested under eccentric loading using the similar method adopted in the study by Hognestad et al [2.39]. The cross section of the specimens was 4 x 6 in (102 x 152 mm) rectangular section, except for two specimens with 3 x 6 in (76 x 152 mm) and 5 x 6 in (127 x 152) sections. The ratios of rectangular hoop volume to concrete core volume were varied from zero to 3.43 %. The specimens were tested under the action of a major and a minor load (P_1 and P_2) such that the neutral axis was always set at the position of longitudinal reinforcing bars near concrete cover in tension side throughout the entire range of loading (see Fig. 2.32 (a)). The method of analysis used to determine the stress-strain relationship was based upon numerical differentiation, following an approach developed by Hognestad

et al [2.39]. The numerical differentiation method used can be explained as follows:

The basic assumptions used were :
(1) The distribution of strains across the section is linear.
(2) All fibres follow the same stress-strain relationship.

With reference to Figs. 2.32 (a) and (b), at any particular stage of loading, the following information can be obtained from the recorded test data.
(1) The strain at the extreme fibre, ε_c.
(2) The average stress over the cross section, f_o, which can be calculated as

$$f_o = \frac{C}{bnd} = \frac{P_1 + P_2 - A_s' f_s'}{bnd} \quad \text{.....} \quad (2.66)$$

where C= resultant compressive force in the concrete
b = width of concrete cross section
d = effective depth of concrete cross section
n = ratio of neutral axis depth to the effective depth
A_s' = total area of the compression reinforcement
f_s' = compressive stress in the compression reinforcement

(3) The moment of the external forces about the neutral axis divided by bn^2d^2, that is, m_0 which can be calculated as

$$m_0 = \frac{M}{bn^2d^2} = \frac{P_1 (a_1 + \delta) + P_2 (a_2 + \delta) - A_s' f_s' (nd - d')}{bn^2d^2} \quad \text{.....} \quad (2.67)$$

where M = applied moment
a_1 = eccentricity pf the major load P_1
a_2 = eccentricity pf the minor load P_2
δ = deflection at the critical section
d'= distance between the centroid of the compression reinforcement and the extreme compression fibre of concrete

C and M can be expressed as

$$C = b \int_0^{nd} \phi(\varepsilon_x)\, dx \qquad \text{.....} \qquad (2.68)$$

$$M = b \int_0^{nd} \phi(\varepsilon_x)\, x\, dx \qquad \text{.....} \qquad (2.69)$$

where $\phi(\varepsilon_x)$ = stress in concrete fibre at strain ε_x

Since

$$x = \frac{\varepsilon_x}{\varepsilon_c}\, nd$$

where x = distance between the neutral axis and the concrete fibre with strain ε_x

assuming that nd is constant,

$$dx = (nd / \varepsilon_c)\, d\varepsilon_x \qquad \text{.....} \qquad (2.70)$$

From Eqs. 2.66, 2.67 and 2.70, Eqs. 2.68 and 2.69 can be put into the following form,

$$\varepsilon_c f_0 = \int_0^{\varepsilon_c} \phi(\varepsilon_x)\, d\varepsilon_x \qquad \text{.....} \qquad (2.71)$$

$$\varepsilon_c^{\,2} m_0 = \int_0^{\varepsilon_c} \phi(\varepsilon_x)\, \varepsilon_x\, d\varepsilon_x \qquad \text{.....} \qquad (2.72)$$

Differentiating both sides of Eqs. 2.71 and 2.72 with respect to ε_c, we get

$$f_c = f_0 + \varepsilon_c \frac{d f_0}{d \varepsilon_c} \qquad \text{.....} \qquad (2.73)$$

$$f_c = 2\, m_0 + \varepsilon_c \frac{d\, m_0}{d\, \varepsilon_c} \qquad \text{.....} \qquad (2.74)$$

The terms $\frac{d\, f_0}{d\, \varepsilon_c}$ and $\frac{d\, m_0}{d\, \varepsilon_c}$ in these equstions represent the slope of the ε_c - f_0 and ε_c - m_0 relationships at any particular strain value ε_c. These terms can be determined by evaluating the change in the values of f_0 and m_0 over small increments of strain. Thus the stress-strain relationships of concrete in the presence of strain gradient can be calculated using Eqs. 2.73 or 2.74. It is noted that Eqs. 2.73 and 2.74 provide two independent methods for calculating the stress corresponding to any strain at the extreme fibre of concrete. Since the eccentricities a_1 and a_2 are very difficult to measure accurately in practice, it is obvious that much more experimental errors is involved in obtaining the values of m_0.

In Fig. 2.33 several stress-strain relations of confined concrete obtained are shown. It may be said that the stress-strain relationships of confined concrete in flexure illustrated by Fig. 2.33 have longer plateaus near maximum stress than the stress-strain models based on axial compression tests shown in Figs. 2.21, 2.31.

It must be noted that the above study by Soliman and Yu contains the following defects. Firstly, no consideration was given to the spalling of the unconfined cover concrete and the calculation of the concrete stress to obtain the stress-strain relationships shown in Fig. 2.33 was based on the total concrete area under compression. In the tests, the area of confined concrete core under compression was about 90 % of the area of cover and core concrete under compression in most specimens. Hence, if the stress-strain relationships were estimated for the confined core area only, the strength and ductility increase might be larger than seen from the stress-strain relationships in Fig. 2. 33. The second defect is that it was assumed that all fibres follow the same stress-strain relationship although the magnitude of confining pressure provided by transverse reinforcement actually varied down the depth of section. Hence the stress-strain relation of core concrete fibres should have been varied down the depth of section. However, it must be emphasized that these two defects cannot be simply solved, due to the mathematical restraint of the numerical differentiation method used.

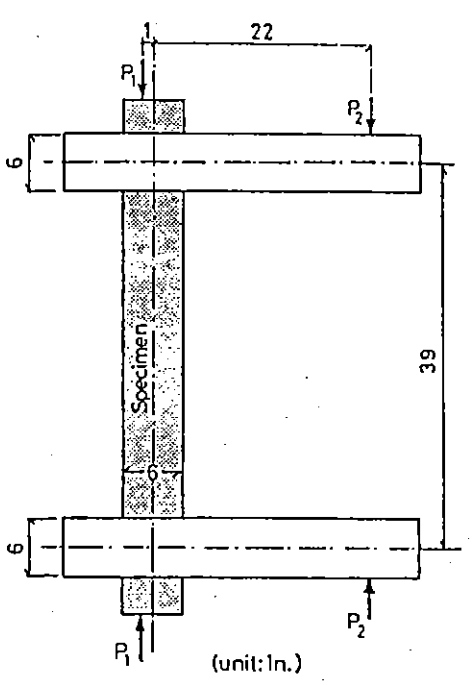

(a) Loading Arrangement

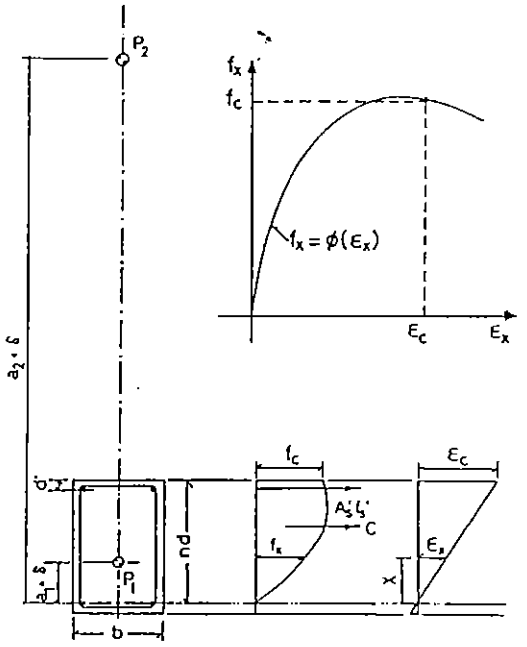

(b) Determination of m_0 and f_0

Fig. 2.32 Loading Condition of the Eccentrically Loaded Column and the Assumed Stress -Strain Relationship of Concrete Used in the Study by Soliman and Yu [2.14].

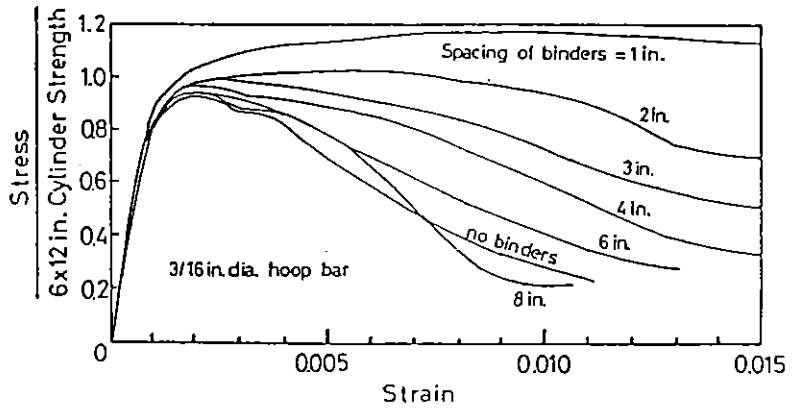

(a) Effect of Spacing of Hoops (Note: 1 in =25.4 mm)

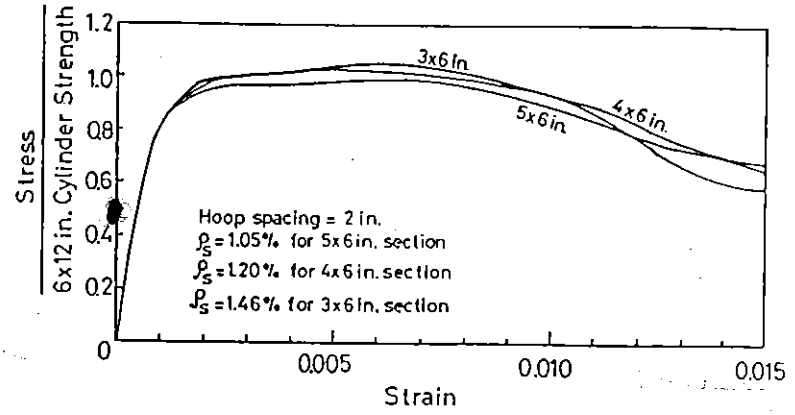

(b) Effect of Shape of Concrete Cross-Section (Note: 1 in =25.4 mm)

Fig. 2.33 Stress-Strain Relationship of Confined Concrete in Flexure, Calculated from Numerical Differentiation of Test Data from Eccentrically Loaded Specimens [2.14].

Unfortunately, in these tests the strains and corresponding stresses induced in the transverse reinforcement were not measured and hence the confining stress condition in the adjacent core concrete was not referred. Since the stress-strain behaviour of the confined concrete is strongly related to the lateral confining stress distribution down the column section depth, which would be determined from the strain gradient, this point is discussed with reference to the study described in the following section.

2.3.2.4 The Influence of the Strain Gradient on the Confining Stress Distribution Down the Column Section Depth

In order to investigate the confining stress condition, and the corresponding stress-strain relationships of the core concrete in flexural members, the following eccentric loading tests on concrete columns were conducted by the author et al at Kyoto University, Japan (1979, [2.8]). Fig. 2.34 (a) shows the detailing of the specimens used for the eccentric loading tests. Square spirals were used, as the transverse reinforcement. For comparison, concrete prisms with 194 mm square section and 400 mm high were also tested under concentric loading. Those prisms were confined with the same square spirals as those used for the eccentric loading tests. The properties of square spirals are listed in Table 2.1 with some of the test results obtained. The loading arrangement and measuring devices are shown in Fig. 2.34 (b). The major and the minor axial loads were controlled so as to induce a triangular strain distribution over the column section until the end of test. That is, the strain at the extreme fibre at the opposite side of the section to the extreme compression fibre was kept zero throughout the entire loading range, as can be seen from the damage to the eccentrically loaded specimens shown in Fig. 2.35. Those concrete strains were measured by a pair of electrical differential transformers with gauge length of 350 mm. The axial tension strains of the square spiral bars were evaluated by averaging the readings from pairs of electrical resistant wire strain gauges which were attached on opposite side of the square spiral bars.

The stress-strain relationships of the concrete for the confined and unconfined columns under eccentric loading were calculated using the same numerical differentiation procedure and the same assumptions adopted in the study by Soliman and Yu [2.14]. The calculated results are

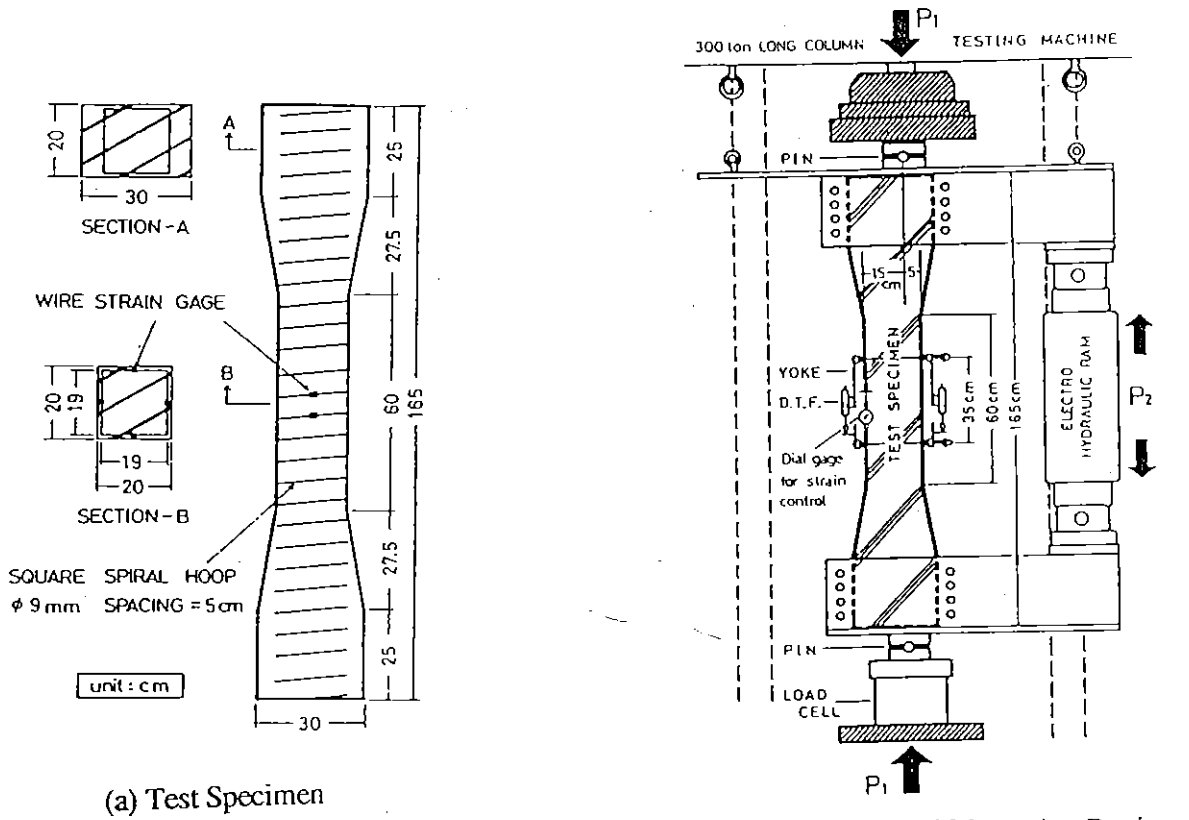

(a) Test Specimen

(b) Loading Arrangement and Measuring Devices

Fig. 2.34 Detailing of Test Specimens, Loading Arrangement and Measuring Devices for Eccentric Loading Tests [2.8].

Table 2.1 Test Column Detailing and Obtained Results

Test Column	Loading Type	Square Spirals				Maximum Concrete Stress (MPa)	Concrete Strain at Maximum Stress (%)
		Bar Dia. (mm)	Yield Strength (MPa)	Pitch (mm)	Volumetric Ratio to Core Volume (%)		
SSM°5	Concen-	8.9	348	50	2.5	36.3	0.65
SSH°5	tric	9.2	1274	50	2.7	42.1	1.20
SS°Plain	Loading					27.2	0.23
SEM°5	Eccentric	8.9	348	50	2.4	33.7	0.34
SEH°5	Loading	9.2	1274	50	2.5	38.1	0.32
SE°Plain						31.7	0.22

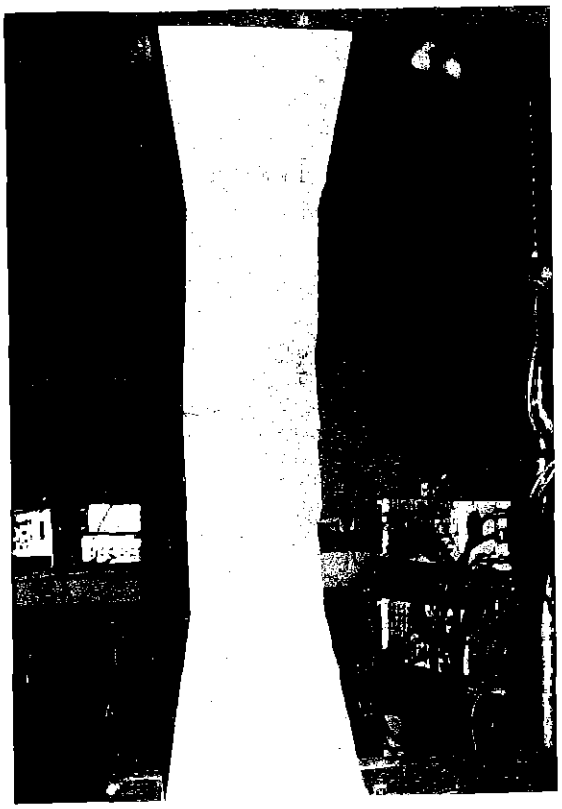

(a) Plain Concrete Specimen (Note: visible tension crack is due to unexpected loading after test)

(b) Confined Concrete Specimen

Fig. 2.35 Damage of Specimens at the End of Eccentric Loading Tests [2.8].

shown in Fig. 2.36. In the strain softening region of concrete, the applied major and minor loads were wiggled due to non-smooth progress of damage of the concrete and hence the calculated points represented by the cross and circular marks were staggered. By applying the least square method the falling branches were represented by straight dashed lines in Fig. 2.36. Also shown in Fig. 2.36 are the confining stresses which were calculated by substituting hoop stresses (which were estimated from the measured hoop strains indicated by the lines with mark (1) in Fig.2.38(a)) into Eq. 2.11. It must be noted that in Fig. 2.38 (a) the lines with mark (1) lie above the other lines, which indicate the hoop strains measured at the locations other than in the extreme compression fibre region, and thus the confining stresses shown in Fig. 2.36 are the maximum likely attained values.

Fig. 2.37 shows a comparison between the stress-strain relations obtained from concentric and eccentric loading tests. It is obvious that the strength and ductility of confined concrete attained in the concentric loading test are greater than those attained in the eccentric loading test, whereas the strength of the plain concrete specimen observed in eccentric loading test is higher than that in the concentric loading test. This can also be seen by comparing the maximum concrete stresses and the corresponding axial compressive strains of concrete shown in Table 2.1.

From these tests, the following observations are notable:

(1) In the eccentric loading tests, the strain increase in the hoop bar located near the neutral axis was negligibly small.

(2) In the eccentric loading tests, the largest increase of hoop tension strain appeared in the hoop bar located near the extreme compression fibre.

(3)The largest hoop strains measured in eccentrically loaded columns were significantly smaller than those attained in concentrically loaded columns, for when the extreme compression fibre strain in the eccentrically loaded column was the same as the compression strain in the concentrically loaded column. Especially in the case of the specimen, SEM°5, with square spirals having a yield strength of 348 MPa, the hoop bar began to be bent outward due to the expansion of core concrete rather than to be axially tensioned from an extreme compression fibre strain of concrete of about 1 % (see dashed lines in Fig. 2.38 (a)).

(4) In the case of SSM°5 with square spirals having a yield strength of 348 MPa, which was tested under concentric load, the axial strain in the hoop

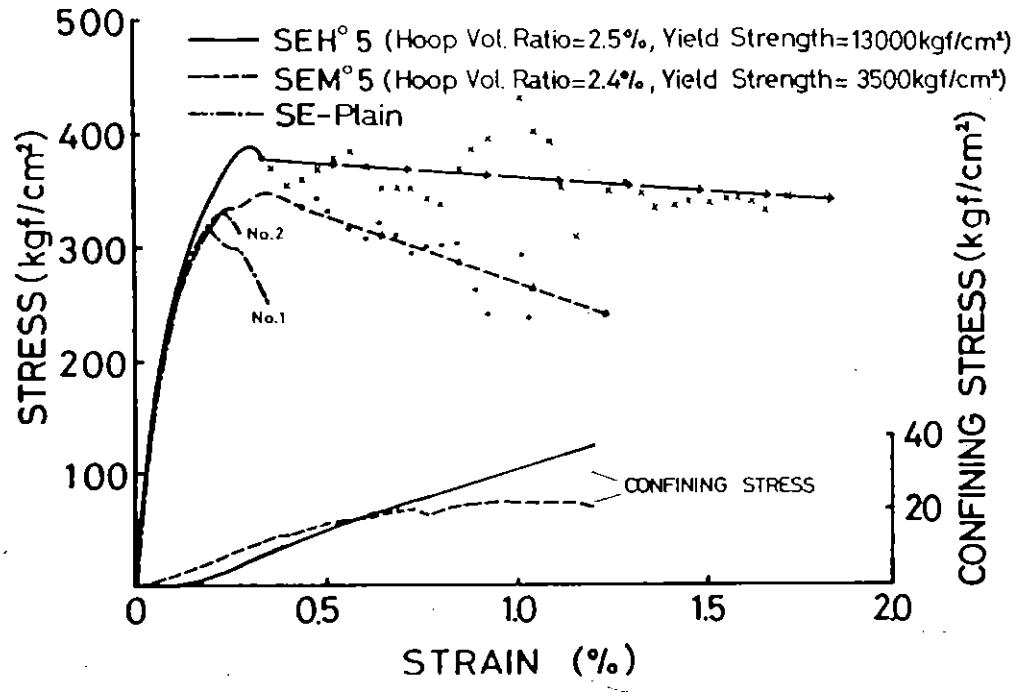

Fig. 2.36 Stress-Strain Relations and Corresponding Confining Stresses Obtained from Eccentric Loading Tests [2.8].

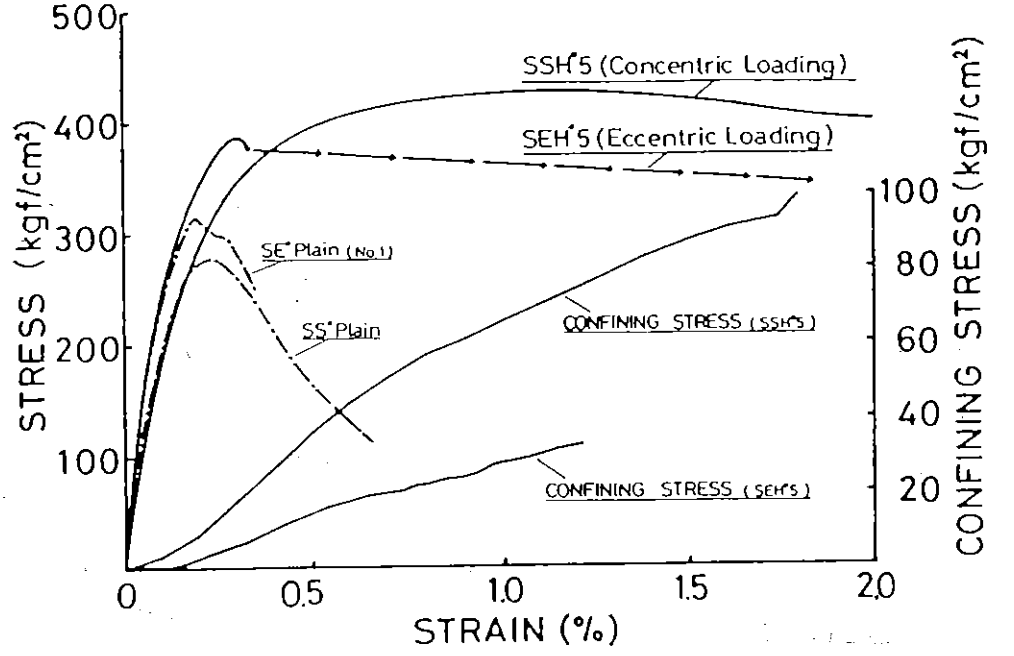

Fig. 2.37 Comparison of Stress-Strain Relations between Concentric and Eccentric Loading Tests [2.8].

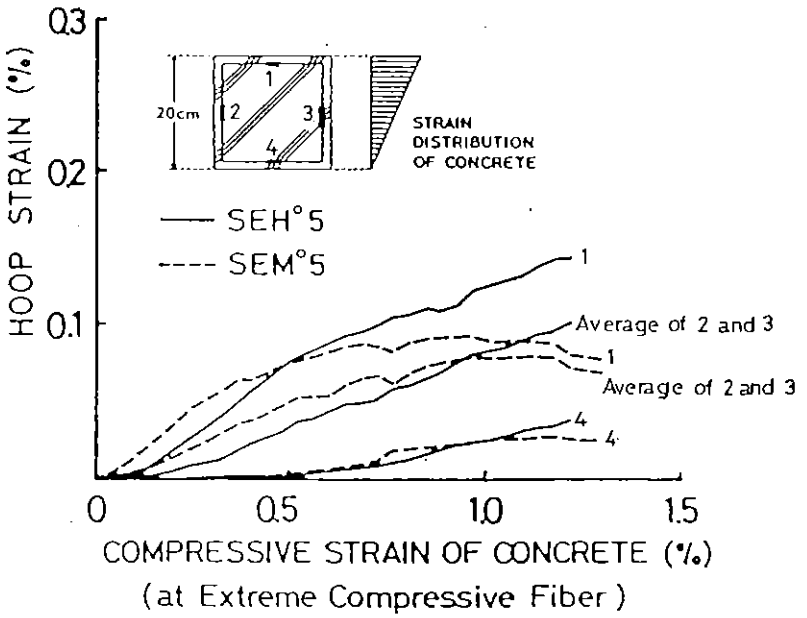

(a) Eccentric Loading Tests

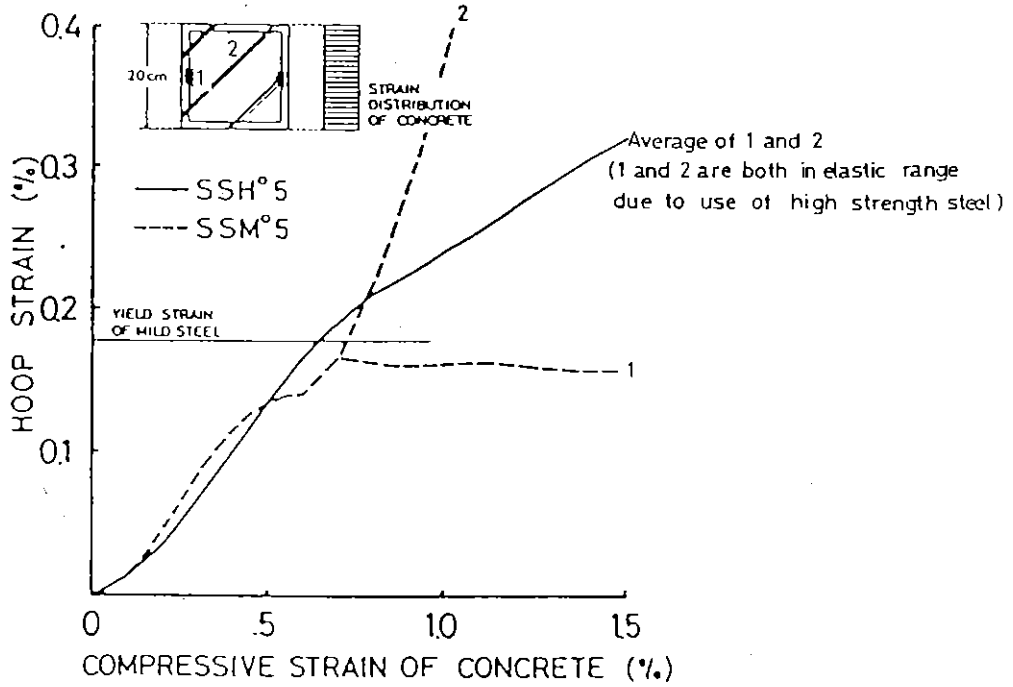

(b) Concentric Loading Tests

Fig. 2.38 Relations between Hoop Tension Strains and Compressive Strains of Concrete [2.8].

bars reached the yield strain from a compressive strain of concrete of about 0.6 %. The concrete strength and the concrete compressive strain at the maximum stress of the confined concrete measured in SSM°5 were, respectively, 1.08 and 1.91 times of those values obtained from the eccentrically loaded SEM°5 confined by the same spirals.
(5) In the case of SSH°5 with square spirals having a yield strength of 1274 MPa, which was tested under concentric load, the concrete strength and the concrete compressive strain at the maximum stress of the confined concrete were, respectively, 1.10 and 3.80 times of those values obtained from the eccentrically loaded SEH°5 confined by the same spirals.

It is notable that the seismic loading tests on rectangular columns confined by rectangular hoops with supplementary cross ties described in Sections 3 and 4 as well as in the reference [2.43, 2.44] have indicated that the axial tension yielding of those transverse reinforcement could occur only at large displacement ductility factors of six or more. From those facts including the above eccentric loading test results, it can be predicted that, when rectangular columns are subjected to bending, at a ductility displacement factor of less than six, the confining lateral pressure provided by the rectangular hoop reinforcement with or without supplementary cross ties will be considerably smaller than that estimated based on concentric loading tests. Hence, when the stress-strain models for confined concrete based on the concentric loading tests are applied to flexural analysis of columns, the strength and ductility enhancement of confined core concrete due to 'lateral pressure' provided by the transverse reinforcement may be overestimated. If those stress-strain models do not result in any overestimation of the strength and ductility increase for a member under flexure, the increase of strength and ductility of the confined concrete may need to be attributed not only to the lateral pressure provided by the transverse reinforcement but also to other factors such as the restraint against damage progress in extreme compression fibre region due to the flexural strain gradient in section, and due to the longitudinal stress gradient suggested by Uppal and Kemp [2.38]. As future research, the effects of those strain gradient and stress gradient on the stress-strain behaviour of the confined concrete must be quantitatively estimated.

2.3.3 Plain Concrete Strength

2.3.3.1 Previous Studies

(a) Strength Enhancement

Based on compression tests on cylinders under fluid lateral pressure, Richart et al [2.3] derived Eq. 2.1 to evaluate the strength increase of concrete due to lateral fluid pressure. Eq. 2.1 can be rewritten in the form of

$$\frac{f'_{cc}}{f'_{co}} = 1 + \alpha_s \frac{f_l}{f'_{co}} \qquad \text{.....} \qquad (2.1')$$

where f'_{cc} = axial compressive strength of confined specimen
f'_{co} = uniaxial compressive strength of unconfined specimen
f_l = confining fluid pressure
α_s = coefficient of strength increase due to lateral pressure
= 4.1 in tests by Richart et al

Eq. 2.1' indicates that a linear relationship exists between f'_{cc}/f'_{co} and f_l/f'_{co}. Values for the coefficient, α_s, vary between researchers [for example, 2.3, 2.4]. An expression like Eq. 2.1' may be traditionally accepted to represent the increase of material strengths tested under bi-axial or tri-axial compressive stress conditions, in order to avoid complications which may be induced from insignificant differences between the uniaxial strengths of materials used. However, when Eq. 2.1 is rearranged in the form of

$$(f'_{cc} - f'_{co}) = \alpha_s f_l \qquad \text{.....} \qquad (2.1")$$

it is obvious that Eq. 2.1 is valid only when the increase of concrete strength from plain concrete strength $(f'_{cc} - f'_{co})$ is independent of the plain concrete strength, f'_{co}.

It is notable that the relationships between $(f'_{cc} - f'_{co})$ and the equivalent fluid pressure, σ_l, proposed by Iyengar et al [2.15], by Watanabe et al [2.17], by Park et al [2.30] and by Sheikh and Uzumeri [2.13], which are expressed by Eqs. 2.15, 2.33, 2.50 and 2.56, respectively, can all be reduced to the same expression as Eq. 2.1". This may mean that, when the range of plain concrete strength is limited within about 20 to 40 MPa, as mostly used

in those studies, the influence of the uniaxial compressive strength of plain concrete on the strength enhancement due to confinement is small.

All the stress-strain models for confined concrete introduced in Section 2.2.3 assume that the enhancement of the ductility of confined concrete decreases as f'_{co} increases. For example, in the case of experimental studies by Iyengar et al [2.15], the ratio of $\varepsilon_{.85}$ to ε_{co} (where $\varepsilon_{.85}$ = strain at 0.85 of the peak stress of a confined concrete specimen in the descending portion of the stress-strain curve and ε_{co} = strain at the ultimate stress of a plain concrete specimen) has been expressed as the function of $\frac{1}{f'_{co}}$ (see Eq. 2.17), while in the case of the study by Sheikh and Uzumeri [2.13, 2.34] it is evaluated as the function of $\frac{1}{\sqrt{f'_{co}}}$ (see Eqs 2.57 and 2.58). Hence, it may be said that it has been assumed that the influence of the uniaxial compressive strength of plain concrete on the enhancement of the ductility of concrete due to confinement is more explicit than on the strength enhancement of concrete due to confinement.

2.3.3.2 Tests Conducted by Author et al.

The author et al [2.8, 2.36, 2.37, 2.46] have conducted axial loading tests on a number of spirally reinforced concrete cylinders, 150 mm diameter by 300 mm high, without concrete cover over several series. Some of those results were used to propose the stress-strain model for the spirally reinforced concrete described in Section 2.2.3. In order to investigate the influence of plain concrete strength on the increase in the strength and ductility of the confined concrete, the data obtained from 29 spirally reinforced concrete cylinders, where the plain concrete strength used was varied from 16.5 to 55.9 MPa, are selected here. The spacing of spirals with bar diameter of 5 to 6.4 mm was varied from 30 to 70 mm and the corresponding ratio of spiral volume to concrete core volume varied from 0.76 to 2.79 %. The yield strengths of spiral steel varied from 161 MPa to 1352 MPa.

(a) Strength Enhancement

In Fig. 2.39 (a), the increase of compressive strength of concrete due to lateral confinement (f'_{cc} - f'_{co}) is plotted against various compressive strength of plain concrete for when the ratio of spiral volume to the core

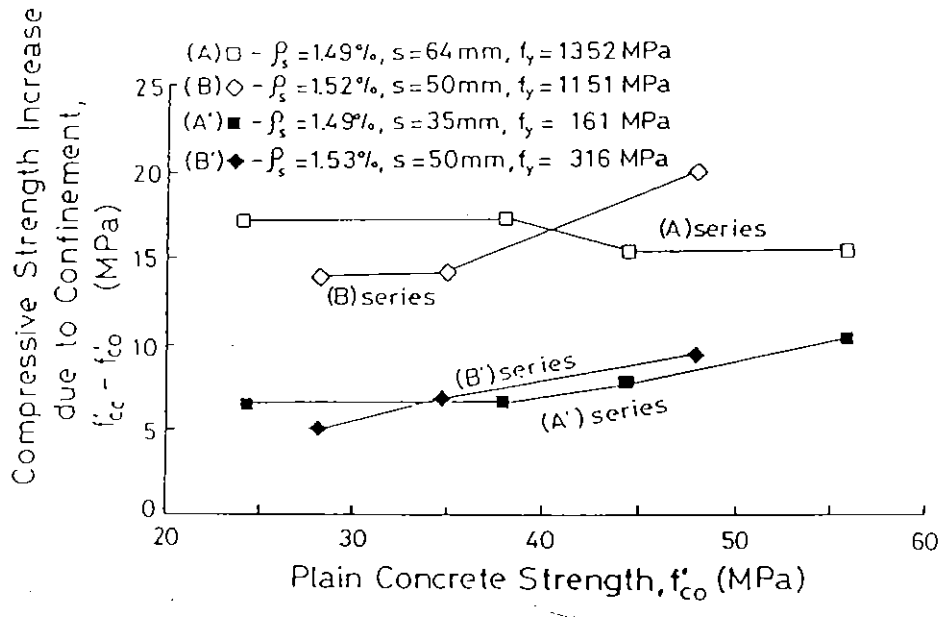

(a) Increase of Compressive Strength

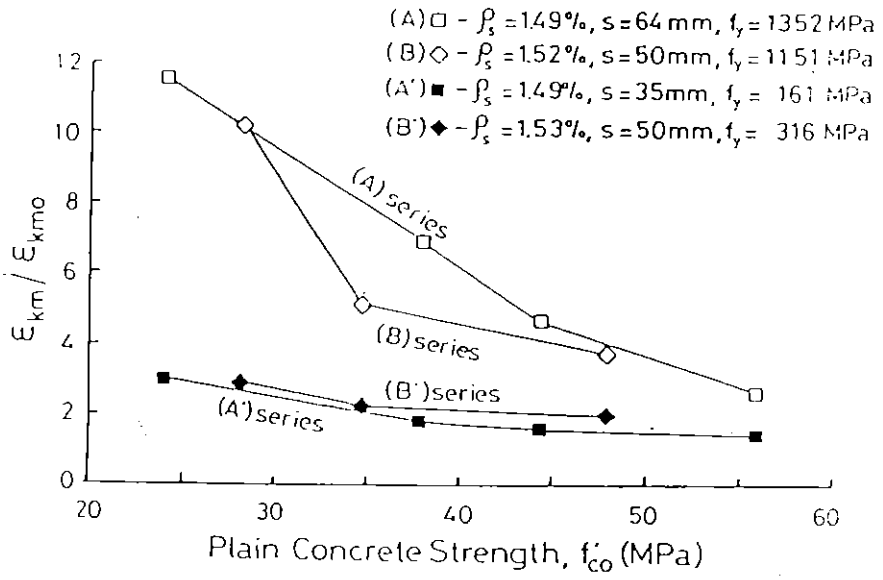

(b) Increase of Strain at the Maximum Value of $k_1 k_3$

Fig. 2.39 Influence of Compressive Strength of Plain Concrete on the Increase in the Strength and Ductility of Confined Concrete.

volume is about 1.5%. The compressive strength of confined concrete, f'_{cc}, is the strength calculated by dividing the maximum axial load by the core area measured to outside of spiral. Fig. 2.39 (a) indicates that the strength increase expressed by f'_{cc} minus f'_{co} is insensitive to the variation of the strength of plain concrete used when the lateral confining pressures provided by the spirals are the same. Hence, it can be said that the relation expressed in the form of Eq. 2.1", which neglects the influence of the compressive strength of plain concrete f'_{co} on the strength enhancement, is adeqaute up to f'_{co} of about 60 MPa.

For practical use, the strength increase of confined concrete is preferably expressed in the form of Eq. 2.1'. As mentioned later in Section 2.4, the failure modes observed in the above tests of the cylinders confined by ordinary strength spirals and high strength spirals were not the same, and hence the relationships between f'_{cc}/f'_{co} and σ_l/f'_{co} are separately plotted for the cases of ordinary strength spirals and high strength spirals in Fig. 2.40 (a) and (b), respectively, where σ_l is the equivalent fluid pressure expressed by Eq. 2.9. The (A), (B), (A') and (B') series shown in Fig. 2.40 correspond to those shown in Fig. 2.39. From the curves shown in Fig. 2.40, it may be said that the influence of the compressive strength of plain concrete on the relationships between f'_{cc}/f'_{co} and σ_l/f'_{co} is not explicit for test cylinders confined by ordinary strength spirals and high strength spirals. For example, the inclinations of the curves of the (A) and (A') series are opposite to those of the curves of (B) and (B') series with respect to the increase of the compressive strength of plain concrete.

In order to check whether peculiar points appear in the plots of (f'_{cc}/f'_{co}, σ_l/f'_{co}) due to the difference of the compressive strength of the plain concrete f'_{co}, all data from the tested cylinders with f'_{co} of from 16.5 to 55.9 MPa were plotted in Fig. 2.41 (a). In this figure, the confined concrete strength f'_{cc} was calculated as the maximum load divided by the critical section area between the spiral bars after spalling of ineffectively confined core area. This definition of f'_{cc} was used in Fig. 2.4 in order to compare the present data with the data obtained by Richart et al [2.3] and Balmer [2.4] from fluid pressure tests where ineffectively confined core is non-existent. The detail of the calculation for the critical section area confined by spirals is described in Section 2.4.4. It is emphasized that any peculiar points due to the difference of the compressive strength of the plain concrete was not

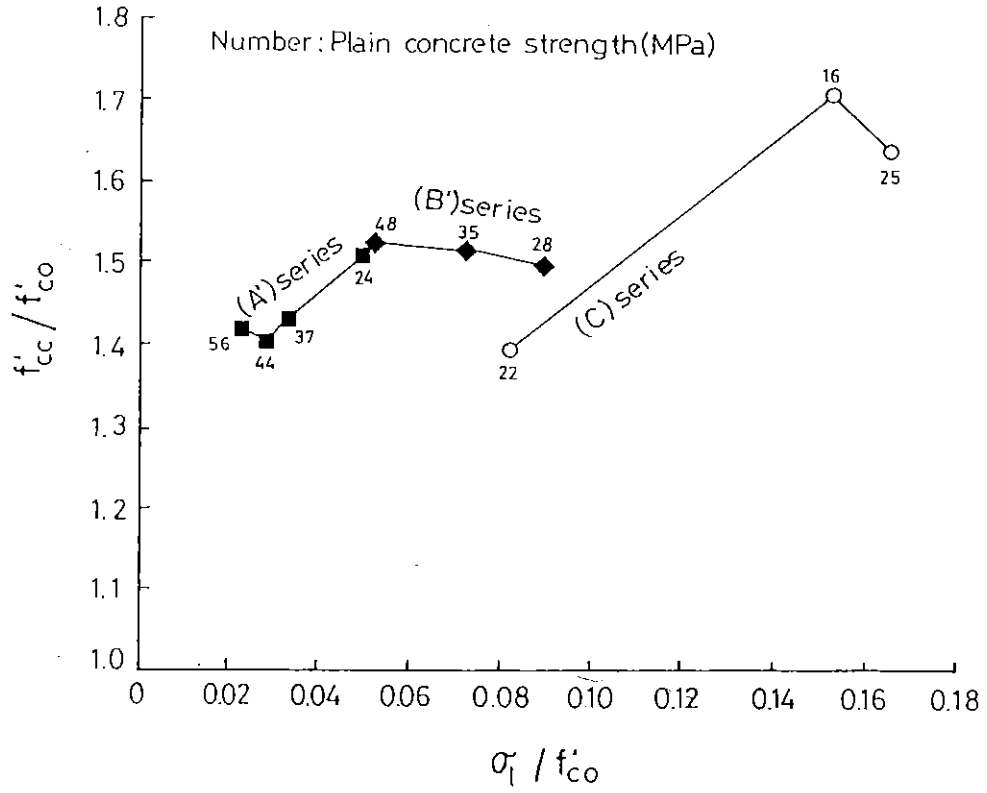

(a) Ordinary Strength Spirals

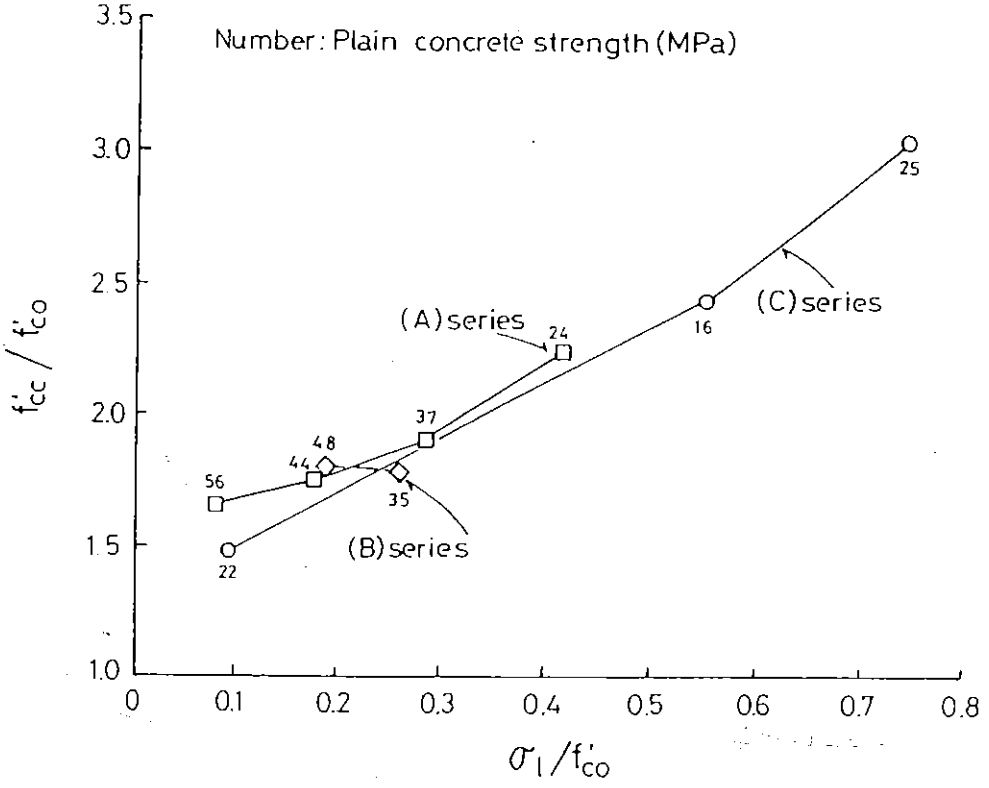

(b) High Strength Spirals

Fig. 2.40 Influence of Compressive Strength of Plain Concrete on the Relation between (f'_{cc} / f'_{co}) and (f'_l / f'_{co}).

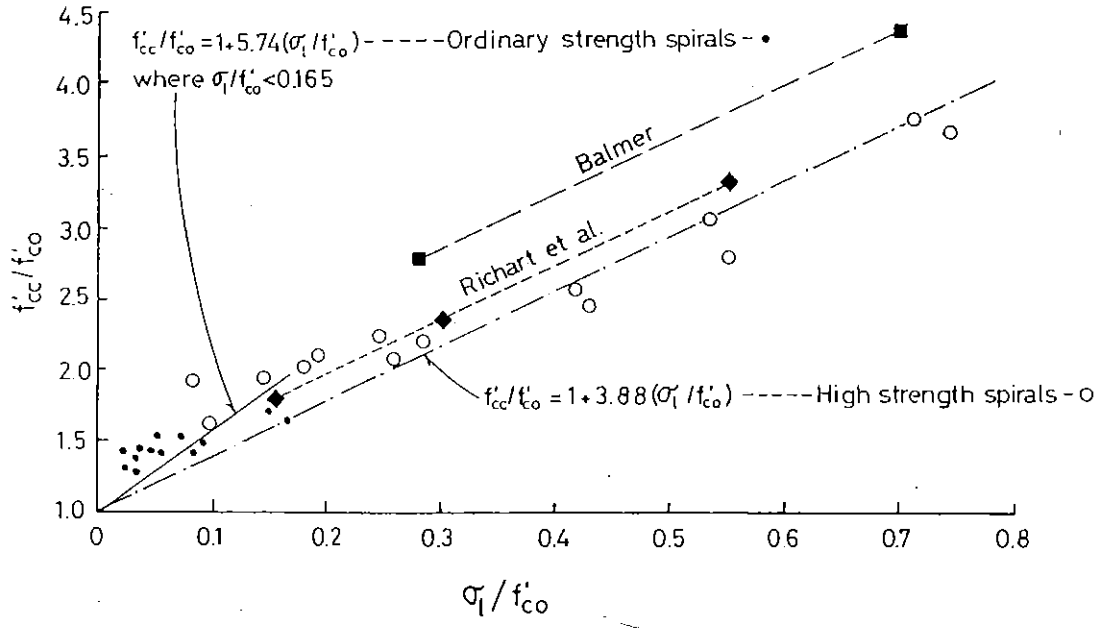

(a) Comparison with Fluid Pressure Tests by Richart et al [2.3] and Balmer [2.4]

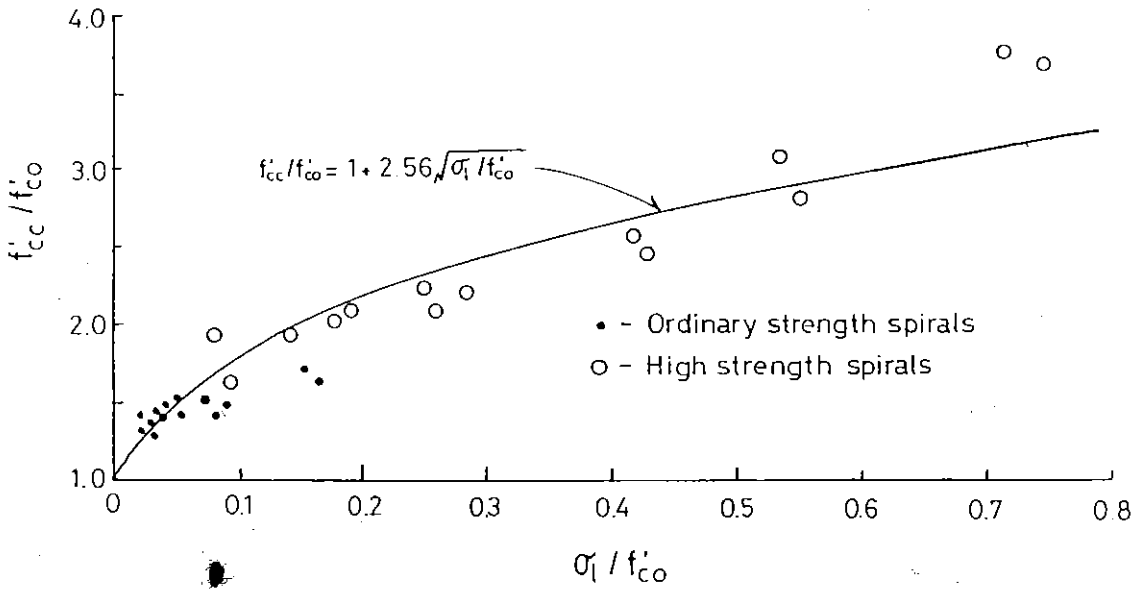

(b) Curve Fitting to All Tested Data

Fig. 2.41 Relationships between (s_l / f'_{co}) and (f'_{cc} / f'_{co}).

recognized while plotting the data. From those results, it may be concluded that the influence of the plain concrete strength, f'_{co}, is not significant when evaluating the increase of the compressive strength of concrete due to confinement for f'_{co} of up to about 60 MPa. Hence the increase of compressive strength of confined concrete can be evaluated using an expression such as Eq. 2.1' or Eq. 2.1".

A regression analysis was conducted using the above test data to express the relationships between f'_{cc}/f'_{co} and σ_l/f'_{co}. When the least square method is applied to the data from the cylinders confined by ordinary strength spirals (the yield strength of which was from 161 to 316 MPa), the best fitting linear curve was found to be

$$\frac{f'_{cc}}{f'_{co}} = 1 + 5.74 \frac{\sigma_l}{f'_{co}} \qquad \text{.....} \qquad (2.75)$$

where $\frac{\sigma_l}{f'_{co}} \leq 0.165$

It may be notable that this estimated value of 5.74 for α_s in Eq. 2.1' is close to that estimated by Mander et al [2.6]. Mander et al suggested using, for practical design, α_s = 5.5 based on the axial load tests on circular columns confined by ordinary strength spirals, where the estimated values of α_s varied from 5.3 to 6.5 for the range of f'_l/f'_{co} (where f'_l is the equivalent fluid pressure expressed by Eq. 2.41) of up to about 0.15.

For the data from the cylinders confined by high strength spirals (the yield strength of which was from 1151 to 1352 MPa), the best fitting linear curve was found to be

$$\frac{f'_{cc}}{f'_{co}} = 1 + 3.88 \frac{\sigma_l}{f'_{co}} \qquad \text{.....} \qquad (2.76)$$

The spiral tension stress which is used to calculate σ_l was estimated from the tension strains measured in the spiral bars when the spirals did not yield. The value of α_s estimated from the tests on the cylinders confined by high strength spirals is smaller than that estimated by Richart et al and by Balmer based on the tests on cylinders confined by fluid pressure. To explain this difference, the following three reasons may be considered.

Firstly, in the case of the cylinders confined by high strength spirals, due to passive confinement the lateral pressure σ_l is gradually increased as the damage of the concrete core progresses, while in the case of the tests by Richart et al [2.3] or Balmer [2.4] constant lateral fluid pressure was applied from the beginning to the end of the tests. This may mean that the damage progress in the concrete core is quicker in the former than in the latter and hence the attained maximum stress might become lower in the former. It may be notable that the strains at the peak stresses of core concrete confined by high strength spirals were from about 1 % to 2.6 % in the above tests. Secondly, in the case of the cylinders confined by high strength spirals, bearing failure of the core concrete may have occurred beneath the spiral bars due to high local pressure, before reaching the maximum load carrying capacity of the core concrete, as mentioned in Section 2.4.3. Thirdly, the effectively confined core area at the critical section used to calculate the confined concrete strength f'_{cc} may be overestimated, although it was estimated from the observed spalling angles of the core concrete (see Section 2.4.4). It may be possible that the minimum section area of the confined core where the magnitude of the lateral pressure can actually reach the equivalent fluid pressure expressed by Eq. 2.9 is significantly less than the critical section area estimated from the observed spalling angles of the core concrete.

When the least square method is applied to the all test data, the best fitting parabolic curve obtained is shown in Fig. 2.41 (b). The curve is expressed as

$$\frac{f'_{cc}}{f'_{co}} = 1 + 2.56 \sqrt{\frac{\sigma_l}{f'_{co}}} \qquad \text{.....} \qquad (2.77)$$

(b) Ductility Enhancement

In Fig. 2.39 (b), to indicate the influence of the compressive strength of plain concrete on the increase of ductility due to confinement, the ratios of ε_{km} to ε_{kmo} are plotted against the plain concrete strength f'_{co}. These ε_{km} and ε_{kmo} values are the same as the available limits of compressive strains of concrete for flexural members, ε_{cu} and ε_{cuo}, respectively, which were defined in the stress-strain model proposed by Watanabe et al [2.17] (see Section 2.2.3). That is, ε_{km} and ε_{kmo} are the axial compressive strains of the

confined concrete and plain concrete at which the average stress in the stress-strain curve of each concrete becomes maximum, respectively. Fig. 2.39 (b) indicates that the ratio of ε_{km} to ε_{kmo}, which expresses the enhancement in ductility of concrete due to confinement, becomes smaller almost linearly as the uniaxial compressive strength of plain concrete increases.

The above mentioned tendency can also be seen from Fig. 2.42, which indicates the relationships between ε_{km} and the ratio of spiral volume to concrete core volume ρ_s. From regression analyses, for the same compressive strength of plain concrete f'_c = 30.8 MPa, the best fitting curves and are expressed by

for 5 mm dia. spirals having a yield strength of 161 MPa,

$$\varepsilon_{km} = 0.538\ \rho_s + 0.110 \quad \text{.....} \quad (2.78)$$

and 6.4 mm dia. spirals having a yield strength of 1352 MPa,

$$\varepsilon_{km} = 1.69\ \rho_s + 0.230 \quad \text{.....} \quad (2.79)$$

When the data from cylinders with f'_c of from 26.2 to 61.3 MPa are also plotted in Fig. 2.42 using diamonds with short solid lines for 5 mm dia. spirals with yield strength of 161 MPa and circles with short dashed lines for 6.4 mm dia. spirals with yield strength of 1352 MPa, those plotted points obviously deviate from the corresponding line expressed by Eq. 2.78 or Eq. 2.79. Thus it is confirmed that ε_{km} becomes smaller as f'_c increases when the same spirals are used as lateral confinement.

In the following section, the influence of compressive strength of plain concrete on the ductile behaviour of the confined concrete is further discussed based on the seismic loading tests on columns with high strength concrete conducted by Muguruma, Watanabe and Komuro [2.47].

2.3.3.3 Tests Conducted by Muguruma et al.

Muguruma, Watanabe and Komuro [2.47] have conducted seismic loading tests on eight columns using high strength concrete. Those

columns had 200 mm square sections and were confined by overlapping hoops as shown in Fig. 2.43. The aspect ratio of the columns (= shear span length / full column depth) was 2.5. The compressive strengths of plain concrete obtained from 10 cm diameter by 20 cm high cylinders were 86 MPa (= 874 kgf/ cm^2) and 116 MPa (= 1181 kgf/ cm^2). Other details of the tested columns are listed in Table 2.2.

Two typical skeleton curves obtained from the measured cyclic moment-curvature relationships for the columns are shown in Fig. 2.44.

In the figure, theoretical moment-curvature curves for monotonic loading, calculated using the modified Kent and Park stress-strain model [2.30] and Watanabe et al model [2.17] for confined concrete, are also plotted. As can be seen from those figures, when high strength concrete is used, the theoretical moment-curvature curves calculated using the modified Kent and Park model for the confined concrete estimates the slope of the falling branch to be more gradual than the measured slope, while those calculated using the Watanabe et al model are steeper than the measured slope. Hence, those models, which were calibrated mainly for the plain concrete strength of up to about 40 MPa, need to be modified to analyse the behaviour of columns when high strength concrete of more than 80 MPa is used.

In the modified Kent and Park model for the confined concrete, tan θ shown in Fig. 2.45 was expressed as

$$\tan \theta = K f'_c Z_m \quad \text{.....} \quad (2.80)$$

where K and Z_m are expressed by Eqs. 2.51 and 2.52, respectively

For this equation, in the study by Muguruma et al [2.47], an additional modification factor β for the modified Kent and Park model was introduced in order to fix the theoretically calculated slope of the falling branch to the measured slope (see Fig. 2.45).

$$\tan \theta' = \beta K f'_c Z_m \quad \text{.....} \quad (2.81)$$

For the eight tested columns, the values of β required to fix the theoretically calculated slope of the falling branch to the measured slope are plotted

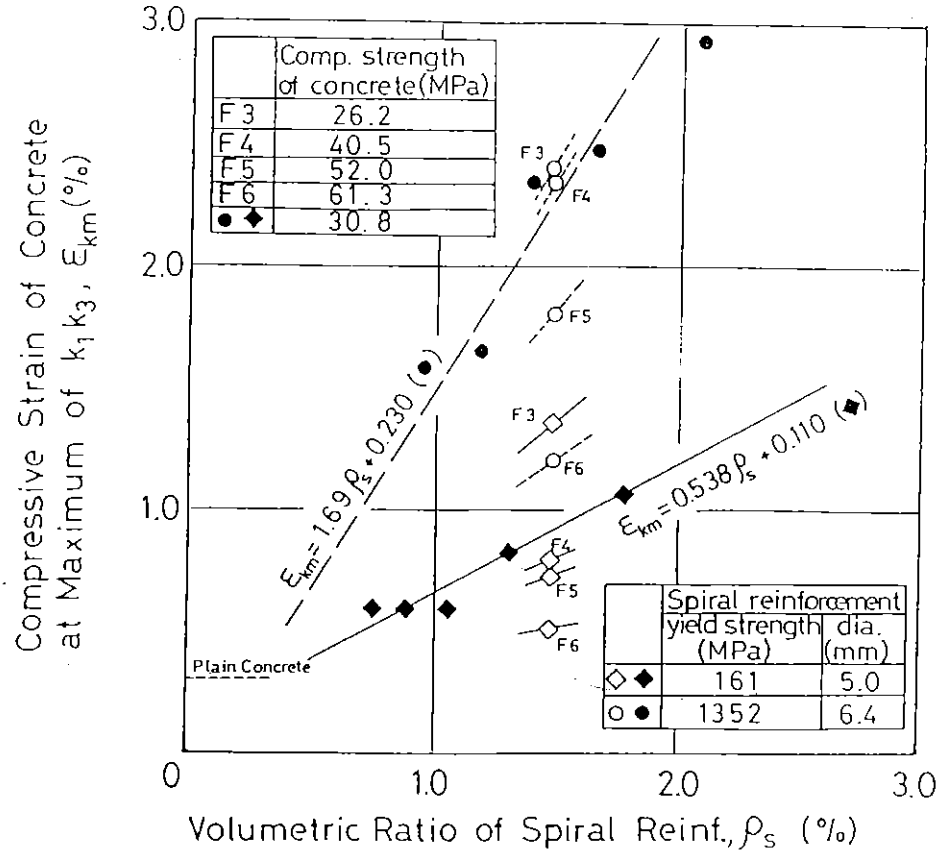

Fig. 2.42 The Influence of the Compressive Strength of Plain Concrete on the Ductile Behaviour of Concrete Confined by Spirals [2.8].

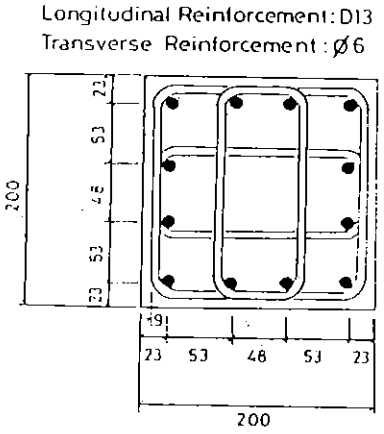

Fig. 2.43 Section of Columns with High Strength Concrete Tested by Muguruma et al [2.47].

Table 2.2 Test Column with High Strength Concrete [2.47]

Test Column	f'_c (MPa)	f_{yh} (MPa)	$P_e / f'_c A_g$	ρ_t (%)	ρ_s (%)
BL-1	116	329	0.254	3.81	4.12
BH-1		792	0.254		
BL-2		329	0.423		
BH-2		792	0.423		
AL-1	86	329	0.400	3.81	4.12
AH-1		792	0.400		
AL-2		329	0.629		
AH-2		792	0.629		

Note: f'_c = compressive strength of plain concrete measured by 10 cm dia. x 20 cm high cylinders
f_{yh} = yield strength of transverse reinforcement
$P_e / f'_c A_g$ = axial load level
ρ_t = ratio of sectional area of longitudinal reinforcement to gross column section
ρ_s = ratio of volume of transverse reinforcement to volume of concrete core

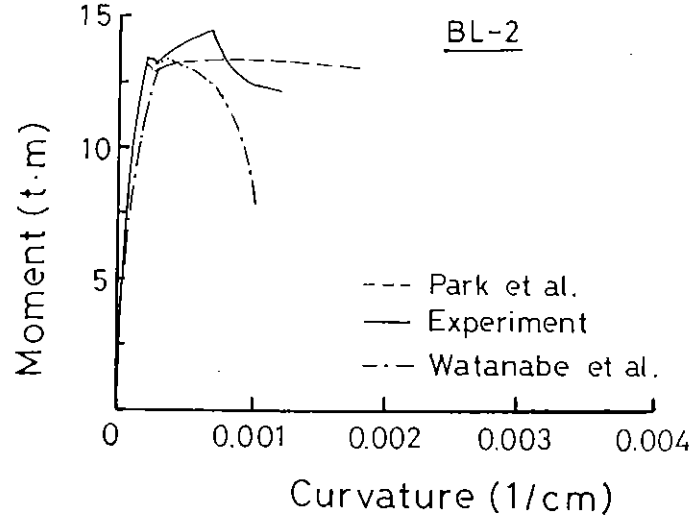

(a) BL-2 Column

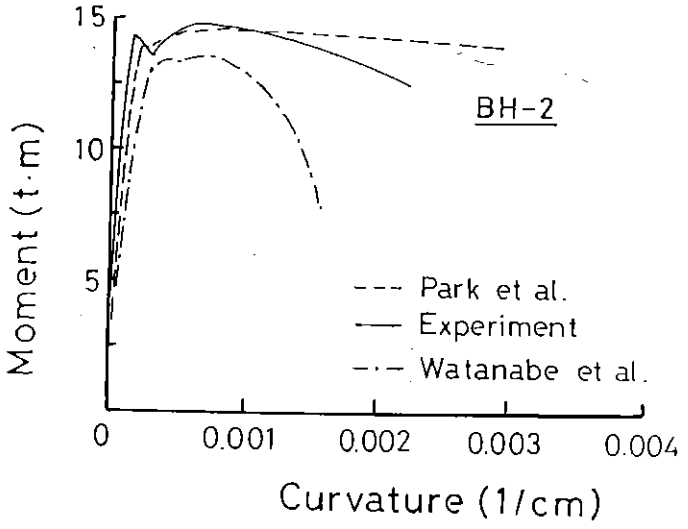

(b) BH-2 Column

Fig. 2.44 Measured Moment-Curvature Relationships for Columns with High Strength Concrete [2.47].

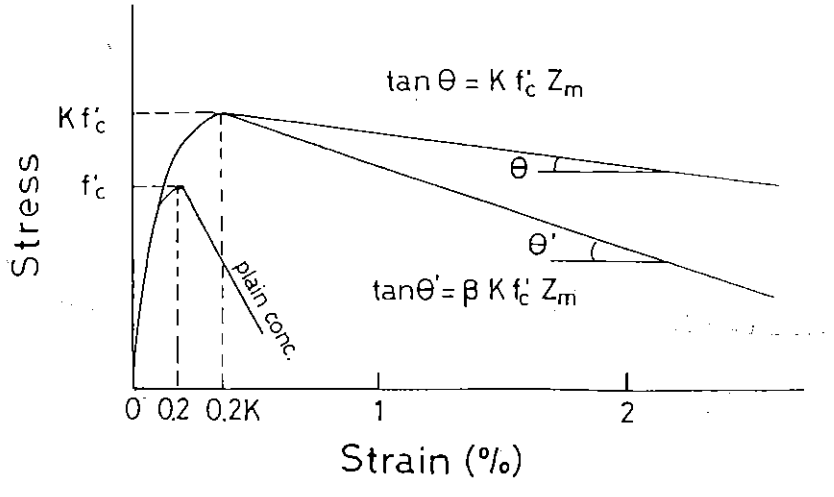

Fig. 2.45 Modification of the Modified Kent and Park Stress-Strain Model for Confined Concrete [2.47]

against f'_c in Fig. 2.46. It is inadequate to directly multiply β into Z_m if β expresses only the effect of the compressive strength of plain concrete f'_c, because Z_m involves not only the effect of plain concrete strength but also the properties of the transverse reinforcement as can be seen from Eq. 2.52. However, Fig. 2.46 is explicitly indicating that, when high strength concrete of more than 80 MPa is used, the ductility enhancement of due to confinement becomes significantly smaller than the estimate based on the Modified Kent and Park Model [2.30] which were calibrated for the concrete strength of up to 40 MPa.

2.3.4 Confining Effects of Longitudinal Reinforcement

2.3.4.1 In the Case of Longitudinal Reinforcement with Circular Hoops or Spirals

For a column with circular section with circular hoops or spirals, NZS 3101 [2.11] specifies that the minimum number of longitudinal reinforcing bars shall be six and that those longitudinal bars shall not be spaced further apart between centres than 200 mm. In practice, generally a greater number of longitudinal reinforcing bars than six are evenly spaced around the circular hoops or spirals especially when the diameter of column is large. In this case, additional confining effect by longitudinal reinforcement may be appreciable.

Based on the axial loading tests on 15 realistically sized concrete columns containing spirals and longitudinal reinforcement, Mander et al [2.6] concluded that an increase in the number of longitudinal reinforcing bars, while maintaining a constant volume of longitudinal steel by the use of smaller diameter bars, made little difference to the efficiency of the concrete confinement. This will mean that the effectiveness of confinement by longitudinal reinforcement is much smaller than that by circular hoops or spirals and hence cannot appear explicitly. This may be attributed to the following two reasons. Firstly, the confining efficiency of longitudinal reinforcement will be rapidly lost from a comparatively small compressive strain of concrete about 0.2 %, due to axial compressive yielding of that steel, because the bending stiffness of the longitudinal reinforcement which determines the degree of confinement is rapidly decreased after axial compressive yielding commences. Secondly, while the bending stiffness of

longitudinal reinforcement is maintained at comparatively small axial compressive strains of less than about 0.2%, the confining effects of the longitudinal reinforcement as well as of lateral reinforcement will be insignificant due to small lateral concrete strains. However, as mentioned using Fig. 2.21 in Section 2.2.3.1, the strength enhancement due to confinement estimated by the Mander et al stress-strain model, which was calibrated using results from spirally reinforced columns with longitudinal reinforcement, was from 1% to 8% higher than estimated by the models based on spirally reinforced concrete cylinders without longitudinal reinforcement. Hence, the strength enhancement due to the presence of longitudinal reinforcement may be appreciable.

2.3.4.2 In the Case of Longitudinal Reinforcement with Rectangular Hoops

The effects of longitudinal reinforcement on concrete confined by rectangular hoops has been investigated in the following experimental studies.

Scott, Park and Priestley [2.29] have tested 22 columns, each having 450 mm square section and containing longitudinal and transverse reinforcement. Fig. 2.47 shows measured stress-strain curves for the core concrete of the 8- and 12- longitudinal bar units with similar amounts of longitudinal steel and various amounts of transverse steel loaded concentrically at the strain rate of 0.0167 per second. In each case the stress-strain curve for the 12-bar unit lies above the curve for the comparable 8-bar unit. Based on this observation, Scott et al concluded that the concrete confinement was improved when a large number of smaller diameter longitudinal bars is used to make up the required area of longitudinal reinforcement. However, the improvement of the concrete confinement cannot simply be attributed to the increased number of longitudinal reinforcement bars for the following reason. As represented in Fig. 2.26, Sheikh et al [2.13] have suggested that the effectively confined concrete area at a critical section varies according to the type of configuration of lateral reinforcement. The 8- and 12- bar columns in Fig. 2.47 correspond to A and D types in Fig. 2.26, respectively. From Fig. 2.26, the ratio of the effectively confined conrete area of 8-bar column to 12-bar column is about 0.85. Therefore, the improvement of the concrete confinement which appeared in 12-bar columns in comparison with 8-bar columns may be attributed to

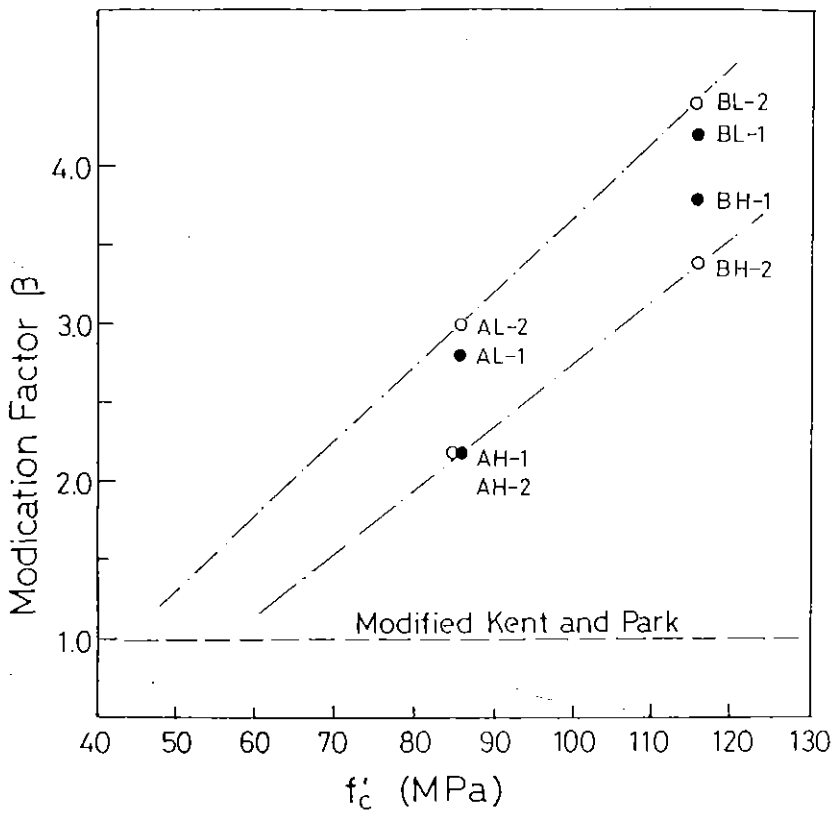

Fig. 2.46 Relationship between f'_c and β [2.47].

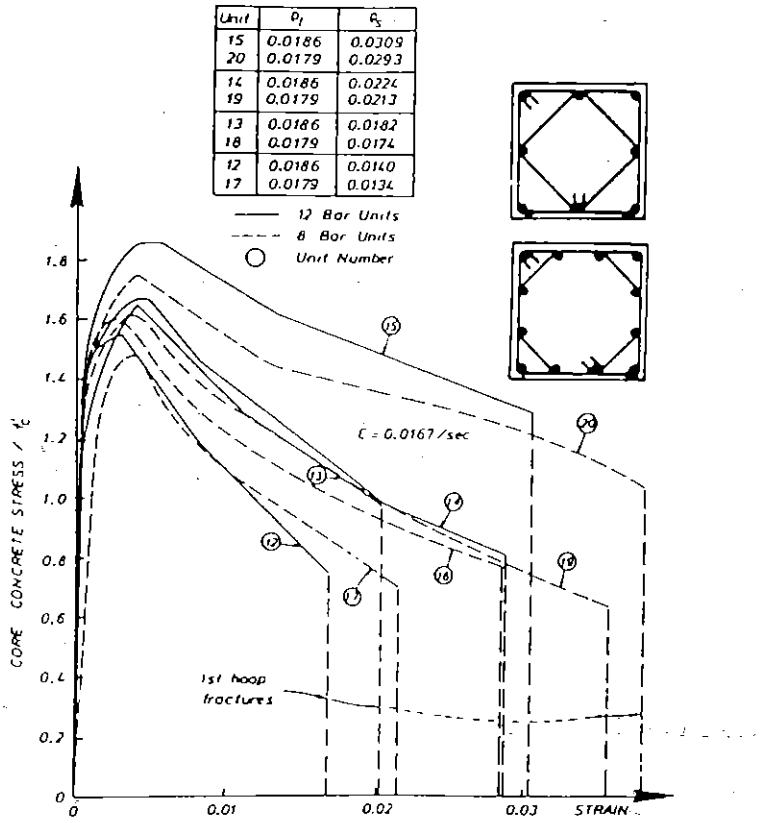

Fig. 2.47 Stress-Strain Curves for Concrete Core of 8- and 12- Bar Columns with Different Transverse Hoops Loaded Concentrically at the High Strain Rate [2.29].

the increase of the effectively confined concrete area due to the configuration of lateral reinforcement resulting from the increased number of longitudinal reinforcement bars. If in this study the columns having sections shown in Fig. 2.48 instead of those in Fig. 2.47 were tested for comparison, the effect of the longitudinal reinforcement might become more clear.

Roy and Sozen [2.10] have conducted axial load tests on 60 concrete prisms of size 5 x 5 x 25 in (127 x 127 x 635 mm) concrete prisms confined by square hoops. Four corner longitudinal bars were provided in some of those prisms in order to investigate the influence of longitudinal reinforcement on the lateral confinement. In this study, it was concluded that there was no consistent effect of longitudinal reinforcement on the strength and ductility of the confined concrete. On the contrary, based on similar axial compression tests on 3 x 3 in (76 x 76 mm) prisms and 4.25 x 4.25 in (108 x 108 mm) prisms Bertero and Felippa [2.9] have indicated that the improvement of ductility of the confined concrete due to the presence of four corner bars was noticeable in the case that premature buckling of the longitudinal bars was avoided by closely spaced ties (see Fig. 2.49).

From the above studies, it cannot be definitely stated that the presence of longitudinal reinforcement appreciably improve the confinement of the core concrete. To improve the strength and ductility of concrete by lateral confinement, the reduction of the ineffectively confined concrete area by adding supplementary cross ties or overlapping hoops as shown in Fig. 2.27 is more significant than the increase of the number of longitudinal bars. However, the presence of this additional lateral reinforcement requires the presence of longitudinal bars to link. As mentioned in the previous section, the confining effects by longitudinal reinforcement will be rapidly lost at a comparatively small compressive strain of concrete about 0.2 % due to its axial compressive yielding, because the bending stiffness of the longitudinal reinforcement which determines the degree of confinement is rapidly decreased after its axial compressive yielding. Moreover, while a comparatively high bending stiffness of longitudinal reinforcement is maintained under axial compressive strains less than about 0.2%, the confining effects of the longitudinal reinforcement as well as of lateral reinforcement may be insignificant at that low strain level since the confinement is passive.

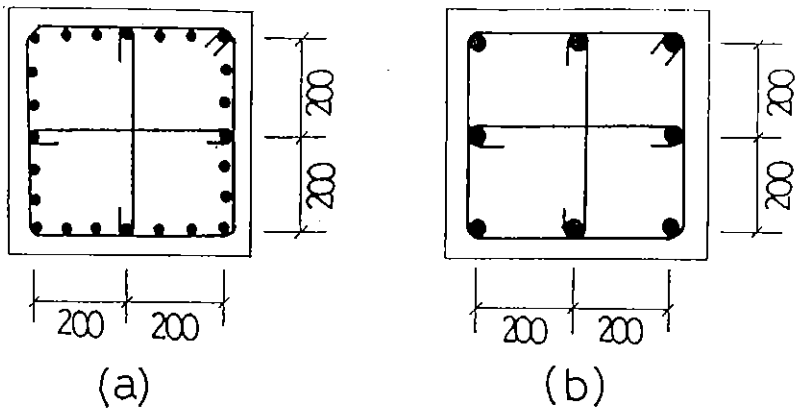

Fig. 2.48 Column Sections Confined by Rectangular Hoops with Supplementary Cross Ties.

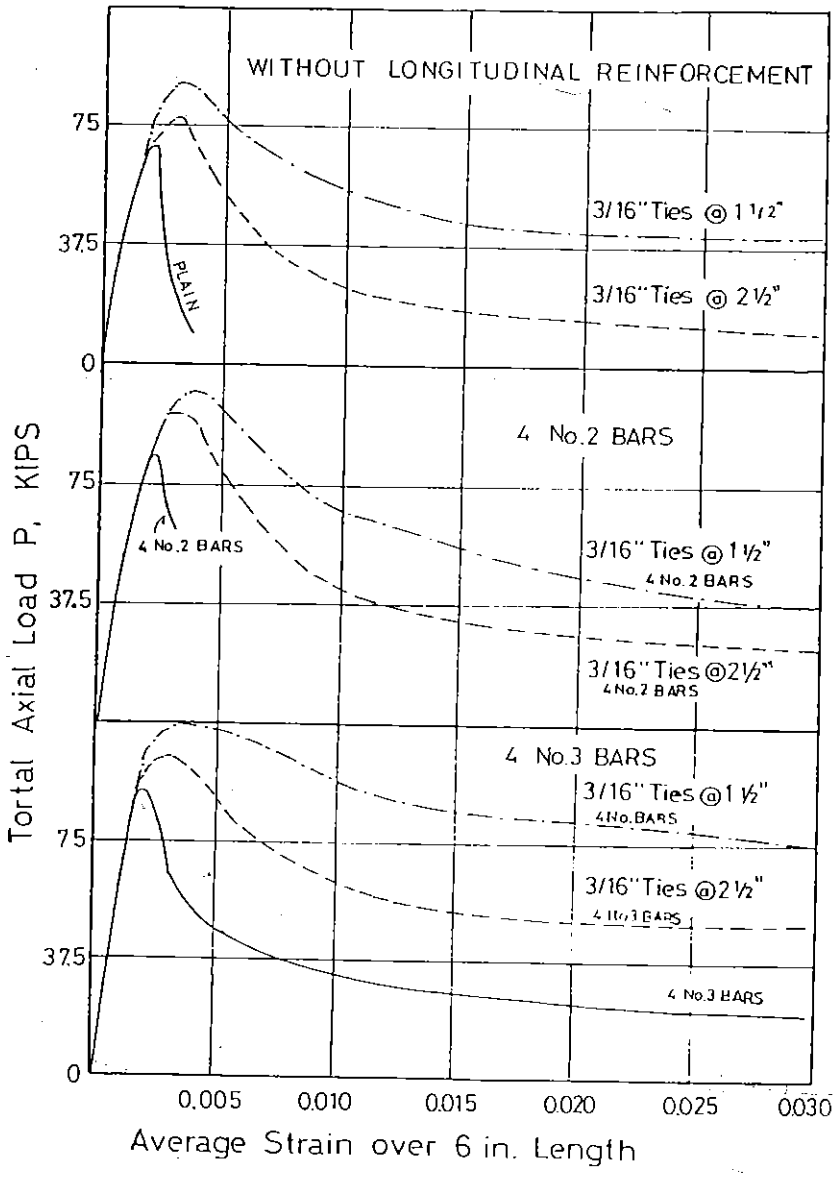

Fig. 2.49 Axial Load-Deformation Curves for 3 x 3 in (76 x 76 mm) Prisms [2.9].

2.4 FAILURE MECHANISM OF CONCRETE CONFINED BY HIGH STRENGTH SPIRALS

2.4.1 Comparison of Failure Modes of Concrete Confined by High Strength Spirals with those by Ordinary Strength Steel Spirals

The difference of the failure modes between concrete cylinders confined by high strength steel spirals and those confined by low strength steel spirals will be considered using the following tests by the author et al [2.8, 2.19]. The tests were conducted on 150 mm diameter by 300 mm high spirally reinforced concrete cylinders without concrete cover and without longitudinal reinforcement. The test specimens are listed with properties of spiral reinforcement in Table 2.3. The uniaxial compressive strength of concrete obtained from 100 mm diameter by 200 mm high cylinders was 30.8 MPa at the test age, while that obtained from 150 mm diameter by 300 mm high concrete cylinders was 27.7 MPa. The loading arrangements and the measuring devices are shown in Fig. 2.50. The axial compressive strain of the cylinders was measured using a pair of linear transformers with gauge length of 250 mm. The spiral strain was mesured using electrical wire strain gauges with gauge length of 2 mm.

The measured stress-strain curves of the confined concrete has already been shown in Fig. 2.3 and the corresponding spiral strains are shown in Fig. 2.51. The test results are also listed in Table 2.4. From Fig. 2.51 (a), it is obvious that the enhancement of the strength and the ductility of concrete due to confinement by high strength steel spirals is remarkably higher than that by low strength steel spirals. This is because the maximum lateral confining pressure in the former is much higher than that in the latter, mainly due to the difference of the yield strength of spirals.

The damage of those spirally reinforced cylinders after testing is shown in Figs. 2.52 to 2.56. Typical failure modes of cylinders with high strength steel spirals and with low strength steel spirals are schematically shown in Fig. 2.57 (a) and (b), respectively. The observed failure conditions of the cylinders with high strength steel spirals and with low strength steel spirals are described as follows;

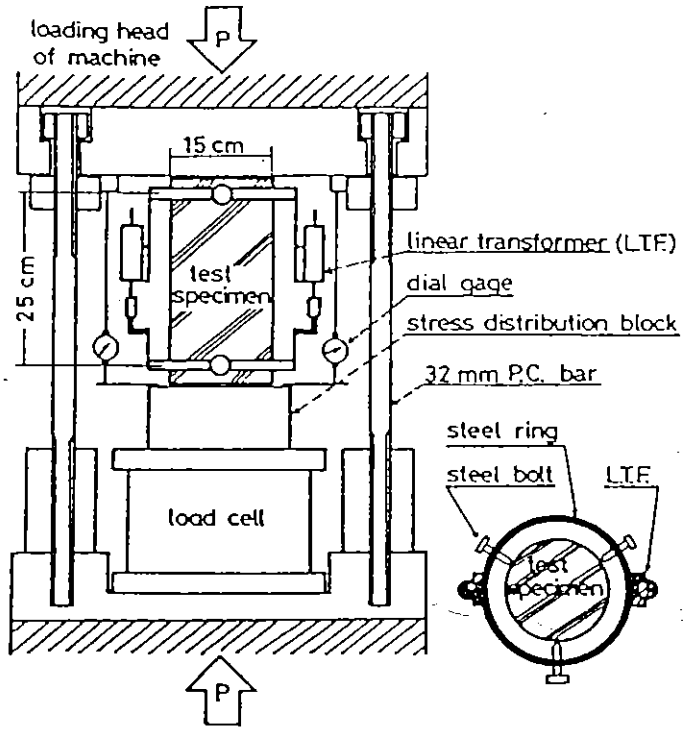

Fig. 2.50 Loading Arrangements and Measuring Devices for Spirally Reinforced Test Cylinders.

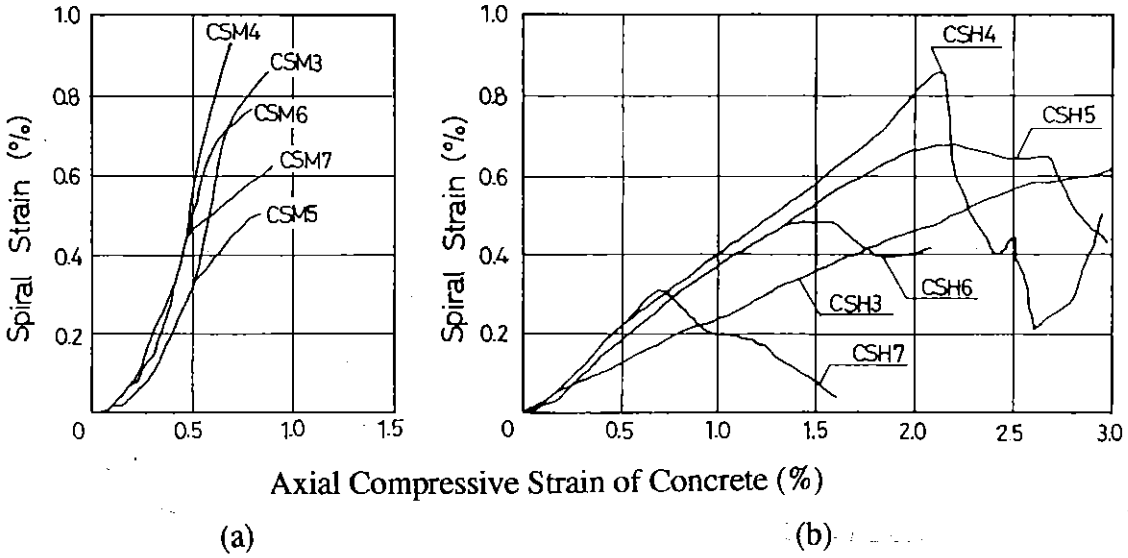

Fig. 2.51 Measured Spiral Strains versus Axial Compressive Strain of Concrete [2.19].

Table 2.3 Test Cylinders with Spiral Reinforcement

Test specimen	Spiral reinforcement			
	bar dia-meter (mm)	pitch (mm)	ratio of spiral volume to core volume (%)	yield strength (MPa)
CSM3	5.0	30	1.78	161
CSM4	5.0	40	1.33	161
CSM5	5.0	50	1.07	161
CSM6	5.0	60	0.89	161
CSM7	5.0	70	0.76	161
CSH3	6.4	30	2.79	1352
CSH4	6.4	40	1.67	1352
CSH6	6.4	60	1.40	1352
CSH7	6.4	70	1.20	1352
CS plain	-	-	-	

Table 2.4 Results from Test Cylinders with Spiral Reinforcement

Test specimen	Measured values at peak load			Axial comp-ressive strain of concrete at spiral yielding (%)
	axial comp-ressive stress of concrete (MPa)	axial comp-ressive strain of concrete (%)	spiral strain (%)	
CSM3	33.6	0.450	0.254	0.24
CSM4	33.1	0.340	0.209	0.22
CSM5	31.0	0.275	0.082	0.28
CSM6	27.6	0.275	0.102	0.25
CSM7	27.4	0.283	0.171	0.19
CSH3	72.2	2.580	0.576	2.60
CSH4	55.7	2.400	0.391	1.65
CSH5	46.2	1.900	0.640	1.80
CSH6	40.8	1.850	0.396	non-yielding
CSH7	35.3	1.000	0.206	non-yielding
CS plain	27.7	0.170		

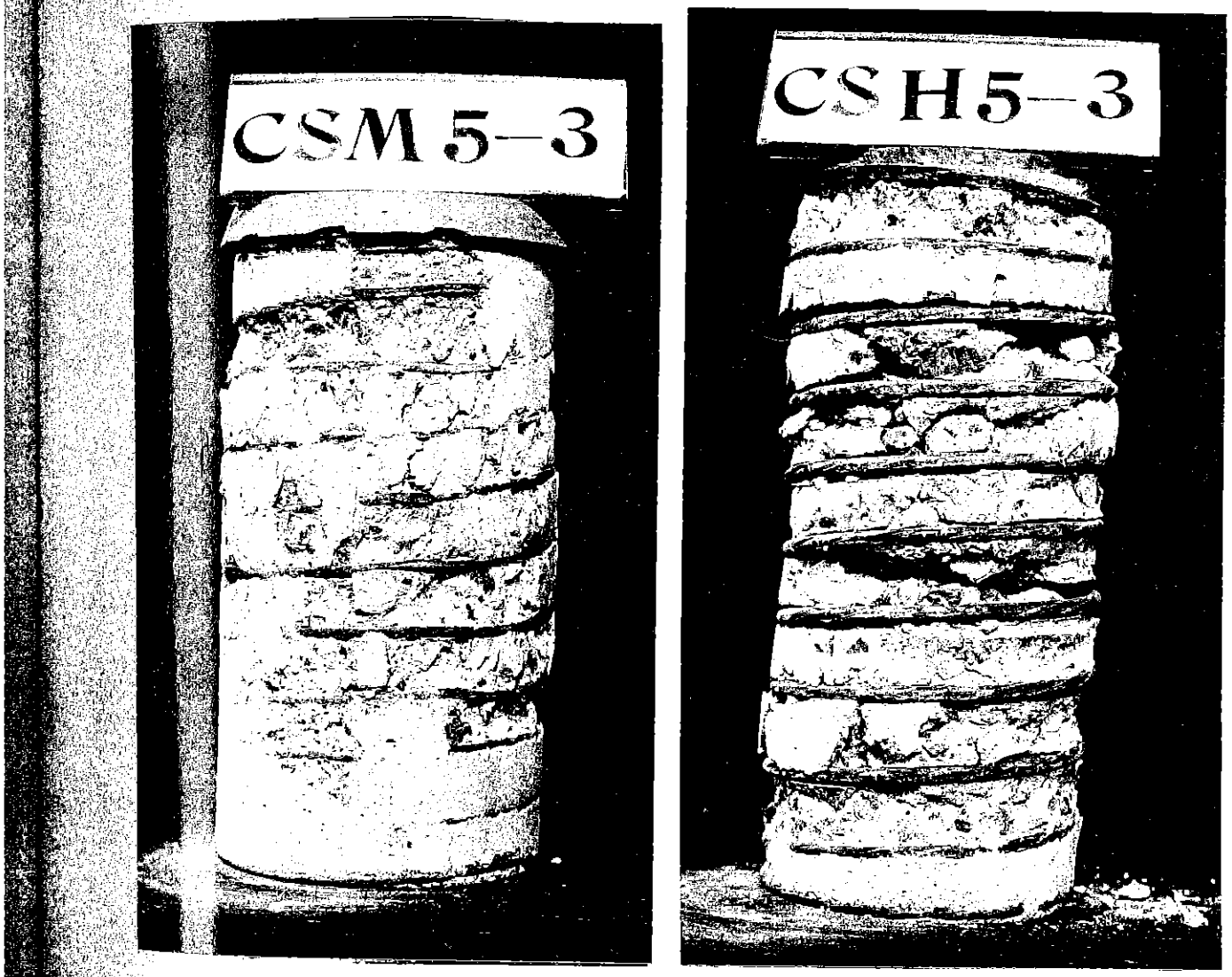

Fig. 2.52 CSM 5-3 and CSH 5-3 after Testing.

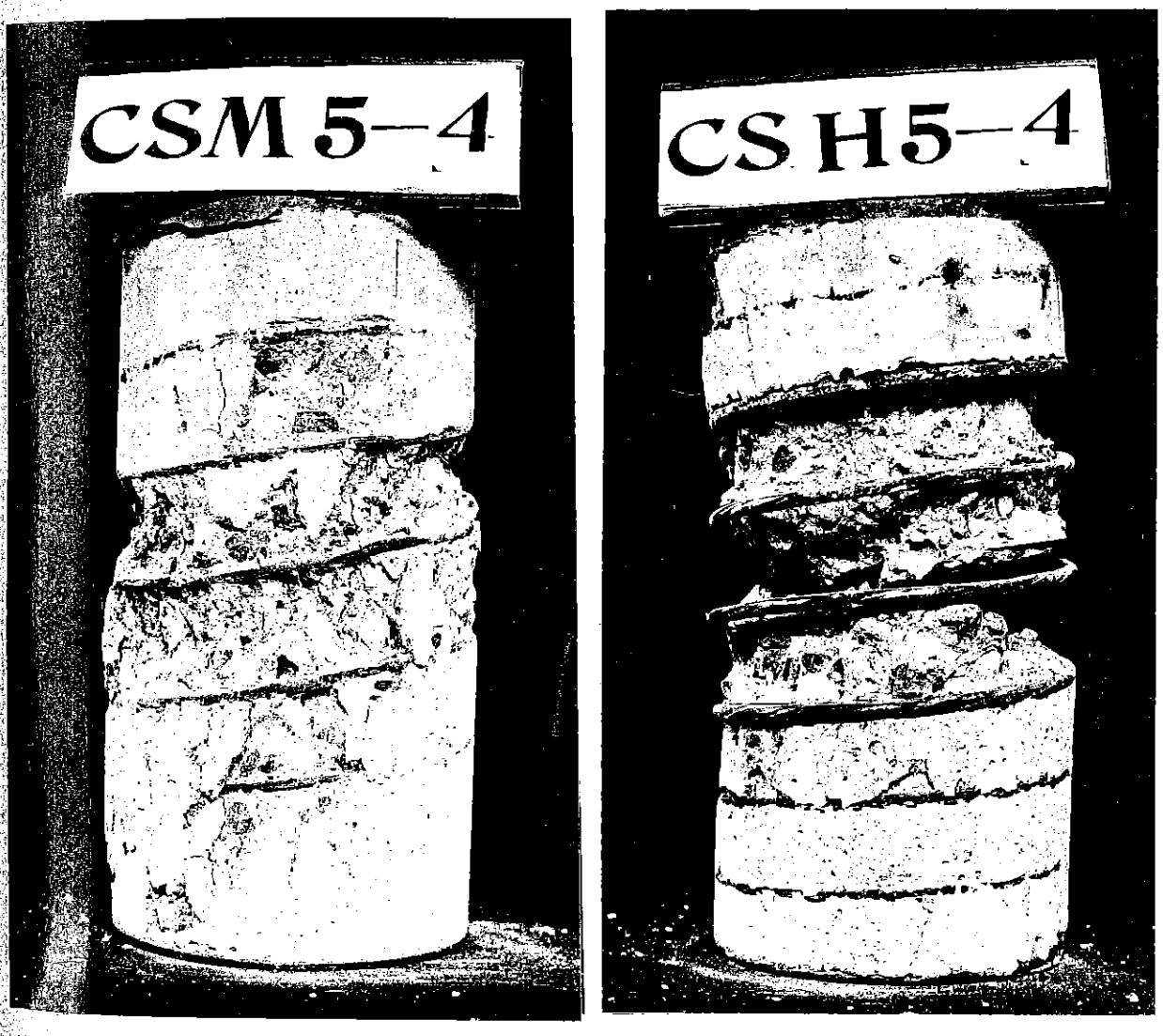

Fig. 2.53 CSM 5-4 and CSH 5-4 after Testing.

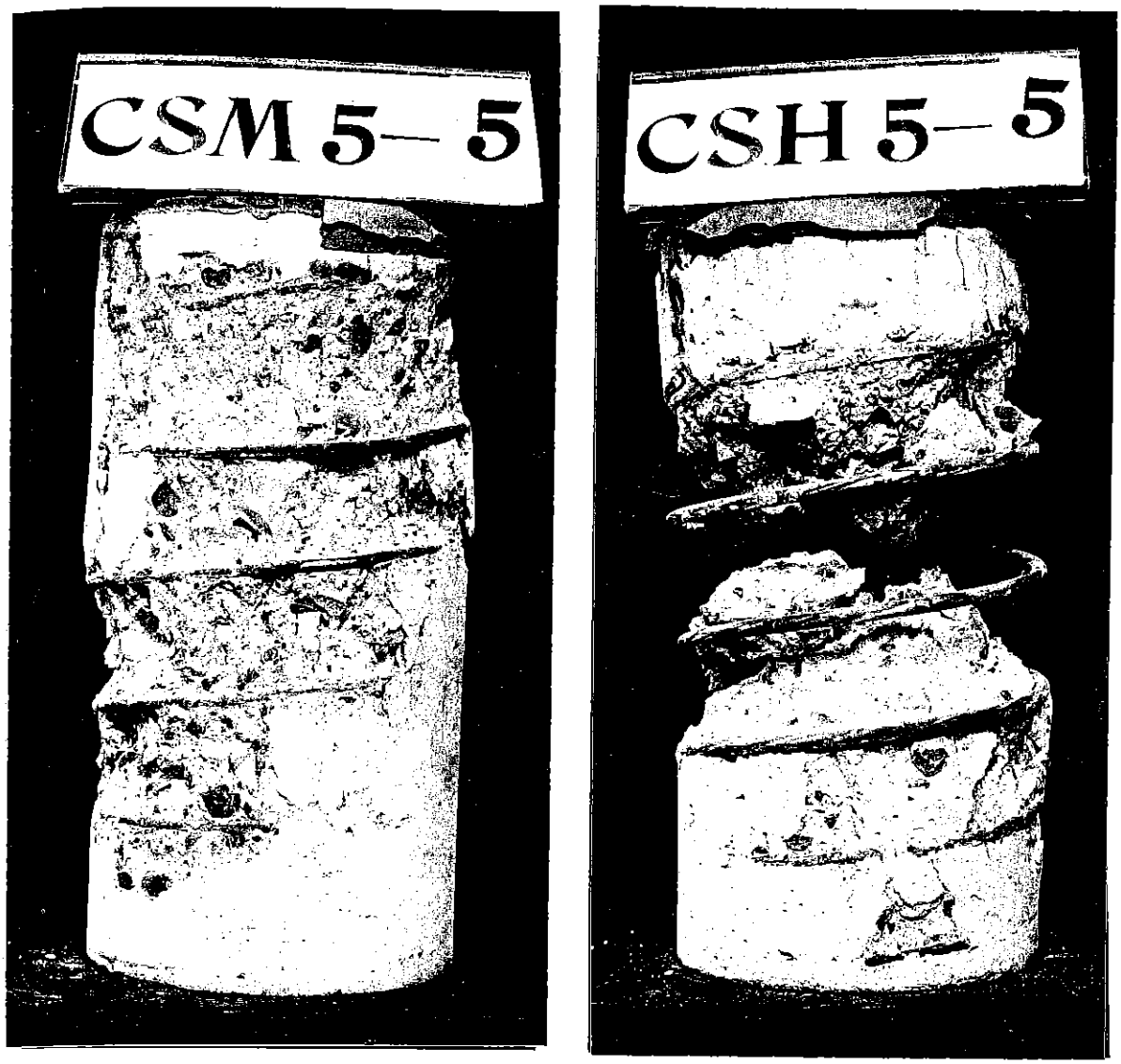

Fig. 2.54 CSM 5-5 and CSH 5-5 after Testing.

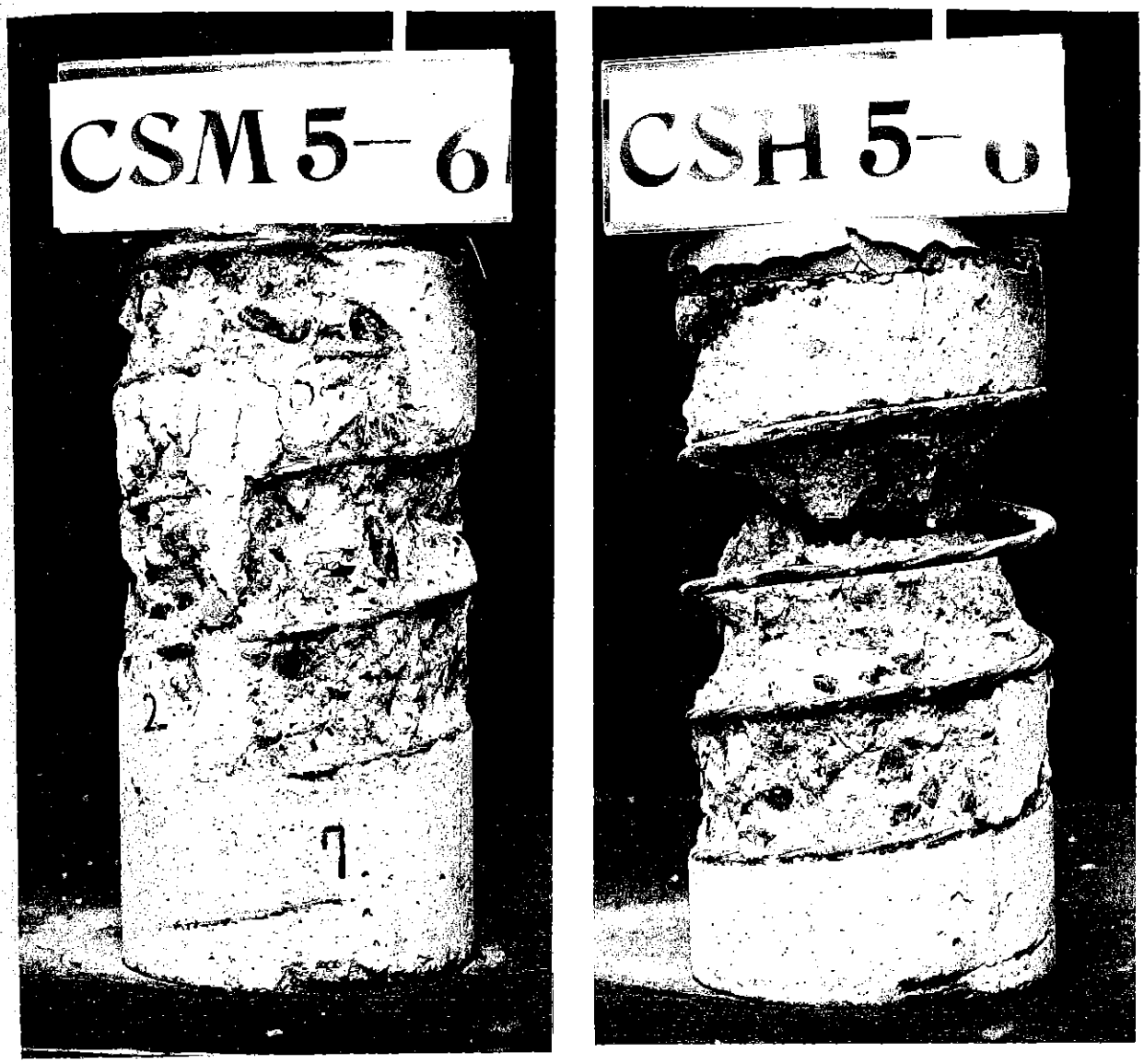

Fig. 2.55 CSM 5-6 and CSH 5-6 after Testing.

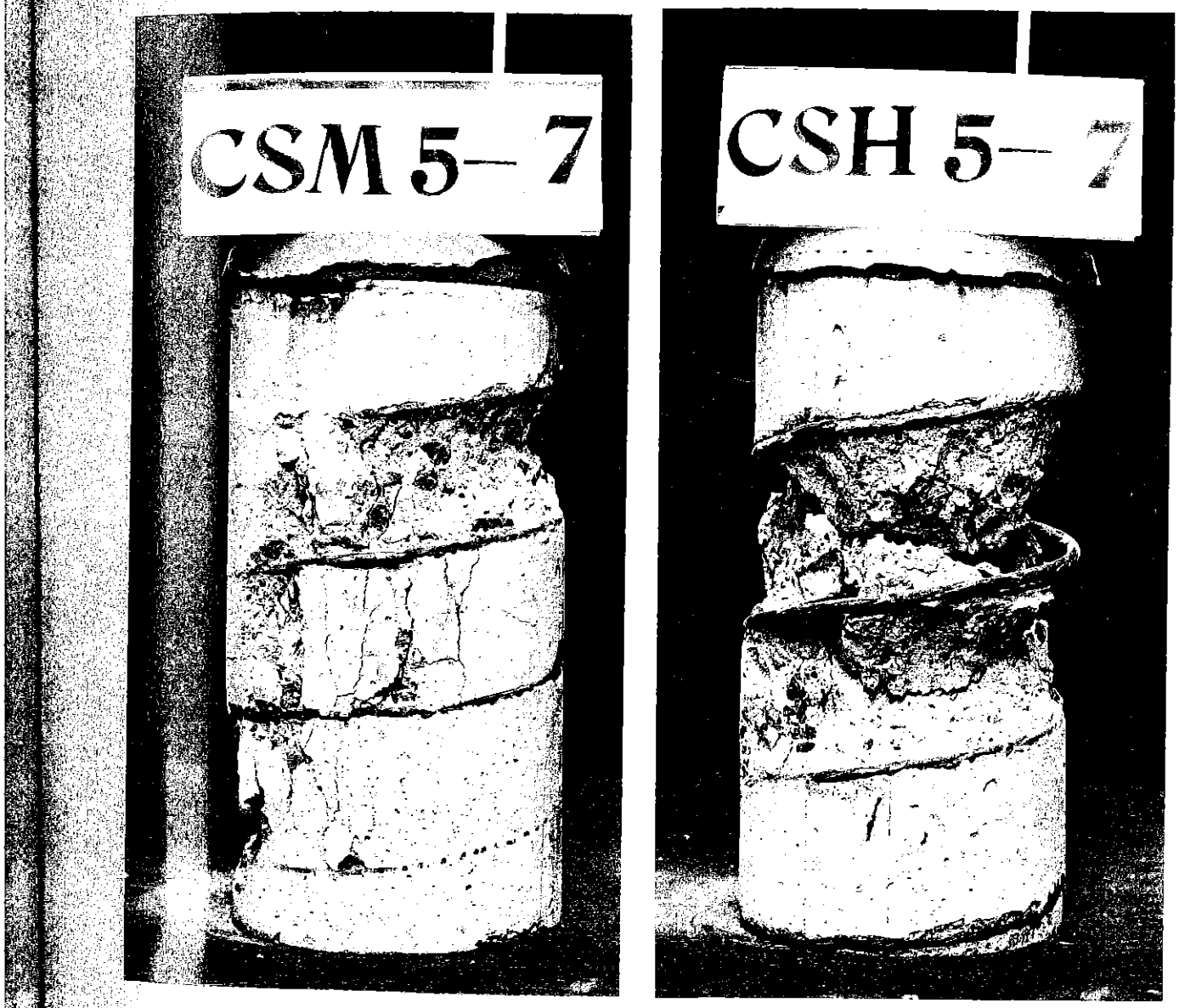

Fig. 2.56 CSM 5-7 and CSH 5-7 after Testing.

Cylinders with high strength steel spirals:
(1) Sudden failure due to crushing of core concrete between spiral bars or beneath the spiral bars occurred with explosive sound (see Fig. 2.57 (a)). Thereafter the load carrying capacity of the cylinders decreased rapidly.
(2) The measured tension strains of the spirals rapidly decreased as the axial compressive strain of the concrete increased after the peak of the axial load applied to the cylinder.
(3) The spalling section of the core concrete at the explosive failure zone was triangular.

Cylinders with low strength steel spirals:
(1) The failure was gradual and gentle with propagation of small longitudinal cracks on the cylindrical surface. The diagonal shear failure plane represented by Fig. 2.23(a) could not be seen from the surface observation.
(2) The measured tension strains of the spirals rapidly increased after the yielding of spiral bar which occurred at around the peak load.
(3) The spalled section of the core concrete was like a parabolic curve (see Fig. 2.57 (b)).

In the case of the cylinders confined by low strength steel spirals, it can be postulated that shear sliding surfaces are formed inside the core concrete with the propagation of micro cracks, as shown in Fig. 2.58 which was used in the reference [2.48] written by the author and Park. Shear sliding surfaces separate the concrete core into top and bottom cones and side shells. This postulation is based on the failure modes usually observed in compression tests on plain concrete cylinders [2.49]. In the assumed failure mode represented by Fig. 2.58, the rapid increase of the spiral tension strains after the peak load on the cylinder can be attributed to the wedging action of the top and the bottom cones which push the side shells outward. The detail of this assumption will be described in Section 6.2. On the contrary, in the case of the cylinders confined by high strength steel spirals, crushing of core concrete represented by Fig. 2.57 (a) takes place around at the peak load and thereafter the spiral bar tension is released as the axial compressive strain of concrete increases, unlike the failure mode of the cylinders with low strength steel spirals.

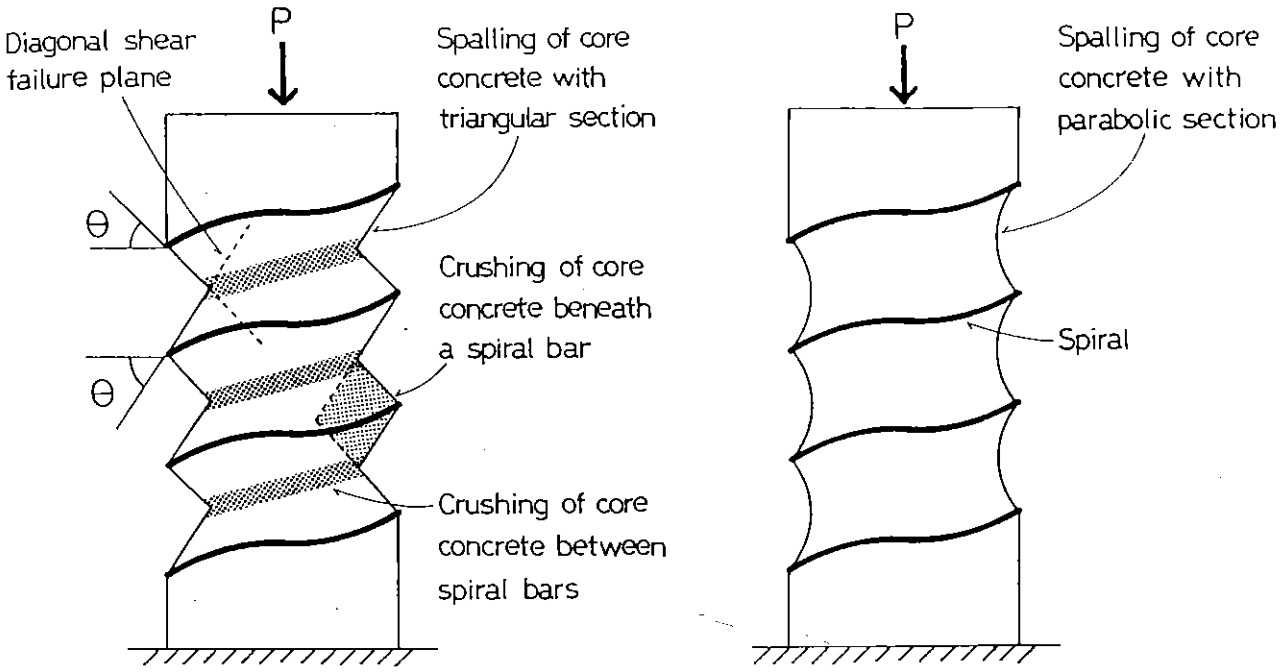

(a) Spiral with High Strength Steel

(b) Spiral with Low Strength Steel

Fig. 2.57 Typical Failure Conditions Observed in Spirally Reinforced Concrete Cylinders.

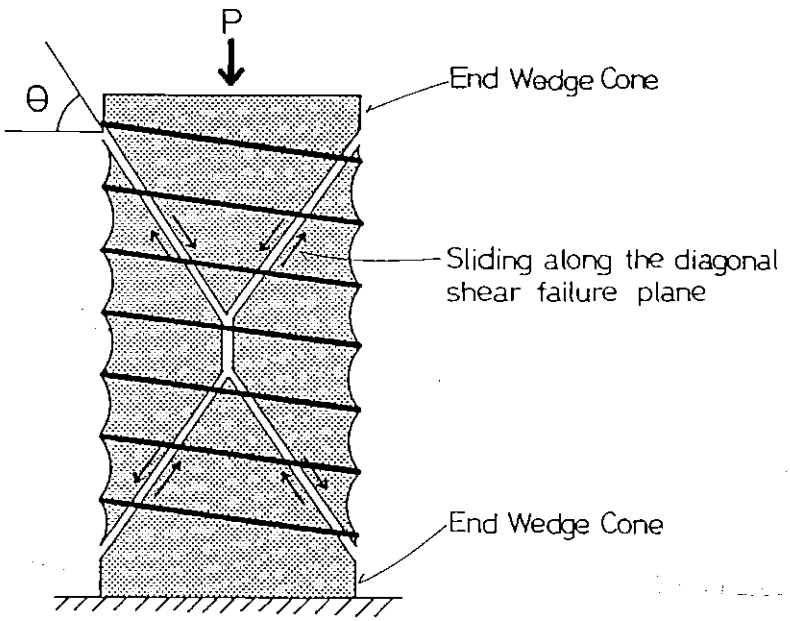

Fig. 2.58 Predicted Failure Mechanism of Concrete Cylinders Confined by Low Strength Steel Spirals.

2.4.2 The Angles of Spalling of Core Concrete in Relation to those of Diagonal Shear Failure Plane

It was observed that when high strength steel spirals were used the spalling angle of the confined core concrete could be smaller than 45°. It is notable that it was assumed that the ineffectively confined concrete area is bounded by a parabolic curve with end slope of 45° in the studies by Mander et al [2.6] or by Sheikh et al [2.13] where ordinary strength steel spirals were used as lateral reinforcement. When the failure mode shown in Fig. 2.58 is assumed, it may be considered that the spalling angle of core concrete is determined only from the local stress condition around the spiral bars. In the case of cylinders confined by high strength spirals, the spalling angle, θ, shown in Fig. 2.57 (a) seems to be affected by not only the local stress condition around the spiral bar but also by the formation of the diagonal shear failure plane of the confined core concrete (dashed lines in Fig. 2.57(a)), judging from the experimental observations. The spalling angle, θ, discussed here is used to evaluate the area of the critical section of spirally confined concrete at failure in Section 2.4.4.

The angles of the diagonal shear failure plane to the transverse section plane, θ, (see Fig. 2.23) depend on the magnitude of lateral pressure provided by the spirals. In the study by Mander et al [2.6], the relation between the plain concrete strength, f'_{co}, and the equivalent lateral pressure, f'_l defined by Eq. 2.41, was expressed by Eq. 2.40 derived from the theoretical ultimate strength surface of Willam and Warnke [2.58] with the triaxial test data of Schickert and Winkler [2.59]. Using the Mohr-Coulomb failure criterion with Eq. 2.40, Mander et al determined the angle of the diagonal shear failure plane θ as follows. The Mohr-Coulomb failure criteria is represented by Fig. 2.59. In the figure, x can be expressed as

$$x = \frac{R}{\sin\phi} - (f'_l + R) \qquad \text{.....} \qquad (2.82)$$

where $R = (f'_{cc} - f'_l)/2$

When $f'_l = 0$ then $R = f'_{co}/2$, therefore

$$x = \frac{f'_{co}}{2 \sin\phi} - \frac{f'_{co}}{2} = \frac{f'_{co}}{2} \frac{(1-\sin\phi)}{\sin\phi} \qquad \text{.....} \qquad (2.83)$$

Thus for confined concrete ($f'_l > 0$)

$$\frac{f'_{co}}{2}\,\frac{(1-\sin\phi)}{\sin\phi} = \frac{(f'_{cc}-f'_l)}{2\sin\phi} - \frac{(f'_{cc}+f'_l)}{2} \quad \text{.....} \quad (2.84)$$

which reduces to

$$f'_{cc} = f'_{co} + f'_l \tan^2(45° + \phi/2) \quad \text{.....} \quad (2.85)$$

But the failure angle $\theta = 45° + \phi/2$, therefore

$$f'_{cc} = f'_{co} + f'_l \tan^2\theta \quad \text{.....} \quad (2.86)$$

Rearranging this,

$$f'_{cc}/f'_{co} = 1 + (f'_l / f'_{co}) \tan^2\theta \quad \text{.....} \quad (2.87)$$

By differentiating,

$$\tan^2\theta = \frac{d(f'_{cc}/f'_{co})}{d(f'_l / f'_{co})} \quad \text{.....} \quad (2.88)$$

Similarly by differentiating Eq. 2.40,

$$\frac{d(f'_{cc}/f'_{co})}{d(f'_l / f'_{co})} = \frac{8.95}{\sqrt{1+7.94\, f'_l/f'_{co}}} - 2 \quad \text{.....} \quad (2.40')$$

From Eqs. 2.79 and 2.40',

$$\tan^2\theta = = \frac{8.95}{\sqrt{1+7.94\, f'_l/f'_{co}}} - 2 \quad \text{.....} \quad (2.89)$$

For the tested cylinders confined by high strength steel spirals (CSH3 to CSH 7), the observed spalling angles are listed in Table 2.5. Also listed in Table 2.5 are the failure plane angles calculated using Eq. 2.89 and assuming that f'_l is approximated by σ_l obtained from Eq. 2.9 . Although the observed spalling angles are always smaller than that the calculated failure angles, it is evident

Table 2.5 Spalling Angles and Diagonal Failure Plane Angles of Confined Core Concrete

Test Specimen	$\frac{\sigma_l}{f'_{co}}$	Measured Angle of Spalling	Average of Measured Spalling Angles	Diagonal Failure Plane Angle (by Eq. 2.80)
CSH3	0.713	30~32°	31°	50.5°
CSH4	0.535	29~46°	36°	54.1°
CSH5	0.429	43~53°	46°	56.4°
CSH6	0.248	48~52°	50°	60.8°
CSH7	0.142	40~64°	55°	63.8°

that both observed and theoretical angles become smaller as the lateral pressure increases.

The effect of the local stress conditions on the spalling angle may be explained as follows. Assume that the spiral bar is sitting on the apex of the wedge formed after spalling of core concrete. When the radius of the cylinder is infinitely large, the stress condition may be considered in the two-dimensional plane with thickness of unity as shown in Fig. 2.60. Using polar coodinates the radial normal stress $\sigma_{r\alpha}$ along the cirular line with radius 'r' can be expressed as,

$$\sigma_{r\alpha} = \frac{k\,\sigma_{lo}\cos\alpha}{r} \qquad \text{.....} \qquad (2.90)$$

where σ_{lo} = local lateral pressure provided by the spiral calculated by taking 's' equals to the spiral bar diameter in Eq. 2.9

k = constant

and tangential normal stress $\sigma_\theta = 0$, shearing stress $\tau_{r\theta} = 0$ [2.7]. Making the resultant of the pressures $\sigma_{r\alpha}$ equal to σ_{lo},

$$\sigma_{lo} = 2\int_0^\theta \frac{k\,\sigma_{lo}\cos^2\alpha}{r}\, r\, d\alpha$$

$$= k\,\sigma_{lo}\left(\theta + \frac{1}{2}\sin 2\theta\right) \qquad \text{.....} \qquad (2.91)$$

From this

$$k = \frac{1}{\theta + \frac{1}{2}\sin 2\theta} \qquad \text{.....} \qquad (2.92)$$

Substituting into Eq. 2.90,

$$\sigma_{r\alpha} = \frac{\sigma_{lo}\cos\alpha}{r\left(\theta + \frac{1}{2}\sin 2\theta\right)} \qquad \text{.....} \qquad (2.93)$$

From Eq. 2.93, the normal stress in x direction at point B, σ_{xB}, can be expressed as

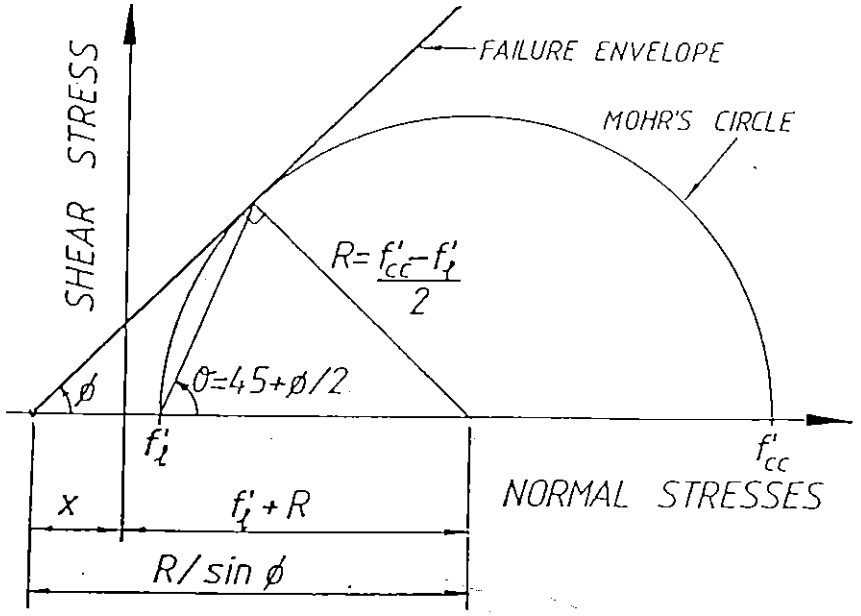

Fig. 2.59 Mohr-Coulomb Failure Criteria Applied to Confined Concrete [2.6]

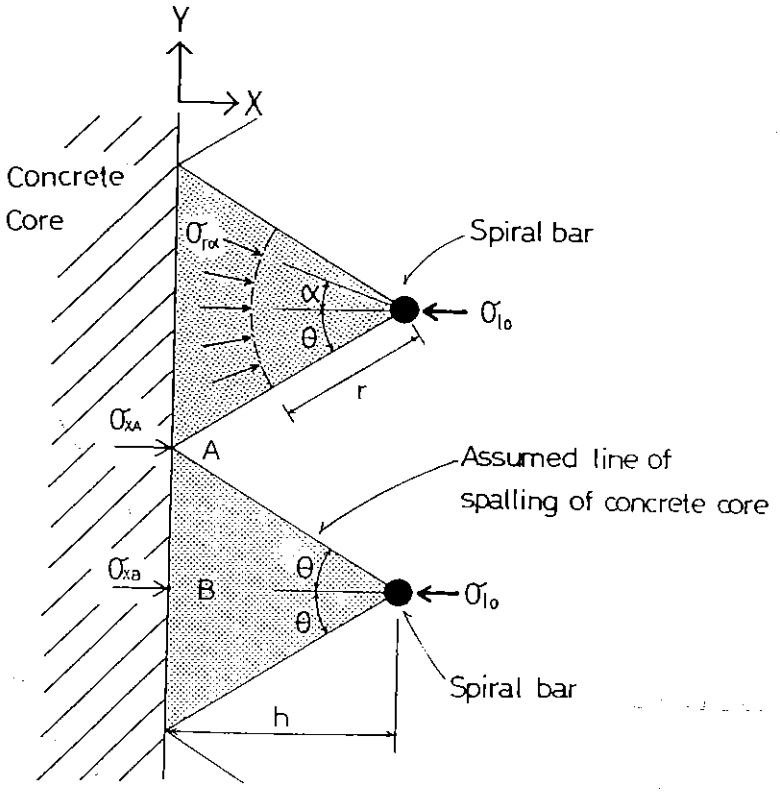

Fig. 2.60 Stresses in a Wedge due to a Concentrated Force at Its Apex.

$$\sigma_{xB} = \frac{\sigma_{lo}}{h\,(\theta + \frac{1}{2}\sin 2\theta)} \qquad \text{.....} \qquad (2.94)$$

Since $\sigma_\theta = 0$ and $\tau_{r\theta} = 0$, the normal stress σ_x in x direction (cartesian coordinates) can be expressed in terms of the radial normal stress $\sigma_{r\alpha}$ (polar coordinates) as

$$\sigma_x = \sigma_{r\alpha}\cos^2\alpha = \frac{\sigma_{lo}\cos^3\alpha}{r\,(\theta + \frac{1}{2}\sin 2\theta)} \qquad \text{.....} \qquad (2.95)$$

At point A, $r = h/\cos\theta$ and $\alpha = \theta$. Hence, the normal stress in x direction at point A, σ_{xA}, as the resultant of two $\sigma_{r\theta}$ can be expressed as,

$$\sigma_{xA} = \frac{2\,\sigma_{lo}\cos^4\theta}{h\,(\theta + \frac{1}{2}\sin 2\theta)} \qquad \text{.....} \qquad (2.96)$$

Assuming that propagation spalling of core concrete inward can be stopped when $\sigma_{xA} = \sigma_{xB}$, and hence equating Eqs. 2.86 and 2.87,

$$2\cos^4\theta = 1 \qquad \text{.....} \qquad (2.97)$$

Eq. 2.97 gives $\theta = 32.8°$. This θ may indicate the smallest spalling angle which is possible when the local lateral pressure provided by spirals is very high. The variations of the observed spalling angles for each tested cylinder listed in Table 2.5 may be indicating the effect of this local stress condition combined with the formation of the diagonal shear failure plane.

In the case of CSM7 to CSM3 confined by low strength steel spirals, σ_l calculated using Eq. 2.9 is from 0.023 to 0.053 times f'_{co}, and when substituted into Eq. 2.89 results in failure plane angle θ from 68.2° to 66.9°. When the failure mode represented by Fig. 2.58 is assumed, the spalling angle may have no relation to the angle of the diagonal shear failure plane and may be determined only from the local stress condition around the spiral bars.

It may be notable that the value of $\tan^2\theta$ in Eq. 2.86 which corresponds to α_s in Eq. 2.1" (Section 2.3.3.1) becomes smaller as the lateral pressure f'_l becomes higher, when $\tan^2\theta$ is given by Eq. 2.89. That is, as listed in Table 2.5, the diagonal failure plane angles for CSH7 to CSH3 calculated using Eq. 2.89 are from 63.8° to 50.5° and the corresponding values of $\tan^2\theta$ (= α_s) are from 4.13 to 1.52 with average of 2.60. This tendency agrees with the test results shown in Fig. 2.41(a) (see Eqs. 2.75 and 2.76) and the results obtained by Richart et al [2.3] and Balmer [2.4], apart from the discrepancy of the absolute values. In the tests by Richart et al [2.3], the measured values of α_s decreased from 5.3 to 3.7 when the lateral fluid pressures f_l was increased from 0.15 f'_{co} to 1.12 f'_{co}. In the tests by Balmer [2.4], the measured values of α_s decreased from 6.4 to 3.0 when f_l was increased from 0.28 f'_{co} to 7.00 f'_{co}.

2.4.3 The Bearing Strength of Concrete Beneath Spiral Bar

As mentioned in Section 2.41, the measured tension strains of high strength steel spirals decrease after the peak of axial load of the cylinders is reached while axial compressive strain of the concrete is increasing. This may indicate that bearing failure of core concrete has occurred beneath the high strength spiral bar due to high lateral pressure, although the bearing failure may be induced by the explosive failure of the central core concrete at the critical section between spiral bars. From the experimental observations, it is difficult to say which occurred first, the crushing of the central core under high triaxial compression or the bearing failure of concrete beneath the spiral bars.

It is notable that any damage of the contact surface of the core concrete beneath the spiral bar could not be observed. Hence, if it is assumed that the bearing failure of the core concrete occurred before the crushing of the central core, the location of the bearing failure may be assumed to be as represented by Fig. 2.61. In the figure, Zone (A) is assumed to be under triaxial compressive stress condition due to lateral pressure by the spiral and the frictional restraint at the interface between the concrete and the spiral. It is noted that the high strength steel spirals used in the tests were formed from deformed steel bars. Zone (B) is assumed to be under biaxial compressive stress condition due to lateral pressure only from the spiral

without influence of the axial stress and the friction between concrete and the spiral. Thus, Zone (B) may be assumed to be the most critical zone when considering the bearing failure of concrete. When it is assumed that the spalling angle of the core concrete is 45° and the distance from the centre of gravity of the spiral bar section to the border between Zones (A) and (B), h_c, equals to the spiral bar diameter, d_{bh}, the width of the plane of the border between Zones (A) and (B), w_c, becomes 2 times d_{bh}. In this case, the average pressure at the plane of the border between Zones (B) and (C), σ_{ave}, is calculated as

$$\sigma_{ave} = \frac{2 A_{sp} f_{sp}}{D' \cdot 2 d_{bh}} \qquad \text{.....} \qquad (2.98)$$

where A_{sp} = area of spiral bar or circular hoop bar
f_{sp} = stress in circular hoop bar or spiral bar
D' = diameter of core section measured to outside of spirals

For the test cylinders CSH3, CSH4, CSH5, the maximum value of σ_{ave} calculated from Eq. 2.98 was 1.67 f'_{co} (where f'_{co} = uniaxial compressive strength of plain concrete) due to yielding of the spiral bar, while the maximum values of σ_{ave} for CSH6 and CSH7 were 1.16 f'_{co} and 0.78 f'_{co}, respectively, from the measured maximum tension strains in the spirals. In Fig. 2.62, most of the experimental values for the biaxial compressive strength of concrete published up to 1973 [2.50, 2.51] are plotted along with the predicted failure envelope proposed by Kotsovos [2.50]. The wide variation of the test data has been attributed mainly to the different testing techniques used and in particular to the degree of frictional restraint at the platen-specimen interfaces [2.50, 2.52]. It may be said that σ_{ave} of 1.67 f'_{co} calculated for CSH3, CSH4 and CSH5 specimens is probably high enough to cause the bearing failure of core concrete beneath the spiral bar, although it cannot be definitely said that this occurred due to the large degree of scatter of the data plotted in Fig. 2.62.

From the above results, when high strength spirals are used in practice, it may be necessary to check the bearing strength of the core concrete beneath the spiral bars. However, to obtain more accurate estimation of the bearing strength of core concrete, further research will be required including the effects of the presence of longitudinal reinforcement which may improve the lateral pressure distribution. When the strength enhancement

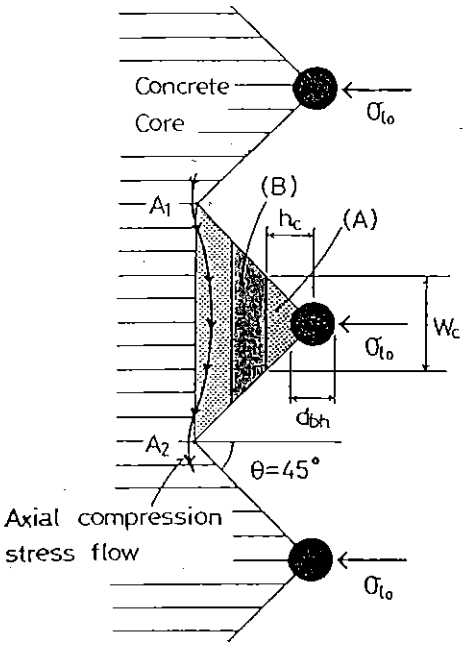

Fig. 2.61 Stress Condition Assumed when Checking the Possible Bearing Failure of Concrete due to Lateral Pressure from Spirals.

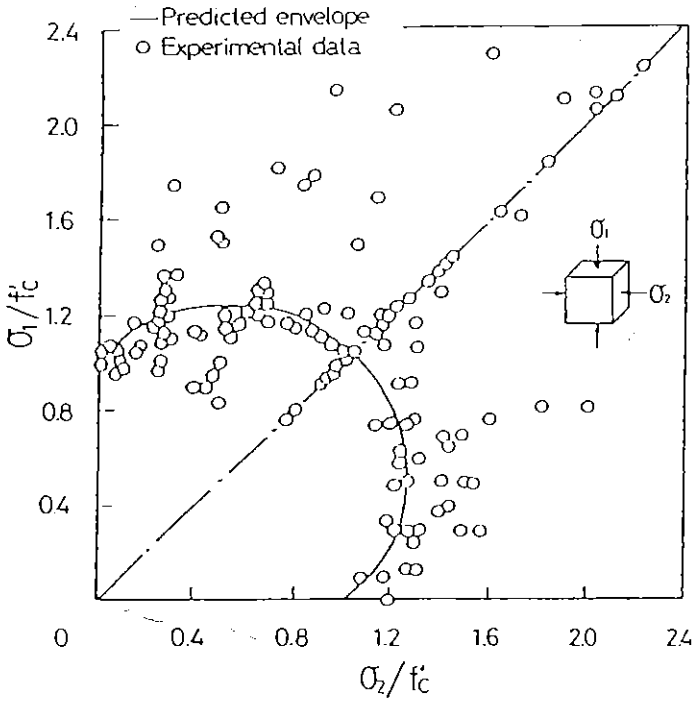

Fig. 2.62 Experimental Values of Biaxial Compressive Strength of Concrete Published up to 1973 and Predicted Failure Envelope Curve by Kotsovos [2.50].

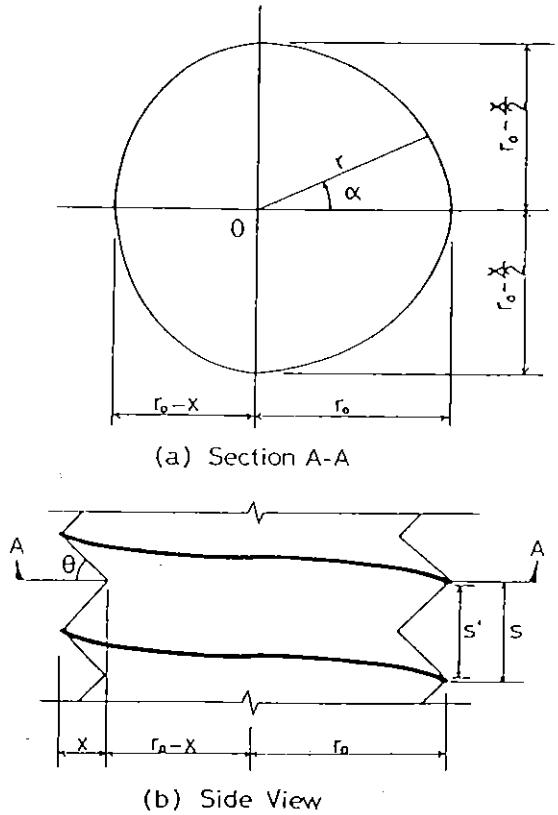

Fig. 2.63 Confined Core Area at the Critical Section Assumed for Cylindrical Specimens with High Strength Steel Spirals.

of confined concrete needs to be estimated for a high lateral pressure condition due to the use of high strength steel spirals, Eq. 2.68 may be tentatively used assuming that this equation is for the case where the bearing failure of the core concrete occurs.

2.4.4 Confined Concrete Core Area at Critical Section after Spalling of Ineffectively Confined Core Concrete

The compressive strength of the confined concrete f'_{cc} was calculated as the maximum load divided by the concrete core area at the critical section after spalling of ineffectively confined core concrete in order to draw Fig. 2.41. This core area at the critical section was determined as follows. In the study by Mander et al [2.6], the effectively confined core area at the critical section was taken at transverse section B-B in Fig. 2.19 and was approximated by Eq. 2.48. Taking the critical transverse section at the same position as in the Mander et al study, it is assumed that 'r' shown in Fig. 2.63 can be expressed in terms of the angle α as

$$r = r_o - \left(\frac{\alpha}{\pi} x \right) \qquad \text{.....} \qquad (2.99)$$

where r_o = radius of the confined core measured to the outside of the spiral bar

x = the depth of the concave after spalling of the core concrete (see Fig. 2.63)

$0 \leq \alpha < \pi$

The area inside the 'r' is calculated as

$$S = 2 \int_0^{\pi} \frac{1}{2} \left[r_o - \left(\frac{\alpha}{\pi} x \right) \right]^2 d\alpha$$

$$= r_o^2 \pi - r_o x \pi + \frac{x^2}{3} \pi \qquad \text{.....} \qquad (2.100)$$

As the ratio to the original core area, $S_o = \pi r_o^2$, Eq. 2.100 is expressed as

$$\frac{S}{S_o} = 1 - \frac{x}{r_o} + \frac{x^2}{3 r_o^2} \qquad \text{.....} \qquad (2.101)$$

For the cylinders confined by high strength steel spirals, it is assumed that 'x' can be expressed as

$$x = \frac{s'}{2} \cot \theta \qquad \text{.....} \qquad (2.102)$$

where s'= clear spacing between spiral or hoop bars

θ = spalling angle of the confined core concrete (see Fig.2.63 (b))

This is because the spalled part of the core concrete was assumed to have a triangular section as mentioned in Sections 2.41 and 2.42.

When plotting the data of the cylinders with high strength spirals in Fig. 2.41, the critical area has been calculated using Eqs. 2.101 and 2.102 with the average of the measured spalling angles for each test specimen listed in Table 2.5. For the cylinders confined by low strength steel spirals, Eq. 2.101 and $x = s'/4$ have been used which assumes a second degree parabola with end slope of 45° as shown in Fig. 2.19.

2.4.5 Fatigue Failure Behaviour of Concrete Confined by High Strength Spirals

In order to investigate the fundamental behaviour of concrete confined by high strength steel spirals under high intensity cyclic loading, the following tests were carried out by the author et al [2.37]. Twenty-four spirally reinforced concrete cylinders and fifteen plain concrete cylinders, each 150 mm diameter by 300 mm high, were tested under monotonic and high intensity cyclic loading. With respect to the spirally reinforced concrete cylinders, as listed in Table 2.6, twelve of them were confined by 6 mm diameter spiral reinforcement with yield strength of 1151 MPa (= 11740 kgf/cm^2) and, for comparison, another twelve were confined by 6 mm diameter spiral reinforcement with yield strength of 316 MPa (= 3225 kgf/cm^2). The pitches of the spirals were all 5 cm. Those test specimens were divided into three series in terms of compressive strength of plain concrete used. That is, the compressive strengths of plain concrete for Series F2, Series F3 and Series F4 were 28.2 MPa (= 288 kgf/cm^2), 34.8 MPa (= 355 kgf/cm^2) and 47.9 MPa (= 489 kgf/cm^2), respectively. Concrete cover was not provided so that the stress-strain relationships of the confined concrete could be obtained simply. The loading arrangements and

Table 2.6 Details of the Spirally Reinforced Cylinders and Maximum Load Level under Cyclic Load

Specimen	Spiral Reinforcement				f'_c (MPa)	Loading type	σ_{ma}/σ_{cu}	σ_{ma}/f'_c	σ_{ma} (MPa)
	b_d (mm)	s (mm)	ρ_s (%)	f_{yh} (MPa)					
F2-M-1.00	6	50	1.53	316	28.3	monotonic	1.00	1.18	33.4
F2-M-0.95						cyclic	0.95	1.12	36.2
F2-M-0.90						cyclic	0.90	1.06	31.6
F2-M-0.85						cyclic	0.85	1.00	29.0
F2-H-1.00	6	50	1.52	1152	28.3	monotonic	1.00	1.50	4.25
F2-H-0.90						cyclic	0.90	1.35	40.0
F2-H-0.85						cyclic	0.85	1.28	38.1
F2-H-0.75						cyclic	0.75	1.12	32.2
F3-M-1.00	6	50	1.53	316	34.8	monotonic	1.00	1.20	41.7
F3-M-0.95						cyclic	0.95	1.14	42.7
F3-M-0.90						cyclic	0.90	1.08	37.6
F3-M-0.85						cyclic	0.85	1.02	35.3
F3-H-1.00	6	50	1.52	1152	34.8	monotonic	1.00	1.41	49.1
F3-H-0.90						cyclic	0.90	1.27	47.0
F3-H-0.85						cyclic	0.85	1.19	42.7
F3-H-0.81						cyclic	0.81	1.14	39.5
F4-M-1.00	6	50	1.53	316	48.0	monotonic	1.00	1.20	57.8
F4-M-0.95						cyclic	0.95	1.14	57.3
F4-M-0.90						cyclic	0.90	1.08	56.6
F4-M-0.85						cyclic	0.85	1.02	48.8
F4-H-1.00	6	50	1.52	1152	48.0	monotonic	1.00	1.42	68.2
F4-H-0.95						cyclic	0.95	1.35	69.0
F4-H-0.90						cyclic	0.90	1.28	63.5
F4-H-0.80						cyclic	0.80	1.14	54.9

Note: b_d = diameter of spiral bar

s = spacing of spiral reinforcement

ρ_s =ratio of volume of spiral reinforcement to volume of concrete core

f_{yh} = yield strength of spiral reinforcement

f'_c = compressive strength of plain concrete measuerd by 15 cm dia. x 30 cm high cylinders

σ_{ma} = maximum compressive stress applied to the specimen

σ_{cu} = compressive strength of the specimen obtained from a monotonic load test

measuring devices used were the same as those used in the tests described in Section 2.4.1 (see Fig. 2.50).

The tests results are listed in Table 2.7. For the cases where the ratios of the maximum stresses applied in cyclic loading to the plain concrete strengths were 1.12 and 1.14, the stress-strain curves for the concrete confined by high strength steel spirals and by ordinary strength steel spirals are shown in Fig. 2.64 and 2.65, respectively. As can be seen from those figures, the concrete cylinders confined by high strength steel spirals indicate significantly higher fatigue strength than those confined by ordinary strength spirals when the ratios of applied maximum stress to the plain concrete strength are the same. This is due to the higher lateral confining pressure provided in the former as can be seen in Fig. 2.66 which shows the envelope curves for the lateral confining pressures versus axial compressive strains of concrete. Those lateral confining pressures were calculated using Eq. 2.9 with the spiral strains as measured by electrical wire strain gauges with gauge length of 2 mm.

In Fig. 2.67, the observed stress fatigue failure points are plotted taking the ratio of the applied maximum stress to the plain concrete strength as the ordinate and the logarithm of cycles to failure as abscissa. As can be seen from the figure, the plotted points showed obvious trends with respect to the yield strength of the spirals but with little effect from the plain concrete strengths used. Hence, regression analysis using the least square method was separately applied to the cylinders confined by high strength spirals, those confined by ordinary strength spirals and the plain concrete cylinders. The best fitting curves are expressed as:

For the cylinders confined by high strength spirals,

$$\frac{\sigma_{cm}}{f'_{co}} = -0.12 \log N_f + 1.41 \quad \text{.....} \quad (2.103)$$

For the cylinders confined by ordinary strength spirals,

$$\frac{\sigma_{cm}}{f'_{co}} = -0.07 \log N_f + 1.17 \quad \text{.....} \quad (2.104)$$

For the plain concrete cylinders,

$$\frac{\sigma_{cm}}{f'_{co}} = -0.04 \log N_f + 0.98 \quad \text{.....} \quad (2.105)$$

where σ_{cm} = the applied maximum stress in the cyclic loading

N_f = number of cycles to failure

Table 2.7 Test Results

Specimen	Cycles to failure	At peak load in final cycle before failure			Axial compressive strain of concrete at yielding of spiral reinforcement (%)
		Spiral strain (%)	Confinig stress by spiral reinforcement (MPa)	Axial strain of concrete (%)	
F2-M-1.00					0.20
F2-M-0.95	1	0.270	2.41	0.40	0.40
F2-M-0.90	11	0.595	2.41	0.61	0.35
F2-M-0.85	133	0.310	2.41	1.07	0.31
F2-H-1.00					non-yielding
F2-H-0.90	8	0.810	8.47	2.01	non-yielding
F2-H-0.85	10	0.535	6.91	1.59	non-yielding
F2-H-0.75	106	0.519	6.77	1.78	non-yielding
F3-M-1.00					0.40
F3-M-0.95	3	0.293	2.41	0.45	0.37
F3-M-0.90	72	0.281	2.41	0.70	0.42
F3-M-0.85	185	1.344	2.41	0.78	0.41
F3-H-1.00					1.14
F3-H-0.90	18	0.906	8.68	1.83	1.77
F3-H-0.85	36	0.658	7.77	1.61	non-yielding
F3-H-0.81	186	0.527	6.88	1.68	non-yielding
F4-M-1.00					0.28
F4-M-0.95	7	1.200	2.41	0.46	0.33
F4-M-0.90	8	0.462	2.41	0.40	0.30
F4-M-0.85	161	1.430	2.41	0.57	0.28
F4-H-1.00					1.03
F4-H-0.95	1	0.317	4.40	0.51	non-yielding
F4-H-0.90	4	0.596	7.40	0.66	non-yielding
F4-H-0.80	145	-		1.29	non-yielding

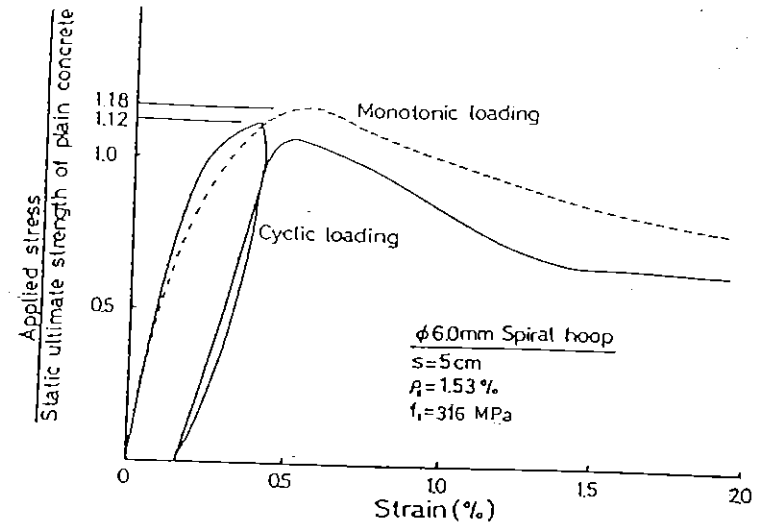

(a) Specimens F2-M-1.00 and F2-M-0.95

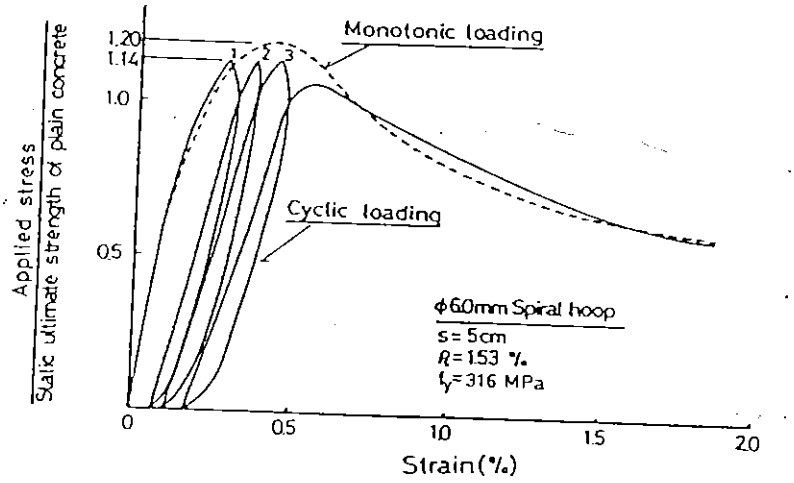

(b) Specimens F3-M-1.00 and F3-M- 0.95

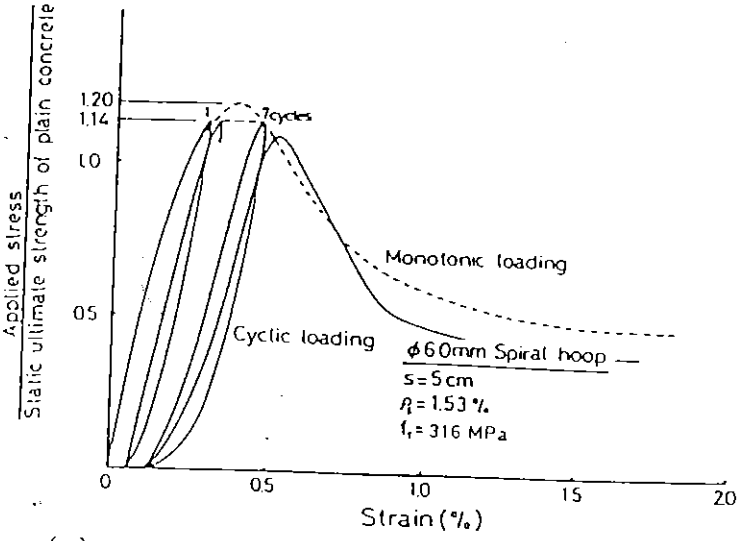

(c) Specimens F4-M-1.00 and F4-M-0.95

Fig. 2.64 Stress-Strain Curves Obtained from the Specimens Confined by Ordinary Strength Steel Spirals.

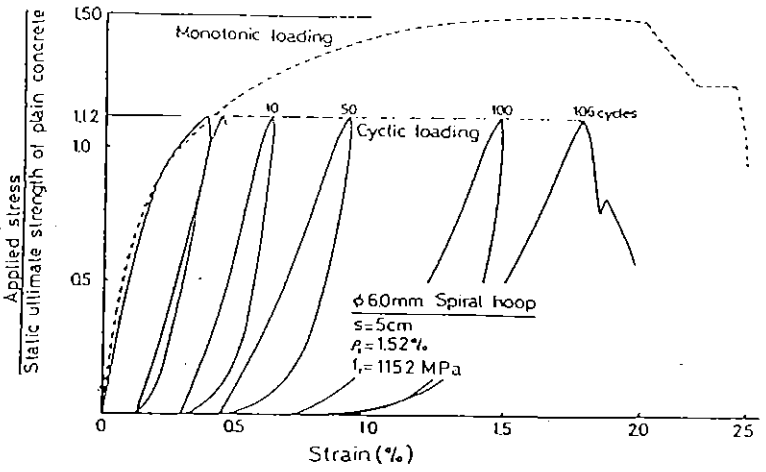

(a) Specimens F2-H-1.00 and F2-H-0.75

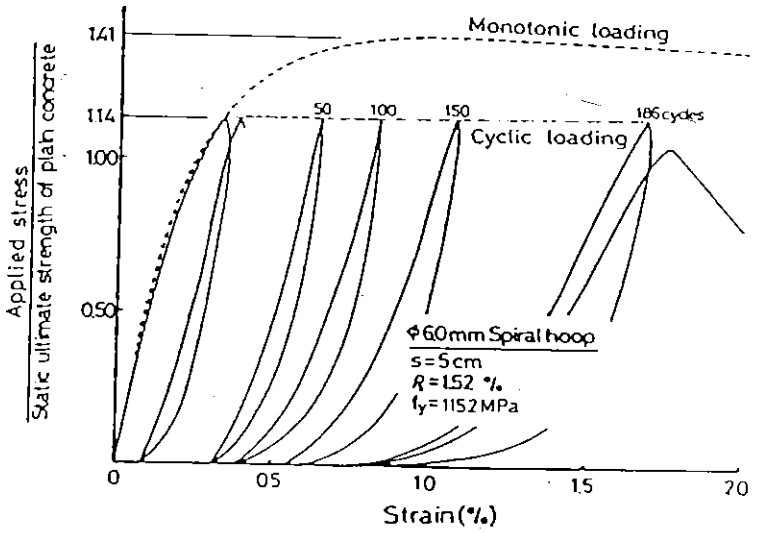

(b) Specimens F3-H-1.00 and F3-H- 0.81

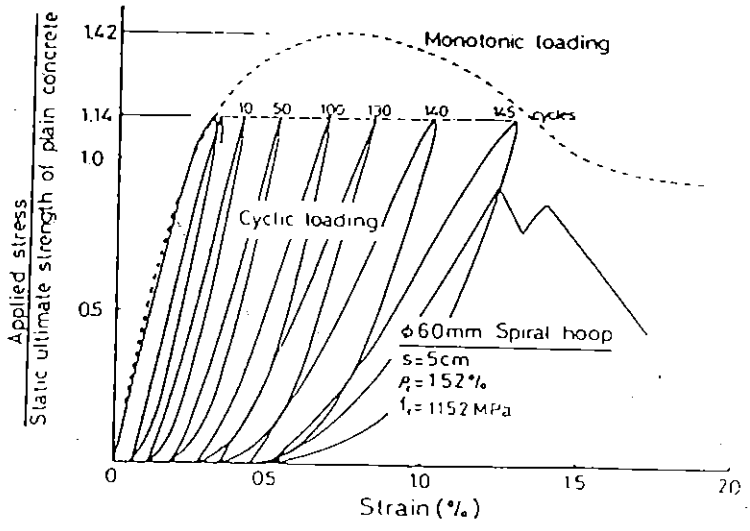

(c) Specimens F4-H-1.00 and F4-H-0.80

Fig. 2.65 Stress-Strain Curves Obtained from the Specimens Confined by High Strength Steel Spirals.

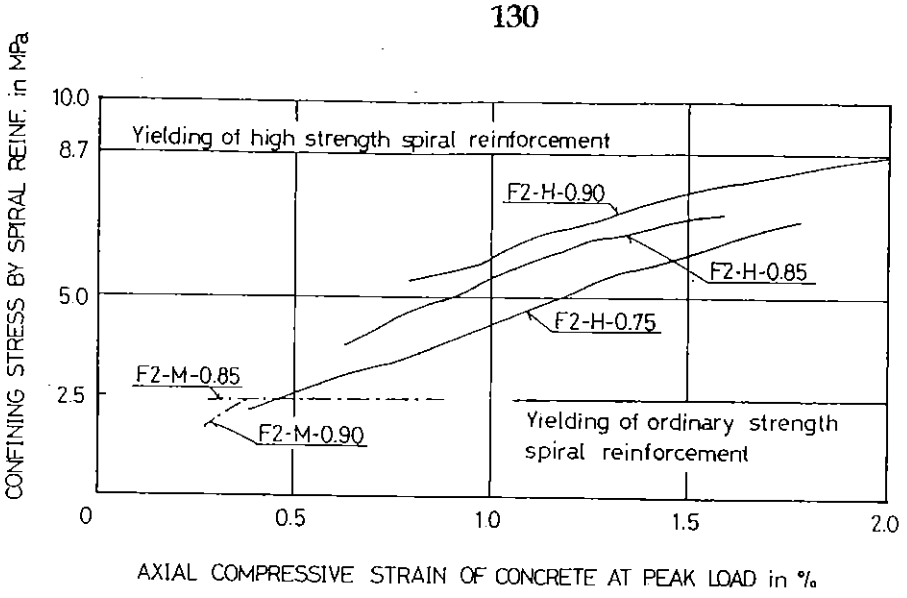

(a) Series F2

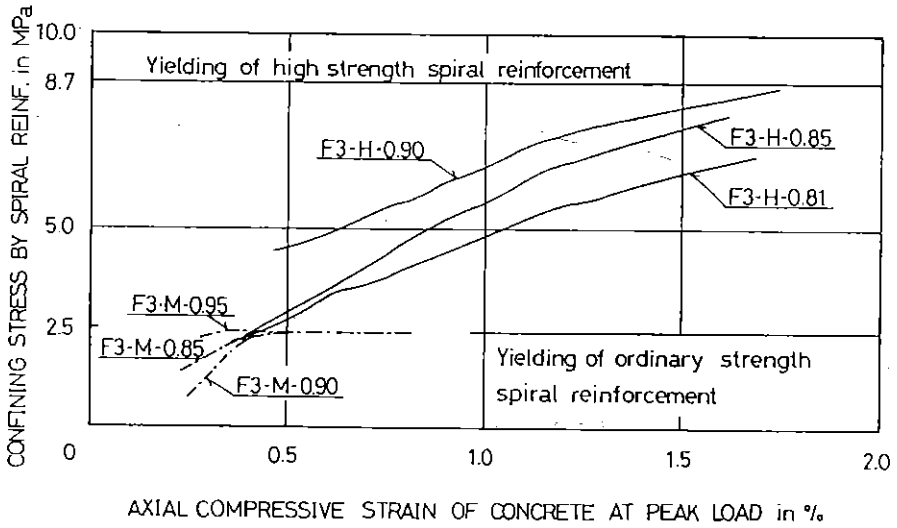

(b) Series F3

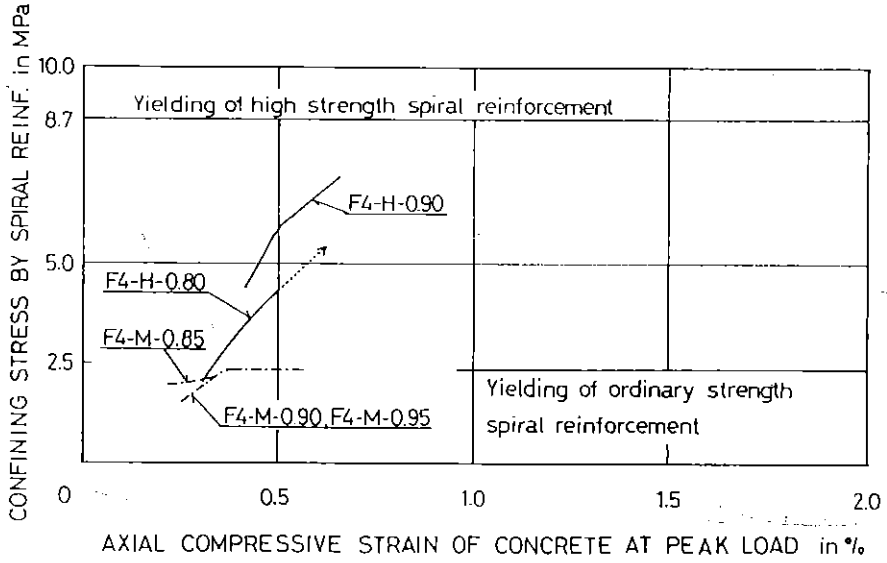

(c) Series F4

Fig. 2.66 Confining Stress by Spirals at Peak Load in Cyclic Loading.

From Eqs 2.103, 2.104 and 2.105, it can be concluded that the fatigue strength of concrete is improved as the degree of lateral confinement becomes higher. However, it must be noted that the cylinders confined by high strength steel spirals fail in a smaller number of loading cycles than those confined by ordinary strength spirals when the ratios of the applied maximum stress in cyclic loading to the ultimate static compressive strength of the corresponding confined concrete are the same. For example, the failure cycles of F3-M-0.90 with ordinary strength spirals and F3-H-0.90 with high strength spirals were 72 cycles and 18 cycles, respectively, as listed in Table 2.7 where the number (= 0.90, in this case) indicated in the last term of each specimen name denotes the ratio of the applied maximum stress to the ultimate compressive strength of the corresponding confined concrete. Hence, when the failure of confined concrete due to cyclic loading of high amplitude, such as earthquake loading, is dicussed in terms of the ultimate strength of the confined concrete rather than in terms of the plain concrete strength, the above fact must be taken into account.

In Fig. 2.68 fatigue failure points are plotted with the measured stress-strain curves of confined concrete under monotonic loading. In the case of the cylinders confined by ordinary strength steel spirals, the fatigue failure ocurred around when the stress-strain curves under cyclic loading come across the corresponding stress-strain curves under monotonic loading. In the studies by Karsan and Jirsa [2.53] and Sinha, Gerstle and Tulin [2.60], it has been shown that, for plain concrete specimens, the envelope curve coincided with the stress-strain curve for a specimen under monotonic loading and that the stress-strain path reached the envelope regardless of the strain accumulated prior to a particular cycle. Hence, it may be said that during cyclic loading the behaviour of concrete confined by ordinary strength steel spirals is close to that of plain concrete. On the other hand, in the case of the cylinders confined by high strength steel spirals the fatigue failure ocurred before the stress-strain curves under cyclic loading came across the corresponding stress-strain curves under monotonic loading, as can be sen from Fig.2.68 as well as from Figs. 2.65 (a) and (b).

In the study by the author and Sakomizu [2.61], spirally reinforced cylinders with the same size as the above were tested under cyclic loading to compare the stress-strain curves with those from monotonic loading tests.

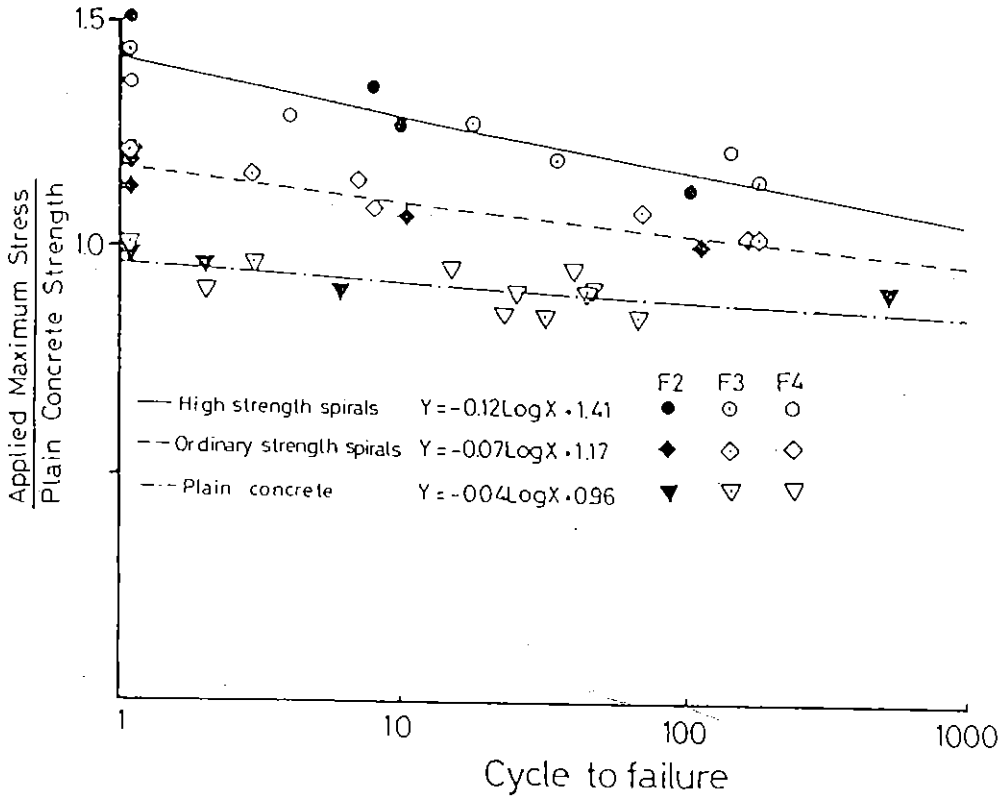

Fig. 2.67 Stress-Fatigue Life Curves for Concrete

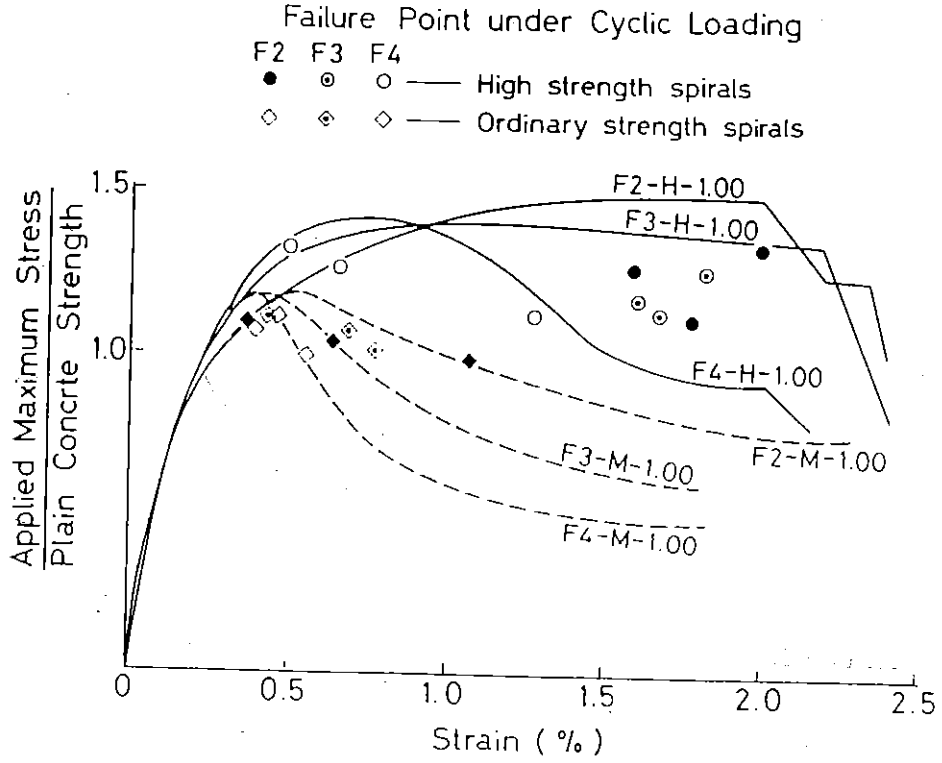

Fig. 2.68 Fatigue Failure Points versus Monotonic Stress-Strain Curves of Confined Concrete

Typical stress-strain curves obtained are shown in Fig. 2.69. For the cylinders shown in the figure, the plain concrete strength at the test age was 206 kgf/cm^2 (= 20.2 MPa), and the F2N-CS-P5 and the F2H-CS-P5 specimens were confined by 6 mm diameter spiral reinforcement having a yield strength of 1151 MPa (= 11740 kgf/cm^2) and 6 mm diameter spiral reinforcement having a yield strength of 316 MPa (= 3225 kgf/cm^2), respectively, with pitch of 5 cm. From these tests, it was found that, in comparison with the monotonic loading curve, the cyclic loading curves of the cylinders with high strength spirals suddenly degradated at a certain concrete strain due to fatigue of the confined core concrete, while those with ordinary strength spirals followed closely the stress-strain curves under monotonic loading.

As a result of the above test results, when high strength spirals are used in practical design it must be remembered that the deformability of the confined concrete under cyclic loading may be significantly less than that predicted from the monotonic stress-strain curve. At this stage there is no precise method available to predict at what strain or cycles the fatigue failure occures under cyclic loading.

2.5 CONCLUSIONS

As a result of the experimental and analytical studies of the behaviour of confined concrete presented in this chapter, along with the review of the stress-strain models previously proposed, the following conclusions are reached:

1. For concrete confined by circular hoops or spirals, the stress-strain model proposed by Mander et al [2.6] gives the largest estimate of the strength and ductility enhancement due to lateral confinement when compared with the models proposed by Desayi et al [2.15], Park and Leslie [2.16] and Watanabe et al [2.17]. For concrete confined by rectangular hoops with or without supplementary cross ties, the Mander et al model [2.6] also gives the largest estimate of the strength and ductility enhacement when compared with the models proposed by Scott et al (the modified Kent and Park model [2.29]) and Sheikh et al [2.13]. Since the stress-strain model proposed by Mander et al has been calibrated by tests on realistically sized columns with realistic reinforcing arrangement, for design purposes this model might be more

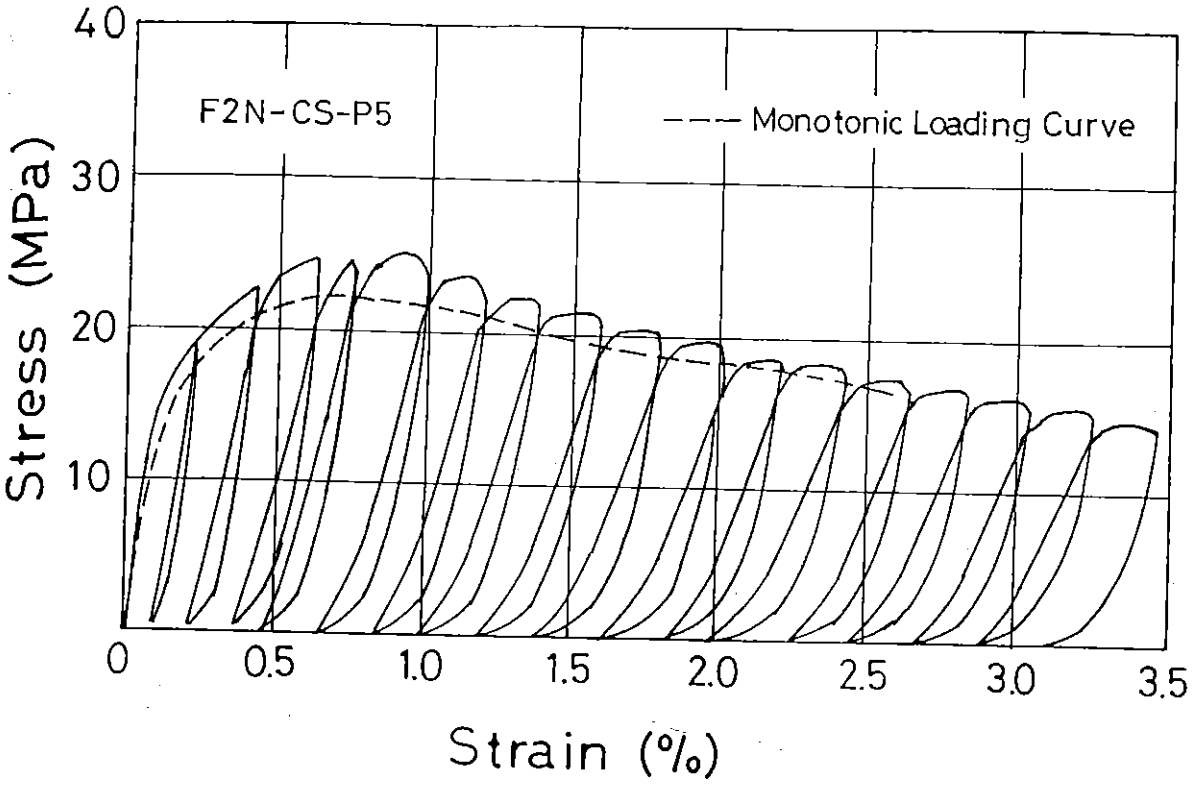

(a) Cylinders Confined by ordinary Strength spirals

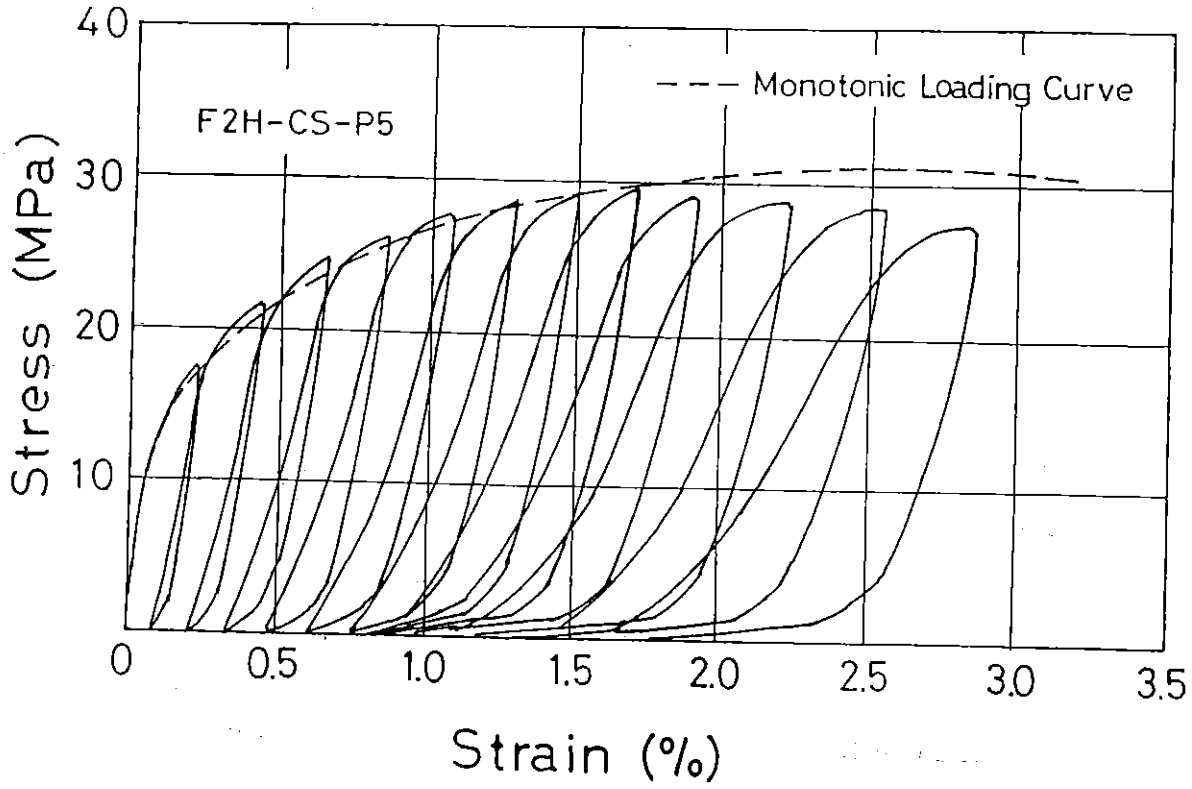

(b) Cylinders Confined by High Strength Spirals

Fig. 2.69 Comparison Between Monotonic and Cyclic Loading Curves [2.61].

reliable than the other models which were calibrated using comparatively small sized columns without longitudinal reinforcement, provided that the strengths of the plain concrete and the transverse reinforcement are within the range ordinarily used.

2. The gauge length used for the strain measurement of concrete significantly affects the slope of the falling branch of the stress-strain curves of confined concrete. This is because, when diagonal failure planes (= diagonal shear sliding planes) are formed after peak load, the strain in the falling branch region is the apparent strain calculated by dividing the gauge length into the relative displacement between the parts separated by those planes. The gauge length used in the Mander et al tests was equal to the least section dimension, which is shorter than that used by other investigations discussed in this chapter. This will be the main reason why the Monder et al model gives the most gentle slope for the falling branch region.

3. The most appropriate gauge length to be adopted in column tests, for application to analyses of columns under combined bending and axial load, cannot be simply stated because the length of compression failure zone along the column axis varies depending on the axial load level and moment gradient imposed. As a future study, a method to appropriately modify the strains measured in axial compression tests with a certain gauge length may need to be established for application to flexural members with various axial load level.

4. The main variables used to determine the stress-strain models for confined concrete introduced in this chapter are; (1) the configuration of transverse reinforcement, (2) the volumetric ratio of transverse reinforcement, (3) the yield strength of the transverse steel, (4) the spacing of the transverse reinforcement, (5) the compressive strength of plain concrete, (6) the content of longitudinal reinforcement and (7) the rate of loading. However, in addition to the above factors, when a member is subjected to flexure and shear with or without axial load, the strain gradient in member section and the stress gradient along the longitudinal axis of the member can also significantly affect the stress-strain relationships of confined core concrete.

5. With respect to the influence of the strain gradient, it is emphasized that the magnitude of the hoop tensile strains observed in extreme compression fibre region in eccentrically loaded columns was significantly smaller than that attained in the columns subjected to axial compression, when the extreme compression fibre strain in the eccentrically loaded columns was the same as the compression strain in the axially loaded columns. Hence, when the improvement in the strength and ductility of confined concrete is evaluated in terms of the lateral pressure provided by the transverse reinforcement, the effectiveness of the transverse reinforcement is significantly reduced by the presence of a strain gradient in the section.

6. The influence of variations in the compressive strength of the plain concrete, f'_{co}, on the strength increase of the confined concrete is not significant at least for f'_{co} up to 60 MPa, when the strength increase of the confined concrete is expressed in terms of the lateral pressure as in Eq. 2.1" in Section 2.3.3.1.

7. The influence of variations in the compressive strength of the plain concrete, f'_{co}, on the ductile behaviour of columns is significant and hence all stress-strain models introduced in this chapter involve this factor. However, those models may need to be modified when applied to cases when f'_{co} is more than 80 MPa, as shown by the study by Muguruma et al [2.47].

8. The evaluation of the confining effect of longitudinal reinforcement is not consistent between researchers. However, even if the effect of the longitudinal reinforcement is appreciable, it is not significant when compared with the other factors. This is because the bending stiffness of longitudinal reinforcement, which determines its efficiency of confinement, is rapidly lost from a comparatively small compressive strain such as 0.2 % due to its yielding in axial compression. A further reason is that when the bending stiffness of longitudinal reinforcement is maintained, under small axial strains less than 0.2 %, the confining effects of the longitudinal reinforcement as well as of lateral reinforcement do not appear explicitly since they apply passive confinement.

9. In axial loading tests on concrete cylinders confined by spirals with yield strength of from 161 MPa to 1352 MPa, the strength and ductility of the

confined concrete were remarkably enhanced as the yield strength of the spiral steel was increased. The observed strength increase of the confined concrete was proportional to the square root of the yield strength of the spiral steel, although most of the stress-strain models assume that it is proportional to the yield strength of the spiral steel. For this fact, the following three reasons can be considered. Firstly, in the case of spirals with yield strength of more than 1000 MPa, due to passive confinement the lateral pressure is gradually increased, as the damage of concrete core progresses, and the maximum lateral pressure which is attained by yielding of the spirals can only be reached at a comparatively large compressive strain of concrete about 2 to 3 %. Secondly, when high strength steel spirals were used, bearing failure of the core concrete may have occurred beneath the spiral bars due to the high local pressure before reaching the maximum possible load carrying capacity of the core concrete. Thirdly, at the ultimate condition, the area of critical section of the concrete core after spalling of the concrete in the ineffectively confined region between spiral bars was significantly smaller in the case of high strength spirals than in the case of ordinary strength spirals. This third reason may be eliminated when the area of the critical section is rigorously evaluated to estimate the real stress condition in the section.

10. The failure of the concrete cylinders confined by the steel spirals with yield strength more than 1000 MPa was sudden and explosive due to crushing of the core concrete between the spiral bars or to the bearing failure beneath the spiral bar, whereas the failure observed for the concrete cylinders with ordinary strength steel spirals was normally gradual and gentle.

11. When cyclic loading was applied to cylinders confined by steel spirals with yield strength less than 400 MPa, the envelope stress-strain curves normally coincided with the stress-strain curves obtained from monotonic loading tests, regardless of the strain accumulated prior to a particular cycle. Hence, for concrete confined by ordinary strength spirals, it can be assumed that the monotonic loading curve represents the skeleton curve of the stress-strain curves under cyclic loading, as is normally assumed for modelling of cyclic loading curves. On the contrary, when cyclic loading with constant maximum load is applied to the cylinders confined by spirals with yield strength of more than 1000 MPa, fatigue failure occurred before

the cyclic loading curves came across the monotonic loading curves. Moreover, when cyclic loading was applied so as to follow the monotonic loading curve, the cyclic loading curves rapidly degraded when a certain compressive strain of concrete was reached and deviated from the monotonic loading curve. Thus, when concrete confined by high strength spirals is subjected to cyclic loading, the compressive strain at failure significantly decreases as the strain accumulated prior to the failure cycle increases. As a future research project, those characteristics of concrete confined by high strength spirals need to be quantitatively evaluated in terms of earthquake design practice, although the relationship between the fatigue cycles to the applied stress level has been evaluated statistically in this study.

CHAPTER THREE

ANCHORAGE DETAILS OF TRANSVERSE REINFORCEMENT

3.1 INTRODUCTION

3.1.1 General Problems in Anchorage of Transverse Reinforcement

Considerable efforts have been made in recent years to develop improved seismic design provisions for reinforced concrete columns in bridge substructures and building frames. The need for effective design provisions has been emphasized by damage caused to bridges and buildings during severe earthquakes. For example, the San Fernando earthquake in Southern California in February 1971 caused extensive damage to a number of recently constructed reinforced concrete columns in bridges and buildings, mainly because of inadequate detailing of those structural members for ductility (see Fig. 3.1). In this earthquake, the anchorage of transverse reinforcement by tension splices in the cover concrete without welding was shown to be a poor detail because circular bridge columns failed due to ineffective anchorage of lapped circular hoops when the cover concrete spalled [3.1]. As another example, it is of note that some bending errors which resulted in hoop bar hooks having a turn of less than 135° at the ends, due to poor execution of work, was listed as one of the causes for the failure and collapse of reinforced concrete columns in the 1968 Tokachi-oki earthquake in Japan [3.2, 3.3]. It can be said that the most important design consideration for ductility in the potential plastic hinge region of reinforced concrete columns is the provision of sufficient transverse reinforcement with adequate anchorage detail, in order to confine the compressed concrete, to prevent buckling of the longitudinal reinforcement, and to prevent shear failure.

In the plastic hinge region of columns, the transverse reinforcement normally yields due to the tension force caused by the lateral expansion of the confined concrete, the outward force from the longitudinal bars, and the

opening of inclined flexural shear cracks, when the columns are loaded far into inelastic condition. Hence, transverse reinforcement needs to be securely anchored in order to be able to sustain the yield force of the hoop and cross tie legs until the final deformation condition of the column is reached, otherwise some loss of effectiveness of the transverse reinforcement due to anchorage failure will occur. For this reason, seismic design codes for concrete structures such as NZS3101:1982 [3.4], CEB-FIP Model Code:1982 [3.5] and JASS-5 :1979 [3.6] specify that hoops and cross ties in the columns shall be anchored by 135° end hooks which turn around longitudinal bars and embedded in the concrete core or by welding of those tie bar ends. However, those anchorage details can sometimes result in a complicated reinforcing fixing job, especially on construction sites. This is because the hoops and cross ties need first to be placed over the ends of longitudinal bars and then shifted along the longitudinal bars to their correct poasition in the reinforcing cage. That is, the hoops and cross ties cannot be inserted directly through the side of the cage into their correct position.

In order to ease the difficulty of placing transverse reinforcement several alternative details for cross ties which simplify the fabrication of reinforcing cages have been used in the United States and other countries. One alternative detail involves the use of cross ties with a 90° hook at one end and a 135° hook at the other end. Such cross ties can be inserted directly into the position from each side of the cage (see Fig. 3.2 (b)) after the hoops are in place. Those end hooks are alternated along the longitudinal bar as shown in Fig. 3.2 (b), in order to avoid the consecutive alignment of 90° end hooks forming weak lines of anchorage along the longitudinal bar. This anchorage detail is permitted by the ACI code: 318-89 [3.7] and the Caltrans code: 1983 [3.8]. Another alternative detail involves the use of 'J' bars which have a 135° end hook and are inserted from each side of the cage and lapped in the core concrete (see Fig. 3.2 (c)), as introduced in the SEAOC code: 1975 [3.9]. Such 'J' bars can be used if the column size permits development of the tension splice. A further alternative detail is to use 'U' bars which are inserted from each side of the cage and lapped in the core concrete (see Fig. 3.2 (d)). Those alternative anchorage details are convenient when fabricating reinforcing cages because they can be inserted from each side of the reinforcing cage rather than being placed over the ends of the longitudinal bars and being brought along those bars. However,

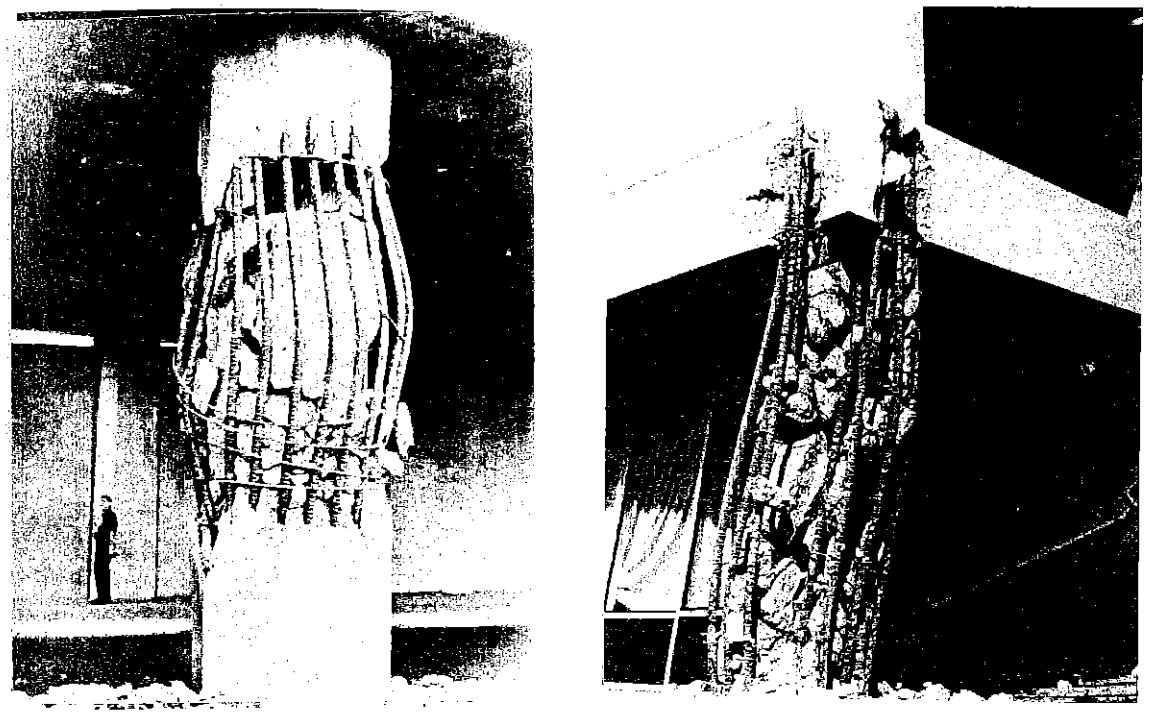

Fig.3.1 Damage Caused to Some Reinforced Concrete Columns in Bridge and Building Structures During the 1971 San Fernando Earthquake.

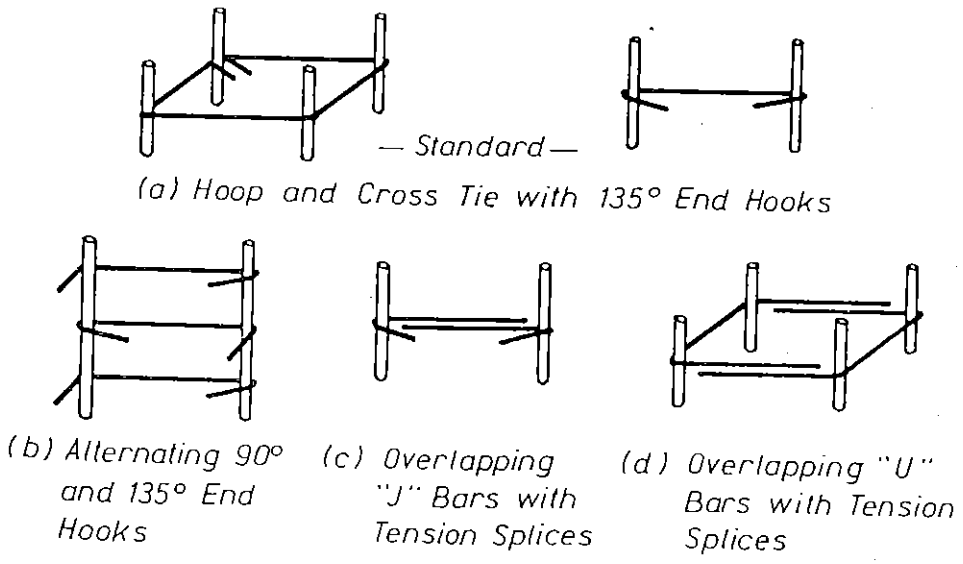

Fig.3.2 Standard and Alternative Details for Anchoring Transverse Reinforcement for Reinforced Concrete Columns.

when those alternative anchorage details for cross ties are used in earthquake design practice, their effectiveness need to be examined with respect to the following points:

[Cross Ties with 90° and 135° End Hooks]

The efficiency of a hoop or a cross tie anchored by a 90° end hook, instead of a conventional 135° or 180° end hook, may be suspect because a 90° end hook can be more easily straightened by the outward force from the confined concrete and longitudinal bar after spalling of cover concrete. The performance of 135° or 180° end hooks is to be better because the end hooks are embedded in the core concrete. When 90° and 135° end hooks of the cross ties are alternated along longitudinal bars as shown shown in Fig. 3.2 (b), buckling of a compressed longitudinal bar may eventually occur over two spacing of tie sets with largest lateral movement of the longitudinal bar at the 90° end hook because the lateral restraint applied by a 90° end hook is weaker than for a 135° or 180° end hook after spalling of the cover concrete. Thus the alternating arrangement of 90° end hooks may not be completely effective and tests are necessary to check the efficiency of this end anchorage detail.

As a matter of course, the cross ties with 90° and 135° end hooks must be restricted for use only as interior cross ties. This is because, when the cross ties with 90° and 135° end hooks are used instead of peripheral rectangular hoops, separation between those cross ties and the concrete core surface can easily occur after spalling of cover concrete, since a 90° end hook will not prevent a tie from moving sideways from the longitudinal bar.

['J' and 'U' Bars with Tension Splices]

The transverse bar details using 'J' and/or 'U' bars must also retestricted for use only as interior cross ties, because the tension splices if placed in the cover concrete lose their effectiveness completely after spalling of the cover conrete. A further requirement for when 'J' and 'U' bars are used for interior cross ties is that the columns section dimension should be large enough to give adequate development length for the tension splices of the tie legs. The length of the lap splices of the tie legs needs to be at least 24 d_b, where d_b= tie bar diameter, when deformed bars with diameter of less than 20 mm and concrete with compressive strength of more than 20 MPa are used, if the provisions for tension splices of longitudinal bars in NZS

3101 [3.4] are applied to tension splices of ties. However, even if the above lap length is provided, the use of tension splices to anchor tie legs may not be fully effective if flexural cracks in the concrete form perpendicular to the longitudinal axis of the column and hence either run along the tie legs or close to and parallel to the tie legs. If wide flexural cracks occur along the tie legs sufficient bond strength to secure the anchorage of the splices may not be available. In such a case, 'J' and 'U' bars may need to be anchored by providing additional end hooks at the tension splice ends as shown in Fig. 3.3. On the other hand, if inclined flexural cracks occur rather than flexural cracks, most of the cracks will not run parallel to the tie bar direction and as a result tension splices in the ties of a such a column could be fully effective. Also, the performance of the tension splices will be affected by the axial compressive load level of the column, since a large axial load level will mean a large neutral axis depth, which in turn means that compression will exist over a significant length of the tension splice thus reducing the effect of cracking. It is evident that tests are necessary to check for spliced cross ties the required length of tension splices, the effect of cracking of the concrete, and the effect of axial compressive load level in the column.

In this chapter, the above mentioned points are investigated by conducting seismic load tests on eight realistically sized columns which contained the various arrangements of transverse reinforcement shown in Fig. 3.2.

3.1.2 Comparison of New Zealand, U. S., European and Japanese Code Provisions for the Anchorage of Transverse Reinforcement

It is of interest to compare the design provisions for the anchorage of rectangular transverse reinforcement given by some current seismic design codes in New Zealand, United States, Europe and Japan. Some code recommendations for the anchorage of the ends of transverse bars which are bent around longitudinal bars are shown in Fig. 3.4.

The New Zealand code , NZS 3101:1982 [3.4] requires at least a 135° turn and an extension at the free end of the bar into the core concrete of either 8 d_b for plain round bars or 6 d_b for deformed bars. Typical arrangements of transverse reinforcement in potential plastic hinge regions of rectangular columns are represented by Figs. 2.8 (Chapter 2) and 3.5 which

(a) 'J' Bars with Additional 90° End Hooks (b) 'U' Bars with Additional 90° End Hooks

Fig.3.3 Alternative Anchorage Details for 'J' and 'U' bars with Additional 90° End Hook.

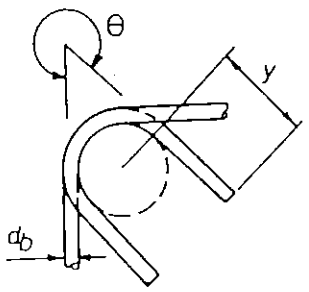

	Minimum Value	
	y	θ
NZS3101[3.4]	8 d_b for plain round bars, 6 d_b for deformed bars	135°
ACI 318 [3.7]	6 d_b	135°
	6 d_b	90°*
SEAOC [3.9]	10 d_b	135°
CEB-FIP [3.5]	10 d_b	135°
AIJ [3.2]	6 d_b	135°

* Where alternated with 135° end hooks

Fig.3.4 Anchorage of Transverse Reinforcement Around a Longitudinal Bar According to Some Codes.

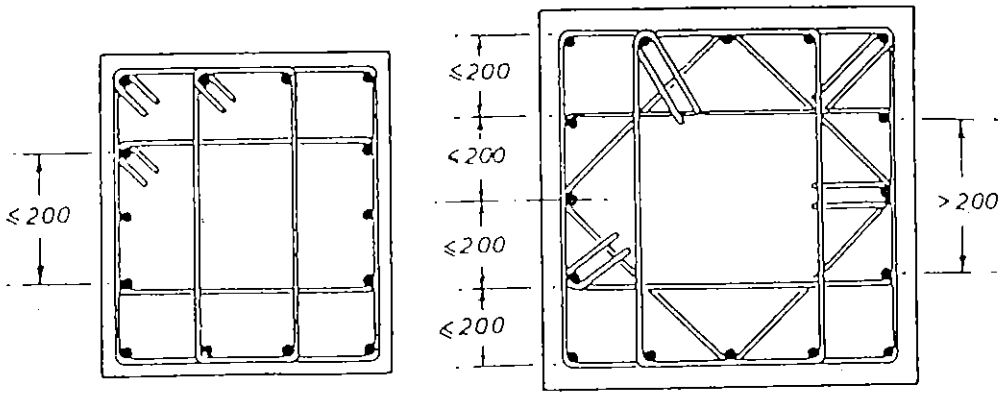

(a) Three overlapping hoops (b) Four overlapping hoops

Fig.3.5 Examples of Transverse Reinforcement in Columns Using Hoops With and Without Cross Ties According to the Commentary on NZS 3101 [3.4]. (Dimensions in mm)

are taken from the commentary of NZS 3101. NZS 3101 also requires that the longitudinal reinforcement be placed not further apart between centres than 200 mm (7.9 in.) and that the center to centre spacing across the column section between cross linked longitudinal bars be not further apart than 200 mm (7.9 in.).

The American Concrete Institute building code, ACI 318-89 [3.7], includes in its Commentary the example of transverse reinforcement by one peripheral hoop and three cross ties in the potential plastic hinge region of a rectangular column shown in Fig. 2.24 in Chapter 2. Anchorage of the hoop bar is achieved with a 135° turn and a 6 d_b extension. The cross ties have a 135° turn and a 6 d_b extension at one end and a 90° turn and a 6 d_b extension at the other end. Consecutive cross ties have their 90° hooks on opposite sides of the column, evidently to counter the possible loss of efficiency of the 90° end hook which is not embedded in the concrete core when the cover concrete spalls. Note that the ACI building code requires the centre to centre spacing across the column section between cross linked bars to be not greater than 14 in. (365 mm).

The recommendations of the Structural Engineers Association of California [3.9] includes in its commentary the example of transverse reinforcement provided in potential plastic hinge regions shown in Fig. 3.6. The use of cross ties with tension splices ('J' bars) is illustrated in this figure.

The second draft of the seismic design appendix to the the model code of the European Concrete Committee - International Federation of Prestressing [3.5] requires the ends of transverse bars to be anchored by at least a 135° turn and a 10 d_b extension of the free end of the bar into the core concrete. Typical details of transverse reinforcement are similar to those shown in Figs. 2.8 and 3.5.

The code of the Architectural Institute of Japan [3.6] requires the ends of transverse bars to be anchored by at least a 135° turn. In the appendix of the commentary a 6 d_b extension of the free end of the transverse bar into the core concrete is specified.

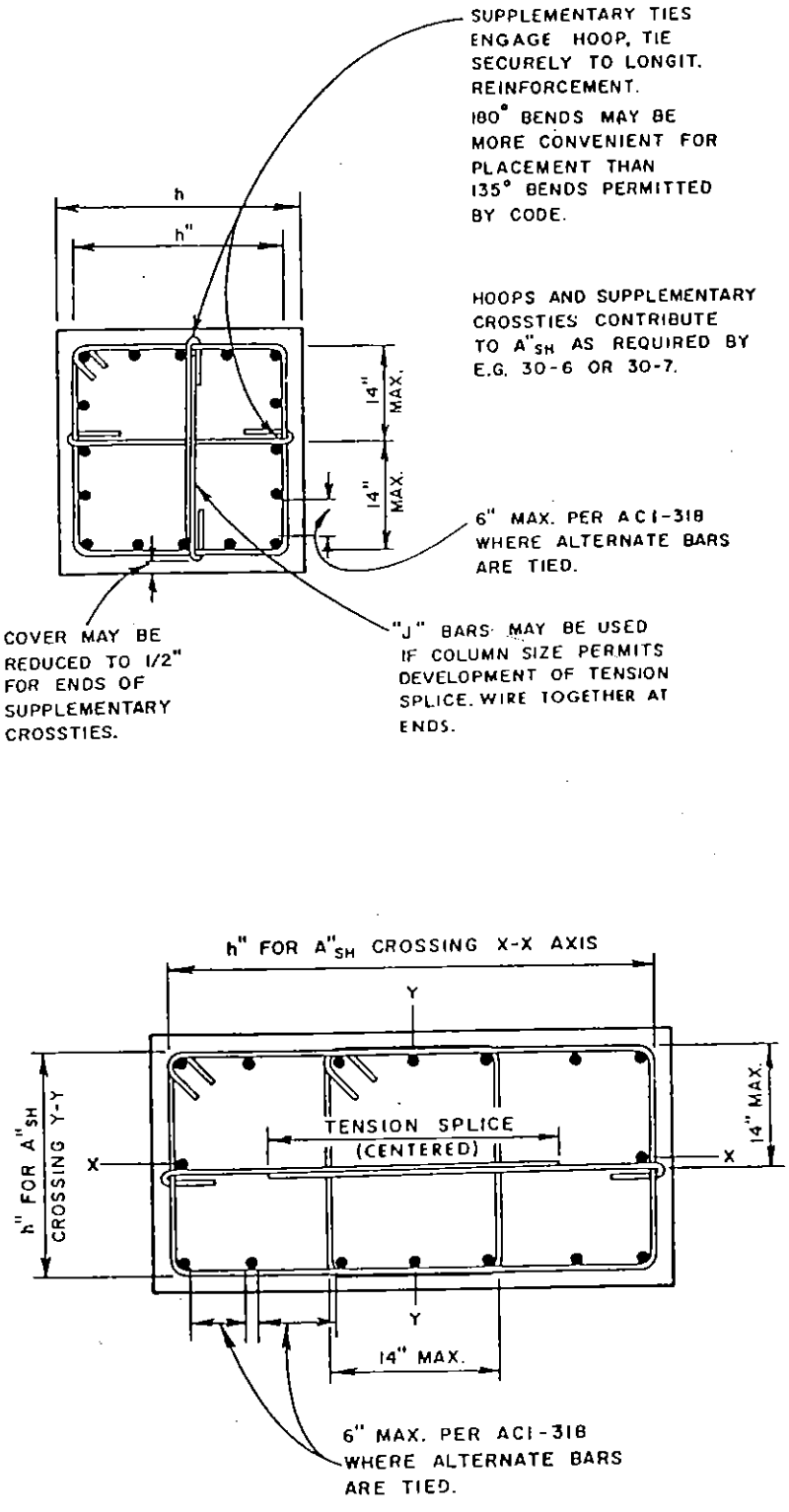

Fig.3.6 Examples of Transverse Reinforcement in Columns According to the Commentary of the SEAOC Recommendations [3.9]. (1 in = 25.4 mm).

3.1.3 Previous Research into Anchorage of Transverse Reinforcement

There has been some previous research into the anchorage of transverse reinforcement in reinforced concrete columns subjected to seismic loading.

The end anchorage for hoops and cross ties from plain round bar comprising a 135° turn and 8 d_b extension at the free end, specified in the New Zealand code, has been found to be effective even at high displacement ductility factors by extensive tests on columns subjected to compressive load and cyclic flexure conducted at the University of Canterbury [3.10]. As far as the author of this thesis is aware, experimental studies on the effectiveness of cross ties anchored by tension splices have not been reported, except for those conducted by the author and Park [3.11, 3.12] which will be described in this Chapter. The effectiveness of cross ties with 90° hooks at one end and 180° hooks at the other end has been investigated in the several studies discussed below.

Moehle and Cavanagh [3.13] have tested reinforced concrete columns under concentric monotonic compression with various types of transverse reinforcement linking the intermediate longitudinal bars. In these tests degradation of column axial load carrying capacity occurred more rapidly in the columns provided with cross ties with 90° and 135° end hooks alternated end for end over the column height than in the columns provided with cross ties with 180° end hooks. However, in this study it was concluded that the differences in confinement effectiveness between those columns appeared not to be significant. This conclusion was derived from theoretical moment-curvature analyses on assumed column sections with axial load levels of 0.1 to 0.6 $f'_c A_g$ (where f'_c = compressive strength of concrete determined from control cylinders and A_g = gross area of column section) using measured stress-strain curves. It must be noted that the columns of Moehle and Cavanagh were tested under monotonic axial compression and it is apparent that axial compression and cyclic flexure, as in seismic loading, would impose a worse loading condition.

Oesterle et al [3.14] have tested several reinforced concrete walls with vertical boundary members containing reinforcement which was detailed in various ways as for columns. Since cyclic horizontal loads were applied to

those walls with no axial load, the boundary elements were subjected to cyclic eccentric tension-compression loading. From the tests on the wall specimens which had the boundary elements reinforced using the transverse detail shown in Fig. 3.7, the use of cross ties with a 90° turn at one end and a 135° turn at the other end, alternated end for end over the height of the boundary members, was found to result in satisfactory behaviour during seismic load reversals in the inelastic range. A measured load versus deflection relationship for one of the tested walls is also shown in Fig. 3.7. Although in these tests a tension splice detail shown in Fig. 3.6 was not used for the boundary elements, Oesterle et al have recommended that a tension splice detail should not be used in the hinging region of vertical boundary elements of walls based on the observation of cracking condition. They state that, because of severe cracking that can develop in the boundary elements under inelastic load reversals, it is likely that the tension splices in the cross ties would eventually become ineffective. This statement is of importance if the spliced cross ties are provided to fully resist the applied shear force for when the boundary element is subjected to eccentric tension load in a particular loading cycle and flexural tension cracks open wide along or parallel to the tie legs. However, the view could be taken that spliced cross ties could be considered reasonable if they are used only to confine the core concrete and to restrain the buckling of longitudinal reinforcement. This assumes that that adequate shear reinforcement is provided in the web of walls to resist the design shear force. The reason for this view can be described as follows. When the spliced cross ties are required to work as confinement of the core concrete and restraint against buckling of the longitudinal reinforcement, the boundary element needs to be under eccentric compressive loading. Under such circumstances the flexural tension cracks formed in the boundary element in the previous loading cycle may be fully closed so as not to significantly degrade the bond condition of the spliced tie legs. Hence, if an adequate amount of shear reinforcement is provided for the web of walls to resist the design shear, the reinforcing detail shown in Fig. 3.6 may be used for boundary elements. It is also noted that, since axial load was not applied to the walls tested by Oesterle et al [3.14], their recommendations may be limited to when a comparatively small axial load is imposed in practical design.

Hanson and Rabbat [3.15] have conducted seismic load tests on sixteen full-scale columns having the sections shown in Fig. 3.8. Light weight concrete was used for thirteen of those columns and normal weight concrete was used for the remainder. The applied axial load was 10 % of column axial load design strength, except for two colums in which 20 and 30 % of the column axial load design strength were applied. Based on the test results, they concluded that cross ties having a 135° end hook at one end and a 90° end hook at the other end, alternated end for end along the column, performed very satisfactorily when confining the column core of both light weight and normal weight concrete columns.

Ozcebe and Saatcioglu [3.16] have tested four reinforced concrete column specimens under simulated severe seismic loading. Those columns had the transverse reinforcing details shown in Fig. 3.9. The applied axial load level corresponded to approximately 12 % of the nominal column capacity, or 20 % of the column design strength. They reached the following conclusions based on the test results; (1) longitudinal bars, if not engaged by a corner of a hoop or a hook of a cross tie, are incapable of providing confinement in hinging regions, (2) cross ties with a 135° hook at one end and 90° hook at the other end perform as satisfactorily as those with 135° hooks at both ends.

In the study by Sheikh et al [3.17], using the various transverse reinforcing details shown in Fig. 3.10, two series of column tests were carried out. In the first series of tests, fifteen columns were tested under montonic axial loading. In the second series, sixteen columns were tested under monotonic flexure to large inelastic deformations, while they were simultaneously subjected to constant axial loads of between 0.40 to 0.78 f'_c A_g. With respect to the cross ties with 90° hooks at one end and 180° hooks at the other end, based on the results of this study, Sheikh et al concluded as follows; (1) cross ties with 90° hooks at one end and 180° hooks at the other end are effective in confining concrete at small deformations, (2) at large deformations when the cover concrete spalled off, the 90° end hooks tend to open out resulting in a rapid loss of column load carrying capacity, (3) this was particularly apparent in specimens tested in flexure under high axial load levels.

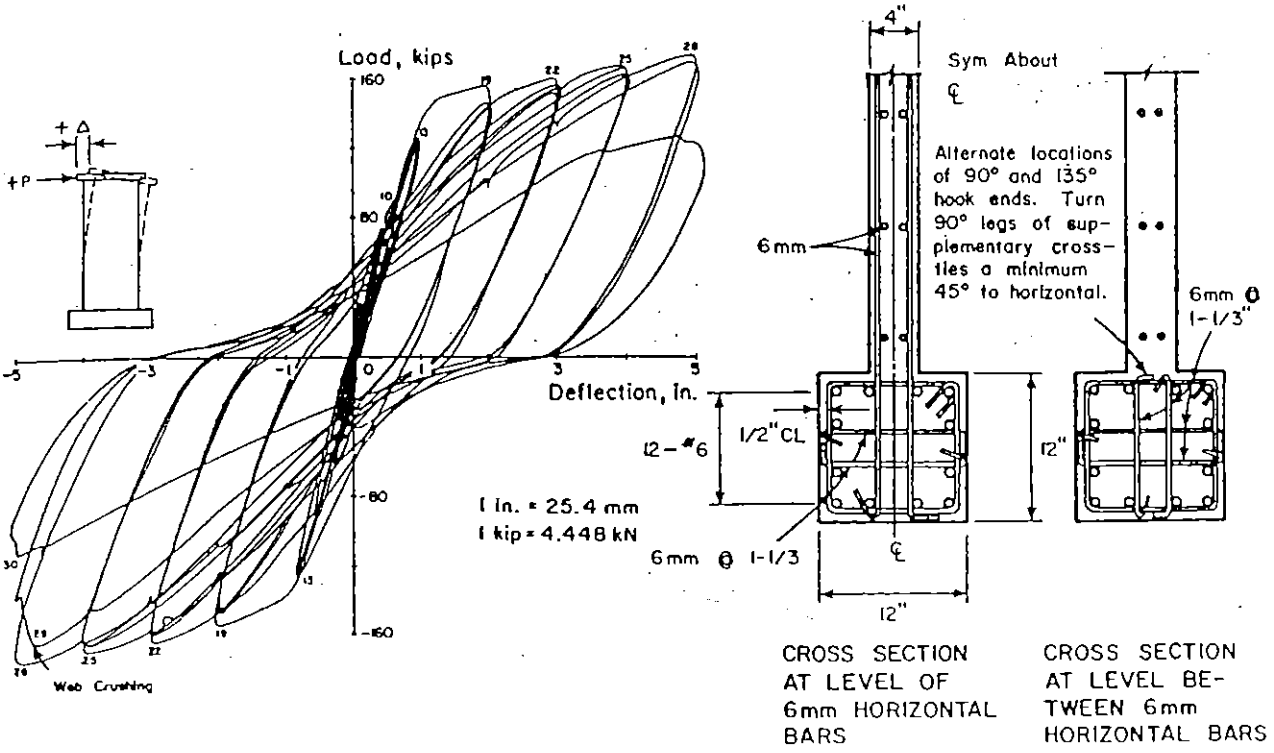

Fig.3.7 Load versus Deflection Relationship Measured for a Wall with Boundary Elements Tested by Oesterle et al [3.14].

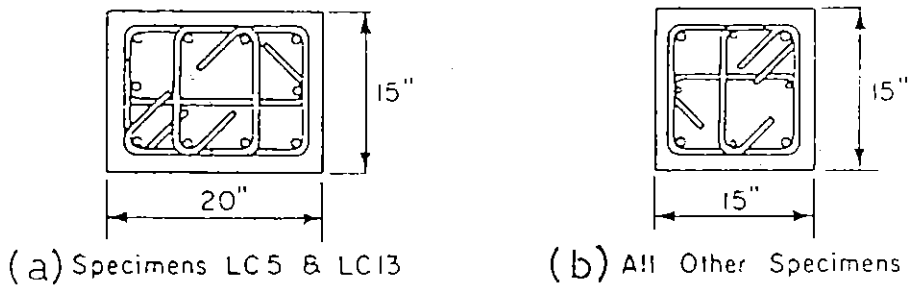

Fig.3.8 Column Sections Used in the Tests of Hanson and Rabbat [3.15].

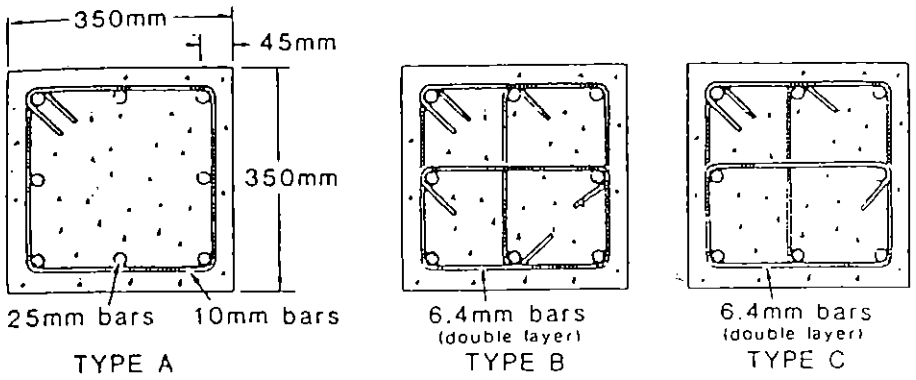

Fig.3.9 Column Sections Used in the Tests by Ozcebe and Saatciglu [3.16].

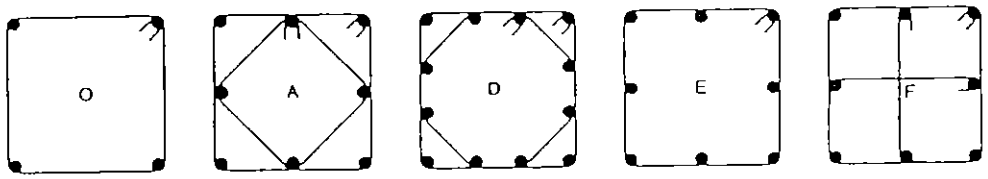

Fig.3.10 Configurations of Transverse Reinforcement Used in the Tests Sheikh et al [3.17].

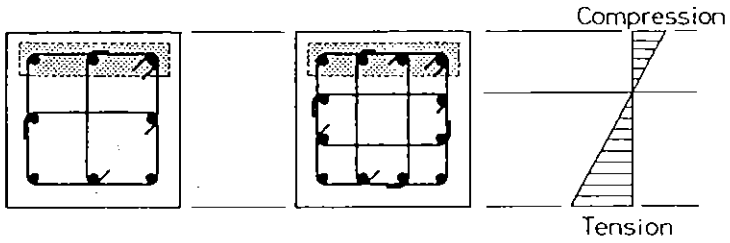

(a) 3-Longitudinal Bars in Compression (b) 4-Longitudinal Bars in Compression (c) Assumed Strain Distribution

Fig.3.11 Compression Reinforcement Corresponding to the Assumed Strain Distributiton.

As is apparent from the above studies, assessments of the performance of cross ties with 90° hooks at one end and 180° hooks at the other end are not always consistent. The inconsistency of the assessments may be attributed not only to the difference in types of loading but also to the different volumetric ratios of compression reinforcement to concrete core, spacings of hoop sets, ratios of compression reinforcement restrained by 90° end hooks to the total compression reinforcement, and so on. For example, the area ratios of compression reinforcement restrained by 90° end hooks to the total compression reinforcement are 33 % and 25 % for the columns illustrated in Fig. 3.11 (a) and (b), respectively.

It is evident that more tests are needed on reinforced concrete columns subjected to seismic loading to compare the performance of various anchorage details for transverse reinforcement. The importance of good detailing of reinforcement in reinforced concrete structures designed for earthquake resistance cannot be overemphasised.

3.2 COLUMN TESTS WITH VARIOUS ANCHORAGE DETAILS FOR TRANSVERSE REINFORCEMENT

3.2.1 Test Programme

3.2.1.1 Details of Column Units

Two series of column units were constructed and tested. The first series of four column units (Units 1 to 4) had a total height of 3.9 m and 400 mm square cross sections, as shown in Fig. 3.12. The second series of four column units (Units 5 to 8) had a total height of 2.75 m and 550 mm square cross sections, as shown in Fig. 3.13. The main variable for the column units was the type of transverse reinforcement and anchorage detail of that reinforcement. Other variables were the level of axial compressive load applied and the aspect ratio of the column. The mechanical properties of the materials and other details of the column units are listed in Table 3.1.

All concrete was normal weight with a maximum aggregate size of 20 mm. The concrete was cast with the columns in a horizontal position in the case of Units 1 to 4. For Units 5 to 8, the concrete for the base block

Table 3.1 Mechanical Properties of Materials and Other Details of Column Units

Column Unit	Concrete		Longitudinal Reinforcement (HD20 - Grade 380)		Transverse Reinforcement (D12 - Grade 275)		Sectional Dimensions of Columns b x h (mm)	Ratio of Shear Span to Full Section Depth	Ratio of Total Area of Longitudinal Reinforcement to Gross Area of Section	Hoop Sets in End Regions		Axial Load Level $\frac{P}{f'_c A_g}$
	Compressive Strength f'_c (MPa)	Modulus of Rupture f_r (MPa)	Yield Strength f_y (MPa)	Ultimate Strength (MPa)	Yield Strength f_{yh} (MPa)	Ultimate Strength (MPa)				Spacing (mm)	Volumetric Ratio (to Concrete Core)	
1 to 4	25.6	3.6	474	721	333	481	400 x 400	4.0	1.57%	80	2.55%	0.2
5 and 6	32.0	4.6	511	675	325	429	550 x 550	3.0	1.25%	110	1.70%	0.1
7 and 8	32.1	4.4	511	675	325	429	550 x 550	3.0	1.25%	90	2.08%	0.3

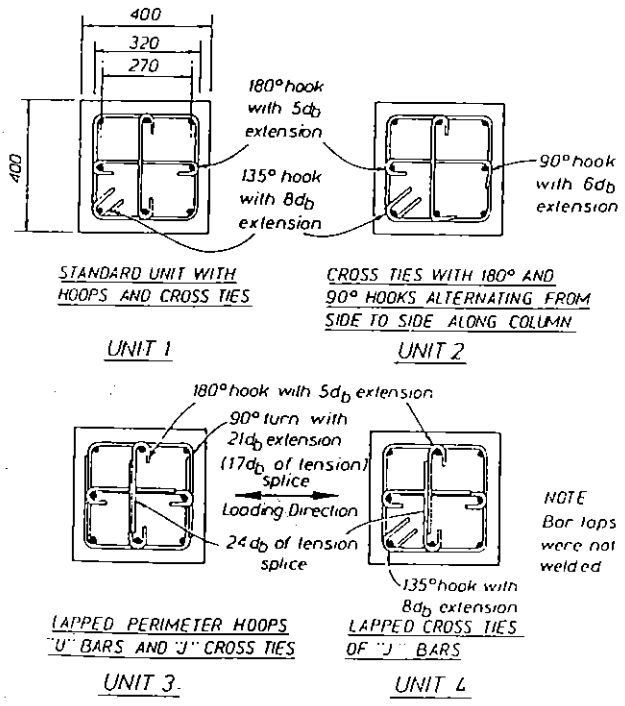

(a) Transverse Sections

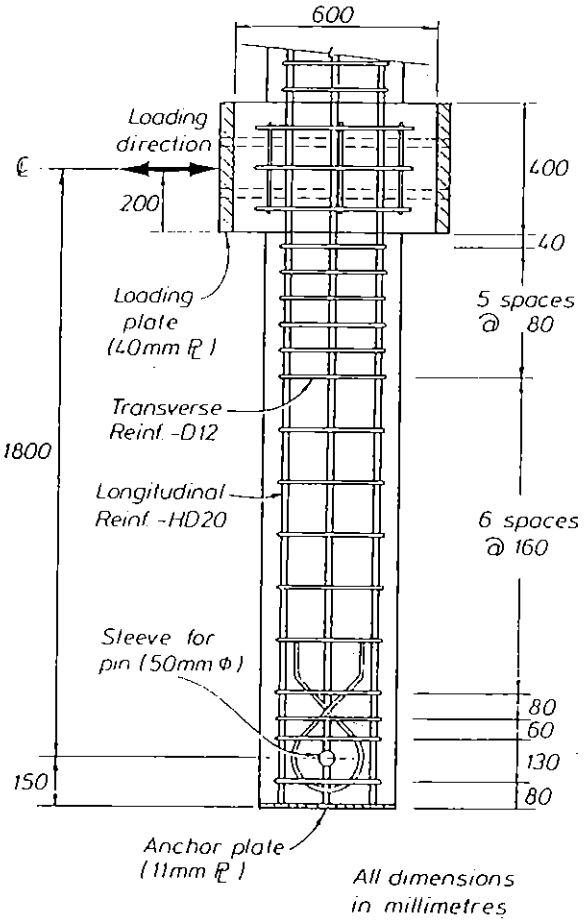

(b) Longitudinal Section

Fig.3.12 Sections of Column Units 1 to 4 Showing Details of Reinforcement.

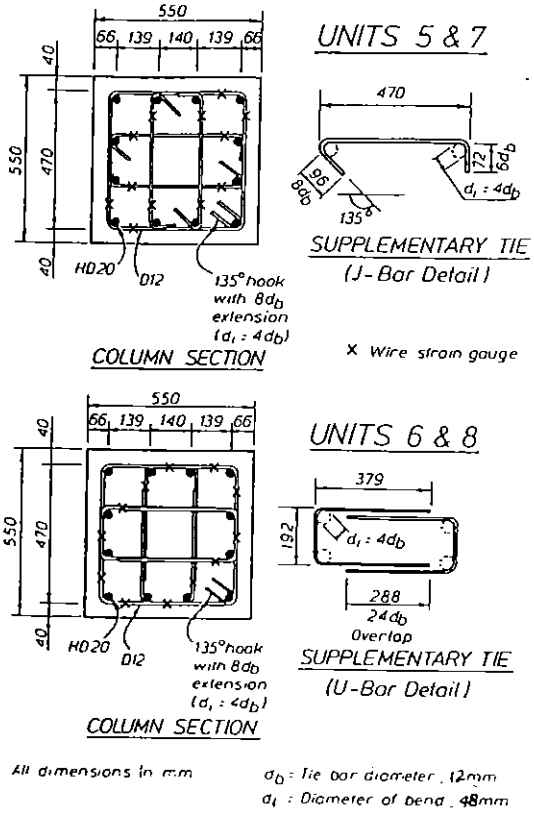

(a) Transverse Sections

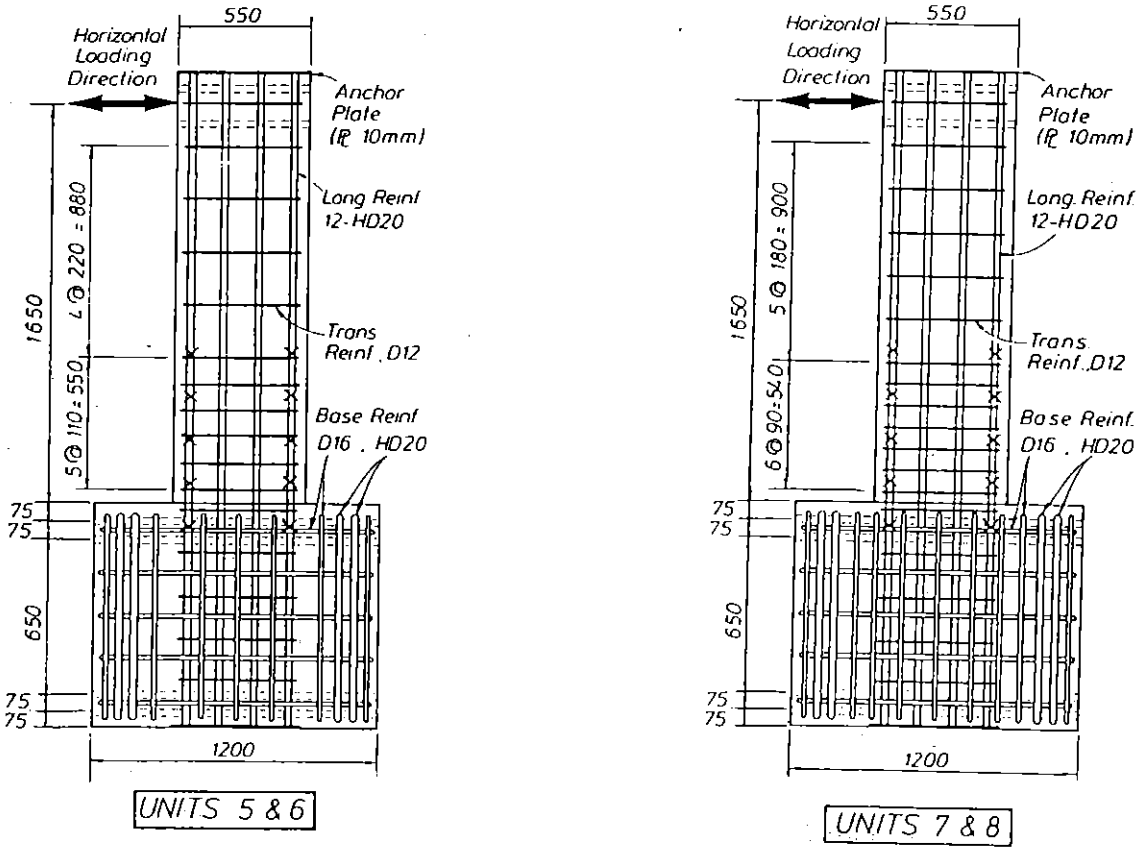

(b) Longitudinal Sections

Fig.3.13 Sections of Column Units 5 to 8 Showing Details of Reinforcement.

which simulated an adjoining footing or pier cap was cast first and 23 days later each column portion was cast with the columns in a vertical position. The compressive strength and modulus of rupture for the column portion of each unit, listed in Table 3.1, were measured from 100 mm diameter by 200 mm high cylinders and 152 x 152 x 473 mm or 120 x 120 x 480 mm prisms. These cylinders and prisms were tested at the stage when the columns were tested, namely, at age 2 months for Units 1 to 4 and at age 4 to 5 months for Units 5 to 8. For the base blocks of Units 5 to 8, concrete with higher strength than that of column portion was used in order to prevent failure occurring in the base blocks. For the base blocks of Units 5 and 6 the control cylinder strength at the test age was 33.2 MPa, and for the base blocks of Units 7 and 8 it was 41.1 MPa.

For each column the longitudinal reinforcement was from 20 mm diameter Grade 380 deformed bar and the transverse reinforcement was from 12 mm diameter Grade 275 deformed bar. The measured stress-strain curves for the reinforcing steel are shown in Fig. 3.14. The strains were measured by a Batty extensometer with a gauge length of 50 mm. The measured steel strengths are also listed in Table 3.1. The amount and spacing of the transverse reinforcement in the plastic hinge regions of the columns was determined to satisfy the provisions of NZS 3101 [3.4] for both confinement and shear. Due to the restriction of hoop spacing, and the limitation of bar sizes available, the transverse reinforcement actually provided in the columns was in excess of the NZS 3101 required quantities by 36 percent in Units 1 to 4, 17 percent in Units 5 and 6, and 2 percent in Units 7 and 8.

In all column units except for Unit 3, the peripheral hoops were anchored by 135° end hooks with a 8 d_b extension which satisfied NZS 3101. In the case of the cross ties used for Unit 1 and 'J' bars used for Units 3 and 4, 180° end hooks with a 5 d_b extension were used, although an extension of more than or equal to 6 d_b has been required for the 135° or 180° end hooks in all codes listed in Fig. 3.4. With respect to the cross ties with a 90° hook at one end and 135° hook at the other end provided for Units 2, 5 and 7, a 6 d_b extension was used for the 90° end hook following the ACI 318-83 code [3.7], and a 8 d_b extension was used for the 135° hook which satified NZS 3101.

The tension splice length of the 'J' bar cross ties for Units 3 and 4 and that of the 'U' bars for Units 6 and 8 were 288 mm (= 24 d_b). The tension splice length of the 'U' bar perimeter hoops for Unit 3 was also intended to be 24 d_b but became 17 d_b due to a manufacturing error in bar cutting. In NZS 3101, it is specified that the development length, l_d, of deformed bars in tension shall be computed as the product of the basic development length, l_{db}, from clause 5.3.7.2 and the applicable modification factor or factors in clause 5.3.7.3, but l_d shall not be less than 300 mm. The basic development length, l_{db}, specified in that code is 24 d_b, when $d_b \leq 20$ mm and $f'_c \geq 20$ MPa, provided that the cover to the bar is not less than 40 mm and the centre-to-centre spacing of such bars is not less than 100 mm. The tension splice length of 'J' and 'U' bar cossties used for Units 3, 4, 6 and 8 was determined to be equal to the above l_{db}, that is 24 d_b, although that is shorter than 300 mm and hence does not satisfy that code provision.

Reinforcing cages and formwork for the first series (Units 1 to 4) and the second series (Units 5 to 8) can partly be seen from Figs. 3.15 and 3.16, respectively. Fig. 3.17 shows the cross ties with 135° and 90° end hooks alternating from side to side along column in Unit 5.

3.2.1.2 Testing Procedure

Constant axial compressive load, at a predetermined level, was applied to each column unit by the 10 MN servo-controlled hydraulic jack in the DARTEC testing machine. The axial load level was either 0.1 $f'_c A_g$ or 0.2 $f'_c A_g$ or 0.3 $f'_c A_g$ as listed in Table 3.1. The cyclic lateral loading was applied by 500 KN or 1000 KN double acting hydraulic jacks. The loading arrangements are shown in Fig. 3.18. The lateral load and displacement history imposed on each column unit consisted of one elastic cycle to a nominal displacement ductility factor $\mu_N = \pm 0.75$ and then two cycles to each of $\mu_N = \pm 2, \pm 4, \pm 6$, etc. The nominal displacement ductility factor μ_N is defined as Δ/Δ_y^M, where Δ= measured lateral displacement at jack and Δ_y^M = calculated lateral displacement at first yield found assuming elastic cracked section behaviour up to the theoretical ultimate horizontal load, H_u. The theoretical ultimate horizontal load H_u was computed using the measured stress-strain relation for the longitudinal reinforcement, the ACI rectangular compressive stress block for the concrete with the measured concrete cylinder strength, an extreme fibre concrete compressive strain of 0.003, and

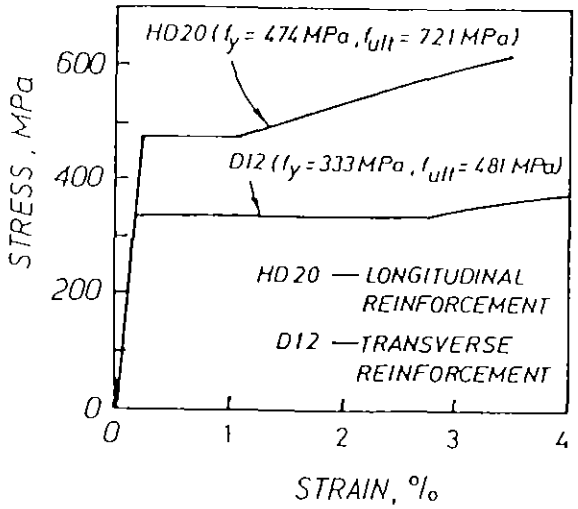

(a) Reinforcing Steel for Units 1 to 4

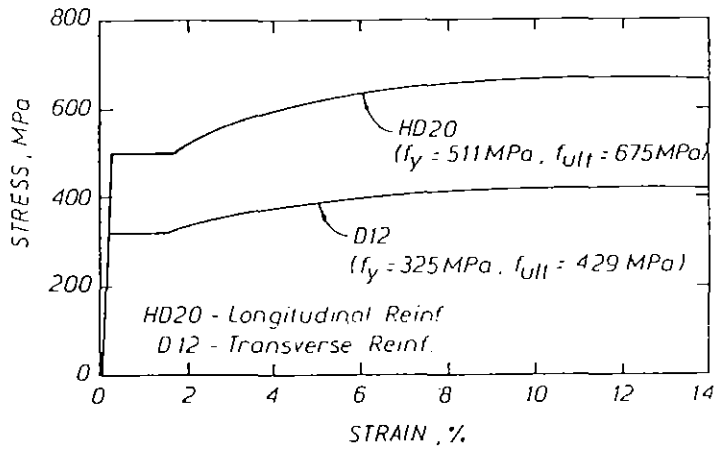

(b) Reinforcing Steel for Units 5 to 8

Fig.3.14 Measured Stress-Strain Curves for the Reinforcing Steel

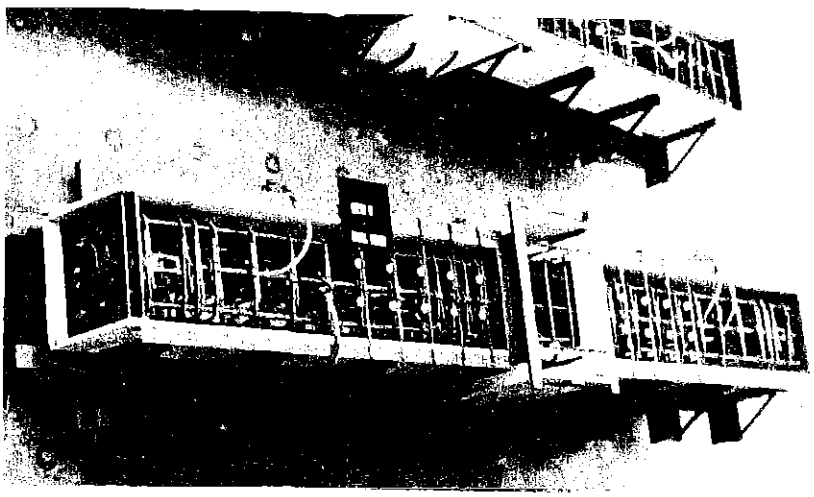

Fig.3.15 Reinforcing Cages and Formwork for Unit 1.

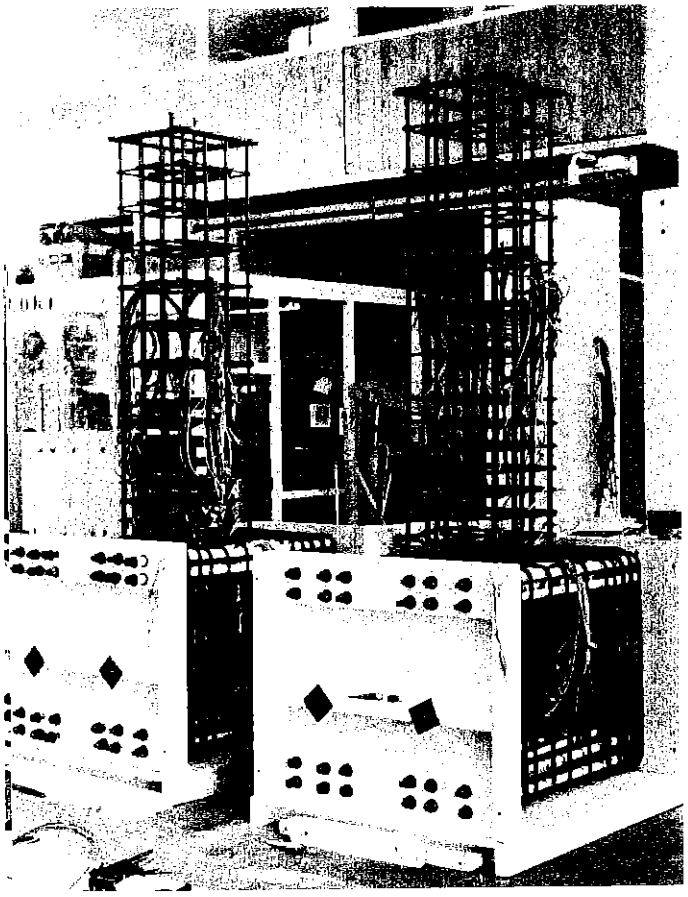

Fig.3.16 Reinforcing Cages with Base Block Formwork for Units 6 and 7.

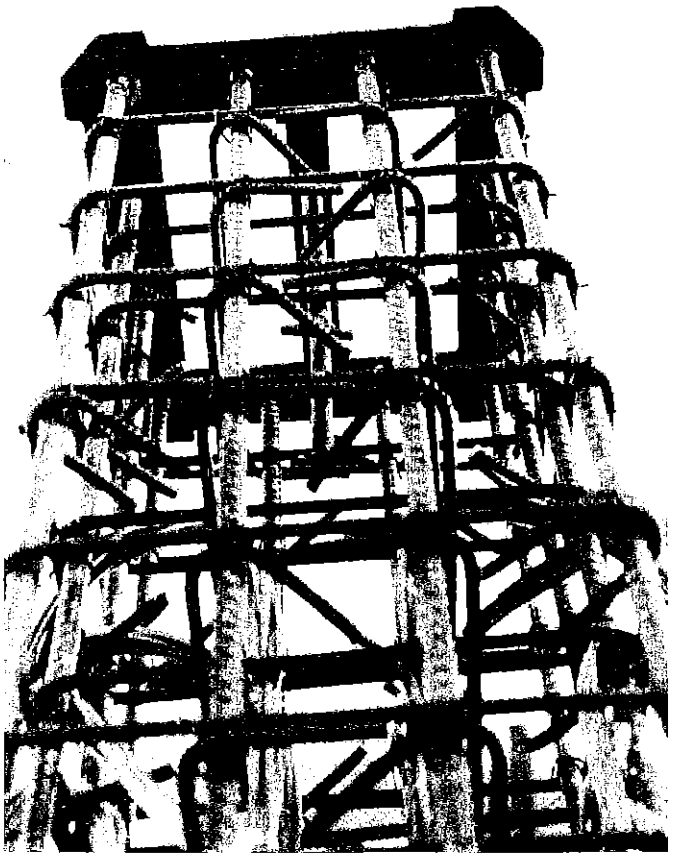

Fig.3.17 Cross Ties with 135° and 90° End Hooks Alternating from Side to Side along the Column, Unit 5.

a strength reduction factor ϕ of unity. The elastic cracked section stiffness was obtained from the initial cycle of lateral loading of up to ± 0.75 of H_u. The horizontal displacement of each column at ± 0.75 of H_u was averaged and divided by 0.75 to find the first yield displacement Δ_y^M. In Table 3.2, the Δ_y^M obtained for each test unit is listed, along with the theoretical value Δ_y^{MKP}. The method to calculate Δ_y^{MKP} is described in Section 3.2.3.

3.2.1.3 Instrumentation

The horizontal displacement of the central stub for Units 1 to 4 and of the column top for Units 5 to 8 were measured by linear potentiometers mounted on a stiff measuring frame as shown in Fig. 3.18. In the case of Units 1 to 4 the rotation of the central stub was also measured using linear potentiometers. The horizontal displacement measured by the potentiometer and the horizontal load measured by a load cell were were used to drive an x-y plotter during testing to trace out the load-displacement hysteresis loops.

In order to obtain the distribution of curvature along the columns and the concrete strains, further pairs of linear potentiometers with gauge length of 160 or 180 mm were placed down the height of the columns. These pairs of linear potentiometers were mounted on 8 mm diameter steel rods which passed through the concrete in the plane of the column section and at right angles to the neutral axis. The rods had been cast in the concrete but the cover concrete surrounding the end of each rod was not present over a depth of 25 mm and a diameter of 30 mm in order to avoid interference by crushed cover concrete. The positions of those potentiometers are also illustrated in Fig. 3.18.

Electrical resistance strain gauges with 5 mm gauge length were attached at various locations on the hoops, cross ties and longitudinal reinforcement within the potential plastic hinge region.

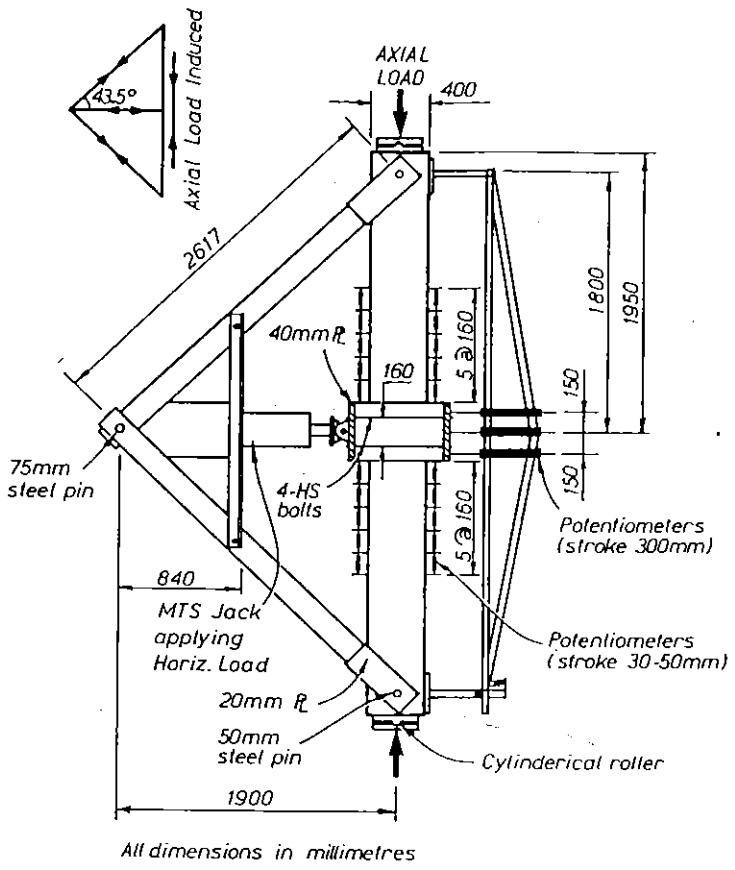

(a) Column Units 1 to 4

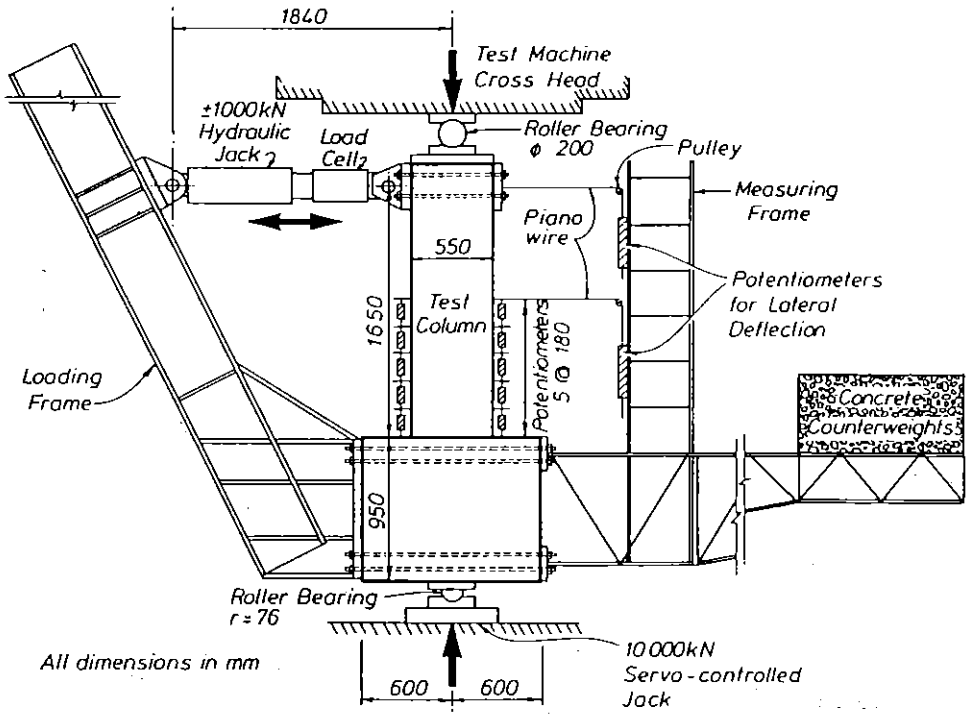

(b) Column Units 5 to 8

Fig.3.18 Loading Arrangements and Potentiometer Positions for Column Units.

3.2.2. Test Results

3.2.2.1 General Observation and Horizontal Load-Displacement Behaviour

Horizontal load versus horizontal displacement hysteresis loops measured for each of the eight column units are shown in Figs. 3.19 to 3.26. The horizontal displacements are also expressed in terms displacement ductility factors and storey drifts (Δ/1600mm for Units 1 to 4 and Δ/1650mm for Units 5 to 8) in those figures. Also shown are the theoretical ultimate horizontal loads H_u calculated by the previously described method using the ACI stress block for concrete. The lines showing H_u slope due to the P-Δ effect.

In Units 1 to 4, the plastic rotation occurred unsymmetrically either above or below the central stub. Further excursions to greater horizontal displacements led to a concentration of the rotation in the plastic hinge which had formed first (see Fig. 3.27). Fig. 3.28 shows the implication of unsymmetrical plastic hinging which was found in Units 1 to 4 by the measured rotation, θ, of each central stub. To account for the concentration of plastic rotation in only one plastic hinge in a column unit, the quantity $\theta \cdot h$ has to be added to the horizontal displacement Δ measured at the centre of the central stub, where h = the distance from centre of the central stub to the horizontal load pins at the ends of each column unit. The displacement ductility factor calculated as $(\Delta + \theta \cdot h)/\Delta_y^M$ is referred to as the real displacement ductility factor, μ_R, and that calculated as Δ/Δ_y^M (ignoring θ) is referred to as the nominal displacement ductility factor μ_N. The real displacement ductility factor μ_R in Figs. 3.19to 3.22 for Units 1 to 4 was thus obtained from the nominal displacement ductility factor μ_N modified to take into account any unsymmetrical plastic rotation that concentrated either above or below the central stub. For Units 5 to 8, $\mu_N = \mu_R$ because plastic hinging only occurred above the base block.

As can be seen from Figs. 3.19 to 3.26, the measured hysteresis loops for each unit, except for Unit 3, indicated stable behaviour, good energy dissipation and limited reduction in strength up to the final stage of each testing. In the case Unit 3, the 90° bends in the square perimeter hoops formed of lapped 'U' bars (the laps were in the cover concrete) commenced to open at a real displacement ductility factor μ_R of about 7, and in the

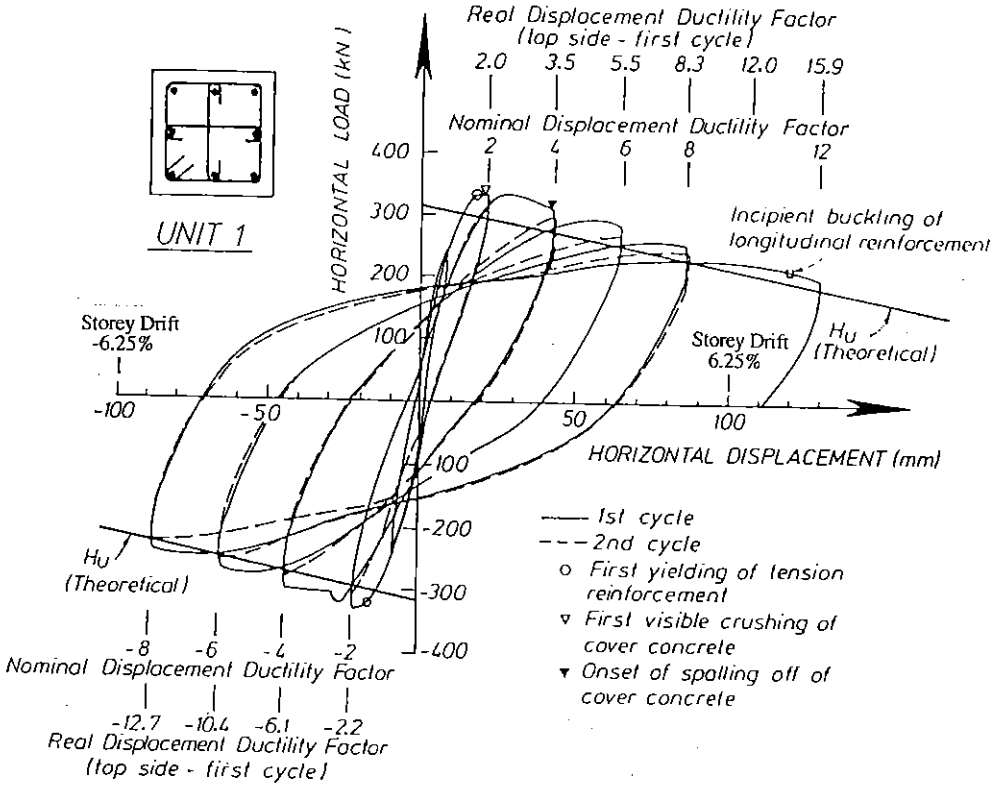

Fig.3.19 Measured Horizontal Load-Displacement Hysteresis Loops for Unit 1.

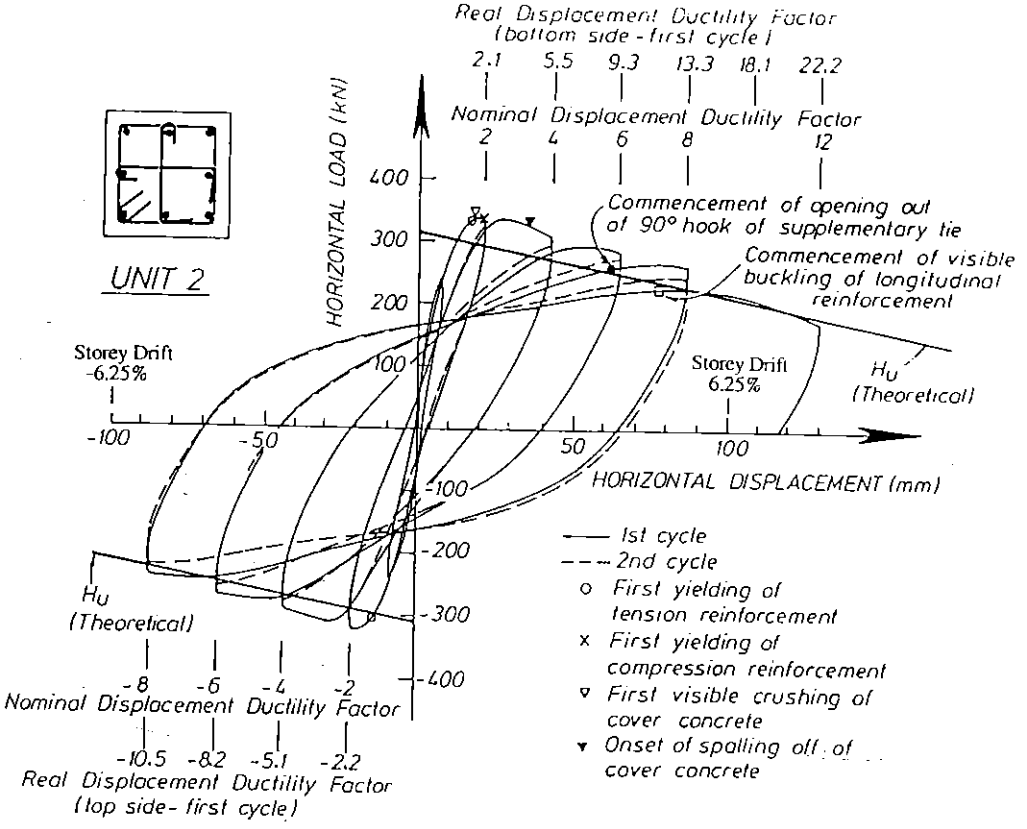

Fig.3.20 Measured Horizontal Load-Displacement Hysteresis Loops for Unit 2.

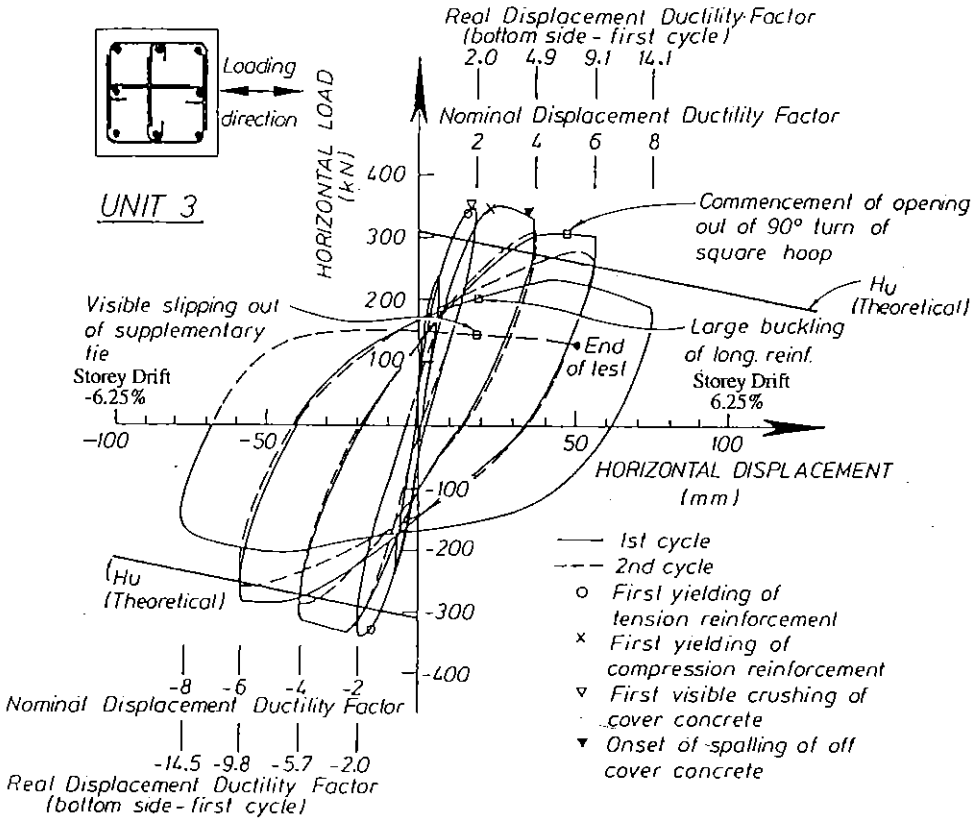

Fig.3.21 Measured Horizontal Load-Displacement Hysteresis Loops for Unit 3.

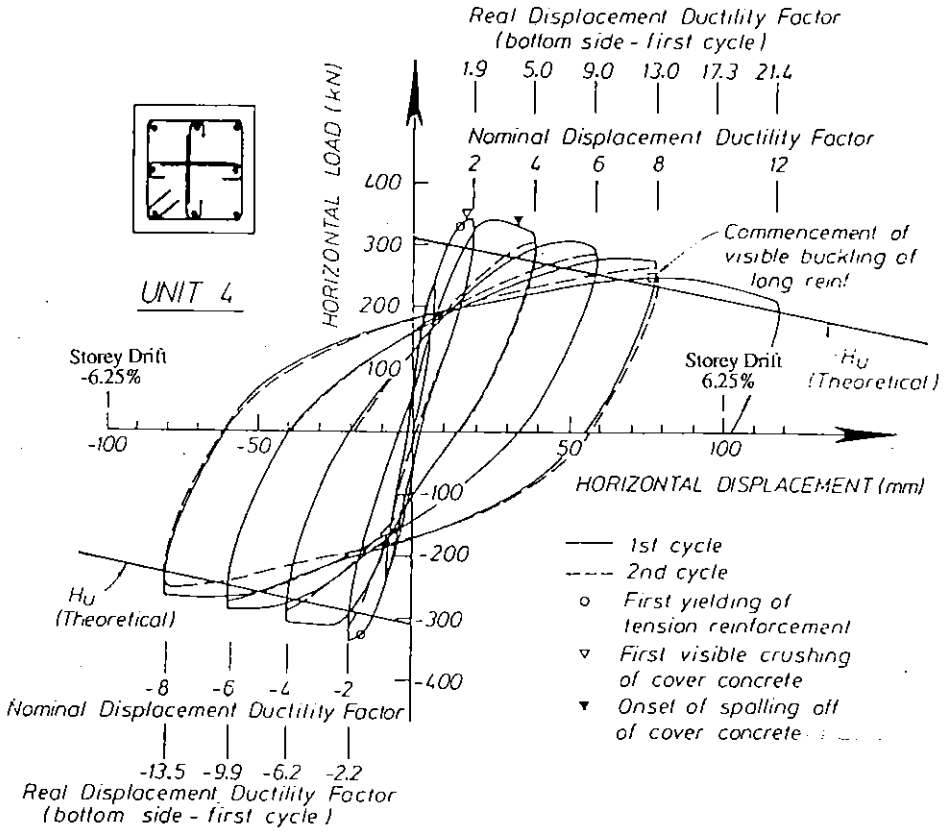

Fig.3.22 Measured Horizontal Load-Displacement Hysteresis Loops for Unit 4.

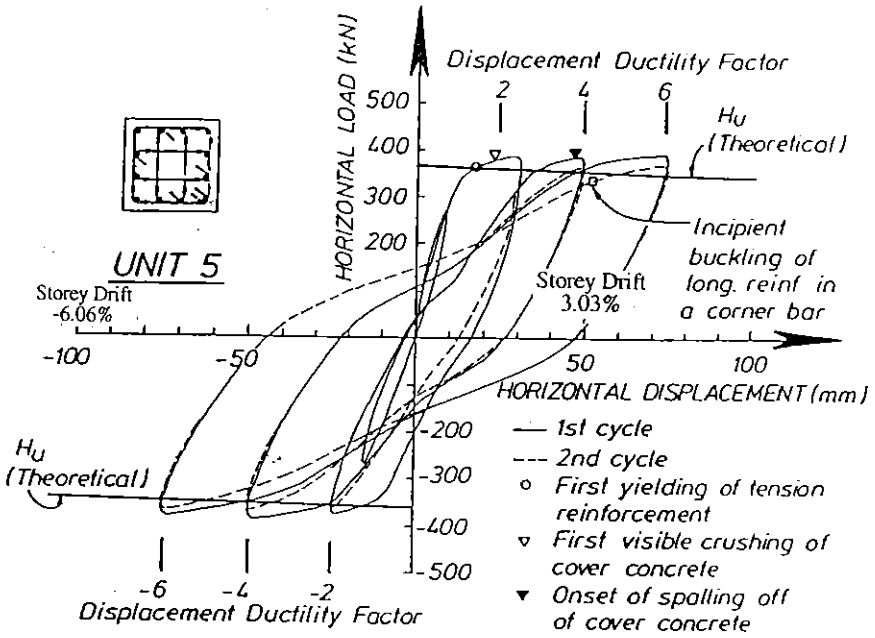

Fig.3.23 Measured Horizontal Load-Displacement Hysteresis Loops for Unit 5.

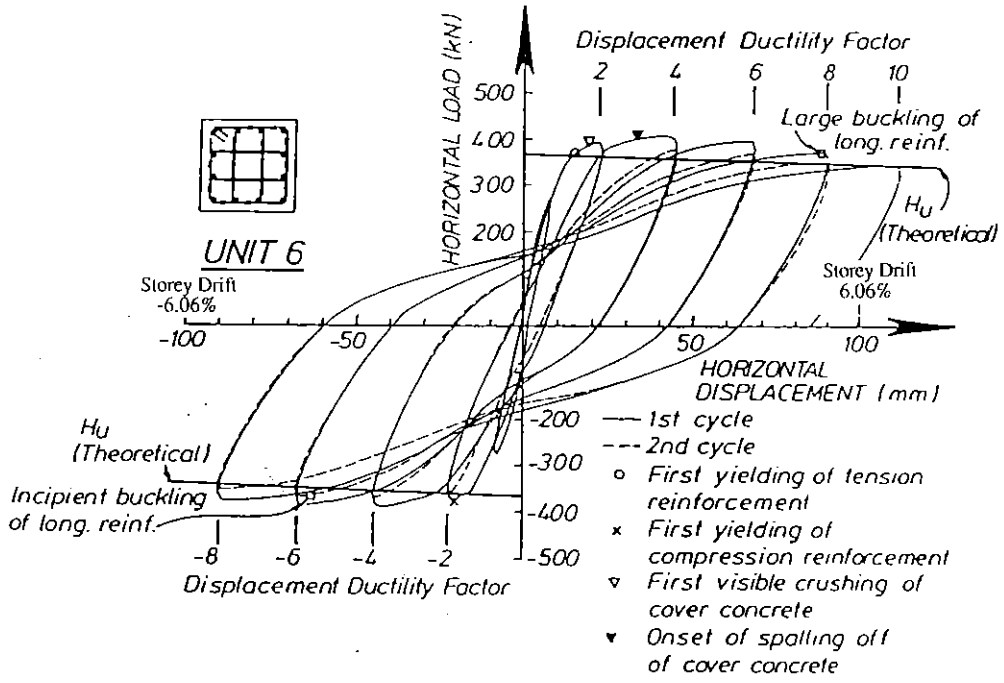

Fig.3.24 Measured Horizontal Load-Displacement Hysteresis Loops for Unit 6.

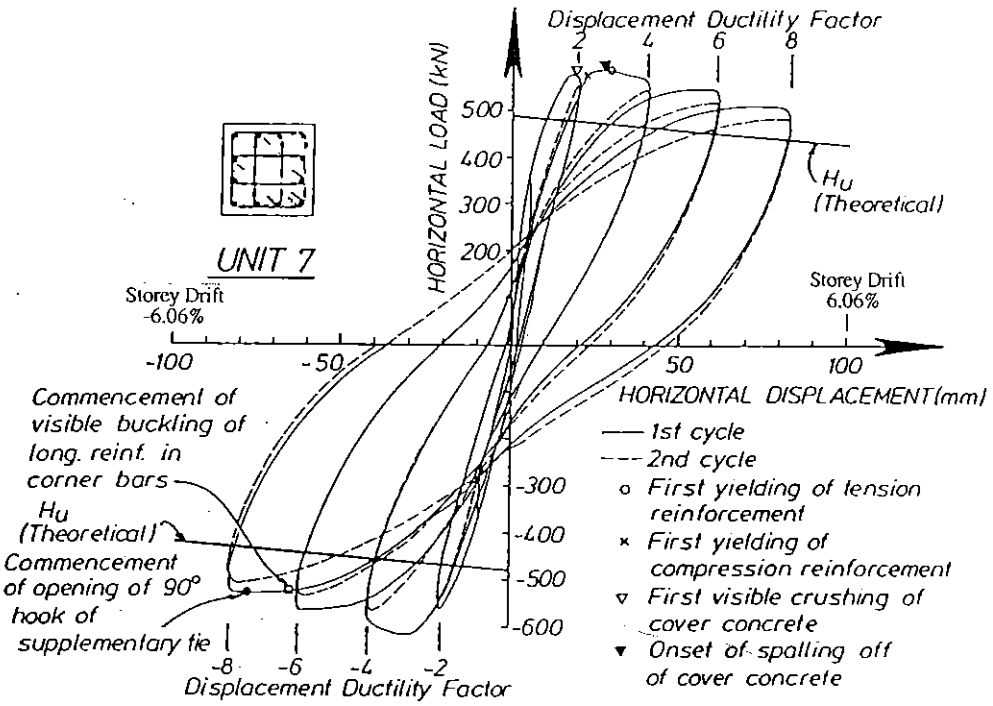

Fig.3.25 Measured Horizontal Load-Displacement Hysteresis Loops for Unit 7.

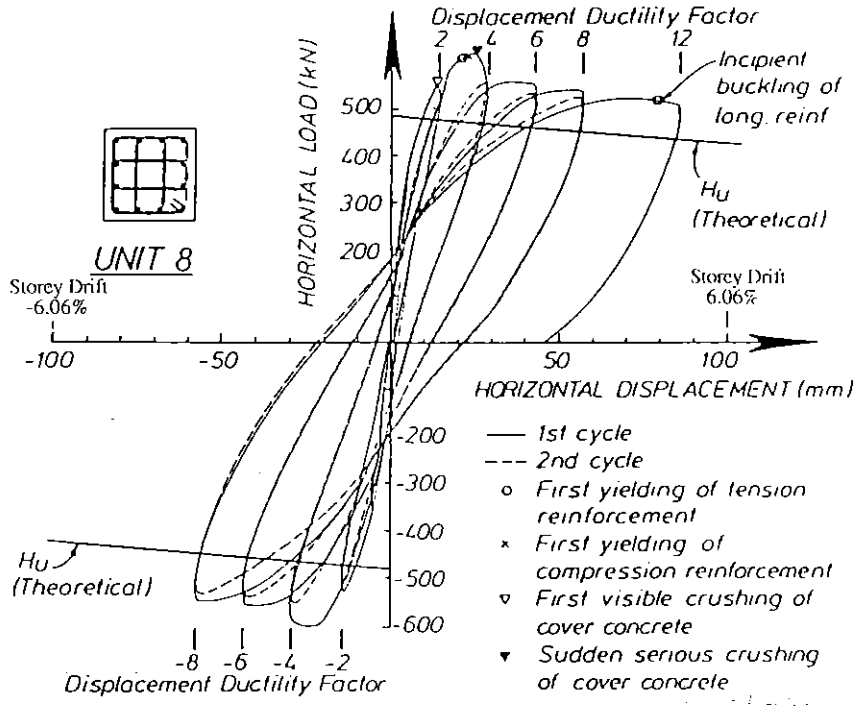

Fig.3.26 Measured Horizontal Load-Displacement Hysteresis Loops for Unit 8.

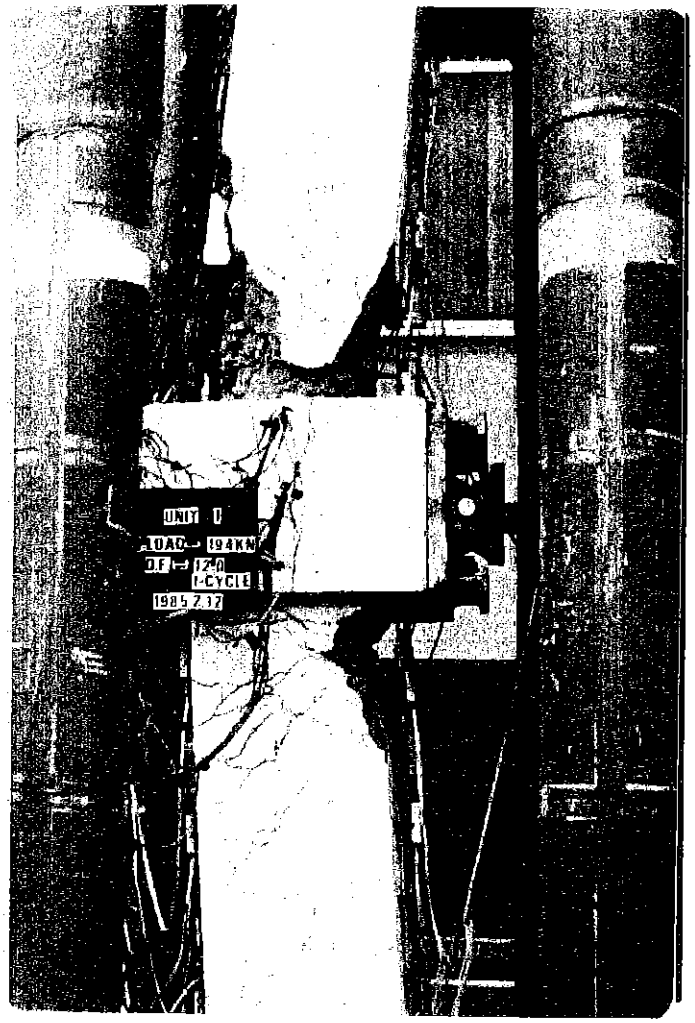

Fig.3.27 Damage Concentrated above the Central Stub of Unit 1.

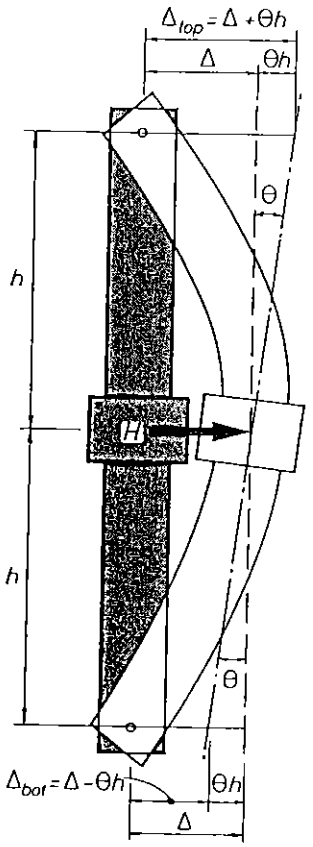

Fig.3.28 Implication of Rotation of the Central Stub of the Column Units.

Table 3.2 Test Results for Column Units 1 to 8

Column Unit	First Yield Displacement (mm)		First Yield Curvature (x 10^{-6} 1/mm)		Maximum Moment			At Nominal Displacement Ductility Factor μ_N = ± 6 in Second Cycle					At Final Stage of Testing				
	Measured Δ_y^M	Theory Δ_y^{MKP}	Measured ϕ_y^M	Theory ϕ_y^{MKP}	Measured M_{max} (1) (kN.m)	Ratio of M_{max} to Theoretical Moment (2) M_{max}/M_{ACI}	Ratio of M_{max} to Theoretical Moment (3) M_{max}/M_{MKP}	μ_N	μ_R^*	M/M_{max} (4)	ϕ/ϕ_y^M	ε_{cc} (%) (5)	μ_N	μ_R	M/M_{max} (4)	ϕ/ϕ_y^M	ε_{cc} (%) (5)
1	10.9	10.2	22.6	15.5	279	1.11	1.05	+6 -6	+ 6.2 -10.6	0.94 0.91	9.2 11.4	2.30 3.57	+12	+15.4	0.94	20.0	6.89
2	10.9	10.2	21.6	15.5	284	1.13	1.07	+6 -6	+ 9.6 - 8.4	0.94 0.88	10.8 12.4	3.61 1.69	+12	+22.3	0.85	32.8	>9.11
3	9.6	10.2	18.4	15.5	290	1.15	1.09	+6 -6	+ 9.4 -10.0	0.91 0.88	11.6 14.6	2.58 4.24	- 8	-14.5	0.66	25.0	8.29
4	10.0	10.2	19.8	15.5	285	1.13	1.08	+6 -6	+ 9.2 -10.0	0.90 0.94	11.9 13.0	3.68 3.58	+12	+21.4	0.94	25.5	7.41
5	12.3	9.0	13.5	16.4	673	1.12	1.08	+6 -6	+6 -6	0.95 0.94	9.9 14.7	1.97 1.69	- 6 (2nd cycle)	- 6	0.94	14.7	1.69
6	11.2	9.0	15.7	16.4	679	1.13	1.09	+6 -6	+6 -6	0.92 0.93	11.3 10.1	2.02 1.63	+10	+10	0.89	20.8	4.85
7	10.3	6.8	9.1	9.6	1043	1.31	1.17	+6 -6	+6 -6	0.87 0.91	10.6 11.3	2.43 1.93	+ 8 (2nd cycle)	+ 8	0.84	15.4	2.66
8	7.1	6.8	8.0	9.6	1045	1.31	1.17	+6 -6	+6 -6	0.88 0.90	9.2 7.6	1.61 1.11	+12	+ 12	0.89	21.9	3.68

Notes: (1) Measured maximum moment at the face of the stub, taking into account the P-Δ moment
(2) Calculated using the actual stress-strain relation of the longitudinal steel and the ACI concrete compressive stress block
(3) Calculated using the actual stress-strain relation of the longitudinal steel and the modified Kent and Park stress-strain relation for the concrete
(4) M = measured moment at face of stub taking into account the P-Δ moment
(5) ε_{cc} = maximum compressive strain on surface of concrete core.

subsequent cycles of loading the strength of the column rapidly degraded due to significant buckling of the longitudinal bars and ineffective confinement of the core concrete.

The measured maximum moments for all column units are listed in Table 3.2 and compared with the theoretical maximum moments M_{ACI} and M_{MKP}. M_{ACI} corresponds to the maximum moment used to calculate Δ_y^M. M_{MKP} was obtained from a section analysis using the stress-strain models for the longitudinal bars shown in Fig. 3.29 and the modified Kent and Park stress-strain models (see Section 2.2.3.2 or reference [3.18]) for confined and unconfined concrete shown in Fig. 3.30. The detail of the section analysis conducted to obtain M_{MKP}, including those stress-strain models used for longitudinal reinforcement and concrete, is described in Section 3.2.3. All column units reached a higher flexural strength than the calculated theoretical strengths M_{ACI} and M_{MKP}. The ratio of the maximum moment measured in the second cycle to $\mu_N = \pm 6$ to the maximum moment measured during the test for each column varied from 0.87 to 0.96 as listed in Table 3.2. It can be concluded that for real displacement ductility factor μ_R up to at least 6 the behaviour of all column units was satisfactory, except perhaps for Unit 3.

3.2.2.2 Concrete Compressive Strains and Buckling of Longitudinal Reinforcement

Crushing of the cover concrete was first obesrved near peak load during the first cycle to a nominal displacement ductility factor of $\mu_N = 2$ when the surface strain was greater than 0.004. Substantial spalling of the cover concrete occurred earlier in Units 7 and 8 than in other units, due to the higher axial load applied. Compressive strains measured at the surface of the core concrete, ε_{cc}, are plotted against the real displacement ductility factors μ_R in Fig. 3.31. Those compressive strains are the values obtained from the readings of the potentiometers located at the closest position to the central stubs in Units 1 to 4 or to the base blocks in Units 5 to 8. From Fig. 3.31, it can be seen that ε_{cc} almost linearly increases up to the final stage of loading corresponding to real displacement ductility factor $\mu_R = 6$ to 12 in all test units except for Unit 3. In case of Unit 3, ε_{cc} has rapidly increased from μ_R = about 9 in accordance with the rapid degradation of the load carrying capacity of the column due to the opening of the 90° bends in the square

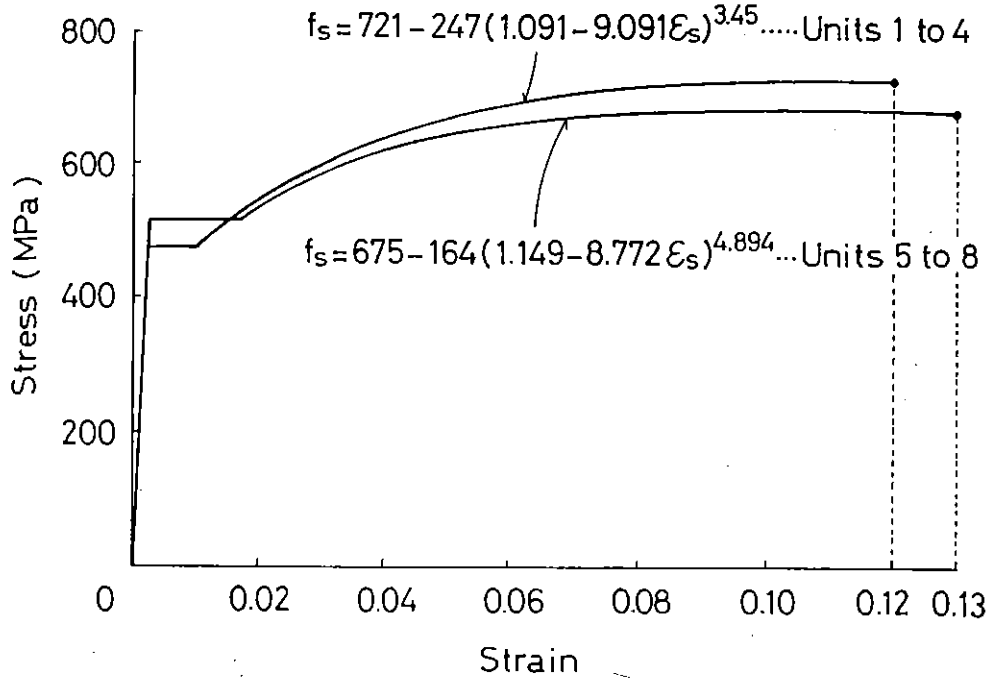

Fig.3.29 Stress-Strain Models for the Longitudinal Bars Used for the Section Analysis.

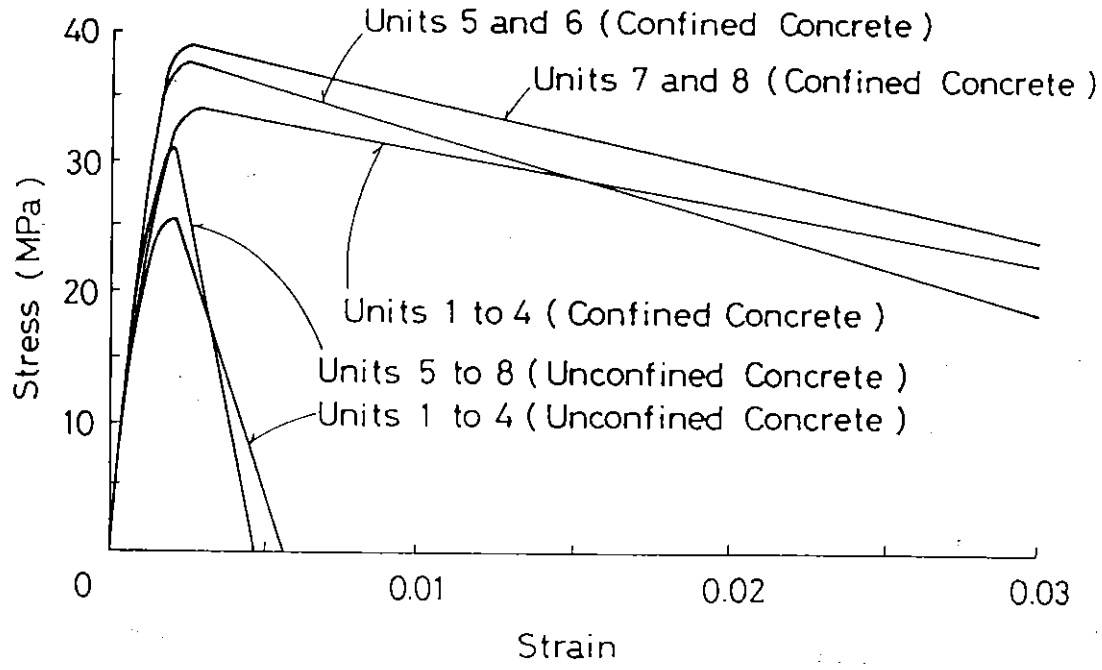

Fig.3.30 Modified Kent and Park Stress-Strain Models for Confined and Unconfined Concrete Used in the Section Analyses.

perimeter hoops formed of lapped 'U' bars. In Table 3.2, the maximum values of ε_{cc} measured at $\mu_N = \pm 6$ in second cycle and at the final stage of testing are listed. The values of ε_{cc} for the final stage of testing were obtained from the readings of the potentiometers located at eventual crushing zone of column and hence do not always correspond to the values shown in Fig. 3.31 which are obtained from the potentiometers located at the closest position to the central stubs or the base blocks.

Slight or serious buckling of longitudinal reinforcement was observed in all column units and commenced at the stages marked in Figs. 3.19 to 3.26. The most serious buckling occurred in the corner bars of Unit 3 over two spacings of the hoop sets, due to the opening out of the 90° bends of the 'U' bars making up the perimeter hoops during the loading immediately after two cycles of $\mu_N = \pm 6$. From this result, the use of 'U' bars for perimeter hoops in which tension splices are placed in the cover concrete is definitely discouraged. In Unit 2, in which interior cross ties with a 90° hook at one end and a 180° hook at the other end were used, serious buckling of the intermediate longitudinal bars occurred over two spacings of the hoop sets with opening of out of the 90° end hook occurring near the final stage of testing at $\mu_R \geq 20$. Those bucklings of longitudinal reinforcement observed for Units 2 and 3 are illustrated in Fig. 3.32. Also illustrated are those bucklings observed for Unit 1 with conventional transvers reinforcing detail and Unit 4 with 'J' bar cross ties, where the buckling occurred between the hoop sets. Slight opening of the 90° end hooks of the interior ties was also observed in Unit 7 at the end of test where $\mu_R = 8$. From those observations, it must be noted that opening out of 90° end hooks of cross ties eventually occurs accompanied by the buckling of the longitudinal reinforcement over two spacings of hoop sets. This is indicating that after spalling of the cover concrete the cross ties with a 90° hook at one end and 135° hook at the other end eventually become less effective than the conventional cross ties with 135° end hooks. However, in the tests conducted in this study the opening of 90° end hooks of the cross ties has not led to a serious degradation of load carrying capacity of the columns within the expected range of deformations of columns under very severe earthquake loading.

In the case of Units 4, 6 and 8, where 'J' or 'U' bars were used as interior cross ties with tension splices in the core concrete, buckling of the

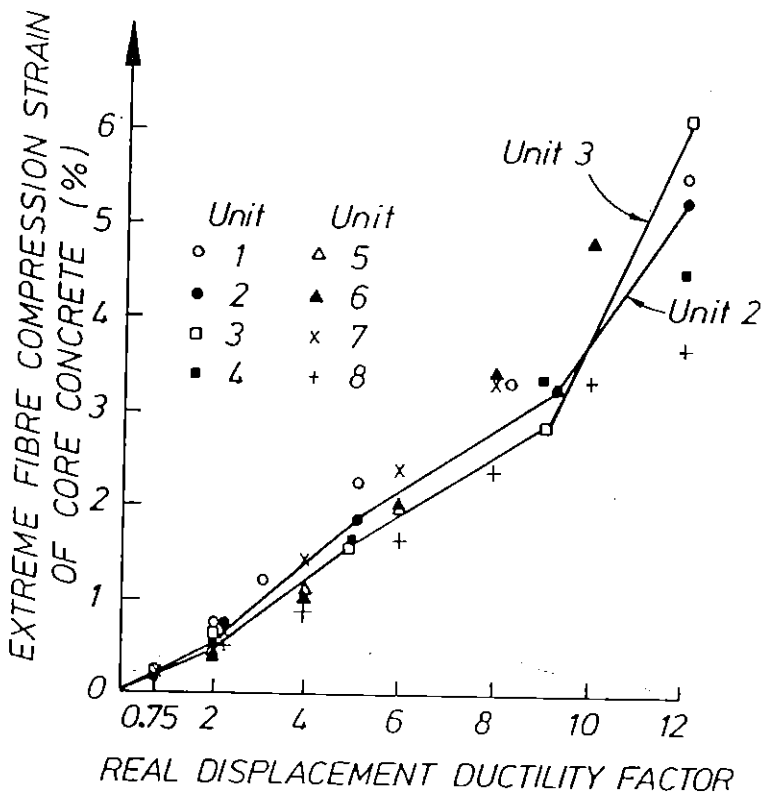

Fig.3.31 Measured Compressive Strain at the Surface of Core Concrete versus Real Displacement Ductility Factor.

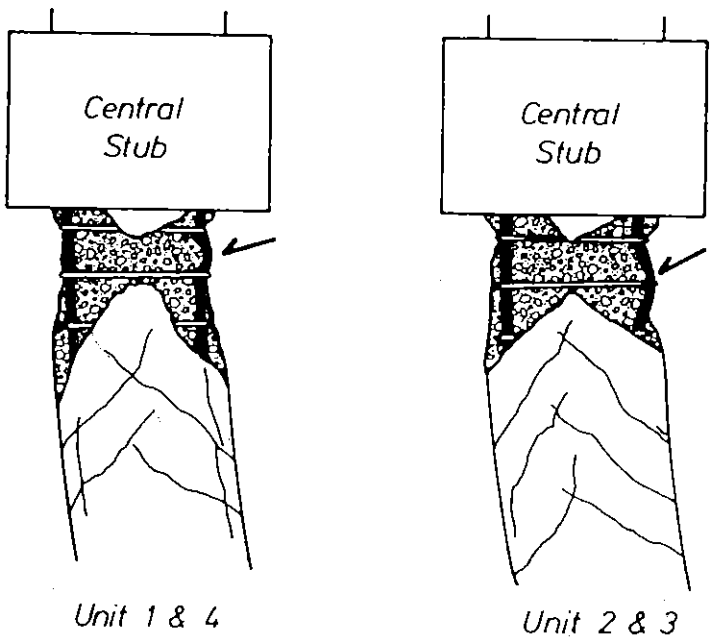

Fig.3.32 Observed Buckling of Longitudinal Reinforcement for Units 1 to 4.

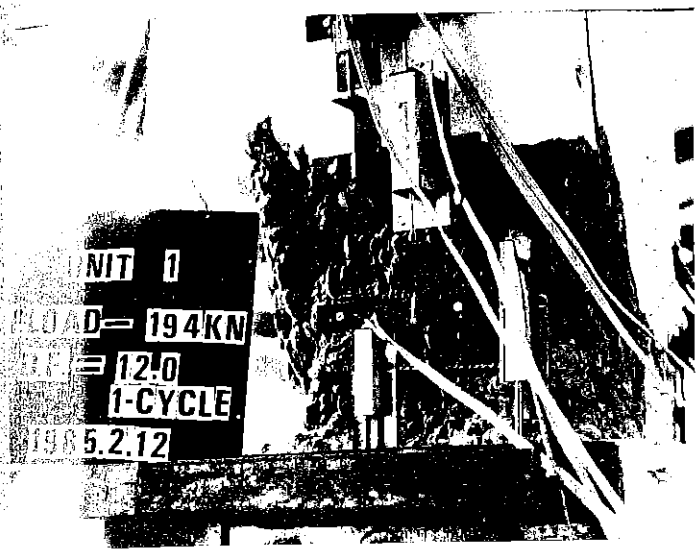

(a) Unit 1 at $\mu_N = 12$. The transverse reinforcement is stll effective.

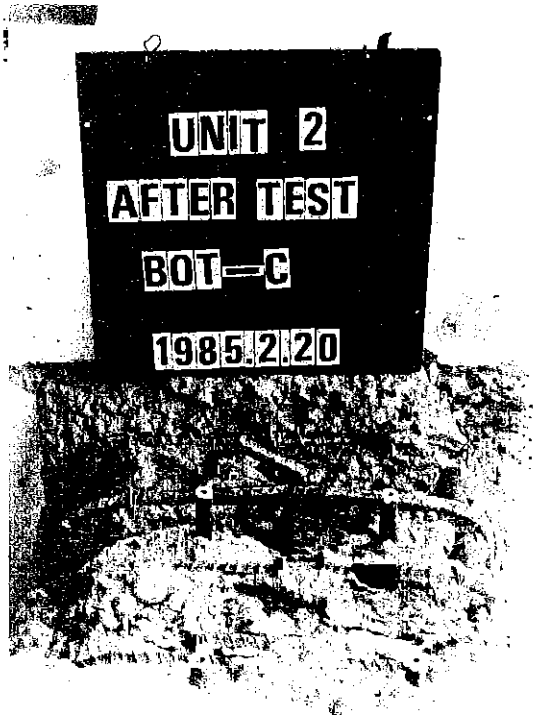

(b) Unit 2 at $\mu_N = 12$. The 90° hooks at one end of the interior cross ties have opened.

(c) Unit 3 at $\mu_N = 8$. The 'U' bar lapped perimeter hoops have become ineffective.

(d) Unit 4 at $\mu_N = 12$. The 'J' bar interior cross ties are still effective.

Fig.3.33 Visible Damage to Column Units 1 to 4 at Final Stages of Testing.

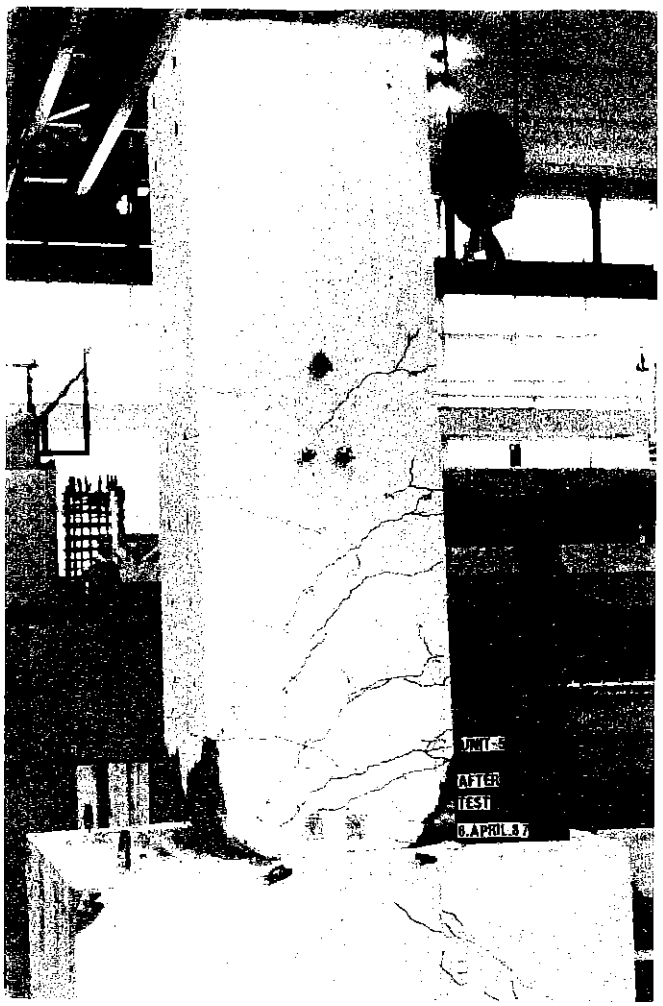

(a) Crack Patterns

(b) The 90° end hooks of the interior cross ties have not opened.

Fig.3.34 Visible Damage to Column Unit 5 after 2 cycles to $\mu_N = \pm 6$.

(a) Crack Patterns

(b) The 'U' bar interior cross ties are still effective.

Fig.3.35 Visible Damage to Column Unit 6 after Loading to $\mu_N = +10$.

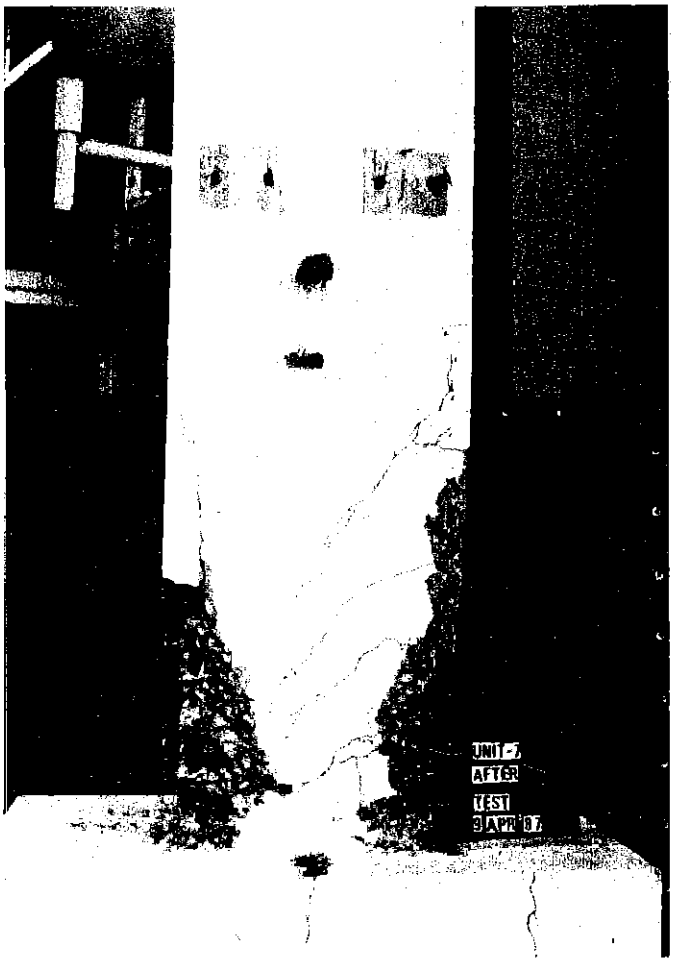

(a) Crack Patterns

(b) The 90° end hooks at one end of the interior cross ties have opened.

Fig.3.36 Visible Damage to Column Unit 7 after 2 cycles to $\mu_N = \pm 8$.

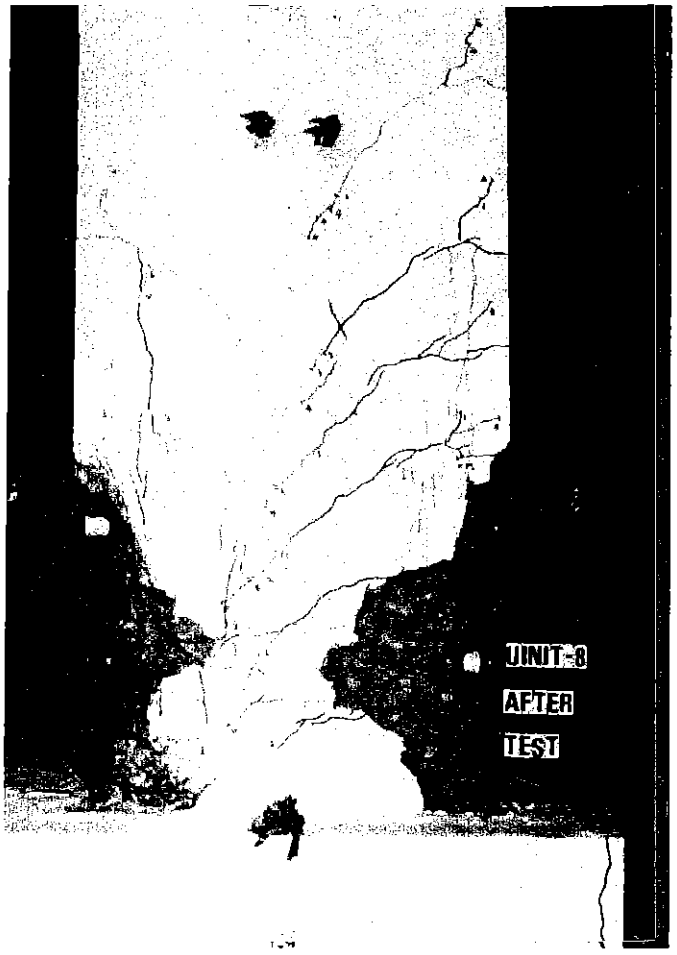

(a) Crack Patterns

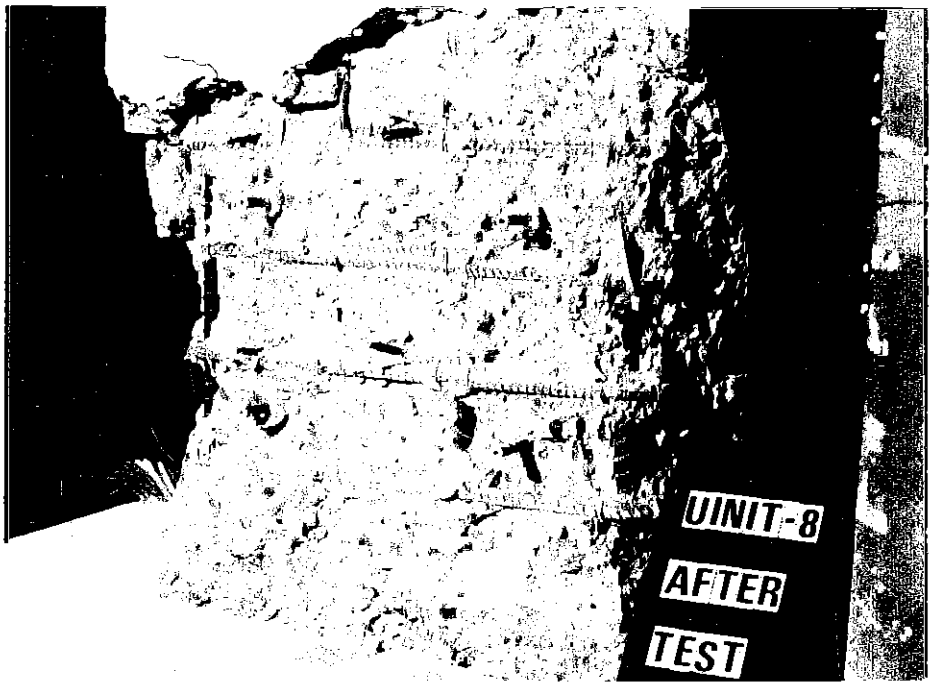

(b) The 'U' bar interior cross ties are still effective.

Fig.3.37 Visible Damage to Column Unit 8 after Loading to $\mu_N = +12$.

longitudinal reinforcement eventually occurred between the hoop sets. Hence, the splice length of 24 transverse bar diameters proved adequate for the Grade 275 steel transverse reinforcement used. It was observed that inclined flexure-shear cracks predominated in the tested columns and hence that the bond conditions along the splices was maintained since most cracks did not run along the splices.

During the final stage of testing the visible damage was crushing of concrete and slight or serious buckling of the longitudinal compression reinforcement as shown in Figs. 3.33 to 3.37.

3.2.2.3 Strains in Transverse Reinforcement

Strains measured by electrical resistance strain gauges on the transverse reinforcement of Unit 1 are shown plotted against the real displacement ductility factors in Fig. 3.38. The strains plotted are the average of pairs of strains measured on opposite sides of the bar in the damage concentrated region of the column. For the peripheral hoops of all test units, in order to avoid picking up strains caused by bending of the hoop bar due to lateral expansion of core concrete, the line connecting a pair of electrical resistance strain gauges on oppsite sides of the bar was parallel to the column axis. This means that strains measured on those opposite sides of the peripheral hoop bar should ideally be equal each other when the bar is bent outward exactly in the transverse direction to the column axis. However, the individual strain readings indicated that there was significant bending of the peripheral hoop bars in random directions. In the same manner, individual strain readings obtained from pairs of electrical resistance strain gauges attached on oppsite sides of cross tie bars also indicated that there was significant bending of the cross tie bars although they were buried inside the concrete core. Hence, averaging of the pairs of strain readings was necessary to obtain the axial tensile strain of the transverse reinforcement.

As can be seen from Fig. 3.38, for Unit 1 thus averaged strains measured in damage concentrated region seldom reached the yield strain, even at the final stages of testing. The highest strains recorded were on the peripheral hoops (gauges A, B and C) and these eventually reached yield strain on the hoop sides in the direction of horizontal load and at right

angles to it. The strains recorded on the cross tie in the direction of loading (gauge D) reached about 59 % of yield but the strains recorded on the other cross tie, which was very close to the neutral axis, reached only about 38% of yield (gauge E).

For Units 1 to 4, pairs of electrical resistance strain gauges attached on opposite sides of transverse reinforcing bars were allocated only for the top half of each column unit, but unfortunately for Units 2 to 4 the plastic rotation concentrated on the bottom half of each column where electrical resistance strain gauges were attached only on one side of each transverse reinforcing bar. As a result, axial tensile strains of transverse reinforcement in the damage concentrated region could not be exactly measured for Units 2 to 4.

For Units 1 to 4, the largest and secondly largest strains of transverse reinforcement recorded by individual electrical resistance strain gauges for each location of transverse section are plotted in Figs. 3.39 (a) to (d). In those figures, a capital letter and a small letter within parentheses by each curve indicates the gauge locations in the transeverse section and the longitudinal section of column, respectively, according to the notations shown in Fig. 3.39 (a). Since those strain readings were obtained from individual electrical resistance strain gauges placed in the regions of column where the damage concentrated, those strains involved the strain due to bending of the transverse bar in addition to the axial tensile strain. For example, the strain readings represented by the curve 'A' in Fig. 3.38 are significantly smaller than those represented by the curve A-(a) in Fig. 3.39 (a), although both of which were measured at the same position of the same hoop. This is because the former curve is a mean curve of the latter curve and the curve obtained from the paired strain gauge attached on oppsite side of the transverse reinforcing bar. Based on this comparison between Figs. 3.38 and 3.39 (a), it may be inferred that the strains of transverse reinforcement shown in Figs. 3.39 (b) to (d) will likely be much larger than the axial tensile strains actually induced in the transverse reinforcement. Thus for Units 2 to 4 exact axial tensile strains of transverse reinforcement in the regions of column where the damage concentrated could not be estimated, since the electrical resistance strain gauges were attached only on one side of transverse reinforcing bars in that region. The behaviour of the

transverse reinforcement durong testing of the columns is described as in the following paragraphs.

For Unit 2, as shown in Fig. 3.39 (b), the strain readings of gauge D-(b) attached on the cross tie bar with 90° and 180° end hooks suddenly decreased at a real displacement ductility factor of about 13. It is notable that this phenomenon coincided with significant opening of the 90° end hook of that cross tie which led to visible buckling of the longitudinal reinforcement marked in Fig. 3.20 and to degradation of load carrying capacity of the column. That is, opening of the 90° end hook of the cross tie has induced the loss of restraint to the buckling of the longitudinal reinforcement and the decrease of confinement of core concrete. On the other hand, the strain measured on a cross tie nearest and parallel to the neutral axis (gauge E-(a)) suddenly began to increase at that displacement ductility factor. This is indicating that the neutral axis position at column section (a) was deepened after buckling of the longitudinal reinforcement, leading to reduction of the lever arm length for the internal moment.

For Unit 3, the strain measured on the lapped 'U' bar peripheral hoop (gauge C-(a) in Fig. 3.39 (c)) showed an abrupt decrease when a real displacement ductility factor of 9 was reached, which coincided with the serious opening of the 90° corner bends of 'U' bars and a degradation of the moment resistance of the column. Corresponding to this decrease of strain in the 'U' bar peripheral hoop, strains in 'J' bar cross ties nearest and parallel to the neutral axis (gauges E-(a) and (b) in Fig. 3.39 (c)) have rapidly increased indicating that the loss of confinement by the peripheral hoops had resulted in a deepening of the neutral axis position. The deepening of the neutral axis position at this stage was confirmed by the change in the calculated position as obtained from the extreme fibre strains measured on the column faces by the pair of linear potentiometers. Moreover, the strains in 'J' bar cross ties in the direction of loading, which were measured by gauges D-(a) and (b) in Fig. 3.39 (c), have also rapidly increased corresponding to the decrease in the peripheral hoop strains. This means that the applied column shear was mainly resisted by those 'J' bar cross ties after the loss of shear resistance of the peripheral hoops due to the serious opening of the 90° corner bends of those bars.

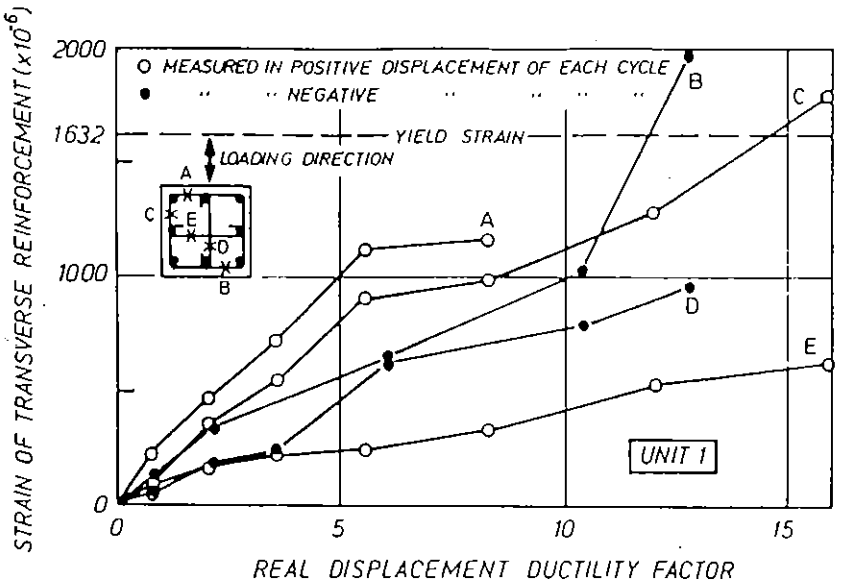

Fig.3.38 Strains Measured on Transverse Reinforcement of the Hoop Sets Nearest the Central Stub Unit 1.

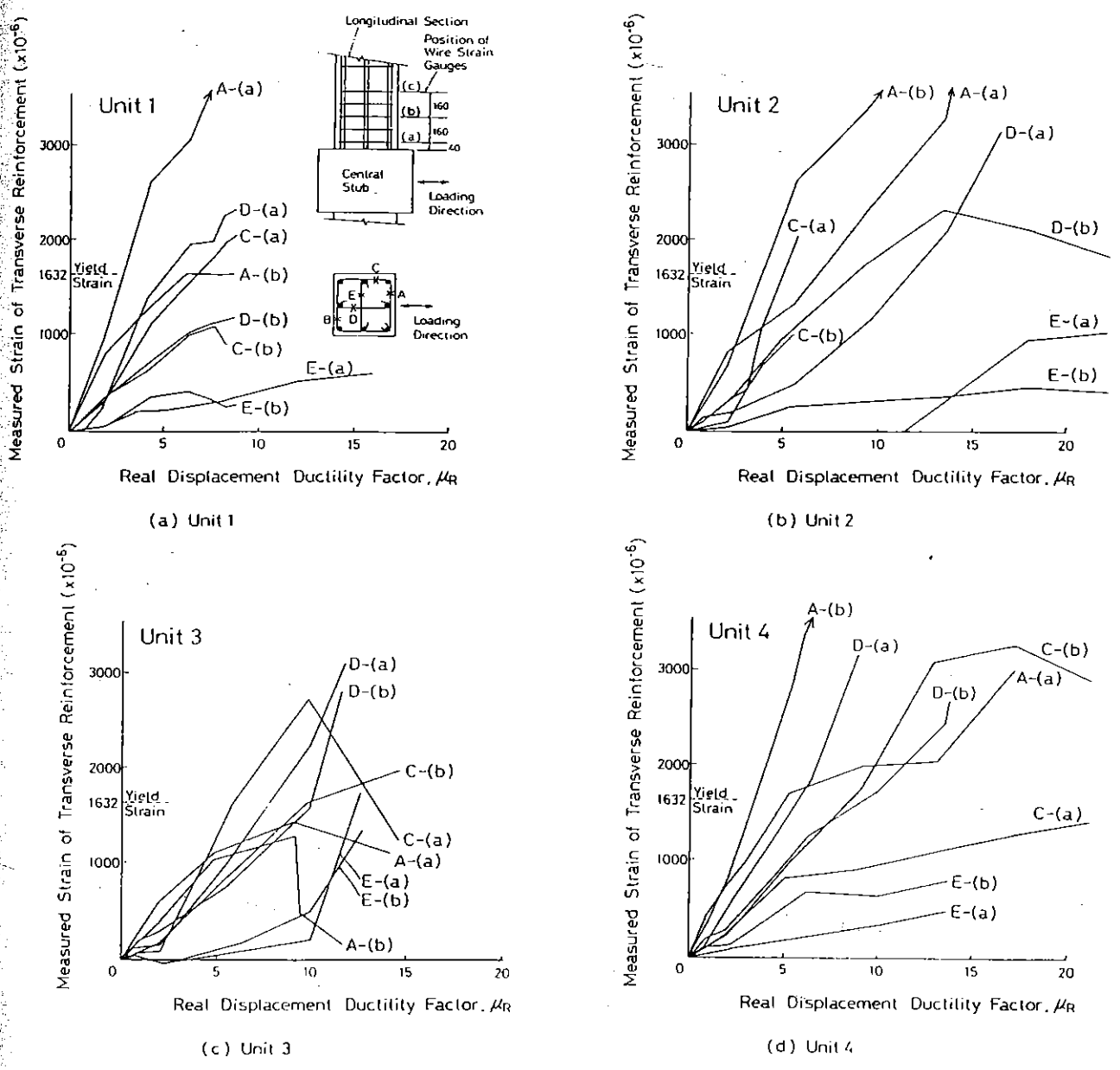

Fig.3.39 Strains Measured on Transverse reinforcement of Units 1 to 4.

For Unit 4, the strain increase observed for the 'J' bar cross ties at position D and E (see Fig. 3.39 (d)) was similar to that observed for the cross ties with a 180° end hook of Unit 1 at the corresponding positions. Therefore, it can be said that the tension splice length of 24 d_b (where d_b = tie bar diameter) was sufficient to effectively anchor the 'J' bar cross ties used for Unit 4. However, it should be noted that the maximum axial tensile strain on the 'J' bars would have likely been up to 60 % of the yield strain. This is because, in the region of Unit 1 where the damage concentrated, the maximum axial tensile strain in the cross ties with 180° end hooks estimated by averaging the pairs of electrical resistance strain gauges attached on the opposite sides of the bars was up to 60 % of the yield strain as shown in Fig. 3.38. This means that the effectiveness of anchorage by tension splices of 'J' bar cross ties might not have been fully investigated in this test, since the axial tensile force induced in the 'J' bar cross ties might have been well below the yield tension force of those transverse bars. It should also be noted that, the measured neutral axis depth at peak moment increased from about 0.3 to 0.6 of the column section depth (= about 10 to 20 d_b) as the displacement ductility factor increased, except for the initial loading to displacement ductility factor of ± 0.75. That is, there was always lateral compressive stress present over part of the length of the tension splices of 'J' bar cross ties in Unit 4 with axial load level $P_e/ (f'_c A_g) = 0.2$.

For Units 5 to 8, the measured strains of transverse reinforcement in the plastic hinge region of each column are shown in Fig. 3.40. The strains plotted are the average of pairs of strains measured on opposite sides of the bar and hence those are indicating axial tesile strains induced. It was confirmed that the cross ties with 90° and 135° end hooks and the 'U' bar cross ties with tension splices reached the axial yield strain at displacement ductility factors of 6 to 8. It should be noted that after spalling of the cover concrete a 90° end hook can only sustain approximately one-tenth of the yield force of the cross tie. This means that the bond conditions along those cross tie legs were satisfactory not only for Units 7 and 8 with axial load level $P_e/(f'_c A_g) = 0.3$ but also for Units 5 and 6 with axial load level $P_e/(f'_c A_g) = 0.1$, otherwise the cross tie could not reach the yield strain near the 90° end hook as measured. It can also be inferred that the inclined flexure-shear cracks were more predominant in Units 5 to 8 than in Units 1 to 4 due to smaller aspect ratio of the former test units and hence the bond conditions

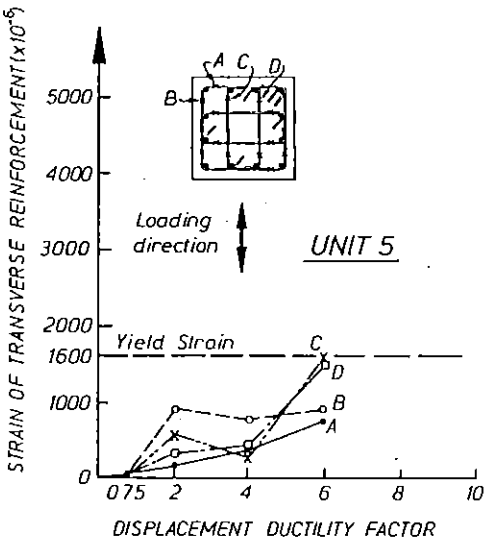

(a) Unit 5

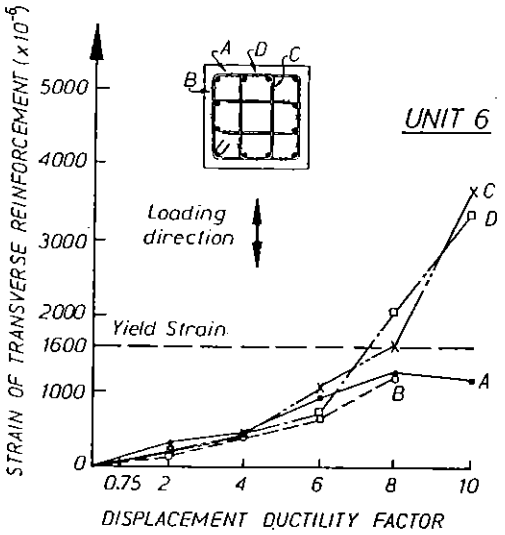

(b) Unit 6

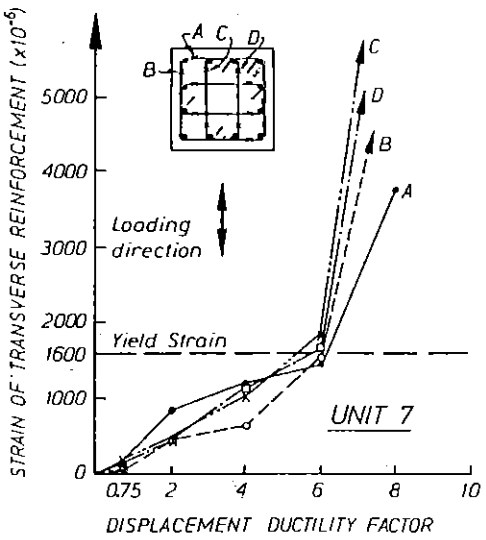

(c) Unit 7

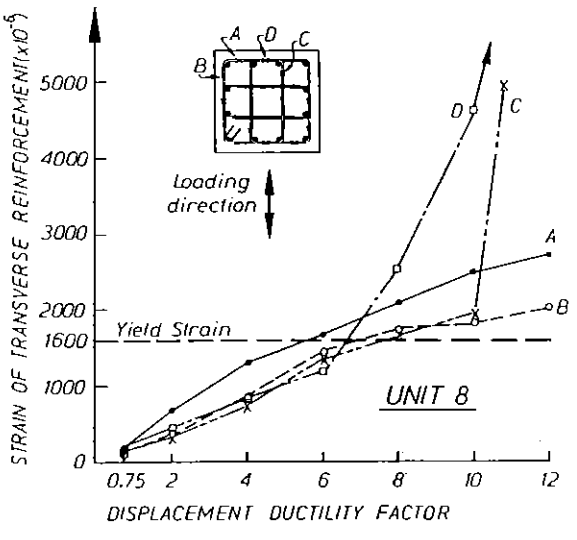

(d) Unit 8

Fig.3.40 Strains Measured on Transverse reinforcement of Units 5 to 8

along the cross tie legs with 90° and 135° end hooks and for the the 'U' bar tension splices were better in the former test units.

For Units 5 and 6 with axial load level $P_e/(f'_cA_g) = 0.1$, the neutral axis depth calculated from the extreme fibre strains measured on the column faces by the pair of linear potentiometers became minimum at displacement ductility factor of 2 to 4 and was about 0.2 of the column section depth. This means that there was lateral compressive stress present at least over about 9 d_b of the cross tie legs in the tests. For Units 7 and 8 with axial load level $P_e/(f'_cA_g) = 0.3$, it became minimum at displacement ductility factor of 4 to 6 and was about 0.35 of the column section depth. Hence, in this case, there was lateral compressive stress present at least over about 16 d_b of the cross tie legs.

For these columns, tested with constant axial load of 0.1 to 0.3 $f'_c A_g$, the alternative anchorage details used for Units 2 and 4 to 8 were as effective as the standard anchorage detail with 135° end hooks. However, it must be noted that exterior columns of a tall building may be subjected to tensile axial load in particular instants of seismic loading and hence the neutral axis depths of such columns may become less than the tested range in this study. In such a case, 'J' and 'U' cross ties with tension splices may become less effective than exhibited in this study from the view point of shear reinforcement, although those cross ties may maintain the effectiveness as confining reinforcement as mentioned in Section 3.1.3 related to the study by Oesterle et al [3.14]. This point must be remembered when these test results are applied to a practical design.

3.2.2.4 Curvature Distribution and Equivalent Plastic Hinge Length

Measured curvature distributions for Units 1 to 8 are shown in Figs. 3.41 to 3.48. As can be seen from those figures, yielding of the column was spread over a length varying between about 0.5 to 1.0 times the section depth of each column, almost in proportion to the axial load level imposed as discussed below.

The curvature at first yield, ϕ_y, defined as the average curvature measured nearest the central stub or the base block in the initial cycle of horizontal loading at $\pm$ 0.75 H_u divided by 0.75 is tabulated in Table 3.2. The

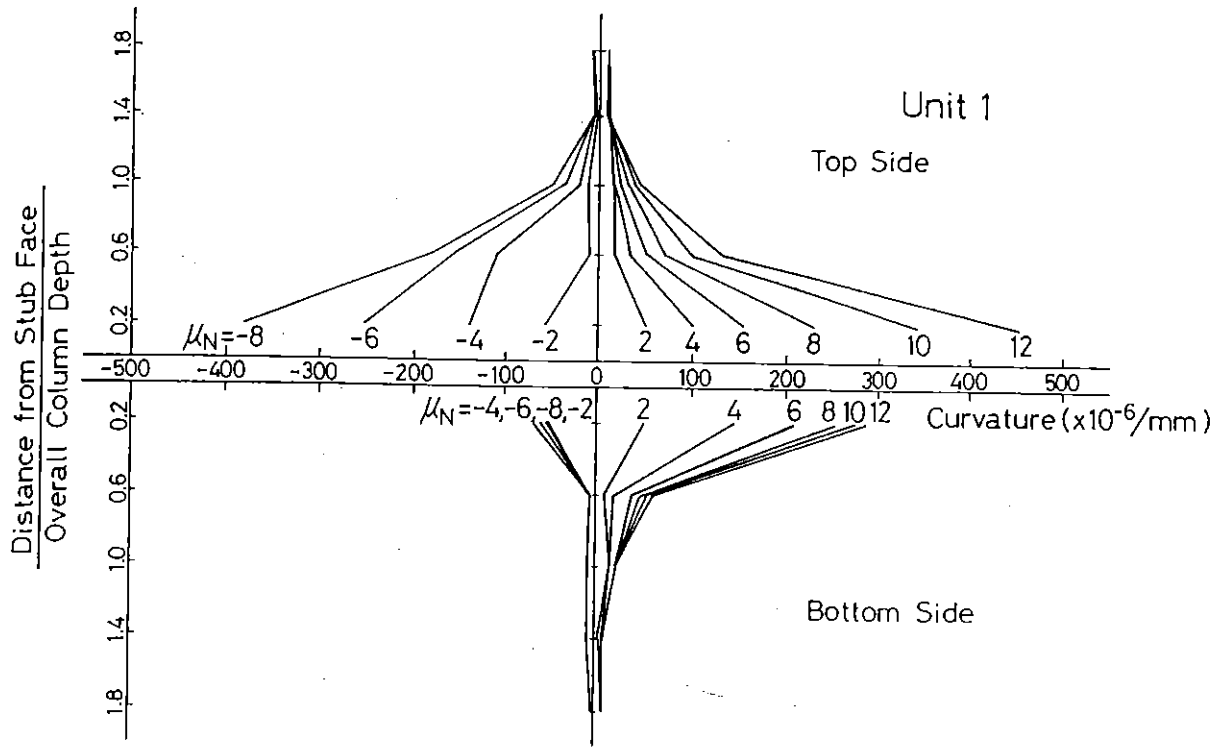

Fig.3.41 Measured Curvature Distribution for Unit 1.

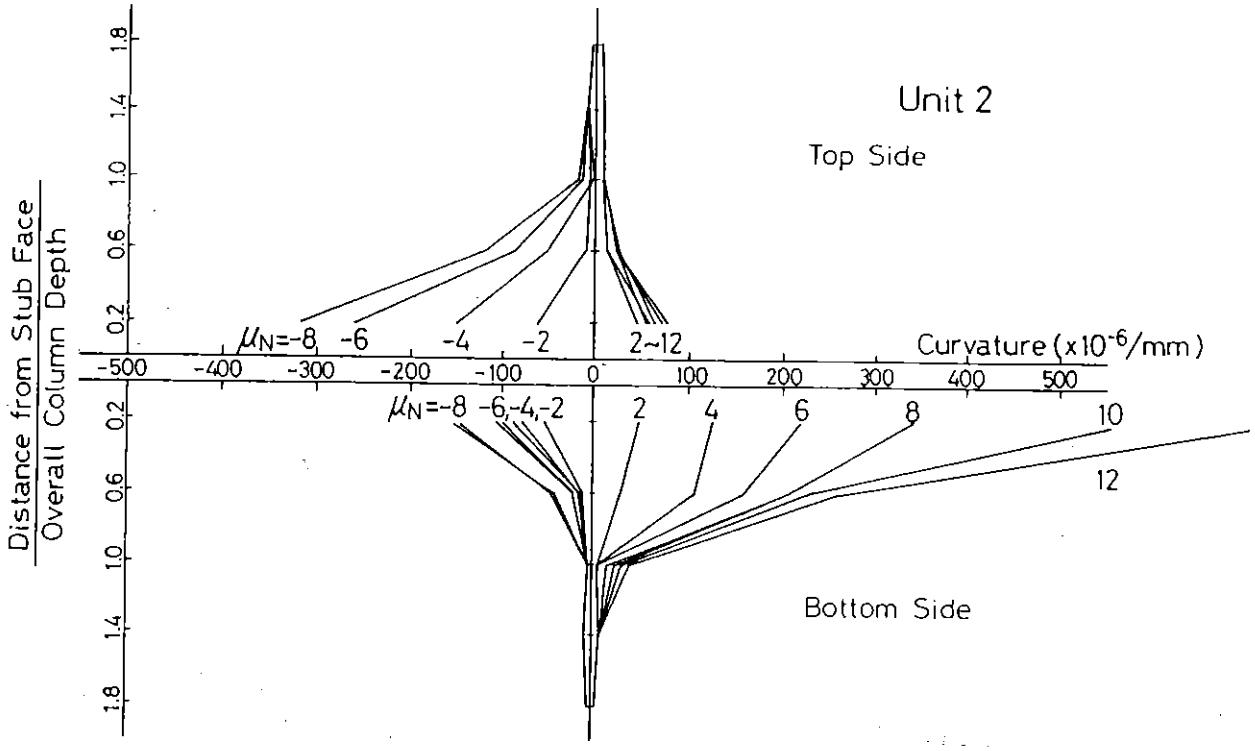

Fig.3.42 Measured Curvature Distribution for Unit 2.

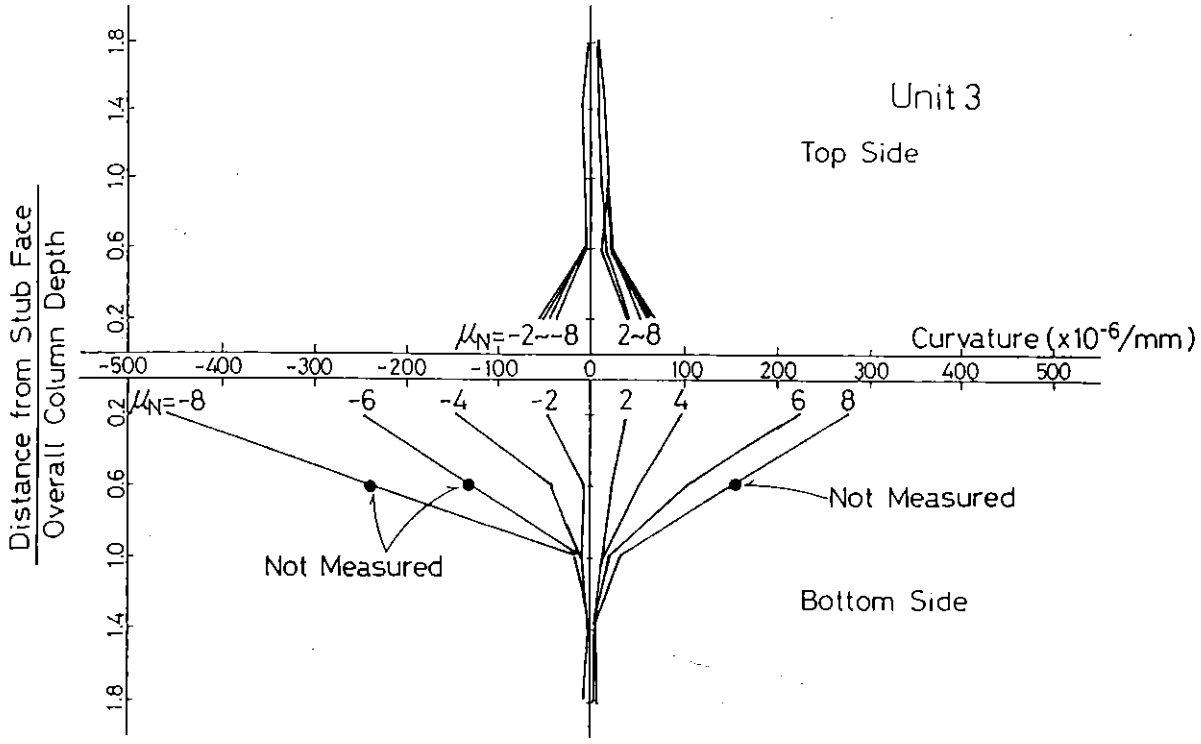

Fig.3.43 Measured Curvature Distribution for Unit 3.

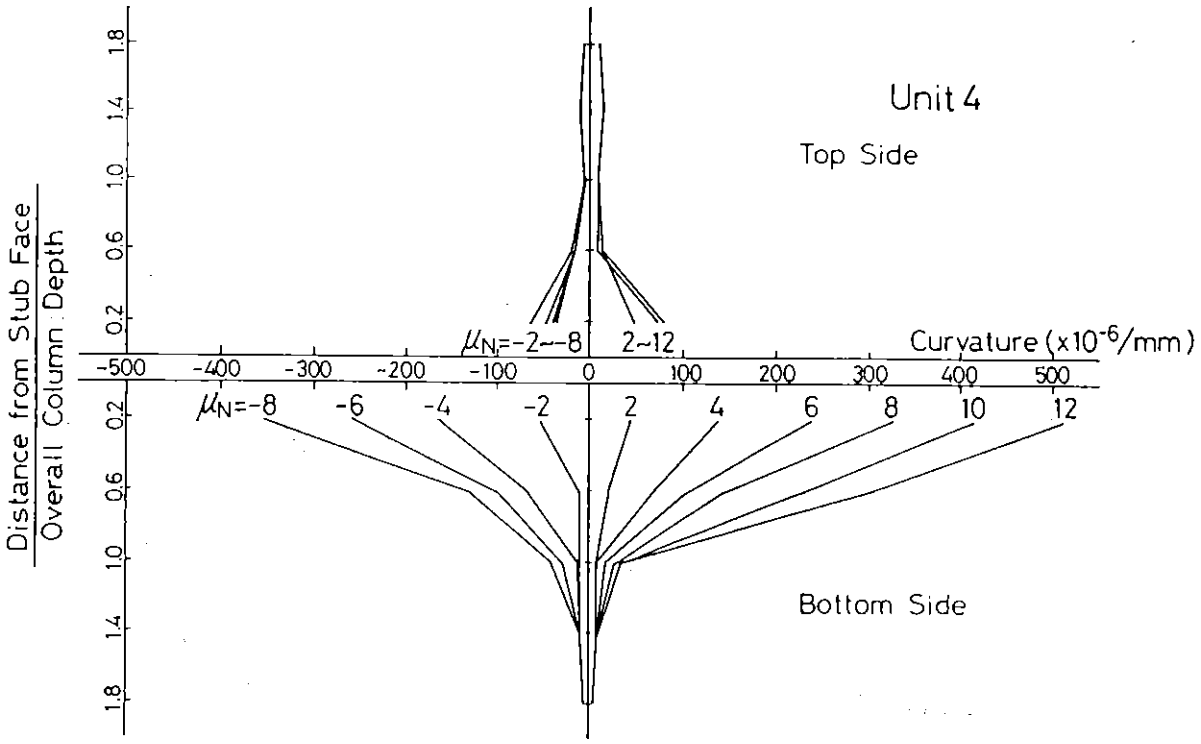

Fig.3.44 Measured Curvature Distribution for Unit 4.

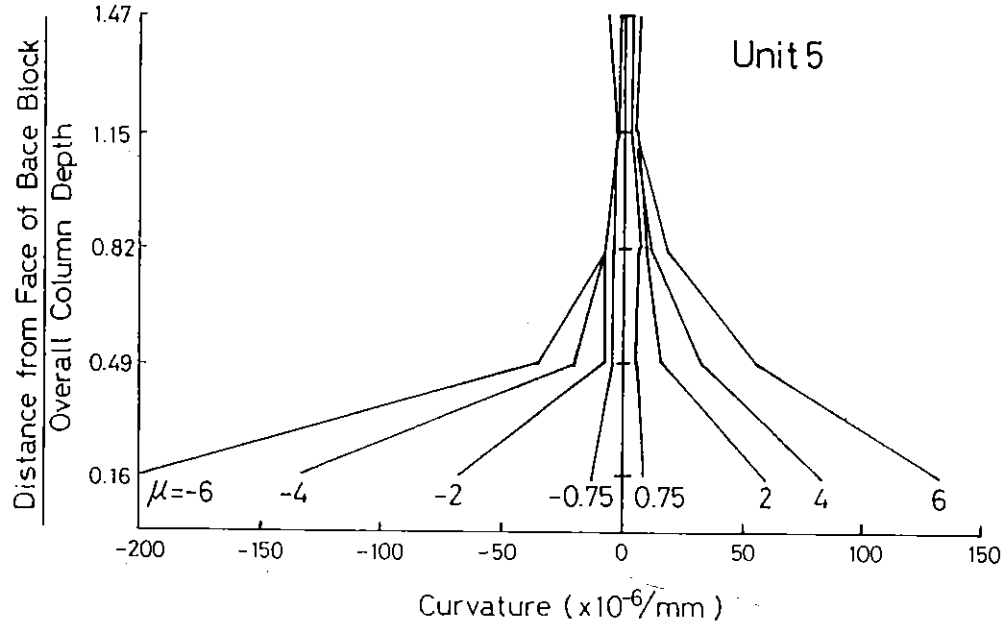

Fig.3.45 Measured Curvature Distribution for Unit 5.

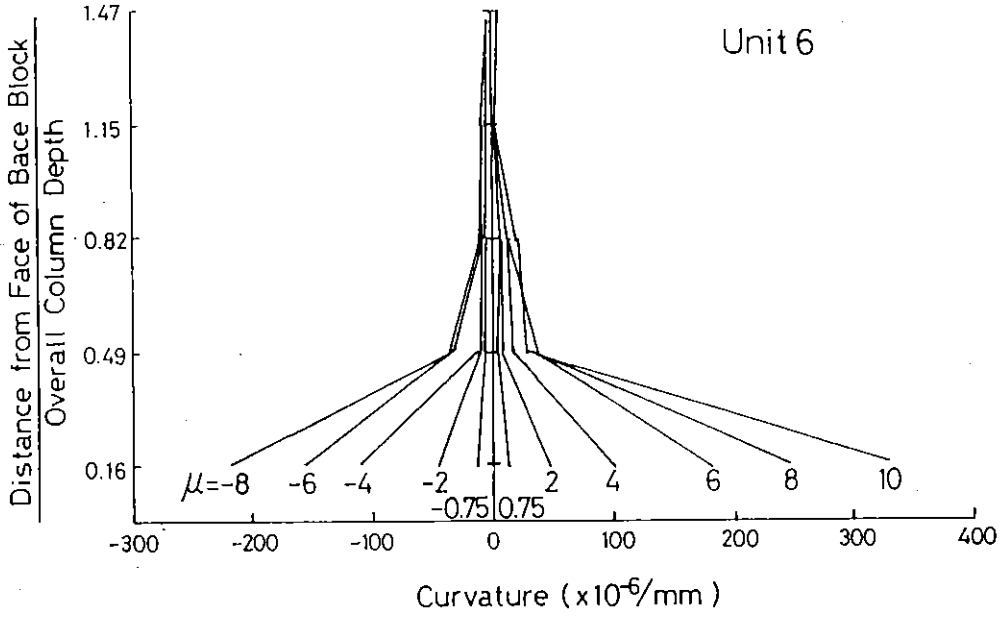

Fig.3.46 Measured Curvature Distribution for Unit 6.

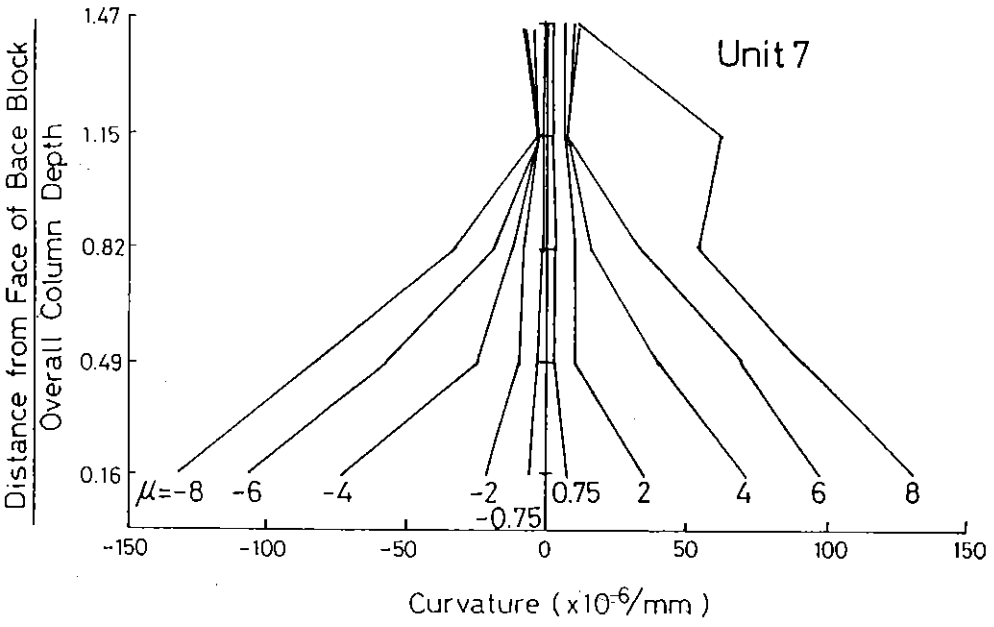

Fig.3.47 Measured Curvature Distribution for Unit 7.

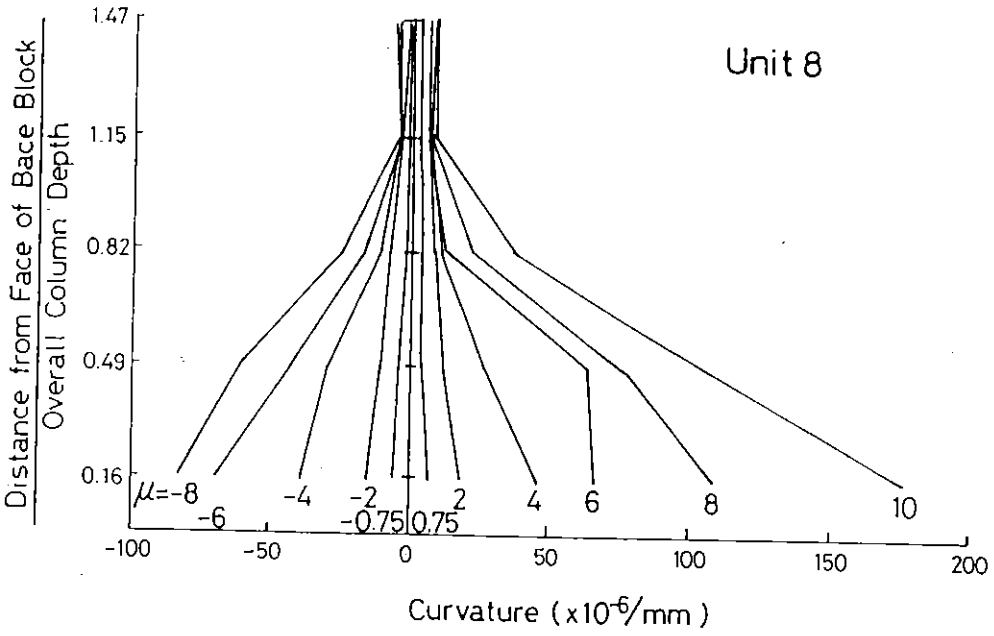

Fig.3.48 Measured Curvature Distribution for Unit 8.

gauge lengths used for the measurement of curvature were 160 mm (0.4 times overall section depth) for Units 1 to 4 and 180 mm (= 0.33 times overall section depth) for Units 5 to 8. The curvature ductility factors ϕ/ϕ_y reached at the critical section in the plastic hinge regions of the column units at various stages of loading is also listed in Table 3.2.

The equivalent plastic hinge length, L_p, was calculated for all test units at measured deformations corresponding to the nominal displacement ductility factor μ_N of ± 6. To calculate L_p, Eq. 3.1 [3.19] was used based on the assumed curvature distribution illustrated in Fig. 3.49, which assumes that the greatest curvature measured within one plastic hinge region was distributed uniformly over L_p.

$$\Delta = \left(\frac{\phi_y L}{2} \cdot \frac{2L}{3}\right) + (\phi - \phi_y) \cdot L_p \cdot \left(L - \frac{L_p}{2}\right) \quad \text{.....} \quad (3.1)$$

where Δ = real horizontal displacement at $\mu_N = \pm 6$ in the second cycle

L= distance from face of the central stub or the base block to point of zero moment at end of column

L_p = equivalent plastic hinge length

For Units 1 to 4 with axial load level $P_e/(f'_c A_g) = 0.2$, the range of values for the equivalent plastic hinge length was 172 to 281 mm, with an average of 234 mm which corresponds to 0.59 of the overall depth of the column section. For Units 5 and 6 with axial load level $P_e/(f'_c A_g) = 0.1$, the range was from 212 to 347 mm with an average of 256 mm which corresponds to 0.46 of the overall depth of the column section. For Units 7 and 8 with axial load level $P_e/(f'_c A_g) = 0.3$, the range was from 367 to 474 mm with an average of 413 mm which corresponds to 0.75 of the overall depth of the column section. Thus, the equivalent plastic hinge length became longer as the imposed axial load level became higher.

The values of equivalent plastic hinge length, which are determined by substituting measured curvatures and deflections into Eq. 3.1, generally exhibit a wide scatter, as can be seen from the above results as well as other researchers' tests, for example, by Zahn et al [3.20]. For this reason, the equivalent plastic hinge length may be approximated as 0.5 times the section depth, when the axial load level is not high.

As a reference, the equivalent plastic hinge lengths were also calculated using Eq. 3.2 which has been proposed by Baker [3.21] for members confined by transverse steel.

$$L_p = 0.8\, k_1\, k_3 \left(\frac{z}{d}\right) c \qquad \text{.....} \qquad (3.2)$$

where k_1 = 0.7 for mild steel or 0.9 for cold worked steel

k_3 = 0.6 when f'_c = 35.2 MPa or 0.9 when f'_c = 11.7 MPa,
assuming that f'_c = 0.85 x cube strength of concrete

z = distance of critical section to the point of contraflexure

d = effective depth of member

c = neutral axis depth at the ultimate moment

The measured neutral axis depths at $\mu_N = \pm 6$ were used for c in Eq. 3.2. It was assumed that k_1 = 0.9 for the used Grade 380 longitudinal reinforcement, since the measured stress-strain curves for that steel indicated comparatively high yield strength with short yield plateau as shown in Fig.3.14. By interpolation, k_3 was determined to be 0.72 for Units 1 to 4 and 0.64 for Units 5 to 8. The values of L_p thus calculated were from 255 to 490 mm with an average of 418 mm (= 1.0 times overall section depth) for Units 1 to 4, compared with the average value of L_p determined experimentally using Eq. 3.1 of 234 mm (= 0.59 times overall section). For Units 5 and 6 the calculated values of L_p were from 224 to 294 mm with an average value of 243 mm (= 0.44 times overall section depth), and for Units 7 and 8 they were from 350 to 458 mm with an average value of 394 mm (= 0.72 overall section depth). Thus, for Units 5 to 8, L_p estimated by Eq. 3.2 agreed well with those determined experimentally using Eq. 3.1 of 0.46 times overall section depth for Units 5 and 6 and 0.75 times overall section depth for Units 7 and 8..

Based on the above results, it can be said that for all test units there was no peculiar curvature distribution or unusual plastic hinge length which could be attributed to the use of alternative anchorage details for transverse reinforcement was not found, at least up to the nominal displacement ductility factor ± 6, except perhaps for Unit 3.

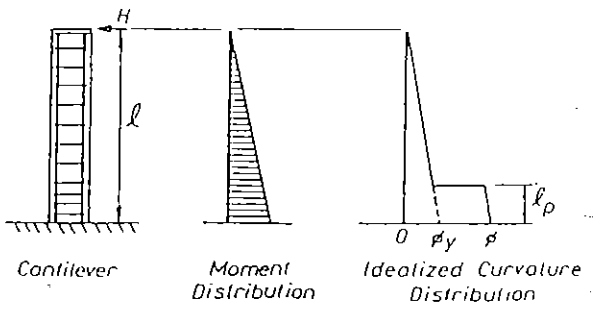

Fig.3.49 Moment and Idealised Curvature Distribution for Columns [3.19]

3.2.3 Theoretical Considerations

3.2.3.1 Flexural Strength of the Tested Columns

As described in Section 3.2.2, theoretical maximum moments M_{ACI} and M_{MKP} were calculated to compare with the test results (see Table 3.2). In the calculation of M_{ACI}, the rectangular stress block for concrete specified in the ACI code [3.7], which neglects the strength and ductility enhancement of core concrete due to lateral confinement, was applied to both cover and core concrete. Hence, M_{ACI} gives a very conservative estimation for the column flexural strength especially when the column axial load is high. M_{MKP} is the theoretical ultimate moment calculated using the modified Kent and Park stress-strain models [3.18] for unconfined cover and confined core concrete. Since the modified Kent and Park stress strain models takes into account the strength and ductility enhancement of the core concrete due to lateral confinement, M_{MKP} gives more realistic estimation for the column flexural strength. The basic procedure of the section analysis used in this chapter is is also used in other chapters. With respect to the influence of various stress-strain models for the confined concrete on the analysed results are referred in Chapter 4.

The stress-strain relationships for longitudinal reinforcement were modelled up to the strain at ultimate strength of steel as shown in Fig. 3.29, based on the measured stress-strain curves. The strains up to about 5 % were measured by a Batty extensometer with a gauge length of 50 mm, where 5 % strain was the measuring limit of that extensometer. From this measurement, the strain ε_{sh} at which strain hardening of steel commences, and the tangent modulus E_{sh} at strain of ε_{sh} in a stress-strain curve was determined (see the notation shown in Fig. 3.51). The strains at the ultimate strength of the longitudinal reinforcing bars were determined as follows. In a tensile test of a steel bar, necking of the steel bar commences after reaching its ultimate strength as illustrated in Fig. 3.50. Under such condition, it may be assumed that the stress-strain relation measured between Points A and B and that measured between Points B and C in Fig. 3.50 follow the curves (1) and (2) in Fig. 3.51, respectively. Based on this assumption, the strain at ultimate strength of a steel bar, ε_{su}, was determined using Eq. 3.3.

$$\varepsilon_{su} = \varepsilon_{sm} + f_{su} / E_s \quad \text{.....} \quad (3.3)$$

where ε_{sm} = strain measured by an ordinary scale with a gauge length of five times the bar diameter in between points B and C in Fig.3.50 after fracture of a steel bar

f_{su} = ultimate strength of a steel bar

E_s = Young's modulus of steel

The strain-hardening curve between the points (ε_{sh} , f_y) and (ε_{su} , f_{su}) in Fig. 3.51 were expressed by Eq. 3.4 using a power function which was proposed by Mander et al [3.22].

$$f_s = f_{su} + (f_y - f_{su}) \left[\frac{\varepsilon_{su} - \varepsilon_s}{\varepsilon_{su} - \varepsilon_{sh}} \right]^p \qquad \ldots\ldots \qquad (3.4)$$

where f_s = stress in the steel bar

f_y = yield strength of the steel bar

ε_s = strain in the steel bar

$$p = E_{sh} \left[\frac{\varepsilon_{su} - \varepsilon_{sh}}{f_{su} - f_y} \right]$$

The stress-strain curves for the longitudinal reinforcement which were used in the tests described in this chapter as well as in other chapters were thus modelled up to the strain , ε_{su}, at which the ultimate strength of steel is reached.

To compute the moment-curvature relationship for a given column section and axial load level, the so-called layers method [eg. 3.23] was used in this study. That is, the column section was divided into a number of discrete laminae, each having an orientation parallel to the neutral axis. For the compressed region of the concrete, the concrete cover area from the extreme compression fibre to the surface of the concrete core was divided into five laminae and the area from that core surface to the neutral axis was divided into twenty laminae. In the analyses, it was assumed that plane sections before bending remain plane after bending. When the modified Kent and Park stress-strain models for concrete shown in Fig. 3.30 were used, the stress-strain models for unconfined and confined concrete were applied to the cover and core concrete, respectively. The moment-curvature relationships were computed by increasing the extreme compressive fibre

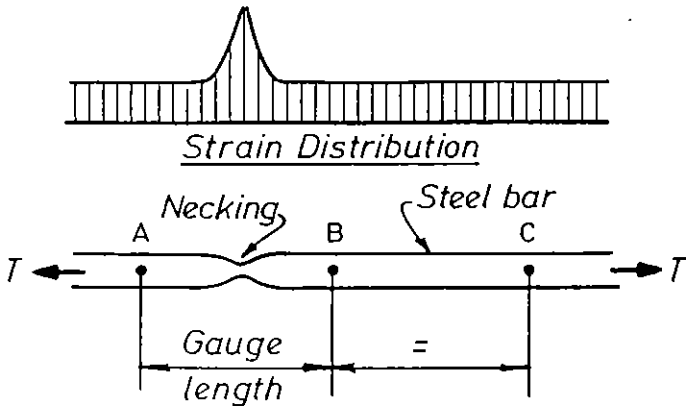

Fig.3.50 Strain Distribution in a Steel Bar with necking.

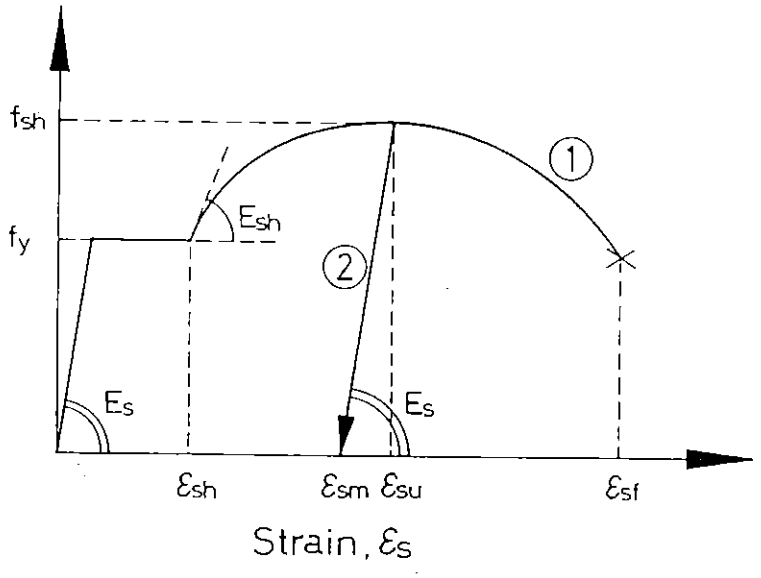

Fig.3.51 Stress-Strain Curves for Steel with Various Gauge Locations.

strain with increments of 0.0001 until the calculated moment became maximum and thereafter with increments of 0.005, satisfying the requirements of strain compatibility and equilibrium [3.19].

With respect to the spalling of the cover concrete, in the study by Park, Priestley and Gill [3.18] the cover concrete was assumed to be effective up to a concrete compressive strain of 0.004 and then to be lost at higher strains. This assumption was also used in this study. In the tests conducted here, the visual impression of the damaged zones of all column units indicated that the cover concrete there was confined and constrained from spalling off untill a real displacement ductility factor of more than 3 was reached (see the solid triangular marks in Figs. 3.19 to 3.26). At real displacement ductility factor of 3, the concrete compressive strain measured at the surface of core concrete reached about 1 % in all test units as shown in Fig. 3.31. Hence, an assumed concrete compressive strain at spalling of 0.004 will give a conservative estimate for the ultimate strength of the tested columns. However, the error due to the assumed concrete compressive strain at spalling is generally insignificant, firstly because the assumption is applied only to cover concrete with small area and secondly because the stress in the cover concrete at a strain greater than 0.004 will be negligible even if it does not spall off.

As shown in Table 3.2, the maximum moments measured in the tested columns exceeded the theoretical values calculated using the modified Kent and Park stress-strain relations for concrete by 5 to 17 %. The difference between those measured and theoretical maximum moments may be attributed to following two reasons. Firstly, the additional confinement of the stiff central stub or base block which would have strengthened the column section adjacent to the stub face. Secondly, the distance between the first hoop set and the central stub face or the base block face was set to be one half of actual spacing in the potential plastic hinge region, as is customarily done in construction practice. For these reasons, the critical section of each tested column was actually away from the stub face or the base block face, although it was assumed that the critical section was located at those faces for the calculation of the theoretical maximum moments listed in Table 3.2. If it is assumed that the theoretical flexural strength calculated using the modified Kent and Park stress-strain models for concrete is exact for the given column section, the critical section at

which this theoretical flexural strength is reached is required to be 77 to 132 mm (= 0.2 to 0.33 times the section depth) from the stub face for Units 1 to 4, 122 to 136 mm (= 0.22 to 0.25 times the section depth) away from the base block face for Units 5 to 6, and 240 mm (= 0.44 times the section depth) for Units 7 to 8. As can be seen from Figs. 3.33 to 3.37, the visually observed location where damage of each tested column concentrated was almost in agreement with the distance calculated above, being further away from the stub or base block face as the applied axial load levels became higher. Previous tests [3.24] have found this critical section to be at about 0.5 c away from the stub face, where c = neutral axis depth. In the current test series, the average value of the measured neutral axis depths measured for Units 1 to 4 was 169 mm (= 0.43 times the section depth) and that for Units 5 to 6 was 155 mm (= 0.28 times the section depth) and that for Units 7 to 8 was 251 mm (= 0.46 times the section depth). Hence, from the results of the current test series, it may be said that the critical section shifted about from 0.5 to 1.0 times c away from the stub face or the base block face.

It is also of note that Ang [3.23, 3.25] has developed empirical relationships for the strength enhancement above the moment predicted by the ACI method for when columns are detailed following NZS 3101 [3.4]. The relationships are in the form of

$$\frac{P_e}{f'_c A_g} < 0.1 \; : \; \frac{M_{max}}{M_{ACI}} = 1.13 \qquad \text{.....} \qquad (3.5)$$

$$\frac{P_e}{f'_c A_g} \geq 0.1 \; : \; \frac{M_{max}}{M_{ACI}} = 1.13 + 2.35 \left(\frac{P_e}{f'_c A_g} - 0.1 \right)^2 \qquad \text{.....} \qquad (3.6)$$

where M_{max} = ultimate moment of column

These equations give $M_{max} = 1.15\ M_{ACI}$ for Units 1 to 4, $M_{max} = 1.13\ M_{ACI}$ for Units 5 and 6, and $M_{max} = 1.22\ M_{ACI}$ for Units 7 and 8. These predicted ultimate moments also resulted in good agreement with the measured ultimate moments of the tested columns.

It is noted that the modified Kent and Park stress-strain models for confined concrete and the above empirical equations proposed by Ang were calibrated by flexure-shear tests on columns confined by ordinary hoops and cross ties with 135° end hooks. Since the measured ultimate moments of

the tested columns agreed well with or exceeded the theoretical ultimate moments M_{MKP} and those predicted by the Ang's empirical equations as shown above, it can be concluded that the hoops and cross ties with the alternative anchorage details used in the current study were as effective as those with the 135° end hooks conventionally used from the view point of attainment of the flexural strength of columns.

3.2.3.2 Moment-Curvature Relationships for the Tested Columns

The monotonic moment-curvature relationships corresponding to a range of extreme fibre concrete compression strains were computed for Units 1 to 8 using the method with the modified Kent and Park stress-strain models for unconfined and confined concrete described in the above section. Those monotonic moment-curvature relationships are shown in Figs. 3.52 to 3.59, compared with the measured moment-curvature curves in the first cycle to nominal displacement ductility factors of μ_N = + 2, + 4, + 6, etc. It has been recognized by many experiments that the envelope curve of moment-curvature responses obtained from low cycle-high amplitude loading on reinforced concrete members coincides with the corresponding monotonic loading curve when those members behave in a ductile manner. For all test units except for Unit 3, the envelope curves of the measured moment-curvarure responses agreed well with or indicated higher load carrying capacities than the corresponding theoretical monotonic moment-curvature relations. Hence, it may be considered that for these columns the transverse reinforcing details using the 'J' or 'U' bar cross ties or the cross ties with 90° and 135° end hooks, combined with the peripheral hoops with 135° end hooks, were as effective as those using the conventional periopheral hoops and cross ties anchored by 135° end hooks specified in NZS 3101 [3.4].

For Unit 3 in Fig. 3.54, the theoretical moment-curvature curves marked (a) and (b) were obtained using stress-strain curves (a) and (b) of Fig. 3.60, respectively. The curve (a) in Fig. 3.60 which was determined by assuming that all transverse reinforcement was effective is the same as that shown for Units 1 to 4 in Fig. 3.30. The curve (b) in Fig. 3.60 was determined by assuming that the confinement from only one-third of the original volumetric ratio of transverse reinforcement was effective, which allows for when the lapped 'U' bars making up the perimeter hoops (the volume of

which corresponds to two-thirds of the total volume of transverse reinforcement) became ineffective after spalling of the cover concrete. The measured moment-curvature curves degraded following the theoretical curve (b) after opening of 90° bends of the lapped 'U' bars, as shown in Fig. 3.54. Hence, it can be concluded that the lapped 'U' bars for perimeter hoops became completely ineffective after spalling of the cover concrete and thus the use of the lapped 'U' bars for perimeter hoops must be discouraged for columns subjected to severe seismic loading.

For the post peak load regions of Units 7 and 8 with axial load of 0.3 f'_c A_g, the load carrying capacities of those test units have obviously been underestimated by the corresponding theoretical monotonic moment-curvature curve. On the other hand, for Units 1 to 4 with axial load of 0.2 f'_c A_g and for Units 5 and 6 with axial load of 0.1 f'_c A_g, the theoretical monotonic moment-curvature curves agreed comparatively well with the envelope curve of the measured moment-curvature curves. With regard to these results, several features can be considered. Firstly, the effect of the strain hardening of longitudinal reinforcement may have appeared more quickly in Units 7 and 8 than other test units because of the higher axial load ratio and because the cyclic loading was applied in smaller curvatures. Secondly, although the theoretical moments were calculated assuming that the critical section was always located at the stub or base block face, the observed critical section gradually shifted away from the stub or base block face as the imposed column displacements increased, and the distance of the critical section from the stub or base block face became larger as the applied axial load level was higher as mentioned in Section 3.2.3.1. Thirdly, since the ratio of the shear span length to the column depth for Units 5 to 8 was smaller than that for Units 1 to 4, the effect of the longitudinal stress gradient mentioned in Section 2.3 might have been more beneficial for Units 7 and 8. On the other hand, it is known that the calculated moment results become more sensitive to the stress-strain model for confined concrete used as the imposed axial load level increases. Hence the results for Units 7 and 8 might be indicating that the modified Kent and Park model underestimates the strength and ductility enhancement of concrete due to lateral confinement. Using several stress-strain models for confined concrete, the adequacy of the modified Kent and Park stress-strain model for the confined concrete is evaluated in Chapter 4. It is noted that the modified Kent and Park model is so easy to use and its accuracy will

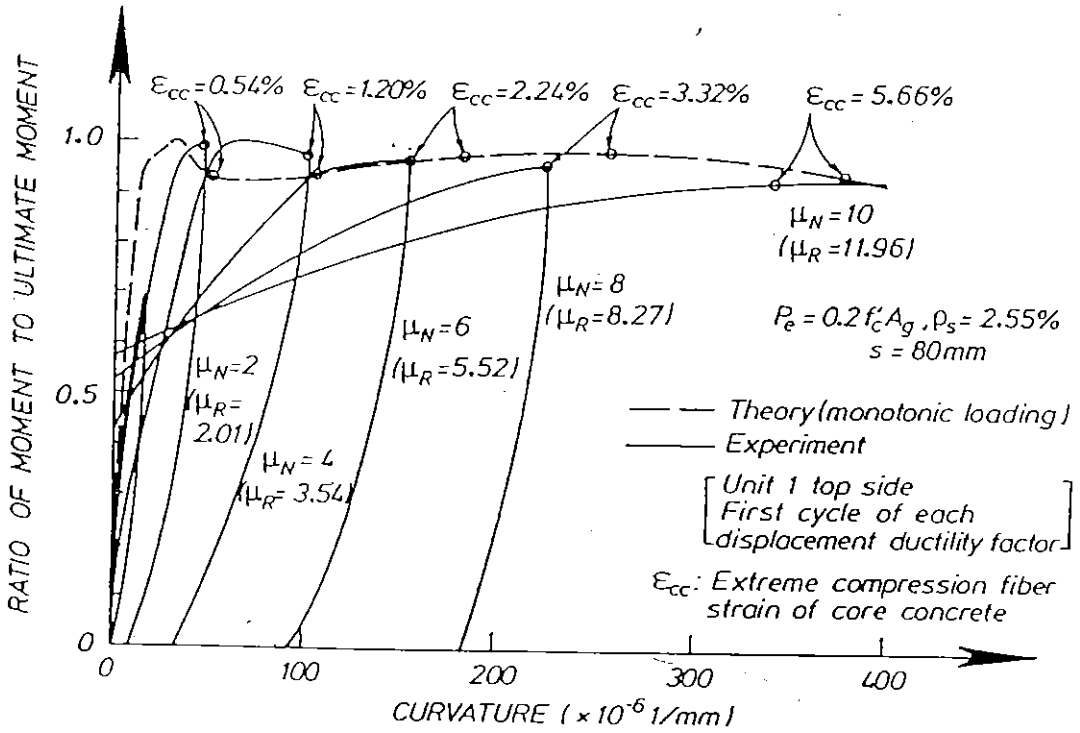

Fig.3.52 Comparison of Theoretical Monotonic and Measured Cyclic Moment Curvature Relations for Unit 1.

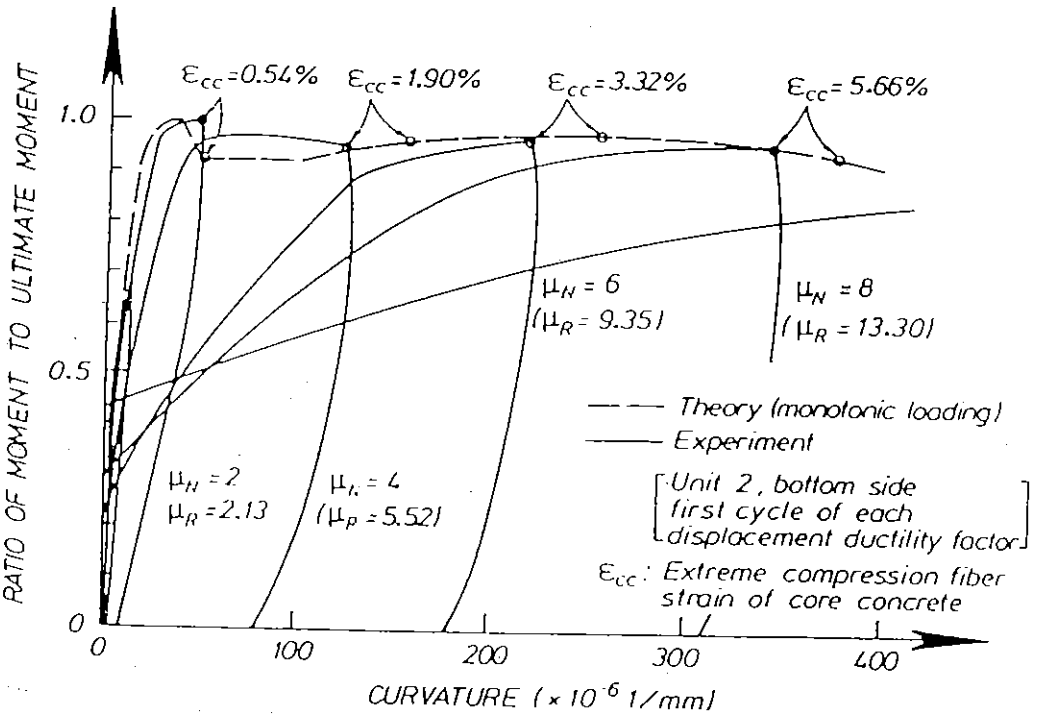

Fig.3.53 Comparison of Theoretical Monotonic and Measured Cyclic Moment Curvature Relations for Unit 2.

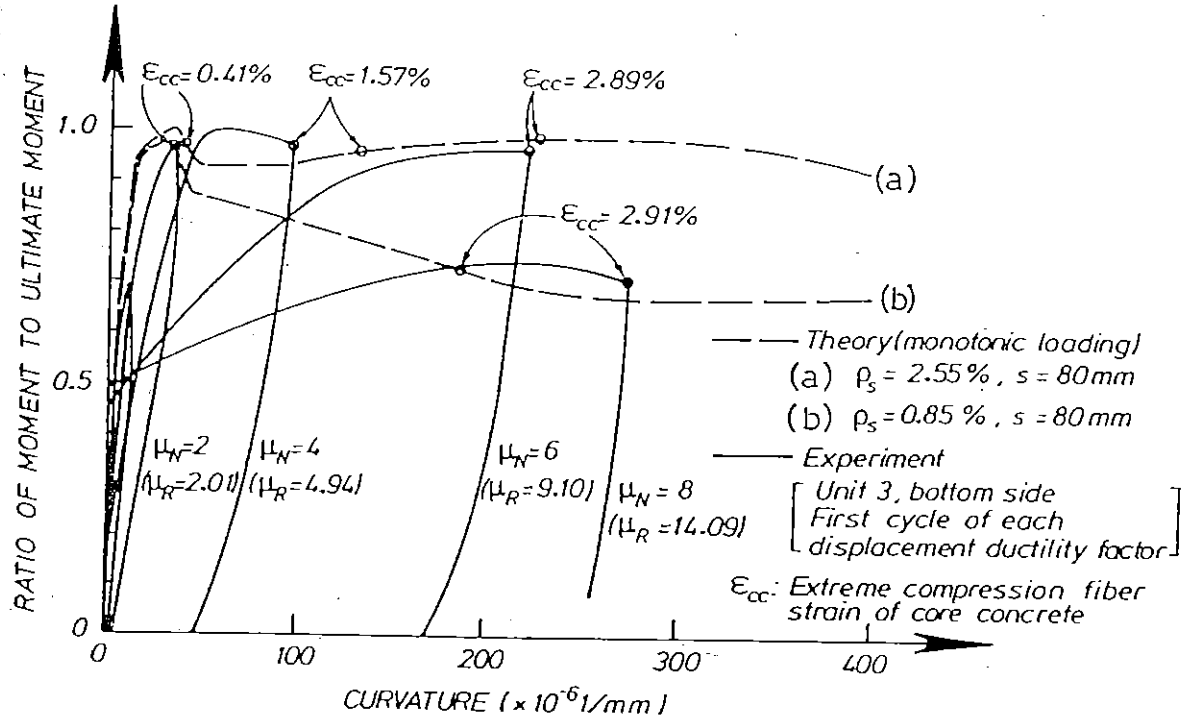

Fig.3.54 Comparison of Theoretical Monotonic and Measured Cyclic Moment Curvature Relations for Unit 3.

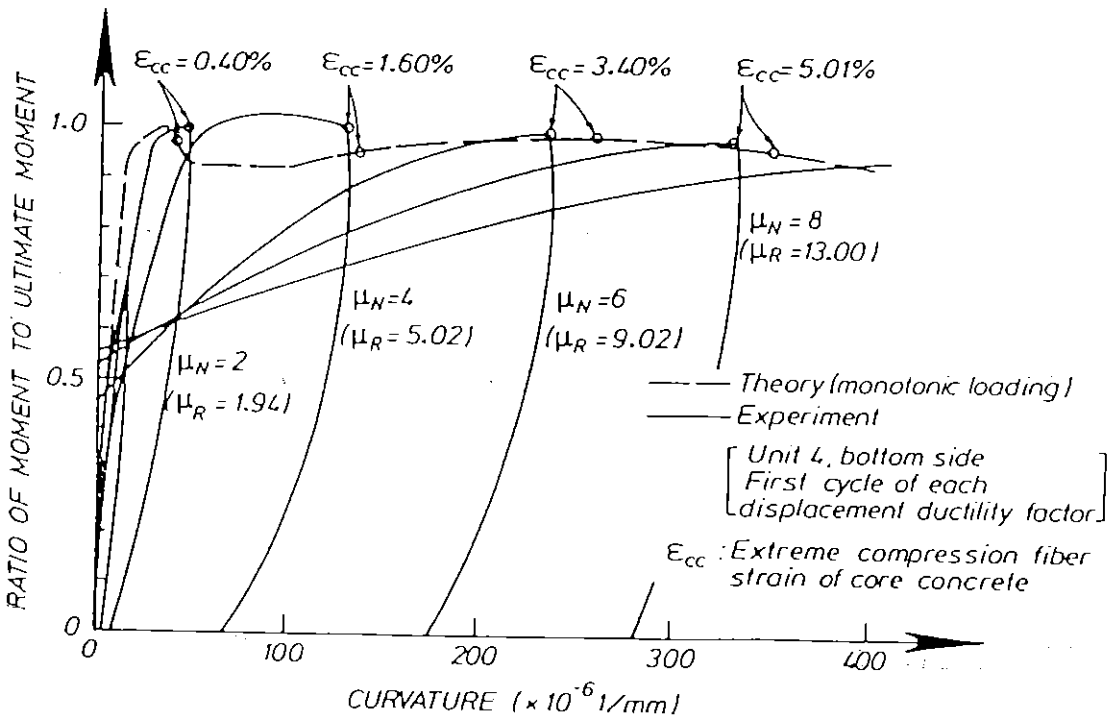

Fig.3.55 Comparison of Theoretical Monotonic and Measured Cyclic Moment Curvature Relations for Unit 4.

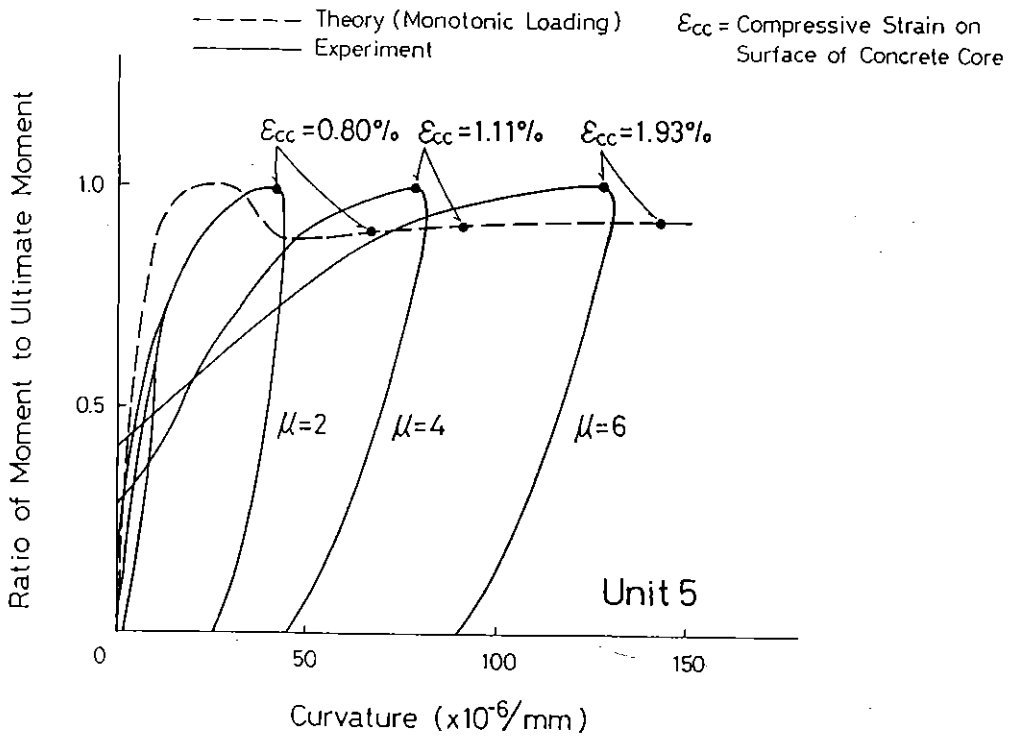

Fig.3.56 Comparison of Theoretical Monotonic and Measured Cyclic Moment Curvature Relations for Unit 5.

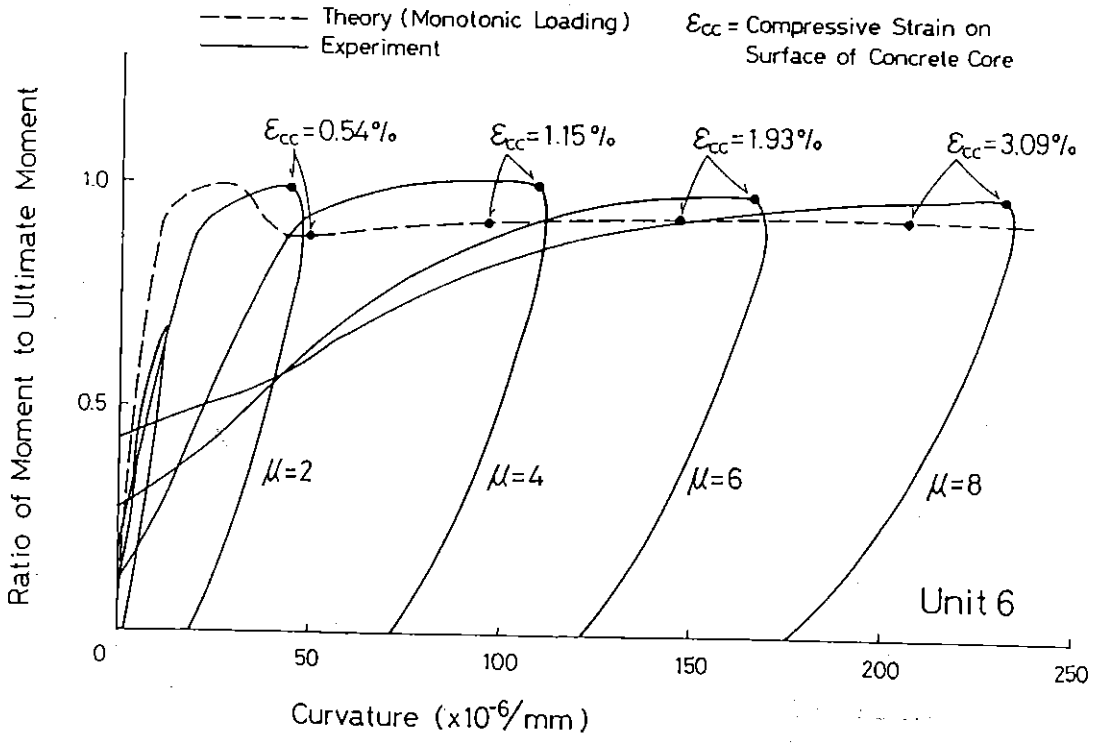

Fig.3.57 Comparison of Theoretical Monotonic and Measured Cyclic Moment Curvature Relations for Unit 6.

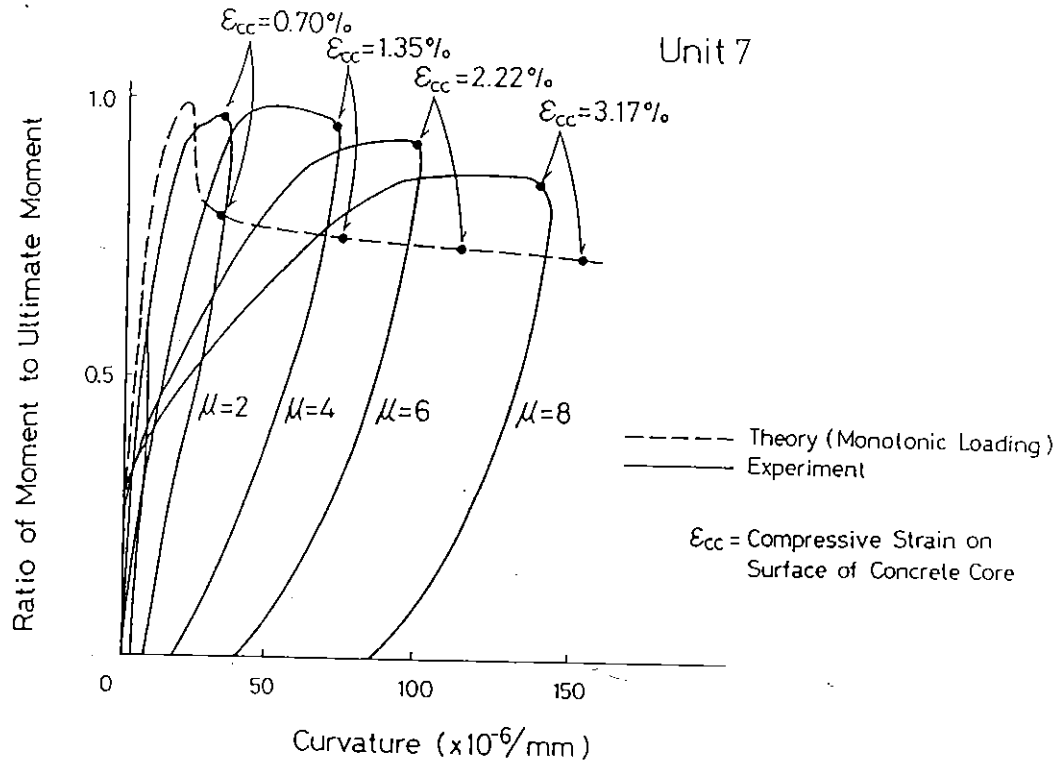

Fig.3.58 Comparison of Theoretical Monotonic and Measured Cyclic Moment Curvature Relations for Unit 7.

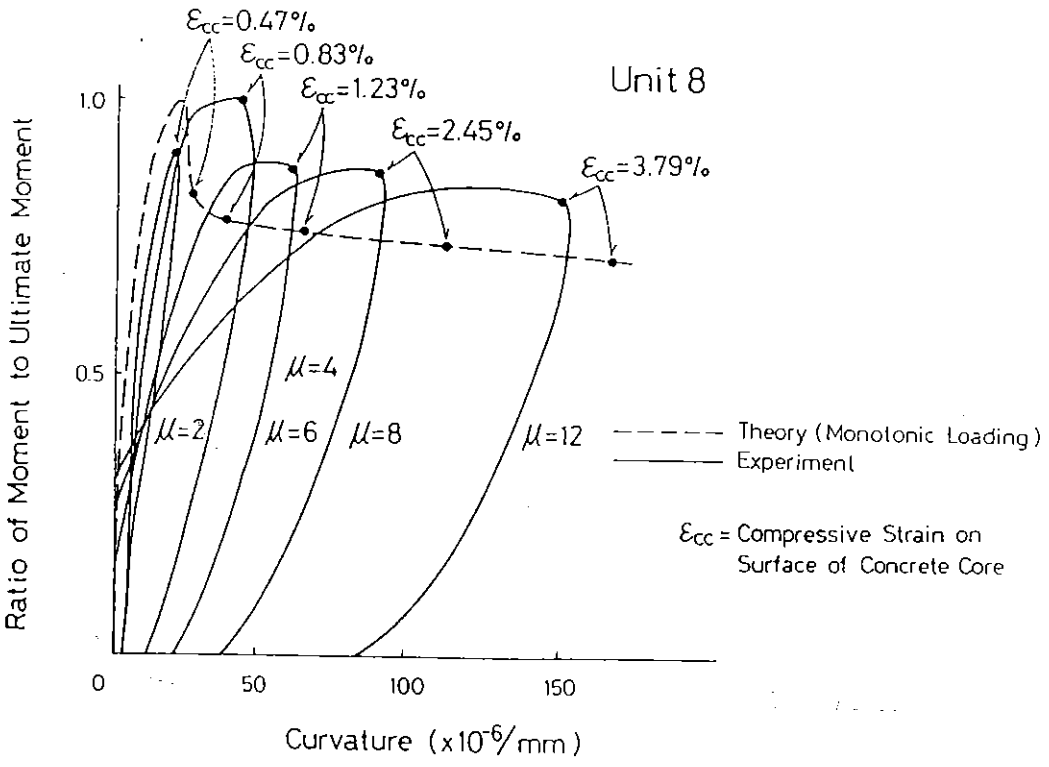

Fig.3.59 Comparison of Theoretical Monotonic and Measured Cyclic Moment Curvature Relations for Unit 8.

normally be satisfactory from the view point of that required in practical design.

3.2.3.3 Initial Stiffness of Column

As can be seen from the values of Δ_y^M shown in Table 3.2, Δ_y^M of Units 2 to 4 agreed well with that of Unit 1, where Δ_y^M = the first yield displacement determined using the measured cracked section stiffness at the 75% of the theoretical ultimate horizontal load, H_u, (see Section 3.2.1.2). Hence, it can be concluded the initial stiffness of column was not affected by the use of alternative anchorage details for the transverse reinforcement for Units 2 to 4. For Units 5 to 8, the same conclusion may be reached since in the early stage of loading any peculiar damage which could be attributed to the use of alternative anchorage details for the transverse reinforcement was not observed, although for Units 5 to 8 no comparison was made with a column having standard transverse reinforcing details.

It is of importance to be able to theoretically estimate the initial stiffness of structural members since it determines the elastic dynamic response of a structure. The theoretical lateral displacement at first yield of each test unit, Δ_y^{MKP} is also listed in Table 3.2. Δ_y^{MKP} was obtained as the sum of :

(a) The flexural deformation calculated by integrating the theoretical curvature distribution determined by section analysis of the cracked region of the column.
(b) The elastic flexural deformation of the uncracked region of the column.
(c) The shear deformation of the cracked region of the column.
(d) The shear deformation of the uncracked region of the column.

In the calculation of (a), the stress-strain models for longitudinal reinforcement shown in Fig. 3.29 and the modified Kent and Park stress-strain model for confined core concrete and unconfined cover concrete were used as used in the calculation of the theoretical moment-curvature mentioned in the previous section. The values of (a) to (d) were calculated using the following equations. The notation used for cracked and uncracked regions of column are illustrated in Fig. 3.61.

The cracking moment M_{cr} was calculated as

$$M_{cr} = f_r \cdot Z_e + \frac{Pe\,D}{6} \quad \text{.....} \quad (3.5)$$

where f_r = modulus of rupture of concrete
Z_e = elastic section modulus
P_e = axial load imposed
D = overall depth of column

Eq. 3.5 can be derived by neglecting the presence of longitudinal reinforcement as follows. As shown in Fig. 3.62, taking the sign of tensile strain as positive, the axial strain of column due to column axial load, ε_{pe}, can be expressed as

$$\varepsilon_{pe} = - \frac{P_e}{E_c \cdot B \cdot D} \quad \text{.....} \quad (3.6)$$

where P_e = column axial load
E_c = Young's modulus of concrete
B = column width

The strain in extreme tension fibre due to moment alone, ε_M, can be expressed as

$$\varepsilon_M = \frac{M_{cr}}{Z_e\,E_c} = \frac{6\,M_{cr}}{B\,D^2\,E_c} \quad \text{.....} \quad (3.7)$$

The strain in extreme tension fibre due to the axial load and the moment, ε_t is expressed in the form of

$$\varepsilon_t = \varepsilon_{pe} + \varepsilon_M = - \frac{P_e}{E_c \cdot B \cdot D} + \frac{6\,M_{cr}}{B\,D^2\,E_c} \quad \text{.....} \quad (3.8)$$

ε_t is also expressed in the form of

$$\varepsilon_t = f_r / E_c \quad \text{.....} \quad (3.9)$$

Equating Eqs. 3.8 and 3.9, Eq. 3.5 is derived. As the value of f_r, the measured values listed in Table 3.1 were used, while fr = 0.6 $\sqrt{f'_c}$ may be used as specified in NZS 3101 [3.4].

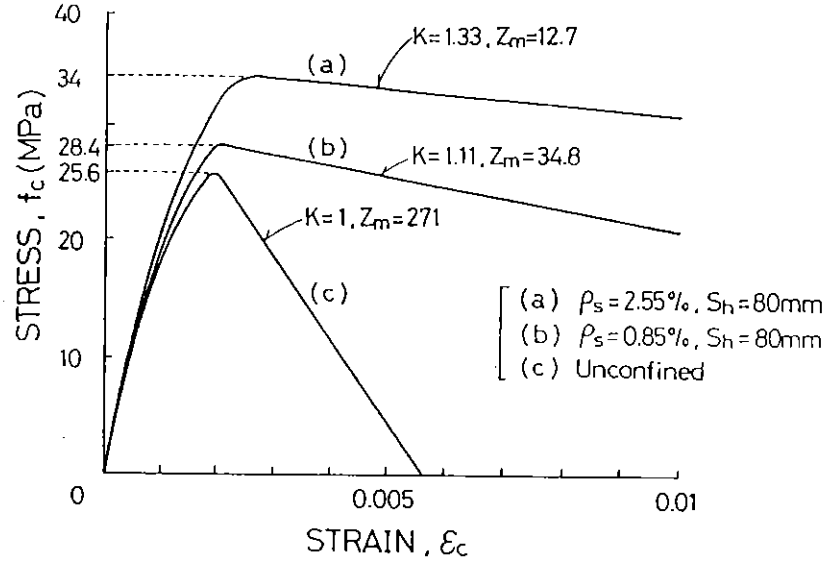

Fig.3.60 Modified Kent and Park Stress-Strain Models for Unit 3.

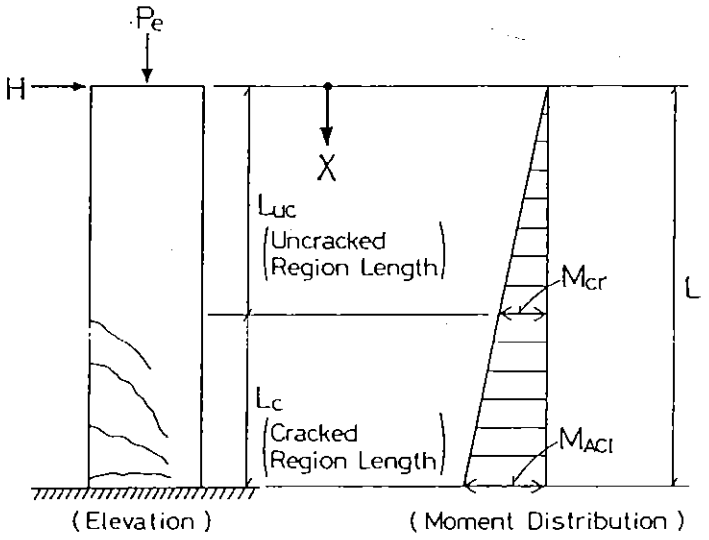

Fig.3.61 Notation Used in the Calculation of Column Deflection.

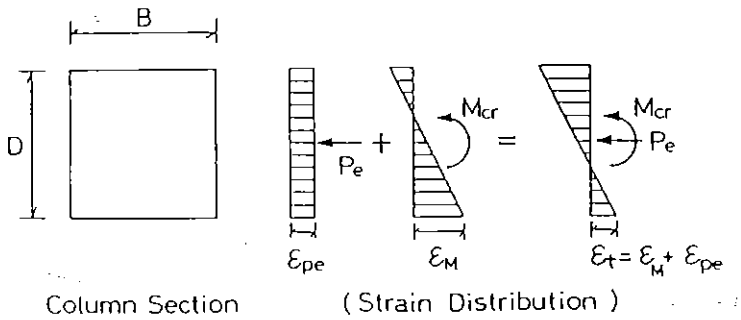

Fig.3.62 Assumed Strain Distribution Used in the Calculation of the Cracking Moment, M_{cr}.

The column deflection due to flexure in uncracked region, Δ_{ucf}, was calculated as

$$\Delta_{ucf} = \frac{M_{cr} L_{uc}^2}{3 E_c I_g} \quad \text{.....} \quad (3.10)$$

where L_{uc} = the uncracked region length of column
I_g = second moment of gross section area of column

The column deflection due to flexure in cracked region, Δ_{cf}, was calculated as

$$\Delta_{cf} = \int_{L_{uc}}^{L} \phi_x \, x \, dx \quad \text{.....} \quad (3.11)$$

where L = shear span length of column
ϕ_x = theoretical curvature of column section at distance x from horizontal loading point when the column end moment = M_{ACI}

The shear deformation of column in uncracked region was calculated taking modulus of rigidity of concrete $G_c = 0.4 E_c$ [3.19]. For the cracked region, the shear deformation was calculated assuming that the modulus of rigidity of concrete is reduced to two-thirds of G_c. That is,

$$\Delta_{ucs} = \frac{H_u}{B D G_c} L_{uc} \quad \text{.....} \quad (3.12)$$

$$\Delta_{cs} = \frac{3 H_u}{2 B D G_c} L_c \quad \text{.....} \quad (3.13)$$

where Δ_{ucs} = column deflection due to shear deformation in uncracked region
Δ_{cs} = column deflection due to shear deformation in cracked region

As the sum of the above deflections, Δ_y^{MKP} was obtained in the form of

$$\Delta_y^{MKP} = \Delta_{ucf} + \Delta_{cf} + \Delta_{us} + \Delta_{cs} \quad \text{.....} \quad (3.14)$$

The obtained Δ_y^{MKP} for Units 1 to 4 was 10.2 mm as shown in Table 3.2 and agreed well with the values of Δ_y^{M}. If theoretical first yield displacement is to be calculated by exactly following the procedure to obtain Δ_y^{M}, firstly the theoretical displacement at 75 % of H_u must be calculated and then divided by 0.75. When Δ_y^{MKP} was calculated following this procedure, it became 9.7 mm for Units 1 to 4. Thus the difference between those values was not so significant and hence the theoretical first yield displacements for Units 5 to 8 were also calculated by the former method using Eqs. 3.5 to 3.14.

As shown in Table 3.2, for Units 5 to 8, the above method gave a conservative estimate of the first yield displacement, especially for Unit 7. In the case of Unit 7, the measured horizontal displacement at - 0.75 H_u, was 1.5 times that at + 0.75 H_u, and as a result for that unit Δ_y^{M} obtained by averaging those values was much larger than Δ_y^{MKP}. The reasons why Δ_y^{MKP} became smaller than Δ_y^{M} for Units 5 to 8 can be considered as follows. Firstly, the concrete near the bottom of those columns may not has been fully compacted compared with the cases for Units 1 to 4. Secondly, since the ratio of shear span length to column depth was three in Units 5 to 8 and was four in Units 1 to 4, the inclined flexure-shear cracks formed in the former units would have contributed more to the column deflection than in the latter units. It is notable that, as a result of the formation of inclined flexure-shear cracks, the shear deformations of those columns would have been significantly larger than those expressed by Eqs. 3.12 and 3.13 even at the first cycle to ± 0.75 H_u. This aspect is discussed in detail in Section 4.3.3.3.

3.3 Conclusions

The following conclusions with regards to the anchorage of the ends of transverse reinforcement, formed from deformed Grade 275 steel bar of diameter d_b, in plastic hinge regions of reinforced concrete columns subjected to severe earthquake loading, are reached based on the test results:

(1) Satisfactory behaviour was observed for: (a) perimeter hoops with 135° end hooks with an 8 d_b extension into the core concrete, (b) interior cross ties formed from 'J' bars in which one end was anchored by a tension splice of 24 d_b in the core concrete and the other end by 180° end hook with a 5 d_b extension, (c) interior cross ties formed from 'U' bars in which the ends were

anchored by tension splices of 24 d_b in the core concrete. In the columns tested inclined flexure-shear cracks were predominant and hence the bond conditions along the tension splices of the 'J' and 'U' bars were not affected by cracking although some cracks did run along the splices.

(2) The interior cross ties with a 90° end hook and 6 d_b extension at one end and a 180° end hook and a 5 d_b extension at the other end, alternating end for end along longitudinal reinforcement, behaved satisfactorily at least up to a displacement ductility factor of 8. Beyond that displacement level the 90° end hooks commenced to open and the effectiveness of those end hooks was reduced gradually. The same conclusion is reached for when the interior cross ties with a 90° end hook and 6 d_b extension at one end and a 135° end hook and 8 d_b extension were used.

(3) The effectiveness of perimeter hoops formed from 'U' bars lapped in the cover concrete with a 17 d_b tension splice degraded rapidly when loss of the cover concrete occurred after loading cycles to nominal displacement ductility factors of 4. This transverse reinforcement detail is definitely to be discouraged. A similar conclusion can be reached regarding rectangular perimeter hoops which are anchored by 90° end hooks, although not tested tested in this study but as revealed in the 1968 Tokachi-oki earthquake and the 1985 Mexican earthquake. This is because perimeter hoops anchored by 90° end hooks can not be held against the longitudinal corner bars at the 90° end hooks after spalling of the cover concrete has occurred.

(4) The influence of the axial load level of the column on the effectiveness of cross tie bars anchored by tension splices was not found to be significant within the tested range of axial load levels between 0.1 and 0.3 $f'_c A_g$. As future research, the effectiveness of cross tie bars anchored by the tension splices needs to be examined for the case of exterior columns of a tall building which can be subjected to cyclic compression and tension axial load at instants during severe earthquake loading.

(5) The equivlent plastic hinge lengths estimated for the tested columns at a nominal displacement ductility factor of 6 were from 0.46 to 0.75 of the overall depth of the column section. The equivalent plastic hinge length was found to become larger as the imposed axial load level increased. Those plastic hinge lengths are in the range normally evaluated for columns

with conventional hoops and cross ties anchored by 135° end hooks. This finding also supports the conclusion that the 'J' or 'U' bar cross ties with tension splices, and the cross ties with 90° end hooks at one end and 135° end hooks at the other end, were as effective as conventional cross ties with 135° end hooks at least up to an imposed nominal displacement ductility factor of 6.

Based on the theoretical considerations, the following conclusions were reached:

(1) With regard to the flexural strength reached by the columns; (a) The maximum measured flexural strength exceeded theoretical nominal flexural strength calculated using the ACI concrete compressive stress block and the measured material strengths by 11 to 31 %. The strength enhancement above the moment estimated by the ACI method was well predicted by the empirical equations proposed by Ang [3.23, 3.25] which takes into account the effect of axial load imposed. (b) A theoretical moment obtained using the modified Kent and Park stress-strain curve for concrete gave more realistic estimate of the ultimate strength of column. This is because the modified Kent and Park models take into accout the enhancement of concrete strength and ductility due to the confinement by transverse reinforcement. Also, it was evident that additional confinement of the critical section was caused by the presence of the adjacent stub or base block which simulated an adjoining beam or other member.

(2) For all test units except for Unit 3, the envelope curves of the measured moment-curvature responses agreed well with or indicated higher load carrying capacities than the theoretical monotonic moment-curvature relationships obtained using the modified Kent and Park stress-strain curves for concrete, at least up to a nominal displacement ductility factor of 6. These results confirmed that the 'J' or 'U' bar cross ties with tension splices, and the cross ties with 90° end hooks at one end and 135°end hooks at the other end, were as effective as conventional cross ties with 135° end hooks, since the modified Kent and Park stress-strain curves for concrete were calibrated by tests on reinforced concrete columns with conventional hoops and cross ties having 139° end hooks. In the case of Unit 3, the measured envelope curve which degraded after opening of 90° bends of the lapped 'U'

bars for the perimeter hoops agreed well with the theoretical monotonic moment-curvature relationship obtained assuming that the lapped 'U' bars were totally ineffective. Thus the ineffectiveness of lapped 'U' bars making up perimeter hoops was also confirmed.

(3) For Units 1 to 4 with the ratio of the shear span length to the column depth of 4, the first yield displacement of column was well predicted by the theoretical method introduced in this study. In this method the first yield displacement of column was calculated as the sum of : (a) The flexural deformation calculated by integrating the theoretical curvature distribution determined by section analysis of the cracked region of the column, (b) The elastic flexural deformation of the uncracked region of the column, (c) The shear deformation of the cracked region of the column, (d) The shear deformation of the uncracked region of the column. For Units 5 to 8 with the ratio of the shear span length to the column depth of 3, the first yield displacement of column was underestimated by that method for two reasons. One reason is that the concrete near the bottom of Units 5 to 8 was not fully compacted compared with the cases for Units 1 to 4. The other reason is that the shear deformations of Units 5 to 8 would be significantly larger than those estimated by the method used in this study due to the comparatively small aspect ratio of column.

CHAPTER FOUR

INTERLOCKING SPIRALS

4.1 INTRODUCTION

When designing reinforced concrete bridge piers or building columns, a column section which is rectangular is sometimes preferable instead of a circular or square section. Figs. 4.1 (a) and (b) illustrate a rectangular column section confined by overlapping rectangular hoops and rectangular hoops with supplementary cross ties, respectively. Those lateral reinforcing details are commonly used in bridge and building construction.

A column section with interlocking spirals shown in Fig.4.2 has been introduced in the standard specifications for highway bridges adopted by the American Association of State Highway and Transportation Officials with revisions by California Transportation Authority (AASHTO:1977 and by CALTRANS:1983 [4.1]). The longitudinal bars inside the interlocking region may be used either to solely interlock the spirals or to provide column load capacity in addition to interlocking the spirals. The CALTRANS code specifies that : (a) If the longitudinal bars are used to solely interlock the spirals, they shall extend into the cap or footing the same distance as the spirals, (b) If the longitudinal bars used for interlocking the spirals are also used to provide column load capacity, they shall be fully developed into the cap and footing. The advantages of this type of column section with the interlocking spirals may be stated as follows:

1. The amount of transverse reinforcement as confinement of the core concrete, which is required to provide adequate ductility in potential plastic hinge regions of the column, may be considerably reduced by using interlocking spirals instead of overlapping rectangular hoops or rectangular hoops with cross ties. This is because spirals can much more effectively confine the core concrete than rectangular hoops. This factor has been taken into account in the New Zealand code, NZS 3101:1982 [4.2].

2. The fixing job of reinforcement may become easier by using interlocking spirals instead of overlapping rectangular hoops or rectangular hoops with cross ties, especially when column sectional dimensions are large in the directions of both principal axes. This is because, if rectangular perimeter hoops are used for a large rectangular column section, many cross ties and/or overlapping hoops are normally required in order to cross-tie the longitudinal bars which are placed between the corners of the section.

The New Zealand code provisions [4.2] and the CALTRANS code provisions [4.1] for spirals are based on experimental and theoretical studies of circular columns with single spirals or circular hoops. These may be acceptable because the basic functions of the spirals in columns are mostly the same in whatever form they are used. However, as a consequence, those codes do not provide all necessary information or specifications for the use of interlocking spirals and hence some decisions are left to the practitioners. The CALTRANS code has some provisions, but the New Zealand code has no provisions, for interlocking spirals.

When designing a column with interlocking spirals in accordance with those codes, the following questions may arise:

1. For a given diameter of spiral, what is the maximum allowable distance between the centres of the adjacent spirals in the transverse section (denoted by d_{il} in Fig.4.2) without losing the efficiency of spirals as shear reinforcement? If the distance between those spiral centres, d_{il}, is too great, the column may have inadequate shear strength and shear stiffness. This is because the efficiency of the spirals as shear reinforcement is considerably reduced in the interlocking region due to the fact that the component of the spiral tension force, in the direction of the applied shear force, is rapidly reduced at this region as shown in Fig.4.2.

2. What is the adequate bar size and spacing of the inner longitudinal bars to securely interlock the spirals? The inner longitudinal bars may be aligned just keeping the maximum allowable spacing of 200mm or 8 inches in accordance with the New Zealand code or the CALTRANS code, respectively. However, the expected functions and the corresponding actions of the inner longitudinal bars to interlock the spirals are different from those required of the outer longitudinal

bars to provide adequate column axial load and flexural capacity. It is obvious that this matter needs to be considered in connection with the mechanisms of the shear transfer by the spirals and the inner longitudinal bars.

3. In the CALTRANS code, the core area of concrete is defined as the core area surrounded by the peripheral line of interlocking spirals, [$2\pi r_1^2 - 2 A_1$ in Fig. 4.3 (a)], instead of each circular core area, when specifying the minimum volumetric ratio of spirals required. This definition may need to be reviewed due to the following reason. Since in columns with interlocking spirals the spirals overlap in the mid-depth region of the column section and the volume of spirals is thus concentrated there, the local volumetric ratio of spirals in that region becomes substantially higher than elsewhere in the column section. As a result, in the extremities of the confined core area, the volume of interlocking spirals provided in accordance with the code specification may be significantly less than that of circular columns with the same volumetric ratio of spirals. Also, the areas marked A_2 in Fig.4.3 (a) are unconfined. These factors may result in insufficient confinement of the column. For example, for a column subjected to combined bending and high axial load, it may result in inadequate confinement in extreme compression region of the column section.

It appears that no past experimental or theoretical study has been conducted to answer the above questions. In this present study, firstly, the general aspects and the related problems of interlocking spirals to provide adequate ductility in the potential plastic hinge region of columns are discussed, referring to the provisions in the New Zealand code, the CALTRANS code and other related codes. Secondly, the effectiveness of interlocking spirals is assessed based on column test results as part of this study. Three columns with interlocking spirals and, for comparison, one rectangular column with rectangular hoops and cross ties, were tested under cyclic horizontal loading which simulated severe earthquake loading. The size of the columns tested was approximately one third of that expected to be used in practical design situations for bridge piers.

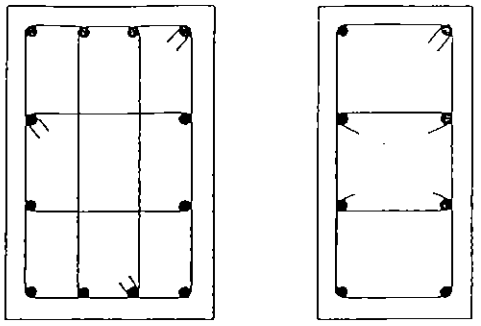

(a) Overlapping Hoops (b) Single Hoop plus Supplementary Cross Ties

Fig. 4.1 Reinforcing Details Using Hoops and Supplementary Cross Ties.

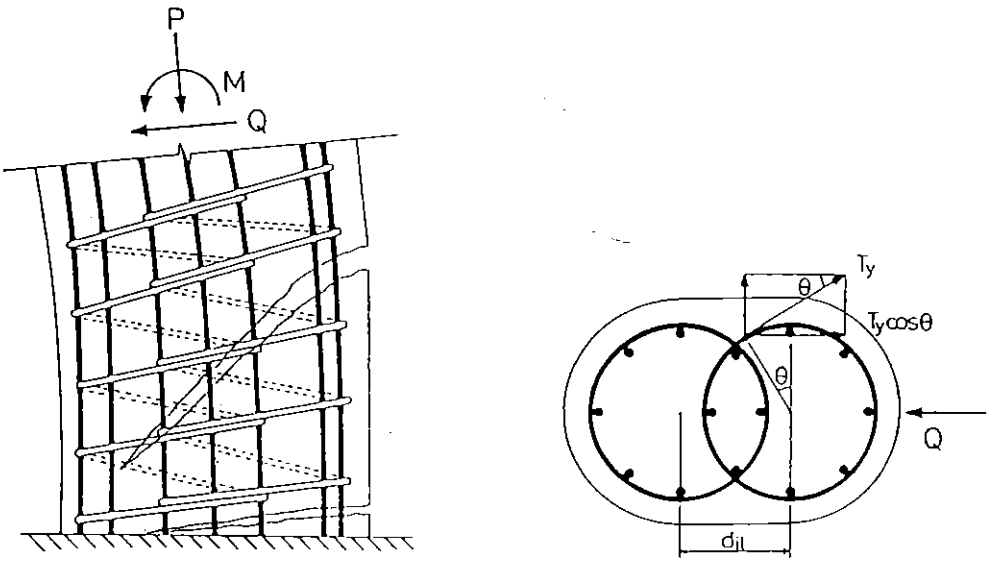

(a) Longitudinal Section (b) Transverse Section

Fig. 4.2 Reinforcing Details Using Interlocking Spirals and Longitudinal Bars.

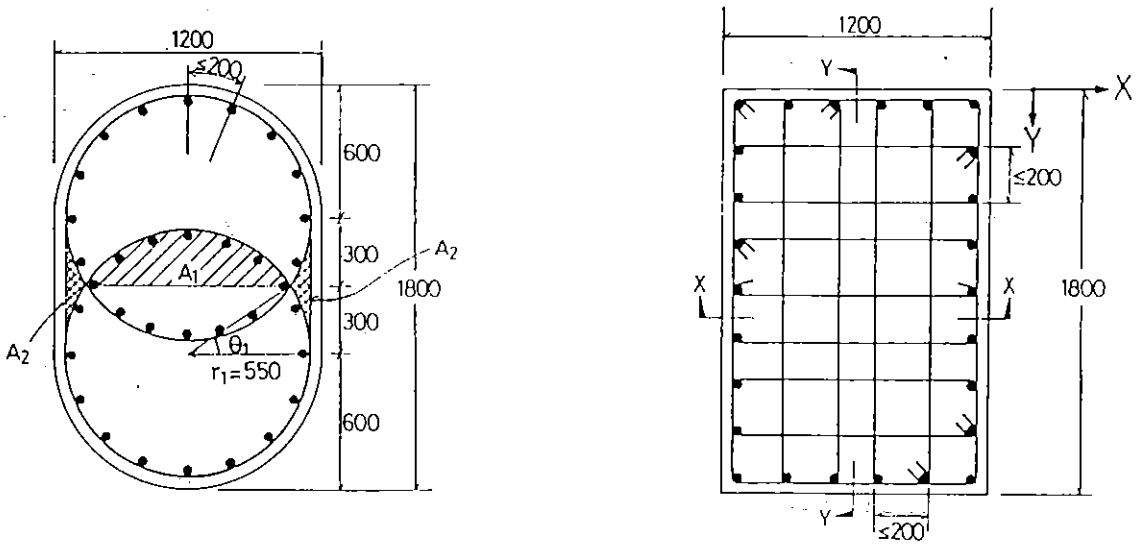

(a) Column with Interlocking Spirals (b) Column with Hoops and Cross-Ties

Fig. 4.3 Assumed Column Sections for Example Calculations of Volumetric Ratios of Transverse Reinforcement

4.2 GENERAL ASPECTS AND RELATED PROBLEMS IN DETERMINING THE REINFORCING DETAILS USING INTERLOCKING SPIRALS

4.2.1 Volumetric Ratio of Interlocking Spirals

4.2.1.1 Comparison with the Volumetric Ratio of Rectangular Hoops with Supplementary Cross Ties

Many experimental studies have demonstrated that spirals, because of their circular shape, confine the core concrete more efficiently than rectangular hoops [4.18]. This factor has been taken into account in the New Zealand code, NZS 3101 [4.2]. It is of interest to know, in practical design based on the code, to what extent the amount of transverse reinforcement can be reduced by using interlocking spirals instead of rectangular hoops with supplementary cross ties. For this purpose, comparative calculations were conducted for the assumed column sections of 1.2 m by 1.8 m shown in Figs. 4.3 (a) and (b).

In ductile structures when plastic hinges are permitted to form in columns under severe earthquake loading, NZS 3101 specifies that the volumetric ratio of spirals ρ_s in the potential plastic hinge regions of columns shall not be less than the greater of :

$$\rho_s = 0.45 \left(\frac{A_g}{A_c} - 1 \right) \frac{f'_c}{f_{yh}} \left(0.5 + 1.25 \frac{P_e}{\phi f'_c A_g} \right) \quad \text{.....} \quad (4.1)$$

or

$$\rho_s = 0.12 \frac{f'_c}{f_{yh}} \left(0.5 + 1.25 \frac{P_e}{\phi f'_c A_g} \right) \quad \text{.....} \quad (4.2)$$

where A_c = area of concrete core of section measured to outside of peripheral spiral, mm^2

A_g = gross area of section, mm^2

f'_c = specified compressive strength of concrete, MPa

f_{yh} = specified yield strength of spiral, MPa

P_e = design axial load in compression due to gravity and seismic loading acting on the column during an earthquake

ϕ = strength reduction factor

For the section shown in Fig.4.3 (a), the relations between ρ_s and the axial load ratio P_e/f'_cA_g expressed by Eqs. 4.1 and 4.2 are plotted in Fig.4.4, assuming that $\phi = 0.9$, $f'_c = 25$ MPa, $f_{yh} = 275$ MPa and a concrete cover of 50 mm to the spirals. In this calculation, in the case of Eq.4.1 the core area A_c as defined by the CALTRANS code was used. That is, the shaded areas marked as A_2 in Fig. 4.3 (a) were excluded from the core area A_c and the area of the spiral interlock was only included once (see above notation of A_c). In the case of this column, Eq. 4.2 governs the volumetric ratio of spirals ρ_s. This is because Eq. 4.1 governs ρ_s only when A_g/A_c is more than 1.27, while the value of A_g/A_c for the assumed section is 1.17.

On the other hand, when rectangular hoops and cross ties, instead of spirals, are used for columns in ductile structures under severe earthquake loading, NZS 3101 specifies as follows. When plastic hinges are permitted to form in those columns, total area of hoop bars and supplementary cross ties in each principal direction of the column cross section within spacing s_h shall not be less than the greater of

$$A_{sh} = 0.3\, s_h\, h''\, \left(\frac{A_g}{A_c} - 1 \right) \frac{f'_c}{f_{yh}} \left(0.5 + 1.25 \frac{P_e}{\phi f'_c A_g} \right) \quad \text{.....} \quad (4.3)$$

or

$$A_{sh} = 0.12\, s_h\, h'' \frac{f'_c}{f_{yh}} \left(0.5 + 1.25 \frac{P_e}{\phi f'_c A_g} \right) \quad \text{.....} \quad (4.4)$$

where A_{sh} = total effective area of hoop bars and supplementary cross ties in direction under consideration within spacing s_h

f_{yh} = specified yield strength of hoops and cross ties, MPa

h''= dimension of concrete core of section measured perpendicular to the direction of the hoop bars to the outside of the peripheral hoop

s_h = centre to centre spacing of hoops

The volumetric ratio of hoops with cross ties required for the section shown in Fig.4.3 (b) was calculated as follows. The values of ϕ, f'_c, f_{yh} and concrete cover thickness were assumed as same as those used for the column with interlocking spirals. As a first step, A_{sh} for each principal direction was calculated using Eqs.4.3 and 4.4. Then, the volumetric ratio of hoops and cross ties to concrete core ρ_{sh} was calculated using the relation

$$\rho_{sh} = \frac{A_{shx}\, h_y'' + A_{shy}\, h_x''}{s_h\, h_x'' h_y''} \quad \text{..... (4.5)}$$

where A_{shx} = A_{sh} in section x-x (see Fig.4.3(b)) determined by Eqs.4.3 or 4.4

A_{shy} = A_{sh} in section y-y determined by Eqs.4.3 or 4.4

h_x'' = dimension of concrete core in x direction (= 1100 mm for the section in Fig.4.3 (b))

h_y'' = dimension of concrete core in y direction (= 1700 mm for the section in Fig.4.3 (b))

The calculated results for various axial load levels are shown plotted in Fig.4.4. As can be seen, Eq. 4.4 governs the value of ρ_{sh} for the assumed section. It is notable that the required ρ_{sh} of the rectangular hoops and cross ties is almost twice the ρ_s of the spirals. As a matter of course, the amount of transverse reinforcement is not simply determined only by the requirements to effectively confine the core concrete. Sometimes, the restriction of the maximum spacing of the hoop sets necessary to prevent premature buckling of the longitudinal reinforcement or to provide adequate shear reinforcement governs the amount of transverse reinforcement. However, Fig.4.4 does indicate that the amount of transverse reinforcement can potentially be reduced to a half by using interlocking spirals instead of rectangular hoops with cross ties.

In the above comparison Eqs.4.2 and 4.4 governed and these equations are independent of the area of the concrete core. Eq. 4.1, instead of Eq. 4.2, will govern the volumetric ratio of spirals when column sectional dimensions are not large. This is because the minimum thickness of concrete cover is restricted by the code specification and hence A_g/A_c increases as the column sectional dimensions decrease. If it is to roughly check which equation, Eq. 4.1 or Eq. 4.2, governs the volumetric ration of the spirals, A_c may be approximated by including the shaded areas A_2 in Fig.4.3 (a). However, when the volumetric ratio of spirals is eventually determined by Eq. 4.1, area of concrete core of the column section needs to be calculated precisely. This follows since the value of A_g/A_c is not much larger than 1, and hence the value of ρ_s which is proportional to $(A_g/A_c - 1)$ in Eq. 4.1 is very sensitive to the estimation of A_c.

In the column section represented by Fig.4.3 (a), the shaded area A_1 is

$$A_1 = \int_{\theta_1}^{\frac{\pi}{2}} 2\, r_1 \cos\theta \, dy$$

where r_1 = radius of circular core section surrounded by spirals in column transverse section (measured to outside of spiral)

$\theta_1 = \sin^{-1} (d_{il} / 2\, r_1)$

$y = r_1 \sin\theta$

Since $dy = r_1 \cos\theta \, d\theta$,

$$A_1 = \int_{\theta_1}^{\frac{\pi}{2}} 2\, (r_1 \cos\theta)^2 \, d\theta$$

$$= r_1^2 \left(\frac{\pi}{2} - \theta_1 - \frac{1}{2} \sin 2\theta_1 \right) \quad \ldots\ldots\ldots\ldots \quad (4.6)$$

Using A_1 obtained from Eq.4.6,

$$A_c = 2 (\pi r_1^2 - A_1) \quad \ldots\ldots\ldots\ldots \quad (4.7)$$

Thus, the exact core area A_c is given by Eq.4.7.

4.2.1.2 Comparison with the Volumetric Ratio of Spirals in Circular Columns

If the volumetric ratios of spirals provided for a column with interlocking spirals and a circular column with a single spiral are the same, their degrees of confinement for the compression zone in the core section are normally considered equivalent. This concept needs to be reviewed for the following reason. When a column with interlocking spirals is subjected to axial compression only, taking a free body surrounded by the semicircular edge and the line X-X as shown in Fig.4.5, the equivalent fluid pressure f_{sl}, after yielding of the spiral bar, is expressed by

$$f_{sl} = \frac{2\, A_{sp}\, f_{yh}}{2\, r_1\, s} \quad \ldots\ldots\ldots\ldots \quad (4.8)$$

where A_{sp} = area of spiral bar

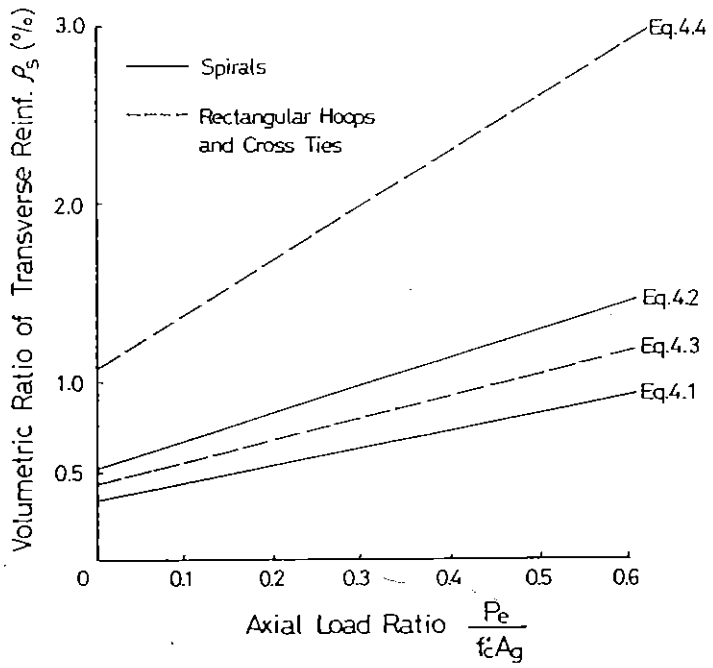

Fig. 4.4 Volumetric Ratios of Spirals and Rectangular Hoops with Cross Ties Required by the New Zealand Code for the Column Sections in Fig. 4.3.

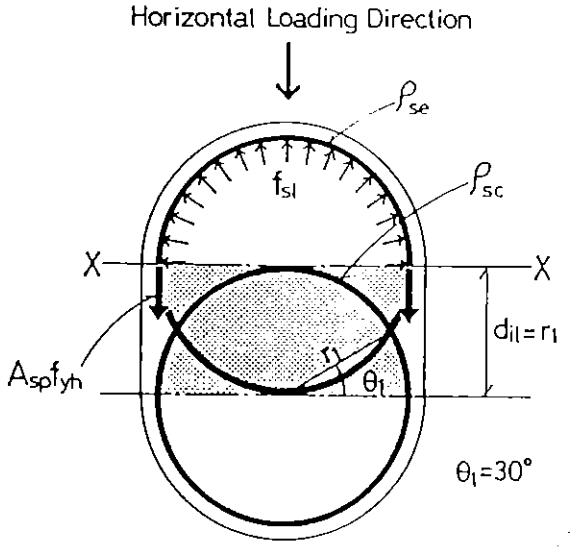

Fig. 4.5 Example of Local Volumetric Ratios of Spirals.

Thus, in the top and bottom of the core section, the maximum confining lateral pressure provided by the spirals is determined by the area of the spiral bar section, the spacing and the yield strength of the spirals placed in those extreme sectional area of the core. It must be noticed that in this case the maximum confining lateral pressure is related to the local volumetric ratio of spirals, not to the overall volumetric ratio of spirals. This means that, for the column with interlocking spirals, the degree of confinement for the compression zone in the core section needs to be counted for the local volumetric ratio in the top and bottom of the core, when column horizontal load is applied in the direction parallel to the longer dimension of the section in Fig.4.5. Since the spirals are intersected at the mid-depth region of the column section and the volume of the spirals is thus concentrated there, the local volumetric ratio of spirals in the region of the interlocking area (the shaded area in Fig. 4.5) may be substantially higher than elsewhere in the column section. Hence, the degree of confinement for the compression zone in the extremities of the core section confined by interlocking spirals may be significantly less than that by the spirals with same ρ_s in a circular column. This may lead to insufficient confinement with interlocking spirals in the top and bottom of the core section.

As an example, the local volumetric ratio of spirals in the top and bottom regions of the concrete core, ρ_{se} , and in the the mid-depth region, ρ_{sc}, will be calculated for the section with $d_{il} = r_1$ (see Fig.4. 5). The ρ_{se} is given by

$$\rho_{se} = \frac{2 \pi r_1 A_{sp}}{s \pi r_1^2} \quad \text{.....} \quad (4.9)$$

where s = centre-to-centre spacing of spirals along a column

Using A_1 calculated from Eq. 4.6, the local volumetric ratio of spirals for the shaded core area, ρ_{sc}, is expressed by

$$\rho_{sc} = \frac{2 \pi r_1 A_{sp}}{(\pi r_1^2 - 2 A_1) s} \quad \text{.....} \quad (4.10)$$

For $\theta_1 = 30°$, A_1 from Eq.4.6 is $0.614\ r_1^2$ and Eqs. 4.10 becomes

$$\rho_{sc} = \frac{2\pi r_1 A_{sp}}{1.91 r_1^2 s} \quad \text{.....} \quad (4.10\ a)$$

The volumetric ratio ρ_s based on the code definition can be expressed as

$$\rho_s = \frac{4\pi r_1 A_{sp}}{2(\pi r_1^2 - A_1)s} \quad \text{.....} \quad (4.11)$$

For $\theta_1 = 30°$, since A_1 is $0.614\ r_1^2$, Eq.4.11 becomes

$$\rho_s = \frac{2\pi r_1 A_{sp}}{2.53 r_1^2 s} \quad \text{.....} \quad (4.11\ a)$$

As a result, the ratios ρ_{se}/ρ_s and ρ_{sc}/ρ_s become 0.81 and 1.32, respectively, for the column section shown in Fig.4.5. Hence, if the volumetric ratio of spirals in a column with interlocking spirals is determined by Eqs.4.1 or 4.2, the local volumetric ratio of interlocking spirals in the core regions outside the area of interlock will become substantially less than that of a circular column with the same ρ_s. This may lead to insufficient confinement of concrete core for the column subjected to flexure and axial compression load when the neutral axis depth of the column section is shallow. Even for a column with high axial load when it is subjected to flexure, the above concept of ρ_{se} may need to be employed from the view point that confinement of the core concrete arises from ρ_{se} in the critical extreme compression fibre region of the section.

The minimum volumetric ratios of spirals expressed by $\rho_s = 0.45\ (A_g/A_c - 1)\ (f'_c/f_{yh})$ and $\rho_s = 0.12\ (f'_c/f_{yh})$ are adopted in the AASHTO code [4.1] and the SEAOC code [4.27], respectively. These expressions have been also adopted in the ACI code [4.6]. The amount of spirals specified in those codes is based on preserving the axial load strength of the section after the cover concrete has spalled rather than aiming to achieve a particular curvature ductility factor for the section. On the other hand, Eqs.4.1 and 4.2 specified in NZS 3101 are also based on the above expressions but with a modification factor $0.5 + 1.25\ P_e/(\phi\ f'_c\ A_g)$ to account for the effect of axial load on the available curvature ductility factor of the column section. This modification factor in NZS 3101 was determined by theoretical moment-curvature analyses, using conservative compression stress-strain curves for confined concrete [4.2]. The analyses recognized

that, if the axial load level is low, and the applied shear force is not large, adequate curvature ductility of the column can be achieved by a relatively small amount of transverse reinforcement. Accordingly, for low axial load levels less than $0.4P_e/(\phi f'_c A_g)$, NZS 3101 requires less transverse reinforcement than the SEAOC and AASHTO codes. On this basis, Eqs.4.1 and 4.2 in NZS 3101, may not provide a margin to cover the reduction in the local volumetric ratio of interlocking spirals from the required ρ_s, although recent studies [4.4, 4.5] have concluded that Eqs.4.1 and 4.2 are still conservative for the low axial load case. Hence, it is considered that, in case of interlocking spirals, ρ_s based on the NZS 3101 equations needs to be increased by a modification factor of ρ_s/ρ_{se}, if the logic of their derivation is pursued.

In the CALTRANS code, the minimum volumetric ratio of spiral reinforcement in the potential plastic hinge region of the column subjected to severe earthquake loading is specified as:

for columns 3 ft (914 mm) or less in least lateral dimension of column,

$$0.45\left(\frac{A_g}{A_c} - 1\right)\frac{f'_c}{f_{yh}}\left(0.5 + 1.25\ \frac{P_e}{f'_c A_g}\right) \quad \text{.....} \quad (4.12)$$

or

for columns larger than 3ft (914mm) in least lateral dimension of column,

$$0.12\ \frac{f'_c}{f_{yh}}\left(0.5 + 1.25\ \frac{P_e}{f'_c A_g}\right) \quad \text{.....} \quad (4.13)$$

but not less than

$$0.45\left(\frac{A_g}{A_c} - 1\right)\frac{f'_c}{f_{yh}} \quad \text{.....} \quad (4.14)$$

Eqs. 4.12 and 4.13 are the same with Eqs. 4.1 and 4.2, respectively, except for the absence of ϕ factor. The CALTRANS code specification is a compromise between the New Zealand code and the AASHTO and SEAOC code. Where the New Zealand code recommendation for ρ_s is less than the AASHTO code one, the AASHTO specification is retained [4.1]. Hence, in the CALTRANS code, confinement for columns with low axial load level is more conservative than the New Zealand code because of the restriction provided by Eq.4.14. Thus the CALTRANS code specifications may cover the reduction of the local volumetric ratio of the interlocking spirals from

the required ρ_s. However, this is not intentionally to cover the reduction, but simply is a result of the compromise between those codes.

4.2.2 Interlocking Spirals as Shear Reinforcement

4.2.2.1 Shear Carried by Concrete

In the New Zealand code, NZS 3101:1982 [4.2], the shear strength of a column section is estimated by a procedure similar to the ACI approach [4.6] which assumes that the ideal strength of the section V_i can be expressed as the sum of the shear "carried by concrete" V_c and that "carried by transverse reinforcement" V_s. In those codes, it is required that the calculated V_i reduced by the strength reductionfactor ϕ shall be larger than or equal to the shear force at the section derived from factored load on the structure, V_u. That is,

$$\phi V_i = \phi (V_c + V_s) \geq V_u \qquad \text{.....} \qquad (4.15)$$

Hence, as the first step, the shear carried by the concrete V_c needs to be estimated. Then, the amount of transverse reinforcement is determined to carry the load V_i minus V_c.

In the New Zealand code as well as the ACI code, the shear carried by the concrete V_c is given by

$$V_c = v_c b_w d \qquad \text{.....} \qquad (4.16)$$

where v_c = ideal shear stress provide by concrete

b_w =web width, or diameter of circular section

d = effective depth of column section

Those codes specify that d be taken as follows: d = distance from extreme compression fibre to centroid of longitudinal tension reinforcement, but need not be less than 0.8 h for prestressed members or 0.8 l_w for walls, and for circular sections need not be less than the distance from extreme compression fibre to centroid of tension reinforcement in opposite half of member (where h = overall thickness of member and l_w = horizontal length of wall).

If the longitudinal reinforcement is uniformly distributed in a circular column, d is calculated as

$$d = 0.5\,D + \left(2\int_0^{\frac{\pi}{2}} r_1^2 \sin\theta\, d\theta\right) / \pi\, r_1$$

$$= 0.5\,D + 0.318\,D' \qquad \text{.....} \qquad (4.17)$$

where $D' = 2\,r_1$

Hence, for large diameter columns, d may be approximated as 0.8 D [4.3].

In case of a column with interlocking spirals, d may become less than 0.8 h when the shear force acts in the direction shown in Fig.4.2 with a comparatively low axial load and hence when the neutral axis depth of the section is not large. However, judging from the treatment of a wall section in the above definition, 0.8 h may be also adopted as d for a column with interlocking spirals. It is notable that an overestimation of d does not result in a similar overestimation of shear carried by concrete given by Eq.4.16. The reason is that an overestimation of d leads to an underestimation of v_c in Eq.4.16 because the tension reinforcement ratio ρ_w (which is expressed by $A_s / b_w\, d$ where A_s = tension reinforcement area) is underestimated and hence the basic concrete shear stress is underestimated. The basic concrete shear stress v_b is given by [4.2]

$$v_b = (0.07 + 10\,\rho_w)\sqrt{f'_c} \le 0.2\sqrt{f'_c} \qquad \text{.....} \qquad (4.18)$$

where $\rho_w = A_s / b_w\, d$

A_s= area of tension reinforcement (for a circular column, a half of total area of longitudinal reinforcement)

The ideal shear stress carried by the concrete of a column v_c is given as the function of v_b and axial load level. v_c for potential plastic hinge regions is determined as follows [4.2]. For axial compression load levels of $P_e \le 0.1f'_cA_g$, v_c is taken as zero. This is because the primary contributions to v_c, namely shear transfer within the compression zone, dowel action and aggregate interlock, are likely to degrade when flexural and diagonal tension cracks open in alternate directions during reversed cyclic inelastic displacements. For axial compression load levels of $P_e \ge 0.1f'_cA_g$, v_c is given by

$$v_c = 4\, v_b \sqrt{\frac{P_e}{f'_c A_g} - 0.1} \qquad \text{.....} \qquad (4.19)$$

Eq. 4.19 presumes that the shear resisting capacity of the concrete increases as the axial load increases. This is based on the concept that a higher axial load level improves shear transfer in the compression zone due to deepening of the neutral axis depth of the section and enhances the shear transferred by aggregate interlock by suppressing the opening of cracks.

4.2.2.2 Shear Carried by Spirals in Circular Columns

Before considering the shear carried by interlocking spirals by truss action, the shear carried by single spirals in circular columns will first be reviewed in this section. According to the ACI code [4.6], the shear force carried by shear reinforcement placed perpendicular to the axis of member is expressed as

$$V_s = \frac{A_v\, f_{yh}\, d}{s} \qquad \text{.....} \qquad (4.20)$$

In the New Zealand code [4.2], the above expression has been modified to enable the direct calculation of the required sectional area of shear reinforcement.

Although the codes allow Eq.4.20 to be used for both rectangular and circular sections, the expression is not rigorous for circular sections. In the study by Priestley and Park [4.3], a more rigorous derivation is given. The basis for Eq. 4.20 is the assumption of a 45° crack crossing the member and all transverse steel reaching the yield strength. For a circular column with spirals, as shown in Fig.4.6, the components of spiral tension force in the direction of the applied shear force, where the spiral bars intercept the 45° crack, must be considered. Assuming that a large number of circular hoops are placed within the region of the 45° crack, the average value of cosθ can be calculated as

$$\text{Average } \sin\theta = \frac{1}{r_1}\int_0^{r_1} \sin\theta \, dy$$

Substituting $dy = - r_1 \sin\theta \, d\theta$ obtained from $y = r_1 \cos\theta$

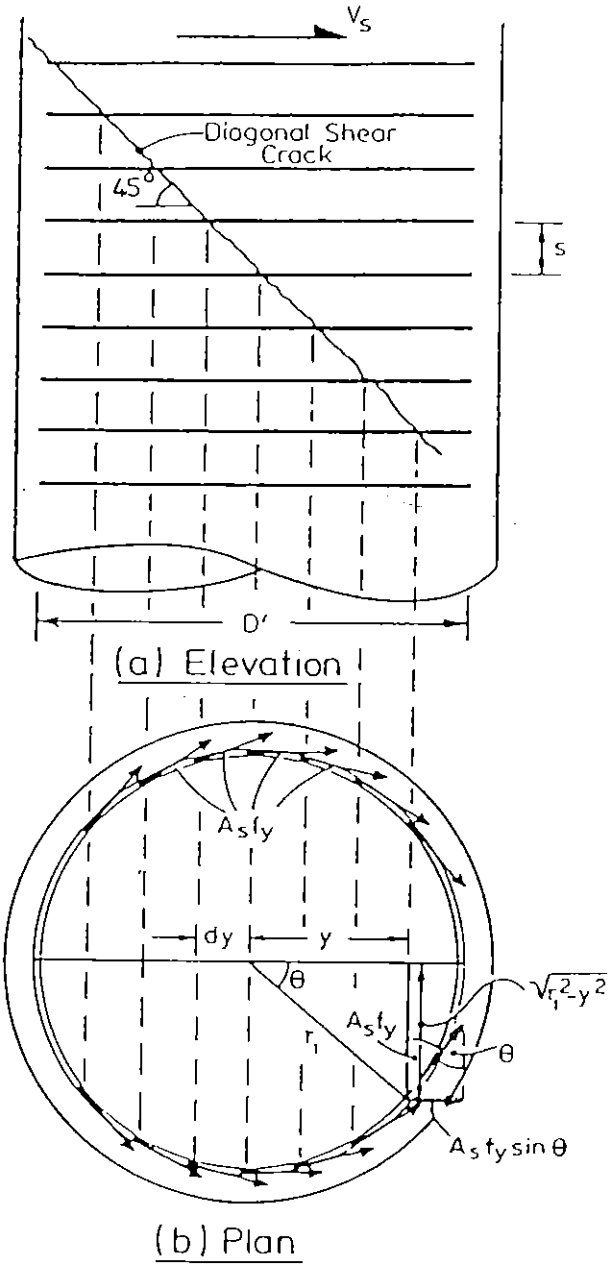

Fig. 4.6 Shear Carried by Single Spirals [4.3].

$$\text{Average } \sin\theta = \frac{1}{r_1}\int_{\frac{\pi}{2}}^{0} r_1 \sin^2\theta \, d\theta = \frac{\pi}{4} \qquad \ldots\ldots\ldots \quad (4.21)$$

Thus the total shear carried by the spiral hoops is

$$V_s = \frac{\pi}{4}(2 A_{sp} f_{yh}) \frac{D'}{s} \qquad \ldots\ldots\ldots\ldots\ldots \quad (4.22)$$

where D'= diameter of circular array of longitudinal reinforcement ($\approx 2 r_1$)

Note the diameter of the core section is taken as a conservative estimate of the diameter of the spiral. Putting $2 A_{sp} = A_v$, since each spiral is cut twice by the 45° crack, and assuming that D'= 0.93 D, which is a good estimate for a column of diameter D = 1.5m, gives

$$V_s = \frac{0.73 A_v f_{yh} D}{s} \qquad \ldots\ldots\ldots\ldots\ldots\ldots\ldots \quad (4.22\ a)$$

On the other hand, from Eq. 4.17

$$d = 0.5 D + 0.318 (0.93 D) = 0.8 D$$

Which on substituting in Eq. 4.20 gives

$$V_s = \frac{0.8 A_v f_{yh} D}{s} \qquad \ldots\ldots\ldots\ldots\ldots\ldots\ldots \quad (4.20\ a)$$

Thus Eq.4.20 will typically overestimate the spiral shear capacity by about 10%. Reference [4.3] has suggested that the more rigorous Eq. 4.22 be used although the difference between the two equations may not be large. The shear carried by interlocking spirals is discussed in the subsequent section on the basis of this suggestion.

4.2.2.3 Shear Carried by Interlocking Spirals

The main assumptions of the design method for spirals as shear reinforcement [4.3], which was introduced in the previous section, may be applicable to interlocking spirals as well. However, the concept used to obtain Eq. 4.22, which assumes that the whole of the spiral reinforcement

reaches its yield strength, may not be applicable to the interlocking parts of the spirals. When a diagonal tension crack runs across the section as shown in Fig.4.7 (a), the stress in the spiral bars outside the area of spiral interlock may rapidly increase to the yield strength immediately after the formation of the cracks. On the other hand, the magnitude of the tension stress attained by the spiral bars bounding the the area of interlock will significantly depend on the spacing of the longitudinal bars inside the area of interlock. If the spacing of these inner longitudinal bars is large, the development of high axial tension stress in the spiral bars bounding the area of interlock may be delayed until the crack opens wide and the straightening deformation of the spirals shown in Fig.4.7 (b) occurs. In this case, it may be prudent to omit the interlocking parts of the spirals from the calculation of the shear carried by the spirals and assume that those parts of the spirals are simply used for the anchorage of the spirals. However, if the longitudinal bars which interlock the spirals are closely spaced, the interlocking parts of the spirals may also be effective as shear reinforcement immediately after opening of the shear crack.

Based on the above considerations, the following three methods to estimate the shear carried by interlocking spirals are considered for the column shown in Fig.4.8.

Method (1):Assuming that the inner longitudinal bars perfectly interlock the spirals and thus all parts of interlocking spirals are effective,

$$V_s = 2\ \frac{\pi}{4}\ (2\ A_{sp}\ f_{yh})\ \frac{b_w'}{s}$$

$$= \pi\ A_{sp}\ f_{yh}\ \frac{b_w'}{s} \qquad \text{.....} \qquad (4.23)$$

where b_w' = diameter of circular core section surrounded by each single spirals ($= 2\ r_1$)

Method (2):Assuming that effectiveness of interlocking spirals is equivalent to that of the transverse reinforcement shown in Fig.4.8(c) and that $d_{il} = b_w / 2$,

$$V_s = \frac{\pi}{4}\ (2\ A_{sp}\ f_{yh})\ \frac{b_w'}{s} + 2\ A_{sp}\ f_{yh}\ \frac{b_w}{2\ s}$$

$$= \left(\frac{\pi}{2}\ b_w' + b_w\right)\ \frac{A_{sp}\ f_{yh}}{s} \qquad \text{.....} \qquad (4.24)$$

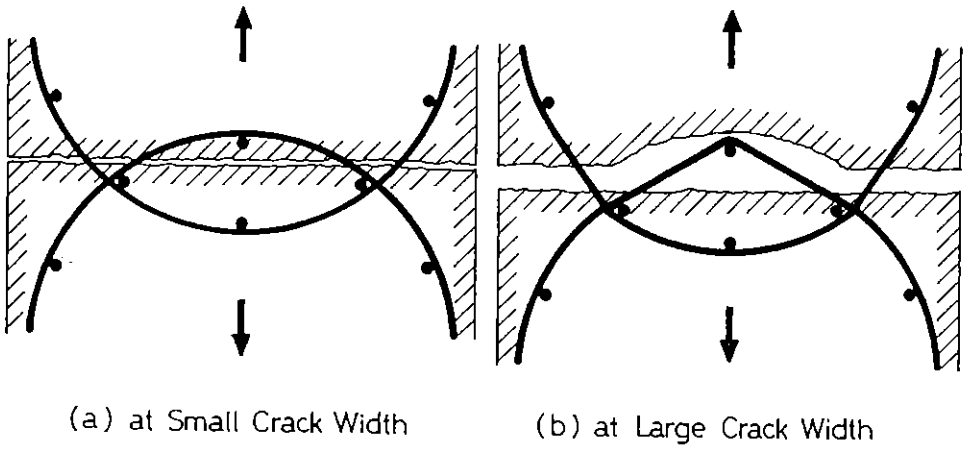

Fig. 4.7 Deformation of Spiral Bars due to Diagonal Tension Cracking.

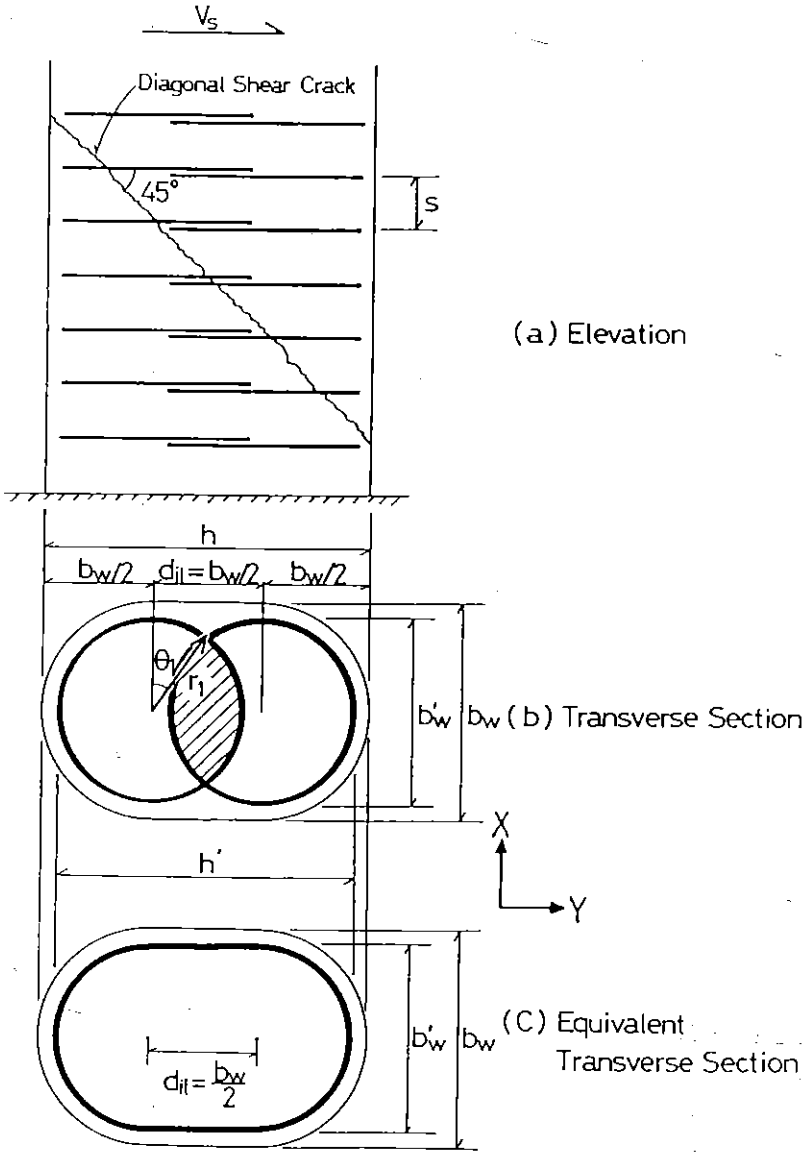

Fig. 4.8 Shear Carried by Interlocking Spirals.

Method (3): Assuming that the parts of the spirals in the interlocking region(the shaded area in Fig.4. 8,(b)) are ineffective against shear and that $d_{il} = b_w / 2$,

In this case, the average cosθ between the angles 0 and θ_1 in Fig.4.8 (b), that is, between y = 0 and $b_w/4$ needs to be calculated.

$$\text{Ave. } \cos\theta = \frac{1}{r_1 \sin\theta_1} \int_0^{\theta_1} r_1 \cos^2\theta \, d\theta$$

$$= \frac{1}{\sin\theta_1} \left(\frac{\sin 2\theta_1}{4} + \frac{\theta_1}{2} \right) \quad \text{.....} \quad (4.25)$$

Hence,

$$V_s = \frac{\pi}{4} (2 A_{sp} f_{yh}) \frac{b_w'}{s} + \text{Ave. } \cos\theta \, (2 A_{sp} f_{yh}) \frac{b_w}{2s}$$

$$= \left(\frac{\pi}{2} b_w' + \text{Ave. } \cos\theta \, b_w \right) \frac{A_{sp} f_{yh}}{s} \quad \text{.....} \quad (4.26)$$

For the column shown in Fig.4.3 (a), $b_w' = 0.92\, b_w$ and $\theta_1 = 0.577$(radian) are estimated. For $\theta_1 = 0.577$(radian), Ave. cosθ = 0.949 is obtained from Eq.4.25. For these values, methods (1),(2) and (3) give $V_s / (A_{sp} f_{yh} b_w/s)$ = 2.89, 2.44 and 2.39,respectively or gives $V_s / (A_v f_{yh} b_w/s)$ = 1.45, 1.22 and 1.20, respectively. As expected, the methods (2) and (3) give almost identical estimations of V_s , for the case when the distance between the centres of the adjacent spirals in the transverse section d_{il} is taken as $b_w/2$. The difference between the value of V_s by method(1) and that by methods (2) or (3) may be also insignificant from the view point of the accuracy of estimation required in practical design. However to properly apply method (1) the inner longitudinal bars are required to perfectly interlock the spirals. Hence methods (2) or (3) may be considered to be more appropriate. In practical design, when d_{il} of about $b_w/2$ is used, method (2) is recommended because Eq.4.24 is simple to calculate and will give a reasonable estimate of V_s.

It is notable that, even when d_{il} of more than $b_w/2$ is used, method (2) does not give a significant overestimation of V_s as long as the spirals are interlocked. This can be demonstrated by an example with the extreme case of $d_{il} = b_w'$(=two times r_1). In this case, the method (3) as well as the method(1) give

$$V_s = \pi A_{sp} f_{yh} \frac{b_w'}{s}$$

and the method (2) gives

$$V_s = \left(\frac{\pi}{2} + 2 \right) A_{sp} f_{yh} \frac{b_w'}{s}$$

Thus V_s by the method (2) results in 1.14 times V_s by the methods (1) and (3) even for such an extreme case. Such a large d_{il} would not be used in practice since it would not permit the spirals to be interlocked effectively.

It must be emphasized that Eqs. 4.23, 4.24 and 4.26 have been derived based on the following assumptions;

(1) An inclined column section along the 45° diagonal tension cracks becomes critical and forms the failure plane.

(2)The amount, spacing and locations of the longitudinal bars inside the interlocking area are adequate to secure the anchorage of each continuous spiral and to interlock neighbouring spirals.

(3) Distance between the centres of the adjacent spirals in the column section, d_{il}, is close enough to provide sufficient interlocking area for placing longitudinal bars to satisfy the assumption (2).

However, as discussed in the subsequent section, vertical splitting cracks parallel with the column axis may be formed in the region of spiral interlocking and induce the failure of the column if interlocking of spirals is insufficient due to inadequately large d_{il} or improper arrangement of longitudinal bars inside the interlocking area. In such case, the amount of interlocking spirals cannot simply be determined only by Eqs. 4.23, 4.24 or 4.26 against the design shear force because the failure mode of the column may be different from that with 45° diagonal tension cracks.

4.2.2.4 A Combined Beam-Arch Action Model for the Column with Weak Interlocking of the Spirals

In order to assess the required distance d_{il} for secure interlocking of the spirals, the reduction of the column strength due to weak interlocking of the spirals needs to be estimated. When the shear carried by the interlocking spirals is estimated using Eqs. 4.23, 4.24 or 4.26, it is necessary to satisfy the condition that d_{il} is adequate to properly interlock the spirals and that the 45° diagonal tension cracks form the failure plane against the applied shear force. However, if d_{il} is relatively large as shown in Fig.4.9,

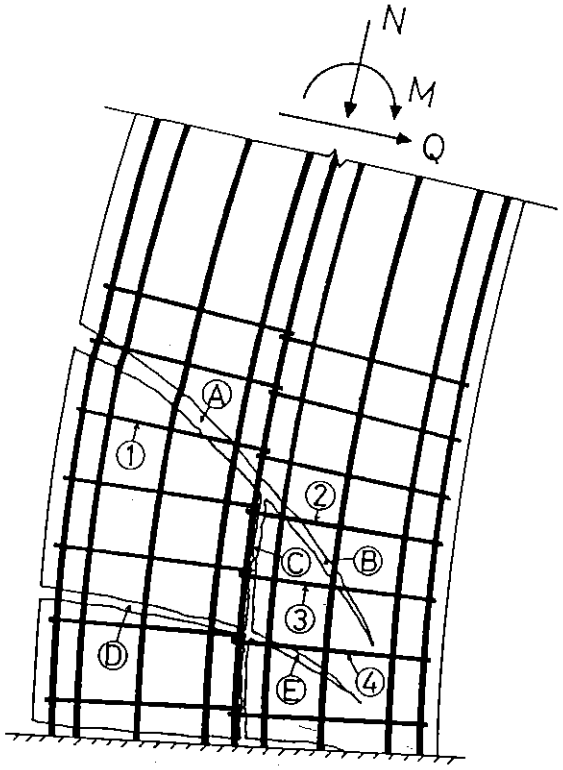

(a) Longitudinal Section

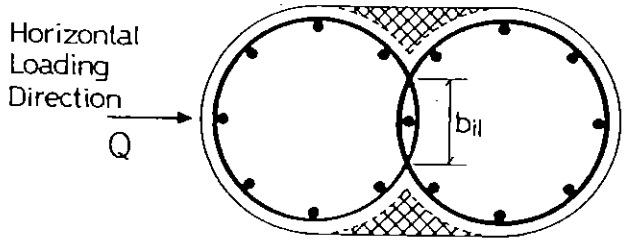

(b) Transverse Section

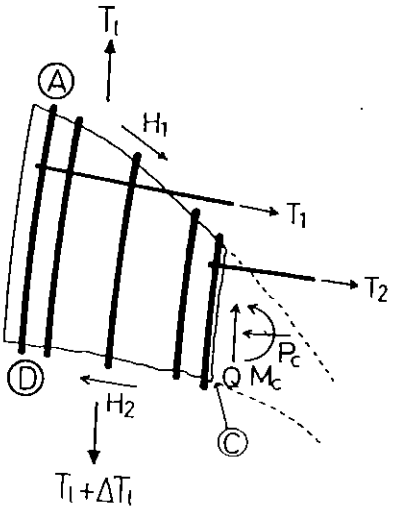

(c) A Concrete Cantilever

Fig. 4.9 Shear Transfer Mechanisms for Spirals with Weak Interlocking.

the vertical crack(C) along the central longitudinal bar may form as well as diagonal tension cracks (A)-(B) and (D)-(E). As a result, the section along the cracks (A)-(C)-(E) may become critical. This is because through the section along the cracks (A)-(C)-(E), only the spiral turn (1) may be effective, since although the spiral turns (2),(3) and(4) are also interconnecting cracks (C)-(E) they are ineffective due to the small magnitude of the spiral tension force component in the applied shear direction. Crack (A)-(B) may be tied by spiral turns (1),(2) and (3) effectively, as estimated by Eqs. 4.23 or 4.26. As a result, the expected shear strength of the column given by Eqs 4.23 or 4.26 may not be reached due to the formation of the weak section line along the cracks (A)-(C)-(E). The reasons why the vertical crack(C) may form can be explained as follows:

The free body of the concrete cantilever can be represented by Fig.4.9(c), as was introduced in the Kani's comb tooth theory [4.8] and in the beam action theory by Park and Paulay [4.18]. In this figure, the tension forces in the longitudinal bars, and the change in those forces due to the bond stresses, are lumped into single forces T_L and $T_L + \Delta T_L$, respectively. The dowel forces acting on the longitudinal bars are not indicated in order to avoid complicating the figure. At the potential vertical crack section(C), a moment M_c is induced to resist the remainder of the moment due to ΔT_L after subtraction of the moments due to the spiral forces T_1 and T_2, the aggregate interlock forces H_1 and H_2, and the dowel forces. The shear force Q is induced mainly by the bond force ΔT_L, although the vertical component of the force H_1 minus that of the force H_2, which are due to the aggregate interlock, may also contribute.

The cover concrete shown as the shaded area in Fig.4.9(b) may spall off in inelastic range of seismic loading, especially when the seismic loading is bi-directional. After the spalling of the cover concrete, the width of the concrete cantilever at the potential cracking section (C) is reduced. This reduction in width weakens the moment of resistance of the section (C) of the concrete cantilever for two reasons. Firstly, the second moment of area decreases and, secondly, the shear stress (Q / the section area) increases. The increase of shear stress decreases the tensile strength of concrete and is one of the important factors to be considered when determining the the cracking moment of the concrete

cantilever section. Accordingly, the moment induced at the section (C) may exceed the moment required to cause cracking of the cantilever. Also the splitting of concrete in the vertical direction may arise from the lateral forces imposed on the longitudinal bars in the region of spiral interlock (see Fig.4.7). Shear transfer from spiral to spiral comes about through dowel action of the longitudinal bars.

Thus the possible formation of the vertical crack at (C) is explained. When crack(C) is developed, due to the weak interlocking of spirals with a relatively large d_{il}, the column actions may eventually become similar to the model shown in Fig.4.10. This model is designated as the combined beam-arch action model in this study. In the figure, the plastic hinge region of the column is modelled by two separated short columns interconnected to the column region which is outside of the plastic hinge region. Outside of the plastic hinge region vertical cracks like crack(C) will not be generated because normally the cover concrete dose not spall off in this region except for squat columns with extremely small aspect ratio of less than 2. It is assumed that the left hand column acts as a tension member (full depth cracking) and the right hand column acts as a member which is subjected to combined axial compression and bending. This model represents arch action [4.18] of the total column with the aid of beam action in the right hand column.

The model in Fig.4.10 is applicable when the column axial load is small enough to make the neutral axis depth significantly less than one half of the overall depth of the column h. The model can be used to estimate the ultimate flexural strength of a column when the interlocking of spirals is weak due to large d_{il}. Assuming that all longitudinal bars have the same size and are evenly spaced, the estimation of the flexural strength can be made as follows;

(1) Regarding the left hand column subjected to axial tension:

In the plastic hinge region, it is assumed that all longitudinal bars have yielded in tension at the ultimate condition. After yielding of the longitudinal reinforcement, the tension force T is expressed by $T= \frac{A_{st}}{2} f_y$, where $\frac{A_{st}}{2}$ = area of the longitudinal reinforcement in the left column, f_y = yield strength of that longitudinal reinforcement. It may be assumed that, even at large deflections of the column, the tension strain in the longitudinal bar does not reach the strain hardening

region because wide propagation of tension yielding is expected due to the left hand column acting as a tension member. This can be examined from the compatibility of deformation at the section A-A, as is described later (see the check-1 below). When all the longitudinal bars in the left hand column have yielded in tension, a bending moment cannot act in the left hand column and hence T is applied to that column centroid. The shear forces carried by the spirals and the concrete mechanisms in the left hand column can be neglected because the axial tension cracks are assumed to be parallel to the spiral bar direction as shown in Fig.4.10 (b). As a consequence, all the shear force H need to be carried by the right hand column.

(2) Regarding the right hand column subjected to combined axial compression and bending:
From the equilibrium requirements, the axial compression force in the right hand column is expressed by $C = P_e + T$. Taking this C as the concentric axial loads of the right hand column, the ultimate moment M_C at the base can be calculated by the conventional section analysis assuming that plain sections before bending remain plane after bending, if the amount of the spirals is sufficient to prevent the shear failure. The required amount of spirals for shear reinforcement can be determined using Eqs. 4.16 and 4.22 for the right hand column alone (that is, neglecting the shear carried by the left hand column.). The shear carried by the concrete V_c will be large due to the high axial load C and hence the required amount of spirals for shear reinforcement will not be so large.

(3)The ultimate moment of the total column at the base , M_u , is expressed by

$$M_u = (T + C)\, d_{il} / 2 + M_C \quad \text{.....} \quad (4.27)$$

(4) The maximum horizontal force H (see Fig. 4.10 (a)) is calculated as

$$H = M_u / (l_1 + l_2) \quad \text{.....} \quad (4.28)$$

where l_1 = length of the column outside of the plastic hinge region

l_2 = plastic hinge length of the column

The plastic hinge length of the column l_2 may be assumed to be a half of the overall depth of the column (that is, 0.5 h) for the case of axial load of up to about $0.3\, f'_c A_g$. The moment in the right hand column at the section A-A, M_A is given by

$$M_A = M_C - H \cdot l_2 \quad \text{.....} \quad (4.29)$$

This M_A, as well as M_C, is used to check the compatibility of the column deformation at the section A-A.

(5) In order to ensure that the model and the assumed actions are valid, the following checks need to be conducted;

check-1: The tension strain in the left hand column

The strain variations in each separated column are represented by Fig.4.11. The elongation of the column Δl_2 at the centre line within the plastic hinge region can be calculated by integrating the strains of the extreme tension fibre in the right hand column, in accordance with the moment variations from M_A to M_C with the axial load C. For compatibility of deformations, the elongation of the left hand column at its right hand edge needs also to be Δl_2 and hence the tension strain at this edge is simply calculated as $\Delta l_2 / l_2$ assuming no bond action within l_2. The calculated strain, $\Delta l_2 / l_2$, needs to be larger than the tension yield strain of the longitudinal bar in order to assume that the longitudinal reinforcement in the left hand column have all yielded.

check-2: The development length of the longitudinal bar

The length of the column outside of the plastic hinge region, l_1 needs to be sufficient to develop the yield force in the tension reinforcement, otherwise the column may suddenly fail before achieving the combined beam-arch action.

check-3: The amount of the spirals in the right hand column

The amount of spirals needs to be sufficient to prevent shear failure of the right hand column.

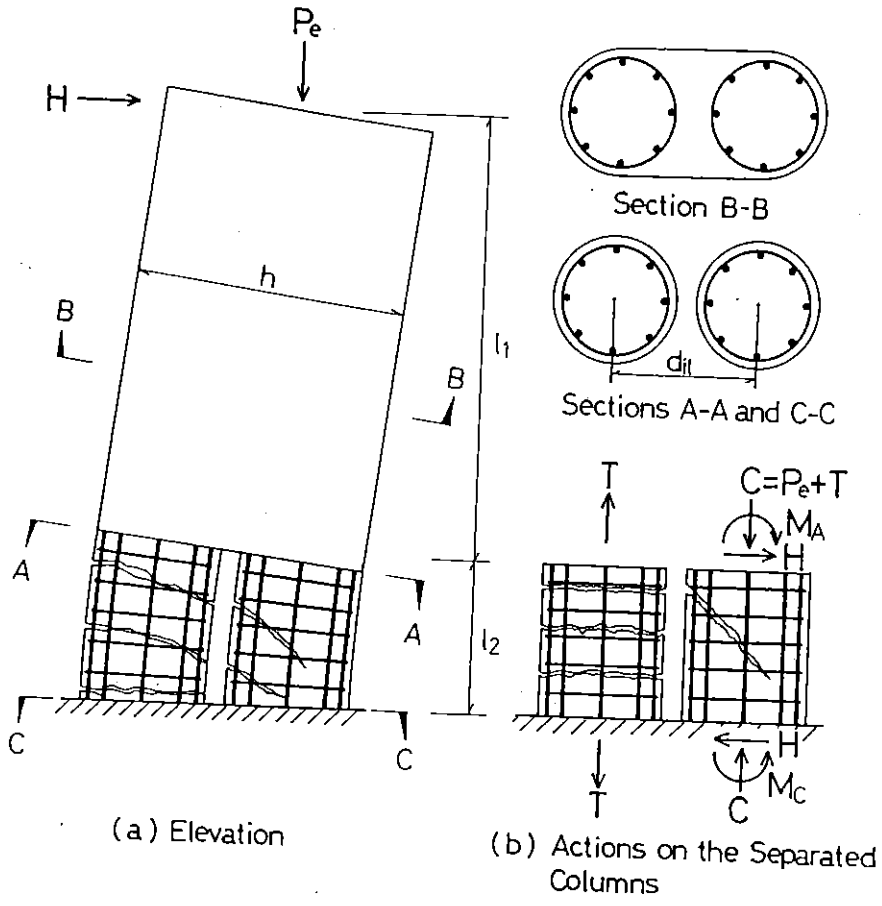

Fig. 4.10 A Failure Model for Column When the Interlocking of Spirals is Weak.

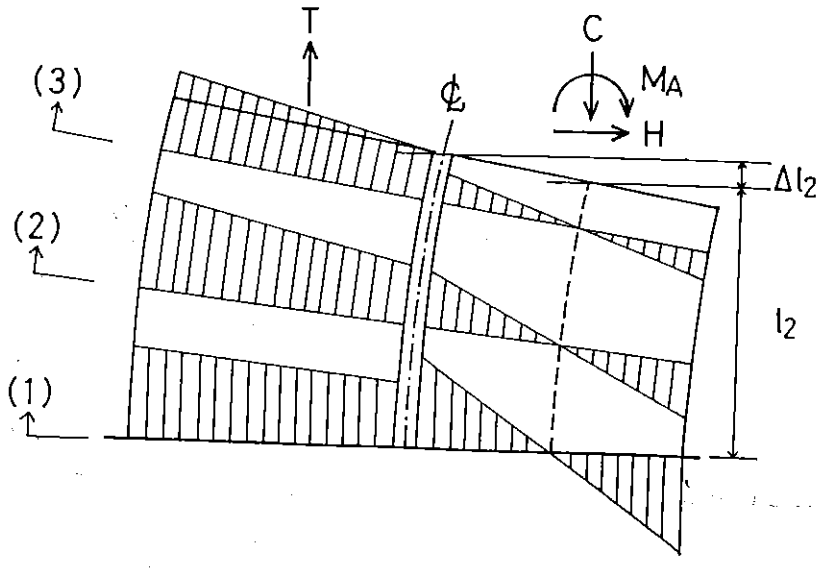

Fig. 4.11 Strain Variations in the Separated Columns.

4.2.2.5 Example Calculation for a Column with Weak Interlocking of the Spirals

For an example calculation, 400mm x 712 mm column section shown in Fig.4.12 will be analyzed. In order to refer to the test results described in Section 4.3.2, similar reinforcing details as Unit 10 have been chosen except for the distance between the centres of the adjacent spirals, d_{il}. The column contains sixteen 20 mm diameter Grade 380 deformed bars (ρ_t = 2.0 % where ρ_t = the ratio of total area of longitudinal reinforcement to A_g) as longitudinal reinforcement. The spirals with pitch of 80 mm are from 10 mm diameter Grade 275 plain bars and the corresponding volumetric ratio ρ_s is 1.08%. The mechanical properties of those reinforcing steels used for the calculation are the same as those for Unit 10 shown in Table 4.2 and Figs. 4.37 and 4.38. The stress-strain relations for the confined core concrete and the unconfined cover concrete (see Fig.4.73) were determined based on the stress-strain model by Mander et al [4.22]. The calculation was conducted for an axial load level, $P_e/(f'_cA_g)$ = 0.1, using two compressive strengths of concrete, 21.2 MPa (the same as Unit 10) and 30 MPa. For the combined beam-arch action, a plastic hinge length, l_2, of one half of the overall column depth, that is, h/2 = 356mm, was assumed.

The calculated results are shown in Fig. 4.13 and in Table 4.1. In the figure, as the axis of abscissa, the concrete strain in the extreme compression fibre, ε_{ef}, is used instead of curvature. This is because, for the combined beam-arch action theory, the concept of the curvature which is based on the hypothesis that plain sections before bending remain plain after bending is not applicable. As the axis of the ordinate in Fig.4.13 the moments at the base of the column are given. A-21 and A-30 denote the obtained curves for combined beam-arch action with f'_c of 21MPa and 30 MPa, respectively. B-21 and B-30 denote the corresponding curves for perfect beam action. In the perfect beam action theory, the concrete strain ε_{ef} of 5 % corresponds to a curvature ductility factor of about 19, as shown in Table 4.1. The yield curvature ϕ_y was defined as the curvature when the calculated moment has reached the ultimate moment calculated using the ACI building code method. After reaching the concrete strain ε_{ef} of about 0.5%, combined beam-arch action could occur, since the check-1 (compatibility check) has passed after reaching that strain. The check-2 is passed if the shear span

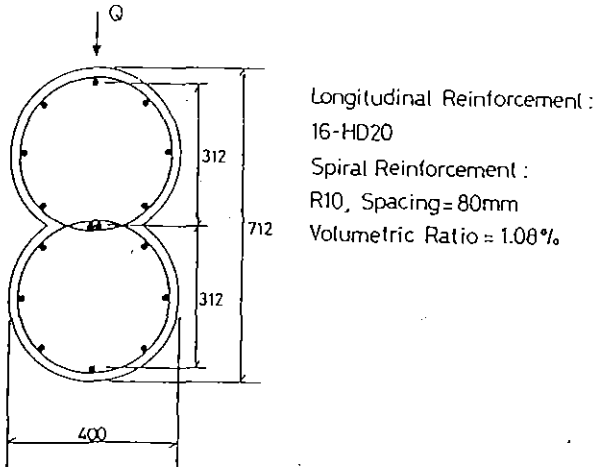

Fig. 4.12 Assumed Column Section with Weak Interlocking of Spirals for Example Calculation.

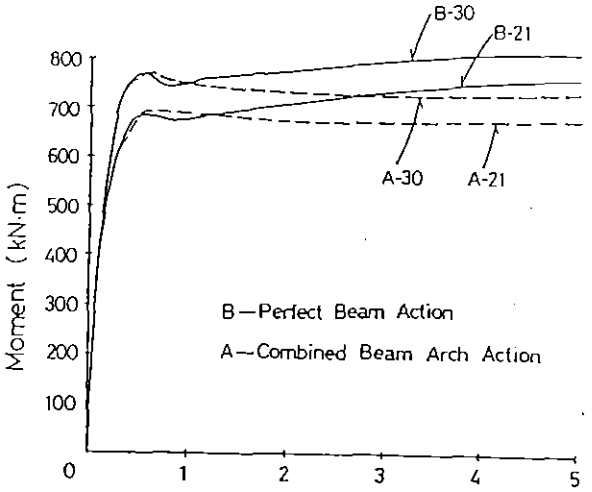

Fig. 4.13 Relationship between Moment at the Base of the Column and Concrete Compressive Strain in Extreme Compression Fibre.

Table 4.1 Comparison of Theoretical Moments between Perfect Beam Action and Combined Beam-Arch Action

$\frac{P_e}{A_g f'_c}$	f'_c (MPa)	M_{ACI} (KN.m)	Concrete Strain in Extreme Compression Fibre, ε_{ef} (%)	Perfect Beam Action		Combined Beam-Arch Action					
				M_1 (KN.m)	$\frac{\phi}{\phi_y}$	$\frac{C}{0.5A_g f'_c}$	M_2 (KN.m)	M_C (KN.m)	M_U (KN.m)	$\frac{M_U}{M_{ACI}}$	$\frac{M_U}{M_1}$
0.1	21.2	599	0.6	685	2.5	0.66	462	237	699	1.17	1.02
			5.0	761	19.9	0.66	462	216	678	1.13	0.89
0.1	30.0	692	0.6	765	2.4	0.52	497	281	778	1.12	1.02
			5.0	810	18.6	0.52	497	229	726	1.05	0.90

Note: M_{ACI} = Moment calculated using the ACI codemethod [6]

M_1 = Moment calculated using ordinary section analysis

M_2 = Moment due to axial loads T and C in each separated column in combined beam-arch action

M_C = Moment of the separated column with the axial load $C/(0.5 A_g f'_c)$ using the same method as in the calculation of M_1.

$M_U = M_2 + M_C$

ϕ/ϕ_y = Ratio of curvature to the yield curvature for perfect beam action

length is more than 1.7 times h, based on the calculation of $l_2 + l_d$ where l_d is the development length required by the NZS 3101:1982.

The shear carried by the spirals was estimated as 334 KN using Eq.4.22 for the whole column depth with a 45° inclined crack. Hence, one half of that, that is, 167 KN can be sustained by the spirals in combined beam-arch action. For a total compressive load of $C/(0.5f'_cA_g) = 0.66$ with $f'_c = 21.2$ MPa, the shear carried by the concrete was estimated as 294 KN using v_c determined by Eq. 4.19 ($0.5\ f'_c\ A_g$ is used since it is assumed that the total axial compressive load is resisted only by the right hand separated column.). The calculated v_c was less than $0.9\sqrt{f'_c}$ and hence no diagonal reinforcement is required according to clause 7.5.4.2 of NZS 3101:1982. Similarly, for a total compressive load of $C/(0.5f'_cA_g) = 0.52$ with $f'_c = 30.0$ MPa, the shear carried by the concrete was estimated as 305 KN. As a result, the total shear carried by the concrete and the spirals during combined beam-arch action could exceed the shear carried only by the spirals in the beam action under $P_e/(f'_cA_g) = 0.1$. Thus, the check-3 has also passed.

For both of the assumed separated columns with different concrete strengths, the calculated moment of resistance of the right hand column in the combined beam-arch action, M_C, reached a maximum at ε_{ef} of about 0.6 %. At this ε_{ef}, the total moment $M_C + M_2$, where M_2 is moment due to axial loads T and C in each separated column, also reached a maximum and was slightly larger than the moment calculated for the same ε_{ef} by assuming perfect beam action. This can be explained using the ultimate moment-axial load interaction curve for the circular column with single spirals, shown in Fig.4.14, which corresponds to the separated column of A-21, in Fig.4.12. In Fig.4.14, the ultimate moment of the column has been defined as the maximum moment attained while ε_{ef} is increased from zero to 5% in a moment-curvature analysis. When axial load level, $P_e/(f'_cA_g)$, is less than 0.3, the maximum moment has been reached at $\varepsilon_{ef} = 5\%$, after spalling of cover concrete, due to strain hardening of longitudinal reinforcement. The reason why the maximum of ε_{ef} is limited to 5% is that buckling of longitudinal reinforcement likely occurs when ε_{ef} exceeds 5%. As can be seen from Fig.4.14, the ultimate moment with $P_e/(f'_cA_g) = 0.66$ is considerably larger than that with $P_e/(f'_cA_g) = 0.1$. Hence, at ε_{ef} of 5.0 % the moment reductions to A-21 from B-21 and to A-30 from B-30, respectively are about 10%. This indicates that the loss of moment resistance due to the

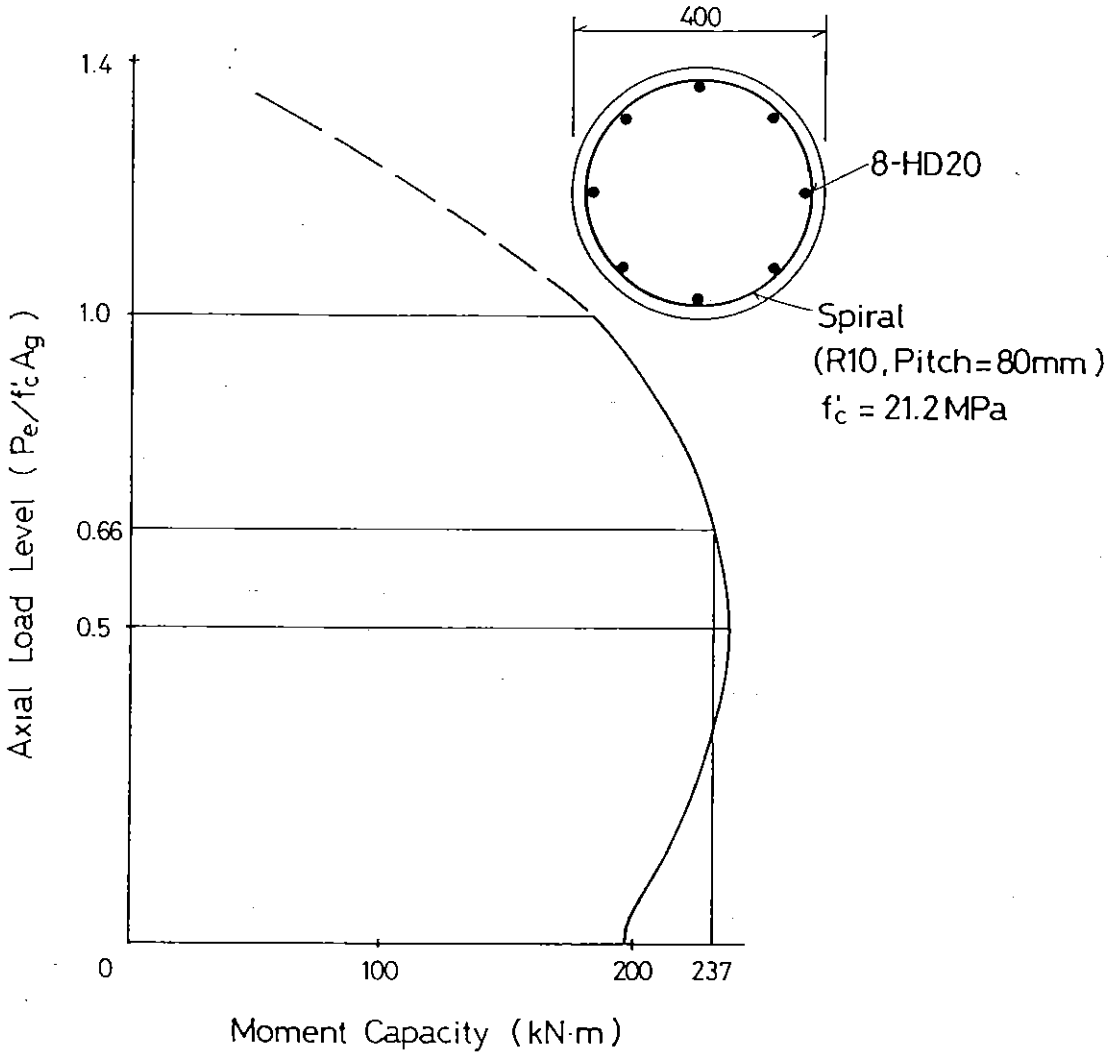

Fig. 4.14 Moment-Axial Load Interaction Curve for the Separated Circular Column with Single Spirals Corresponding to A-21.

weak interlocking of the spirals may not be particularly significant if the concrete core is well confined so as to achieve adequate strength and ductility under high axial load.

However, it must be emphasized that, in the combined beam-arch action, the load carrying capacity and the stiffness of the column under cyclic loading may be rapidly decreased. This reduced stiffness of the column may lead to pinching of the hysteresis loops and hence result in a loss of some hysteretic energy dissipation during severe seismic loadings. If the above design method, in which the combined beam-arch action is assumed, is required to be used, the column may need to be given the category of limited ductility. Otherwise, it is recommended that supplementary ties with 90° and 135° end hooks [4.6] are provided as shown in Fig.4.15 in order to reinforce the mid-depth region of the column section against shear and to reduce the concrete area unconfined.

4.2.2.6 Review of Previous Research to Evaluate Dowel Action of Longitudinal Reinforcement

Secure interlock of spirals may be interpreted as the prevention of neighbouring spirals from tearing apart when transferring shear from spiral to spiral. The shear transfer from spiral to spiral in the interlocking area may be by shearing action of core concrete at the initial stage of loading as shown in Fig. 4.16 and probably by dowel action of the longitudinal bars in the inelastic range of cyclic loading. Those actions to transfer the shear may be too complicated to rigorously evaluate the strength and stiffness of the interlock considering all aspects of dowel behaviour, especially for a case of columns subjected to severe earthquake loading. This is because under such circumstances the core concrete in the interlocking area is subjected to multi-axial stresses along with the presence of inclined shear cracks, and the longitudinal bars are significantly stressed in axial tension or compression in addition to dowel forces. In other words, the stress and strain of each constituent at critical condition, which are to be applied to the corresponding failure criteria, cannot be simply estimated since equilibrium and compatibility are variable for every particular failure mode which likely occurs.

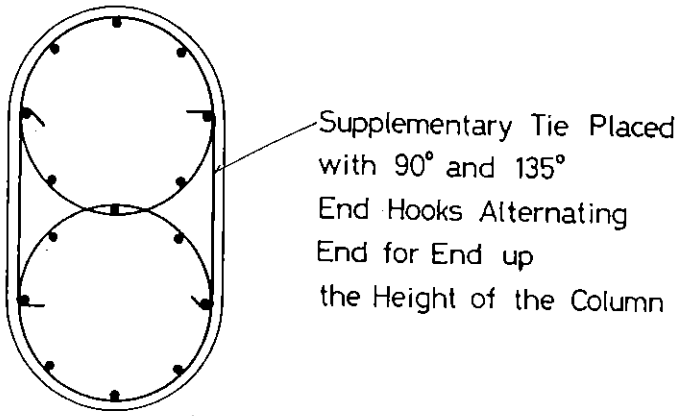

Fig. 4.15 Interlocking Spirals with Supplementary Ties.

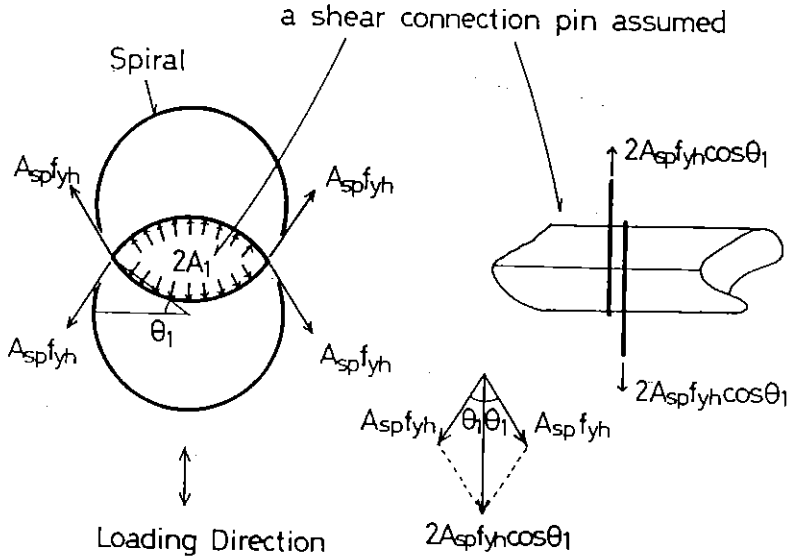

Fig. 4.16 Core Concrete to Interlock Spirals Acting as a Shear Connection Pin.

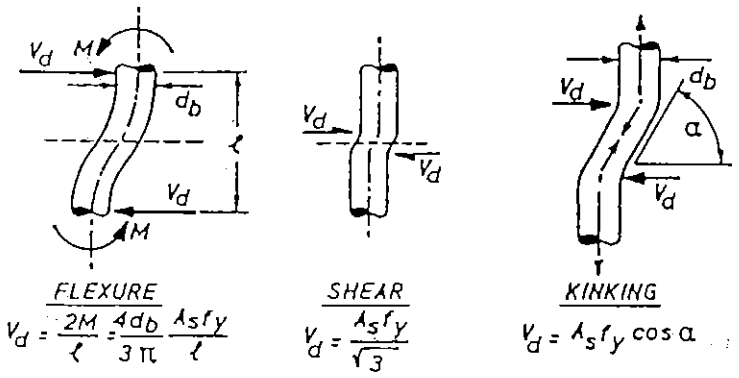

Fig. 4.17 Mechanisms of Dowel Action across a Shear Interface [4.17, 4.18].

Generally speaking, the dowel action of a steel bar across a shear interface is classified into three mechanisms, that is, flexure, direct shear and kinking as shown in Fig.4.17 [4.17, 4.18]. The mechanism actually induced in a particular longitudinal bar within the interlocking area will depend on the shear crack width, pitch of the spirals, axial strain induced in the longitudinal bar, bearing strength of concrete, etc. When the longitudinal bars to interlock the spirals are well developed or anchored to provide the column load capacity as well, they will most likely yield during severe seismic loading except for the case when the neutral axis of the column section nearly coincides with those bar locations. When longitudinal bars yield in axial tension or compression, it is normally considered that only kinking is effective to transfer shear force. Both flexural and direct shear strengths of the longitudinal bars are normally taken to be zero or negligible after their axial yielding unless strain hardening of steel is taken into account and the assumption of isotropic or kinematic hardening [4.10] is applied to the failure criteria for steel. For example, when the von Mises criterion expressed by Eq.4.30 or the Tresca criterion expressed by Eq.4.31 is used as the failure criterion for steel (they have been commonly used for ductile metals), the maximum shear stress τ_{xy} is estimated as zero after axial stress σ_x reaches the yield stress σ_o.

$$\text{(von Mises)} \qquad \left(\frac{\sigma_x}{\sigma_o}\right)^2 + 3\left(\frac{\tau_{xy}}{\sigma_o}\right)^2 = 1 \quad \text{.....} \qquad (4.30)$$

$$\text{(Tresca)} \qquad \left(\frac{\sigma_x}{\sigma_o}\right)^2 + 4\left(\frac{\tau_{xy}}{\sigma_o}\right)^2 = 1 \quad \text{.....} \qquad (4.31)$$

where σ_x = axial stress in material
τ_{xy} = shear stress in material
σ_o = yield strength of material

In a reinforced concrete member, the capacity of the dowel to carry shear force is governed by either material failure or support failure of the dowel. As an example, when a reinforced concrete beam subjected to combined shear and bending is considered, material failure of the dowel is characterized by the yielding of the longitudinal reinforcement under combined tension and shear or under combined tension and bending. Support failure may result from horizontal cracking of the concrete cover or yielding of the stirrup. Johnston and Zia [4.11] assumed five failure modes

of dowel action with various positions of an inclined shear crack against stirrups (see Fig.4.18) and mathematically analyzed each failure mode by applying the corresponding failure criteria to both dowel support failures and dowel material failures. A typical interaction curve between dowel strength and axial tension in a longitudinal bar obtained in that study is represented by Fig. 4.19. In the figure, V_d , T and T_y indicate shear force carried by dowel, total tension force in longitudinal bars and tension yield force of longitudinal bars, respectively. This theoretical study is notable because various failure modes of dowel action were considered. However, the basic equation used in that study was a fourth-order differential equation and hence solutions were too complicated for design purposes. Moreover, in order to predict failure at instant of cover cracking, it was necessary to assume a value for the deflection of the dowel which causes horizontal cracking of cover, y_c , such as to be 0.001 to 0.004 in (=0.0254 to 0.102 mm). Therefore, it was stated that further study was needed to evaluate y_c as influenced by the various parameters such as cover thickness, concrete strength, stirrup arrangement and placement of longitudinal reinforcement. It should be noted that in the study dowel strength was evaluated to be zero after axial yielding of longitudinal reinforcement as can be seen from Fig. 4.19. This is because the dowel strength provided by kinking of longitudinal bars was neglected.

A number of experimental studies on shear transfer by dowel action have been conducted to establish empirical equations for evaluating the dowel strength. Those studies are conveniently grouped according to the type of specimens used (see Fig. 4.20 [4.12]) as :

(a) direct dowel tests
(b) divided beam tests
(c) beam end tests

Most of the direct dowel tests [eg. 4.13] apply shear to adjacent short corbels in order to investigate details such as the bearing for a precast beam and column face plates as introduced in clause 11.7 (Shear-friction) of the ACI Building Code [4.6], or to estimate the shear strength of construction joins [4.17]. In those direct dowel tests, it is considered that shear resistance is provided by friction against shear sliding between the faces of shear cracks due to aggregate interlock and also by dowel effect of reinforcement. In the shear-friction design method introduced in ACI Building Code [4.6], the

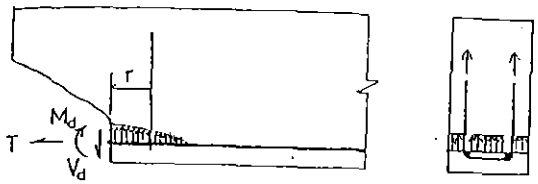

Mode A ($r \neq 0$), Mode D ($r = 0$)

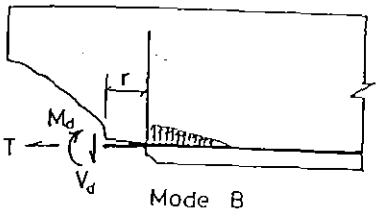

Mode B

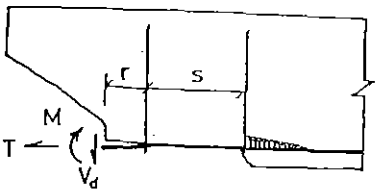

Mode C ($r \neq 0$), Mode E ($r = 0$)

Fig. 4.18 Typical Failure Modes of Dowel Action in a Beam [4.11].

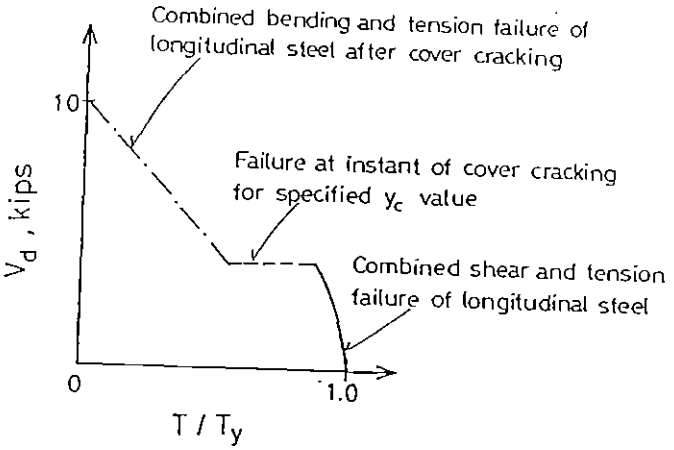

Fig. 4.19 Typical Interaction Curve for Dowel Action in a Beam [4.11].

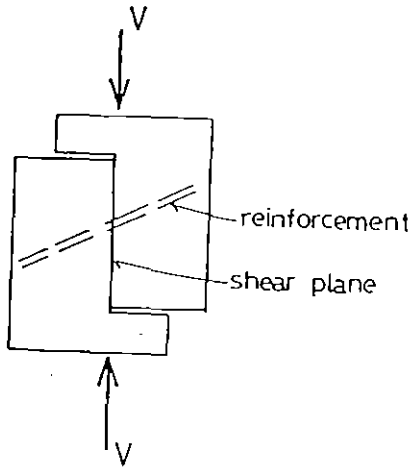

(a) Direct Dowel Test

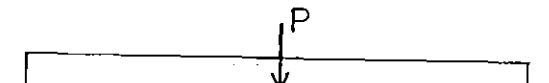

(b) Divided Beam Test

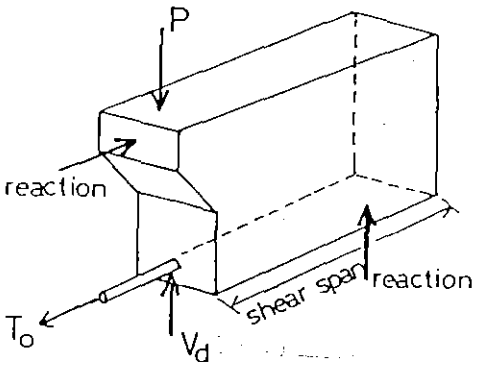

(c) Beam-End Test

Fig. 4.20 Various Dowel Tests.

shear friction reinforcement is considered to produce frictional resistance against sliding between the faces of crack by providing a compression force acting across the crack [4.13, 4.17]. This compression force is generated to balance the tension force induced in shear frction reinforcement when the crack faces are forced to separate. The shear friction method can be representatively expressed by Eq. 4.32, assuming that reinforcement are perpendicular to shear plane,

$$V_n = A_{vf} f_y \mu \quad \text{.....} \quad (4.32)$$

where V_n = nominal shear strength
A_{vf} = area of shear friction reinforcement
f_y = yield strength of shear friction reinforcement
μ = coefficient of friction; for normal weight of concrete placed monolithically, μ =1.4

It is notable that in those direct dowel tests the kinking effect of reinforcement also contributes to the shear transfer to some extent [4.13]. However, shear transfer by kinking is normally appreciable only after a considerable relative displacement across the shear interface is attained [4.18].

On the other hand, in direct dowel tests carried out by Dulácska [4.14] (see Fig.4.21), the dowel effect of reinforcement was investigated by eliminating friction between the crack faces by inserting two layers of 0.2 mm thick brass in the shear plane as a smooth simulated crack. The aim was to evaluate the dowel strength provided by reinforcement assuming that the shear force was counteracted only by the crosswise bars, when the crack opens, due to loss of the friction effect. The angle of reinforcement across the shear plane, δ, was varied from 10° to 40°. Based on the experimental observations it was stated that; (1) the bar across the simulated crack became distorted and broke the sharp concrete edge, (2) skewed shear cracks developed in the middle of the concrete, (3) the behaviour of the dowel action was almost ideally elasto-plastic. It can be presumed that the dowel strength capacity was determined by local fracture of concrete in elasto-plastic dowel behaviour. This is because, the failure strengths reported in that study are only about one-third of the estimated dowel strength of reinforcement calculated using Eqs 4.30 assuming the direct shear

mechanism of the reinforcement shown in Fig.4.17. Taking into account the test results the following equation was proposed in that study to estimate the dowel strength.

$$T_f = \rho \phi^2 \gamma \sigma_y n \sin\delta \left[\sqrt{1 + \frac{\sigma_c}{3 \rho \gamma^2 \sigma_y n \sin^2\delta}} - 1 \right] \quad \text{..... (4.33)}$$

where T_f = dowel failure force

ϕ = bar size

δ = angle of dowel reinforcement (see Fig. 4.21)

σ_y = yield stress of steel

σ_c = cube strength of concrete

n= coefficient of local compression of concrete

γ = constant

$\rho = 1 - N^2 / N_y^2$

N= tension force in bar

N_y = tensile force inducing yield in pure tension

It is noticed that Eq. 4.33 is inconvenient when $\delta = 0$, that is, dowel reinforcement is placed perpendicularly to the shear plane because $\sin\delta$ goes to zero but $1/\sin^2\delta$ goes to ∞, although in such a case reasonable value of T_f seems to be obtained by substituting very small value of δ instead of zero.

The above study by Dulácska [4.14] may be inadequate to evaluate effectiveness of longitudinal reinforcement to interlock spirals. This is because cracks at the mid-depth of the column section, where longitudinal bars to interlock spirals are located, should not be allowed to open so wide as to lose friction between crack faces. If such a wide crack is generated at the mid-depth of column section, an unacceptably large shear displacement may be required at the extreme fibre region in the column section from compatibility. However, it is noteworthy that those tests involve axial load in reinforcement as an experimental parameter and that Eq.4.33 was derived, based on the test results, using an assumption that the dowel strength is reduced to zero as the tension force in bar N increases to the yield tension force N_y.

To evaluate dowel strength in beams, divided beam tests [eg. 4.15] and beam end tests [eg. 4.16] (see Fig. 4.20) have been conducted focussing on the

splitting failure of cover concrete. Referring to those tests, Jimenez, White and Gergely [4.12] have proposed the following empirical equation to evaluate dowel strengths in beams based on a regression analysis of 87 specimens.

$$V_{do} = 0.75 \frac{b_n}{n} d_b \quad \text{.....} \quad (4.34)$$

where V_{do}= dowel force in reinforcement required for a splitting failure (in kips)

n = number of bars in one layer of reinforcement

d_b = bar diameter in inch

b_n = net beam width (= beam width - n d_b) in inch

It is notable that V_{do} is reduced as the number of bars increases. This typical example indicates that in the beam tests V_{do} has been determined by the splitting failure of the cover concrete. Hence, dowel strength cannot be improved by simply increasing the amount of longitudinal reinforcement.

In beam tests only a few test results are available where tension and dowel forces of significant magnitude were applied simultaneously. Hence, Jimenez, White and Gergely [4.12] also proposed that until further data becomes available, an elliptic interaction curve given by Eq. 4.35 may tentatively be assumed for specimens without transverse reinforcement.

$$\frac{T^2}{T_o^2} + \frac{V_d^2}{V_{do}^2} = 1 \quad \text{.....} \quad (4.35)$$

where T= tensile force in reinforcement

T_o = tensile force in reinforcement required for a splitting failure

V_d= dowel force in reinforcement

Eq. 4.35 might not be changed significantly if transverse reinforcement is provided, since studies based on divided beam tests [4.12] have indicated that stirrups are beneficial in increasing the ultimate dowel strength only when they are placed within one inch of the transverse crack. A notable point is that these studies also indicate the importance of including the tensile force in reinforcement when estimating dowel strength.

In the case of the longitudinal bars which interlock spirals, test results obtained from direct dowel tests, rather than those from beam tests, may be more suitably utilized to evaluate the contribution of those bars to shear transfer, for the following reasons:

(1) Since longitudinal bars which interlock spirals are positioned deep inside the core concrete, splitting failure or local fracture of concrete surrounding those bars is unlike that of cover concrete in beams. Empirical equations obtained from beam tests are probably valid only when the thickness of cover concrete is up to several times the longitudinal bar diameter.

(2) In divided beam or beam end tests, only a few test results are available where tension and dowel forces of significant magnitude were simultaneously applied to longitudinal reinforcement. On the other hand, longitudinal bars which interlock spirals are significantly stressed when resisting column actions under severe seismic loading.

(3) It may be acceptable to consider that the shear transfer from spiral to spiral in an interlocking concrete core area is similar to that can be achieved by direct dowel tests or in a shear connection pin as represented by Fig. 4.16.

If the shear-friction method [4.6] based on direct dowel tests is used to evaluate the contribution of longitudinal bars for interlocking spirals, some modification of the method will be required. This is because the longitudinal bars which interlock spirals may be significantly stressed when resisting column loads before cracks due to direct shear force from spirals are formed. It must be emphasized that those cracks due to direct shear are different from diagonal shear cracks due to column bending and shear. The compression force to induce shear friction, which is provided by counteraction of the longitudinal bars in tension, is to be reduced in proportion to the magnitude of tension force induced previously in the longitudinal bars. This can be expressed by Eq. 4.36, assuming that the longitudinal bars which interlock the spirals are perpendicular to shear plane,

$$V_n = A_{vf} (f_y - f_s) \mu \qquad \text{..... (4.36)}$$

where V_n = nominal shear strength

A_{vf} = area of longitudinal reinforcement to interlock spirals

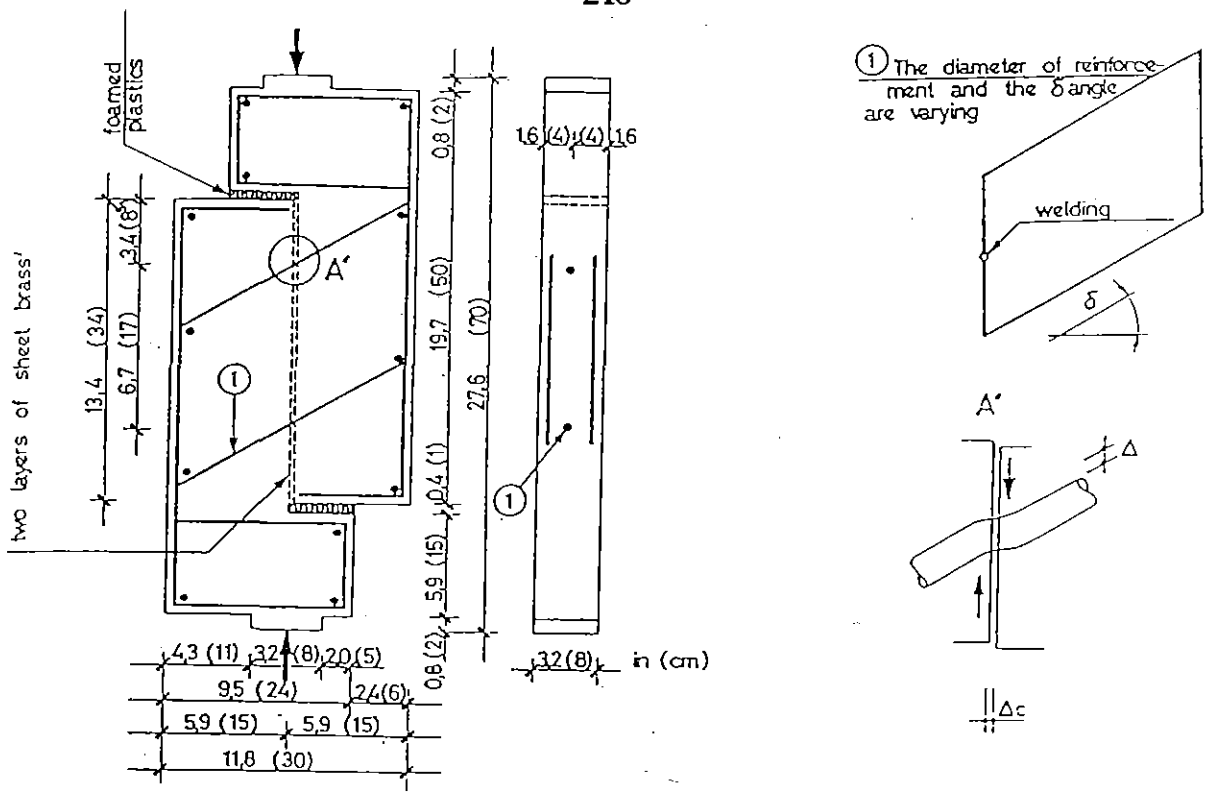

Fig. 4.21 Details of a Test Specimen Used in Direct Dowel Tests [4.14].

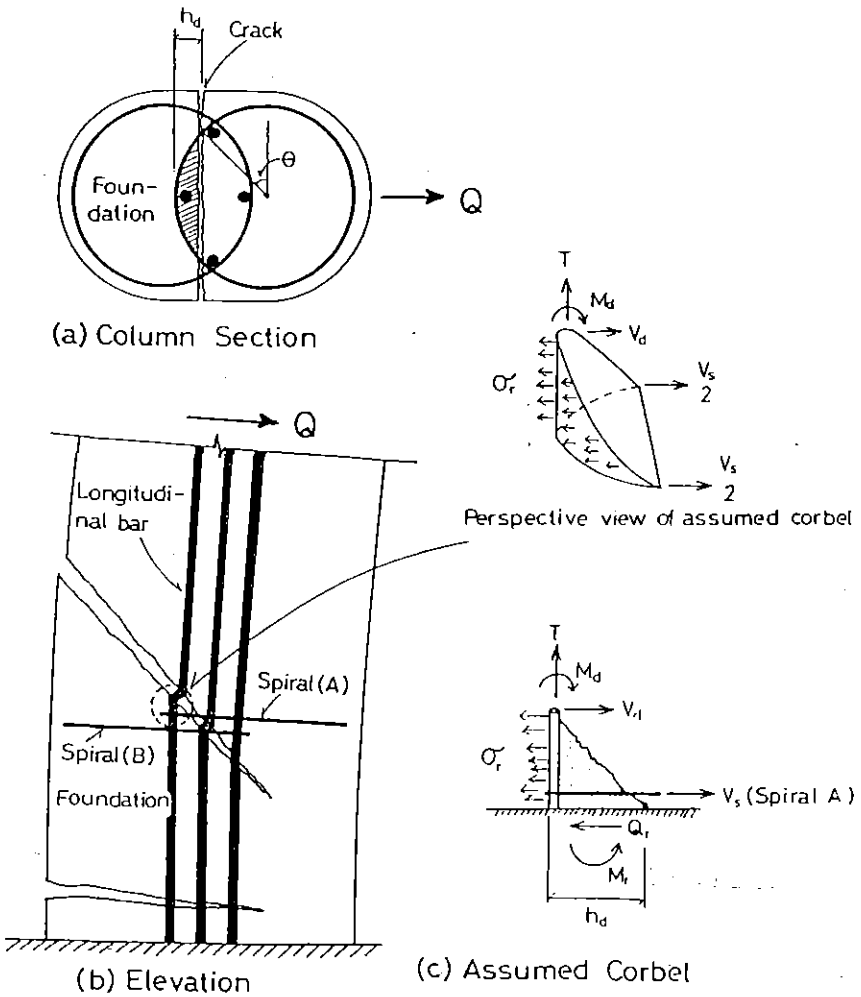

Fig. 4.22 Assumed Corbel with an Elastic (Winkler) Foundation - Case (1).

f_y = yield strength of longitudinal steel

f_s =tension stress in longitudinal reinforcement which interlock the spirals due to column load

μ = coefficient of friction; for normal weight of concrete placed monolithically, μ =1.4

Based on these considerations, adequate distance between the centres of the adjacent spirals, d_{il}, and arrangement of longitudinal bars to adequately interlock spirals are discussed in the following sections. However, it must be emphasized that, as mentioned above, the dowel action is so complicated that the following discussions in Sections 4.2.2.7 to 4.2.2.9 only suggest a possible design method rather than proposing a rational design method. It should also be noted that reinforcing details shown in Fig.4.15, involving supplementary ties, result in a shear design procedure more simple and clear, and does not rely on dowel action of the reinforcement.

4.2.2.7 Adequate Distance between the Centres of the Adjacent Spirals

Since core concrete in the interlocking region is likely to be separated by diagonal shear cracks as shown in Fig. 4.7, it is considered that core concrete without the aid of longitudinal bars to interlock the spirals is not a dependable method to transfer shear from spiral to spiral in the inelastic range of cyclic loading. However, in order to secure initial stiffness of the interlock, the area of concrete core for the interlock may need to be adequate. This is because appreciable shear transfer from spiral to spiral due to dowel action of longitudinal bars is achieved only after cracks (which are different from diagonal shear cracks due to column bending and shear as mentioned in the previous section) are formed across shear interface.

At the initial stage of loading of a column when only a few diagonal shear cracks appear, a cracked condition of column may be represented by Fig. 4.22. The region bounded by a diagonal tension crack, core concrete outside interlocking area and spiral (B) may be modelled by a corbel shown in the figure, where σ_r is the counteracting stress from the core concrete outside the interlocking area assumed to be an elastic (Winkler) foundation. The critical loading condition of the corbel can be significantly changed in accordance with the assumed position and width of the diagonal tension

crack which affects the tension force and dowel force in the longitudinal bar represented by T, M_d and V_d in Figs. 4.22 and 4.23. Moreover, the direction of the bond stress along the longitudinal bar is also altered at some point as shown in Fig. 4.24. When taking the shaded area in Fig. 4.25 as a free body and assuming that M_d and V_d are negligible, the above fact leads to the finding that a resultant force V_r from τ_{cl} (due to bond action) and τ_{ch} (provided by spiral shear, V_s) can act either across or along the concrete cantilever, depending on the direction of bond force, $\int \tau_{cl}\, d_{ld}$, as can be seen form case (a) and case (b), respectively. Those situations make the problem too complicated to be rigorously solved taking every failure mode into account. Hence, in this study, it is assumed that initial stiffness of interlocking spirals can be secured by providing adequate strength for this modelled corbel for a particular loading condition.

As a particular loading condition, to give a target for adequate strength of the modelled corbel, it is assumed that in Fig. 4.23 the moment M_d and the shear V_d due to dowel action of longitudinal reinforcement is just balanced by σ_r obtained from a Winkler foundation and that $\int \tau_{cl}\, d_{ld}$ is zero. V_r then is in the direction of V_s. In this case, the shear from spiral (A) needs to be resisted by direct shear in the arch-shaped area between spirals (A) and (B), that is, in the shaded area of column section shown in Fig.4.22 (a). The average shear stress τ_{ave} in the shaded area can be expressed by Eq. 4.37 assuming that spiral reinforcement has yielded.

$$\tau_{ave} = \frac{2\, A_{sp}\, f_{yh} \cos\theta}{r_1^{\,2}\,[\pi / 2 - (\sin 2\theta)/2 - \theta]} \qquad \text{.....} \qquad (4.37)$$

where $\theta = \sin^{-1}[(r_1 - h_d)/r_1]$

h_d = distance between a diagonal shear crack and outer edge of core concrete in interlocking area (see Fig. 4.22 (a))

The relationship between θ and $\tau_{ave} \cdot [r_1^{\,2}/(2A_{sp}f_{yh})]$ is drawn in Fig.4.26. It is notable that τ_{ave} becomes infinitely large as the angle θ increases to $\pi/2$, although the shear force Q expressed by $2\, A_{sp}\, f_{yh} \cos\theta$ (that is, the numerator in Eq.4.37) decreases to zero as the angle θ increases to $\pi/2$. This

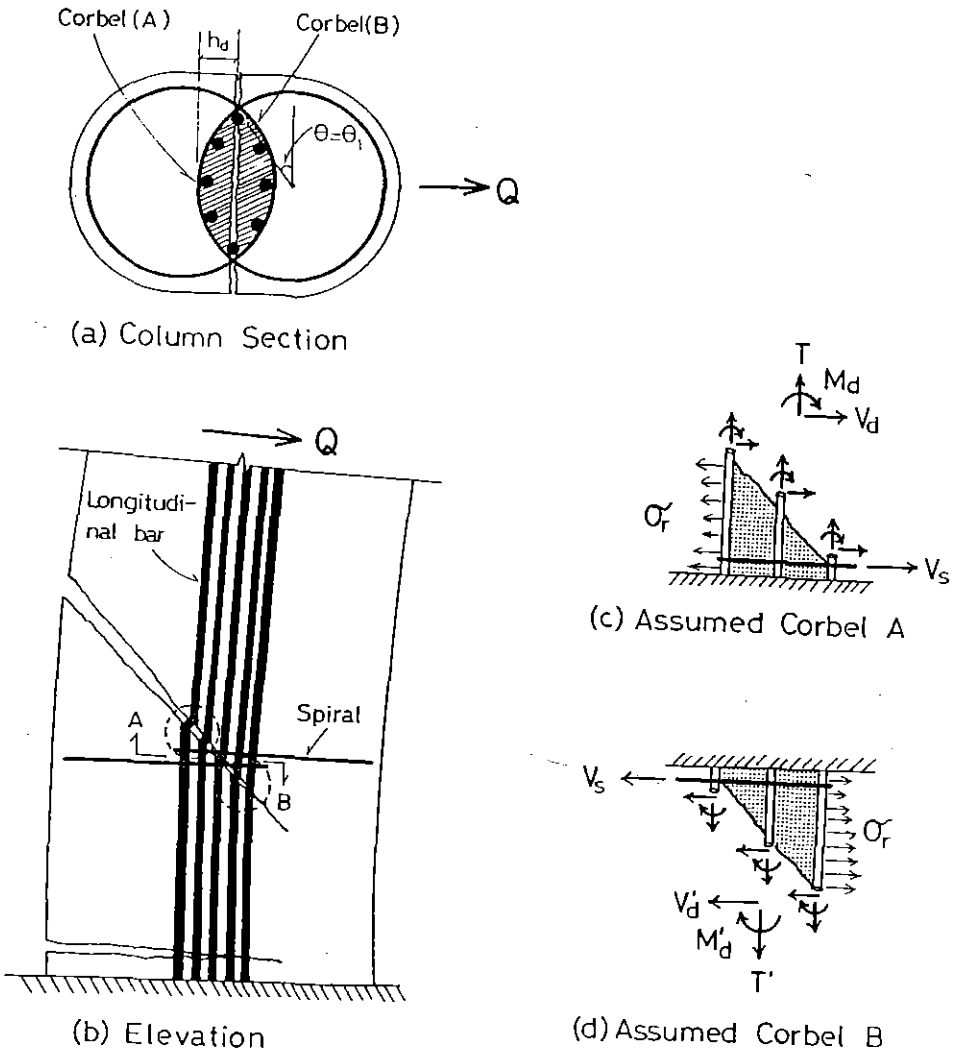

Fig. 4.23 Assumed Corbel with an Elastic (Winkler) Foundation - Case (2).

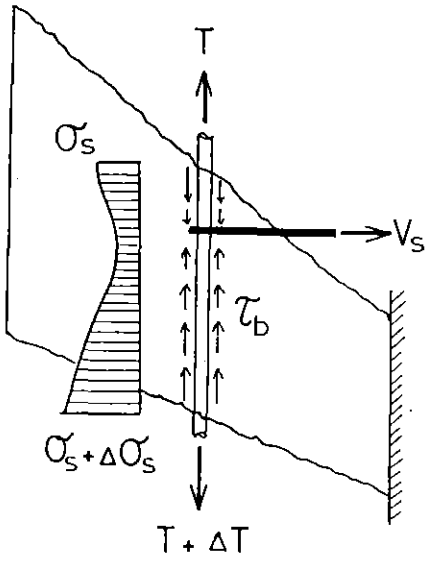

Fig. 4.24 Bond Stress Distribution τ_b and Steel Stress Distribution σ_s for a Longitudinal Bar.

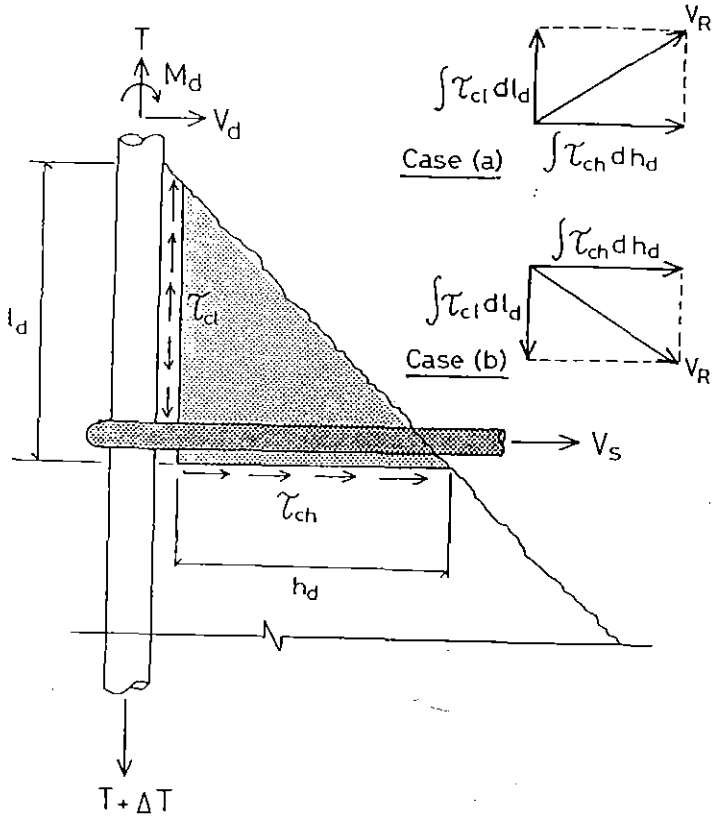

Fig. 4.25 Direction of Resultant Force V_R at Local Fracture of Concrete Core.

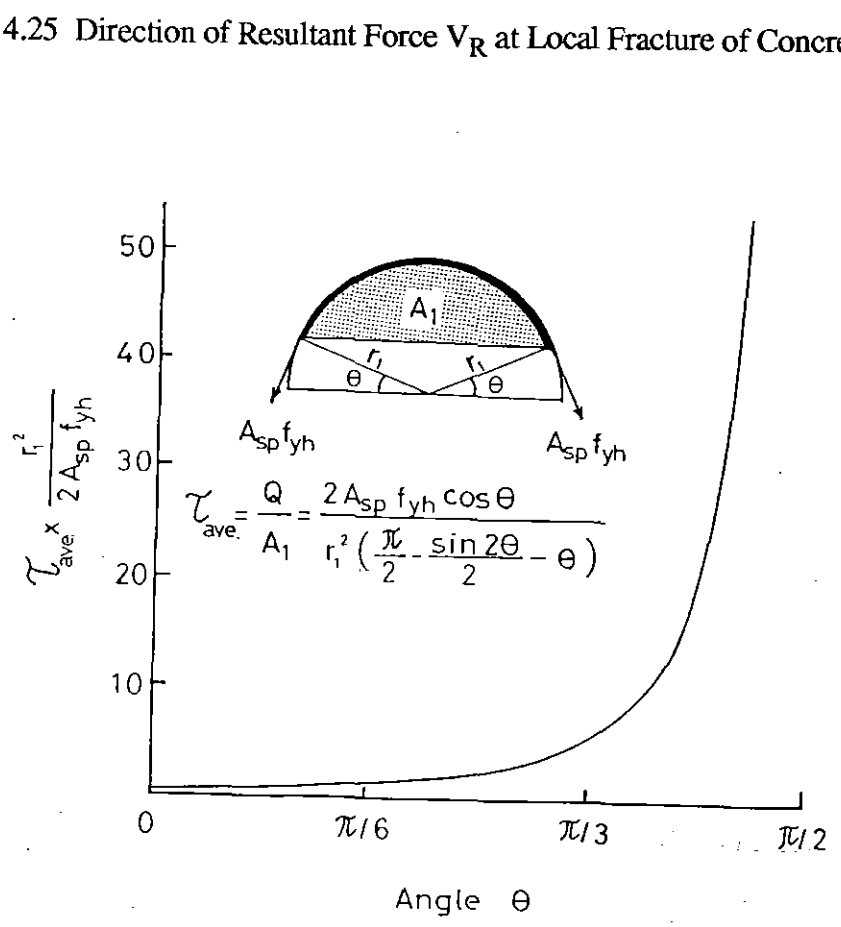

Fig. 4.26 Relationship between Angle θ and Average Shear Stress τ_{AVE}.

demonstrates that fracture of the assumed corbel cannot be avoided when the distance, h_d, is reduced to zero. However, when the diagonal shear crack runs so as to make h_d small, shear transfer from spiral to spiral could be achieved by the outer spiral bars as discussed in Section 4.2.2.3 (see Fig. 4.7). Hence, it may be assumed that the most critical case is when the diagonal tension crack runs across the center of the interlocking area as shown in Fig.4.23, because the assumed corbels (A) and (B) may possibly fail at the same time.

The shear strengths of concrete obtained by direct shear tests (of the type shown in Fig.4.20 (a)) are about a quarter to one-eighth of compression strength of concrete [4.13, 4.19]. Hence, assuming that the direct shear strength of concrete is $\frac{f'_c}{n}$ and taking $\theta = \theta_1$, adequate initial stiffness of interlock may be provided by requiring that;

$$\frac{f'_c}{n} \geq \frac{2 A_{sp} f_{yh} \cos\theta_1}{r_1^2 [\pi / 2 - (\sin 2\theta_1)/2 - \theta_1]} \qquad \text{.....} \qquad (4.38)$$

where n = ratio of direct shear strength of concrete to compressive strength f'_c.

As a reference, for Units 10 to 12 tested in this study τ_{ave} calculated from Eq.4.37 with $\theta = \theta_1 = 35°$ was about 3.3 MPa and the corresponding ratio to f'_c was about from 6 to 9. Hence, it may be considered that for those test units the initial stiffness of the interlocking core area was adequate.

On the other hand, to prevent wide opening of diagonal tension cracks in the interlocking region, it may become a reasonable target to keep 80% of the yield force of the peripheral spiral bar for the component in the applied shear direction at the mid-depth of the section (see Fig.4.27), although this target has no theoretical background. To meet this target, d_{il} needs to be 0.6 b_w' (where $b_w' = 2 r_1$) with $\theta_1 = 37°$, where the web width of 0.8 b_w' can be maintained even after spalling of cover concrete. It is notable that Units 10 to 12 with $\theta_1 = 35°$ showed satisfactory behaviour as described in Section 4.3.

4.2.2.8 Minimum Area of Longitudinal Bars Required to Interlock Spirals

The following discussion assumes that the longitudinal bars which interlock spirals are well developed or securely anchored. When a column is loaded into the inelastic range, longitudinal bars which interlock spirals sooner or later yield in tension or compression depending on the level of the axial load imposed. This is described in detail for Units 10 to 12 in Section 4.3.2.3. After yielding of those longitudinal bars, shear transfer from spiral to spiral due to dowel action of those bars is neither effective nor able to be evaluated unless strain hardening of steel is taken into account as discussed in Section 4.2.2.6.

At first yield displacement of column, the axial strains induced in the longitudinal bars which interlock the spirals may significantly be less than the yield strain because those longitudinal bars are located at mid-depth region of the column section. It is of importance to securely interlock spirals at least until the column displacement reaches first yield displacement. When the strength design method [4.2, 4.6] is used, secure interlocking of spirals may be required at least until strain in extreme concrete compression fibre reaches 0.003. This is because in the strength design method the maximum usable strain at extreme compression fibre, ε_c, is assumed to be equal to 0.003. Taking this loading condition on a column as a target, the modified shear friction method represented by Eq.4.36 may tentatively be used to determine the adequate amount of longitudinal bars required to interlock the spirals, until a more satisfactory method is established. Here, at ε_c of 0.003 average stress in the longitudinal bars in interlocking area is denoted by f_{s3}. Replacing f_s by f_{s3}, Eq.4.36 is rewritten as

$$V_n = A_{vf} (f_y - f_{s3}) \mu \qquad \text{.....} \qquad (4.39)$$

For the assumed corbel represented by Fig. 4.23, the shear force applied by the spiral is estimated to be $2 A_{sp} f_{yh} \cos \theta_1$ assuming that spirals have yielded. Since this shear force needs to be less than or equal to V_n from Eq. 4.39, it is required that,

$$2 A_{sp} f_{yh} \cos \theta_1 \leq A_{vf} (f_y - f_{s3}) \mu$$

Rearranging the terms gives

$$A_{vf} \geq \frac{2\, A_{sp}\, f_{yh} \cos\theta_1}{(f_y - f_{s3})\,\mu} \qquad \text{.....} \qquad (4.40)$$

Thus, the amount of longitudinal reinforcement to interlock the spirals is determined as the shear friction reinforcement by Eq. 4.40.

For example, in case of Unit 10 A_{vf} required by Eq.4.40 is more than 121 mm^2 assuming that A_{sp} = 78.5 mm^2 (for spiral bar diameter of 10 mm), f_y = 485 MPa (measured strength of Grade 380 steel used), f_{yh}= 308 MPa (measured strength of Grade 275 steel used), f_{s3} = 252 MPa (from moment curvature analysis, at ε_c = 0.003), θ_1=35° and μ = 1.4. In the interlocking area two times A_{vf}, that is, 242 mm^2 is required because Eq.4.40 is applied to the corbel, area of which at the assumed critical section is a half of the interlocking area as shown in Fig.4.23. If specified yield strengths are used for f_y and f_{yh} instead of measured strengths, A_{vf} required by Eq.4.40 becomes more than 221 mm^2 and the corresponding total area of longitudinal bars required to interlock the spirals thus becomes more than 442 mm^2. Hence, when a 20mm diameter bar of Grade 380 steel (A_s= 314 mm^2) is used to interlock the spirals, Eq.4.40 is satisfied by providing one or two bars for Unit 10.

It is notable that longitudinal bars in the interlocking area reach their yield strain before ε_c reaches 0.005 in a moment-curvature analysis and before the column displacement reaches 2 times first yield displacement in a load-displacement analysis conducted for Unit 10. This implies that during the inelastic range of loading shear transfer from spiral to spiral by longitudinal bars in the interlocking area will not be improved in practice unless a large number of longitudinal bars are added. As mentioned in Section 4.2.2.6, after yielding of longitudinal bars in axial tension or compression, the dowel strength of those bars can be expected to be achieved only by kinking. However, shear transfer by kinking is normally appreciable only after a considerable relative displacement across the shear interface is attained [4.18].

The option of placing the longitudinal bars in the interlocking area which are not well anchored, and hence serve mainly to interlock the spirals

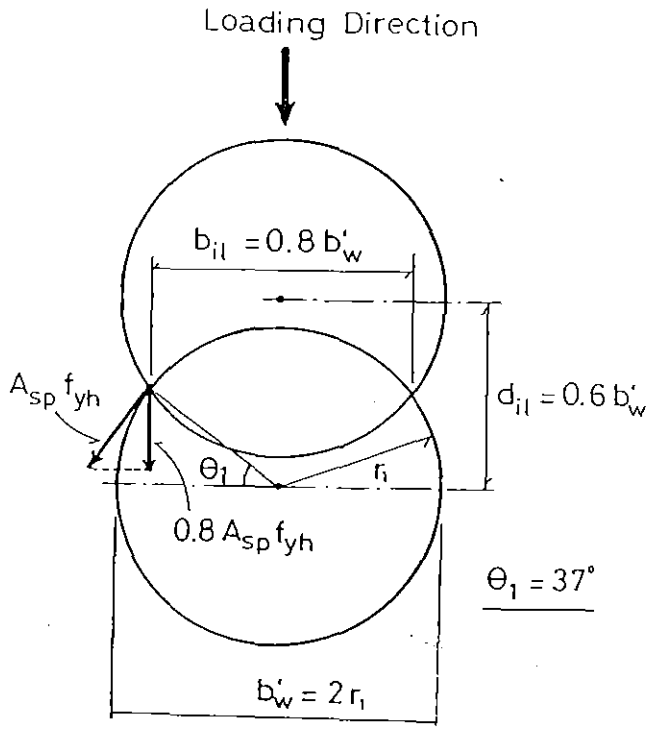

Fig. 4.27 Dimensions of Column Section when $\theta_1 = 37°$.

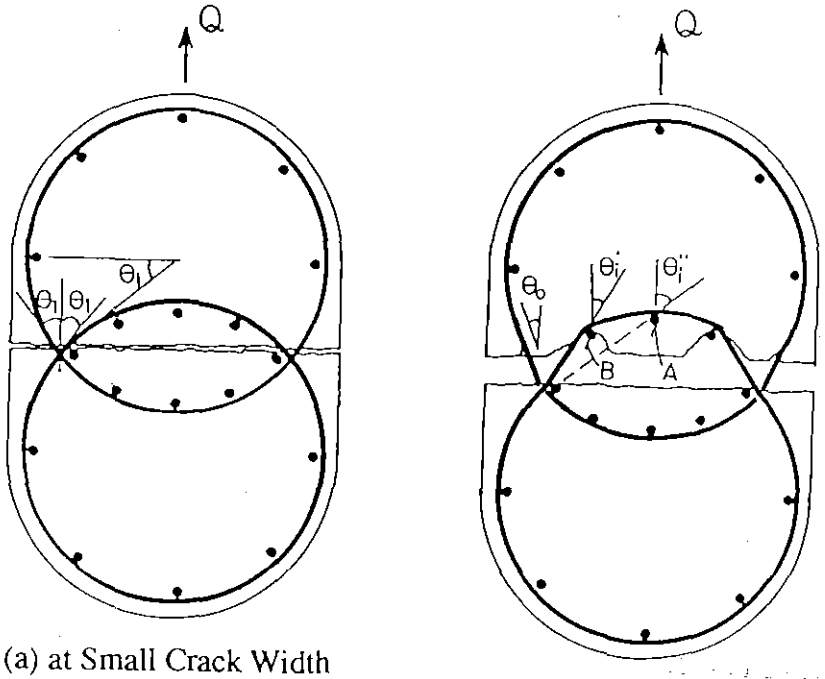

(a) at Small Crack Width

(b) at Large Crack Width

Fig. 4.28 Change of Inclination in Spiral Tension Force from the Direction of the Applied Shear as Crack Width Increases.

[4.1], may be advantageous because f_s in Eq. 4.36 or f_{s3} in Eq.4.40 will thus be smaller than the magnitude calculated from a moment-curvature analysis where it is hypothesized that plain sections before bending remain plane after bending. However, it must be emphasized that those longitudinal bars need to be at least bonded where the shear friction method is applied, so as to be able to attain their yield strength when clamping the concrete across the cracks.

4.2.2.9 The Spacing of the Longitudinal Bars to Interlock the Spirals

When local fracture of the core concrete occurs due to the bearing stresses created by highly stressed spirals after the formation of shear cracks, the spirals need to be anchored by the suspension mode as shown in Fig.4.7 (b). To attain this suspension mode, a fundamental requirement is that the longitudinal bars are to be placed at each corner of the intersection of interlocking spirals and at each centre of the arch of the inner spiral bar. Hence, at least four longitudinal bars are required inside the interlocking area.

When a diagonal tension crack with small width separates the column section at mid depth as shown in Fig.4.28(a), it may be considered that the inclinations of the spiral tension forces of both the outer and inner spiral bars are the same θ_1 measured to the direction of the shear force applied to the column. However, when the crack opens wide and the suspension mode is attained with local fracture of core concrete, the inclination of the outer spiral bar is reduced to θ_o and that of the inner spiral bar is increased to θ_i', as represented by Fig.4.28 (b). If the longitudinal bar (B) is not placed, the inclination is further increased to θ_i''. This geometrical consideration indicates that smaller spacing of the longitudinal bars to interlock spirals will produce the following two benefits. Firstly, the suspension mode which can make the inner spiral bar effective after the local fracture of the core concrete is more quickly attained. Secondly, after completion of the suspension mode, the inclination of the inner spiral bar force to the direction of the shear force on column is smaller. Thus, as the spacing of the longitudinal bars decreases, the efficiency of the inner spiral bars is enhanced. Hence, it may be recommended that the spacing of longitudinal bars inside the interlocking area should be as small as possible. However, it is not necessary to make the spacing of those longitudinal bars

uneconomically small provided that the amount of the interlocking spirals is determined by Methods (2) or (3) described in Section 4.2.2.3. This is because Method (3) assumes that the inner spiral bars in the interlocking area are ineffective against shear and Method (2) is a simplified method which gives similar result with Method (3).

4.3 TESTS ON COLUMNS WITH INTERLOCKING SPIRALS

4.3.1 Test Programme

4.3.1.1 Principal Dimensions of Test Column Units and Details of the Reinforcement and Concrete

The principal dimensions of Units 9 to 12 which were constructed and tested are shown in Fig.4.29. Those column units had a total height of 2.884 m. In the column region shown in the figure as section B-B, Unit 9 had 400 mm x 600 mm rectangular cross section and Units 10 to 12 had 400 x 600 mm^2 cross section with semicircular edges on two sides. The top block with 600 mm square cross section and the base block of dimensions 914 mm x 950 mm x 1200 mm simulated a pier cap and a footing, respectively.

For Unit 9, the longitudinal reinforcement was from 24 mm diameter deformed bar of Grade 380 steel and the transverse reinforcement was from 12 mm diameter plain round bar of Grade 275 steel. For Units 10 to 12, the longitudinal reinforcement was from 20 mm diameter deformed bar of Grade 380 steel and the transverse reinforcement was from 10 mm diameter plain round bar of Grade 275 steel. The measured steel strengths are listed in Table 4.2 and reinforcing details for each test column unit are shown in Figs. 4.30 to 4.34. The axial load ratios $P_e/(f'_cA_g)$ used in the tests for Units 9 and 10 were 0.1, for Unit 11 was 0.3 and for Unit 4 was 0.5.

The amount and spacing of transverse reinforcement in the potential plastic hinge region of the tested columns were determined to satisfy the provisions of NZS 3101 [4.2] for both confinement and shear, except for Unit 11 where the spacing of spirals in that region was 100mm. In clause 6.5.4.3 of NZS 3101, a provision requires that the spacing of spirals needs to be equal to or less than one-fifth of the least lateral dimension of the cross section

and the spiral spacing of 80 mm is thus required of Unit 11. However, the spirals provided in Unit 11 satisfy all other provisions of that code. The amount of transverse reinforcement was governed by the confinement requirement for Units 9, 11 and 12 and by the shear requirement for Unit 10. It is notable that the shear carried by the interlocking spirals was estimated using Method (1) described in Section 4.2.2.3, which may provide an unconservative estimate of the shear strength.

The reinforcing details in the base blocks of all column units were determined to resist more than 1.5 times the corresponding column load carrying capacity, in order to avoid failure in those base blocks during testing.

The concrete was cast with the test column units in a vertical position. All concrete was normal weight with a target slump of 100mm and a maximum aggregate size of 13mm. The column region of the units were cast one by one from different batches of concrete with the same target strength of 25 MPa. For the base block part of each column unit, a higher concrete strength of 35 MPa was specified in order to avoid excessive propagation of crushing of concrete into the base block during testing. Moulds were dismantled one week after casting and all test columns were damp cured for 28 days. At the test age of two to three months, the compressive strengths of the concrete of the column regions for all test units were measured from 100mm diameter by 200mm cylinders and varied between 21.2MPa to 29.7MPa as listed in Table 4.2. The compressive strengths of concrete placed in the base block were also measured in the same way and were 42.3MPa for Units 9 and 10 , 45.0MPa for Unit 11 and 40.5MPa for Unit 12. The moduli of rupture of the column region concrete, as measured from 152mm x 152 mm x 473 mm prisms, are also listed in Table 4.2.

4.3.1.2 Loading Arrangements and Testing Procedure

The concentric axial load was applied to each test column unit by a 10 MN DARTEC electro-hydraulic universal testing machine through cylindrical steel bearings which allowed free rotation at the ends of column, as shown in Fig. 4.35. During the tests, using the servo-control system of the machine the axial load was kept constant at a predetermined level for each

column unit. As the main experimental variable, the axial load level imposed on each test column unit varied from 0.1 to 0.5 $f'_c A_g$, where f'_c = concrete compressive cylinder strength and A_g = gross area of column cross section, as listed in Table 4.2.

A reversible horizontal load was applied to the top block of each column unit by a ± 1000 KN hydraulic jack. The lateral load and displacement history imposed on each column unit consisted of one elastic cycle to a displacement ductility factor $\mu = \pm 0.75$ and then two cycles to each of $\mu = \pm 2, \pm 4, \pm 6, \pm 8$, etc. The displacement ductility factor μ is defined as Δ/Δ_y^M, where Δ = measured lateral displacement at the hydraulic jack and Δ_y^M = calculated lateral displacement at first yield found assuming elastic cracked section behaviour up to the theoretical ultimate horizontal load, H_u. The theoretical ultimate horizontal loads, H_u , for the test columns were computed using the stress-strain models for the longitudinal reinforcement shown in Fig.4.38, the ACI rectangular compressive stress block for the concrete with the measured concrete cylinder strength, an extreme fibre concrete compressive strain of 0.003, and a strength reduction factor ϕ of unity. The stress-strain models for longitudinal bars shown in Fig.4.38 were based on the measured stress-strain relations. Strains of up to about 6% were measured by a Batty extensometer with a gage length of 50 mm and the strains at the ultimate strength of the steel and at bar fracture were measured by an ordinary scale with a gauge length of five times bar diameter. The elastic cracked section stiffness was obtained from the initial cycle of loading of up to ± 0.75 of H_u , as mentioned in Section 3.2. The horizontal displacement of each column at ± 0.75 H_u was averaged and divided by 0.75 to find the first yield displacement Δ_y^M. In Table 4.4, the Δ_y^M obtained for each test column unit is listed along with theoretical values. Those theoretical values are discussed in Sections 4.3.2 and 4.3.3.

4.3.1.3 Instrumentation

The horizontal displacements at the hydraulic jack and at mid-height of the test columns were measured by linear potentiometers mounted on a stiff measuring frame as shown in Fig.4.35. The latter displacements were also used to estimate the shear deformation of each column by investigating the relation between those displacements and the flexural deflections which are calculated using the measured curvature distribution along column axis.

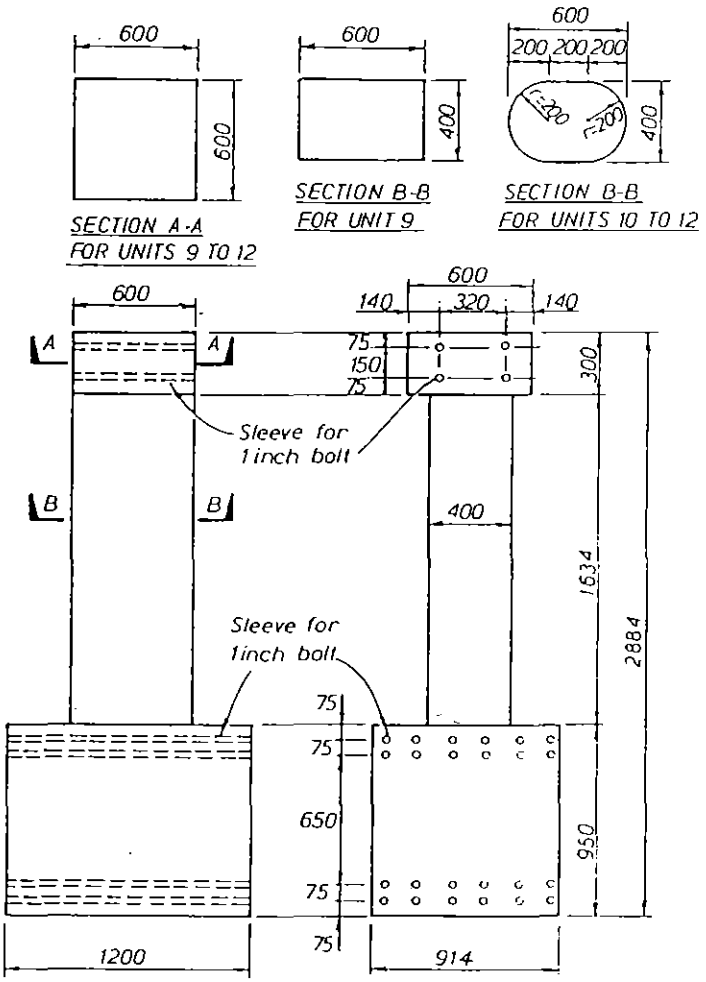

Fig. 4.29 Principal Dimensions of Units 9 to 12.

Table 4.2 Mechanical Properties of Materials and Other Details of Column Units 9, 10, 11 and 12.

Column Unit	Concrete		Longitudinal Reinf.			Transverse Reinf.			Sectional Dimensions of Column, B x D	Ratio of Shear Span Length to D	Ratio of Total Area of Longitudinal Reinf. to Gross Area of Section,	Hoop Sets in End Region			Axial Load Level $\frac{P_e}{f'_c A_g}$
	f'_c	f_t	Bar Type and Dia.	f_y	f_{su}	Bar Type and Dia.	f_y	f_{su}				Spacing	Volumetric Ratio to Concrete Core		
	(MPa)	(MPa)		(MPa)	(MPa)		(MPa)	(MPa)	(mm)		ρ_t (%)	(mm)	ρ_s (%)	ρ_{se} (%)	
9	26.9	4.1	HD24	432	588	R12	305	446	400x600	2.97	1.88	80	2.17	-	0.1
10	21.2	3.0	HD20	485	644	R10	308	431	400x600	2.97	2.14	80	1.29	1.08	0.1
11	29.7	4.6	HD20	485	644	R10	308	431	400x600	2.97	2.14	100	1.03	0.92	0.3
12	24.6	3.8	HD20	485	644	R10	308	431	400x600	2.97	2.14	75	1.38	1.15	0.5

Note: f'_c = compressive strength of plain concrete

f_t = modulus of rupture of plain concrete

f_y = yield strength of a steel bar

f_{su} = ultimate strength of a steel bar

B = column width

D = overall depth of column

HD = Grade 380 steel, deformed bar.

R= Grade 275 steel, plain round bar.

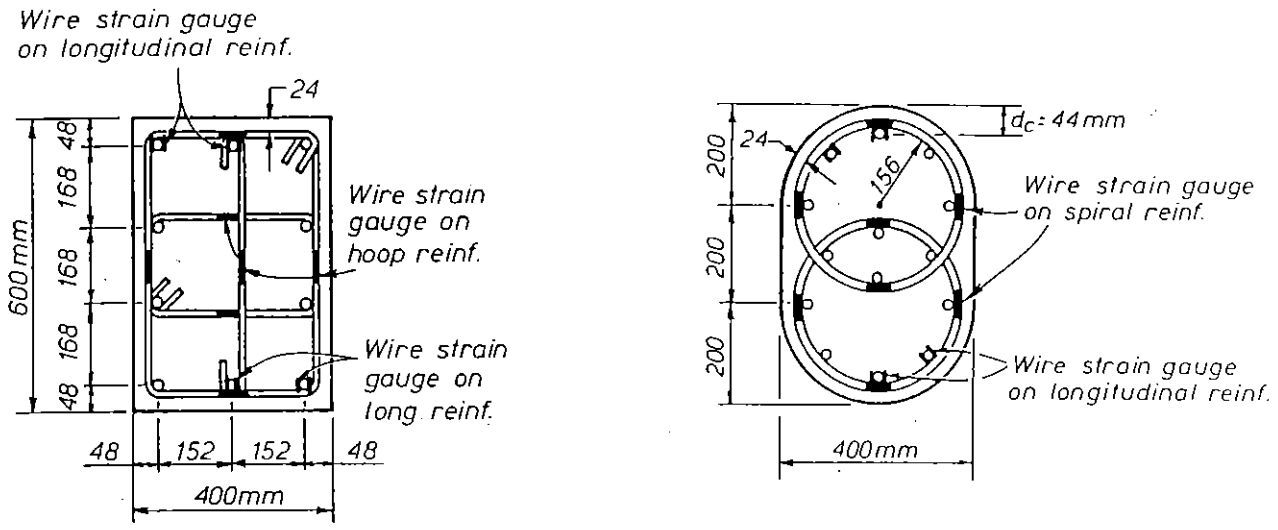

(a) Unit 9 (b) Units 10 to 12

Fig. 4.30 Transverse Sections of Column Units 9 to 12.

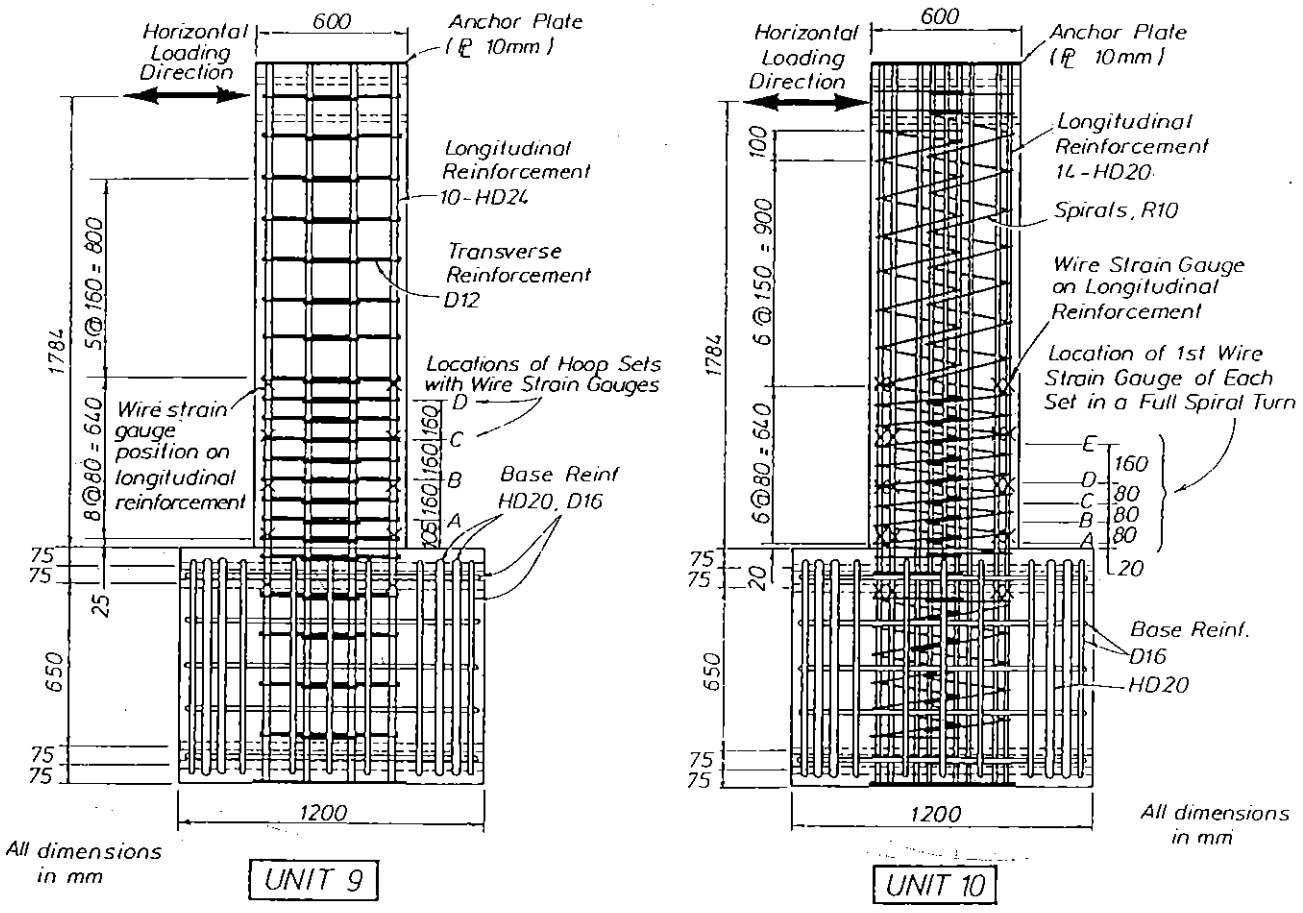

Fig. 4.31 Longitudinal Sections of Column Units 9 and 10 Showing Details of Reinforcement.

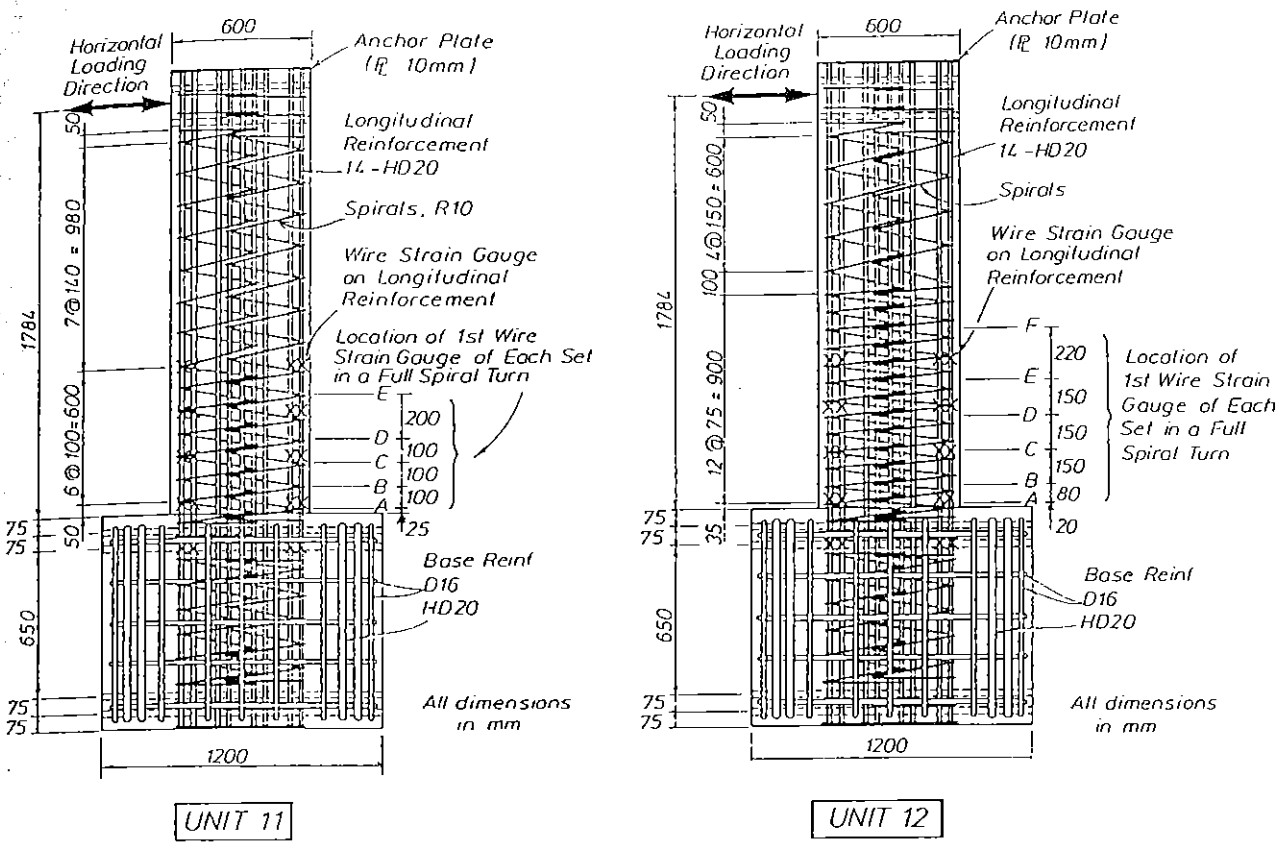

Fig. 4.32 Longitudinal Sections of Column Units 11 and 12 Showing Details of Reinforcement.

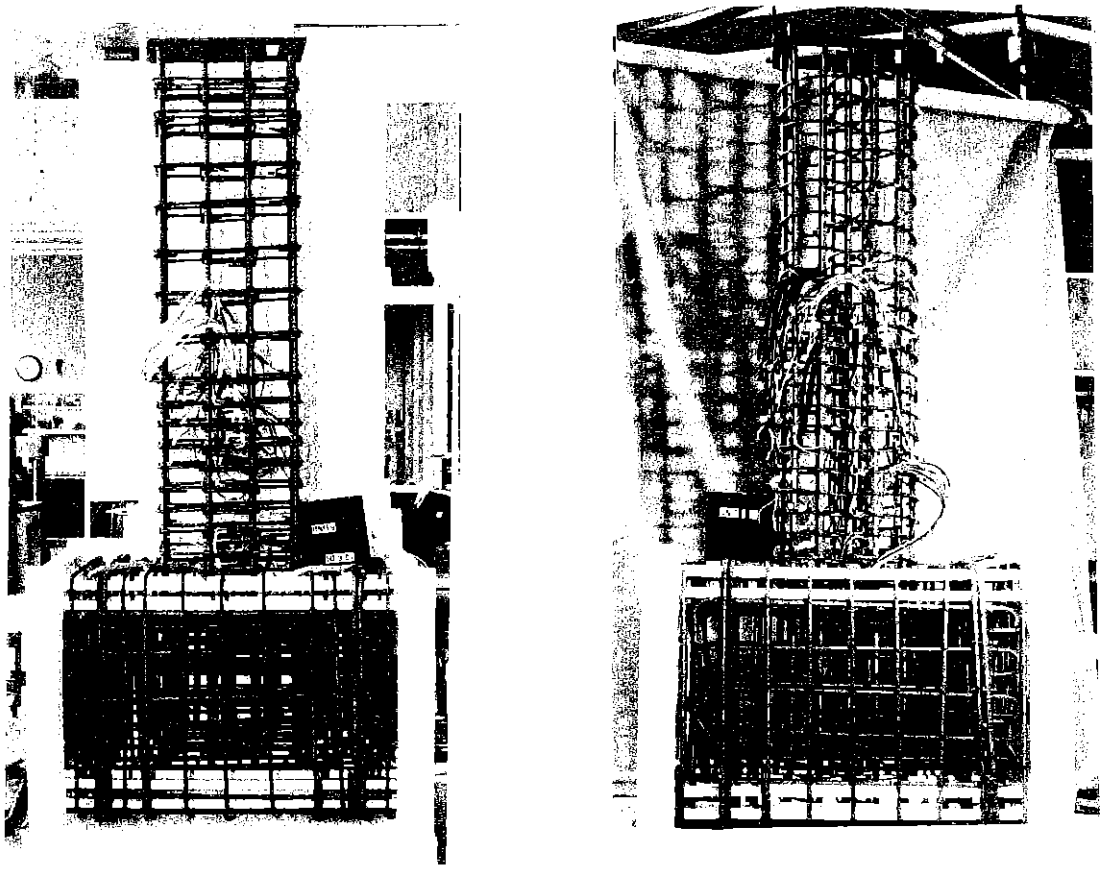

(a) Column with Rectangular Hoops and Cross Ties

(b) Column with Interlocking Spirals

Fig. 4.33 Reinforcing Cages for Columns and Base Blocks.

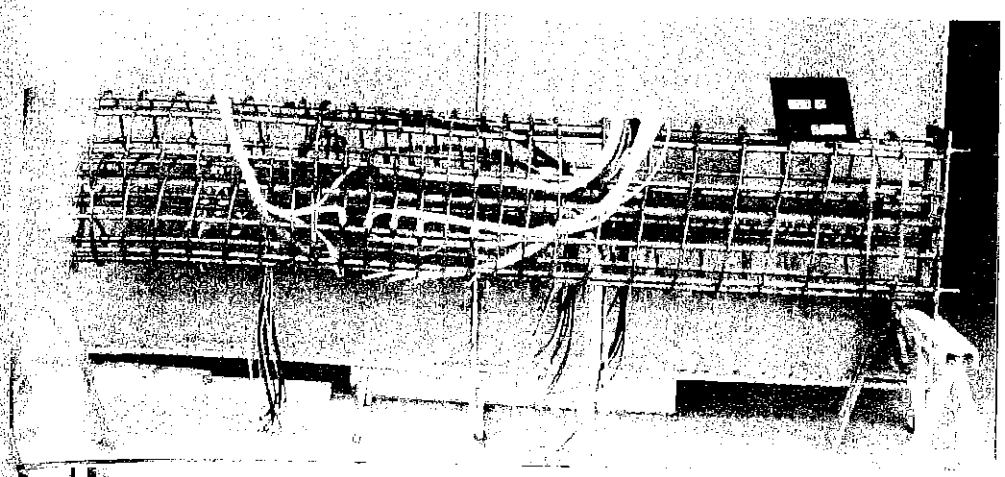

(a) Side View

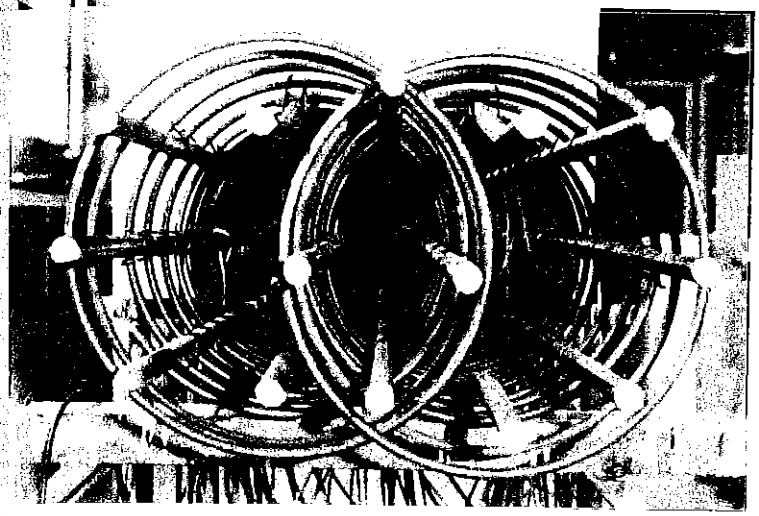

(b) Top View

Fig. 4.34 A Reinforcing Cage for Column with Interlocking Spirals.

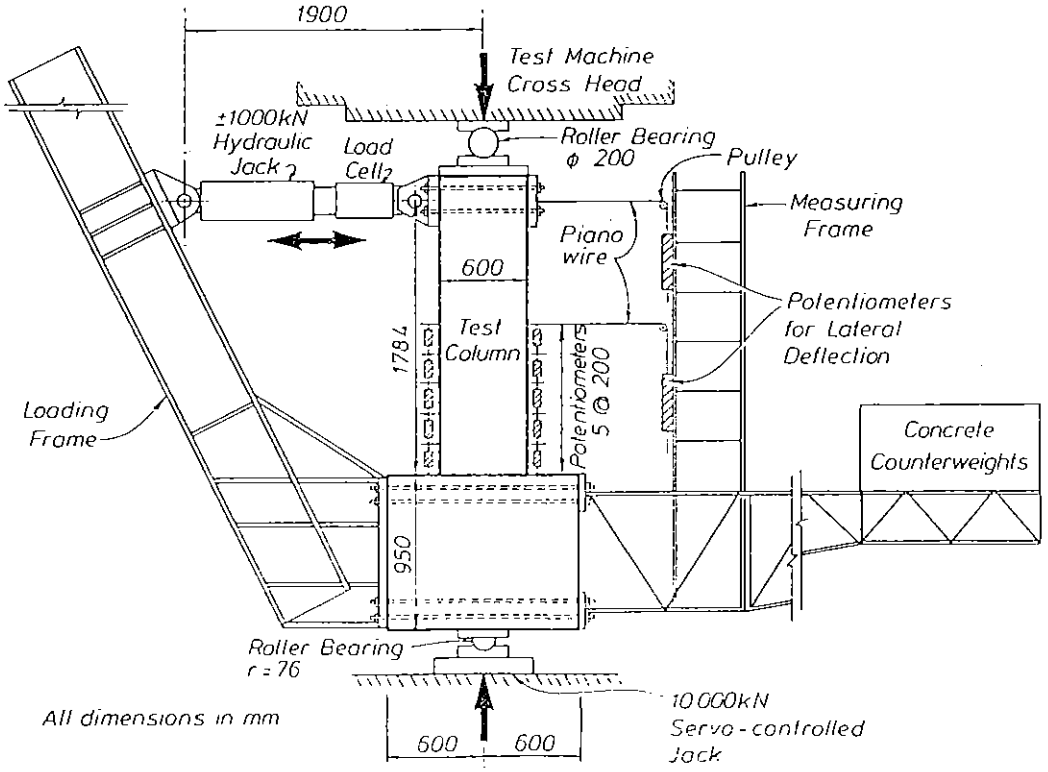

Fig. 4.35 Loading Arrangements and Potentiometer Positions for Column Tests.

(a) View of Side Parallel with Loading Direction

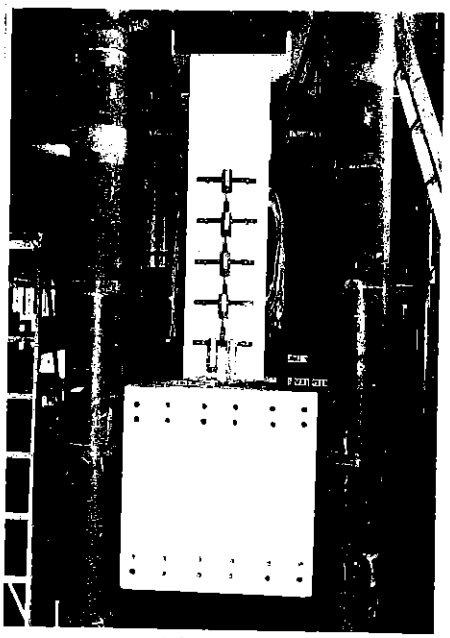

(b) View of Loading Side before Attaching Loading Frame

Fig.4.36 Column Unit Set Up in the DARTEC Machine.

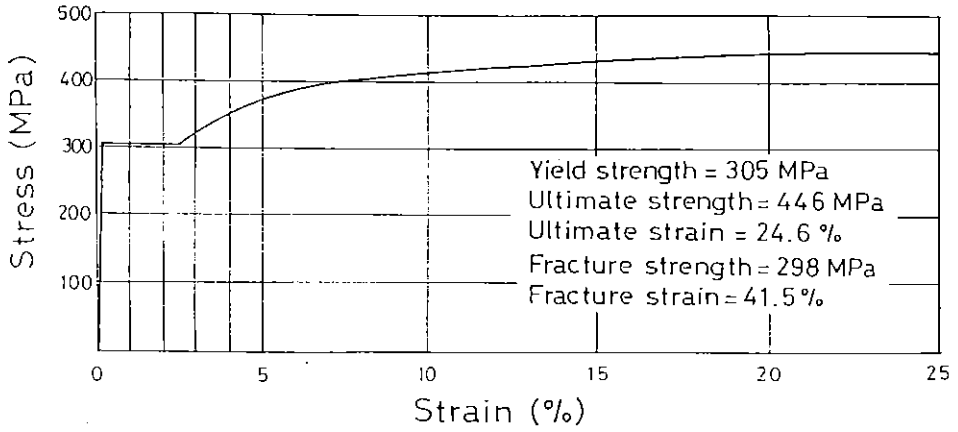

(a) 12 mm Dia. Round Bar for Rectangular Hoops and Cross Ties (Unit 9)

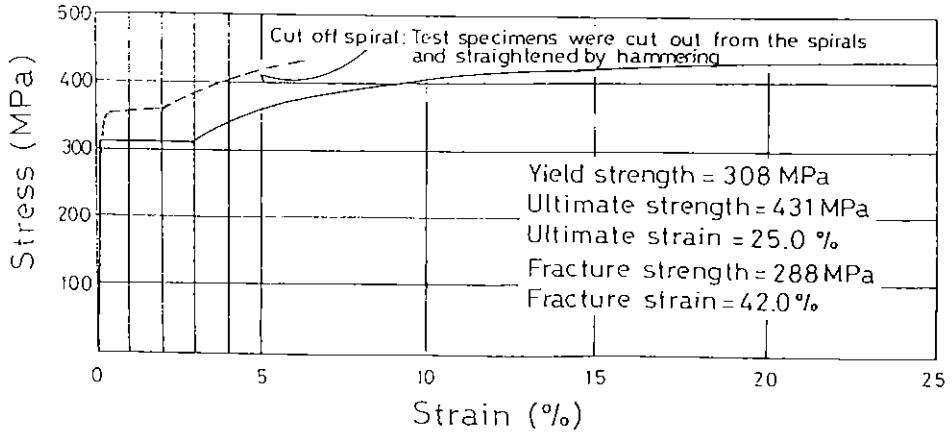

(b) 12 mm Dia. Round Bar for Spirals (Units 10 to 12)

Fig. 4.37 Measured Stress-Strain Relationships for Transverse Reinforcement from Grade 275 Steel.

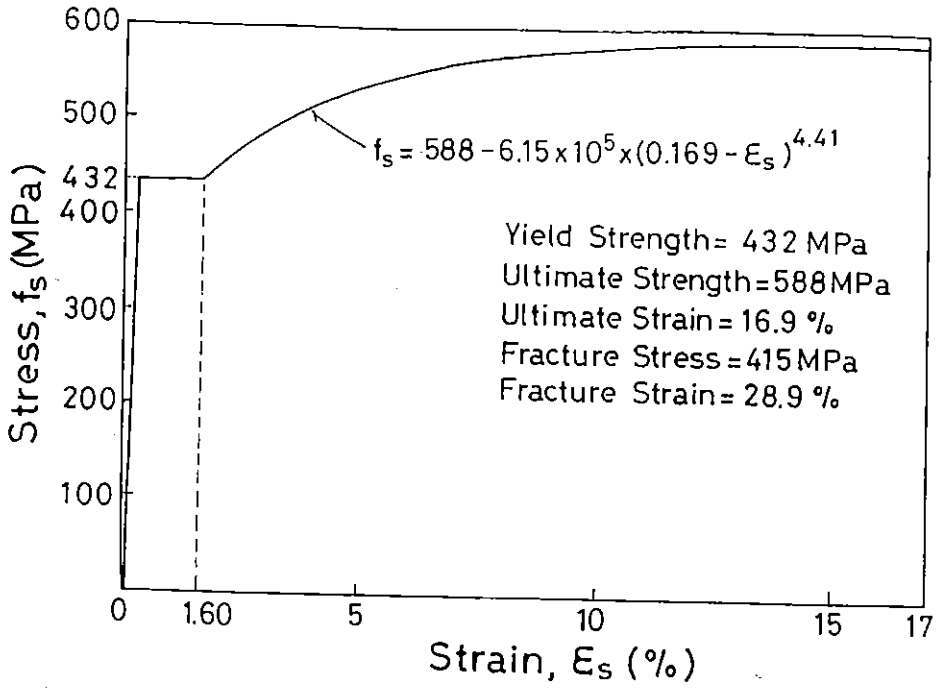

(a) 24 mm Dia. Deformed Bar for Longitudinal Reinforcement for Unit 9

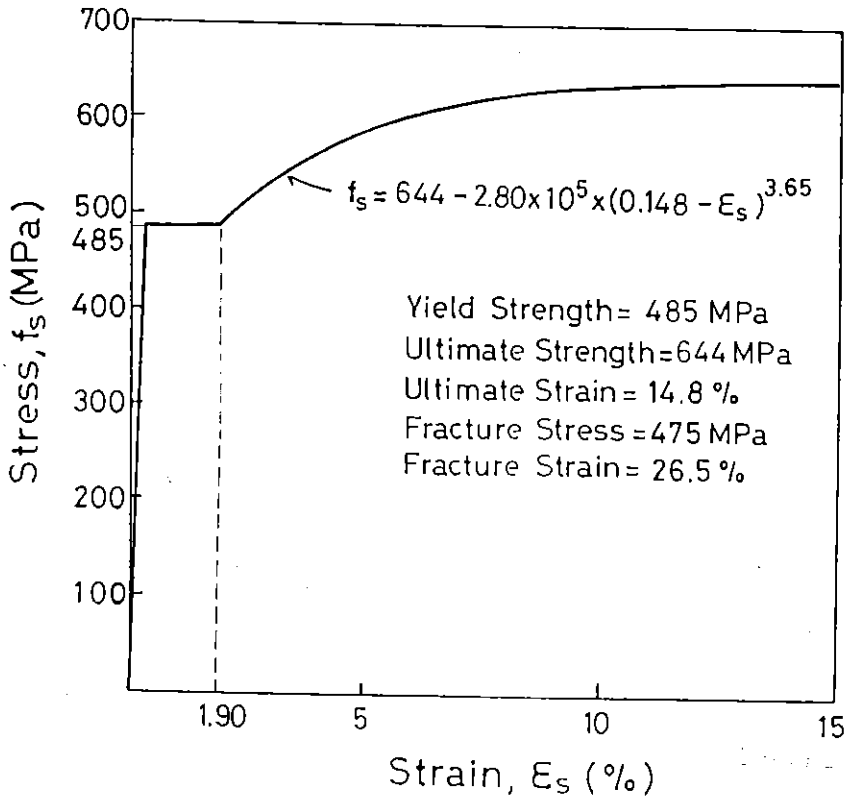

(b) 20 mm Dia. Deformed Bar for Longitudinal Reinforcement for Units 10 to 12

Fig. 4.38 Measured Stress-Strain Relationships for Longitudinal Bars from Grade 380 Steel.

The measured horizontal displacement minus the calculated deflection due to flexure can be taken to be the deflection mainly due to shear deformation of the column as discussed later in Section 4.3.3.3.

To measure the curvature distributions and the concrete strains, five pairs of linear potentiometers, of guage length 200 mm, were placed down the height of the columns. Those potentiometers were mounted on 10 mm diameter steel rods which passed through the concrete in the plane of the column section and at right angles to the neutral axis. The rods were cast in the concrete but the cover concrete surrounding the end of each rod was not present over a depth of 25 mm and a diameter of 30 mm in order to avoid interference by crushed cover concrete.

Electric resistance strain gauges were attached at various locations on the longitudinal reinforcement, hoops and cross ties, and spirals as indicated by cross marks in Figs. 4.30 to 4.32. At each location, a pair of electric wire gauges were attached on opposite sides of the bar and their strain readings were averaged to estimate the axial strain induced in the bar. This is because the longitudinal and transverse reinforcement can significantly be bent in the inelastic range of loading.

4.3.2 Test Results

4.3.2.1 General Observation and Horizontal Load-Displacement Behaviour

Horizontal load versus horizontal displacement hysteresis loops measured for all the column units are shown in Figs. 4.39 to 4.42. Also shown in those figures are the theoretical ultimate horizontal loads, H_u, which were calculated as described in Section 4.3.1.2. The slope of the lines of theoretical ultimate horizontal load is due to the P-Δ effect which decreases the horizontal load carrying capacity of the column with increasing horizontal displacement. The test on Unit 9 was terminated when the displacement ductility factor μ reached 10 in order to prevent damaging the measuring devices. For Units 10 to 12 the tests were terminated when first spiral fracture occurred. All measured hysteresis loops shown in Figs. 4.39 to 4.42 illustrate stable behaviour, good energy dissipation and limited reduction in strength up to the end of the test end and the displacement ductility factor μ reached more than 10. However, it

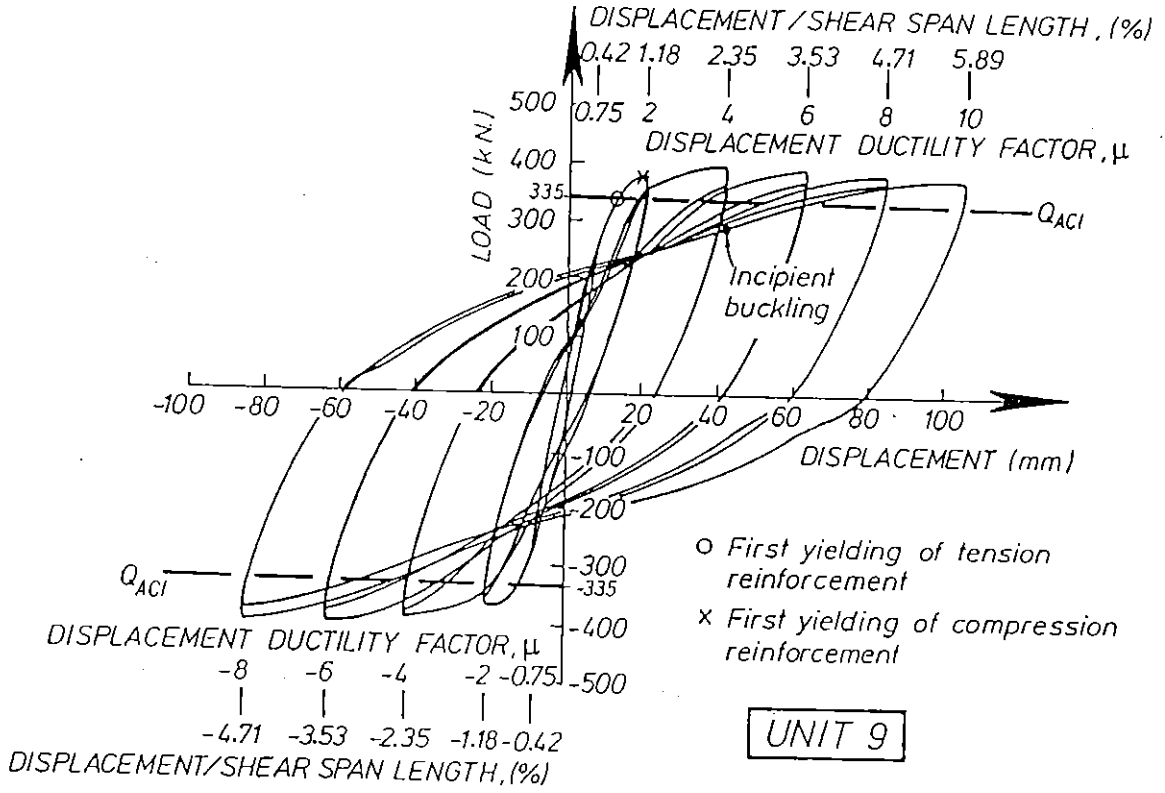

Fig. 4.39 Measured Horizontal Load-Displacement Hysteresis Loops for Unit 9.

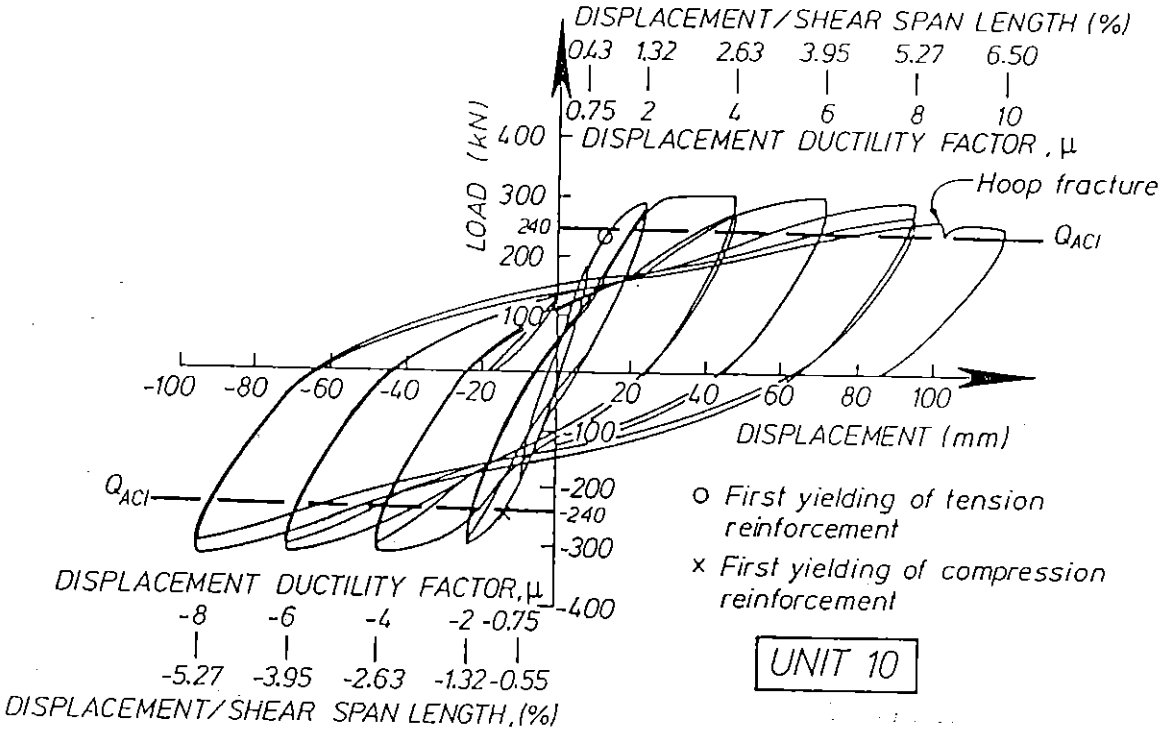

Fig. 4.40 Measured Horizontal Load-Displacement Hysteresis Loops for Unit 10.

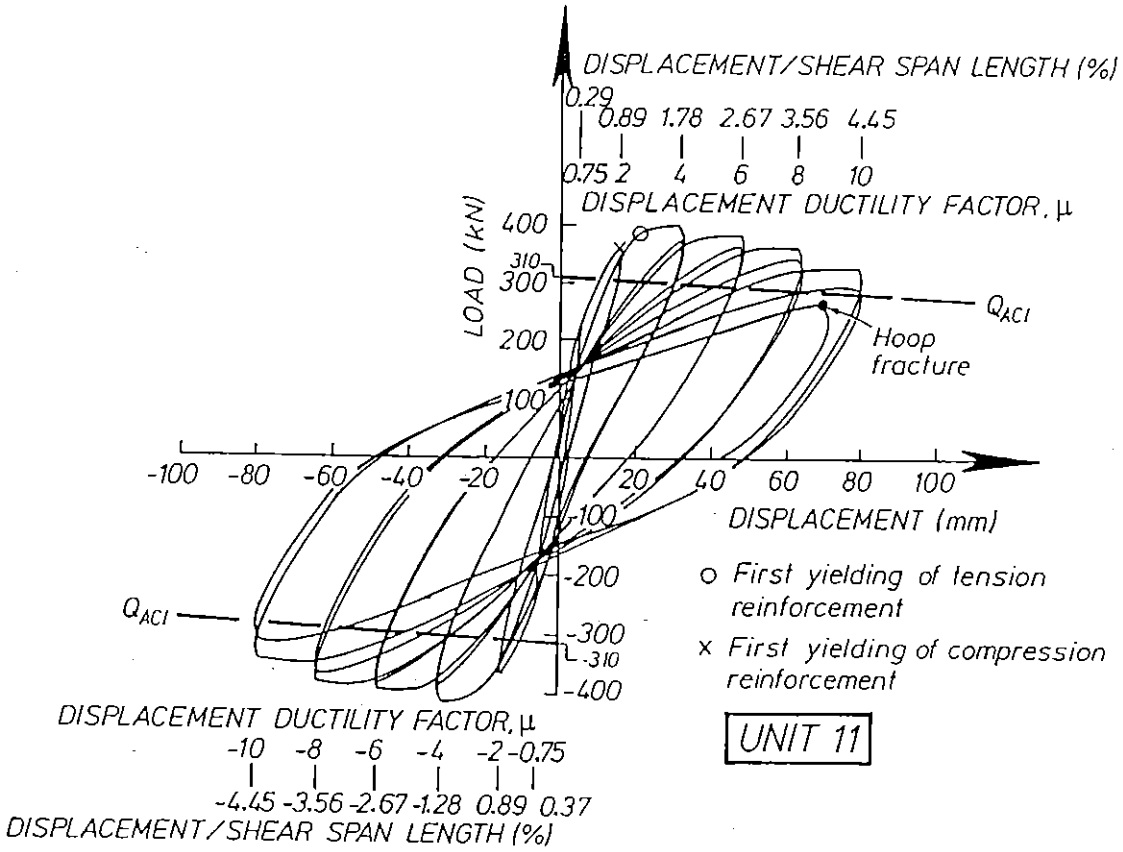

Fig. 4.41 Measured Horizontal Load-Displacement Hysteresis Loops for Unit 11.

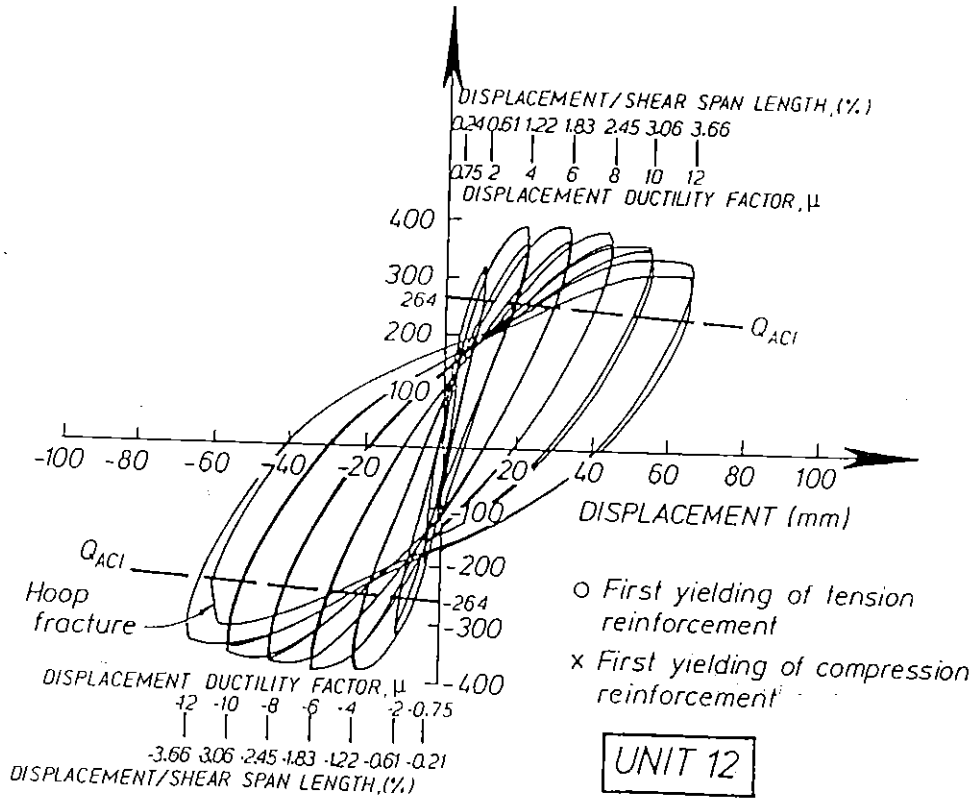

Fig. 4.42 Measured Horizontal Load-Displacement Hysteresis Loops for Unit 12.

is notable that slight pinching of hysteresis loops is observed for Unit 10 compared with Unit 9. The reason for this is discussed later with theoretical considerations.

In each of Figs. 4.39 to 4.42, a scale for Δ/L, where Δ = horizontal displacement and L= shear span length (= 1.784 m), is also shown. The value of Δ/L may nearly correspond to the storey drift in a building which is designed based on a strong column-weak beam approach [4.20, 4.21] to achieve a beam sidesway mechanism where column plastic hinges form only at the base and possibly at the column top in the top storey. For ductile moment resisting frames of reinforced non-prestressed concrete, NZS 4203 code [4.20] requires that the storey drift, which is computed for the design seismic loading and assuming that the frame remains elastic, should not exceed 0.0032 of the storey height when those frames are located in the worst seismic zone in New Zealand [4.21]. This means that, assuming the structure yields at the design static seismic loading, the permitted horizontal deflection at a displacement ductility factor μ of 4 is 1.3 % of the storey height. It is notable that for all test columns the values of Δ/L reached more than 3.7 % while keeping stable hysteresis loops.

Table 4.3 lists measured maximum moments (M_{max}) with corresponding theoretical values. M_{max} is the measured maximum moment which was reached including the moment due to P-Δ effect during the cyclic loading on each column unit. Table 4.4 lists first yield displacements (Δ_y^M) and first yield curvatures (ϕ_y^M) with corresponding theoretical values. The first yield displacement Δ_y^M was calculated as described in Section 4.3.1.2. That is, column displacements at $\pm$ 0.75 H_u in the initial cycle of loading to $\mu = \pm$ 0.75 were measured and then those measured displacements were averaged and divided by 0.75 to obtain Δ_y^M. In like manner, the first yield curvature ϕ_y^M corresponding to Δ_y^M was calculated using measured curvatures. That is, the measured curvatures at $\pm$ 0.75 H_u in the initial cycle of loading to $\mu = \pm$0.75 were averaged and divided by 0.75 to obtain ϕ_y^M, where curvature measurements were conducted using a pair of potentiometers of gauge length 200 mm and located at the first position counting from the base block side shown in Fig. 4.35.

For comparison, theoretical maximum moments, first yield displacements and first yield curvatures are also listed in Tables 4.3 and 4.4. To calculate those theoretical moments, the perfect beam action was assumed. That is, it was hypothesized that plane sections before bending remain plane after bending. M_{ACI} is the theoretical moment calculated using the ACI rectangular compressive stress block for concrete as described in Section 4.3.1.2. M_{MND}, M_{MKP} and M_{PL} are also the theoretical maximum moments obtained from section analyses where unconfined and confined concrete stress-strain models proposed by Mander et al [4.22], by Kent and Park (the modified Kent and Park model) [4.3], and by Park and Leslie [4.23] were used for cover and core concrete. Those stress-strain models for concrete are shown in Figs. 4.72 to 4.75 in Section 4.3.3.1. For longitudinal bars the modelled stress-strain curves shown in Fig. 4.38 were used and the strength reduction factor ϕ was taken as unity. In those section analyses to obtain M_{MND}, M_{MKP} and M_{MKP}, the extreme compressive fiber strain of concrete, ε_{ef}, was increased from zero to 6 % with increment of 0.02% for ε_{ef} of up to 1% and 0.2% for ε_{ef} of between 1% and 6% in order to find the maximum moment which may be reached after spalling of cover concrete due to strain hardening of longitudinal reinforcement. It was assumed that cover concrete spalls at strain of 0.6 % [4.22].

It is notable that for all tested columns the measured maximum moments exceeded the corresponding theoretical maximum moments calculated using above various theoretical stress-strain relations for concrete. With respect to the modified Kent and Park stress-strain model, it is available only for concrete confined by rectangular hoops with or without supplementary ties and hence it was applied only to Unit 9. The model by Park and Leslie is available only for concrete confined by circular hoops or spirals and hence it was applied to Units 10 to 12. The stress-strain model for confined concrete proposed by Mander et al was determined according to the lateral pressure provided by rectangular hoops or spirals and hence was applied to both Unit 9 and Units 10 to 12 using lateral pressure estimated for each type of confining reinforcement.

Two theoretical values for the first yield displacement were calculated, Δ_y^A and Δ_y^B. The theoretical value of the first yield displacement, Δ_y^A, was obtained using the method mentioned in Section 3.2.3. That is, Δ_y^A was obtained as the sum of ; (a) the flexural deformation calculated by integrating

the theoretical curvature distribution determined by section analysis of the cracked region of the column, (b) the elastic flexural deformation of the uncracked regions, and (c) the shear deformations of the cracked and uncracked regions. All contributions (a) to (c) towards $\Delta_y{}^A$ were calculated for when the lateral load reached the theoretical value H_u. In the calculation of the flexural deformation (a), the Mander et al stress-strain models for confined core concrete and unconfined cover concrete, and the stress-strain models for longitudinal bars shown in Fig. 4.38, were used.

Theoretical value of the first yield displacement, $\Delta_y{}^B$, was obtained as the sum of (a), (b) and (c) for when the lateral load reached 75 % of the theoretical value H_u (calculated using the same stress-stain relations for concrete and reinforcement as that used to obtain $\Delta_y{}^A$) divided by 0.75. This procedure is the same as that used to obtain $\Delta_y{}^M$ except for that in the calculation of $\Delta_y{}^M$ the measured displacement at 0.75 H_u was used instead of the above theoretical displacement.

The theoretical value for the first yield curvature $\phi_y{}^A$ is the calculated maximum curvature for when the theoretical lateral load reached H_u in the computation of $\Delta_y{}^A$. The theoretical values of the first yield curvature $\phi_y{}^B$ is the curvature for when the theoretical lateral load reached 75% of H_u divided by 0.75 to obtain $\phi_y{}^B$. This procedure is also the same as that used to obtain $\phi_y{}^M$ except that the measured curvature at 0.75 H_u is used in the calculation of $\phi_y{}^M$.

As can be seen from Table 4.4, theoretical values of $\Delta_y{}^B$ and $\phi_y{}^B$ which were obtained by following the procedure to obtain $\Delta_y{}^M$ and $\phi_y{}^M$, respectively, are significantly less than the measured values. The main reason for this may be attributed to overestimation of the initial stiffness of concrete in the stress-strain models for concrete, as demonstrated by the previous test results in Section 3.2.3.2. That is, the initial stiffness of the stress-strain model for concrete, which is based on the measured values from small concrete cylinders, is likely to be higher than that in a full size column due to the scale effect. In addition, in the case of the theoretical first yield displacement $\Delta_y{}^B$, shear deformation due to initial flexural shear cracks may actually be larger than the estimated contribution of the shear deformation to $\Delta_y{}^B$. The contribution of shear deformation to $\Delta_y{}^B$ was simply calculated by assuming the modulus of rigidity of concrete for an

uncracked section and an analogous truss [4.18] for a cracked section (see Section 3.2.3). The shear deformation of the tested columns will be discussed in Section 4.3.3.3.

On the other hand, as can be seen from Table 4.4, the theoretical values of Δ_y^A and ϕ_y^A agree well with the measured values of Δ_y^M and ϕ_y^M, although they are calculated directly at the theoretical horizontal load H_u and not by the procedure used to obtain Δ_y^M and ϕ_y^M. As mentioned in Section 3.2.3, for Units 1 to 8 the theoretical values of Δ_y^A and ϕ_y^A also agreed well with the measured values. Hence, the method used to obtain Δ_y^A and ϕ_y^A may tentatively be adopted to estimate Δ_y^M and ϕ_y^M until a more adequate method is achieved.

In Table 4.5, the following measured values at the displacement ductility factor $\mu = \pm 6$ in second cycle of loading and at the final stage of testing are listed; (1) ratios of measured displacement to shear span length, (2) ratios of measured moment M to the measured maximum moment M_{max}, (3) ratios of measured curvature ϕ to the measured first yield curvature ϕ_y^M, and (4) the measured maximum compressive strain on the surface of concrete core ε_c. The values of ε_c were obtained from readings of a pair of potentiometers of gauge length 200 mm and located at the first position counting from the base block side shown in Fig 4.35, except for the values in parentheses. The ε_c values in parentheses were obtained from readings of the second pair of potentiometers counting from the base block side. This is because the damage in compression zone of Units 11 and 12 spread upwards from the column bottom as the deflection of the column increased and eventually concentrated in the region where the second pair of potentiometers were located. It is notable that the very bottom part of column is additionally confined by the adjacent stiff base block and hence the column damage normally concentrated a distance away from the face of the base block as can be seen from Figs. 4.44 to 4.50.

As listed in Table 4.5, the ratios of measured moment to M_{max} varied between 87 to 96 % at the peak of the second cycles of loading to $\mu = \pm 6$ and between 77 to 97 % at the final stage of loading. The maximum compressive concrete strain measured on the surface of the concrete core, ε_c, was more than 3.9% in all columns. From these measurements, it can be concluded that all columns tested could maintain sufficient load carrying capacity to perform in a ductile manner at all stages of loading.

Table 4.3 Comparison between Measured and Theoretical Maximum Moments for Units 9,10, 11 and 12

Colum Unit	Maximum Moment			
	Measured Maximum Moment, M_{MAX} (1) (KN.m)	Ratio of M to Theoretical Moment, $\frac{M_{MAX}}{M_{ACI}}$ (2)	Ratio of M to Theoretical Moment, $\frac{M_{MAX}}{M_{MND}}$ (3)	Ratio of M to Theoretical Moment, $\frac{M_{MAX}}{M_{MPK\ or\ PL}}$ (4)
9	712	1.19	1.01	1.13 (M_{MPK})
10	553	1.29	1.01	1.10 (M_{PL})
11	737	1.33	1.13	1.15 (M_{PL})
12	739	1.57	1.14	1.22 (M_{PL})

Table 4.4 Comparison between Measured and Theoretical Values for First Yield Displacements and Curvatures for Units 9, 10, 11 and 12.

Col-umn Unit	First Yield Displacement				First Yield Curvature			
	Measured Δ_y^M (mm)	Theory(A) Δ_y^A (5) (mm)	Theory(B) Δ_y^B (6) (mm)	Ratio $\frac{\Delta_y^B}{\Delta_y^M}$	Measured ϕ_y^M ($x10^{-6}$ 1/mm)	Theory(A) ϕ_y^A ($x10^{-6}$ 1/mm)	Theory(B) ϕ_y^B ($x10^{-6}$ 1/mm)	Ratio $\frac{\phi_y^B}{\phi_y^M}$
9	10.4	9.2	7.2	0.69	13.3	15.0	7.3	0.55
10	11.7	10.2	8.9	0.76	14.8	12.0	9.0	0.61
11	7.9	8.2	6.3	0.80	9.8	9.4	7.2	0.73
12	5.4	6.0	4.8	0.89	6.0	6.8	5.1	0.85

Table 4.5 Measured Moments, Curvatures and Concrete Strains in Inelastic Range of Loading for Units 9, 10, 11 and 12.

Colum Unit	At Displacement Ductility Factor $\mu = \pm 6$ in Second Cycle					At Final Stage of Testing				
	μ	Δ/L(%) (7)	M/M_{max} (8)	ϕ/ϕ_y^M	ε_c(%) (9)	μ	Δ/L(%) (7)	M/M_{max} (8)	ϕ/ϕ_y^M	ε_c(%) (9)
9	6 -6	3.5	0.93 0.92	6.99 8.85	1.84 2.51	10 (1st Cycle)	5.9	0.97	13.2	3.90
10	6 -6	4.0	0.89 0.96	7.85 8.76	2.76 2.30	10 (1st Cycle)	6.6	0.85	13.9	5.61
11	6 -6	2.7	0.96 0.92	6.72 9.50	1.82 3.01	-10 (2nd Cycle)	4.4	0.77	16.5	3.45 (5.41)
12	6 -6	1.8	0.93 0.87	7.23 7.35	1.76 1.33	12 (2nd Cycle)	3.7	0.79	13.1	(4.07)

Note:

(1)Measured maximum moment at the face of the baseblock, taking into account P-Δ effect

(2)Calculated using the actual stress-strain relation of the longitudinal steel and the ACI concrete stress block

(3)Calculated using the actual stress-strain relation of the longitudinal steel, and the stress-strain relation for concrete modelled by Mander et al.

(4)Calculated using the actual stress-strain relation of the longitudinal steel, and the moidfied Kent and Park stress strain relation for the concrete of Unit 9 and the Park and Leslie stress-strain relation for the concrete of Units 10 to 12.

(5)Theoretical first yield displacement when the calculated moment reached M_{ACI} using the stress-strain relations in note (3)

(6)1.33 times theoretical displacement when the calculated moment reached 0.75 M_{ACI}, using the stress-strain relations in note (3)

(7)The ratio of measured displacement, Δ, to the shear span length, L

(8)M = measured moment at the face of the baseblock, taking into account P-Δ effect

(9) ε_c = maximum compressive strain on surface of concrete core

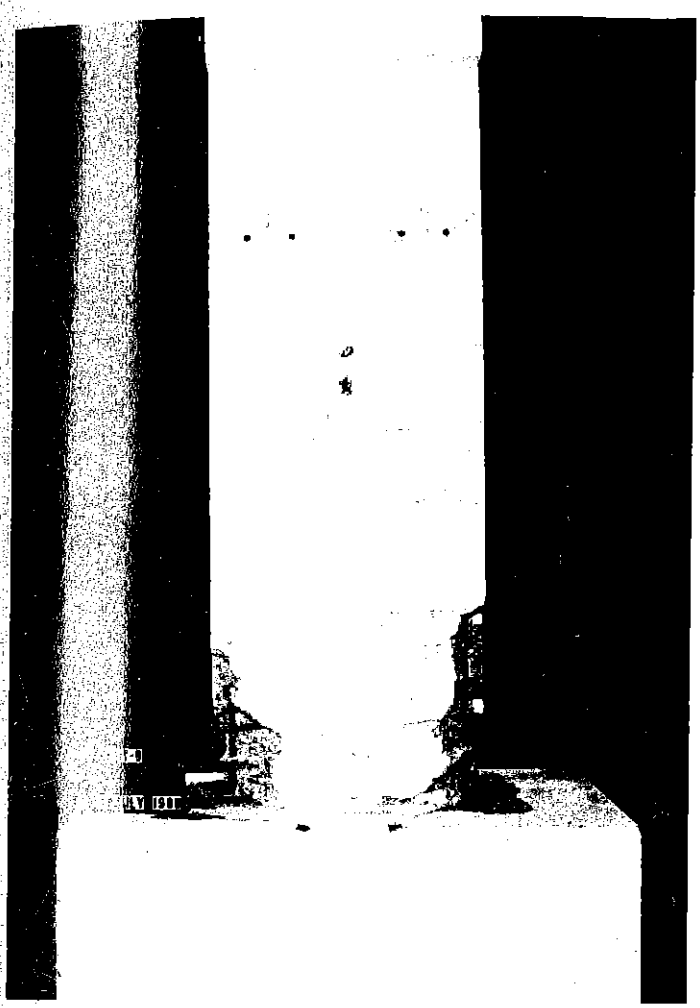

Fig. 4.43 Unit 9 after Testing.

Fig. 4.44 Unit 10 after Testing.

Fig. 4.45 Unit 11 after Testing.

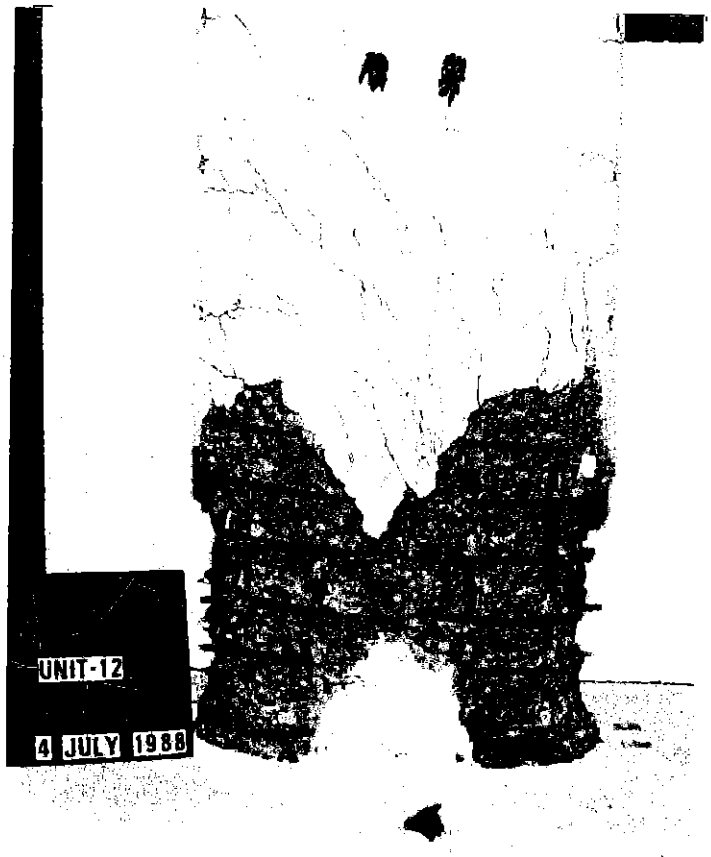

Fig. 4.46 Unit 12 after Testing.

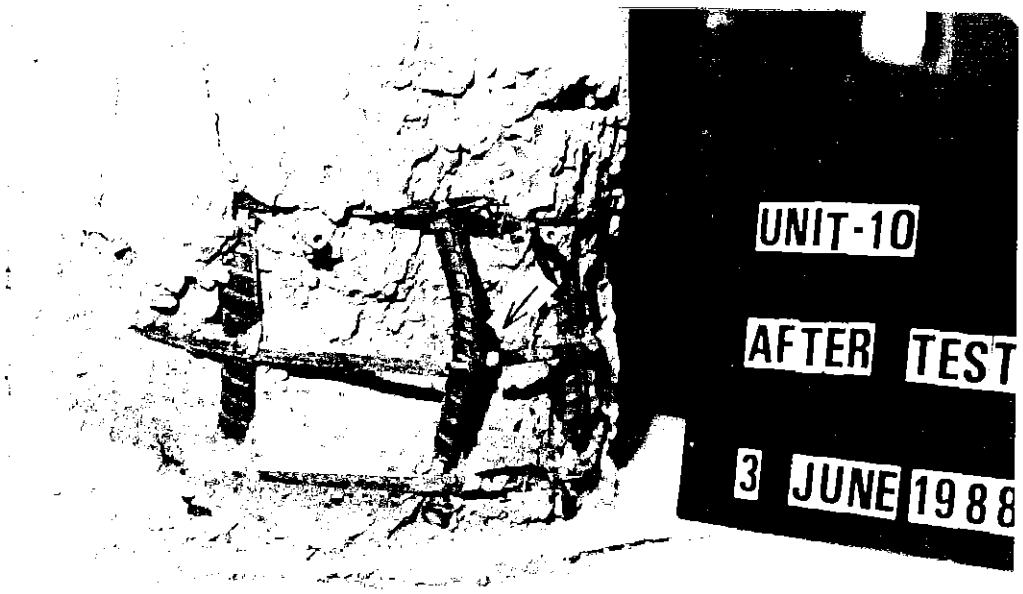

Fig. 4.47 Spiral Fracture in Unit 10.

Fig. 4.48 Unit 10 at Displacement Ductility Factor of 8 in Second Cycle. (Arrow shows a gap between spiral and longitudinal bar in tension zone of column.)

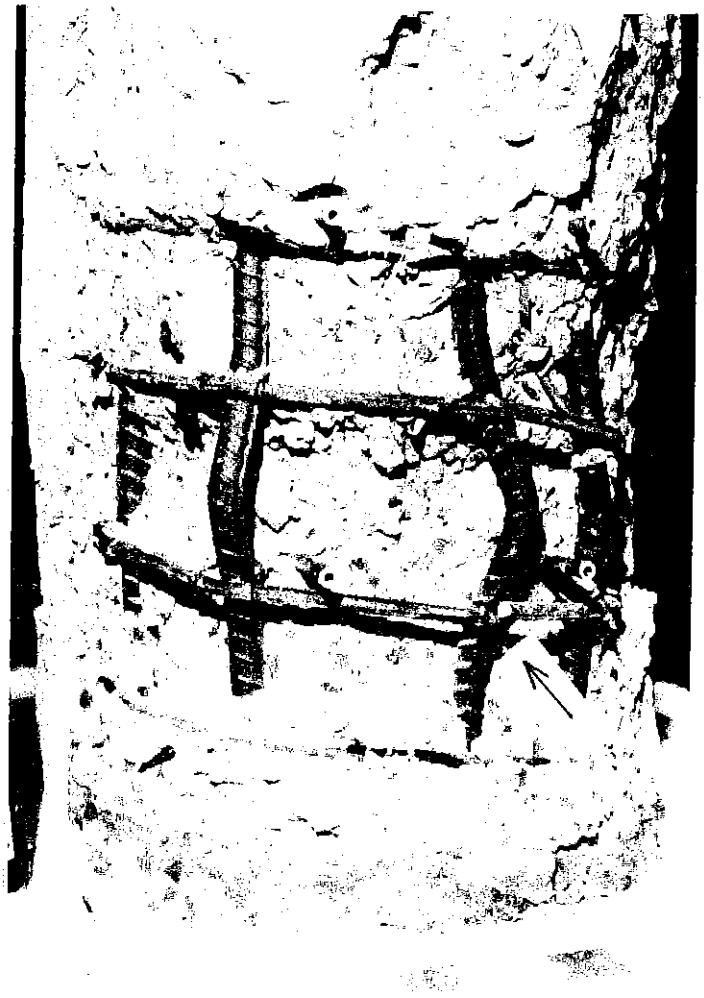

Fig. 4.49 Spiral Fracture in Unit 11.

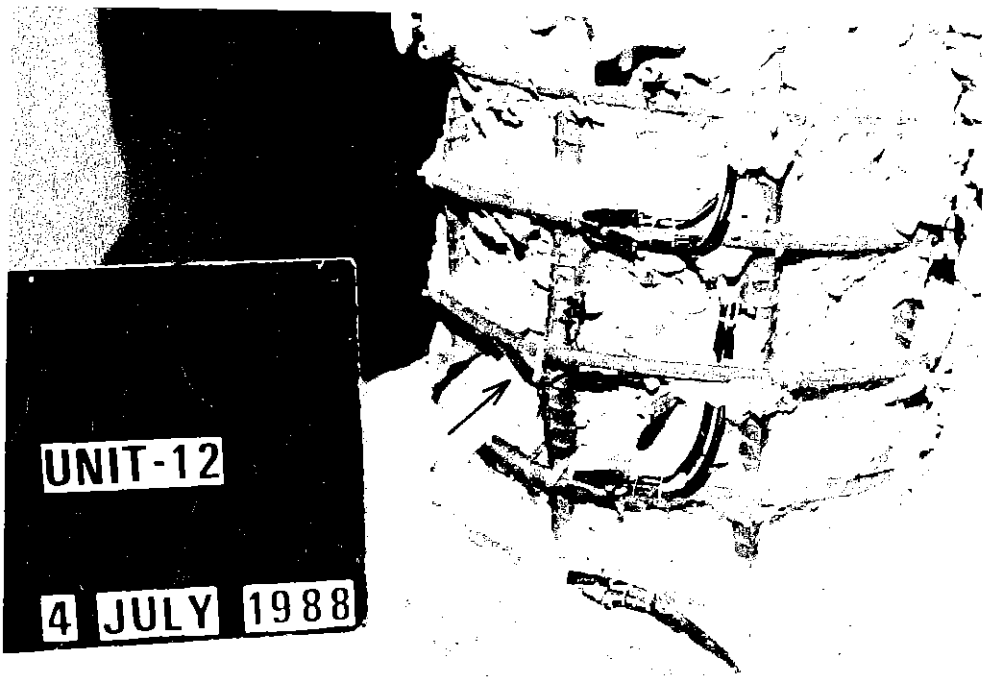

Fig. 4.50 Spiral Fracture in Unit 12.

4.3.2.2 Curvature Distribution

The measured horizontal load versus curvature hysteresis loops for Units 9 to 12 are shown in Figs. 4.51 to 4.54, respectively. Those curvatures were measured by a pair of potentiometers which were of gauge length of 200 mm and located at the first position from the base block side shown in Fig. 4.35. In those figures, theoretical ultimate horizontal loads, H_u , are also indicated in a similar manner as in Figs.4.39 to 4.42. The theoretical ultimate load lines were drawn by straight lines connecting the point of H_u at zero curvature with the point of H_u at each final curvature, reduced by taking P-Δ effect into account. Strictly speaking, those theoretical ultimate horizontal load lines can be straight only when the measured curvatures are exactly proportional to the corresponding horizontal displacements. However, it can be said that those measured curvatures were nearly proportional to the corresponding displacements and hence the errors involved in assuming straight ultimate load lines are insignificant.

Since the main purpose of these column tests was to investigate the effectiveness of interlocking spirals as shear reinforcement, the moment-curvature relations are discussed focussing on this point in this paragraph. It can be said that all of the hysteresis loops shown in Figs. 4.51 to 4.54 show stable behaviour and good energy dissipation up to the final stages of loading. However, it is notable that, when those loops for Units 9 and 10 are compared, slight pinching of the loops can be recognized in Unit 10 as well as in the horizontal load versus displacement hysteresis loops shown in Figs. 4.39 and 4.40. This indicates that the slight pinching recognized in the horizontal load versus displacement hysteresis loops for Unit 10 in Fig. 4.40 can be attributed to the moment-curvature (that is, flexural) characteristics of the column section rather than to the characteristics of shear deformation, assuming that the measured curvatures are not affected by shear deformation. The measured spiral strains in Unit 10 indicated that serious yielding of the spirals was due to the bending moment of the column rather than shear, as discussed later in Section 4.3.2.5. Moreover, as also mentioned later in Section 4.3.3.3, in all columns tested shear deformation significantly contributed to the horizontal displacement but there was no significant difference between Units 9 and 10 with respect to the ratio of shear deformation to the horizontal displacement. Hence, from the view point of shear reinforcement, it cannot be said that the interlocking spirals provided in Unit 10 were less effective than the rectangular hoops

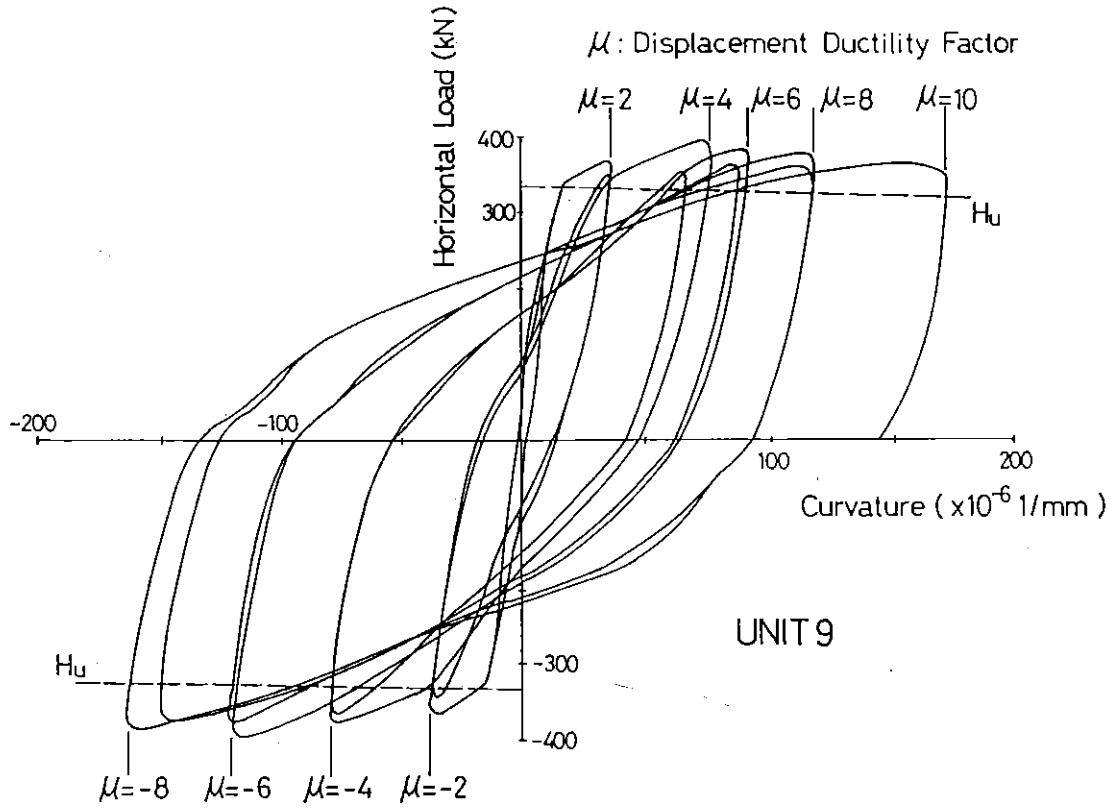

Fig. 4.51 Measured Horizontal Load-Curvature Hysteresis Loops for Unit 9.

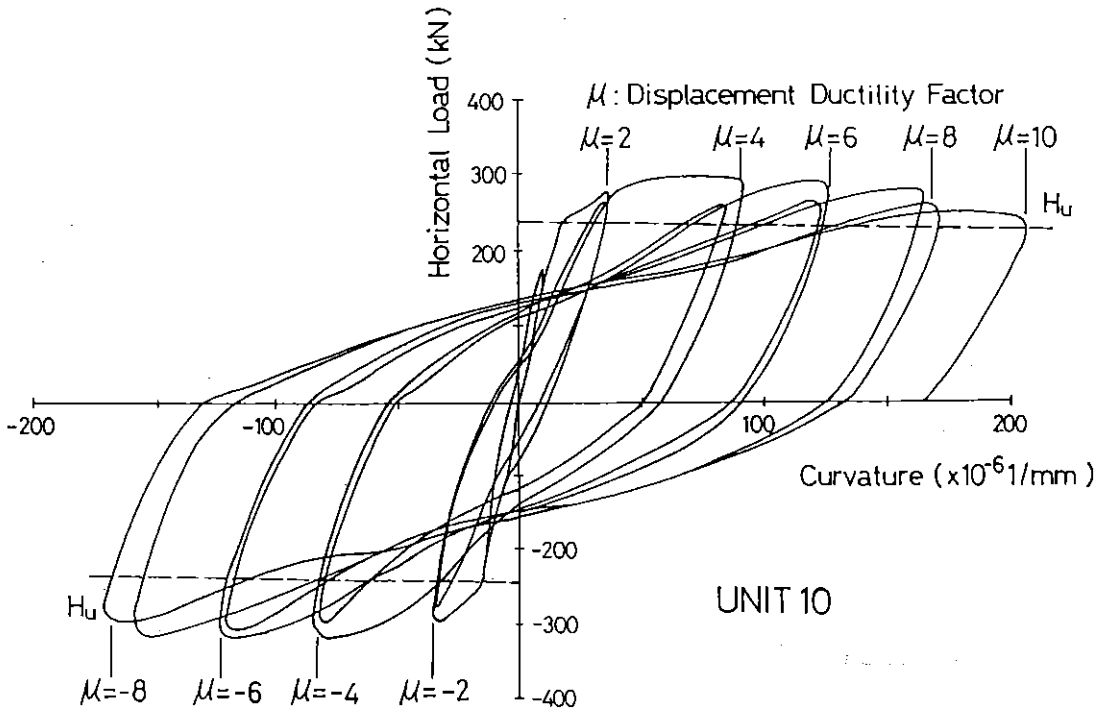

Fig. 4.52 Measured Horizontal Load-Curvature Hysteresis Loops for Unit 10.

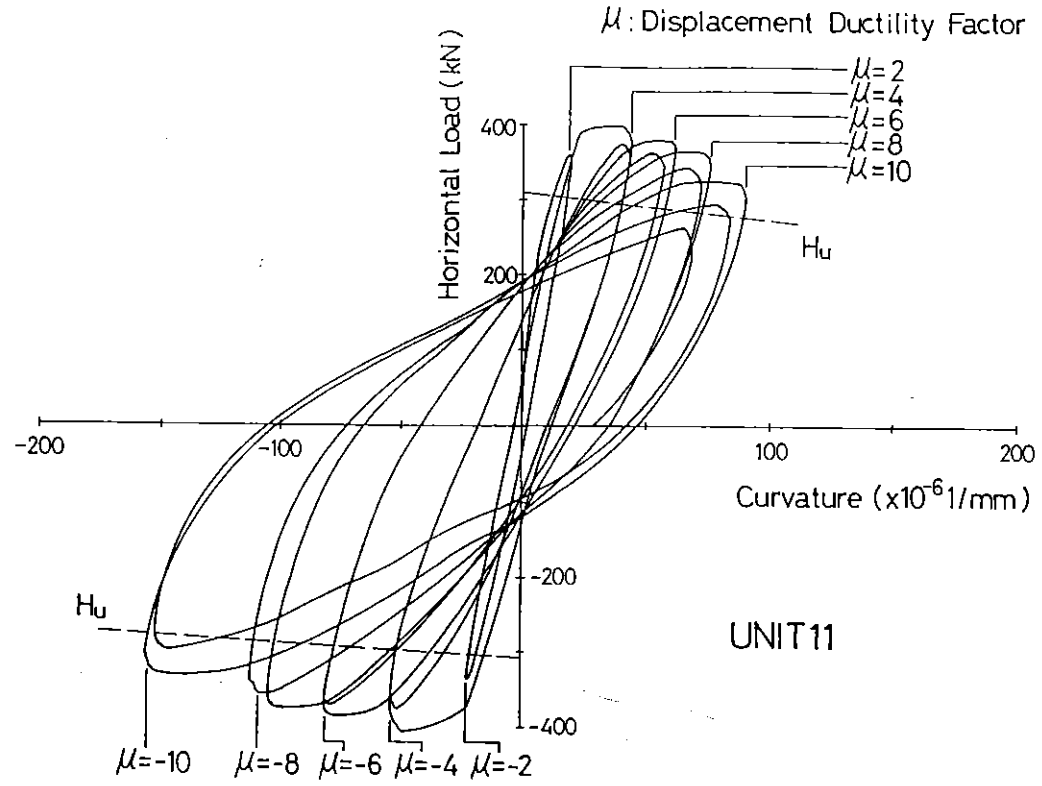

Fig. 4.53 Measured Horizontal Load-Curvature Hysteresis Loops for Unit 11.

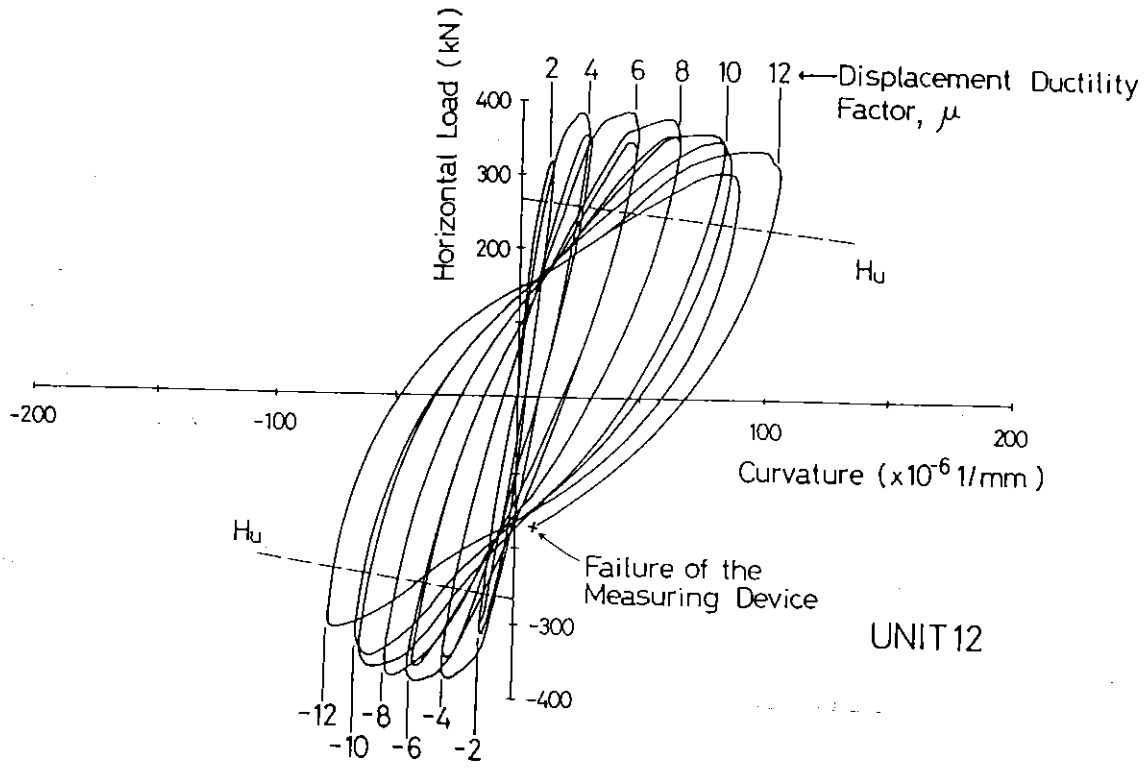

Fig. 4.54 Measured Horizontal Load-Curvature Hysteresis Loops for Unit 12.

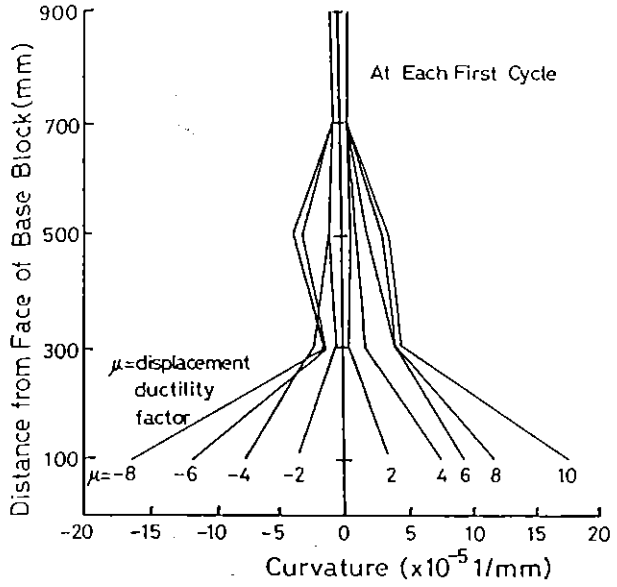

Fig. 4.55 Curvature Distributions in Unit 9.

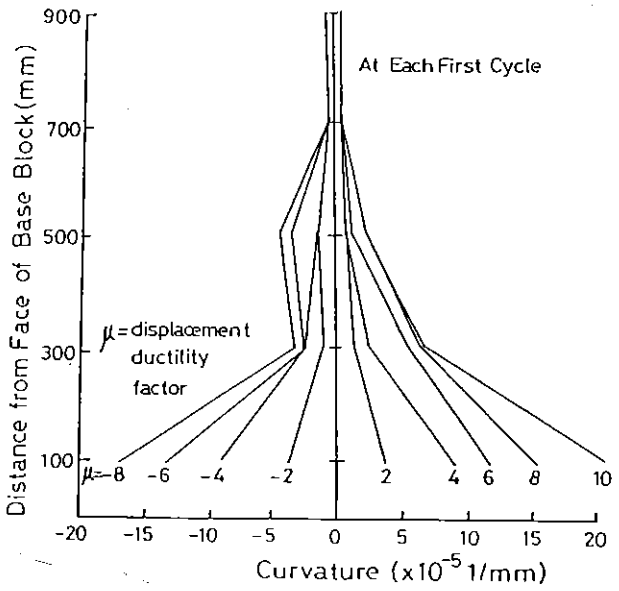

Fig. 4.56 Curvature Distributions in Unit 10.

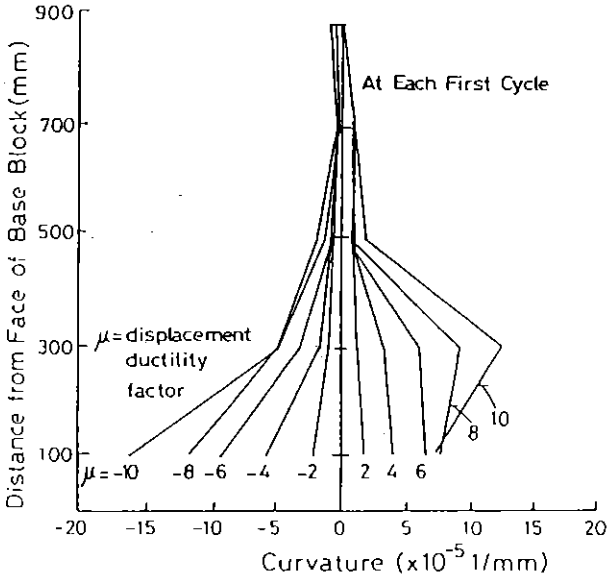

Fig. 4.57 Curvature Distributions in Unit 11.

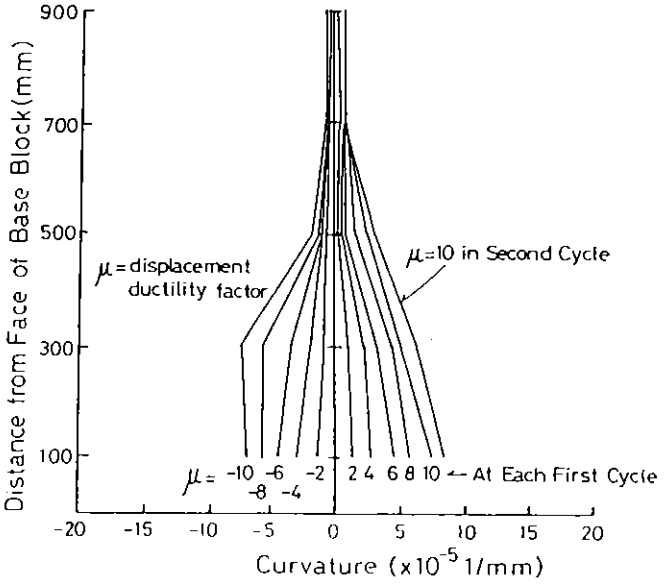

Fig. 4.58 Curvature Distributions in Unit 12.

and cross ties provided in Unit 9, although slight pinching of the hysteresis loops can be recognized in Unit 10.

Curvature distribution profiles measured along the columns for Units 9 to 12 are shown in Figs. 4.55 to 4.58. Those curvatures were measured by five sets of potentiometers of gauge length 200 mm as shown in Fig. 4.35. From Figs. 4.55 and 4.56 it can be seen that for Units 9 and 10 with axial load level $P_e/f'_c A_g$ of 0.1, large inelastic curvature is concentrated in the region within 200 mm (= one-third of full column depth) from the face of the base block. It is notable that the curvature distribution profiles for Units 9 and 10 are very similar. On the other hand, Figs. 4.57 and 4.58 for Units 11 and 12 with axial load level $P_e/f'_c A_g$ of 0.3 and 0.5 , respectively, indicate that large inelastic curvature region spreads over a length corresponding to two-thirds to full column depth. Based on this fact, it can be said that the region of large inelastic curvature spreads along a greater length of column as the axial load increases.

4.3.2.3 Concrete Strains and Longitudinal Bar Strains

Figs. 4.59 to 4.62 present the variations in concrete strain measured along the column axis by potentiometers for Units 9 to 12, respectively. The positive values indicate compressive strains at the extreme compression fibre of the core concrete and the negative values indicate apparent tension strains of core concrete at the position of outermost tension reinforcement. It is notable that for Units 9 and 10 those tension strains increased significantly over about 600 mm (= a full column depth) from the face of the base block as the imposed displacement ductility factor μ increased. On the contrary, the significant increase of the measured compressive strains was limited in the region within about 200 mm (=one-third of column depth) from the base block face in accordance with the measured curvatures shown in Figs. 4.55 and 4.56. This indicates that the column deformation cannot adequately be expressed by section curvatures alone in case of the columns tested having relatively small aspect ratio (ratio of shear span length to full column depth = 2.97). Based on the above observation, a deformation

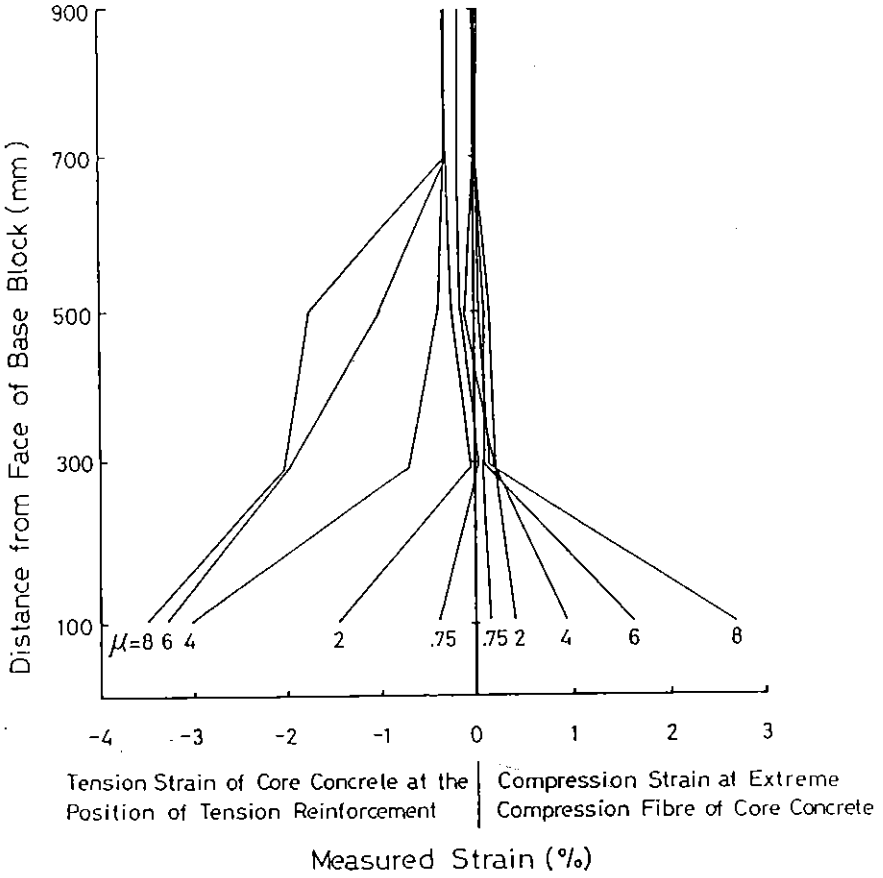

Fig. 4.59 Concrete Strain Variation Measured along Column Axis by Potentiometers in Unit 9.

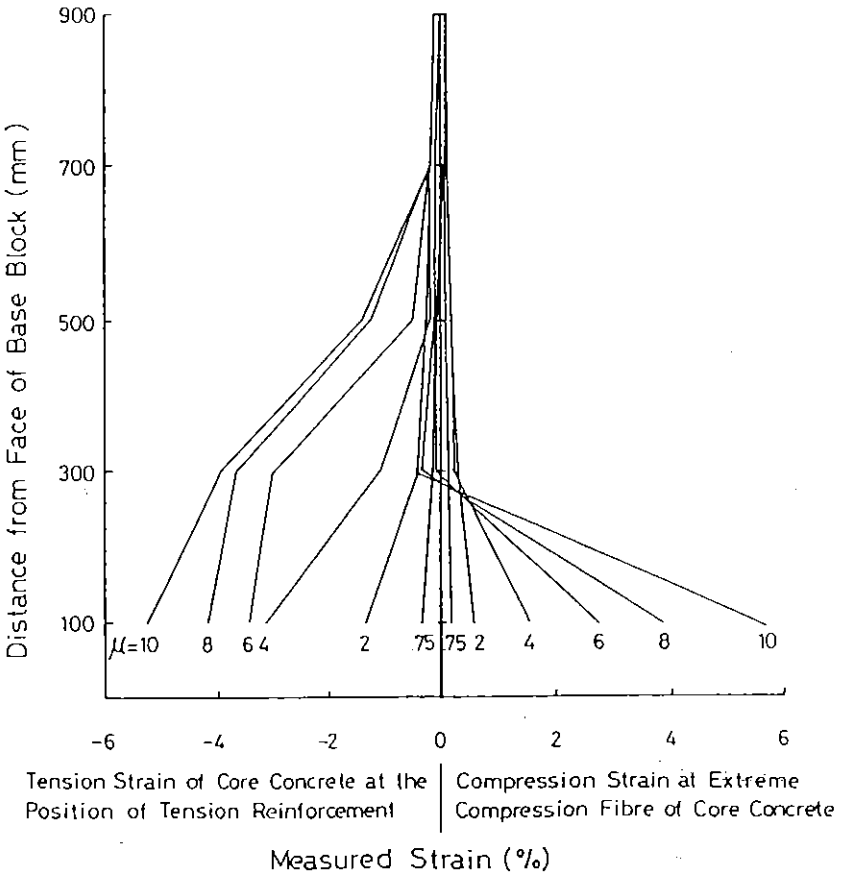

Fig. 4.60 Concrete Strain Variation Measured along Column Axis by Potentiometers in Unit 10.

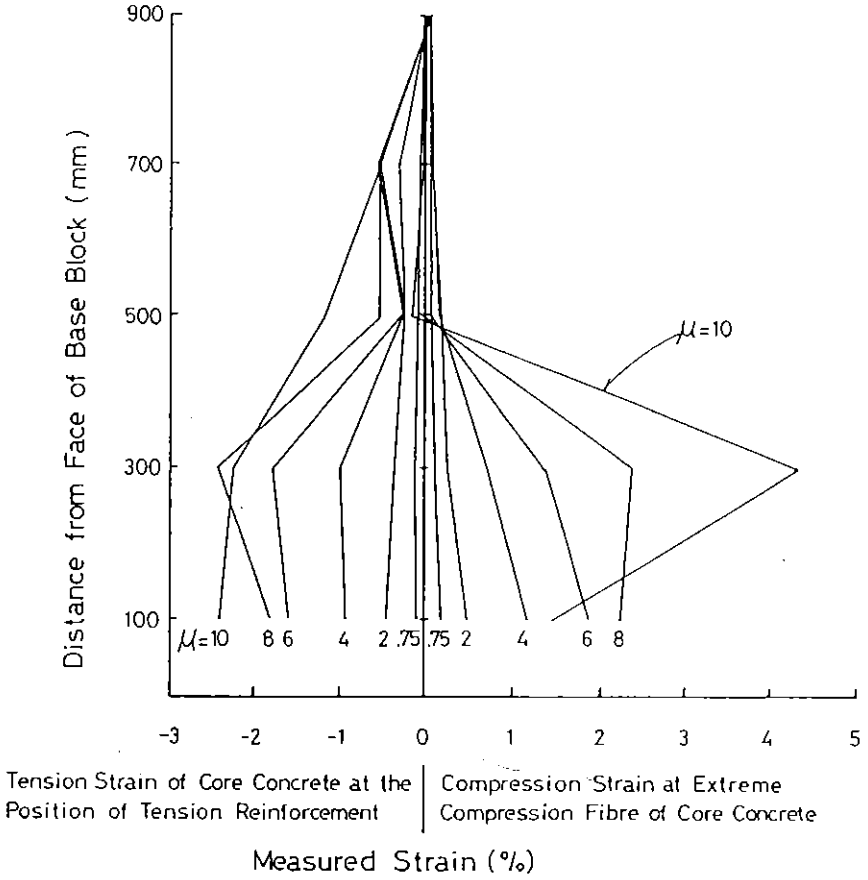

Fig. 4.61 Concrete Strain Variation Measured along Column Axis by Potentiometers in Unit 11.

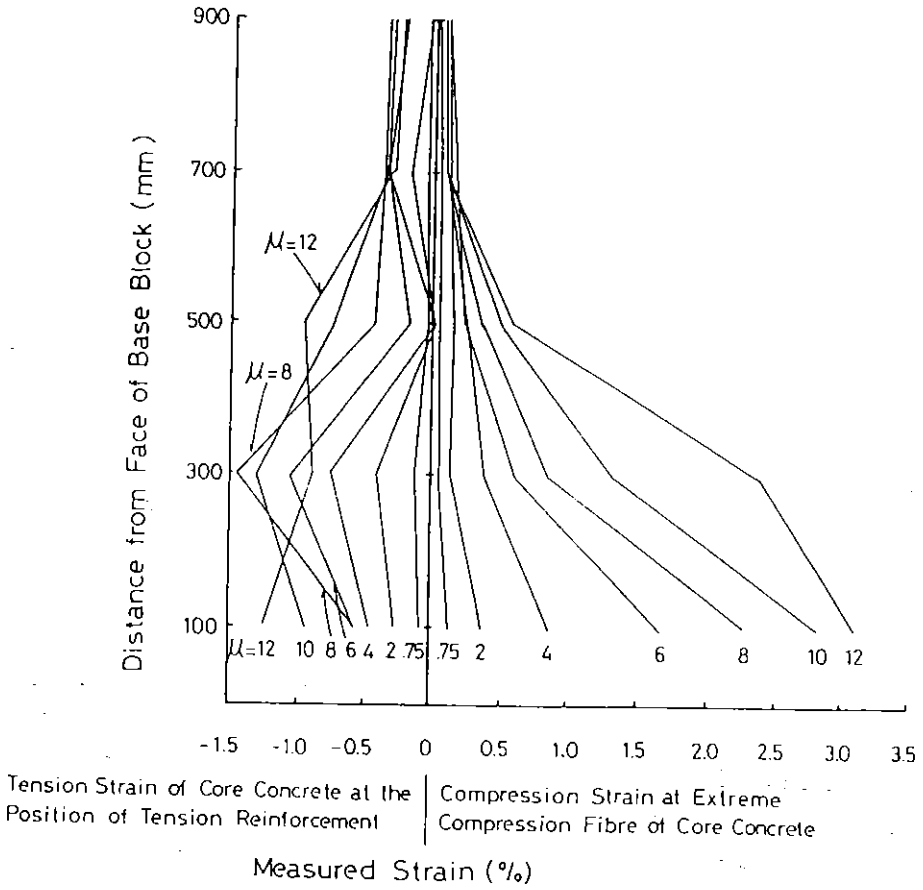

Fig. 4.62 Concrete Strain Variation Measured along Column Axis by Potentiometers in Unit 12.

model to estimate column deflection is proposed in Section 4.3.3.3. On the other hand, in Units 11 and 12, a large increase of both compressive and tensile strains in inelastic range was observed over more than 400 mm from the face of the base block as well as in the measured curvatures.

The strain distributions measured for the longitudinal bars of Units 9 to 12 are shown in Figs. 4.63 to 4.66, respectively. The first yielding of longitudinal reinforcement in tension and in compression are also marked in the horizontal load versus displacement hysteresis loops shown in Figs. 4.39 to 4.42. Those strains were measured by electric resistance wire strain gauges, of 5 mm gauge length, located at various positions along each longitudinal bar. The positive and negative values are tension and compressive strains, respectively. That is, the signs are opposite against those used for concrete strains. In Figs. 4.63 to 66, those measured strains are shown only up to a displacement ductility factor μ of $\pm$ 6 or $\pm$8 . This is because any significant increase of measured strains could not be observed for further loading to larger μ. This is probably due to bond slip of longitudinal reinforcement or in some cases due to slip or peeling off of the wire strain gauges. For all columns tested, it may be said that the strain distribution profiles obtained from the wire strain gauge readings are analogous to those obtained from the potentiometers readings when the displacement ductility factor μ is small. However, the absolute values of the strains measured by the wire strain gauges were less than those by the potentiometers from the early stage of loading. This is also attributed to bond slip of longitudinal reinforcement including the yield penetration into the base block assuming that there was no slip of wire strain gauges due to deterioration of glue at least in the early stage of loading.

It is notable that, when longitudinal reinforcement in concrete has been stretched far into the inelastic range by a loading excursion in tension, the strains in the longitudinal reinforcement remain in tension strain or shows only small compression strain when the loading direction is reversed. This phenomenon can be seen from Figs. 4.63 to 4.66. This is due to the concrete causing some compression and cracks not closing completely due to uneven bearing at the crack faces. It is well known that, when beams or columns with relatively small axial load are tested under cyclic flexural loading, they elongate during testing due to permanent elongation of longitudinal reinforcement. At the final stage of loading, a large

elongation of Units 9 and 10 (in the order of cm) was indicated by the readings of the ram stroke position of the Dartec Machine which was used to apply the axial loads.

Yield penetration of the longitudinal reinforcement into the base block was checked by wire strain gauges located 150 mm inside the base block from the column-base block interface (see the strains correspond to -150 mm in the abscissa in Figs.4.63 to 4.66). In Unit 9, the measured strains in that position exceeded the yield strain from μ=6 onwards and increased little or decreased during further loading. The maximum measured strain was 0.407 % at μ = 6. In Unit 10, the strains in the longitudinal reinforcement at that position reached the yield strain from μ=8 and during further loading increased rapidly. The maximum strain was 1.06 % at μ=10. In Units 11 and 12 yielding of longitudinal reinforcement at that position was not observed during the testing. From these measurements, it is evident that the relatively low stiffness observed in the horizontal load versus displacement hysteresis loops for Unit 10 may be partly attributed to the yield penetration of longitudinal reinforcement into the base block.

As discussed in Section 4.2.2.8, the secure interlocking of spirals depends on whether the longitudinal bars in the interlocking area yield or not. When Unit 10 was loaded to a displacement ductility factor of 2, the longitudinal bars placed to interlock the spirals seemed to have yielded in tension, judging from the measured extreme compressive fibre strains of concrete and the corresponding neutral axis depths. In case of Unit 11, those bars possibly yielded in tension or in compression during loading to a displacement ductility of 4 or more, although this is not clear because the neutral axis depth of column section was very close to the position of those bars. In case of Units 12, those longitudinal bars yielded in compression at least during loading to a displacement ductility factor of 4 due to the large axial load imposed. Hence, it may be said that in Units 10 to 12 the longitudinal bars in the interlocking area were effective to interlock the spirals only during the elastic range or during the early part of the inelastic range of loading. However, the effect of the yielding of that reinforcement may not have been so significant because cracks due to direct shear from the spirals could not be observed in the test units. This means that the interlocking of spirals may have been achieved by the concrete corbel shown in Figs.4.22 and 4.23 or that the column deformation mechanisms that

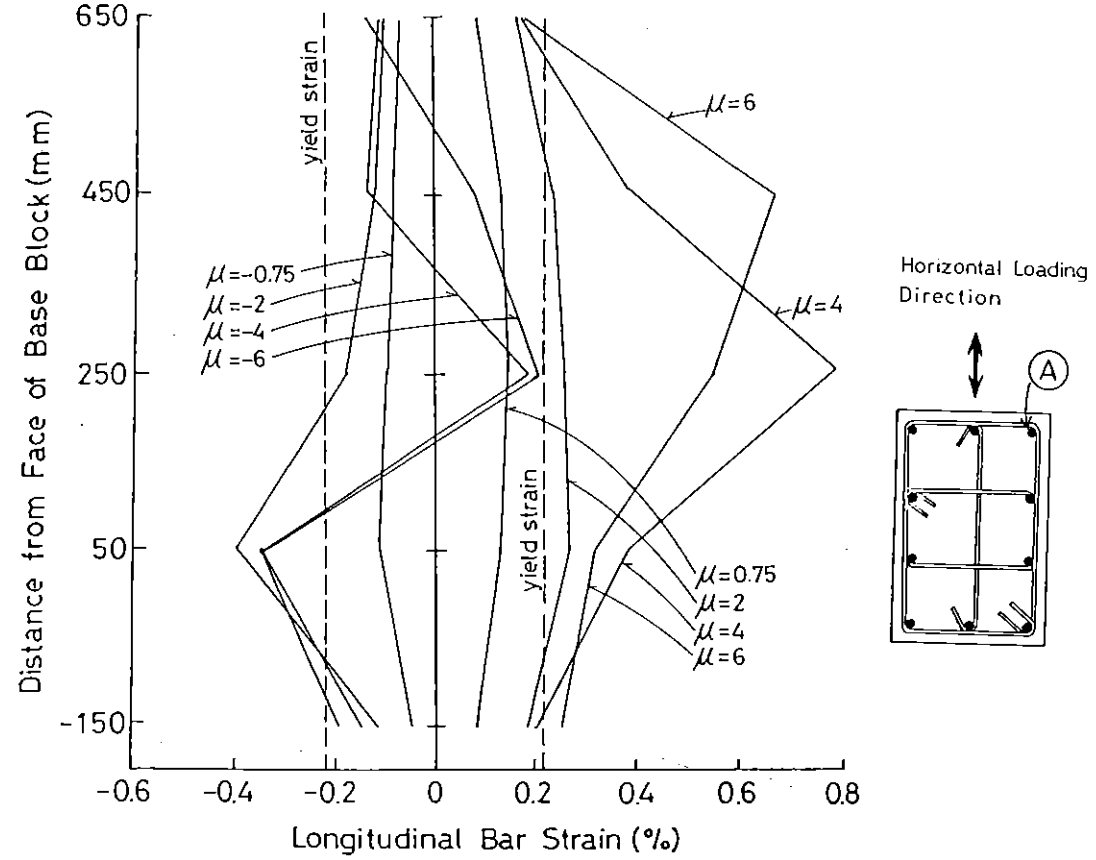

(a) Corner Longitudinal Bar Ⓐ

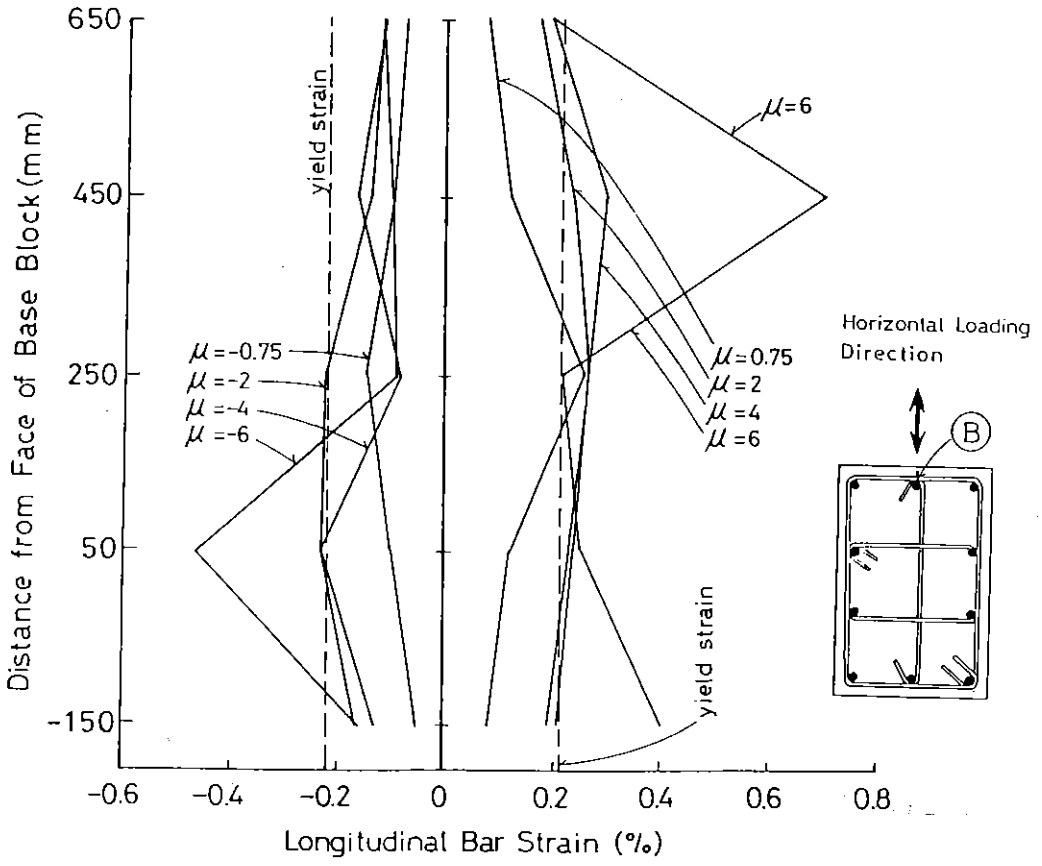

(b) Middle Longitudinal Bar Ⓑ

Fig. 4.63 Longitudinal Bar Strains Measured in Unit 9.

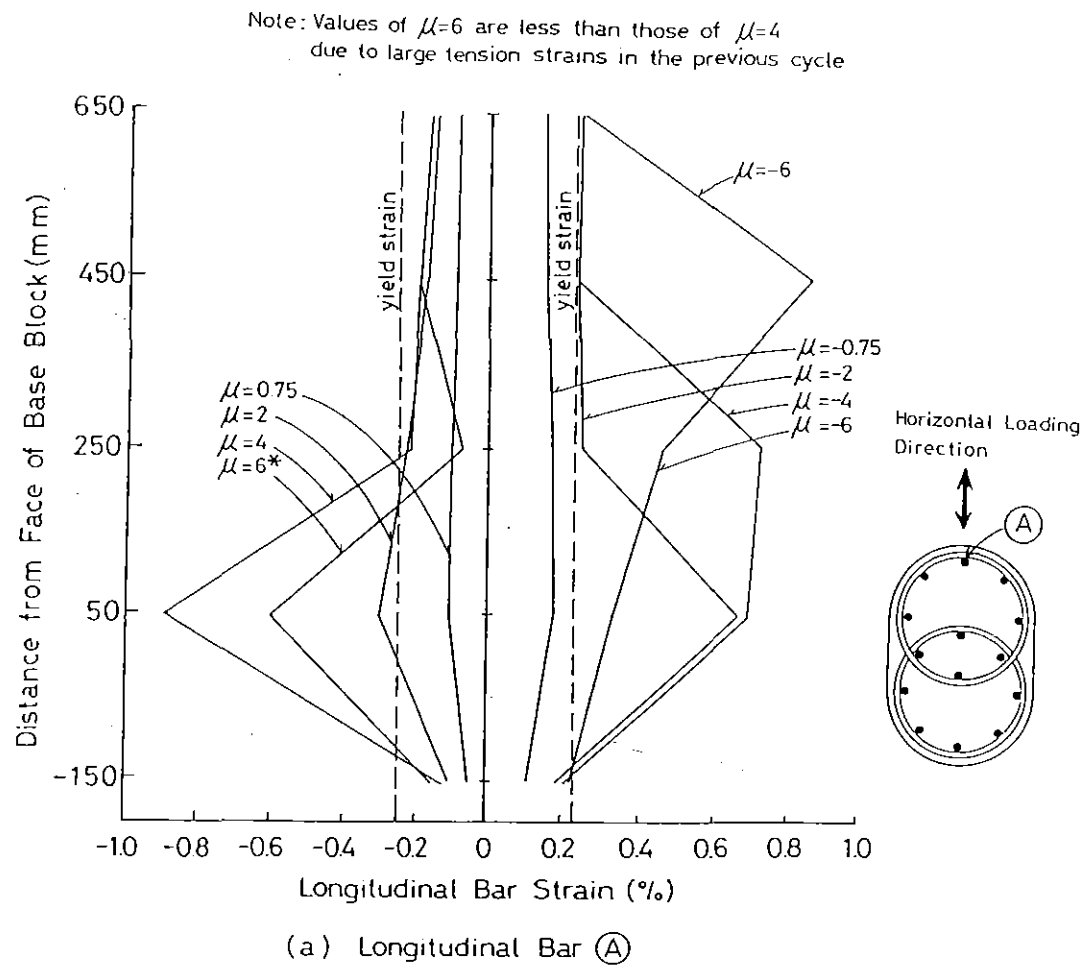

(a) Longitudinal Bar Ⓐ

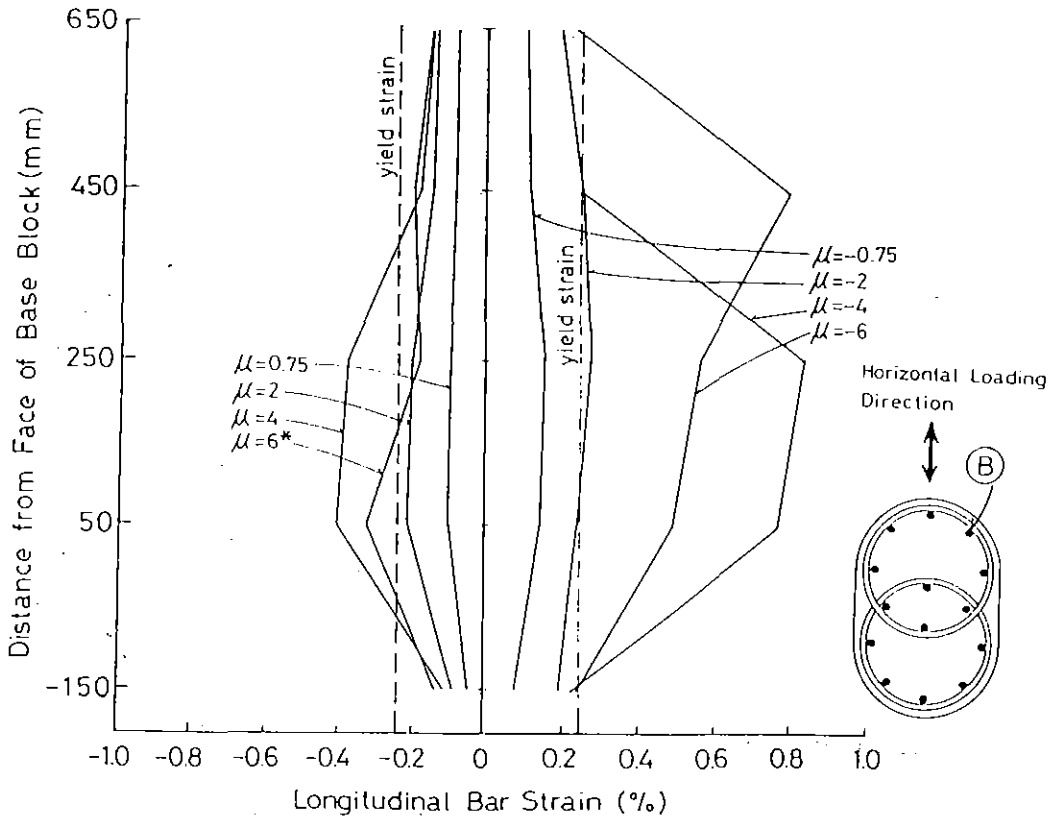

(b) Longitudinal Bar Ⓑ

Fig. 4.64 Longitudinal Bar Strains Measured in Unit 10.

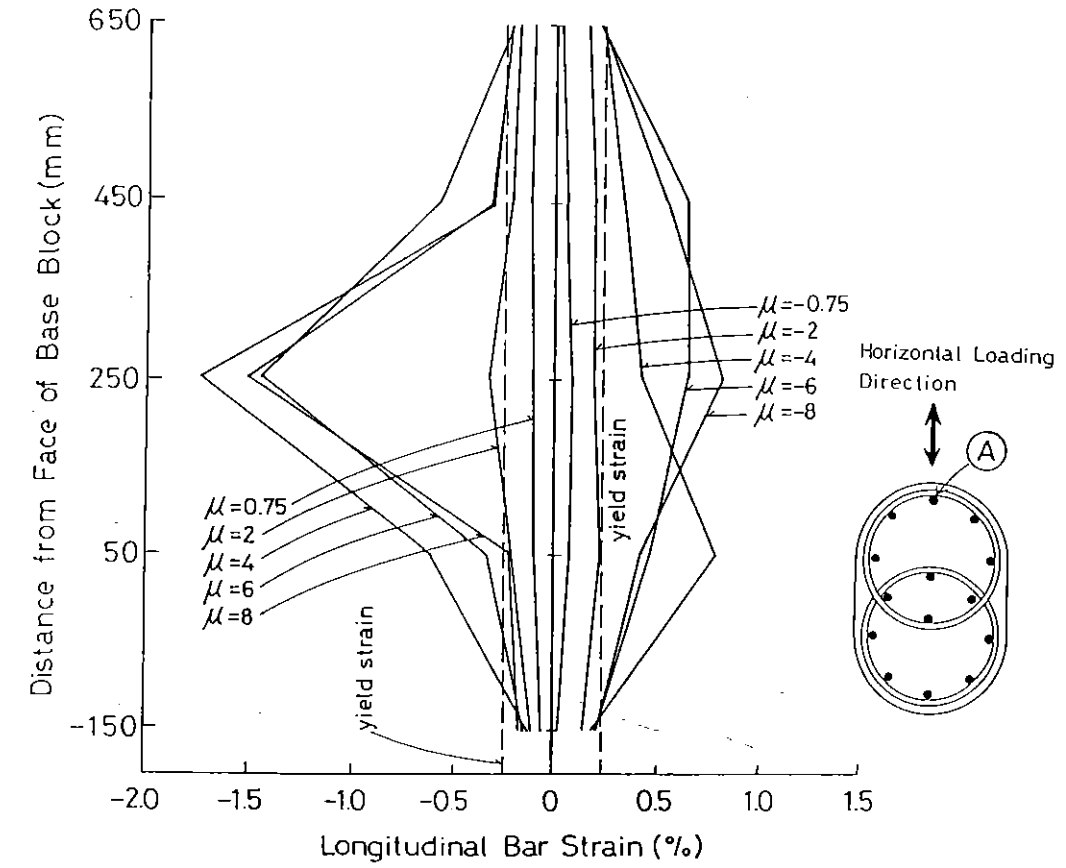

(a) Longitudinal Bar Ⓐ

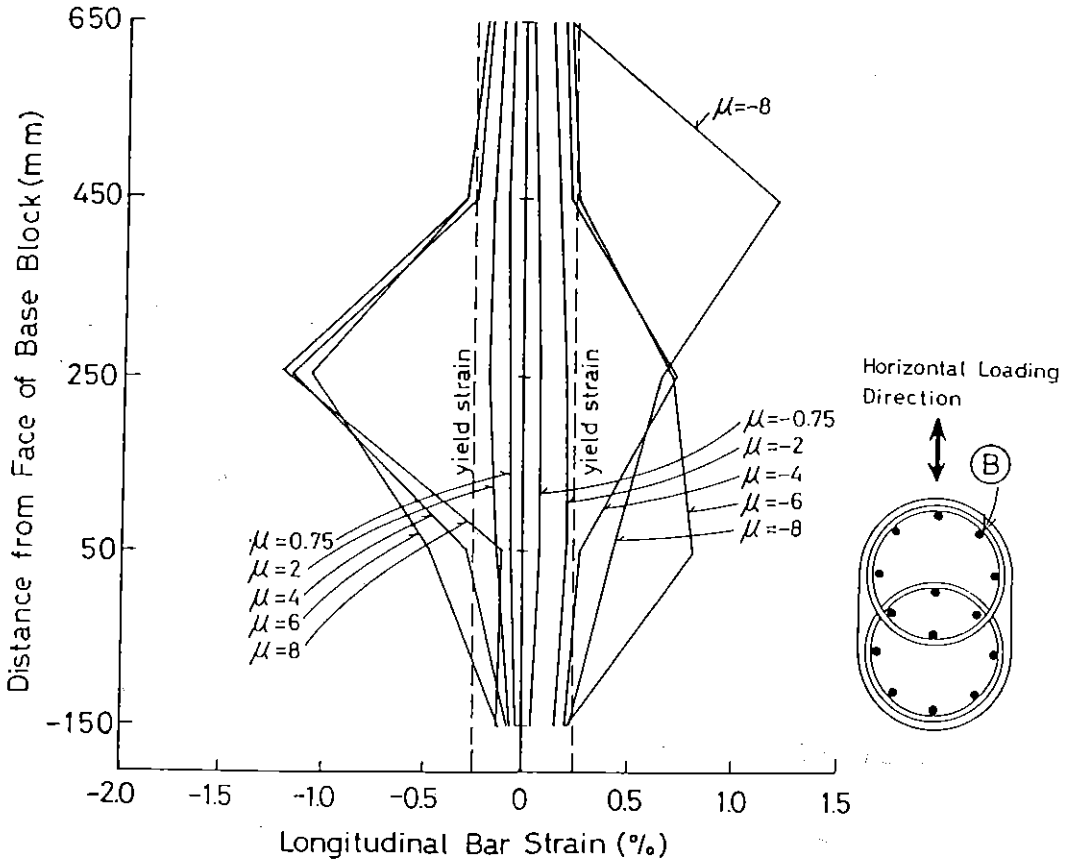

(b) Longitudinal Bar Ⓑ

Fig. 4.65 Longitudinal Bar Strains Measured in Unit 11.

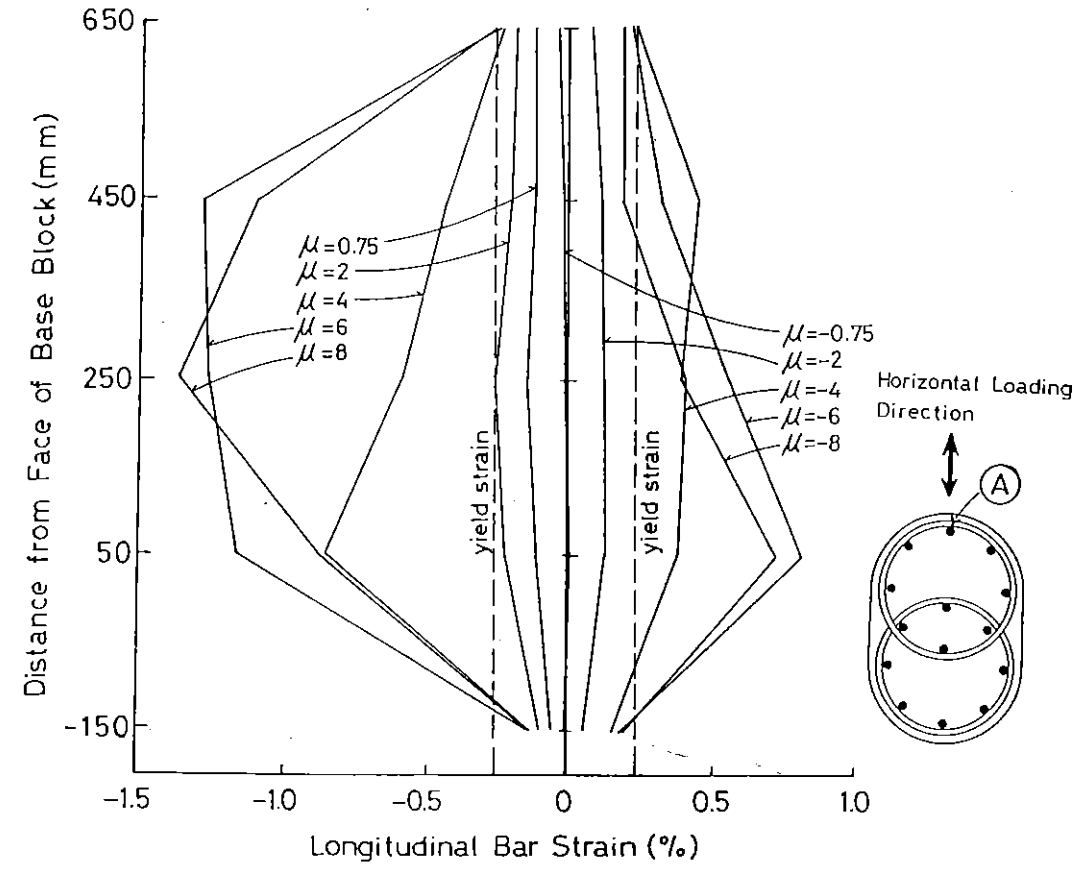

(a) Longitudinal Bar Ⓐ

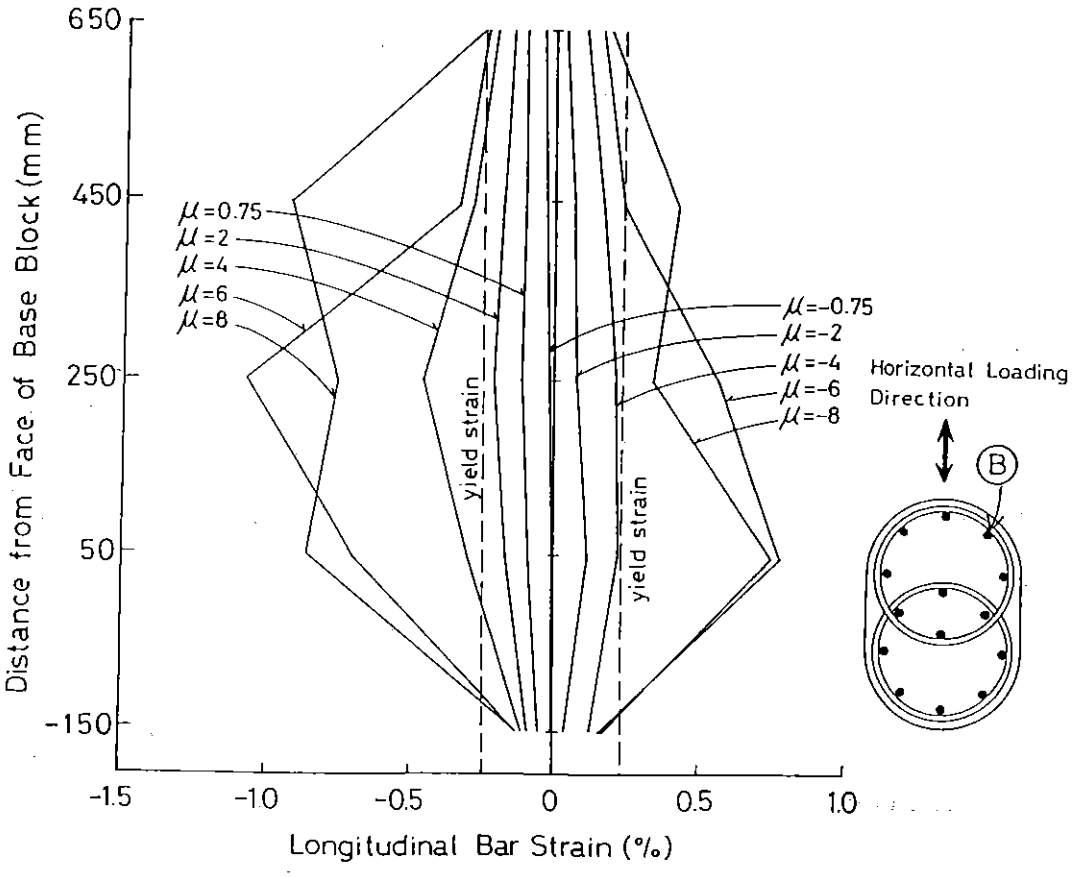

(b) Longitudinal Bar Ⓑ

Fig. 4.66 Longitudinal Bar Strains Measured in Unit 12.

actually occurred in Units 10 to 12 may not have necessarily relied on those longitudinal bars to interlock the spirals. Later in Section 4.3.3.3, the crack pattern of Unit 10 at displacement ductility factor $\mu = 4$ shown in Fig. 4.83 (b), is used to propose a shear deformation model. It is notable that the flexural shear cracks shown in the figure are almost perpendicular to the column axis from extreme tension fibre to the interlocking area and hence only a small shear force was required to be transferred in the interlocking area by the spiral tension.

4.3.2.4 Buckling of Longitudinal Reinforcement

Buckling of the longitudinal reinforcement was eventually observed in all column units and commenced or became visible at the stages marked in Figs. 4.39 to 4.42. In the case of Unit 9, only incipient buckling of longitudinal reinforcement was observed in the final stage of loading to a displacement ductility factor $\mu = +10$. In the case of Units 10 to 12, incipient buckling was observed in the loading cycle to a displacement ductility factor of 8 to 12, and finally the buckling of longitudinal reinforcement was so serious as to fracture the spiral bar at the last stage of testing . The buckled condition of the longitudinal reinforcement in Units 10 to 12 can be seen from Figs. 4.47, 4.49 and 4.50, respectively.

The ratios of the hoop or spiral spacing to the longitudinal bar diameter in Units 9, 10, 11 and 12 were 3.3, 4.0, 5.0 and 3.8, respectively. Those ratios are small enough to prevent premature buckling of longitudinal reinforcement when undergoing yield reversals in tension and compression. NZS 3101[4.2] requires the ratio to be less than 6 for that purpose. In fact, in all columns tested the buckling of the longitudinal reinforcement did not occur until the displacement ductility factor μ reached more than 8 and the compressive strain of the core concrete surface measured by the potentiometers exceeded 2 % (the corresponding compressive strains in the longitudinal reinforcement measured by wire strain gauges reached up to 1.8 % or less due to bond slip).

4.3.2.5 Strains in Transverse Reinforcement

Strains measured by electrical resistance wire strain gauges on the transverse reinforcements of Units 9 to 12 are shown plotted against the

displacement ductility factors in Figs. 4.68 to 4.71, respectively. The locations of those wire strain gauges are illustrated in Figs. 4.30 to 4.32. The notation attached to the curves in Figs. 4.68 to 4.71 indicates the gauge locations in accordance with the stress condition in each column section shown in Fig.4.67. In case of the spirals, a number which follows an alphabet letter indicates the distance of the gauge location from the face of the base block. For example, E-120 indicates that the wire strain gauge located at E in the column transverse section is 120 mm away from the face of the base block. The strains plotted are the average of pairs of strains measured on opposite sides of the bar. The individual strain readings indicated that there was significant bending of the transverse reinforcing bars and hence averaging of the pairs of strain readings was necessary to obtain the axial tensile strain. It is to be noted that those bar sides where the wire strain gauges were attached were so selected as to prevent large core concrete pressure from acting on the wire strain gauge surface. That is, the plane of each wire strain gauge film is vertical to the plane of concrete core surface. If the surfaces of those wire strain gauges were facing core concrete, significant pressure from the core concrete caused by expansion of the core concrete due to Poisson's effect could induce errors in the measured strains.

Yielding of the spiral bars in axial tension could be observed from a relatively small displacement ductility factor such as μ= 3 to 4 in Units 10 to 12. However, in Unit 9, yielding of hoops and supplementary ties in axial tension could not be observed at any of the loading stages of the column. This would be because the transverse reinforcement provided in Unit 9 was governed by the NZS 3101 requirement for confinement and was 24 % in excess of that required for shear by NZS 3101. It is known that the NZS 3101 code for confinement by rectangular hoops with or without supplementary ties, NZS 3101 code provisions are conservative when the axial load level is less than 0.5 $P_e/(f'_cA_g)$ [4.5]. Hence with respect to both shear and confinement, Unit 9 probably had enough margin to avoid the yielding of transverse reinforcement. It is notable that the volume of transverse reinforcement provided for Unit 9 was almost twice of that for each of Units 10 to 12, as listed in Table 4.2.

In Unit 9, the strain readings at A_1 and B (see Fig. 4.68) indicate lateral expansion of the core concrete due to the Poisson's effect. The readings at A_2 and C mainly correspond to opening and widening of shear cracks. As a

matter of course, the strain readings at A_2 and C could also involve the Poisson's effect of core concrete but probably with small effect. This is because at the peaks in the loading cycles the measured neutral axis depths were mostly much less than 200 mm and hence the gauge locations at A_2 and C were in tension zone of core concrete. As can be seen from Fig.4.68, the hoops and supplementary cross ties worked more significantly as shear reinforcement than as confining reinforcement when the location of each hoop set became farther from the face of base block. It is notable that the strain readings atA_1, which indicate the confinement of the core concrete, became largest at hoop set A located at 105 mm from the face of the base block. These observations correspond to the fact that significant compression of the core concrete concentrated in the region within 200 mm from the face of the base block but the zone of serious inclined shear cracks spread over about 600 mm as shown in Fig.4.59.

In Unit 10, as can be seen from E-120 in Fig. 4.69 (b), first yielding of the spiral bar occurred at between μ= +2 and +3 on the way to the first cycle of loading to μ= +4. The measured spiral strain of E-120 reached 0.781% at μ= +4 and as a consequence a large permanent elongation of the spiral remained in the reversed cycle of loading to μ= -4. The strain of E-120 measured at μ= -4 was 0.686 %, indicating elastic strain recovery from the strain at μ= +4 in the previous cycle of loading. This yielding can be attributed to the Poisson's effect of core concrete due to the following two reasons; (1)E-120 was located in the extreme compression zone of core concrete for the loading at μ= +4, (2) In the following reversed cycle of loading to μ= -4, in which E-120 was located in the tension zone of the core concrete, the strain of E-120 was reduced and showed elastic strain recovery. If the yielding was due to opening or widening of shear cracks, the spiral strain reading increases during the reversed loading to μ of negative sign for which the wire strain gauge is located in the tension zone of concrete core section. This is because a flexural shear crack opens from tension zone of column section and the width normally becomes smaller towards compression zone. The strain readings of S_b-310 in Fig.4.69 (d) indicate the effect of inclined shear cracks. That is, the strain reading of S_b-310 at each peak of positive cycle of loading always increased in the following peak of negative cycle of loading. For example, the strain of S_b-310 was 0.122 % at μ= 8 and increased to 0.183% at μ= -8 exceeding the yield strain of the spiral bar.

It can be said that the spiral bars in Unit 10 did not yield due to shear at least until the displacement ductility factor μ exceeded $\pm$ 6 because strains denoted by S_a, S_b or I remained in elastic range when μ is less than 6 (see the gauge locations shown in Fig.4.67). It is notable that within a full spiral turn in section D (see Fig.4.31 Unit10) the measured spiral strains of I-260 also increased significantly as the displacement ductility factor μ increased in the same manner as E-280, S_a-270, S_b310. This may be indicating that the inclined shear cracks are predominant in this region. However, it is emphasized that the spirals were not seriously stretched to high yield strain by shear force. This is because normally the hysteresis loops deteriorate when yield of the transverse reinforcement is due to shear [4.28].

The strains measured by the wire strain gauges which were located in the full spiral turn in section E (= 420 mm away from the base block face) were small and only reached about 0.04% at their maximum. Hence it is not shown here.

As mentioned in Section 4.3.2.2, when the horizontal load versus curvature (or displacement) hysteresis loops for Units 9 and 10 are compared, lower stiffness with slight pinching can be observed in the inelastic range of loading for Unit 10. This can be attributed to the yielding of the spiral bars which were located in the compression zone of the core concrete based on the above observations. It must be emphasized that in the case of Unit 10 the yielding of spirals in an early stage of loading is mainly due to the Poisson's effect of core concrete rather than due to the shear. Hence, it is suggested that the provisions against confinement may need to be reviewed for the interlocking spirals. This can be further explained by the following observation. Fig.4.48 shows a large gap between a spiral bar and a longitudinal reinforcement bar in the tension zone of the column section at μ= - 8. The large elongation of the spiral bar shown in the figure was due to the buckling of longitudinal reinforcement in the previous positive cycle of loading. The figure explains how the effectiveness of confinement is lost when a permanent elongation occurred in spiral bar whether it is due to the expansion of core concrete or due to the buckling of the longitudinal reinforcement. The photographed region is close to the face of the base block and hence flexural cracks which are vertical to the column axis were predominant there. Therefore, the gap would have little effect on the shear strength of the column. However, it is obvious that such gap due to the

permanent elongation of the spirals makes the spirals less effective when acting as confinement of the core concrete in the following positive cycle of loading.

The measured spiral strains for Units 11 and 12 also indicate that the role of the spirals changes from confining reinforcement to shear reinforcement as the distance from the base block face becomes farther (see Figs.4.70 and 4.71). In those column units the yielding of spirals due to the lateral expansion of core concrete occurred from the loading cycles of μ= +4 and the yielding due to the shear cracks occurred from the loading cycles of μ= -6 or -8. These judgements are made noting the gauge locations in the column transverse section and whether the measured strain increased or decreased when the applied column load was reversed, as mentioned previously. Those figures also indicate that the damage of core concrete due to compression spread over 400 mm or more from the face of the base block (see E-400 for Unit 11 in Fig. 4.70 and E-435 for Unit 12 in Fig. 4.71). This fact corresponds to the measured concrete strains shown in Figs. 4.61 and 4.62.

In the concentric loading tests (monotonic and cyclic loading) on concrete cylinders confined by spirals, conducted by the author et al [4.25], there can be found a series of tests in which the material strengths were similar as those of Units 10 to 12. In that series of tests, the yield strength of the spiral and the compressive strength of the concrete were 316MPa and 28MPa, respectively, and the volumetric ratio of the spirals was 1.53%. In those tests, first yielding of the spiral was observed at an axial compressive concrete strain of 0.2 % to 0.4% for both cyclic and monotonic loading tests and thereafter the load carrying capacity of the confined core concrete was reduced. For Units 10 to 12, it may be said that the loading condition in the compression zone of the column section confined by a half part of the interlocking spirals may be close to the above test cylinders. Therefore it can be concluded that, in Units 10 to 12 yielding of the interlocking spirals due to expansion of the core concrete could not be avoided from an early stage of loading such as μ =3. However, it is notable that in Units 11 and 12 any significant deterioration of horizontal load-versus displacement hysteresis loops due to the yielding of spirals could not be recognized. This indicates that those hysteresis loops are not so susceptible to the deterioration of stress-strain relation of the confined core concrete induced by the yielding of confining reinforcement. This can be confirmed by a section analysis conducted in Section 4.3.3.2.

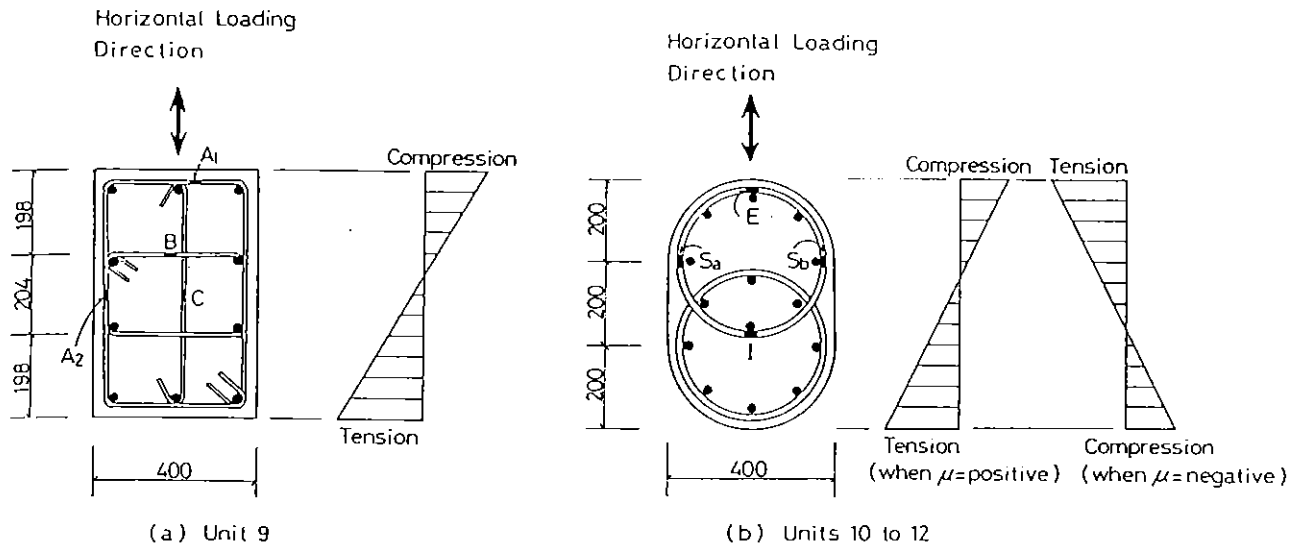

Fig. 4.67 Wire Strain Gauge Locations on Transverse Reinforcement and Axial Strain Variations in Column Transverse Section, Corresponding to Measured Strains Shown Figs. 4.68 to 4.71.

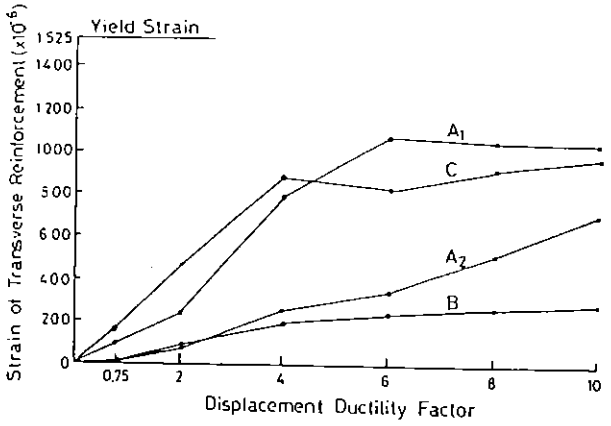

(a) Hoop Set A (Distance from face of base block = 105mm)

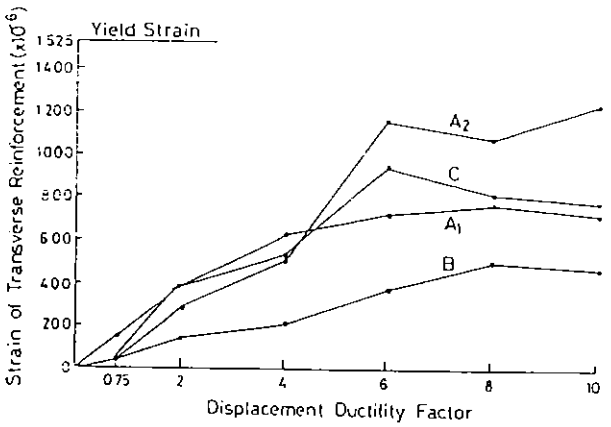

(b) Hoop Set B (Distance from face of base block = 265mm)

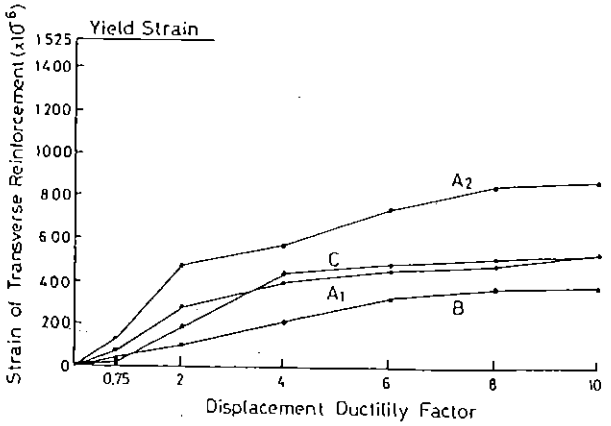

(c) Hoop Set C (Distance from face of base block = 425mm)

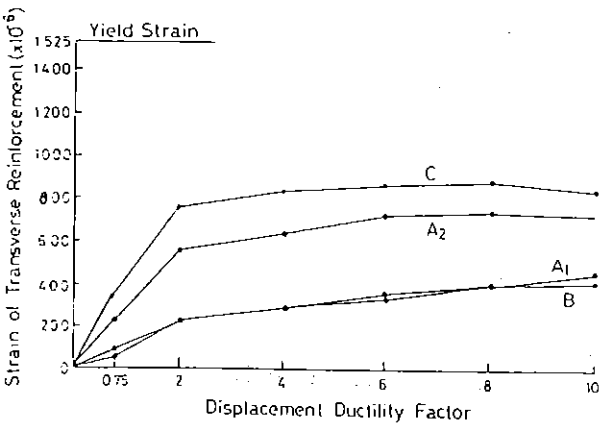

(d) Hoop Set D (Distance from face of base block = 585mm)

Fig. 4.68 Measured Hoop and Tie Bar Strains in Unit 9.

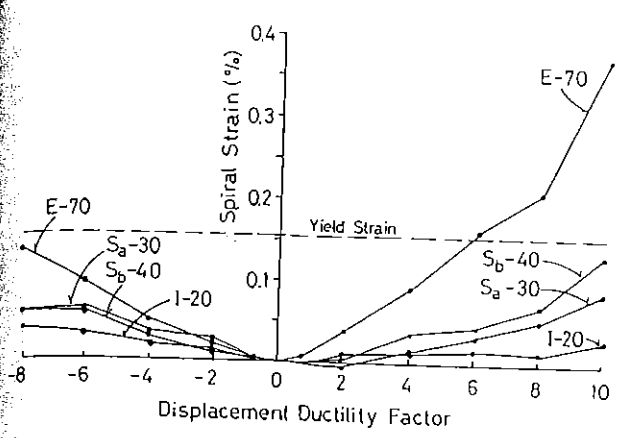

(a) Spiral Strains Measured in a Full Spiral Turn at Section A

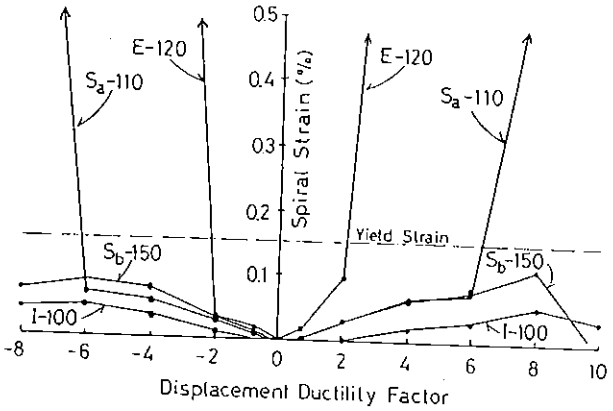

(b) Spiral Strains Measured in a Full Spiral Turn at Section B

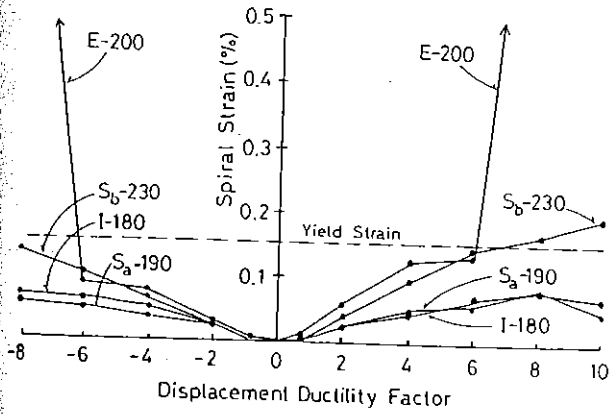

(c) Spiral Strains Measured in a Full Spiral Turn at Section C

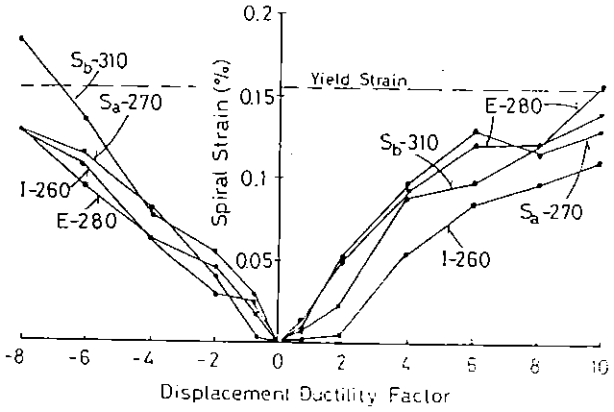

(d) Spiral Strains Measured in a Full Spiral Turn at Section D

Fig. 4.69 Measured Spiral Strains in Unit 10.

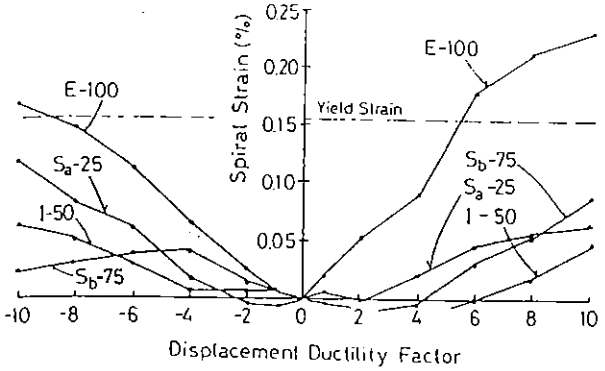

(a) Spiral Strains Measured in a Full Spiral Turn at Section A

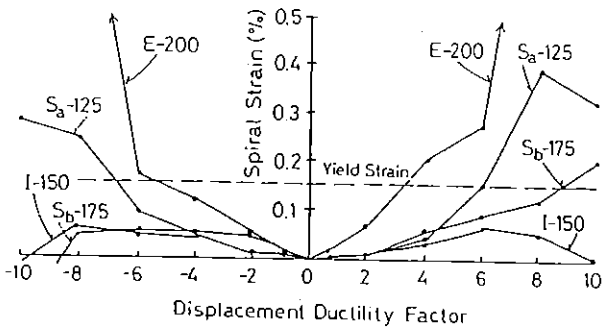

(b) Spiral Strains Measured in a Full Spiral Turn at Section B

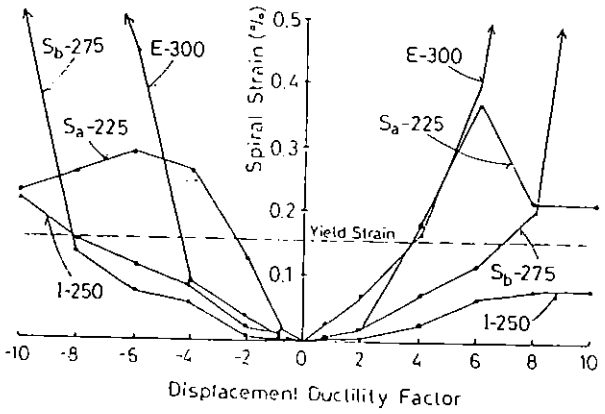

(c) Spiral Strains Measured in a Full Spiral Turn at Section C

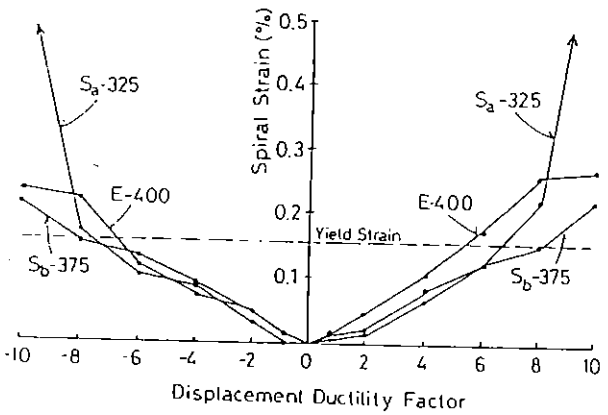

(d) Spiral Strains Measured in a Full Spiral Turn at Section D

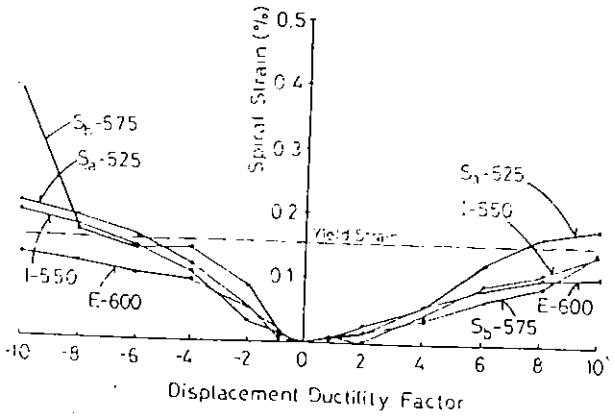

(e) Spiral Strains Measured in a Full Spiral Turn at Section E

Fig. 4.70 Measured Spiral Strains in Unit 11.

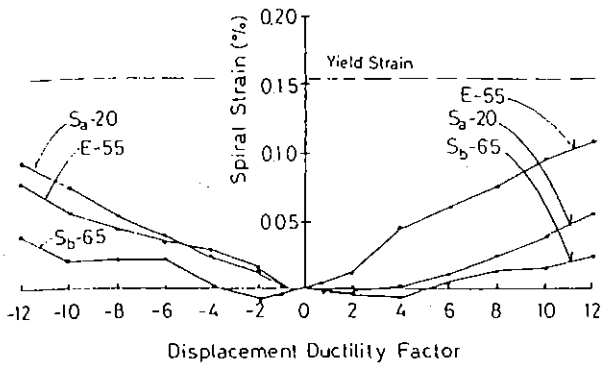

(a) Spiral Strains Measured in a Full Spiral Turn at Section A

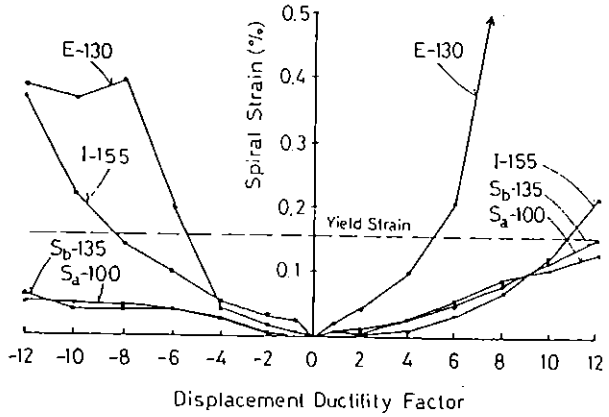

(b) Spiral Strains Measured in a Full Spiral Turn at Section B

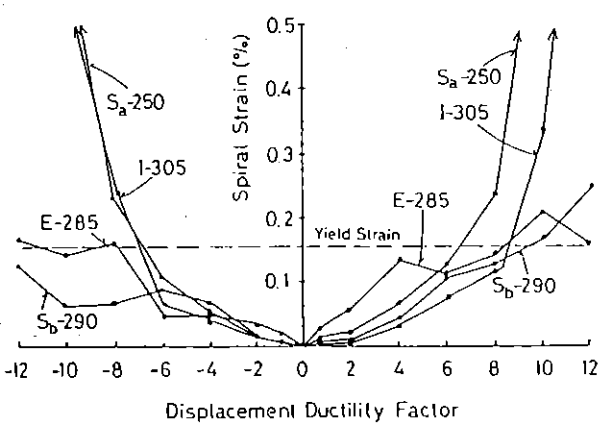

(c) Spiral Strains Measured in a Full Spiral Turn at Section C

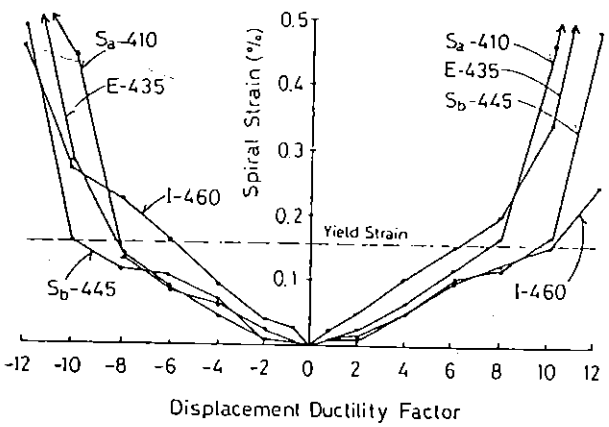

(d) Spiral Strains Measured in a Full Spiral Turn at Section D

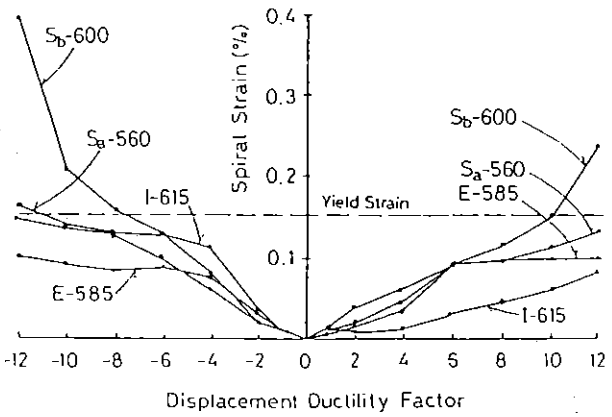

(e) Spiral Strains Measured in a Full Spiral Turn at Section E

Fig. 4.71 Measured Spiral Strains in Unit 12.

4.3.3 Theoretical Considerations

4.3.3.1 Flexural Strength

As has been described in Section 4.3.2.1 and Table 4.3, theoretical moments M_{MND}, M_{MKP} and M_{PL} were calculated using the stress-strain models for confined and unconfined concrete which were proposed by Mander et al [4.22], by Kent and Park [4.6] and by Park and Leslie [4.23], respectively. Those stress-strain models for confined and unconfined concrete are shown in Figs.4.72 to 4.75. It is notable that for Unit 9 with rectangular hoops and cross-ties, those models indicate not only ductility improvement but also considerable strength enhancement of core concrete due to the confining effect, especially in case of the model by Mander et al. Another notable feature is that the difference between ρ_{se} (=the local volumetric ratio of interlocking spirals, see Section 4.2.1.2) and ρ_s (= the volumetric ratio of interlocking spirals as defined by NZS 3101 [4.2]) affected insignificantly the stress-strain relations of confined concrete so far as Units 10 to 12 concerned. In Fig. 4.73 the effect of the difference between ρ_{se} and ρ_s on the stress-strain curves for confined concrete are shown taking the model of Mander et al as an example. The difference between ρ_{se} and ρ_s affected the maximum moments calculated using these stress-strain curves for confined concrete by only up to about 1%. This can be seen in the moment versus concrete strain curves calculated by assuming the perfect beam action, shown later in Fig. 4.78. Hence, ρ_s was used in the following analyses neglecting the difference from ρ_{se}, except for the case where it is noted otherwise. However, this does not mean that the difference between ρ_{se} and ρ_s always has a insignificant effect on the behaviour of columns.

From Table 4.3 it is evident that the ACI method [4.6], which neglects the concrete strength enhancement due to the lateral confinement, gives a very conservative estimation for the column flexural strength especially when the column axial load is high. This tendency has already been pointed out by Ang et al [4.3] who derived the following empirical

relationships for the flexural strength enhancement above the moment predicted by the ACI method.

$$\frac{P_e}{A_g f'_c} < 0.1 : \frac{M_{max}}{M_{ACI}} = 1.13 \qquad \text{.....} \qquad (4.41)$$

$$\frac{P_e}{A_g f'_c} \geq 0.1 : \frac{M_{max}}{M_{ACI}} = 1.13 + 2.35 \left(\frac{P_e}{A_g f'_c} - 0.1 \right)^2 \qquad \text{.....} \qquad (4.42)$$

Although no experimental data from columns with interlocking spirals were used to obtain Eqs. 4.41 and 4.42, the measured maximum moments for Units 10 to 12, as well as for Unit 9, agree well with the predicted maximum moments obtained using those equations. Hence, it may be said that the ACI method combined with the above equations can predict, with satisfactory accuracy, the ultimate flexural strength of a column with interlocking spirals.

The stress-strain models for confined concrete proposed by Mander et al [4.22], by Kent and Park [4.6] and by Park and Leslie [4.23] gave a more realistic calculated value for the column flexural strength. However, the calculated maximum moments using those stress-strain models for concrete are still less than the measured values. This can be attributed to the additional confinement of the stiff base block which would have strengthened the column section adjacent to the face of the base block and as a result have made the critical section of the column shift away from the base block face. Previous tests [4.25] have found this critical section to be at about 0.5 c away from the stiff stub or base block face where c = neutral axis depth. The effect of the additional confinement of the stiff base block can be recognized visually from Figs.4.43 to 4.50. The measured and theoretical values of the neutral axis depth c varied from about one-third to two-third of the full column depth at the maximum moments corresponding to the axial loads P_e of 0.1 to 0.5 $A_g f'_c$. When the theoretical moments M_{MND} are modified assuming that the critical section shifts 0.5 c from the face of the base block, the values of M_{MAX}/M_{MND} in Table 4.3 become about 0.95, 0.95, 0.97 and 1.01 for Units 9, 10, 11 and 12, respectively. The values of M_{MND} show better fit with test results than the values of M_{MKP} and M_{PL}. Hence, for the analyses shown in the following sections, the stress-strain model for concrete proposed by Mander et al is mainly used.

4.3.3.2 Moment versus Concrete Compressive Strain Relations Based on the Perfect Beam Action and Combined Beam-Arch Action

In Section 4.3.3.1, perfect beam action was assumed when calculating the theoretical maximum moments. That is, it was assumed that plane sections before bending remain plane after bending according to Bernoulli's principle. However, it must be emphasized that the validity of Bernoulli's principle was lost at $\mu = \pm 2$ in all columns tested due to the bond slip of longitudinal reinforcement including the yield penetration into the base block. This can be seen by comparing the strain distribution profiles of the longitudinal reinforcement (shown in Figs. 4.63 to 4.66) with those profiles for the concrete at the position of longitudinal reinforcement (shown in Figs. 4.59 to 4.62). Therefore, to logically analyse the behaviour in the inelastic range of Units 9 to 12, a section analysis using Bernoulli's principle may be meaningless, because the assumed strain distribution in column section based on Bernoulli's principle became fictitious in the inelastic range of loading for these columns.

On the other hand, when a column is very ductile and shows almost elasto-plastic behaviour, the accuracy of the assumed strain distribution in the column section may not be so significant from an engineering point of view when estimating the load carrying capacity of the column. This is because, when the strains in the concrete and longitudinal reinforcement have exceeded their each elastic limits, the moment of resistance of such a ductile column becomes unsusceptible to change of strain as long as the strains are increasing. This can be seen from many studies [eg. 4.4, 4.5, 4.22] which have indicated that most theoretical moment-curvature relations calculated for ductile reinforced concrete members agree with test results, although the assumed strain distribution in the column section based on the Bernoulli's principle would likely be different from that actually occuring during severe cyclic loading.

In this study, noting that significant bond slip of longitudinal reinforcement occurred from an early stage of loading, the combined beam-arch action model proposed in Section 4.2.2.4 is applied to Units. 9 to 12. The assumed column sections are shown in Fig. 4.76. For Unit 9 and for Units 10 to 12, it is assumed that the bottom three and the bottom five longitudinal bars, respectively, are subjected to constant tension force over

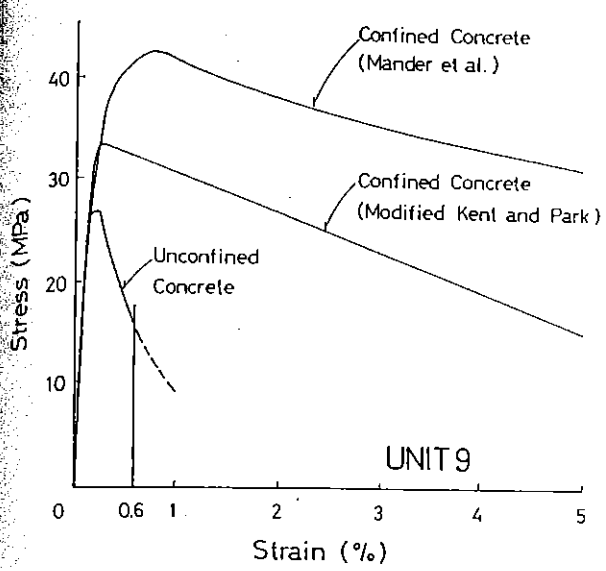

Fig. 4.72 Stress-Strain Models for Concrete Used for Unit 9.

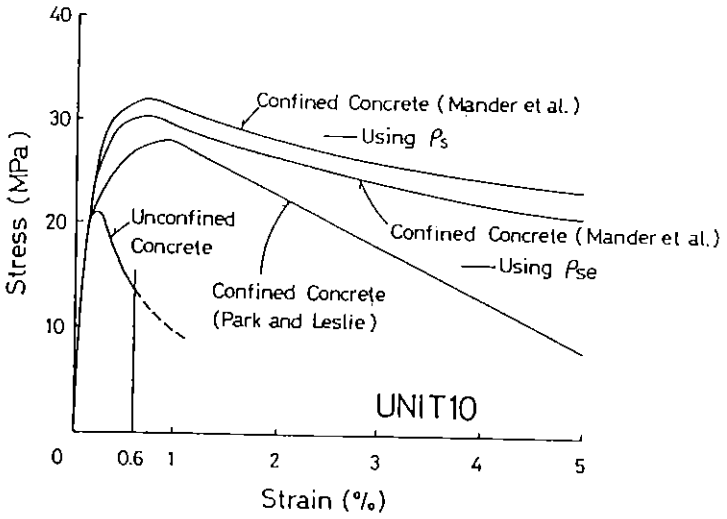

Fig. 4.73 Stress-Strain Models for Concrete Used for Unit 10.

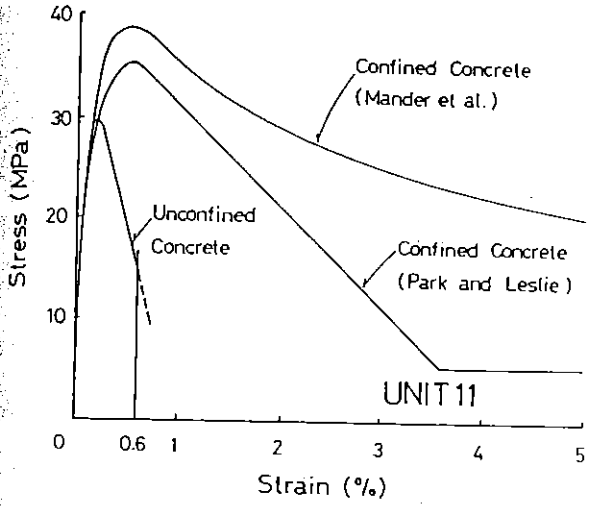

Fig. 4.74 Stress-Strain Models for Concrete Used for Unit 11.

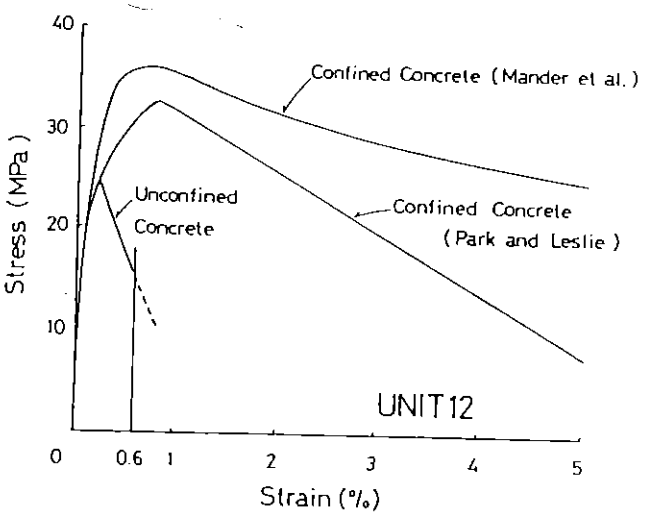

Fig. 4.75 Stress-Strain Models for Concrete Used for Unit 12.

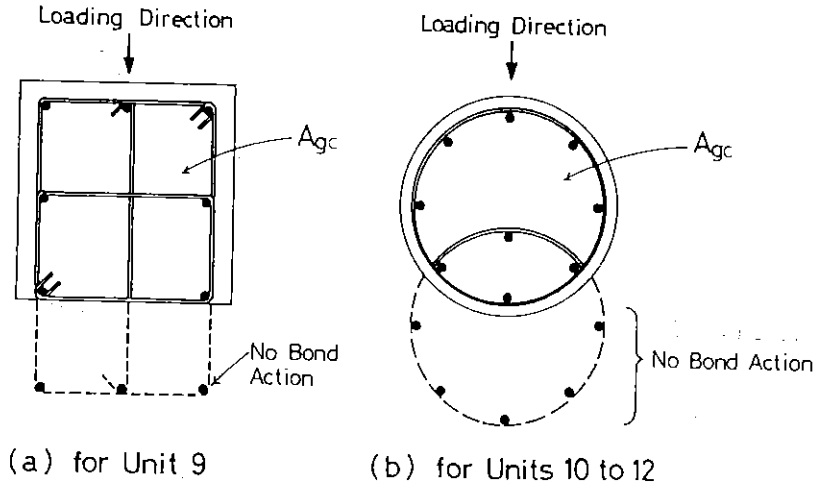

Fig. 4.76 Combined Beam-Arch Action Models for Units 9 to 12.

the plastic hinge length of the column, l_2. It is also assumed that after yielding of those bars the bar strains did not reach the strain hardening region because of the bond slip. In Fig. 4.76, the part of column section surrounded by solid lines is assumed to be subjected to the axial compression load C (= P_e + T) and bending moment. For this part of column section Bernoulli's principle is applied and hence the strain of tension reinforcement can increase into the strain hardening region as the column deformation increases. The stress-strain models for unconfined and confined concrete proposed by Mander et al are used for the cover and core concrete, respectively (see Figs. 4.72 to 4.75). The compressive strain of cover concrete at spalling is assumed 0.6 %. In combined beam-arch action, the concept of curvature is not valid as mentioned in Section 4.2.2.4. Hence, variations in the moment of resistance for Units 9 to 12 were plotted against the concrete compressive strain in the extreme compression fiber as shown in Figs. 4.77 to 4.80. The starting point of each curve indicates the concrete compressive strain at which the strain compatibility check (see check-1 in Section 4.2.2.4) is satisfied. In those figures, the measured skeleton curves and the results calculated by assuming the perfect beam action are also indicated. Some of those calculated results are listed with the calculated curvatures for perfect beam action in Table 4.6.

As can be seen from Figs. 4.78 to 4.80, in case of the columns tested with interlocking spirals, the curves predicted by assuming the combined-beam arch action show better fit with the measured skeleton curves than the curves obtained assuming perfect beam action. On the other hand, in case of Unit 9 with rectangular hoops and supplementary cross-ties (see Fig. 4.77), the curve of the combined beam arch action indicates poor fit. Hence, it may be presumed that the mechanism of deformation was closer to that of combined beam-arch action for Units 10 to 12 than for Unit 9. If this presumption is correct, the slip of longitudinal reinforcement was more serious in Units 10 to 12 than in Unit 9, although it is not evident from the strain distribution profiles of longitudinal reinforcement measured along the column axes.

The possibility of more serious slip of tension reinforcement in Units 10 to 12 than in Unit 9, may be explained as follows. When inclined shear cracks open, the bond force acting on the tension reinforcement is resisted by the combination of aggregate interlock, dowel, flexural action of the concrete

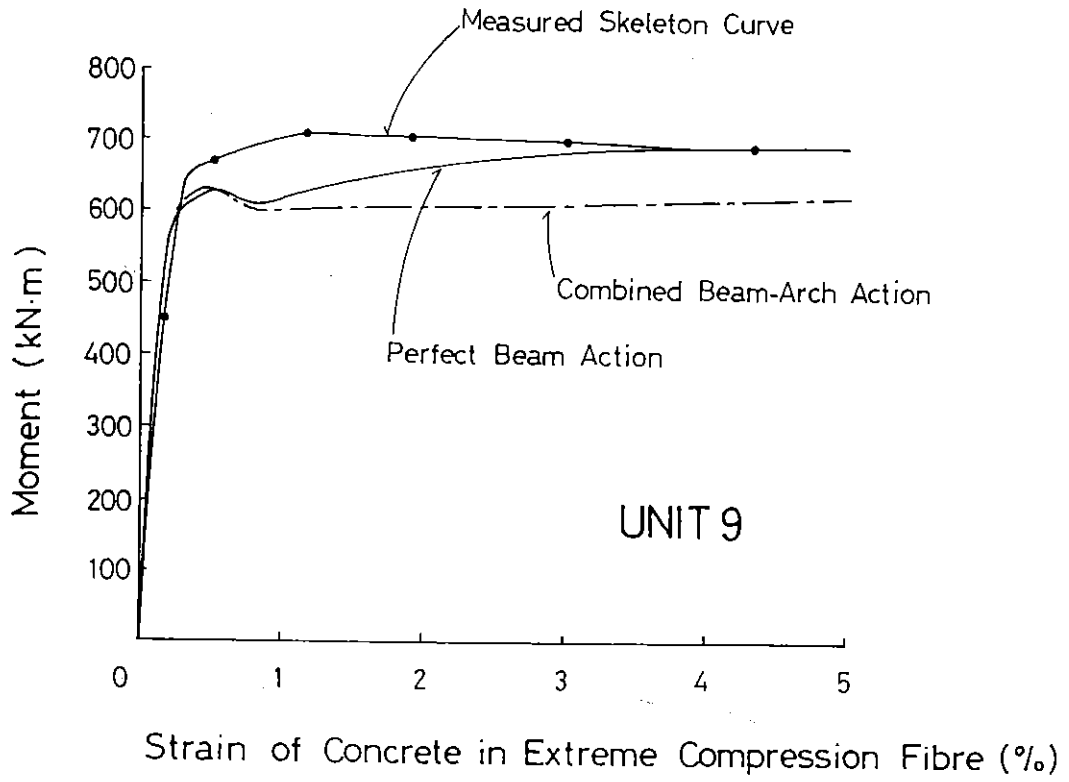

Fig. 4.77 Comparison between Theoretical and Measured Moment-Concrete Strain Relations for Unit 9.

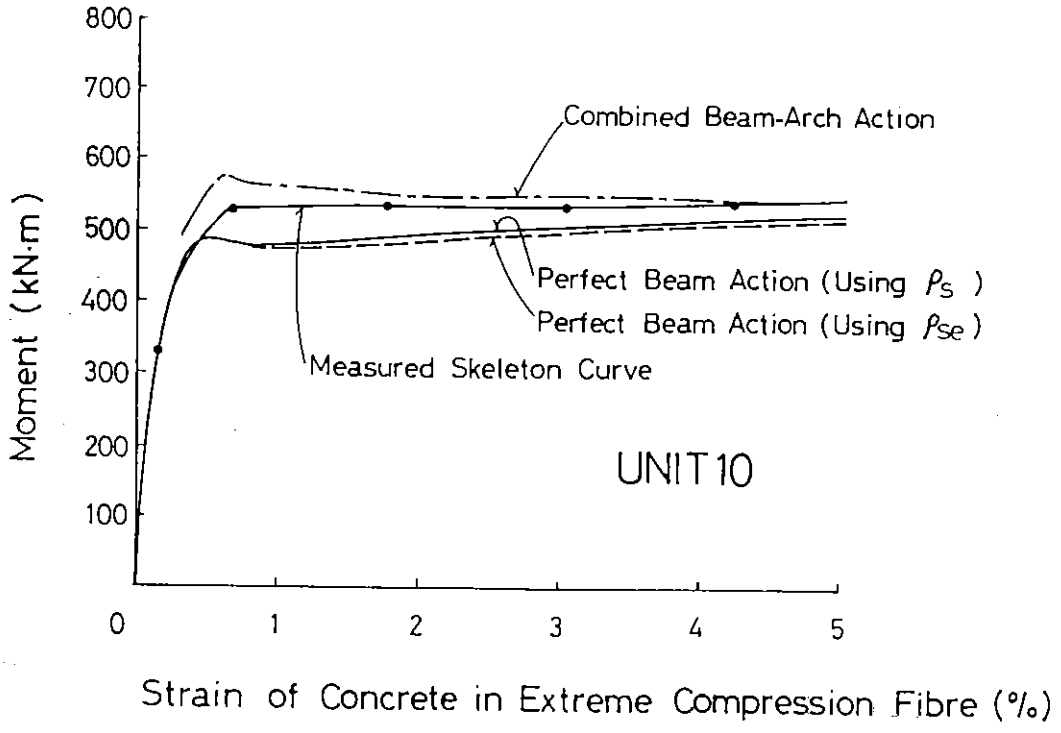

Fig. 4.78 Comparison between Theoretical and Measured Moment-Concrete Strain Relations for Unit 10.

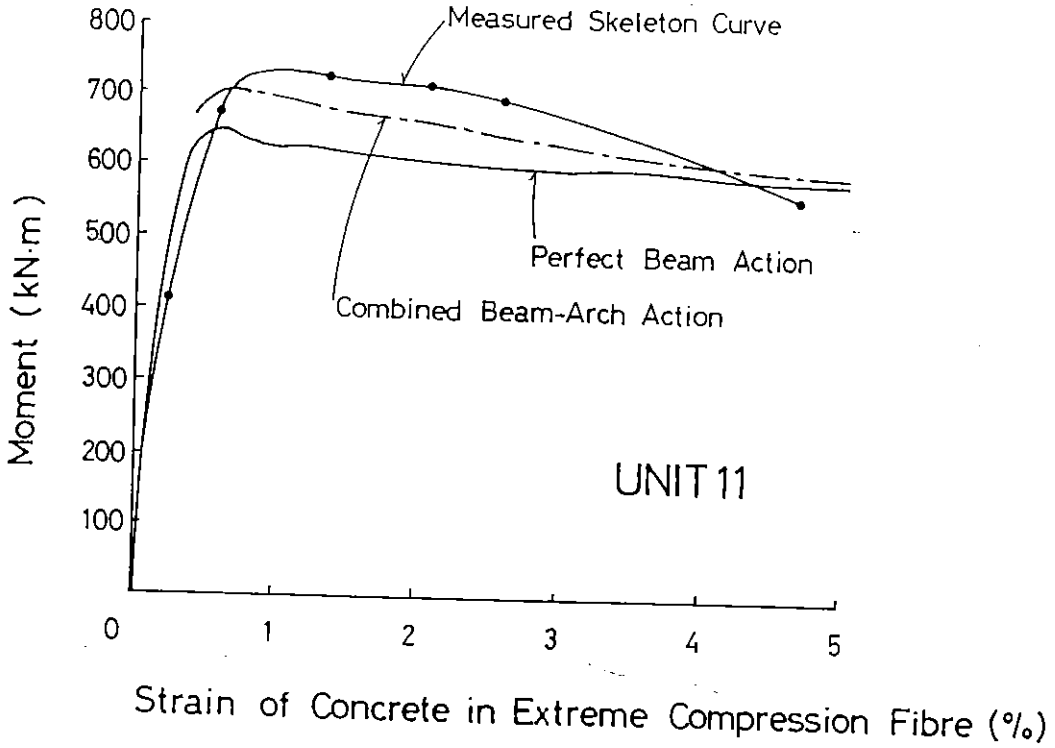

Fig. 4.79 Comparison between Theoretical and Measured Moment-Concrete Strain Relations for Unit 11.

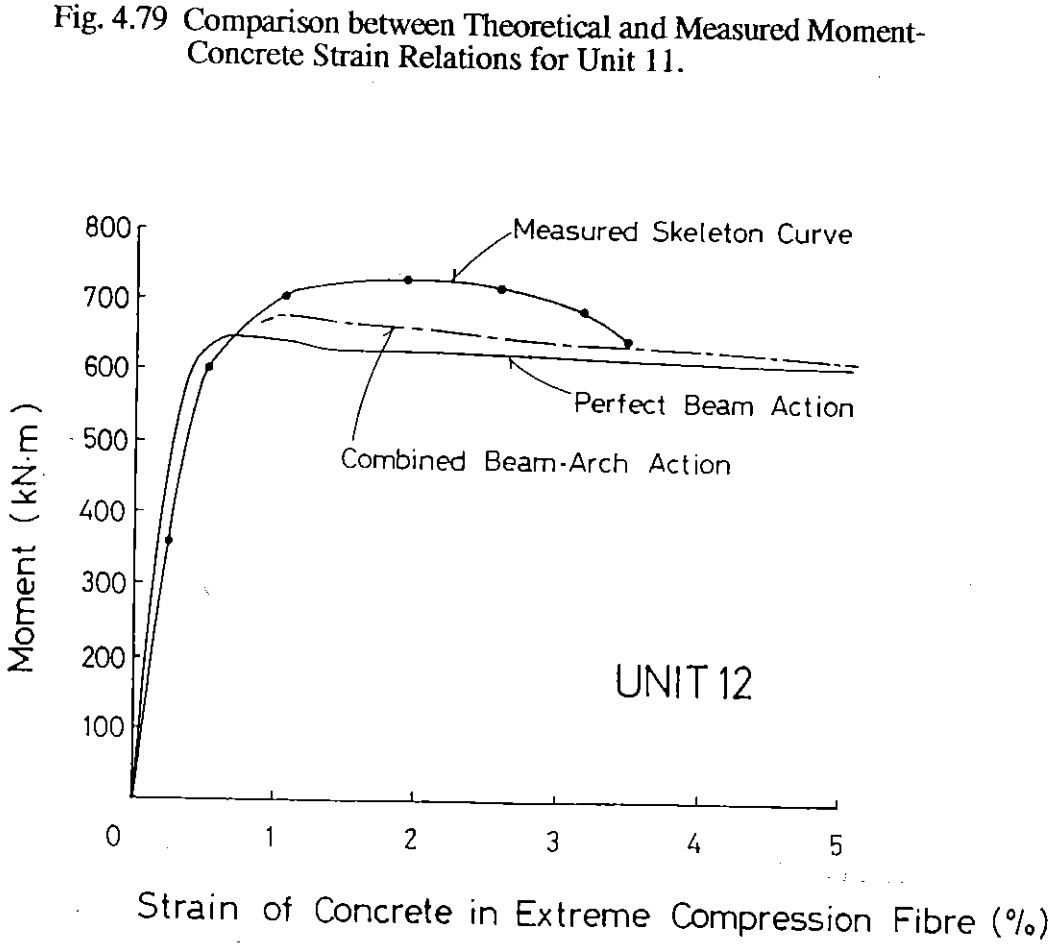

Fig. 4.80 Comparison between Theoretical and Measured Moment-Concrete Strain Relations for Unit 12.

Table 4.6 Theoretical Moments Calculated Assuming Perfect Beam Action and Combined Beam-Arch Action for Units 9, 10, 11 and 12.

Col-umn Unit	$\frac{P_e}{f'_c A_g}$	M_{ACI} (KN·m)	μ	Concrete Strain in Extreme Comp. Fibre, ε_{cf} (%)	Measured Moment M_m (KN·m)	Perfect Beam Action M_1 (KN·m)	ϕ_y ($\times 10^{-6}$ 1/mm)	$\frac{\phi}{\phi_y}$	Combined Beam-Arch Action $\frac{C}{A_{gc} f'_c}$	M_2 (KN·m)	M_c (KN·m)	M_u (KN·m)	Comparison of Moment ratio $\frac{M_1}{M_m}$	$\frac{M_u}{M_m}$
9	0.1	597	2	0.51	674	627	16.00	2.2	0.29	266	354	620	0.93	0.92
			-8	4.32	697	702		16.1			358	624	1.01	0.90
10	0.1	429	2	0.65	528	480	12.10	2.8	0.45	253	316	569	0.91	1.08
			8	4.22	546	531		17.2			310	563	0.97	1.03
11	0.3	552	4	1.32	737	626	9.38	5.7	0.70	393	276	669	0.85	0.91
			10	4.65	636	601		18.6			218	611	0.94	0.96
12	0.5	471	4	1.04	711	646	6.80	5.2	1.06	463	217	680	0.91	0.96
			12	3.42	644	626		17.2			184	647	0.97	1.00

Note: A_g = gross area of column section

A_{gc} = gross area of separated column section subjected to combined axial load C and beding moment M_c in combined beam-arch action, shown in Fig. 4.76.

$P_e / A_g f'_c$ = axial load level

μ = displacement ductility factor

M_{ACI} = moment calculated using the ACI method [4.6]

M_1 = moment calculated using ordinary section analysis

M_2 = moment due to axial loads T and C in each separated column

M_c = moment of the separated column with the axial load level $C/A_{gc} f'_c$

$M_u = M_2 + M_c$

ϕ / ϕ_y = ratio of curvature to the yield curvature for perfect beam action, where ϕ_y = curvature when calculated moment reaches M_{ACI}.

cantilever and tension force in transverse reinforcement (see Fig. 4.9). In case of spirals, the component of tension force in spirals which is parallel with the direction of the shear force applied to column can contribute to the bond force. This component of spiral tension force is small when the intersection of an inclined shear crack with a spiral bar is close to the extreme tension fibre region of the column section (see Fig. 4.6). As described in Sections 4.2.2.2 and 4.2.2.3, when the amount of spirals required as shear reinforcement is to be determined by assuming a 45° inclined shear crack, the reduction in the spiral force component due to the spiral bar inclination has to be taken into account. However, this was determined only by considering the equilibrium of the forces acting in the direction parallel to the column shear force. With respect to the bond force, it is determined from the equilibrium of moment at the end of the concrete cantilever as can be seen from Fig. 4.9 (c). It must be emphasized that the component of spiral force which contributes to the bond force is small at where the moment arm length is large and vice versa. Hence, the potential capacity of bond force provided by spiral tension force is less than that by rectangular hoops and cross ties when the amounts of those two types of transverse reinforcement are that required by the design shear force. Moreover, in case of Units 10 to 12, as was described in Section 4.3.2.5, the spirals have yielded from an early stage of loading due to the Poisson's effect of the core concrete in compression zone. As a result, large inelastic elongation of spiral bars occurred. Consequently, the inelastically elongated spiral bars could have been ineffective to generate bond force, when the horizontal column load was reversed and when the compression zone of the column section became theß tension zone. On the contrary, in case of Unit 9, the strains in hoops and cross ties remained in elastic range until the end of test.

4.3.3.3 Shear Deformation

To fully evaluate the deflections of reinforced concrete members, the shear deformation and slip of longitudinal reinforcement need to be considered, as well as flexural deformations. Normally, it is not simple to estimate the contribution of each deformation factor, especially in the inelastic range of loading. To estimate the inelastic deflections of members, the concept of plastic rotation within a plastic hinge length l_p [4.3, 4.18] has commonly been used. This can be explained for the cantilever shown in

Fig.4.81, where ϕ_y = yield curvature and ϕ_u= ultimate curvature. The vertical deflection at A is calculated as

$$\Delta_A = \left(\frac{\phi_y l}{2}\,\frac{2l}{3}\right) + (\phi_y - \phi_u)\, l_p \left(l - \frac{l_p}{2}\right) \quad \text{.....} \quad (4.43)$$

When the values of ϕ_y and ϕ_u can be obtained from a section analysis or from an experiment, l_p can be determined by substituting an experimentally measured deflection Δ_A into Eq. 4.43. Thus the determined value for l_p involves the effects of shear deformation, yield penetration of longitudinal reinforcement and concrete damage propagation into the base block, in addition to the flexural deformation of column. The contributions of deformations other than flexural deformation are sometimes negligible, but can sometimes be significant, depending on aspect ratio of the member, material characteristics and reinforcing details including the anchorage of longitudinal reinforcement. The plastic hinge length l_p also is significantly affected by the assumed value of ϕ_u. In order to estimate member deflection more rigorously, it is necessary to evaluate the contributions of each deformation factor corresponding to the mechanisms of deformations. In this section, the contribution of shear deformation to the total column deflection is investigated using the test data obtained from Units 9 to 12 and, for comparison, Units 5 to 8 described in Section 3. It must be noted that Units 5 to 8 are square columns with square hoops and supplementary cross-ties. The aspect ratio (= ratio of shear span length to full column depth) of those units was 3, which was the same as in Units 9 to 12, and the axial load level ($=P_e / f'_c A_g$) was 0.1 for Units 5 and 6 and was 0.3 for Units 7 and 8.

As has been shown in Fig. 4.35, the curvature distributions along the column axis were measured using five pairs of potentiometers. The measured curvatures by those potentiometers are schematically illustrated as ϕ_1 to ϕ_5 in Fig.4.82. It is notable that the curvatures measured at the bottom of columns include slip of the longitudinal reinforcement from the base block. In the figure, Δ^M_{top} and Δ^M_{mid} denote the column displacement measured at the column top and the column displacement measured at the column mid-height, respectively. Using the measured curvatures the flexural deflection at the column mid height Δ^B_{mid} can be calculated as

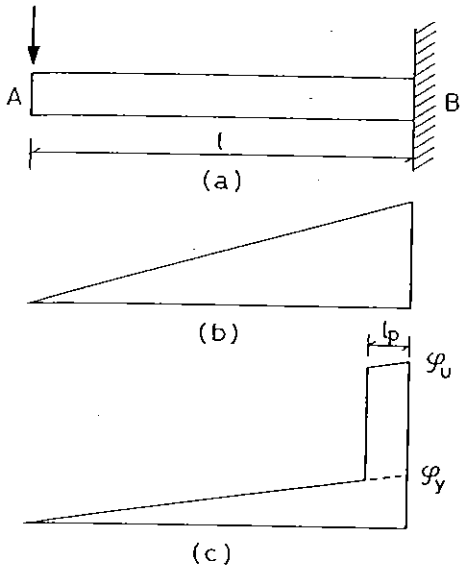

(a) Cantilever
(b) Bending Moment Distribution
(c) Curvature Distribution

Fig. 4.81 Flexural Deflection of a Cantilever.

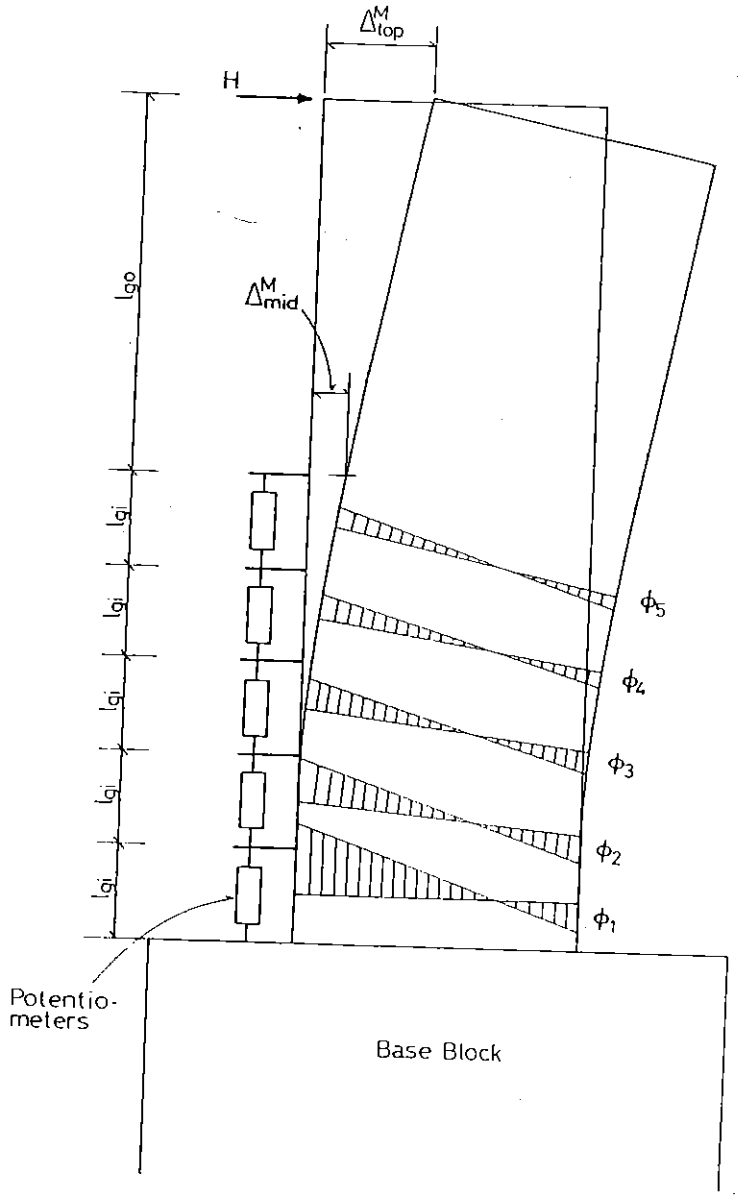

Fig. 4.82 Curvature Variation Used for Calculation of Column Deflection due to Bending.

$$\Delta^{B}_{mid} = \sum_{i=1}^{5} \phi_i \, l_{gi} \, l_i \qquad \text{.....} \qquad (4.44)$$

where l_{gi} = gauge length for potentiometers
= 180 mm for Units 5 to 8 and 200 mm for Units 9 to 12
l_i = distance between the measuring point of Δ_{mid}^{M} and the center position of i-th pair of potentiometers

The displacement at the column top Δ^{B}_{top} after yield displacement is calculated as

$$\Delta^{B}_{top} = \sum_{i=1}^{5} \phi_i \, l_{gi} \, l_i' + \frac{1}{(1+5\, l_{gi}/l_{go})} \; \phi_y \; \frac{l_{go}}{2} \frac{2\, l_{go}}{3} \qquad \text{.....} \quad (4.45)$$

where l_{go} = length of column where potentiometers are not placed
= 750 mm for Units 5 to 8 and 784 mm for Units 9 to 12
l_i'= distance between the measuring point of Δ^{M}_{top} and the center position of i-th pair of potentiometers

The last term in the right hand side of Eq.4.45 is the deflection due to the elastic deformation over the length l_{go} and is negligible for the case of the tested columns in this study. Hence, it was neglected in the calculation of Δ^{B}_{top} for Units 5 to 12. Those calculated results for Units 9 to 12 and Units 5 to 8 are listed in Tables 4.7 to 4.10 and Tables 4.11 to 4.14, respectively. In the tables, the calculated displacements using the method shown below are also listed.

In Fig. 4.83, the crack pattern of Unit 10 at a displacement ductility factor μ = 4 is shown. It can be seen that the flexural cracks vertical to the column axis begin to incline at the central region of the column and hence those cracks are referred to as flexural shear cracks. A flexural shear crack can be modelled as shown in Fig.4.84 where the notation is as follows ;

c = distance of the rotation centre from the extreme compression fibre
D = full depth of a column
l_o = vertical distance between the rotation centre and the column top
l_c = vertical distance between the opening edge of crack and the column top
$h_1 = D - c - h_2$

Table 4.7 Comparison between Measured and Theoretical Displacements for Unit 9

Displacement Ductility Factor,μ	For Column Displacement at Mid-Height					For Column Displacement at Top-Height				
	Δ^{M}_{mid} (mm)	Δ^{B}_{mid} (mm)	$\frac{\Delta^{B}_{mid}}{\Delta^{M}_{mid}}$	Δ^{S}_{mid} (mm)	$\frac{\Delta^{S}_{mid}}{\Delta^{M}_{mid}}$	Δ^{M}_{top} (mm)	Δ^{B}_{top} (mm)	$\frac{\Delta^{B}_{top}}{\Delta^{M}_{top}}$	Δ^{S}_{top} (mm)	$\frac{\Delta^{S}_{top}}{\Delta^{M}_{top}}$
0.75	3.38	2.79	0.83	3.34	0.99	7.50	6.42	0.86	6.88	0.92
-0.75	-3.83	-2.94	0.77	-3.60	0.94	-8.03	-6.80	0.85	-6.96	0.87
2	10.35	8.37	0.81	9.65	0.93	20.85	17.99	0.86	18.82	0.90
-2	-10.73	-8.47	0.79	-9.77	0.91	-21.30	-17.96	0.84	-17.97	0.84
4	21.60	17.54	0.81	21.07	0.98	41.93	35.82	0.85	39.60	0.94
-4	-22.58	-18.04	0.80	-22.25	0.99	-42.53	-36.59	0.86	-40.02	0.94
6	32.93	24.84	0.75	33.51	1.02	62.63	50.82	0.81	63.44	1.01
-6	-34.50	-26.32	0.76	-33.78	0.98	-63.23	-53.32	0.84	-62.30	0.99
8	44.63	30.64	0.69	43.55	0.98	83.70	62.62	0.75	83.72	1.00
-8	-46.80	-35.49	0.76	-47.50	1.01	-84.23	-70.90	0.84	-89.58	1.06
10	57.38	42.14	0.73	53.69	0.94	105.23	84.56	0.80	99.50	0.95
average			0.77		0.97			0.83		0.95

Table 4.8 Comparison between Measured and Theoretical Displacements for Unit 10

Displacement Ductility Factor,μ	For Column Displacement at Mid-Height					For Column Displacement at Top-Height				
	Δ^{M}_{mid} (mm)	Δ^{B}_{mid} (mm)	$\frac{\Delta^{B}_{mid}}{\Delta^{M}_{mid}}$	Δ^{S}_{mid} (mm)	$\frac{\Delta^{S}_{mid}}{\Delta^{M}_{mid}}$	Δ^{M}_{top} (mm)	Δ^{B}_{top} (mm)	$\frac{\Delta^{B}_{top}}{\Delta^{M}_{top}}$	Δ^{S}_{top} (mm)	$\frac{\Delta^{S}_{top}}{\Delta^{M}_{top}}$
0.75	3.53	3.20	0.91	3.70	1.05	8.03	6.85	0.85	7.00	0.87
-0.75	-4.50	-3.67	0.82	-4.81	1.07	-9.53	-8.23	0.86	-9.31	0.98
2	11.18	9.76	0.87	11.38	1.02	23.70	20.36	0.86	21.50	0.91
-2	-11.55	-9.23	0.80	-11.33	0.98	-23.55	-19.77	0.84	-21.33	0.91
4	23.25	20.87	0.90	25.04	1.08	46.80	41.68	0.89	46.29	0.99
-4	-24.60	-20.67	0.84	-25.74	1.05	-47.10	-41.82	0.89	-47.13	1.00
6	36.08	30.50	0.85	43.06	1.19	70.65	61.11	0.86	80.66	1.14
-6	-37.58	-30.14	0.80	-38.08	1.01	-70.43	-61.00	0.87	-70.14	1.00
8	48.53	39.55	0.81	58.30	1.20	93.90	79.15	0.84	110.07	1.17
-8	-50.48	-38.83	0.77	-49.15	0.97	-93.98	-78.19	0.83	-90.53	0.96
10	61.58	49.62	0.81	72.84	1.18	117.68	98.03	0.83	137.08	1.16
average			0.83		1.07			0.86		1.01

Table 4.9 Comparison between Measured and Theoretical Displacements for Unit 11

Displacement Ductility Factor,μ	For Column Displacement at Mid-Height					For Column Displacement at Top-Height				
	Δ^{M}_{mid} (mm)	Δ^{B}_{mid} (mm)	$\frac{\Delta^{B}_{mid}}{\Delta^{M}_{mid}}$	Δ^{S}_{mid} (mm)	$\frac{\Delta^{S}_{mid}}{\Delta^{M}_{mid}}$	Δ^{M}_{top} (mm)	Δ^{B}_{top} (mm)	$\frac{\Delta^{B}_{top}}{\Delta^{M}_{top}}$	Δ^{S}_{top} (mm)	$\frac{\Delta^{S}_{top}}{\Delta^{M}_{top}}$
0.75	2.55	1.96	0.77	2.50	0.98	5.63	4.29	0.76	5.00	0.89
-0.75	-2.88	-2.47	0.86	-2.50	0.87	-6.15	-5.22	0.85	-4.61	0.75
2	7.65	6.14	0.80	8.01	1.05	16.20	13.35	0.82	15.89	0.98
-2	-7.43	-5.95	0.80	-6.73	0.91	-15.68	-12.89	0.82	-12.82	0.82
4	15.83	13.25	0.84	17.83	1.13	32.33	27.70	0.86	34.82	1.08
-4	-15.75	-13.99	0.89	-18.96	1.20	-31.20	-28.96	0.93	-37.42	1.20
6	23.78	21.57	0.91	28.37	1.19	48.15	44.12	0.92	54.46	1.13
-6	-24.30	-22.41	0.92	-31.09	1.28	-47.10	-45.32	0.96	-61.10	1.30
8	31.80	28.20	0.89	36.63	1.15	63.83	57.71	0.90	70.43	1.10
-8	-32.70	-29.79	0.91	-36.75	1.12	-63.08	-60.00	0.95	-70.86	1.12
10	39.60	33.11	0.84	33.80	0.85	79.65	68.63	0.86	64.10	0.80
-10	-40.73	-38.43	0.94	-41.80	1.03	-78.90	-76.33	0.97	-78.13	0.99
average			0.87		1.07			0.89		1.02

Table 4.10 Comparison between Measured and Theoretical Displacements for Unit 12

Displacement Ductility Factor, μ	For Column Displacement at Mid-Height					For Column Displacement at Top-Height				
	Δ^M_{mid} (mm)	Δ^B_{mid} (mm)	$\frac{\Delta^B_{mid}}{\Delta^M_{mid}}$	Δ^S_{mid} (mm)	$\frac{\Delta^S_{mid}}{\Delta^M_{mid}}$	Δ^M_{top} (mm)	Δ^B_{top} (mm)	$\frac{\Delta^B_{top}}{\Delta^M_{top}}$	Δ^S_{top} (mm)	$\frac{\Delta^S_{top}}{\Delta^M_{top}}$
0.75	1.88	1.46	0.78	2.10	1.12	4.20	3.22	0.77	4.38	1.04
-0.75	-1.88	-1.41	0.75	-1.19	0.63	-3.90	-3.01	0.77	-2.17	0.56
2	5.18	4.20	0.81	5.78	1.12	10.80	9.25	0.86	11.49	1.06
-2	-5.25	-4.33	0.82	-4.55	0.87	-11.10	-9.25	0.83	-8.42	0.76
4	10.58	8.65	0.82	12.89	1.22	21.83	19.00	0.87	26.78	1.23
-4	-10.80	-8.91	0.83	-9.56	0.89	-21.83	-18.91	0.87	-18.14	0.83
6	16.13	13.58	0.84	22.85	1.42	32.78	29.08	0.89	48.34	1.47
-6	-16.58	-14.03	0.85	-14.49	0.87	-32.70	-29.36	0.90	-27.40	0.84
8	21.53	18.04	0.84	34.18	1.59	43.58	38.33	0.88	72.59	1.67
-8	-22.58	-19.39	0.86	-20.24	0.90	-43.73	-40.43	0.92	-38.48	0.88
10	26.85	22.74	0.85	35.72	1.33	54.30	47.82	0.88	73.95	1.36
-10	-28.20	-24.70	0.88	-24.17	0.86	-54.83	-51.38	0.94	-45.93	0.84
12	32.18	27.02	0.84	34.48	1.07	65.10	56.42	0.87	70.07	1.08
-12	-33.83	-30.26	0.89	-29.45	0.87	-65.55	-62.42	0.95	-56.64	0.86
average			0.83		1.05			0.87		1.03

Table 4.11 Comparison between Measured and Theoretical Displacements for Unit 5

Displacement Ductility Factor, μ	For Column Displacement at Mid-Height					For Column Displacement at Top-Height				
	Δ^M_{mid} (mm)	Δ^B_{mid} (mm)	$\frac{\Delta^B_{mid}}{\Delta^M_{mid}}$	Δ^S_{mid} (mm)	$\frac{\Delta^S_{mid}}{\Delta^M_{mid}}$	Δ^M_{top} (mm)	Δ^B_{top} (mm)	$\frac{\Delta^B_{top}}{\Delta^M_{top}}$	Δ^S_{top} (mm)	$\frac{\Delta^S_{top}}{\Delta^M_{top}}$
0.75	4.62	2.31	0.48	4.90	1.02	9.23	5.46	0.59	11.40	1.24
- 0.75	-8.66	-2.85	0.33	-3.88	0.45	-14.50	-6.25	0.43	-7.69	0.53
2	15.21	11.21	0.74	14.30	0.94	29.40	23.74	0.81	27.90	0.95
- 2	-23.42	-11.58	0.49	-13.82	0.59	-24.68	-24.01	0.97	-26.40	1.07
4	15.85	16.68	1.05	22.32	1.41	49.40	34.80	0.70	43.10	0.87
-4	-37.20	-22.55	0.61	-26.13	0.70	-49.20	-45.61	0.93	-49.12	1.00
6	29.24	26.92	0.92	36.67	1.25	73.90	55.65	0.75	70.44	0.95
-6	-51.17	-33.60	0.66	-40.32	0.79	-73.80	-67.26	0.91	-75.41	1.02
average			0.66		0.89			0.76		0.95

Table 4.12 Comparison between Measured and Theoretical Displacements for Unit 6

Displacement Ductility Factor, μ	For Column Displacement at Mid-Height					For Column Displacement at Top-Height				
	Δ^M_{mid} (mm)	Δ^B_{mid} (mm)	$\frac{\Delta^B_{mid}}{\Delta^M_{mid}}$	Δ^S_{mid} (mm)	$\frac{\Delta^S_{mid}}{\Delta^M_{mid}}$	Δ^M_{top} (mm)	Δ^B_{top} (mm)	$\frac{\Delta^B_{top}}{\Delta^M_{top}}$	Δ^S_{top} (mm)	$\frac{\Delta^S_{top}}{\Delta^M_{top}}$
0.75	3.89	2.79	0.72	3.44	0.88	7.65	6.26	0.82	6.96	0.91
-0.75	-4.13	-2.72	0.66	-3.69	0.89	-8.78	-6.07	0.69	-7.48	0.85
2	11.55	8.28	0.72	9.78	0.85	22.60	17.88	0.79	19.30	0.85
-2	-11.43	-8.26	0.72	-10.29	0.90	-22.60	-17.33	0.77	-20.03	0.89
4	23.48	17.31	0.74	20.70	0.88	44.80	35.76	0.80	39.61	0.88
-4	-23.63	-18.06	0.76	-21.02	0.89	-44.80	-36.33	0.81	-39.44	0.88
6	35.74	30.88	0.86	37.88	1.06	67.20	62.51	0.93	71.42	1.06
-6	-36.15	-27.31	0.76	-33.19	0.92	-67.20	-54.77	0.82	-62.11	0.92
8	47.46	41.50	0.87	50.84	1.07	89.80	83.44	0.93	95.90	1.07
-8	-48.67	-37.13	0.76	-45.17	0.93	-89.60	-74.05	0.83	-84.58	0.94
10	59.86	52.96	0.88	63.83	1.07	112.00	105.27	0.94	119.96	1.07
average			0.77		0.94			0.83		0.94

Table 4.13 Comparison between Measured and Theoretical Displacements for Unit 7

Displacement Ductility Factor,μ	For Column Displacement at Mid-Height					For Column Displacement at Top-Height				
	Δ^{M}_{mid} (mm)	Δ^{B}_{mid} (mm)	$\frac{\Delta^{B}_{mid}}{\Delta^{M}_{mid}}$	Δ^{S}_{mid} (mm)	$\frac{\Delta^{S}_{mid}}{\Delta^{M}_{mid}}$	Δ^{M}_{top} (mm)	Δ^{B}_{top} (mm)	$\frac{\Delta^{B}_{top}}{\Delta^{M}_{top}}$	Δ^{S}_{top} (mm)	$\frac{\Delta^{S}_{top}}{\Delta^{M}_{top}}$
0.75	3.00	1.74	0.58	2.08	0.69	6.08	3.99	0.66	4.11	0.68
-0.75	-5.38	-1.45	0.27	-1.61	0.30	-9.34	-3.19	0.34	-3.09	0.33
2	10.43	7.40	0.71	9.18	0.88	20.63	16.56	0.80	18.67	0.90
-2	-11.21	-5.15	0.46	-6.12	0.55	-20.60	-11.70	0.57	-12.50	0.61
4	20.95	16.46	0.79	21.15	1.01	41.20	35.62	0.86	41.84	1.02
-4	-21.90	-14.61	0.67	-16.36	0.75	-41.20	-30.90	0.75	-31.70	0.77
6	31.19	25.09	0.80	35.54	1.14	61.80	54.24	0.88	71.13	1.15
-6	-32.56	-23.81	0.73	-27.09	0.83	-61.80	-50.00	0.81	-52.20	0.84
8	41.15	36.90	0.90	53.95	1.31	82.60	83.80	1.01	113.08	1.37
-8	-43.22	-31.58	0.73	-36.50	0.84	-82.40	-66.56	0.81	-70.79	0.86
average			0.66		0.83			0.75		0.85

Table 4.14 Comparison between Measured and Theoretical Displacements for Unit 8

Displacement Ductility Factor,μ	For Column Displacement at Mid-Height					For Column Displacement at Top-Height				
	Δ^{M}_{mid} (mm)	Δ^{B}_{mid} (mm)	$\frac{\Delta^{B}_{mid}}{\Delta^{M}_{mid}}$	Δ^{S}_{mid} (mm)	$\frac{\Delta^{S}_{mid}}{\Delta^{M}_{mid}}$	Δ^{M}_{top} (mm)	Δ^{B}_{top} (mm)	$\frac{\Delta^{B}_{top}}{\Delta^{M}_{top}}$	Δ^{S}_{top} (mm)	$\frac{\Delta^{S}_{top}}{\Delta^{M}_{top}}$
0.75	2.53	1.71	0.68	2.05	0.81	5.33	3.96	0.74	4.12	0.77
-0.75	-2.88	-1.46	0.51	-1.50	0.52	-5.40	-3.27	0.61	-2.88	0.53
2	7.05	4.94	0.70	6.76	0.96	14.30	11.44	0.80	14.19	0.99
-2	-7.37	-4.24	0.58	-5.65	0.77	-14.30	-9.55	0.67	-11.40	0.80
4	13.81	10.87	0.79	12.62	0.91	28.10	23.81	0.85	25.02	0.89
-4	-14.91	-10.17	0.68	-13.37	0.90	-28.60	-22.22	0.78	-26.58	0.93
6	21.18	18.27	0.86	21.25	1.00	42.90	39.37	0.92	41.51	0.97
-6	-21.93	-16.44	0.75	-17.66	0.81	-42.90	-35.20	0.82	-34.29	0.80
8	28.29	26.44	0.93	32.00	1.13	57.20	56.00	0.98	62.74	1.10
-8	-29.03	-21.29	0.73	-22.83	0.79	-57.20	-45.64	0.80	-44.55	0.78
12	42.08	40.91	0.97	47.79	1.14	85.80	85.75	1.00	92.78	1.08
average			0.74		0.88			0.81		0.88

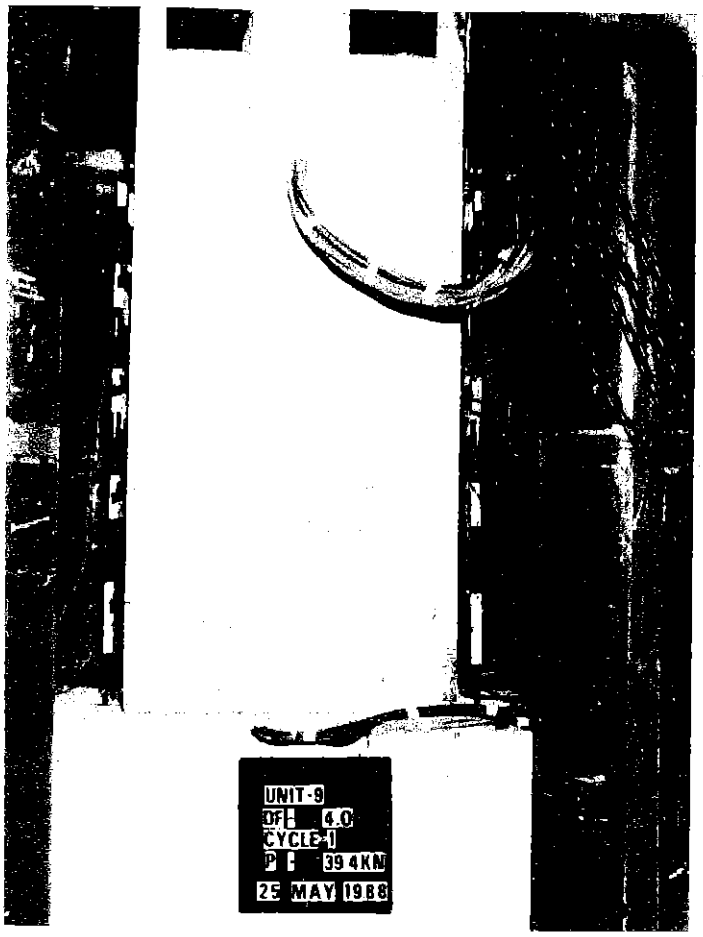

Fig. 4.83 (a) Crack Pattern of Unit 9 at Displacement Ductility Factor $\mu = 4$.

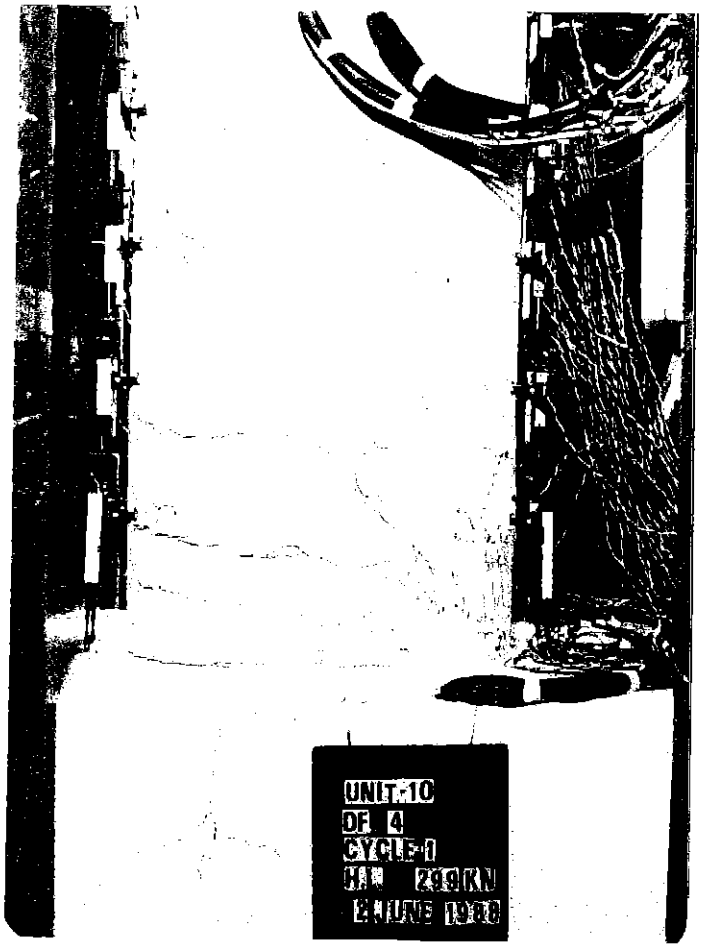

Fig. 4.83 (b) Crack Pattern of Unit 10 at Displacement Ductility Factor $\mu = 4$.

h_2 = length of the part of crack perpendicular to the column axis
Δ_d = distance between the opening edges of the flexural shear crack
Δ_h = vertical distance between crack opening edges when a horizontal flexural crack is formed and the column rotates with angle θ.
$\Delta_{h'}$ = vertical distance between the opening edges of a flexural shear crack
α = angle between the column axis and the inclined part of the crack
β = angle between horizontal line and the line connected from the rotation centre to the opening edge of the flexural shear crack
θ = rotation angle of the column

It may be assumed that the potentiometer readings indicate $\Delta_{h'}$ rather than Δ_d, judging from the comparatively large gauge length, l_{gi}, used in this study. From a geometrical condition, $\Delta_{h'} \approx \Delta_h$ when the column rotates with angle θ. This can be examined as follows;

Δ_h, Δ_d and cos β are expressed as

$$\Delta_h = (h_1 + h_2) \theta$$

$$\Delta_d = \theta \sqrt{(h_1 + h_2)^2 + (h_1 \cot \alpha)^2}$$

$$\cos \beta = (h_1 + h_2) / \sqrt{(h_1 + h_2)^2 + (h_1 \cot \alpha)^2}$$

From geometry, $\Delta_{h'} = \Delta_d \cos \beta$. Substituting the above relations,
$\Delta_{h'} = (h_1 + h_2) \theta$ and hence $\Delta_{h'} = \Delta_h$

As can be seen from Fig. 4.83, most of the flexural shear cracks propagated into the almost same depth over the column region where the potentiometers were placed. Based on this observation, the crack pattern was modelled as shown in Fig. 4.85. Using this model and strain at the extreme tension fibres measured by the potentiometers, the column deflections were calculated for Units 5 to 12. In the calculation following assumptions were used;

(1) The distance c of each rotation centre from the extreme compression fiber is all the same along the column axis as shown in Fig. 4.85. The distance c is equal to the neutral axis depth measured by the bottom set of potentiometers.
(2) The angle $\alpha = 45°$.
(3) $h_1 = h_2$

(4) When the position of the rotation centre calculated using the above assumptions is located inside the base block, the rotation centre is set at the face of the base block assuming that the crack is an inclined straight line (see the bottom crack in Fig. 4.85).

(5) All cracks within a potentiometer gauge length are represented by one crack and its crack opening position is set at the centre of the gauge length of each potentiometer .

The column displacement at the column mid-height, Δ^S_{mid} , is calculated as

$$\Delta^S_{mid} = \sum_{i=1}^{5} \theta_i \, l_i^r \qquad \text{.....} \qquad (4.46)$$

where θ_i = rotation angle of i-th flexural shear crack assumed

l_i^r = vertical distance between the measuring point of Δ^M_{mid} and i-th rotation centre

The column displacement at the column top, Δ^S_{top} , is calculated neglecting elastic deformation in the uncracked region of the modelled column in Fig.4.85.

$$\Delta^S_{top} = \sum_{i=1}^{5} \theta_i \, l'^r_i \qquad \text{.....} \qquad (4.47)$$

where θ_i = rotation angle of i-th flexural shear crack assumed

l'^r_i = vertical distance between the measuring point of Δ^M_{top} and i-th rotation centre

The calculated results for Units 5 to 12 are listed in Table 4.7 to 4.14.

It can be considered that the difference between Δ^M_{top} and Δ^B_{top} is the shear deformation, because the deformation due to the slip out of longitudinal reinforcement from the base block has been included in Δ^B_{top} as mentioned previously. To some extent, the large compression against the face of the base block may have caused an additional rotation in the columns tested but this rotation is also likely to have been included in Δ^B_{top}. This is because the face of the base block in contact with the bottom pair of potentiometers remained undamaged until the displacement ductility factor reached six or more in all tested columns. Moreover, when concrete damage began to propagate into the base block due to large compression, the

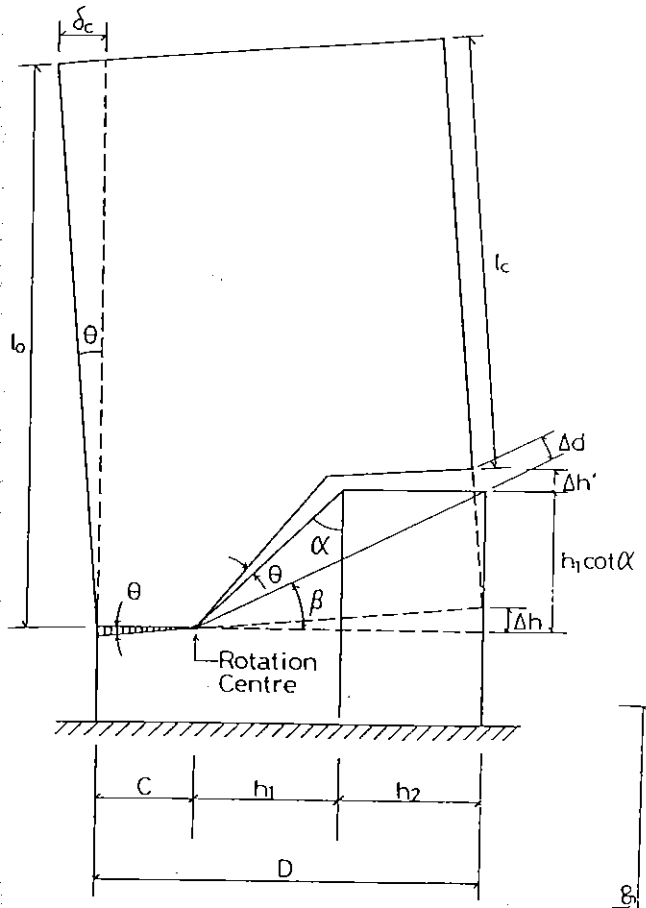

Fig. 4.84 Deflection due Opening of a Flexural Shear Crack.

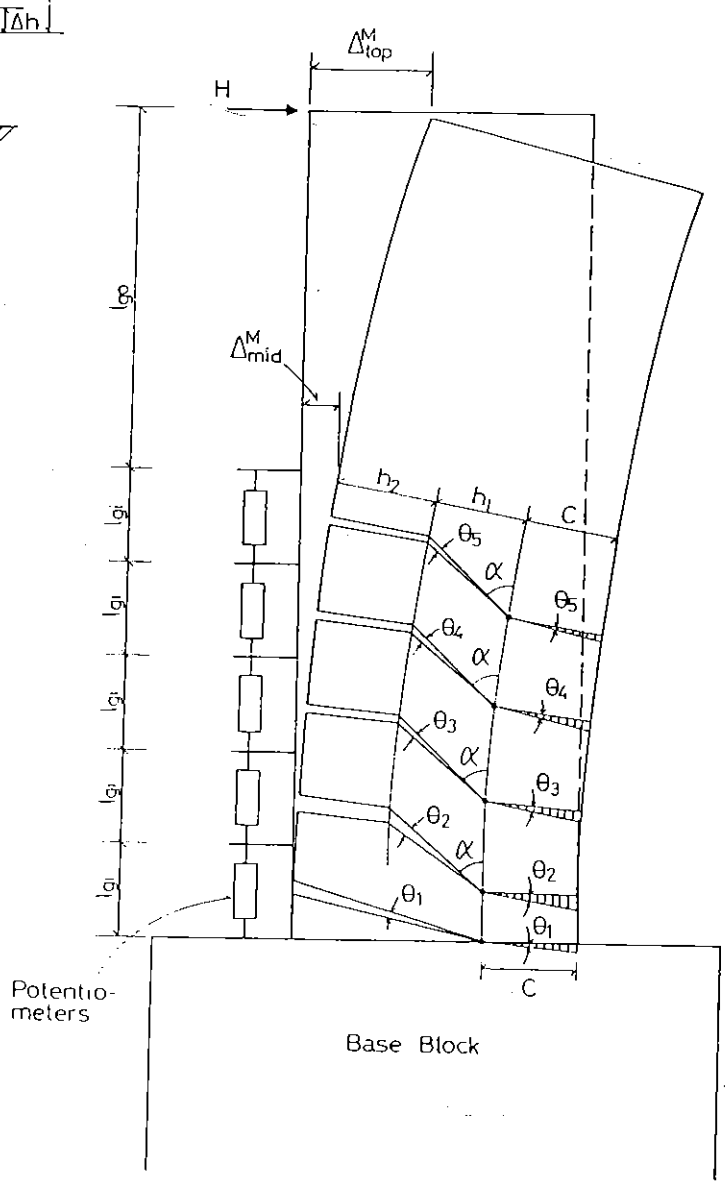

Fig. 4.85 Rotation Angle Variation Used for Calculation of the Column Deflection due to Flexural Shear Cracking.

concrete cover of the base block began to deform outwards and made compression strain readings of the bottom potentiometer larger than reality. Hence, in such a case Δ^B_{top} may have been overestimated, although the concrete surface of the base block was always repaired to make the potentiometer readings correct when the outward movement of cover concrete from the base block face was recognized. For this reason, the shear deformation estimated by the difference between Δ^M_{top} minus Δ^B_{top} might be underestimated when the displacement ductility factor was more than six. Similar remarks can be made concerning the relation between Δ^M_{mid} and Δ^B_{mid}. In this section, the shear deformation is defined as Δ^M_{top} minus Δ^B_{top} or Δ^M_{mid} minus Δ^B_{mid}.

As can be seen from Table 4.7 to 4.14, Δ^B_{top} and Δ^B_{mid} are always significantly less than the corresponding Δ^M_{top} and Δ^M_{mid} from displacement ductility factor $\mu=\pm$ 0.75 to the final stage of loading. It is normally considered that the ratio of shear deformation to the flexural deformation is smaller in the elastic range of loading. However, for all units tested, the ratios of shear deformation to the column displacement at ductility factor $\mu=\pm$ 0.75 are almost comparable with those at the final stage of loading. As has been mentioned in Section 4.3.2.1, the theoretical values of the initial stiffness were significantly greater than the measured values. One of the reason for the overestimation of the initial stiffness by theory can be attributed to the underestimation of the shear deformation. It is suggested that, for the columns with aspect ratio of three or less, the shear deformation must be adequately evaluated even for the load of 0.75 H_u.

For each test unit the shear deformation defined as Δ^M_{top} minus Δ^B_{top} or Δ^M_{mid} minus Δ^B_{mid} varied from 11% to 34 % of the measured column displacement at the load peaks. On the contrary, Δ^S_{top} and Δ^S_{mid} calculated using the shear deformation model shown in Fig. 4.85 agreed well with the corresponding Δ^M_{top} and Δ^M_{mid}. This indicates that the deformation mechanism of the columns tested were close to the shear deformation model shown in Fig. 4.85. This also indicates that the combined beam-arch action model applied to Units 9 to 12 in Section 4.3.3.2 was adequate from the view point of the column deformation mechanism. This is because the basic column deformation mechanism assumed in the shear deformation model is the same with that in the combined beam-arch action model.

The axial load level (=P_e / f'_cA_g) was varied from 0.1 to 0.3 for Units 5 to 9 and from 0.1 to 0.5 for Units 9 to 12 but the effect of the axial load level on the shear deformation defined here is little as far as those test results are concerned. On the other hand, when the results of Units 5 to 9 with hoops and supplementary cross ties are compared with those of Units 10 to 12 with interlocking spirals, the shear deformations of the former units are a little larger than those of the latter units. This may be attributed to the slight difference in the flexural shear crack pattern. When Figs. 4.83 (a) and (b) are compared, it can be seen that the actual ratio of h_1 to h_2 is a little larger for Unit 9 than for Unit 10. It is obvious that, when calculating Δ^S_{top} and Δ^S_{mid} for Unit 5 to 9 with rectangular hoops and cross-ties, better agreement with the test results could be obtained if a larger value was assumed for the ratio of h_1 to h_2. Hence, it can be concluded that the shear deformation defined here is a little larger in columns with rectangular hoops and cross-ties than in columns with interlocking spirals.

From the above observations, the following point is emphasized. For the columns tested with aspect ratio of 3, the ratio of column deflection due to shear to total column deflection reached 10 to 30 % and this ratio was almost constant from displacement ductility factor μ = 0.75 to the final stage of loading where μ was more than 8. Hence, it is suggested that for a column with an aspect ratio of 3, when the column deflection is calculated based on curvature distribution assuming that plane sections remain plane, the calculated column deflection should be increased by about 20 % or more due to shear deformation. This suggestion is on the premise that the concept of curvature does not involve any shear deformation.

In this study, the shear deformation model was used to explain the deformation mechanism which actually occurred in the columns tested and the same model supported the validity of combined beam-arch action theory. For future research, it is suggested that, for columns with weak interlocking spirals or with comparatively small aspect ratio, the deflection can be estimated on the basis of combined beam-arch action with the shear deformation model. The distance of the rotation centre from extreme compression fibre in the shear deformation model , c, can be estimated as the neutral axis depth of the separated column subjected to $C = P_e + T$ in combined beam-arch action theory. The ratio of h_1 to h_2 may be taken as unity and θ may be as 45°. The only difficulty may be how to estimate the

spread of the inelastically tensioned zone but it may tentatively be taken as the plastic hinge length l_p which has normally been adopted for ordinaly flexural deflection analysis.

4.4 CONCLUSIONS

In this chapter general aspects and related problems associated with determining appropriate reinforcing details using interlocking spirals as transverse reinforcement were first discussed. Then, the effectiveness of the interlocking spirals was considered using the results of the column tests conducted in this study. From these theoretical studies and experimental observations following conclusions are reached:

1. The amount of transverse reinforcement required for the confinement of core concrete in the potential plastic hinge region of a column can considerably be reduced by using interlocking spirals instead of rectangular hoops and supplementary cross-ties, when the amount of transverse reinforcement is determined by NZS 3101 code.

2. The local volumetric ratio of interlocking spirals in the extreme compression region of column section, ρ_{se} can become significantly less than the volumetric ratio ρ_s required for the case of single spirals, when it is determined following the normal code approach. This result affects the stress-strain relationship for confined core concrete. A proposal is made for an appropriate definition of the volumetric ratio of interlocking spirals for use in codes.

3. The shear carried by interlocking spirals can be estimated by a proposed method which considers the equivalent transverse reinforcement. This method is referred to as Method (2).

4. When the interlocking of spirals is weak, due to a small overlap distance between adjacent spirals, the load carrying capacity of the column can be estimated by the combined beam-arch action theory proposed in this study. However, the distance between adjacent spirals, d_{il}, should not be made inadequately large because the load carrying capacity and stiffness of the column under cyclic loading can rapidly decrease as a result. If an

inadequately large d_{il} needs to be adopted because of some architectural requirement, it is recommended that a proposed reinforcing detail be used in which ties are provided in addition to the interlocking spirals.

5. In order to determine an adequate overlap distance for the adjacent interlocking spirals an approach is proposed. This approach is based on the concept that the initial stiffness of interlocking must be secured by the concrete core in the interlocking area, since dowel action of the longitudinal bars to interlock the spirals can only be expected after cracking of the concrete. In the proposed approach, the interlocking concrete core is modelled by a concrete corbel under a particular loading condition and the sectional area of the corbel is determined to resist direct shear from spirals.

6. The amount of longitudinal bars required to interlock the spirals can be determined by using the shear friction method in a proposed modified form. However, it must be emphasized that the longitudinal bars become largely ineffective for such purpose when they yield due to column bending.

7. At least four longitudinal bars should be provided inside the interlocking area of the spirals in order to attain the suspension mode of resistance of the spirals suggested in this study. This is because the anchorage of the spirals can only be achieved by the suspension mode when local fracture of core concrete occurs.

8. The columns tested with interlocking spirals satisfied all of the above requirements and the checks. The behaviour of those columns under simulated severe earthquake loading was very satisfactory. That is, all the measured hysteresis loops displayed good energy dissipation and limited reduction in strength up to the end of the test at a displacement ductility factor μ of more than 10. Hence, it can be said that all the above requirements and the checks are adequate as far as the columns tested were concerned.

9. Yielding of interlocking spirals due to Poisson's effect of core concrete occurred at a displacement ductility factor μ of three to four in all tested columns and those spiral strains rapidly increased during further loading. Yielding of interlocking spirals due to shear began to occur at a displacement ductility factor μ of six or more but was not serious. Deterioration of the

horizontal load-displacement hysteresis loops due to the yielding of spirals was not obvious. This indicates that most of the yielding of the spirals was due to Poisson's effect of the core concrete, since the hysteresis loops normally deteriorate when transverse reinforcement yield due to shear.

10. The longitudinal bar strains measured by electric resistance wire strain gauges indicated rapid deterioration of bond between longitudinal reinforcement and concrete in the plastic hinge region of the tested columns. Based on this fact, the combined beam-arch action theory was applied to the tested columns. For the columns with interlocking spirals, the behaviour predicted by the combined beam-arch action theory showed good agreement with the test results.

11. Using the shear deformation model proposed here, the deformation mechanism that actually occurred in the tested columns was satisfactorily interpreted.

12. For the columns tested with an aspect ratio of 3, the shear deformation defined in this study reached 10 to 30 % of the column deflection and this ratio was almost constant from displacement ductility factor $\mu = 0.75$ to the final stage of loading where μ of more than 8 was applied. This indicates that the deflection of a column cannot always be predicted by curvature distribution found assuming that plane sections remain plane within acceptable error. It is suggested that for a column with aspect ratio of 3, when the theoretical column deflection is calculated based on curvature distribution, the calculated column deflection needs to be increased by about 20 % or more to take shear deformations into account.

CHAPTER FIVE

BUCKLING MODEL FOR LONGITUDINAL REINFORCEMENT

5.1 INTRODUCTION

In seismic design codes for reinforced concrete structures, the minumum spacing of transverse reinforcement has normally been specified not only to provide shear capacity of a member and to confine the core concrete in potential plastic hinge region but also to prevent premature buckling of longitudinal reinforcement. Premature buckling means either elastic buckling or inelastic buckling which occurs at an early stage of inelastic loading on the member. That is, in order to provide reinforced concrete members with adequate ductility, it is essential to prevent or sufficiently delay buckling of longitudinal reinforcement by limiting the spacing of transverse reinforcement. For example, the NZS 3101 code: 1982 [5.1] requires hoop sets to be spaced no farther apart six times the longitudinal bar diameter in the potential plastic hinge region of columns. As another example, in the case of the ACI code: 318-89 [5.2], closed ties are required to be spaced no farther apart than eight times the longitudinal bar diameter in the potential plastic hinge region of beams. In the ACI code it is considered that for columns the spacings of hoop sets are normally governed by the requirements to provide adequate confinement of the core concrete and to prevent shear failure.

It must be noted that in the above codes the minimum spacing of transverse reinforcement specified to prevent the premature buckling of longitudinal reinforcement have normally been determined implicitly, assuming that the restraint by transverse reinforcement is strong enough to ensure that longitudinal bars buckle between hoop or stirrup sets, with each longitudinal bar acting as a fixed-fixed column. Hence, when restraint against movement of longitudinal reinforcement, provided by transverse reinforcement, is too weak to generate such assumed mode of buckling, those specified minimum spacings of transverse reinforcement become inadequate. As mentioned in Chapter three, in order to make the fixing of cross ties to longitudinal bars easier, the ACI code:318-89 [5.2] and the

Caltrans code:1983 [5.3] have introduced the alternative anchorage detail for cross ties shown in Figs. 3.2 (b) and 3.11. The 90° end hooks and 135° end hooks of the cross ties are alternated along longitudinal bars in order to avoid the consecutive alignment of 90° end hooks foming weak lines of anchorage along the longitudinal bars. The efficiency of cross ties anchored by 90° end hooks may be suspect because the 90° end hooks could be straightened by the outward forces from the core concrete and the buckled longitudinal bars after spalling of the cover concrete. For this reason, the effectiveness of the transverse reinforcing details shown in Fig. 3.11 has been investigated by several experimental studies including the study conducted for this thesis. However, the conclusions reached in those studies were not always consistent (see Chapter three). The inconsistency of the conclusions of those studies may be attributed to the difference in types of loading, the different volumetric ratios of the transverse reinforcement to the concrete core, spacings of hoop sets, ratios of compression reinforcement restrained by 90° end hook to the total compression reinforcement, and so on. Hence, to obtain a more consistent assessment of the effectiveness of the above transverse reinforcing details, it is necessary to conduct theoretical studies which can reveal aspects unseen in experiments or can confirm the experimental evidences.

The main objective of this present study conducted for this chapter is to theoretically assess the effectiveness of the transverse reinforcing details shown in Figs. 3.2 (b) and 3.11 as restraint against buckling of longitudinal reinforcement. For this purpose, analytical models to investigate the buckling behaviour of an intermediate longitudinal bar restrained by peripheral hoops and cross ties with 90° and 135° end hooks are proposed. Moreover, a method to check whether premature buckling of longitudinal reinforcement using this type of lateral reinforcement details can occur or not is also proposed for use in practical design.

5.2 REVIEW OF PREVIOUS RESEARCH

5.2.1 Classic Theories of Inelastic Buckling

With respect to elastic buckling theory, Euler [5.4] developed the formula expressed by Eq. 5.1 more than 200 years ago, and it is still very much in use.

$$P_{ecr} = \frac{\pi^2 E I}{L^2} \quad \text{.....} \quad (5.1)$$

where P_{ecr} = the Euler load
E = the modulus of elasticity
I = the moment of enertia of the cross section of column
L = the length of column between the hinged-ends

Modifications in the Euler formula to adapt it to the inelastic range of metal behaviour came between 1889 and 1910 with the development of the tangent modulus theory [5.5] and the double-modulus theory (or referred to as the reduced modulus theory) [5.6, 5.7]. In 1889, Engesser [5.5] suggested that if column failure occurred at a stress above the elastic limit of the material, the column strength could be obtained by simply replacing E by E_t, the tangent modulus, in the Euler formula expressed by Eq. 5.1 (see Fig. 5.1 (b)). However, he recognized that the theoretical contradictions involved in the tangent modulus theory and, in 1895, suggested that the substitution for E in the Euler formula should not be by E_t, but by a 'reduced' modulus E_r, intermediate between E and E_t. It is evident that, when an axially loaded column begins to bend at the tangent modulus load, there are corresponding increases and decreases in compressive strain toward the concave and convex sides, respectively, of the bent column. Hence, the reversal strain in the convex side will unload following the elastic modulus E, whilst the compressive strain in the concave side will continue to increase following the tangent modulus E_t (see Fig. 5.1 (c)). By considering force and moment equilibrium across the section, the equivalent reduced modulus, E_r, can be determined for any given section shape. In 1910, von Kármán [5.7] derived an explicit solution for E_r for a rectangular section as

$$E_r = \frac{4 E E_t}{(\sqrt{E} + \sqrt{E_t})^2} \quad \text{.....} \quad (5.2)$$

Shanley [5.8] clarified the conceptual significance of these theories in 1947 and also showed that, after initial deflection at the tangent-modulus load, a theoretical maximum load would be reached between the tangent-modulus and the reduced-modulus loads [5.9]. That is, Shanley suggested that the

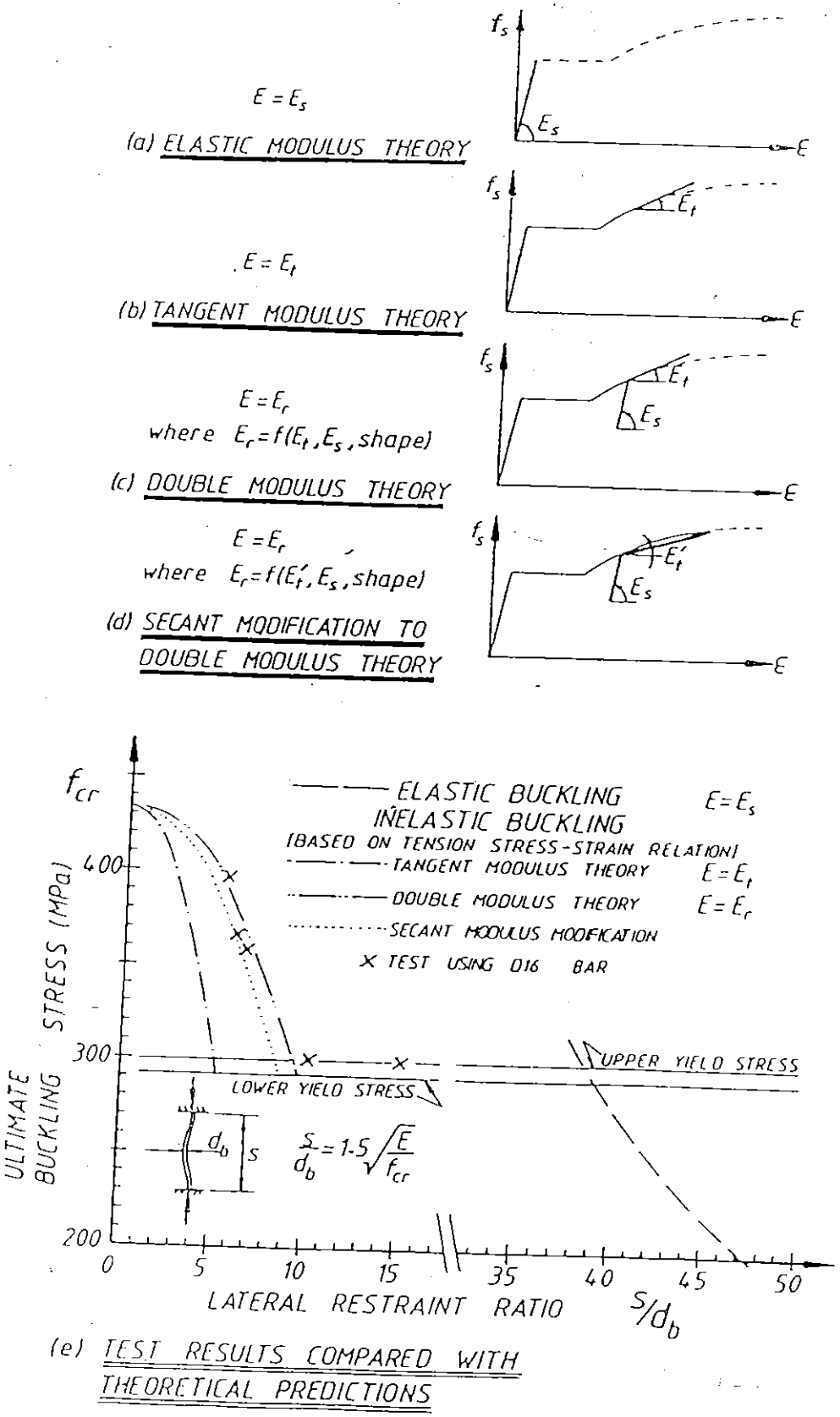

Fig. 5.1 Inelastic Buckling Theories and Test results Obtained in the Study by Mander et al [5.10].

tangent modulus theory and the reduced modulus (= double modulus) theory would give the lower and the upper bounds, respectively, for the buckling load.

The following studies conducted to clarify the inelastic buckling behaviour of longitudinal reinforcement basically used those classical inelastic buckling theories.

5.2.2 Previous Studies at University of Canterbury

Mander, Priestley and Park [5.10], University of Canterbury, investigated inelastic buckling behaviour of longitudinal reinforcement by conducting axial compression tests on 16 mm diameter Grade 275 deformed reinforcing bars with various support length. The test results are shown in Fig. 5.1 (e) compared with the theoretical predictions. In those tests, some of the measured buckling stresses lie somewhere between the buckling stresses predicted by the tangent-modulus and reduced modulus theories as suggested by Shanley [5.8], although some other results agree well with the solution by the double modulus theory.

Based on the above experimental observations, Mander, Priestley and Park proposed a secant modification to the double modulus theory, considering the practical situation of the longitudinal reinforcement in the compression zone of reinforced concrete columns. Because the double modulus theory uses only the instantaneous tangent modulus for the concave side of the buckled bar, as depicted in Fig. 5.1 (c), sudden buckling on reaching the double modulus stress is implied together with very small curvature. However, it may be more realistic to consider that the section of the longitudinal bar has a steeper strain gradient, that is, a larger curvature at ultimate buckling load, than that assumed in the double modulus theory. Fig. 5.1 (d) shows a secant modulus of elasticity E_t' calculated between two stress-strain coordinates separated by a probable strain variation of say ε_{sh}, where ε_{sh} = steel strain at the commencement of strain-hardening. They recommended that such a secant modulus of elasticity E_t' be used instead of the instantaneous tangent modulus to determine the reduced modulus E_r.

It is noted that the objective of the above study by Mander, Priestley and Park was to determine the maximum spacing of the transverse reinforcement which would prevent longitudinal reinforcement from buckling until reaching a particular ultimate compressive steel strain which was to be determined in terms of the ductility of reinforced concrete members required in the seismic design. Fig. 5.2 (a) [5.11] shows an idealized mechanical model of the interaction between the compressed longitudinal bar, the supporting core concrete and the hoops or spirals in the plastic hinge region of a reinforced concrete column. If it can be assumed that the compressed longitudinal bar is strongly restrained by stiff hoops and that lateral pressure from the ineffectively confined core concrete between hoops is negligible, the model in Fig. 5.2 (a) may be further simplified to that of a bar of length s with full rotational and lateral fixty at both ends, as shown in Fig. 5.2 (b) [5.11]. For the case of the compressed bar fully fixed at both ends shown in Fig. 5.2 (b), the effective buckling length becomes $\frac{s}{2}$ due to double curvature imposed and hence the critical stress f_{cr}, for the Euler case expressed by Eq. 5.1, is then given by

$$f_{cr} = \frac{4\pi^2}{s^2}\frac{EI}{A_s} \qquad \text{.....} \qquad (5.3)$$

where A_s = area of steel bar section

The radius of gyration r is defined as

$$r = \sqrt{\frac{I}{A_s}} \qquad \text{.....} \qquad (5.4)$$

Therefore from Eq. 5.3 the slenderness ratio is

$$\frac{s}{r} = 2\pi\sqrt{\frac{E}{f_{cr}}} \qquad \text{.....} \qquad (5.5)$$

For a circular section with a diameter d_b, the radius of gyration is

$$r = \frac{d_b}{4} \qquad \text{.....} \qquad (5.6)$$

However, deformed reinforcing bars which are normally used for longitudinal reinforcement are not truly circular. Hence, by measuring the actual sectional dimensions of the deformed bars tested, Mander et al found that

$$r = 0.955 \frac{d_{bn}}{4} \quad \text{.....} \quad (5.7)$$

where d_{bn} = nominal bar diameter of the deformed bar

They indicated that, by substituting Eq. 5.7 into Eq. 5.5, the ratio of lateral support spacing for a reinforcing bar in double curvature became

$$\frac{s}{d_{bn}} = 1.5 \sqrt{\frac{E}{f_{cr}}} \quad \text{.....} \quad (5.8)$$

If it is required that buckling of longitudinal bars in the plastic hinge region of reinforced concrete column be prevented until the strains in those bars reach the inelastic range, the maximum spacing of hoops is obtained by replacing E by adequately determined E_r. That is,

$$\frac{s}{d_{bn}} = 1.5 \sqrt{\frac{E_r}{f_{cr}}} \quad \text{.....} \quad (5.9)$$

Using Eq. 5.9, Mander et al have also shown that the maximum hoop spacing to prevent longitudinal bars from buckling becomes approximately six times d_{bn}, as specified in the NZS 3101 code [5.1], for E_r and f_{cr} at compressive strain of 0.05 which were determined from a stress-strain relationship measured on a 16 mm diameter Grade 275 deformed reinforcing bar. In this calculation, the reduced modulus E_r was determined using the elastic modulus E and the secant modulus E_t' expressed by

$$E_t' = \frac{[f_{su} - f(\varepsilon_{su} - \varepsilon_{sh})]}{\varepsilon_{sh}} \quad \text{.....} \quad (5.10)$$

where f_{su} = ultimate strength of steel

$f(\varepsilon_{su} - \varepsilon_{sh})$ = steel stress at strain of $(\varepsilon_{su} - \varepsilon_{sh})$

ε_{su} = steel strain at the ultimate strength
ε_{sh} = steel strain at the commencement of strain-hardening

Zahn, Park and Priestley [5.11] extended the above study conducted by Mander et al as follows. The maximum expected compressive strains, ε_{suc}, will vary in accordance with the intensity of ducitility required for a column and with the grade of steel used for the longitudinal reinforcement. For various maximum expected compressive strains, ε_{suc}, the minimum hoop spacings s/d_{bn} necessary to control bar buckling can be determined by solving Eq. 5.9. In this determination the corresponding steel stresses from the monotonic tension stress-strain curve were substituted for f_{cr}. By plotting the results of these calculations for a range of ε_{suc} they obtained Figs. 5.3 (a) and 5.4 (a) for Grade 275 deformed bars and for Grade 380 deformed bars, respectively. Figs. 5.3 (b) and 5.4(b) show the corresponding ratios of the buckling stress to the yield strength, notated f_{suc}/f_y. For each steel type two cases were considered. For case 1 the guaranteed yield strength (275 MPa and 380MPa), an average ultimate tensile strength, f_{su}, and average strain hardening tangent modulus, E_{sh}, were assumed. The material properties assumed in the calculations for case 2 were the average yield strength, the average ultimate tensile strength and the lowest value for E_{sh}. Those were based on the data obtained from monotonic tension tests on Grade 275 and 380 defomed bars with various diameters which were carried out at University of Canterbury between 1978 to 1985. A linear expression was chosen to represent a lower bound for the strains and stresses calculated for the two cases, and the increase of the buckling stress and strain for s/d_{bn} <4 was neglected. Unfortunately, in the reference [5.11] it is not stated how the reduced modulus E_r in Eq. 5.9 was determined to draw Figs. 5.3 and 5.4. If the used test data involved the complete stress-strain relationships of those bars, or were sufficient to model the stress-strain relationships of those bars, the secant modulus of elasticity E_t' for each ε_{suc} might have been calculated between two stress-strain coordinates separated by a strain of ε_{sh}, following the method proposed by Mander et al [5.10]. If not, the average strain hardening tangent modulus, E_{sh}, and the lowest value for E_{sh} may have been directly used as the secant modulus E_t' for case 1 and case 2, respectively, regardless of the magnitude of ε_{suc}.

Thus, for design practice the minimum hoop spacings s/d_{bn} necessary to control bar buckling were determined in those studies conducted at

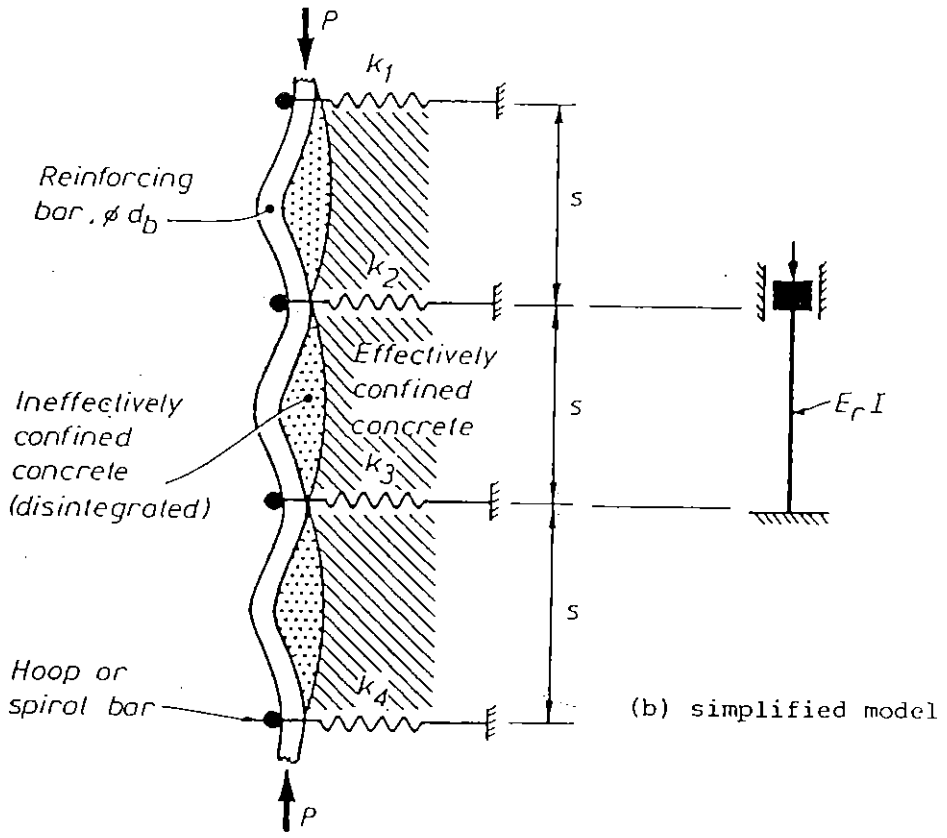

Fig. 5.2 Mechanical Models for Buckling of a Longitudinal Bar Braced by Hoops or Spirals [5.11].

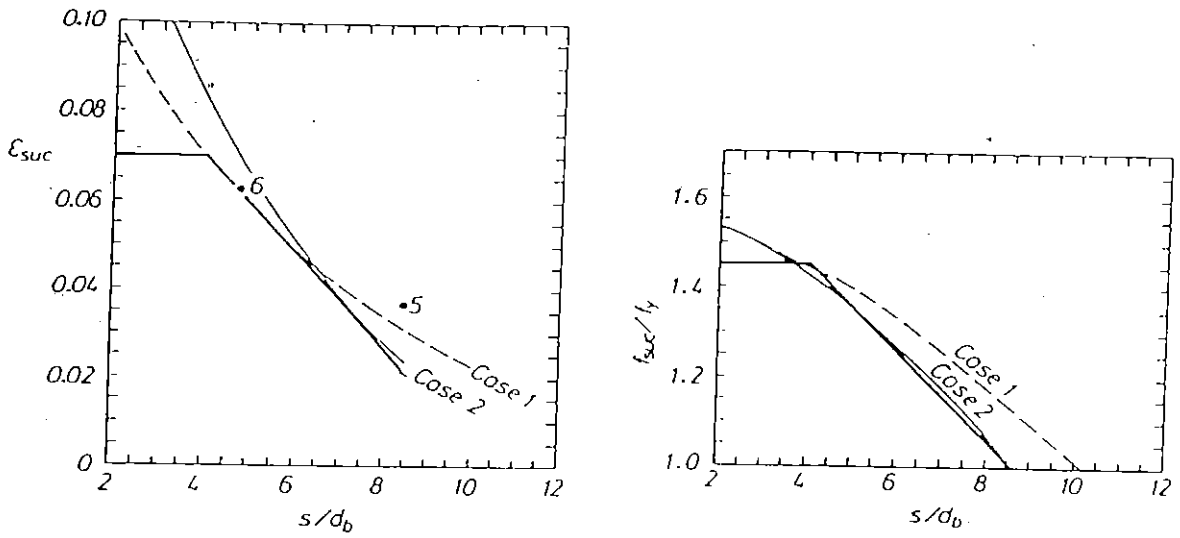

Fig. 5.3 Grade 275 Steel - Ultimate Compressive (Buckling) Strain and Stress of Reinforcing Bars with Diameter d_b versus Hoop or Spiral Bar Spacing Along the Column Axis [5.11].

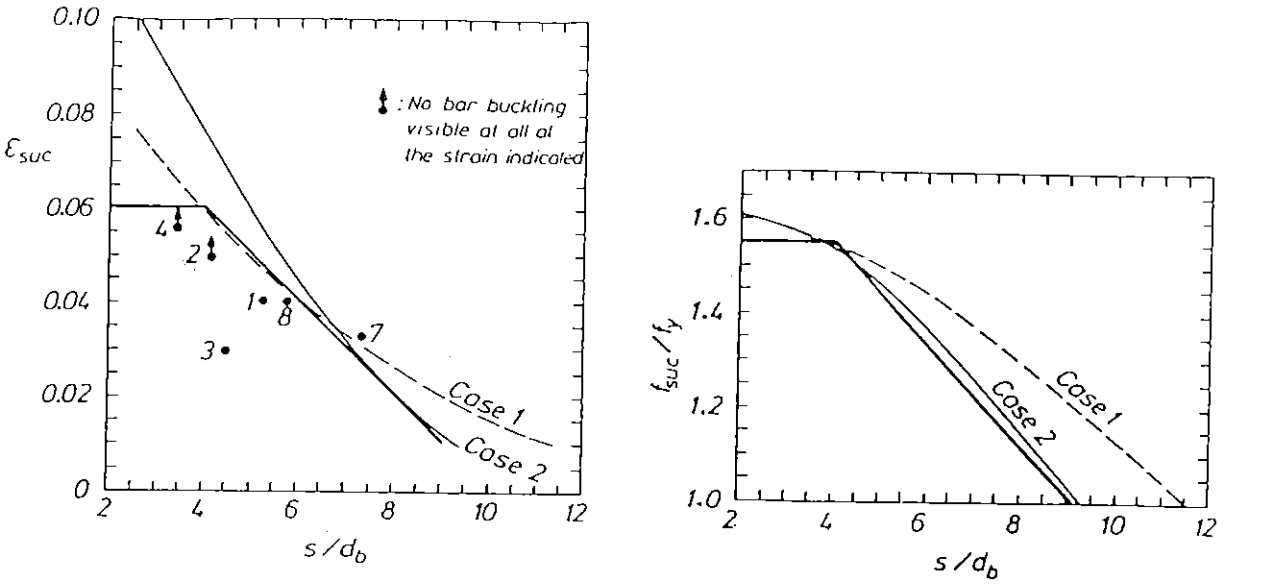

(a) Theoretical and Experimental Buckling Strain (Test Units 1 to 4 and 7, 8)

(b) Theoretical Buckling Stress to Yield Strength Ratio

Fig. 5.4 Grade 380 Steel - Ultimate Compressive (Buckling) Strain and Stress of Reinforcing Bars with Diameter d_b versus Hoop or Spiral Bar Spacing Along the Column Axis [5.11].

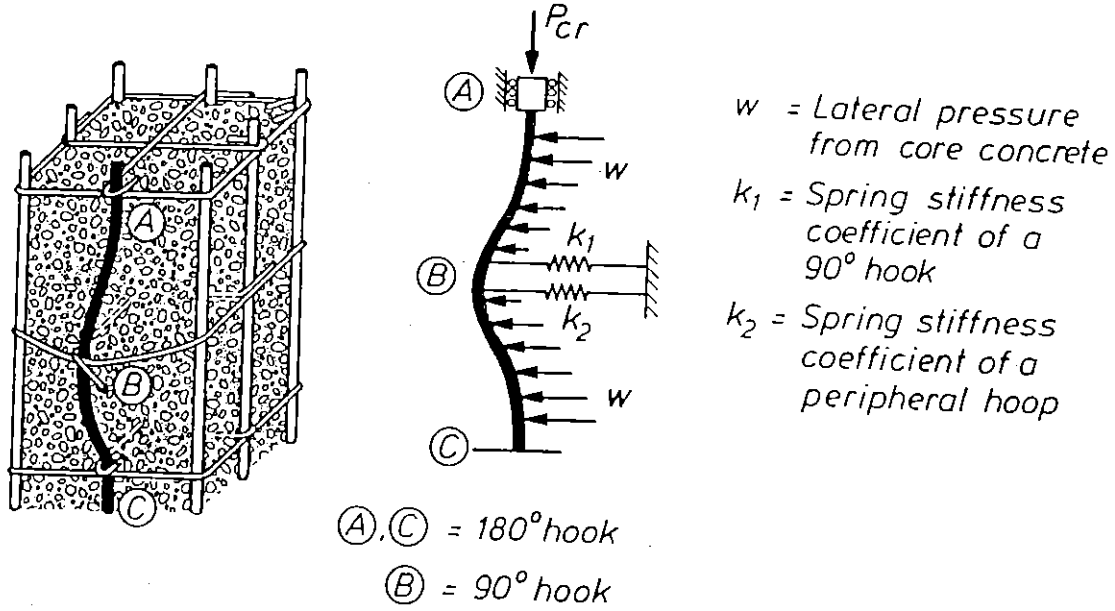

(a) Buckling Mode

(b) Buckling Model

Fig. 5.5 Buckling of Intermediate Longitudinal Bar Restrained by Cross Ties with 90° and 135° or 180° End Hooks Alternating along Column.

University of Canterbury. However, it should be noted that the results of those studies may not always give adequate minimum hoop spacings to control longitudinal bar buckling as expected. This is because in those studies it was assumed that longitudinal reinforcement was completely fixed at the position of hoop sets with respect to rotation and lateral displacement and that the lateral pressure from the ineffectively confined core concrete between hoops had a negligible effect on the buckling of longitudinal reinforcement. However, when the cover concrete spalls over several hoop spacings in the plastic hinge region of a member and yielding of transverse reinforcement spreads over that region, longitudinal reinforcement can buckle in a mode shape that spans several hoop spacings as can be seen from Figs. 4.47 to 4.50 in Chapter four. For this type of buckling, analytical and experimental study conducted by Scribner [5.12] is notable, although that study focussed on the buckling behaviour of intermediate longitudinal bars restrained only by perimeter stirrups, without cross ties hooked around, in beams. Also, lateral pressure from the ineffectively confined core concrete between hoops may not be negligible when longitudinal reinforcement is compressed far into inelastic range and hence when the bending stiffnes of longitudinal reinforcement is significantly reduced. In the following study conducted for this thesis, lateral pressure from the ineffectively confined core concrete between hoop sets, and the actual stiffness of perimeter hoops and the hooks of cross ties as restraint of longitudinal bar buckling, were taken into account.

5.3. BUCKLING OF AN INTERMEDIATE LONGITUDINAL BAR RESTRAINED BY PERIMETER HOOPS AND CROSS TIES WITH 90° AND 135° END HOOKS

5.3.1 A Buckling Model for an Intermediate Longitudinal bar Restrained by Cross Ties with 90° and 135° End Hooks

If cross ties with 90°end hooks at one end and 135° or 180° end hooks at the other end are provided in a reinforcing cage, with these end hooks alternating along the intermediate longitudinal bars, buckling of the intermediate longitudinal bars may eventually occur over two spacings of hoop sets with the largest lateral deflection at the position of the 90° end

hooks as shown in Fig. 5.5 (a). This is because after spalling of cover concrete the restraint by the 90° end hooks against the buckling of the longitudinal bar becomes much weaker than that by the 135° or 180° end hooks which are embedded in the core concrete and as a result the longitudinal bar can easily deflect at the position of the 90°end hook. In fact, this type of deformation of the intermediate longitudinal bars was observed with opening out of the 90° end hooks in several column tests (see Fig. 5.6) and can be considered as the most probable mode of buckling when such type of lateral reinforcement detail is used.

Based on the above observation, the intermediate longitudinal bar was modelled as shown in Fig. 5.5 (b) in order to analyze the buckling behaviour . In the model, the intermediate longitudinal bar was assumed to be completely restrained against rotation and lateral movement at the points (A) and (C) of each 135° or 180° end hook. At the point (B), the 90° end hook and the peripheral hoop were represented by springs with stiffnesses of k_1 and k_2 respectively. It should be noted that this model can be adequate only in case when the spring stiffness of the cross ties with 135° or 180° end hooks is considerably larger than that of the 90°end hooks. The spring stiffness of the cross ties with 135° or 180° end hooks may be governed by the bond condition along their tie legs rather than the bending stiffness of those end hooks embedded in the core concrete. A method to estimate the stiffness of the cross ties with 135° or 180° end hooks is introduced in Section 5.3.8. If it is considered that the spring stiffness of the cross ties with 135° or 180° end hooks is not large enough to apply the above assumption, points (A) and (C) also need to be restrained by suitable spring models. However, the spring stiffnesses of the cross ties with 135° or 180° end hooks are normally large enough to consider the above assumption adequate.

The longitudinal bars in a reinforced column are normally subjected to not only axial load but considerable lateral pressure from the core concrete under severe earthquake loading. The axial load in the longitudinal bars are caused by both the axial load and the bending moment applied to the column. The lateral pressure along the longitudinal bars is due to the lateral expansion of the core concrete referred to as Poisson's effect. Hence, in the consideration of the buckling of those longitudinal bars the following two factors need to be taken into account in addition to

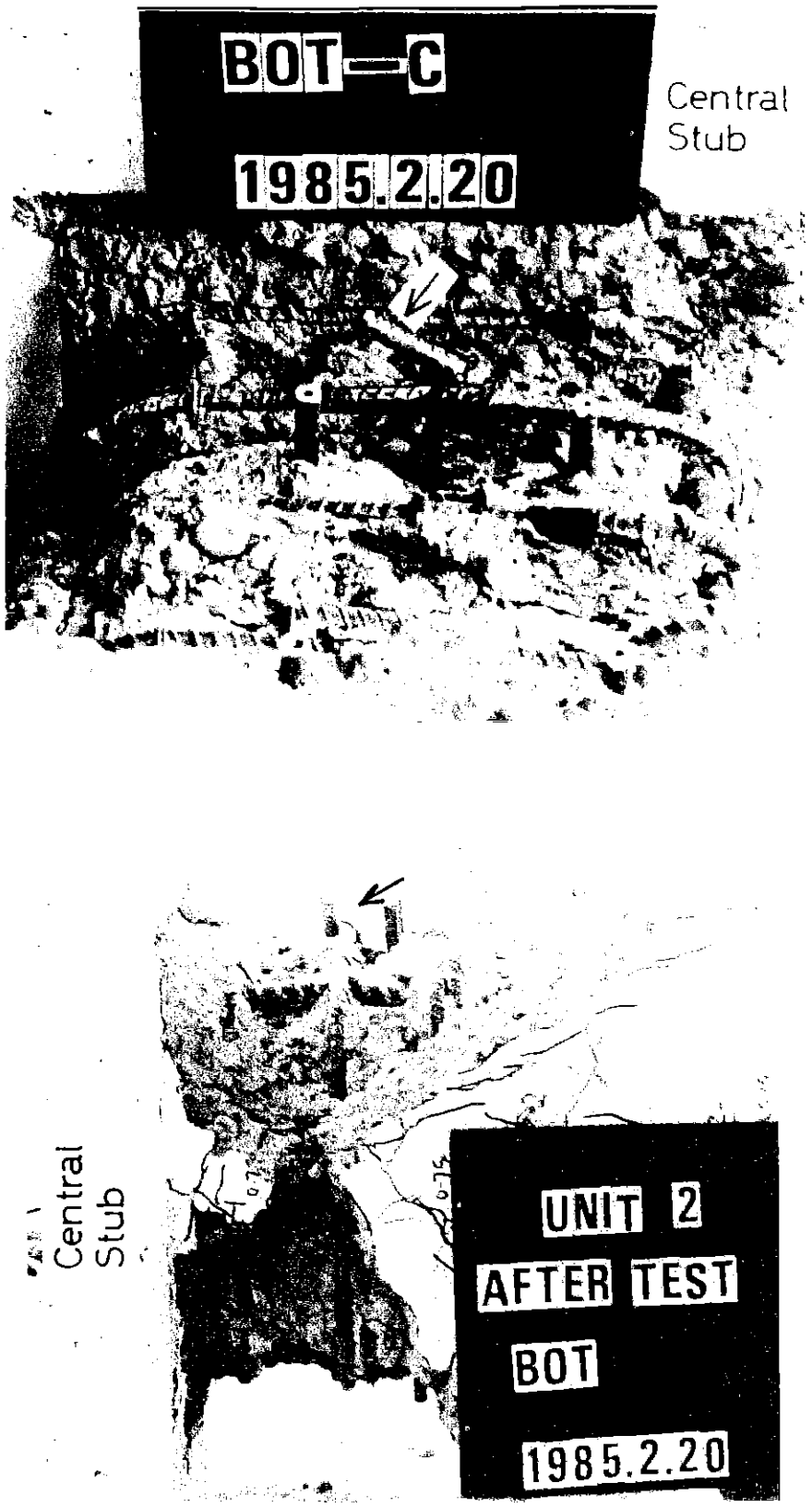

Fig. 5.6 Buckling of Intermediate Longitudinal Bar with Opening Out of 90° End Hook [5.14].

the ordinary factors such as the slenderness ratio, end restraint condition and so on.

(1) The magnitude and the distribution of the lateral pressure imposed on the longitudinal bar from the core concrete.

(2) The inelastic moment of resistance of the longitudinal bar under high axial compression which may already have reached the strain hardening condition by axial compression only. This factor has a significant influence.

To deal with the above factors, the following three stages of deformation and loading conditions in the intermediate longitudinal bar were considered. These stages are schematically shown in Fig. 5.7. In the figure, the definition of a plastic hinge is where the longitudinal bar section has reached the maximum inelastic moment of resistance including strain hardening of steel. As a matter of course, the presence of an axial load in the longitudinal bar reduces the maximum moment of resistance of the bar section and was therefore taken into account in the following analysis. Each stage can be described as follows.

Stage(1): At small lateral deflection of the intermediate longitudinal bar ,

(a)The longitudinal bar has not developed a plastic hinge although it may have already yielded longitudinally by high axial compression due to the combined axial load and bending moment applied to the column.

(b)The lateral pressure from the core concrete is uniformly distributed along the longitudinal bar.

(c)The 90° end hook works as an elastic brace.

(d)The bracing effect of the peripheral hoop crossing over the longitudinal bar may be negligible.

Stage(2): At large lateral deflection of the intermediate longitudinal bar,

(a)The longitudinal bar has developed two plastic hinges at both ends restrained by 135° or 180° end hooks.

(b)The lateral pressure from the core concrete commences to concentrate at the position of the 135°or 180° end hooks.

(c)The 90° end hook works as an elastic brace or an inelastic brace.

(d)The bracing effect of the peripheral hoop may still be negligible or slightly noticeable.

Stage(3): At the final deflected condition of the longitudinal bar,

(a)Another plastic hinge has been generated in the longitudinal bar at mid-span in addition to at the both ends.
(b)The lateral pressure from the core concrete becomes more concentrated at the position of the 135°or 180° end hooks.
(c)The 90° end hook works as an elastic brace or as an inelastic brace.
(d)The peripheral hoop may become effective.

5.3.2 Definition of Buckling

It is of importance to define what is meant by buckling of the longitudinal bar in this study. In general, the buckling is defined as a state of unstable equilibrium for a compression member. A state of unstable equilibrium may be expressed as when the member suddenly bows out sideways by changing its state of velocity after reaching a certain critical load [5.13]. In case of a steel column subjected to axial load, commencement of lateral deflection usually leads to its entire collapse because there is no way to stop increasing lateral deflection unless the axial load is reduced. This is a typical example of a state of unstable equilibrium. Hence, for a structural steel column lateral deflection must be avoided as far as possible. From this point of view, a buckling check using infinitesimal deformation theory is normally adequate.

On the contrary, it is hard to elucidate a state of unstable equilibrium for the longitudinal reinforcement in a reinforced concrete member, especially when the core concrete is well confined by closely spaced transverse reinforcement. The combined lateral pressure and axial load on the longitudinal bar may give rise to a significant lateral deflection in the longitudinal bar. However, this lateral deflection in the longitudinal bar does not always mean a state of unstable equilibrium. In fact it has been observed that the commencement of lateral deflection in the longitudinal compression bars did not result in a rapid increase of the bar deflection or in serious degradation of load carrying capacities in reinforced concrete columns where the amounts of lateral reinforcement were adequate [5.14]. Two explanations can be considered for the reason why the load carrying capacities of those columns could be maintained in spite of the occurrence of lateral deflection in the longitudinal bars. One is that the axial forces in the laterally deflected longitudinal bars were not reduced due to the bracing

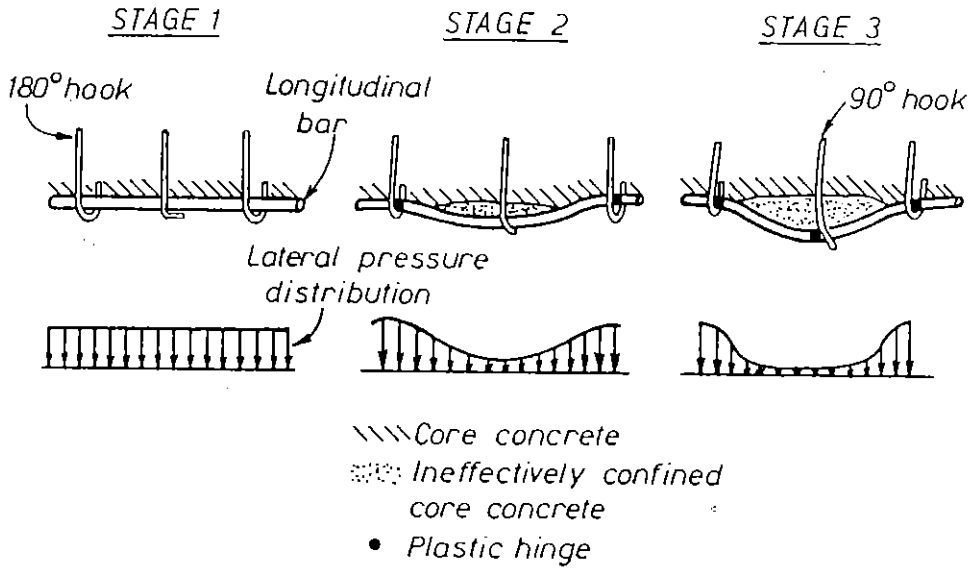

Fig. 5.7 Change of Lateral Pressure Distribution along Longitudinal Bar with Progress of Lateral Deflection of Longitudinal Bar.

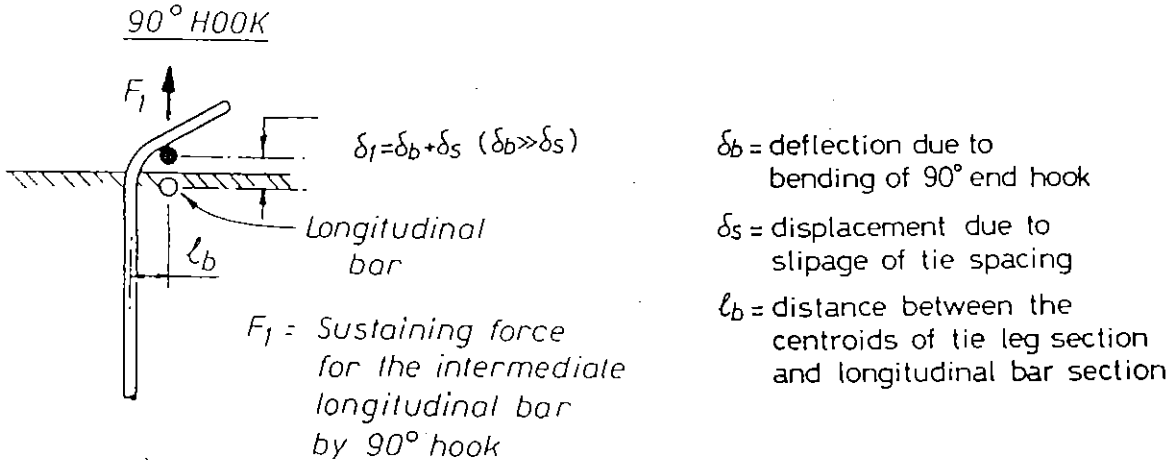

Fig. 5.8 Deflection Due to Opening of a 90° End Hook Caused by Outward Force from a Intermediate Longitudinal Bar.

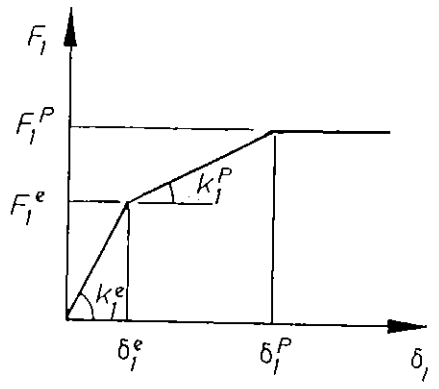

Fig. 5.9 Spring Model of 90° End Hook.

effect of the transverse reinforcement. The other is that a certain reduction of axial stress in each deflected longitudinal bar actually occurred but was compensated by a stress increase in the well confined concrete.

In this study, the buckling of a longitudinal bar is defined as a sudden increase in the lateral deflection of the longitudinal bar associated with a rapid decrease in the axial stress in it. Hence, if the stress reduction in the longitudinal bar under increasing lateral deflection is small or negligible, because of the bracing effect of the transverse reinforcement, such a condition of the longitudinal bar is not considered as buckling in this study.

However, it must be noted that the lateral deflection of the longitudinal bar needs to be limited to as small as possible, even if the axial stress in the bar is maintained by the bracing effect of the transverse reinforcement. This is because a large lateral deflection of the longitudinal bar leads to the departure of both longitudinal bar and the transverse reinforcement from the concrete core surface and thus results in their loss of confining effect on the core concrete. From this point of view, the magnitude of the lateral deflection of the longitudinal bar in each of the stages mentioned above was also determined in the following analyses.

5.3.3 Spring Models for a 90° End Hook and a Peripheral Hoop

The relation between the outward force applied to the 90° end hook by the longitudinal bar, F_1, and the corresponding displacement of the 90° hook at the contact point with the longitudinal bar, δ_1, is illustrated in Fig. 5.8. δ_1 can be expressed as the sum of δ_b and δ_s, where δ_b is the deflection of 90° hook due to bending and δ_s is displacement of 90° end hook due to slippage of the tie leg from the core concrete. In this study, δ_s was neglected because δ_s can be considered negligibly small compared with δ_b, especially when deformed bars are used for tie bars. The slippages of the peripheral hoop legs have also been neglected in this study. This matter is discussed in Section 5.3.8.

The spring characteristic k_1 representing the 90° end hook was modelled as shown in Fig. 5.9. In the figure, δ_1^e indicates the the 90° hook deflection (at the contact point with the longitudinal bar) when the moment at the bent corner of the 90° hook reaches the maximum elastic moment of

resistance of the hook bar, M_e^t. δ_1^p indicates the 90° hook deflection where extreme fiber strain at the bent corner of the 90° end hook reaches the steel strain at commencement of strain-hardening, ε_{sh}. The moment of resistance at deflection of δ_1^p, which is denoted by M_p^t, is represented by the full plastic moment of the bar section. F_1^e and F_1^p denote the outward forces applied to the 90° hook by the longitudinal bar at deflections of δ_1^e and δ_1^p, respectively. During further deflection of the 90°end hook, it is assumed that F_1 is constnt at F_1^p. That is, the increase of inelastic moment of resistance due to strain hardening is neglected. In the following calculations, it was also assumed that the reduction of the moment resistance of the tie bar due to the presence of axial tension is small enough to be neglected because F_1^e and F_1^p are normally far below the yield force of the tie bar.

The elastic moment of resistance of the 90° end hook section, M_e^t, can be written as,

$$M_e^t = f_{yt} Z = f_{yt} \frac{\pi d_b^3}{32} \quad \text{.....} \quad (5.11)$$

where f_{yt} = yield strength of tie bar steel
Z = elastic section modulus
d_b= tie bar diameter

For equilibrium, $M_e^t = F_1^e \cdot l_b$, where l_b = distance between the centroids of the tie leg section and the longitudinal bar section (see Fig. 5.8). Hence,

$$F_1^e = \frac{M_e^t}{l_b} = f_{yt} \frac{\pi d_b^3}{32 l_b} \quad \text{.....} \quad (5.12)$$

Using this F_1^e, δ_1^e can be calculated as

$$\delta_1^e = \frac{F_1^e l_b^3}{3EI_t} \quad \text{.....} \quad (5.13)$$

where E = Young's modulus of steel
I_t = moment of inertia of the tie bar section

Hence, the initial stiffness of the 90° end hook, k_1^e, can be calculated as

$$k_1^e = \frac{F_1^e}{\delta_1^e} = \frac{3 E I_t}{l_b^3} \quad \text{.....} \quad (5.14)$$

In case of a round bar, M_p^t can be approximated as 1.7 M_e^t based on the ratio of plastic section modulus to the elastic section modulus. Hence,

$$F_1^p = 1.7\, F_1^e \quad \text{.....} \quad (5.15)$$

In order to calculate δ_1^p , the bending moment and curvature distribution of the 90° hook and the corresponding stress-strain relation of the tie bar were assumed as shown in Fig. 5.10. Accordingly, δ_1^p can be expressed as follows.

$$\delta_1^p = \int_0^{0.59 l_b} \phi_1(x)\, x\, dx + \int_{0.59 l_b}^{l_b} \phi_2(x)\, x\, dx$$

$$= \int_0^{0.59\ l_b} \frac{F_1^p\, x^2}{E I_t}\, dx + \int_{0.59\ l_b}^{l_b} \frac{1}{d_b}\left[2\,\varepsilon_y + \frac{2(\varepsilon_{sh} - \varepsilon_y)}{0.41\, l_b} (x - 0.59\, l_b) \right] x\, dx$$

$$= \frac{F_1^p\, (0.59\, l_b)^3}{3 E I_t} + \frac{1}{d_b}\left[(4.88\,\varepsilon_y - 2.88\,\varepsilon_{sh}) \frac{x^2}{2} + \frac{4.88\,(\varepsilon_{sh} - \varepsilon_y)}{l_b} \frac{x^3}{3}\right]_{0.59\ l_b}^{l_b} \quad \text{... (5.16)}$$

where ε_y = yield strain of tie bar steel

ε_{su} = strain at the ultimate strength of tie bar steel

$\phi_1(x)$, $\phi_2(x)$ =assumed curvature distribution along the 90° hook at x from free end

Using the values calculated above, the stiffness of the 90° end hook at lateral deflections of longitudinal bar between δ_1^e and δ_1^p can be written in the form

$$k_1^p = \frac{F_1^p - F_1^e}{\delta_1^p - \delta_1^e} \quad \text{.....} \quad (5.17)$$

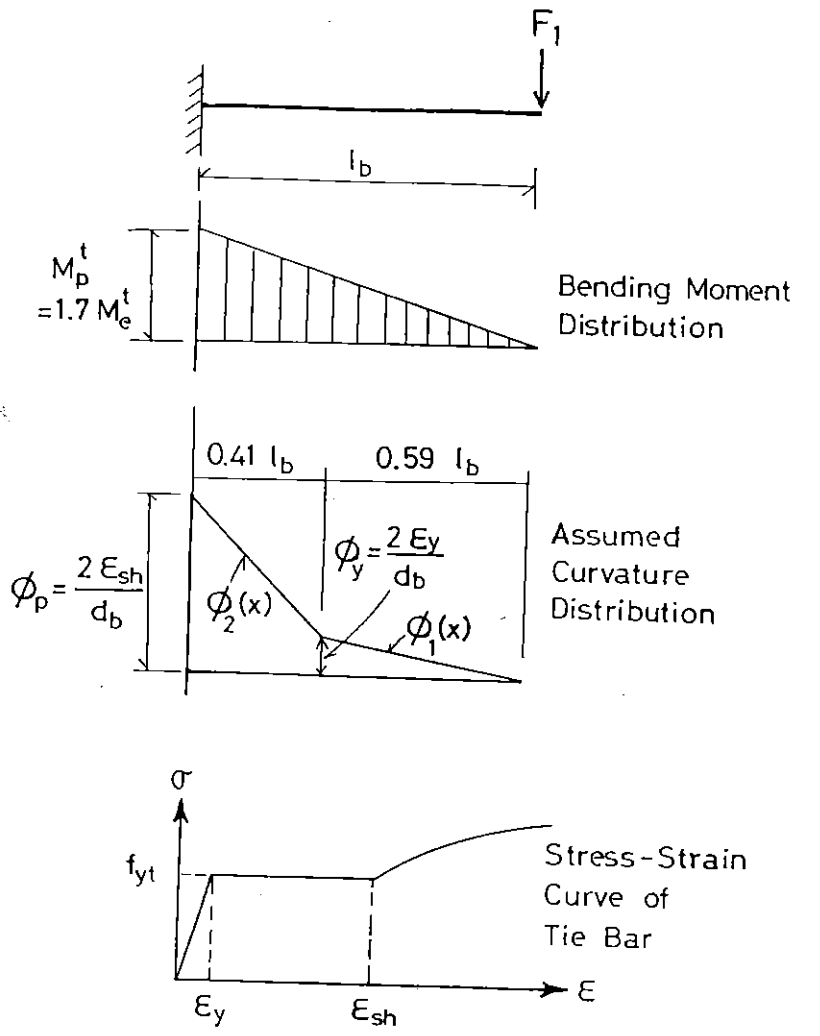

Fig. 5.10 Bending Moment and Assumed Curvature Distribution Along End of 90° Hook, and Stress-Strain Curve Used to Calculate Deflection of 90° End Hook in Inelastic Range of Steel.

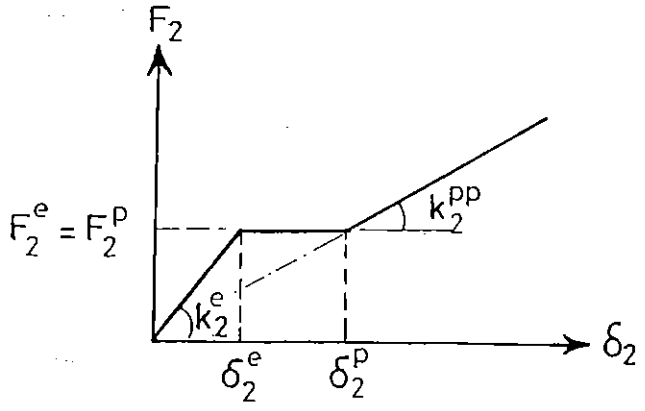

Fig. 5.11 Spring Model for Peripheral Hoop when $K_2^e > K_2^{pp}$

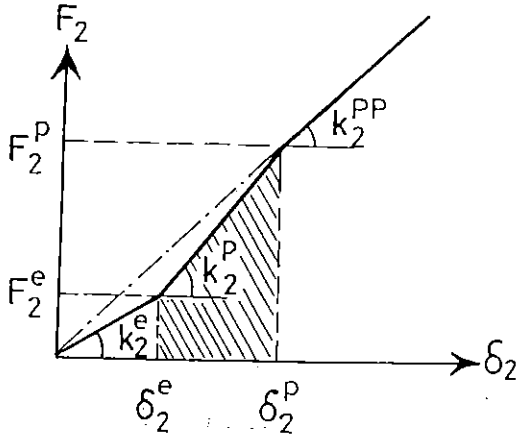

Fig. 5.12 Spring Model for Peripheral Hoop when $K_2^e < K_2^{pp}$

A spring model for the peripheral hoop which crosses over the intermediate longitudinal bar at the position of the 90° end hook is shown in Figs. 5.11 and 5.12. To determine the initial stiffness of the peripheral hoop against the lateral movement of the intermediate longitudinal bar, it is assumed that the tension force generated in the hoop bar is much smaller than its yield force until flexural plastic hinges have formed at both ends and at the centre of the peripheral hoop bar. This assumption means that the lateral pressure from the core concrete and the outward force from the intermediate longitudinal bar mainly work to bend the hoop bar until those yield hinges are generated.

In Figs. 5.11 and 5.12, δ_2 and F_2 denote the central deflection of the peripheral hoop bar and corresponding outward force applied to the mid-span of the peripheral hoop bar by the longitudinal bar, respectively. δ_2^e indicates the central deflection of the peripheral hoop bar where the moment at the corner bents of the peripheral hoop bar has reached the maximum elastic moment of resistance of the peripheral hoop bar, M_e^h. The outward force F_2 corresponding to δ_2^e is denoted by F_2^e.

The upper bound value of the initial stiffness of the peripheral hoop bar, k_2^{eu}, can be calculated by neglecting the lateral pressure along the hoop bar from the core concrete, w, shown in Fig. 5.13. In this case, three plastic hinges (at both ends and the centre of the hoop bar) are formed at the same time because the central moment is same as those at the corner bents. Hence, the outward force applied to the centre of the peripheral hoop by the longitudinal bar F_2^{eu} at displacement of δ_2^e can be calculated as

$$F_2^{eu} = \frac{8\, M_e^h}{l_h} = f_{yh}\, \frac{\pi\, d_{bh}^3}{4\, l_h} \qquad \text{.....} \qquad (5.18)$$

where l_h= the length of peripheral hoop bar between corner longitudinal bars

f_{yh} = yield strength of hoop bar steel

d_{bh} = hoop bar diameter

The relationship between the central deflection δ_2^{eu} and the corresponding outward force from the longitudinal bar F_2^{eu} can be expressed in the form

$$\delta_2^{eu} = \frac{F_2^{eu} l_h^3}{192 E I_h} \quad \text{.....} \quad (5.19)$$

where I_h = moment of inertia of the peripheral hoop bar section

Hence, k_2^{eu} can be written as

$$k_2^{eu} = \frac{F_2^{eu}}{\delta_2^{eu}} = \frac{192 E I_h}{l_h^3} \quad \text{.....} \quad (5.20)$$

If a uniform distribution of lateral pressure, w, along the hoop bar from the core concrete is assumed as shown in Fig. 5.13, the initial stiffness of the peripheral hoop bar with regard to the restriction against lateral deflection of the longitudinal bar, k_2^e, may be calculated as follows. In this case, it must be noticed that magnitude of w is not proportional to the central deflection of peripheral hoop bar δ_2^e. This means that w may increase or be reduced as the hoop deflection of δ_2^e increases because it depends on the velocity of the lateral expansion of the core concrete due to Poisson's effect. However, it may be assumed that, at the initial stage in the column loading, w increases as δ_2 increases. If so assumed, the increment of the central deflection $\Delta\delta_2^w$ due to the increment of w can be expressed in the form

$$\Delta\delta_2^w = \frac{\Delta w\, l_h^4}{384 E I_h} \quad \text{.....} \quad (5.21)$$

where Δw = increment of uniform lateral pressure along the peripheral hoop from the core concrete

Based on Eq.5.19, $\Delta\delta_2^F$ which denotes increment of the central deflection due to the increment of F_2 can be written as

$$\Delta\delta_2^F = \frac{\Delta F_2\, l_h^3}{192 E I_h} \quad \text{.....} \quad (5.22)$$

where ΔF_2 = increment of F_2

Hence, k_2^e can be expressed in the form

$$k_2^e = \frac{\Delta F_2}{(\Delta\delta_2^F + \Delta\delta_2^w)} = \frac{384 E I_h}{(2 l_h^3 + (\Delta w\, l_h / \Delta F_2) l_h^3)} \quad \text{.....} \quad (5.23)$$

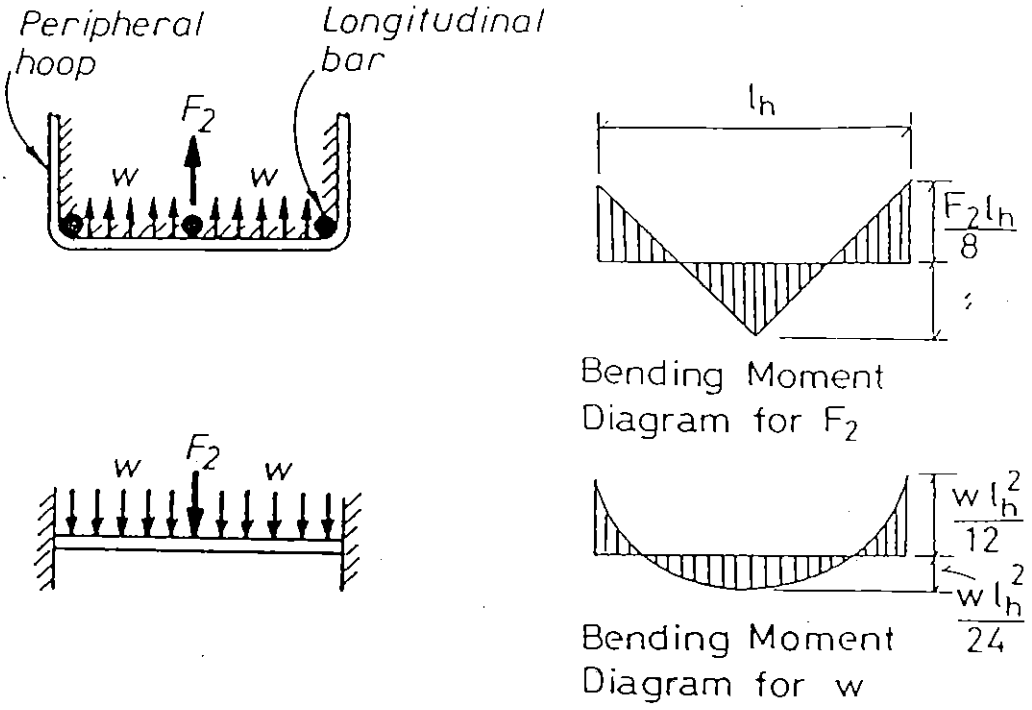

Fig. 5.13 Loading Condition of Peripheral Hoop at Small Deflection.

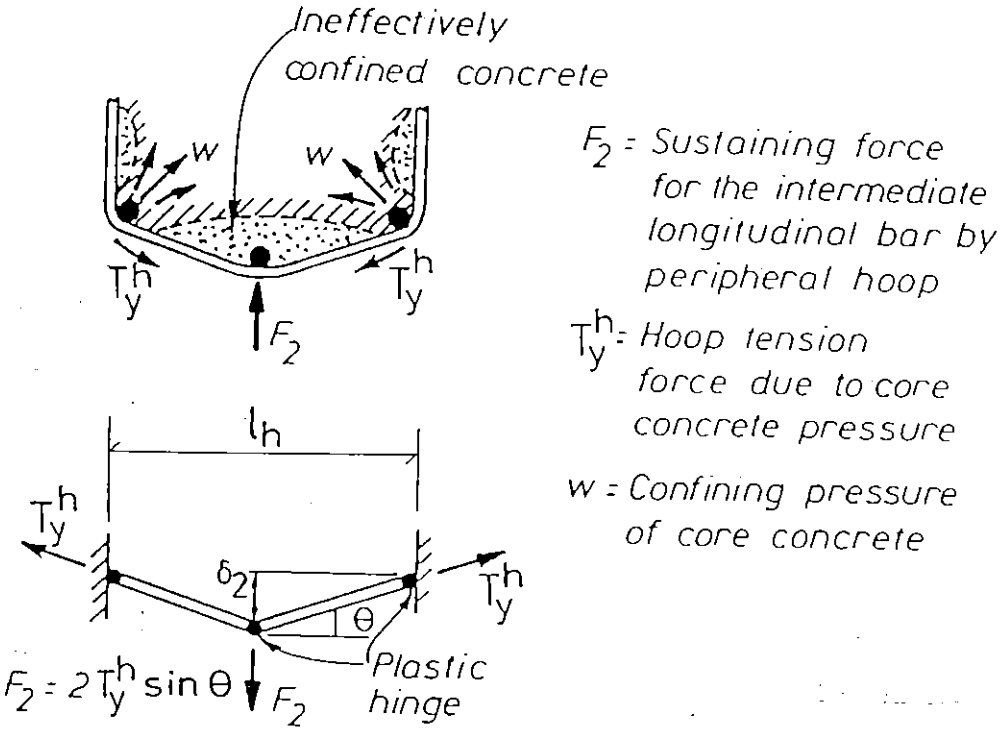

Fig. 5.14 Loading Condition of Peripheral Hoop at Large Deflection.

As can be seen from Eq. 5.23, k_2^e depends on the ratio of $\Delta w\, l_h/\Delta F_2$ in this case. k_2^e can be almost zero if the increase of lateral pressure of w due to Poisson's effect of core concrete is rapid. On the other hand, w may be decreased or not increase if increase of the hoop deflection of δ_2 is rapid. In this case, Δw may be taken as zero and thus Eq.5.23 becomes equivalent to Eq. 5.20 which neglects the presence of lateral pressure along the peripheral hoop bar.

It is notable that the value of k_2^e is considerably smaller than k_1^e for a 90° end hook even if k_2^{eu} is adopted as k_2^e, in practical cases. For example, if $d_b = d_{bh}$, $I_t = I_h$, $l_b = 3\ d_b$ and $l_h = 40\ d_b$, the ratio of $k_1^e\ /\ k_2^{eu}$ becomes about 37. Hence, the restraint by the peripheral hoop against the intermediate longitudinal bar may normally be neglected in the initial stage of column loading. To simply represent the spring characteristic of the peripheral hoop, k_2^{eu} was adopted as k_2^e in Figs. 5.11 and 5.12.

Since it was assumed that the tension force generated in the hoop bar is much smaller than its yield force until flexural yield hinges are formed at both ends and at the centre of the peripheral hoop bar, the reduction in the moment capacity of the peripheral hoop bar due to the presence of the tension force was neglected in the calculation of δ_2^{eu}. M_e^h $(= f_{yh}\, \pi d_{bh}^3/32)$ can be used as the fixed end moment of the peripheral hoop bar of $F_2^{eu}\, l_h/8$. Hence, Eq.5.19 can be rewritten as

$$\delta_2^{eu} = \frac{M_e^h\, l_h^2}{24\, E\, I_h} \qquad \text{.....} \qquad (5.24)$$

In Figs. 5.11 and 5.12, δ_2^p indicates the central deflection at which the axial force in the peripheral hoop bar has just reached the axial yield tension force T_y^h due to the lateral expansion of core concrete. It is assumed that at this stage the three plastic hinges in the peripheral hoop have already formed at the centre and at both ends as shown in Fig. 5.14. As the central deflection δ_2 increases over δ_2^p, the moment resistance of the plastic hinges of hoop bar will rapidly decrease due to the increase of axial tension strain above the yield strain. Under such condition, the force F_2 may be assumed

to be balanced only by the vertical component of T_y^h . In this case, the relation between F_2 and δ_2 can be expressed as

$$F_2 = \frac{2\, T_y^h\, \delta_2}{\sqrt{l_h^2/4 + (\delta_2)^2}} \approx \frac{4\, T_y^h\, \delta_2}{l_h} \quad \ldots\ldots \quad (5.25)$$

From Eq. 5.25, the stiffness k_2^{pp} at deflections beyond δ_2^p was estimated as

$$k_2^{pp} = \frac{F_2}{\delta_2} = \frac{4\, T_y^h}{l_h} \quad \ldots\ldots\ldots\ldots \quad (5.26)$$

The estimation of δ_2^p is not easy because the axial tension yielding of the peripheral hoop bar depends on the development of the lateral pressure from the core concrete which eventually concentrates at the corners of the column section. That is, the axial tension yielding of the peripheral hoop bar is likely to be not related to the magnitude of the hoop central deflection. However, δ_2^p can be approximated as follows. If k_2^{pp} calculated by Eq. 5.26 is smaller than k_2^{eu} by Eq. 5.20 as represented by Fig. 5.11, it may be assumed that F_2^p corresponding to δ_2^p is equal to F_2^{eu} . This is because F_2 will hardly increase after the formation of plastic hinges in the hoop bar. Using Eq. 5.25, F_2^p can be expressed in the form

$$F_2^p = \frac{4\, T_y^h\, \delta_2^p}{l_h} = f_{yh} \frac{\pi\, d_{bh}^2\, \delta_2^p}{l_h} \quad \ldots\ldots \quad (5.27)$$

Equating Eq. 5.27 to Eq. 5.18,

$$\delta_2^p = \frac{d_{bh}}{4} \quad \ldots\ldots\ldots \quad (5.28)$$

If k_2^{pp} calculated by Eq. 5.26 is larger than k_2^{eu} by Eq. 5.20 as represented by Fig. 5.12, δ_2^p may be estimated as follows. The work due to the rotations of plastic hinges W_r can be expressed in the form

$$W_r = M_y^h\, (\theta^p + \theta^p + 2\theta^p) = 4\, M_y^h\, \theta^p \quad \ldots\ldots\ldots \quad (5.29)$$

where M_y^h = moment of resistance of the peripheral hoop bar at the plastic hinges

θ^p = rotation of plastic hinge of hoop bar expressed by $2(\delta_2^p - \delta_2^e)/ l_h$ (assuming that θ is small)

The corresponding work W_f due to the outward force of the longitudinal bar is represented by the shaded area in Fig. 5.12. Hence, W_f can be written as,

$$W_f = (F_2^p + F_2^e)(\delta_2^p - \delta_2^e) / 2 \quad \ldots\ldots \quad (5.30)$$

Equating W_r and W_f,

$$4 M_y^h [2(\delta_2^p - \delta_2^e)/ l_h] = (F_2^p + F_2^e)(\delta_2^p - \delta_2^e) / 2$$

Rearranging this,

$$8 M_y^h / l_h = (F_2^p + F_2^e)/ 2 \quad \ldots\ldots\ldots\ldots \quad (5.31)$$

Substituting $F_2^p = 4 T_y^h \delta_2^p / l_h$ (see Eq.5.27) and rearranging it,

$$\delta_2^p = \frac{4 M_y^h}{T_y^h} - \frac{F_2^e l_h}{4 T_y^h} \quad \ldots\ldots\ldots\ldots \quad (5.32)$$

In Eq. 5.32, M_y^h may be approximated by the maximum elastic moment of resistance of the peripheral hoop bar M_e^h used in Eq. 5.18. This is because M_y^h may be smaller than the plastic moment of resistance, due to the axial tension yielding of the hoop bar, but not so small at δ_2^p where the hoop bar has just yielded. This will be explained based on Fig. 5.18 in the subsequent section. If so approximated, Eq. 5.32 can be rewritten as

$$\delta_2^p = \frac{d_{bh}}{2} - \frac{F_2^e l_h}{4 T_y^h} \quad \ldots\ldots\ldots\ldots \quad (5.33)$$

In this case, k_2^p, which denotes the stiffness of peripheral hoop at lateral deflections of longitudinal bar between δ_2^e and δ_2^p, can be expressed in the form

$$k_2^p = \frac{F_2^p - F_2^e}{\delta_2^p - \delta_2^e} \quad \ldots\ldots\ldots\ldots \quad (5.34)$$

The value of δ_2^p obtained by Eq.5.28 or Eq. 5.33 may contain some error due to the neglect of the contribution of the lateral pressure from the core concrete. However, the contribution of the lateral pressure from the core concrete to δ_2^p will be smaller than that to δ_2^e. This is because, in the case of rectangular hoop reinforcement, the lateral pressure from the core concrete normally concentrates at the corners of the column section at large deformation [eg. 5.15].

5.3.4 Moment of Resistance of a Longitudinal Bar under High Axial Compression

Usually, the slenderness ratios of longitudinal reinforcing bars restrained by hoop sets specified in the NZ 3101 code[5.1] are small enough to result in inelastic buckling of the longitudinal bars. In order to estimate the moment of resistance of the longitudinal bar under high axial compression, the following assumptions, which are similar to those used in the inelastic buckling theory by von Kármán called "double modulus theory" [5.7], were adopted.

1. At first, the longitudinal bar is axially loaded up to axial stress of σ_r as shown in Fig. 5.15.
2. Secondly, bending moment is applied until the extreme compression fibre reaches the strain of the ultimate strength of steel ε_{su} , without reducing the axial load originally applied.

To use a computer for the moment calculation, the bar section was divided into 200 layers with the same thicknesses as shown in Fig. 5.15. The layer where the stress is unchanged after bending is referred to as the pseudo-neutral axis in this study. If i-th layer is located above the pseudo-neutral axis, the compression stress increase in the layer, σ_c^i, is expressed by Eq. 5.35. If j-th layer is located below the pseudo-neutral axis, the stress decrease σ_t^j is expressed by Eq. 5.36.

$$\sigma_c^i = f_c(\varepsilon_i) - \sigma_r \quad \text{.....} \quad (5.35)$$

where ε_i= strain of i-th layer in the longitudinal bar section

$f_c(\varepsilon_i)$ = stress of i-th layer above the pseudo-neutral axis in the bar section

σ_r = axial stress at the position of the pseudo-neutral axis in the bar section

$$\sigma_t^j = f_t(\varepsilon_j) - \sigma_r \quad \text{.....} \quad (5.36)$$

where ε_j = strain of j-th layer in the bar section

$f_t(\varepsilon_j)$ = stress of j-th layer above the pseudo-neutral axis in the bar section

If the longitudinal bar did not experience any cyclic loading in the yield range, the stress-strain relation obtained from monotonic tensile tests on the longitudinal bar steel could be applied to the layers above pseudo-neutral axis, assuming that the stress-strain curve in compression is same as that in tension. For this case, the following equation was adopted for the strain hardening region in the stress-strain curve, based on the study by Mander et al [5.10].

$$f_c(\varepsilon_s) = f_{su} - \alpha_1(\varepsilon_{su} - \varepsilon_s)^{\beta} \quad \text{.....} \quad (5.37)$$

where f_{su} = ultimate strength of steel

ε_s = steel strain

ε_{su} = strain at the ultimate strength of bar steel

α_1, β = constants to determine stress-strain curve in the strain hardening region of steel

The layers below pseudo-neutral axis are subjected to reversed loadings. In order to model the stress-strain curve under reversed loading, the following method was used in this study. The stress-strain relation obtained from monotonic tensile tests was used just as a skeleton curve, taking into account the Bauschinger effect as shown in Fig. 5.16. The skeleton curve was always set to begin at the strain,

$$\varepsilon_{ro} = [\varepsilon_r - f_c(\varepsilon_r)/E] \quad \text{.....} \quad (5.38)$$

where ε_r is the compression strain at pseudo-neutral axis.

The function $f_t(\varepsilon_j)$ was expressed by a combination of $f_1(\varepsilon_s)$ and $f_2(\varepsilon_s)$. That is,

$$f_t(\varepsilon_s) = f_1(\varepsilon_s) + f_2(\varepsilon_s) \quad \text{.....} \quad (5.39)$$

where $f_1(\varepsilon_s)$ represents the skeleton curve.

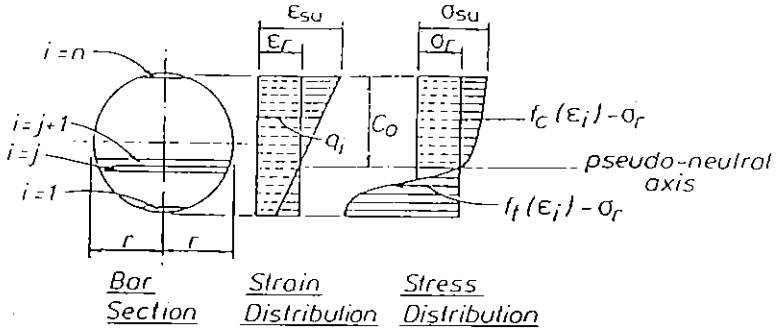

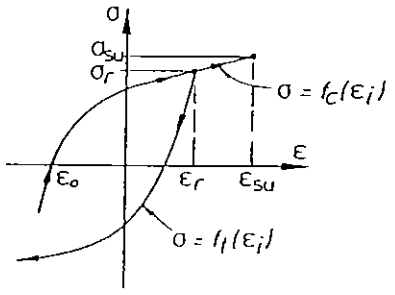

Stress-Strain Relation of Steel

C_o — Distance of pseudo-neutral axis from the extreme compression fibre of the bar

$f_c(\varepsilon_i)$ — Stress of ith segment above the pseudo-neutral axis

$f_t(\varepsilon_i)$ — Stress of ith segment below the pseudo-neutral axis

$f_c(\varepsilon_i)-\sigma_r$ — Stress increment of ith segment above the pseudo-neutral axis

$f_t(\varepsilon_i)-\sigma_r$ — Stress decrement of ith segment below the pseudo-neutral axis

Fig. 5.15 Stress Distribution for a Longitudinal Bar Subjected to Combined Axial Load and Bending, and Segmentation of Bar Section for Moment Calculation Using the Layer Method.

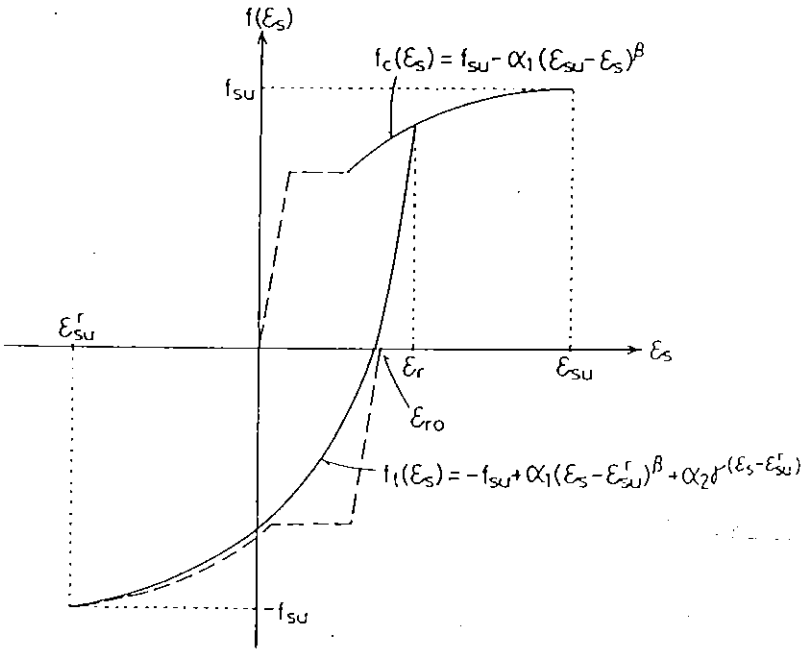

Fig. 5.16 Stress-Strain Model for Steel Subjected to Reversed Loading.

Hence, in Eq. 5.39, $f_1(\varepsilon_s)$ needs to become more predominant as the strain increases toward tension side in the reversed loading curve. This can be achieved by making $f_2(\varepsilon_s)$ a function which rapidly approaches its asymptote parallel to the strain axis as the strain increases toward tension side in the reversed loading curve. To satisfy this condition, the following functions were selected respectively.

$$f_1(\varepsilon_s) = -f_{su} + \alpha_1 (\varepsilon_s - \varepsilon^r_{su})^{\beta} \quad \ldots\ldots\ldots \quad (5.40)$$

where ε^r_{su} = strain at ultimate stress in the reversed loading curve ($= \varepsilon_{ro} - \varepsilon_{su}$)

$$f_2(\varepsilon_s) = \alpha_2 \gamma^{(\varepsilon s - \varepsilon^r su)} \quad \ldots\ldots\ldots \quad (5.41)$$

where α_2, γ = constants

The initial tangent modulus of the curve under reversed load was assumed to be equal to the Young's modulus of the steel, E = 200,000 MPa. Hence, differentiating Eqs. 540 and 5.41, respectively

$$f_1'(\varepsilon_s) = \alpha_1 \beta (\varepsilon_s - \varepsilon^r_{su})^{\beta-1} \quad \ldots\ldots\ldots \quad (5.42)$$

$$f_2'(\varepsilon_s) = f_2(\varepsilon_s) \ln \gamma \quad \ldots\ldots\ldots \quad (5.43)$$

where $\ln \gamma$ = natural logarithm of γ

and at the point $\varepsilon_s = \varepsilon_r$,

$$E = f_1'(\varepsilon_r) + f_2'(\varepsilon_r) \quad \ldots\ldots\ldots \quad (5.44)$$

The curve expressed by Eq. 5.39 intersects the curve of Eq. 5.37 at the point $\varepsilon_s = \varepsilon_r$. Hence,

$$f_c(\varepsilon_r) = f_1(\varepsilon_r) + f_2(\varepsilon_r) \quad \ldots\ldots\ldots \quad (5.45)$$

From Eqs. 5.44 and 5.45,

$$E - f_1'(\varepsilon_r) = \alpha_2 \gamma^{(\varepsilon r - \varepsilon^r su)} \ln \gamma \quad \ldots\ldots\ldots \quad (5.46)$$

$$f_c(\varepsilon_r) - f_1(\varepsilon_r) = \alpha_2 \gamma^{(\varepsilon r - \varepsilon^r su)} \quad \ldots\ldots\ldots \quad (5.47)$$

Solving Eqs. 5.46 and 5.47,

$$\ln \gamma = \frac{E - f_1'(\varepsilon_r)}{f_c(\varepsilon_r) - f_1(\varepsilon_r)} \qquad \text{.....} \qquad (5.48)$$

and hence γ can be obtained as exponential of $\{\frac{E - f_1'(\varepsilon_r)}{f_c(\varepsilon_r) - f_1(\varepsilon_r)}\}$.
Substituting this γ value into Eq. 5.46 or Eq.5.47, α_2 can also be obtained.

As an example, for a typical HD 20 longitudinal bar, $f_c(\varepsilon_i)$ and $f_t(\varepsilon_j)$ determined using above equations are shown in Fig. 5.17. Using the stress-strain relations shown in Fig. 5.17, the inelastic moment of resistance of the HD 20 longitudinal bar was calculated for each corresponding axial compression strain of ε_r. The calculated results are shown in Fig. 5.18 and Table 5.1. It can be seen that the inelastic moment of resistance of the bar is not small up to ε_r of about 3 % compared with the maximum elastic moment of resistance, if the longitudinal bar is monotonically loaded up to ε_r. However, if the bar was already tensioned up to strain of 3% in the previous cycle, during cyclic loadings of a column, the inelastic moment of resistance under the axial compression strain ε_r of 3 % becomes close to zero. This is because each fiber in the bar travels totally 6 % and already reaches almost the ultimate strength before bending.

For reference, using the bi-linear stress-strain model for the reversed loading part shown in Fig. 5.19 (a), the inelastic moments of resistance of the HD 20 longitudinal bar were also calculated and are listed in Table 5.1. It can be seen that the difference of calculated results due to the use of the bi-linear stress-strain model is very small. Hence, in practice, it may be sufficient to use the bi-linear stress-strain model for the reversed loading part. In the case where the linear curves shown in Fig. 5.19 (b) were applied to $f_c(\varepsilon_i)$ and $f_t(\varepsilon_j)$, respectively , the calculated moment of resistance at ε_r of 3 % was 0.321 kN·m which is about 15 % larger than that calculated by the above method. This is due to significant overestimation of tension stresses in the layers near extreme tension fiber.

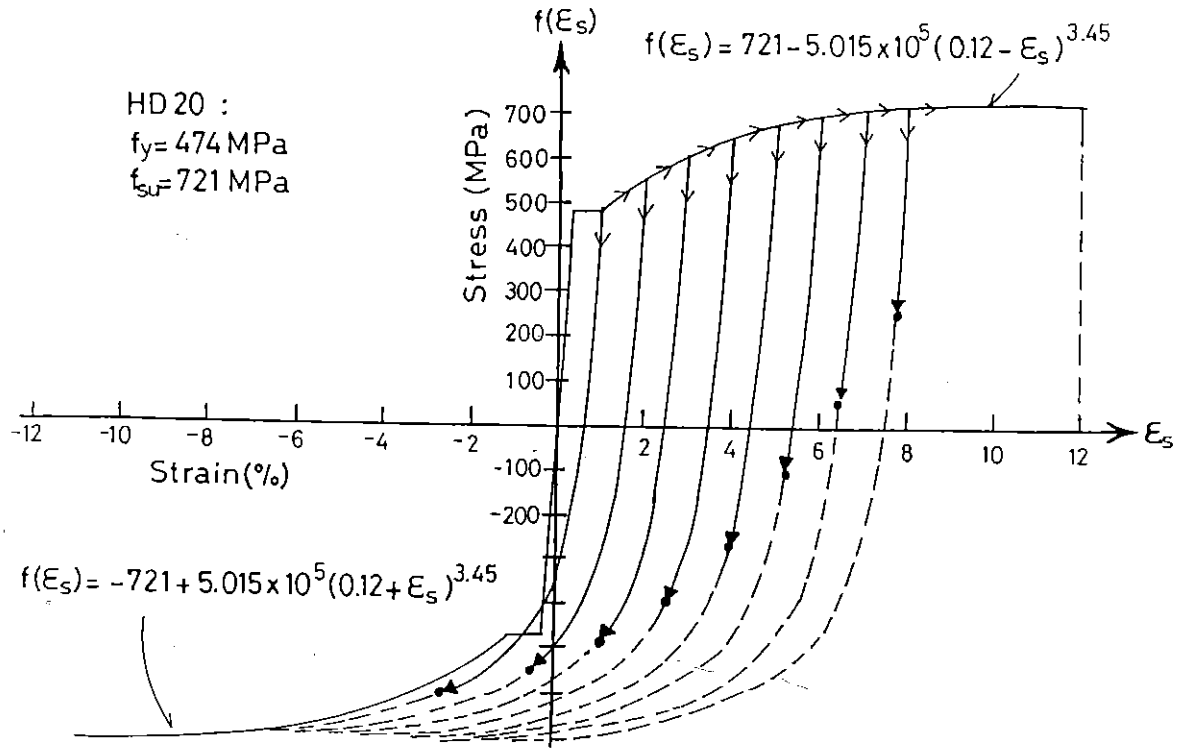

Fig. 5.17 Stress-Strain Model for HD 20 Bar Subjected to Reversed Loading.

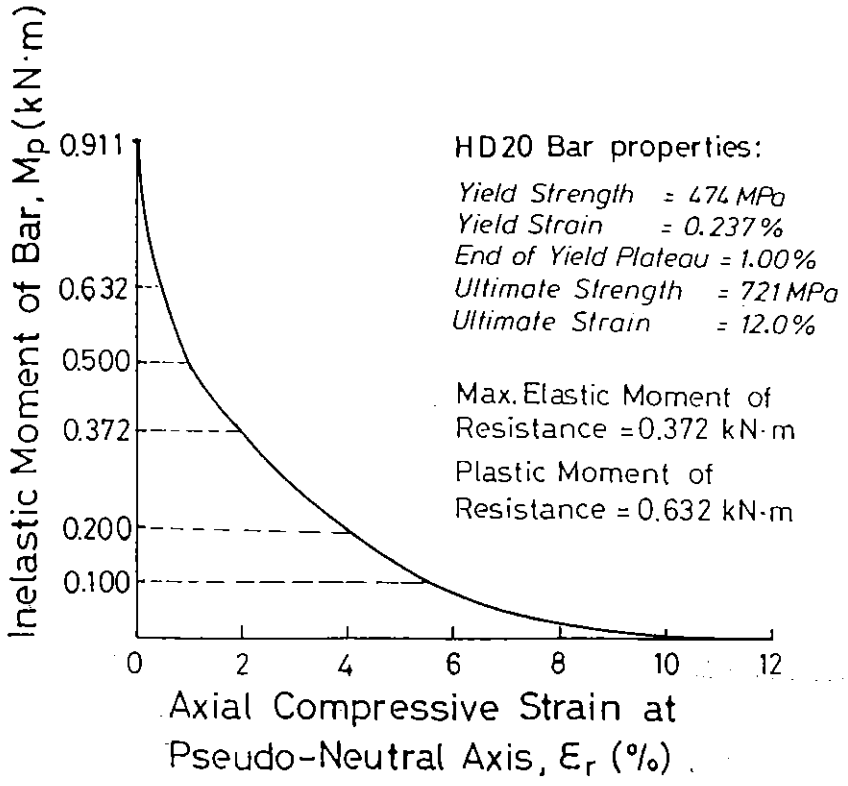

Fig. 5.18 Decrease of Moment Resistance of a HD 20 Bar Subjected to Axial Compression Load.

Table 5.1 Inelastic Moment of Resistance of a HD 20 Bar.

Compression Strain at Pseudo-Neutral Axis, ε_y, in %	Reversed Loading Curve: $f_t(\varepsilon_s) = f_1(\varepsilon_s) + f_2(\varepsilon_s)$		Reversed Loading Curve: $f_t(\varepsilon_s)$ = bilinear	
	C_o / d_{bl}	Moment of Resitance in KN· m	C_o / d_{bl}	Moment of Resitance in KN· m
0.0	0.500	0.911	-	-
1.0	0.760	0.495	0.770	0.497
2.0	0.785	0.381	0.810	0.386
3.0	0.825	0.280	0.845	0.285
4.0	0.855	0.195	0.870	0.199
5.0	0.875	0.127	0.890	0.130
6.0	0.885	0.077	0.905	0.078
7.0	0.915	0.042	0.920	0.043
8.0	0.935	0.020	0.935	0.020

Note: C_o = pseudo-neutral axis depth from extreme compression fibre
d_{bl} = longitudinal bar diameter
HD 20 : f_y = 474 MPa, ε_y = 0.237 %, ε_{sh} = 1.0 %
f_{su} = 721 MPa, ε_{su} = 12.0 %
maximum elastic moment of resistance = 0.372 KN· m
maximum plastic moment of resistance = 0.632 KN· m

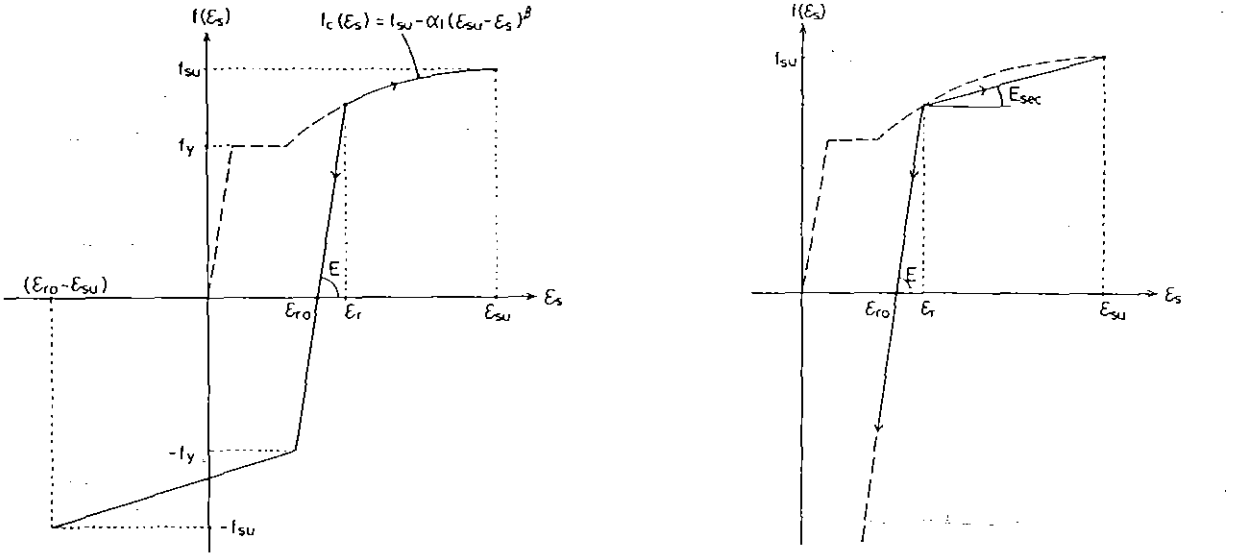

(a) Using Bilinear Curve for Reversed Loading

(b) Using Linear Curves for Both Increased and Reversed Loadings

Fig. 5.19 Alternative Stress-Strain Models for Steel.

5.3.5 Buckling of the Intermediate Bar at Small Deflection in Stage (1)

At Stage (1), when deflection of the intermediate longitudinal bar is small, it was assumed that lateral pressure on the intermediate longitudinal bar was distributed uniformly as shown in Figs. 5.7 and 5.20. It was also assumed that the restraint provided by the peripheral hoop against lateral deflection of the intermediate longitudinal bar is negligible at this stage. The following relation must be satisfied at the position of the maximum moment in order to avoid an unstable condition. At the positions of the intermediate longitudinal bar restrained by 135° or 180° end hooks,

$$\frac{F_1 l_s}{8} + M_p \geq \frac{w l_s^2}{12} + P_{cr} \frac{\delta}{2} \qquad \text{.....} \qquad (5.49)$$

where F_1 = load sustained by 90° end hook

M_p=inelastic moment of resistance of the intermediate longitudinal bar

P_{cr} = critical axial load of the intermediate longitudinal bar

δ = deflection of longitudinal bar at position of 90° end hook

l_s = spacing between 135° or 180° end hooks

w= pressure from core concrete, assumed to be uniformly distributed

If w is small enough to satisfy $M_p \geq (w\ l_s^2/12)$, the relation represented by Eq. 5.49 can be simplified as

$$\frac{F_1 l_s}{8} \geq \frac{P_{cr} \delta}{2} \qquad \text{.....} \qquad (5.50)$$

Substituting $F_1 = k_1^e \delta$ into Eq. 5.50 and rearranging gives,

$$k_1^e \geq \frac{4 P_{cr}}{l_s} \qquad \text{.....} \qquad (5.51)$$

Using k_1^e calculated from Eq. 5.14, the maximum value of P_{cr} can be estimated from Eq. 5.51. If the estimated P_{cr} can reach the ultimate compression force of the intermediate longitudinal bar P_u or at least its compressive yield force P_y , k_1^e may be considered large enough to avoid premature buckling of the intermediate longitudinal bar.

However, it should be noted that Eq. 5.51 is valid only when the initial deflection due to imperfection of the intermediate longitudinal bar is negligible. It is also notable that the maximum elastic deflection of the 90° end hook δ_1^e given by Eq. 5.13 will be in the order of 0.01 to 0.1 mm in practice. This can be recognized from the example calculation described in Section 5.3.7. Hence, imperfection of the longitudinal bar is likely to affect the initial buckling condition. If there is already an initial deflection due to the imperfection, δ_o , Eq. 5.50 needs to be modified as follows

$$\frac{F_1 l_s}{8} \geq \frac{P_{cr}(\delta + \delta_o)}{2} \qquad \text{.....} \qquad (5.52)$$

and thus Eq. 5.51 is replaced by

$$k_1^e \geq \frac{4 P_{cr}}{l_s}\left(1 + \frac{\delta_o}{\delta}\right) \qquad \text{.....} \qquad (5.53)$$

In Eq. 5.53, $\frac{\delta_o}{\delta}$ becomes infinitely large at the initial condition of $\delta = 0$ and hence an unstable condition occurs for any magnitude of k_1^e until δ reaches a certain value.

In this case, the relationship between $F_1 l_s/8$ and $P_{cr}(\delta + \delta_o)/2$ against δ can be represented as in Fig. 5.21. In the figure, δ_{st} indicates the deflection where $F_1 l_s/8$ and $P_{cr}(\delta + \delta_o)/2$ can be balanced. Hence, if the value of δ_{st} is less than δ_1^e given by Eq. 5.13, a state of stable equilibrium can be expected. δ_{st} can be calculated as

$$\delta_{st} = \frac{\delta_o}{\frac{k_1^e l_s}{4 P_{cr}} - 1} \qquad \text{.....} \qquad (5.54)$$

The maximum magnitude of δ_o to be able to satisfy Eq. 5.54 can be calculated by taking $\delta_{st} = \delta_1^e$ in Eq. 5.54. Hence,

$$\delta_o^c = \delta_1^e \left(\frac{k_1^e l_s}{4 P_{cr}} - 1\right) \qquad \text{.....} \qquad (5.55)$$

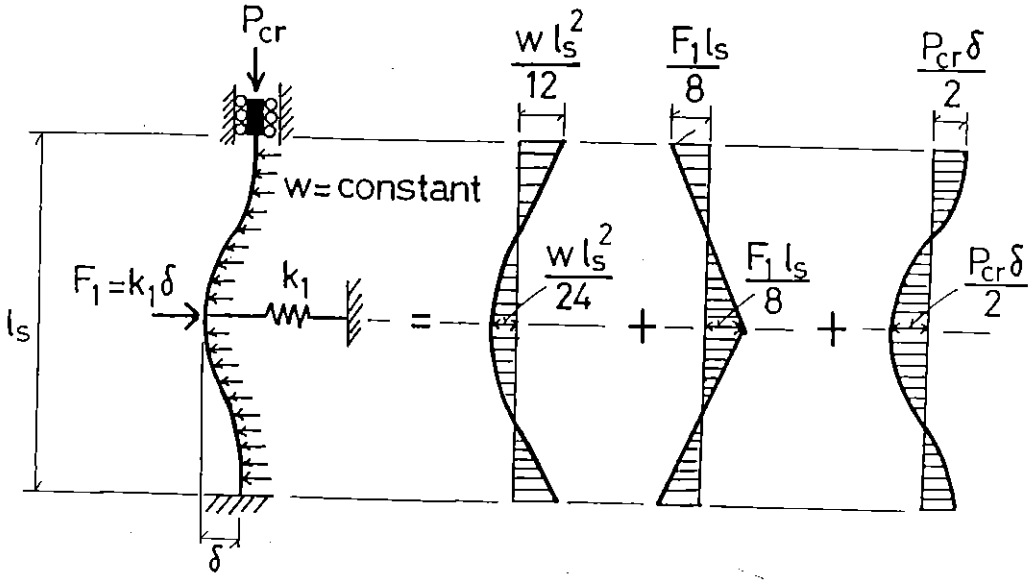

Fig. 5.20 Moment Distribution along Longitudinal Bar for Each Assumed Load in Stage (1).

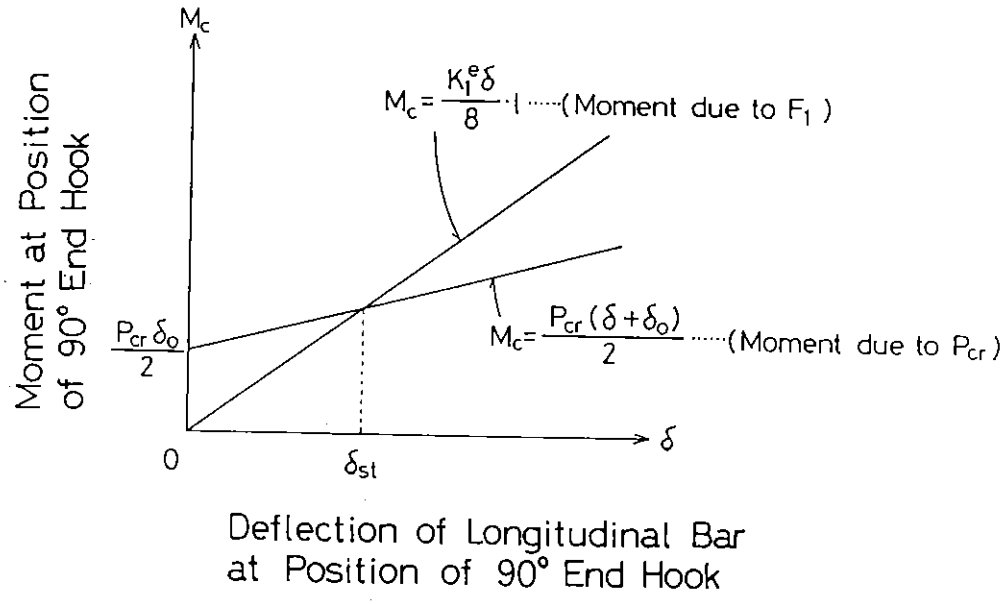

Fig. 5.21 Moment due to Axial Load of Longitudinal Bar (Which Has Initial Deflection due to Imperfection) versus Moment due to Sustaining Force of 90° End Hook.

where δ_o^c = maximum magnitude of δ_o to satisfy a state of stable equilibrium in the longitudinal bar

In practical design, δ_o^c can be evaluated by substituting δ_1^e and k_1^e of the provided 90° end hook (which are calculated using Eqs. 5.13 and 5.14, respectively) and an adequate value of P_{cr} (which may be P_y or P_u) into Eq. 5.55. Hence, if the calculated δ_o^c, which is required to prevent premature buckling of the intermediate longitudinal bar in Stage (1), is impractically small it means that the stiffness of 90° hook is too small. It is noted that δ_o^c which is calculated using ordinary values for strength and dimensions of reinforcement may be impractically small. This is discussed later in the example calculation shown in Section 5.3.7.

5.3.6 Buckling of the Intermediate Bar at Large Deflection in Stages (2) and (3)

In order to represent the loading condition on the intermediate longitudinal bar at the stage of large lateral deflection in Stages (2) and (3), a combination of simplified loading models was used as shown in Fig. 5.22. Triangularly distributed lateral pressure with maximum load per unit length q was placed on the both ends of the longitudinal bar to express the concentration of the lateral pressure at the position of 135° or 180° end hooks. It was assumed that no concentration of the lateral pressure at the position of the 90° end hook occurred at large deflections of the longitudinal bar in Stage (2) or (3). This assumption is based on the experimental observation that the core concrete beneath the 90° end hook could not be well confined and began to crush at large deflection, because of the low stiffness of the 90° end hook. Moreover, it seemed that separation between core concrete and the longitudinal bar at the position of the 90° end hook occurred at the final stage [5.14].

If the lateral deflection of the longitudinal bar, restrained by those ties, reached the ultimate magnitude, δ_{cr}, where a state of stable equilibrium against these combined loading models can be maintained in an ultimate condition, it may be assumed that:

(a)The bending moment due to the lateral pressure from the core concrete is resisted only by the bending resistance of the intermediate longitudinal bar with the restraint of 135° or 180° end hooks.

(b)The buckling moment due to the axial load P_{cr} with corresponding central deflection δ_{cr} is balanced by the moment due to the sustaining load of the 90° end hook F_1 and that of the peripheral hoop F_2.

These assumptions correspond to the previous assumption that the concentration of lateral pressure does not occur at the position of the 90° end hook.

A check whether the intermediate longitudinal bar is in a state of stable equilibrium or not is conducted in the following order of steps.

(Step 1.) Calculation of the ultimate deflection δ_{cr}.

If the central deflection in the longitudinal bar reaches the ultimate deflection δ_{cr} able to maintain the axial load P_{cr}, the following relation must be satisfied as can be seen from Fig. 5.22 (d) and (e),

$$\frac{(F_1 + F_2)}{4} l_s = P_{cr} \delta_{cr}$$

Rearranging the terms:

$$\delta_{cr} = \frac{(F_1 + F_2)}{4 P_{cr}} l_s \quad \text{.....} \quad (5.56)$$

Both F_1 and F_2 are function of δ and hence, to solve Eq. 5.56 with regard to δ_{cr}, a trial and error method or a diagram such as shown in Fig. 5.27 (See an example calculation in Section 5.3.7) is required.

(Step 2.) Calculation of the uniform load w, and the triangular load with maximum load per unit length q with its load acting length $a \cdot l_s$:

It is assumed that the ties with 135°or 180° end hooks has yielded by tension force due to those distributed loads w and q , in Stages (2) and (3). It is also assumed that the distributions of w and q in the neighbouring spans (outside of the positions of 135° or 180° end hooks) are same as

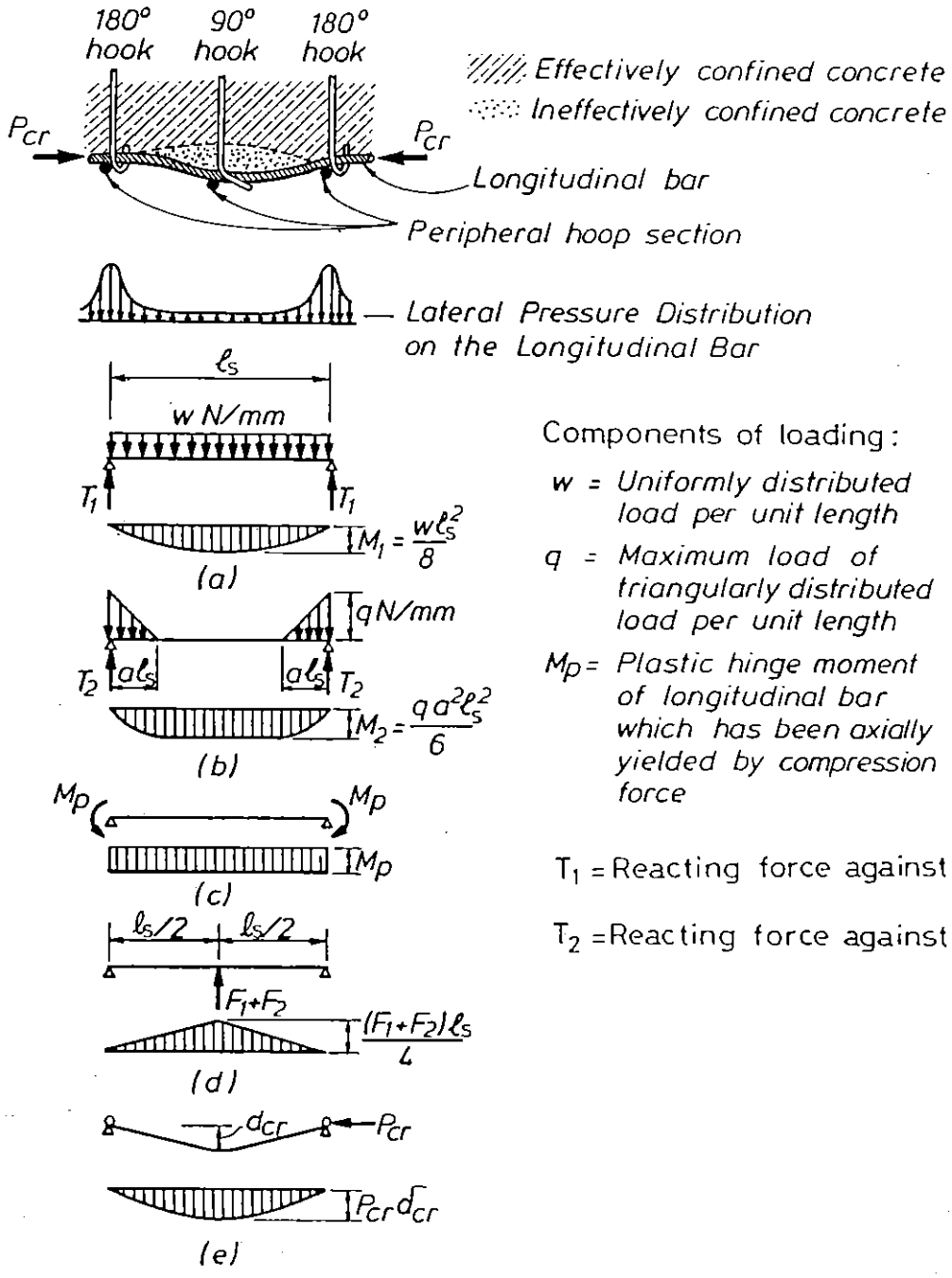

Components of loading:

- w = Uniformly distributed load per unit length
- q = Maximum load of triangularly distributed load per unit length
- M_p = Plastic hinge moment of longitudinal bar which has been axially yielded by compression force

T_1 = Reacting force against w, $(= \frac{w\ell_s}{2})$

T_2 = Reacting force against q, $(= \frac{qa\ell_s}{2})$

Fig. 5.22 Loading Models for Intermediate Longitudinal Bar in Stages (2) and (3).

those inside the span under consideration. Hence, from the equilibrium of vertical component of loads,

$$T_y = 2(T_1 + T_2) - 2\frac{(F_1 + F_2)}{2}$$

where T_1 = Reacting force against w at pin support in Fig. 5.22
T_2 = Reacting force against q at pin support in Fig. 5.22

Substituting $T_1 = \frac{w l_s}{2}$ and $T_2 = \frac{q a l_s}{2}$,

$$T_y = 2\left(\frac{w l_s}{2} + \frac{q a l_s}{2}\right) - 2\frac{(F_1 + F_2)}{2} \quad \text{.....} \quad (5.57)$$

where T_y = yield force of the tie bar leg with 135° or 180° end hook.

If steel bars with same strength and with same sectional dimensions are used for all lateral reinforcement, $(F_1 + F_2)$ is normally much smaller than T_y and hence may be neglected in Eq. 5.57 in practice. In this case, Eq. 5.57 may be replaced by

$$T_y = 2\left(\frac{w l_s}{2} + \frac{q a l_s}{2}\right) \quad \text{.....} \quad (5.58)$$

It was assumed that the triangularly distributed loads become zero at the inflection point of the longitudinal bar which is calculated using w, q and the fixed end moment M_b at the positions of 135° or 180° end hooks. As a consequence, the following equation must be satisfied at the inflection point where the moment is zero.

$$\frac{T_y}{2} a l_s - M_b - \frac{1}{2} w (a l_s)^2 - \frac{q a l_s}{2} \cdot \frac{2}{3} a l_s = 0 \quad \text{.....} \quad (5.59)$$

For the Stage 2, it was assumed that the end moment M_b has just reached the maximum inelastic moment of resistance of the longitudinal bar M_p. Hence,

$$M_b = M_p = \frac{w l_s^{\,2}}{12} + \frac{(2-a)}{12} q a^2 l_s^{\,2} \quad \text{.....} \quad (5.60)$$

Solving Eqs. 5.58, 5.59 and 5.60

$$q = \frac{(T_y l_s - 12 M_p)}{(a-1)^2 a l_s^2} \qquad \text{.....} \qquad (5.61)$$

$$w = [T_y - \frac{(T_y l_s - 12 M_p)}{(a-1)^2 l_s}] \cdot \frac{1}{l_s} \qquad \text{.....} \qquad (5.62)$$

$$(3 T_y l_s) a^4 - (9 T_y l_s) a^3 + 6 (T_y l_s + 7 M_p) a^2 - (T_y l_s + 36 M_p) a + 6 M_p = 0$$

$$\text{.....} \qquad (5.63)$$

At Stage 3, it was assumed that the moment at the mid-span M_c has also reached M_p. Hence,

$$M_c = M_b = M_p = \frac{w l_s^2}{8} + \frac{q a^2 l_s^2}{6} - M_p \qquad \text{.....} \qquad (5.64)$$

Rearranging this equation,

$$2 M_p = \frac{w l_s^2}{8} + \frac{q a^2 l_s^2}{6} \qquad \text{.....} \qquad (5.65)$$

Solving Eqs. 5.58, 5.59 and 5.65,

$$a = \frac{3 (16 M_p - w l_s^2)}{4 (T_y - w l_s) l_s} \qquad \text{.....} \qquad (5.66)$$

$$q = \frac{4 (T_y - w l_s)^2}{3 (16 M_p - w l_s^2)} \qquad \text{.....} \qquad (5.67)$$

$$l_s^4 w^3 + (4 T_y l_s^3 - 128 M_p l_s^2) w^2 + (4 T_y^2 l_s^2 - 128 T_y M_p l_s + 2304 M_p^2) w - 32 M_p T_y^2 = 0$$

$$\text{.....} \qquad (5.68)$$

If T_y and M_p can be adequately estimated, the values of w, q and a in Stages (2) and (3) are calculated using above equations. T_y can be easily estimated using a measured or a specified yield strength of the tie bar steel. The estimation for M_p is not easy because it depends on the

hysteresis of the axial strain in the longitudinal bar during the cyclic loading of the column. However, M_p may be approximated as follows. Firstly, estimate the axial strain in the longitudinal bar where the tie bar leg anchored by 135° or 180° end hooks yields based on experimental results or other adequate methods. Secondly, for the estimated axial strain of the longitudinal bar, M_p is evaluated using a diagram like Fig. 5.18 drawn by the method described in Section 5.3.4.

(Step 3.) Calculation of the central deflection δ :

In order to calculate the central deflection δ due to loads w, q, P_{cr}, M_p, F_1 and F_2, it is necessary to estimate the bending stiffness of the longitudinal bar E_p I at the axial compression strain ε_r under consideration. A tangent modulus of elasticity E_t at ε_r in the stress-strain curve of the steel may be adopted as E_p. An alternative method is to use the relation,

$$E_p I = M_p / \phi_p \qquad \text{.....} \qquad (5.69)$$

where ϕ_p = curvature of the longitudinal bar subjected to combined high axial load and moment M_p

ϕ_p in Eq. 5.69 is calculated using the procedure of calculation for M_p described in Section 5.3.4. It is notable that value of E_p calculated from Eq. 5.69 is a secant modulus between zero moment and M_p as shown in Fig. 5.23. That is, the calculated E_p is an underestimate in the region of the bar where moment is close to zero along the longitudinal bar. It is also notable that values of E_p from Eq. 5.69 and the tangent modulus E_t at ε_r in the stress-strain curve of the steel are not significantly different in practice. This is because M_p and ϕ_p used in Eq. 5.69 includes tension stiffness below pseudo-neutral axis in the bar section which is much higher than compression stiffness above pseudo-neutral axis. On the other hand, the compression stiffness above pseudo-neutral axis estimated using Eq. 5.69 is smaller than E_t. As a result, E_p from Eq. 5.69 becomes sometimes smaller and sometimes larger than E_t, depending on magnitude of ε_r.

The central deflection δ can be expressed as the sum of deflections δ_w due to w, δ_q due to q, δ_m due to M_p, δ_f due to F_1 and F_2,

and δ_p due to P_{cr}, based on moment distribution shown in Fig. 5.22. That is,

$$\delta = \delta_w + \delta_q + \delta_m + \delta_f + \delta_p \qquad \text{.....} \qquad (5.70)$$

δ_w can be expressed as

$$\delta_w = \frac{5\, w\, l_s^4}{384\, E_p\, I} \qquad \text{.....} \qquad (5.71)$$

δ_q may be approximated using an equivalent point load of q a $l_s/2$ with the distance of a $l_s/3$ from the position of the 135° or 180° end hook. In this case,

$$\delta_q = \frac{q\, a^2\, l_s^4}{E_p\, I}\left(\frac{1}{48} - \frac{a^2}{324}\right) \qquad \text{.....} \qquad (5.72)$$

δ_m can be expressed as

$$\delta_m = -\left(\frac{M_p\, l_s^2}{8\, E_p\, I}\right) \qquad \text{.....} \qquad (5.73)$$

It was assumed that $\delta_f + \delta_p \approx 0$, based on the following assumption and approximation. The central moment due to F_1 and F_2 and that due to P_{cr} were assumed to be balanced in a state of stable equilibrium as already described in the assumption (b). The moment distribution along the longitudinal bar due to P_{cr}, which is used to calculate the deflection δ_p, is not quite same as that due to F_1 and F_2 but may be similar. Hence, δ_f and δ_p almost cancels each other.

(Step 4.) Buckling check:

If δ calculated in Step 3 is larger than δ_{cr} in Step 1, buckling of the longitudinal bar is known to have occurred.

Through the above steps, occurrence of buckling of the longitudinal bar can be examined for the Stages (2) and (3) where the lateral pressure on the longitudinal bar due to Poisson's effect of core concrete is not negligible.

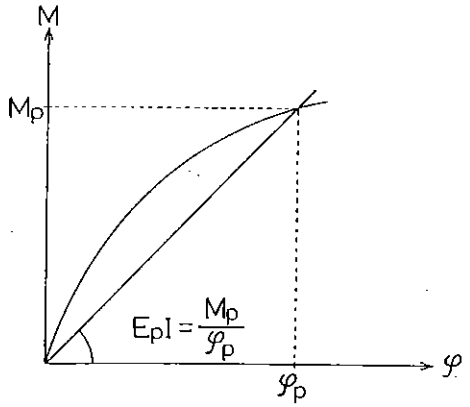

Fig. 5.23 Moment Curvature Relation in Inelastic Range for a Longitudinal Steel Bar.

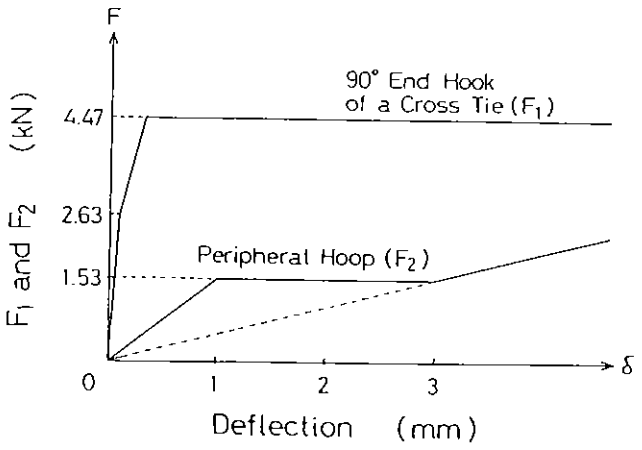

Fig. 5.24 Spring Models for 90° End Hook of a Cross Tie and a Peripheral Hoop for the Tested Column (Unit 2).

Table 5.2 Constants of Modelled Springs.

90° End Hook of Cross Tie	Peripheral Hoop
$k_1^e = 77.4 \times 10^3$ N/mm	$k_2^e = 1.52 \times 10^3$ N/mm
$k_1^p = 7.7 \times 10^3$ N/mm	$k_2^p = 0$
$\delta_1^e = 0.034$ mm	$k_2^{pp} = 0.51 \times 10^3$ N/mm
$\delta_1^p = 0.274$ mm	$\delta_2^e = 1.005$ mm
$F_1^e = 2.63$ KN	$\delta_2^p = 3.00$ mm
$F_1^p = 4.47$ KN	$F_2^e = 1.53$ KN
	$F_2^p = 1.53$ KN

Note: Transverse Steel Bar : D 12

$f_y = 333$ MPa

$\varepsilon_y = 0.167$ %

$\varepsilon_{sh} = 2.74$ %

$f_{su} = 481$ MPa

$\varepsilon_{su} = 18.0$ %

$l_b = 20$ mm

$l_h = 295$ mm

However, it must be emphasized that, in the case when the calculated value of δ_{cr} is large, the loss of confining effect on core concrete by the longitudinal bar and lateral reinforcement must be considered even if buckling is prevented. In such case, ductile behaviour of a column cannot be secured.

5.3.7 Example Calculation and Assessment of the Effectiveness of 90° End Hooks of Cross Ties

As an example of the application of the above theory, the following calculations were conducted for the tested column, Unit 2, described in Chapter three. The sectional dimensions and the reinforcement details for Unit 2 are shown in Fig. 3.12. A reversible horizontal load was applied to the central stub of Unit 2 (see Fig. 3.18 (a)). The column axial load was held constant at 0.2 $f'_c A_g$, where f'_c = concrete compressive cylinder strength and A_g = gross area of column. The measured compressive strength of concrete at the test age was 25.6 MPa. The longitudinal reinforcement composed of eight 20mm deformed bars of Grade 380 steel (HD 20), being 1.57 % of the gross area of the column cross section. The measured yield and ultimate strengths were 474 MPa and 721 MPa, respectively. The transverse reinforcement was from 12 mm diameter deformed bar of Grade 275 steel, the measured yield and ultimate yield strengths of which were 333 MPa and 481MPa, respectively. Fig. 3.14 (a) shows measured stress-strain curves of those bars. The centre to centre spacing of the transverse reinforcement sets was 80 mm (= $l_s/2$) in the plastic hinge region. This spacing was based on the requirements of NZS 3101 [5.1]. Measured horizontal load-displacement loops of the column are shown in Fig. 3.20. Commencement of opening of the 90° end hooks was observed at a displacement ductility factor of about 9. Lateral deflection of the intermediate longitudinal bars became visible at displacement ductility factor of about 11. Thereafter, lateral load carrying capacity of the column gradually decreased. The appearance of the plastic hinge region of the column at the final stage of testing is shown in Fig. 5.6.

The 90° end hook of the cross tie and the peripheral hoop were modelled using the method described in Section 5.3.3. The spring models for the 90° end hook and peripheral hoop are shown in Fig. 5.24 and the calculated constants for that reinforcement are listed in Table 5.2. It is notable that the maximum deflection of the 90° end hook in elastic range is

only 0.034 mm. It is also notable that the initial stiffness of the peripheral hoop is negligibly small in comparison with the 90° end hook. Inelastic moments of resistance of the longitudinal bar for various axial compression strains were calculated as described in Section 5.3.4 and the results are shown in Fig. 5.18.

(a) Buckling Check for Stage (1)

From Eq. 5.51, maximum value of P_{cr} can be calculated as

$$k_1^e \, l_s \, / \, 4 = 77.4 \times 10^3 \text{N/mm} \times 160 \text{ mm} \, / 4 = 3096 \text{ KN}$$

Since the ultimate compression force of the HD 20 bar used is 226 KN, buckling could therefore be prevented if there was no initial deflection of longitudinal bar due to imperfection, δ_o.

Using Eq. 5.55, maximum value of initial deflection of the HD 20 bar due to imperfection, δ_o^c, which could satisfy a state of stable equilibrium in the HD 20 bar, was calculated as 0.67 mm for a spacing between 180° end hooks, l_s, of 160 mm. This magnitude of imperfection of the bar corresponds to about 4 mm of δ_o^c per meter length of the bar. Such order of imperfection of longitudinal reinforcement would be likely to occur in a construction site due mainly to two reasons (See Fig. 5.25). One is that hoops and cross ties which are fixed to longitudinal reinforcement, to keep the longitudinal reinforcement in the correct position, normally have variations of a few mm in their leg length due to manufacturing error. Another reason is that reinforcing bars can be easily bent during site operations. From this point of view, if the calculated value of δ_o^c becomes only a few mm for l_s of 200 mm or so, it is recommended that the initial stiffness of the 90° hook be considered to be not sufficiently dependable to prevent buckling of the longitudinal bar.

In the column test shown in Fig. 3.20, at a displacement ductility factor μ of about $\pm$ 4, the measured strain in the longitudinal reinforcement was in the range of $\pm$ 1.0%. This means that the longitudinal reinforcement had a total strain range of about 2.0 % during cyclic loading. Hence, in Eq. 5.49 the inelastic moment of resistance of the longitudinal bar M_p at μ of about $\pm$ 4 may be approximated as 0.38 KN m, based on the calculated value

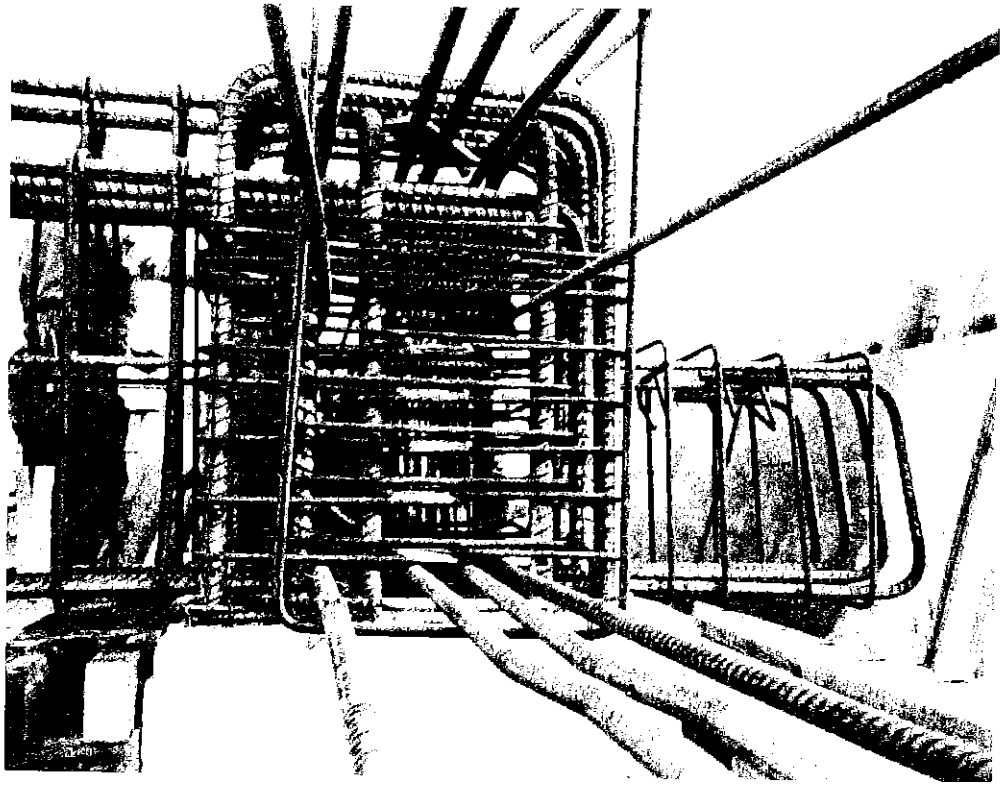

Fig. 5.25 Reinforcing Bar Condition at a Construction Site.

Table 5.3 Calculated Conditions for an Intermediate Longitudinal Bar Using the Buckling Model for Stages (2) and (3).

ε_r (%)		2.0	3.0	4.0	5.0	6.0
M_p ($\times 10^3$ N· mm)		381	280	195	127	77
$E_p I$ ($\times 10^6$ N· mm^2)		50.5	38.5	27.8	18.5	11.5
Two Plastic Hinges	w (N/mm)	145	76	30	9	2
	q (N/mm)	456	852	1284	1939	3150
	a	0.204	0.190	0.162	0.118	0.075
	δ (mm)	5.5	4.3	3.1	1.9	1.1
Three Plastic Hinges	w (N/mm)	-	162	101	58	31
	q (N/mm)	-	585	1190	2039	3369
	a	-	0.129	0.115	0.088	0.061
	δ (mm)	-	16.1	16.3	16.6	16.8

of M_p when ε_r = 2.0 % in Table 5.1. A possible maximum value of w can be estimated as 179 N/mm, assuming that $M_p = w\, l_s^2/12$. The tension force in the cross tie, T_w, corresponding to this magnitude of w is evaluated as

$$29\ \text{KN}\ (= w\, l_s) > T_w > 24\ \text{KN}\ (= w\, l_s - F_1^p)$$

It can be shown that this range of T_w causes a tension strain ε_s of between 0.106 % and 0.128 % in the tie bar leg, based on the relation $\varepsilon_s = (T_w/A_s)/E$. In the test, the measured tie bar strains at μ of $\pm$ 4 were less than 0.1% as indicated in Fig. 5.26. This means that the magnitude of w imposed on the longitudinal bar in the test was small enough to satisfy $M_p \geq w\, l_s^2/12$ in Eq. 5.49 at least up to $\mu = \pm 4$. Hence, Eq. 5.50 is applicable instead of Eq.5.49 up to μ of $\pm$ 4 in the case of this column test.

From these calculations, it may be concluded that the buckling model shown in Fig. 5.20 for Stage (1) is adequate for the early stage of loading of up to displacement ductility factor of about $\pm$ 4 as far as this column test concerned.

(b) Buckling Check for Stages (2) and (3)

As the first step, δ_{cr} (=ultimate central deflection of longitudinal reinforcement able to maintain an axial load P_{cr}) can be determined from Fig. 5.27 or by a trial and error method using Eq.5.56. For the tested column, δ_{cr} of 1.61mm can be obtained taking P_{cr} as the yield force of the longitudinal bar.

In Table 5.3, the calculated results for Stages 2 and 3 in Section 5.3.6 are listed for various ε_r from 2 to 6 %. It must be noted that, in the calculation, the cross ties with 180° end hooks were always assumed to have yielded due to the lateral pressure from the core concrete for each ε_r value.

In the case when ε_r = 2% was assumed, plastic hinges in the longitudinal bar could form only at both bar ends restrained by 180° end hooks. This is because the inelastic moment of resistance of the longitudinal bar was still large at this stage. However, the calculated central deflection d for ε_r = 2% is much larger than δ_{cr}. This indicates that the longitudinal bar could have buckled if the cross ties with 180° end hooks had actually yielded due to the lateral pressure from the core concrete. However, as mentioned in the

buckling check for Stage (1), the measured strains in the cross ties were up to 0.1%, which is less than the yield strain of 0.163 %, at this loading stage of the tested column.

As can be seen from Table 5.3, δ could be smaller than δ_{cr} in the case when the cross ties with 180° end hooks were assumed to have yielded at ε_r = 6 % assuming that two plastic hinges formed in the longitudinal bar. In the tested column, the yielding of the cross ties with 180° end hooks were observed at μ of about 9, as shown in Fig. 5.26. At this stage, the maximum longitudinal bar strains measured by electric wire strain gauges indicated a strain range from 0.7 % tension strain to 2.0 % compression strain due to cyclic loading. On the other hand, the maximum longitudinal bar strains, which were calculated from curvatures measured by potentiometers, indicated a strain range from 1.0 % tension strain to 3.0 % compression strain. This calculation was based on the assumption that plane sections before bending remain in plain after bending. As a matter of course, this assumption may be incorrect in the inelastic range of cyclic loading. However, measurements by electric wire strain gauges are also unreliable at high inelastic strains. Hence, the real strain in the longitudinal bars would lie between those values. Based on these strain measurements, an estimate for ε_r of more than 5 % might be reasonable if the Bauschinger effect on steel due to cyclic loading consisting of two cycles to each of μ =±2, and ±5 and one cycle to μ_d = +9 was taken into account. From this point of view, it may be said that lateral deflection of the longitudinal bar δ could possibly be smaller than the critical deflection δ_{cr} under the condition of longitudinal bar with two plastic hinges, even though lateral pressure from core concrete was large enough to make the cross ties with 180° end hooks yield. In effect, the occurrence of buckling of the longitudinal bar could not be observed until the displacement ductility factor μ was about 11 in the test.

However, it could be considered that the lateral pressure distribution had changed and shifted the longitudinal bar from a two plastic hinge condition to a three plastic hinge condition. The central deflection δ could have thus exceeded the critical value of δ_{cr}. Accordingly, at μ of more than 11, the lateral deflection of the longitudinal bar was observed to become large in the test. After the central deflection exceeded δ_{cr}, the axial load in the longitudinal bar reduced as the deflection increased, in accordance with the magnitude of F_1 plus F_2 as can be seen from Fig. 5.27.

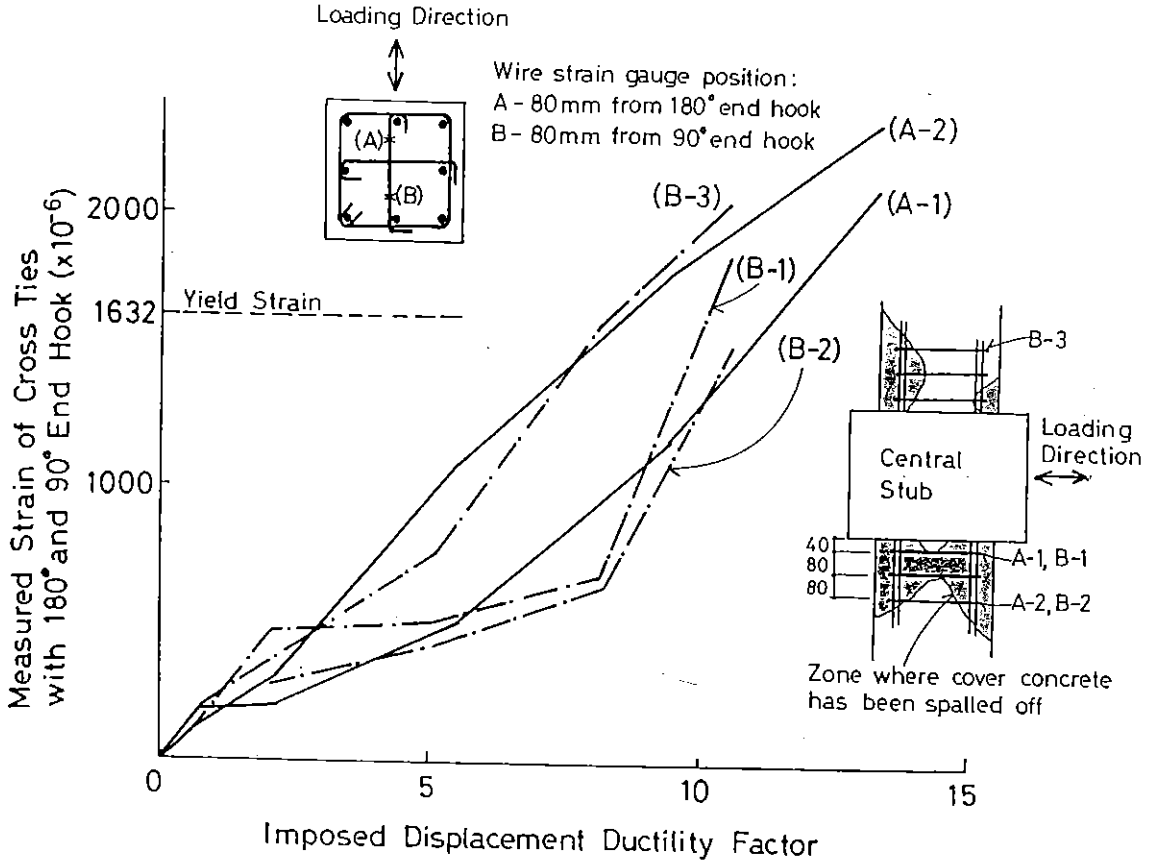

Fig. 5.26 Measured Strains on Cross Ties with 90° and 180° End Hooks at Each End for Unit 2.

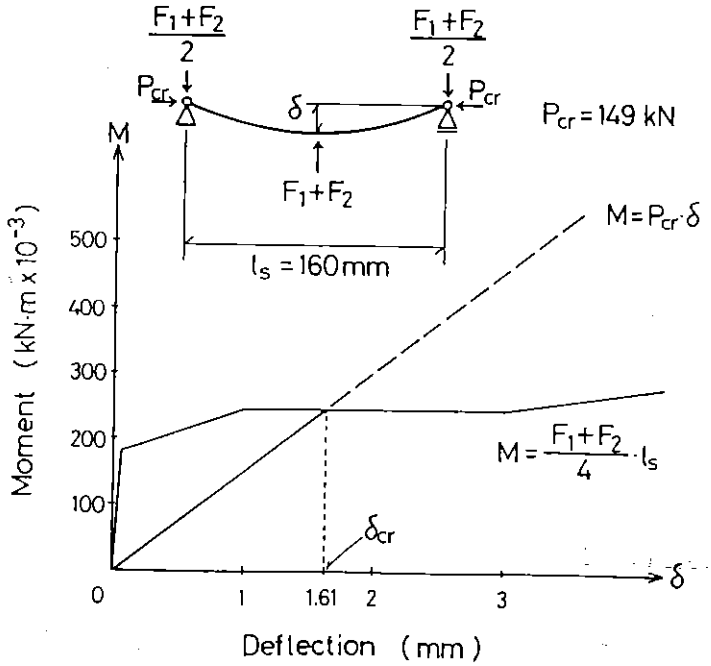

Fig. 5.27 Theoretical Maximum Deflection Able to Maintain the Axial Load, P_{cr}.

Fig. 3.20 shows that the loss of load carrying capacity of the column is gradual even after buckling of the intermediate longitudinal bar with the opening of the 90° end hook. In order to explain this situation, moment-curvature analyses were conducted for the tested column section shown in Fig. 5.28. In the analyses, the modified Kent and Park stress-strain model for confined concrete [5.16] was used. For the longitudinal bars, the stress-strain model shown in Fig. 5.17 was used. In Fig. 5.28, curve (A) indicates the case when all peripheral hoops and cross ties are adequately anchored using 180° end hooks. Curve (B) corresponds to the case when the intermediate longitudinal bar has buckled and totally lost its load carrying capacity, using the same stress-strain relation of confined concrete as in curve (A). Curve (C) indicates the case when one third of the lateral reinforcement became ineffective in addition to the total loss of load carrying capacity of the buckled intermediate longitudinal bar. From the comparison between curves (A) and (B), it may be said that decrease in the load carrying capacity of the column due to buckling of a longitudinal bar is not so significant providing that the core concrete is well confined,.

It must be emphasized that measured strain in the tie legs with the 90° end hooks could also reach the yield strain, as shown in Fig. 5.26, although the maximum sustaining force of a 90° end hook F_1^p is only about 12 % of the yield force of the tie leg. This may mean that core concrete was confined to some extent as a result opf the bond effect of the deformed bar cross tie legs. This has been observed by other investigations. For example, axial compression tests on columns in reported reference [5.17] have demonstrated that straight deformed bars without any end hooks and without any connection between bars can also effectively confine the core concrete if the amount of the straight deformed bars is sufficient. Hence, it can be considered that ductile behaviour of the column might be lost more quickly if plain bars were used for cross ties with 90° and 180° end hooks at the ends. It is notable that deformed bars seem to have been used for the cross ties in all the column tests appeared in references [5.14, 5.18, 5.19, 5.20, 5.21 5.22], although most of the American studies do not clearly state whether deformed bars or plain bars were used. This conjecture is based on the requirement in ACI 318-83 [5.2] to use deformed bars for reinforcement except for spirals and prestressing tendons, while in NZS 3101 [5.1] plain bars are allowed to use for ties and stirrups as well.

The question, "plain bar or deformed bar, which is the more effective for cross ties with 90° and 135° or 180° end hooks at the ends ?", it is not easy to answer . The minimum diameter of bends for ties with plain bars can be one half of that with deformed bars according to NZS 3101. This means that the use of plain bar can make the distance between the centroids of the tie leg section and the longitudinal bar section, l_b, shorter in comparison with when the deformed bar is used. As a consequence, a larger stiffness of 90° end hook against lateral deflection of the longitudinal bar can be achieved when plain bar is used if the bar size and Young's modulus of steel are same. On the contrary, cross ties from deformed bars may possibly confine the core concrete in the compression zone more effectively due to the higher bond strength than for plain bars. Moreover, cross ties from deformed bars may effectively prevent the wide opening of the diagonal tension cracks which occur around the mid-depth of the column, without relying much on the end hooks, due to the good bond of the tie legs. On the other hand, cross ties from plain bars will be anchored mainly by the end hooks due to lack of bond strength in the tie leg, and hence may prevent wide opening of the inclined diagonal tension cracks due to significant elongation in the plain bar tie legs from the crack position to the end hook, especially after yielding of the tie.

5.3.8. Limits of Application of the Model

The model presented in the previous sections is derived for intermediate longitudinal bars restrained by peripheral hoops and cross ties with alternating 90° and 135° or 180° end hooks along the longitudinal bar. The following two conditions must be satisfied in order that this model is used in an adequate manner.

(1)Yielding of the tie legs anchored by the 135° or 180° end hooks, due to the outward force from the longitudinal bars, does not take place at such anearly stage of loading, such as in Stage (1).

(2)The stiffness of the 135° or 180° end hooks against the longitudinal bar buckling is considerably larger than that of the 90° end hooks.

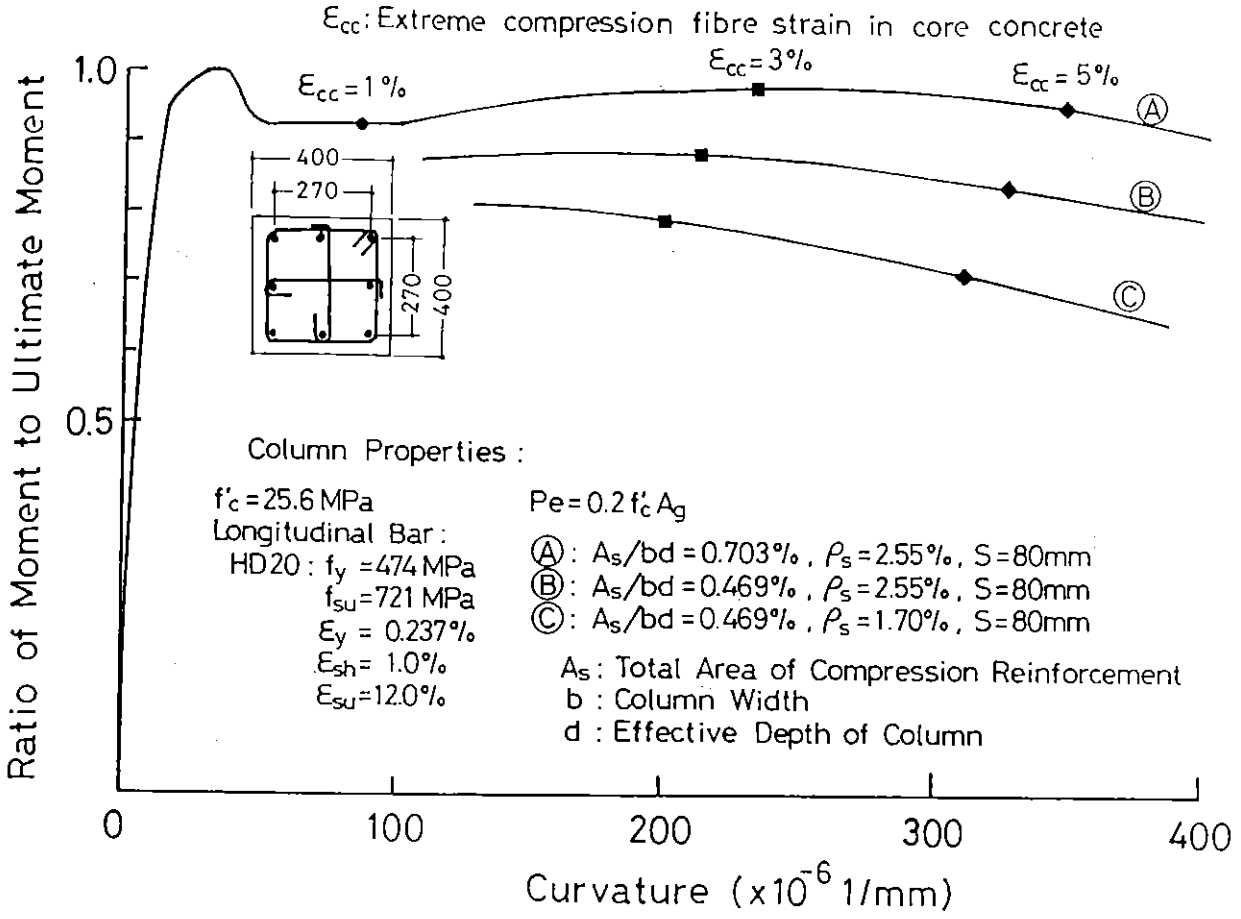

Fig. 5.28 Theoretical Monotonic Moment-Curvature Relations for Unit 2.

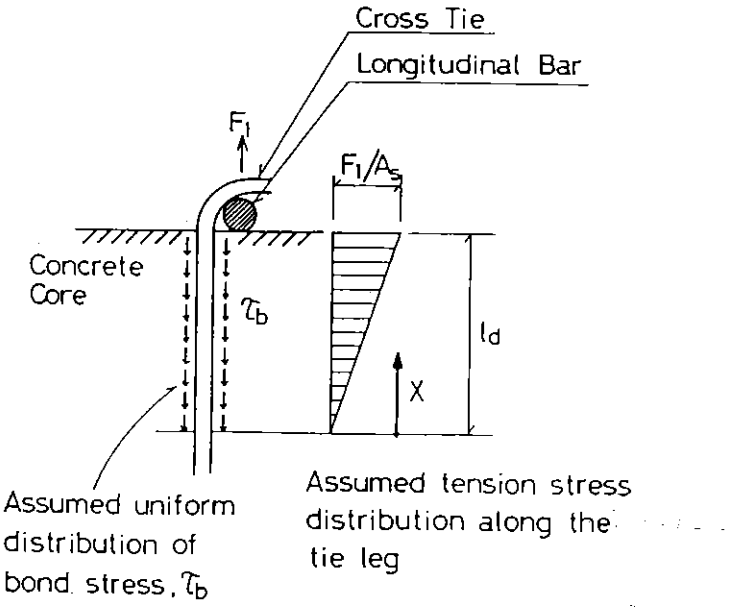

Fig. 5.29 Assumed Bond Stress Distribution for Estimating the Tie Leg Stiffness Against Pull-out Force.

If the above conditions can not be satisfied, it is necessary that points (A) and (C), at the 135° or 180° end hooks in Fig. 5.5 are also restrained by suitable spring models.

The meaning of condition (1) is that, if yielding of the tie legs occurrs from the early stage of loading , the displacements of the 135° or 180° end hooks due to pull out from the concrete core may not be negligible. Such a situation will possibly occur in the case when the amount of lateral reinforcement is considerably small. However, condition (1) is normally satisfied if the amount of lateral reinforcement is determined in compliance with the ductility design method of NZS 3101.

Whether condition (2) can be satisfied or not may be checked as follows.

The outward force applied to the end hooks and the reacting bond stresses in the tie legs may be assumed to be as in Fig.5.29. As a matter of course, the tie bar is to be stretched not only by the outward force from the longitudinal bar but by expansion of core concrete due to Poisson's effect and also by shear force. However, for the purpose of checking, the assumption represented by Fig. 5.29 may be acceptable.

The deflection of the 90° end hook due to bending, δ_b, in the elastic range of the steel can be expressed in a form similar to Eq. 5.13 Hence,

$$\delta_b = \frac{F_1 l_b^3}{3EI_t} \qquad \text{.....} \qquad (5.74)$$

The displacement of the 90° end hook due to slippage of the tie leg from the core concrete, δ_s , may be calculated assuming that the bond stress distribution along the tie leg is uniform. In this case, δ_s can be expressed in the form

$$\delta_s = \int_0^{l_d} \varepsilon_x \, dx = \int_0^{l_d} \frac{F_1}{A_s E} \frac{x}{l_d} \, dx = \frac{F_1 l_d}{2 A_s E} \qquad \text{.....} \quad (5.75)$$

where l_d = development length required to resist outward force from longitudinal bar

x = coordinate of a point along tie bar leg.
A_s = area of tie bar section
ε_x = tension strain in the tie bar leg at point x

The stiffness of the cross tie with 90° end hook (k_1^e) can be expressed as

$$k_1^e = \frac{F_1}{(\delta_b + \delta_s)} \qquad \text{.....} \qquad (5.76)$$

Substituting Eqs. 5.74 and5.76 into Eq. 5.76,

$$k_1^e = \frac{1}{(\frac{l_b^3}{3EI_t} + \frac{l_d}{2A_s E})} \qquad \text{.....} \qquad (5.77)$$

In case of the cross ties with 135° or 180° end hook, the hook itself may be assumed to be not deformable since the hook end is embedded into the core concrete with adequate length extension. Hence, the initial stiffness of the cross tie with a 135° or 180° end hook, k_3^e, may be determined only from the pull out displacement $\delta_{s'}$ and thus,

$$k_3^e = \frac{F_3}{\delta_{s'}} = \frac{2A_s E}{l_d} \qquad \text{.....} \qquad (5.78)$$

where F_3 = outward force on 135° or 180° end hook from longitudinal bar
$\delta_{s'}$= displacement of 135° or 180° end hook due to slippage of tie leg from core concrete

Then the ratio of k_1^e to k_3^e designated by R_e can be calculated in the form

$$R_e = \frac{k_1^e}{k_3^e} = \frac{l_d}{2AE\left(\frac{l_b^3}{3EI_t} + \frac{l_d}{2AE}\right)}$$

Substituting $A_s = \pi d_b^2/4$ and $I_t = \pi d_b^4/64$ where d_b = tie bar diameter,

$$R_e = \frac{1}{\left[\frac{32\, l_b^3}{3\, l_d\, d_b^2} + 1\right]} \qquad \text{..... (5.79)}$$

In Eq. 5.79, l_b and l_d can be written as a function of d_b as described in the subsequent paragraphs.

Since the longitudinal bar diameter is normally 2 to 3 times the tie bar diameter, the distance between the centroids of the tie bar leg section and the longitudinal bar section, l_b, may possibly be in a range of 3 to 4 times the tie bar diameter. Hence, $l_b = 3 \sim 4\ d_b$.

The development length, l_d, depends on the magnitude of F_1 or F_3 and the bond condition of the core concrete. If l_d is estimated for the stage when the extreme fiber of the 90° end hook bar section at the bent corner has just reached the yield strain, it can be calculated as follows. In Eq. 5.12, the corresponding F_1^e has already been expressed. F_1^e can also be expressed as the function of the bond stress in the tie leg τ_b. Assuming that the bond stress distribution is uniform,

$$F_1 = \tau_b\, \pi\, d_b l_d \qquad \text{..... (5.80)}$$

Equating Eqs. 5.12 and 5.80,

$$\frac{f_{yt}\, \pi\, d_b^3}{32\, l_b} = \tau_b\, \pi\, d_b l_d$$

Rearranging,

$$l_d = \frac{f_{yt}\, d_b^2}{32\, \tau_b\, l_b} \qquad \text{..... (5.81)}$$

If plain bars were used for the cross ties, the average bond stress may be assumed about 0.3 to 1.0 MPa based on the static pull-out tests of plain bars from concrete blocks in reference [5.23]. As an example, if f_{yt} = 300 MPa and $l_b = 3\ d_b$ are assumed, Eq. 5.81 gives $l_d = 3\sim10\ d_b$ for the above bond stress. Substituting these values into Eq. 5.79, R_e = 0.01~0.03 can be

obtained. If deformed bars were used for the cross ties, R_e has a much smaller value because the average bond stress in a deformed bar can normally reach more than 2 times that in a plain bar .

From above considerations, it may be concluded that, in comparison with the stiffness of a cross tie with the 135° or 180° end hook, the stiffness of a cross tie with a 90° end hook is normally small enough for the buckling model shown in Fig. 5.5 to be considered adequate. However, it should be noted that the stiffness ratio R_e expressed by Eq. 5.79 can be rapidly increased by making the the tie bar diameter closer to the longitudinal bar diameter. For example, if the tie bar diameter is same as the longitudinal bar diameter, the distance between the centroids of the tie leg section and the longitudinal bar section, l_b, can be close to d_b if the code provision for the minimum inside diameters of bends for ties is neglected. In such a case, l_d calculated from Eq. 5.81 becomes 10 to 30 d_b for f_{yt} = 300 MPa and τ_b = 0.3 to 1.0 MPa and Re from Eq.5.79 becomes 0.48 to 0.74. Moreover, if the bond condition of the tie leg degrades under cyclic loading, the development length l_d becomes longer and consequently the value of R_e becomes larger.

From the above check, if the calculated ratio R_e becomes less than about 0.1, it may consider that the model represented by Fig. 5.5 is adequate.

5.4 CONCLUSIONS

Based on the above analytical study, the following conclusions are reached with regard to the effectiveness of cross ties with a 90° end hook at one end and a 135° or 180° end hook at the other end alternating along the longitudinal reinforcement:

1. The initial stiffness of the 90° end hook can be large enough to prevent buckling of the intermediate longitudinal bar in the early stages of loading. However, the maximum elastic deflection of the 90° end hook at the contact point with the longitudinal bar, which is estimated by Eq. 5.13, is in the order of 0.01 to 0.1 mm, in practice. Hence, the initial deflection of the longitudinal reinforcement due to imperfection must be considered.

2. The maximum allowable initial deflection of the longitudinal bar due to imperfection $\delta_o{}^c$ can be calculated using Eq. 5.55. If the calculated value of

$\delta_o{}^c$ is impractically small, lateral restraint by the 90° end hook against longitudinal bar buckling should not be expected. In such case, the cross ties with a 90° end hook at one end and a 135° or 180° end hook at the other end should be neglected in the evaluation of the total amount of effective transverse reinforcement.

3. The initial stiffness of a peripheral hoop, with regard to the lateral restraint of an intermediate longitudinal bar, is negligibly small compared with that of a cross tie with a 90° end hook. Hence, it is not necessary to take the restraint of peripheral hoops into account in the early stage of loading of the column.

4. If the amount of transverse reinforcement is large enough to delay tensile yielding of the transverse reinforcement until the column reaches a large displacement ductility factor (e.g. more than 6), buckling of the longitudinal bar may be adequately delayed by the restraint of a 90° end hook and the peripheral hoop. This can be explained as follows. When a displacement ductility factor of more than 6 is reached, the longitudinal reinforcement has already been loaded far into the inelastic range. As a result, the bending stiffness of the longitudinal bar degrades rapidly as its compression strain increases. Under such condition, the lateral pressure from the core concrete concentrates at the positions of the 135° or 180° end hooks. As a consequence, the deflection of the longitudinal bar due to lateral pressure can remain small in magnitude, which results in a moment due to deflection can be balanced by a small sustaining force from the 90° end hook and the peripheral hoop. However, such a state of stable equilibrium in the longitudinal bar may be only temporary. That is, buckling of the longitudinal bar can eventually occur as the pressure distribution along the longitudinal bar changes.

5. In a numerical example it was found that a 90° end hook on a cross tie could only sustain about 12 % of the yield force of the cross tie.

6. The transition of loading conditions on the longitudinal bar, which includes the lateral pressure from the core concrete, is well predicted for stages of loading on the column using the model proposed in this study .

7. In the inelastic range of behaviour of the column, the effective confinement of the core concrete may be a more critical requirement than the prevention of buckling of the longitudinal reinforcement, except for the case when the column has an extremely large amount of longitudinal reinforcement. If the buckling of the intermediate longitudinal reinforcement restrained by a 90° end hook results in a rapid decrease in the load carrying capacity of the column, it may be mainly because the effective confinement of the core concrete is lost due to large deflection of the bar. Therefore, decrease in the load carrying capacity of of the column caused by buckling of an intermediate longitudinal bar can be insignificant providing that the core concrete is adequately confined. Hence, it is recommended that an adequate margin for the amount of transverse reinforcement be provided if cross ties with 90° and 135° or 180° end hooks are used.

8. In order to reduce the ratio of the area of compression reinforcement restrained by 90° end hooks to the area of compression reinforcement securely restrained by 135° or 180° end hooks, the transverse reinforcement detail shown in Fig.3.11(b) is preferable rather than that shown in Fig. 3.11 (a).

9. In the previous column tests with axial load level of up to 0.3 $f'_c A_g$, which are reported in references [5.14, 5.18, 5.19,5.20, 5.21], the effectiveness of the cross ties with a 90° end hook at one end and a 135° or 180° end hook at the other end alternating along longitudinal reinforcement was generally as satisfactory as that of conventional cross ties with 135° or 180° end hooks. The analytical study developed in this chapter also also indicates the possibility of such a result, since bond between the tie leg and the confined concrete aids the anchorage of the cross tie. However, it should be noted that deformed bars were used for the cross ties in those previous column tests and hence the tie legs might have confined the core concrete by bond without relying significantly on the end hooks for anchorage. Further research on the effectiveness of cross ties with a 90° end hook at one end and a 135° or 180° end hook at the other end is recommended for the case where plain bar is used.

10. It should be noted that only cross ties with 90° end anchorages are considered here. Peripheral hoops with 90° end hooks are definitely inadequate as transverse reinforcement since once the cover concrete spalls

such perimeter hoops can move away (outwards) from the longitudinal bars and render the anchorage useless.

CHAPTER SIX

AVAILABLE LIMIT STRAIN OF CONFINED CONCRETE IN REINFORCED CONCRETE COLUMNS

6.1 INTRODUCTION

When a ductile design approach is used for the seismic design of reinforced concrete frame structures, the deformability of the constituent structural members needs to be assessed. In NZS 4203:1984 [6.1], regular symmetrical frame buildings designed to dissipate seismic energy by ductile flexural yielding, are required to be capable of deflecting laterally through at least eight load reversals so that the total horizontal deflection at the top of the main portion of the building under the specified design loads is at least four times that at first yield, without the horizontal load carrying capacity of the building being reduced by more than 20 %. NZS 4203 also states that the performance of the primary members of the seismic resisting system subjected to the displacement or curvature ductility demand determined in accordance with the above requirement, is acceptable if they lose no more than 30 % of their strength and provided the overall building ductility requirements are met. The derivation of those criteria for the limitation of the degradation of the load carrying capacity is not clearly stated in NZS 4203 but may be from engineering judgement based on dynamic analyses of frame structures [eg. 6.2] or lessons from earthquake damage at Tokachi-oki (1968), San Fernando (1971) and so on.

When seismic resisting ductile members are designed in accordance with the requirements specified in NZS 4203, the critical (ultimate limit) deformation of those members may be defined as the deformation where the strength of the member is reduced to 70 % of the maximum load carrying capacity during simulated severe seismic loading. At the University of Canterbury, cyclic loading which consists of two cycles each to displacement ductility factors of ± 2, ± 4, ± 6, ±8 etc. is commonly adopted as the simulated severe seismic loading, when deformation capabilities of earthquake resistant members need to be examined by experiments. Since such experiments cannot always be conducted, because of economical

reasons or available limit of experimental facilities, it is desirable to theoretically estimate the critical deformations of earthquake resistant members, if this can be achieved with satisfactory accuracy. In effect, theoretical cyclic load-displacement hysteresis loops for a member are often calculated in order to find the critical deformation of the member at which the calculated load-displacement hysteresis loops degrade to a predetermined level [6. 3]. However, normally this type of analysis is not an easy task. If the critical (ultimate limit) deformation can be defined as a particular value for the extreme compression fibre strain of concrete, the calculation of the limit (ultimate) deformation becomes much simpler. Hence, the previous research [6.4, 6.5, 6.7, 6.8] described in the next section has tried to establish empirical equations for an ultimate compressive strain of concrete in the extreme compression fibre of member as a function of the volumetric ratio and yield strength of the transverse reinforcement, the volumetric ratio of the longitudinal reinforcement and so on. However, it has been found that those empirical equations can be very conservative for well confined concrete, when the critical (ultimate limit) deformation of a member is defined as the deformation where the strength of the member is reduced to 70 % or 80 % of the maximum load carrying capacity during simulated severe seismic loading.

When a reinforced concrete column is loaded far into the inelastic range to failure, fracture of the hoop reinforcement eventually occurs and results in a sudden drop in the load carrying capacity of the section due to a reduction in confinement of the core concrete and a loss of buckling restraint for the longitudinal bars. This stage of failure signals the destruction of the column. For this reason, hoop fracture should definitely be avoided within the expected range of column deformation under any design load condition, especially for the deformations imposed by a severe earthquake. In order to provide such a restriction to the column deformation, a method for the prediction of the available maximum deformation of the column section limited by the occurrence of hoop fracture has been proposed by Mander et al [6.3, 6.10]. In this chapter, a modified method for the prediction of the occurrence of hoop fracture is proposed referring to the method proposed by Mander et al.

6.2 PREVIOUS RESEARCH

6.2.1 Empirical Equations for Ultimate Compressive Strain of Concrete

Early experimental work on the deformability of reinforced concrete beams led to the development of empirical equations for the ultimate concrete compression strain, ε_{cu}, to predict the rotational capacity of plastic hinges in beams. For example, Baker [6.4] proposed that

$$\varepsilon_{cu} = 0.0015 \, [\, 1 + 150 \, \rho_s + (0.7 - 10 \, \rho_s) \, d/c \,] \leq 0.01 \quad \ldots\ldots\ldots \quad (6.1)$$

where ρ_s =volumetric ratio of transverse reinforcement to confined concrete core

d = effective depth of the section

c = neutral axis depth

and Corley [6.5] proposed that

$$\varepsilon_{cu} = 0.003 + 0.02 \, \frac{b}{z} + \left[\frac{(\rho_s + \rho_{cc}) \, f_{yh}}{138} \right]^2 \quad \ldots\ldots\ldots \quad (6.2)$$

where ρ_{cc} = volumetric ratio of the longitudinal reinforcement to the confined concrete core

f_{yh} = yield strength of transverse reinforcement in MPa

z = distance from critical section to point of contraflexure

Since Eq. 6.1 limits the maximum value of ε_{cu} to 1 % and Eq. 6.2 estimates that ε_{cu} is up to about 1.5 % for an ordinary range of values used for the variables, it is evident that those equations are very conservative for well confined reinforced concrete columns in which the extreme compression fibre strain of the core concrete normally reaches more than 2% at a displacement ductility factor of six without significant decrease of the load carrying capacity. This can be seen from many experimental studies [eg. 6.7] as well as from the test results shown in Chapters three and four.

From the results of concentric and eccentric column compression tests Scott, Park and Priestley [6.6] proposed the following equation to predict

the maximum available compressive strain for concentrically loaded columns.

$$\varepsilon_{max} = 0.004 + 0.9\,\rho_s \left[\frac{f_{yh}}{300}\right] \qquad \text{.....} \qquad (6.3)$$

where f_{yh} = yield strength of transverse reinforcement in MPa

This value for ε_{max} is a lower bound value for hoop fracture for columns with transverse reinforcement. When Eq. 6.3 was established, the enhancement in strain capacity of the concrete due to the presence of a strain gradient was ignored, although it was found by Scott, Park and Priestley [6.6] that for eccentrically loaded columns with a strain gradient (such that the strain at one face was approximately zero and the other ε_{max}) the strain at first hoop fracture approximately doubled. Therefore, in the context of predicting the rotational capacity of a column Eq. 6.3 will also be conservative.

In the study by Muguruma et al [6.8, 6.9], the available limit of compressive strain of concrete in a flexural member with or without axial load was defined as the axial compressive strain at which the average stress in the monotonic stress-strain curve of concrete becomes a maximum (see Section 2.2). This definition was applied to both confined and unconfined concrete. As shown in Fig. 2.17, the available limit of compressive strain of concrete determined by this definition is also conservative when used to predict the rotational capacity of plastic hinges in columns or beams. The details of determining the limit of the compressive strain of concrete using the stress-strain models of confined and unconfined concrete proposed by Muguruma et al have been described in Section 2.2.

6.2.2 The Energy Balance Theory Proposed by Mander et al

In recent studies conducted at the University of Canterbury, the ultimate compressive strain of concrete ε_{cu} has been defined as the longitudinal compressive strain corresponding to first fracture of the transverse reinforcement [6.7]. Mander et al [6.3, 6.7, 6.10, 6.11] have established that it is possible to predict this strain with reasonable accuracy on the basis of energy considerations, as described in the following paragraphs.

Many experimental studies have demonstrated that the compressive strength and ductility of the core concrete in a reinforced concrete member can be enhanced using closely spaced transverse confining reinforcement in the form of spirals or hoops with or without cross ties, as described in Chapter two. Schematic stress-strain curves of confined and unconfined concrete can be represented by Fig. 6.1 [6.3]. The area under each curve represents the total strain energy per unit volume required to 'fail' the concrete and the shaded area indicates the increase in strain energy at failure resulting from confinement. Here the failure of the confined concrete is defined as the stage of first hoop fracture.

In the energy balance theory proposed by Mander et al [6.3, 6.7, 6.10], it was assumed that the ultimate strain energy capacity of the transverse confining reinforcement per unit volume of core concrete core (U_{sh}) could be equated to the difference in area between the confined (U_{cc}) and unconfined (U_{co}) stress-strain curves (that is, the shaded area in Fig. 6.1) plus the stored strain energy in the compressed longitudinal reinforcement per unit volume of concrete core (U_{sc}). This was expressed in the form

$$U_{sh} = (U_{cc} - U_{co}) + U_{sc} \qquad \text{.....} \qquad (6.4)$$

The theory indicates that Eq. 6.4 can be rewritten for per unit volume of concrete core in terms of strains and stresses as

$$\rho_s \int_0^{\varepsilon_{sf}} f_{sh}\, d\varepsilon_{sh} = \left(\int_0^{\varepsilon_{cu}} f_{cc}\, d\varepsilon_c - \int_0^{\varepsilon_{sp}} f_{co}\, d\varepsilon_c \right) + \rho_{cc} \int_0^{\varepsilon_{cu}} f_{sl}\, d\varepsilon_c \qquad \text{.....} \qquad (6.5)$$

or for per unit length of the column,

$$A_{cc}\rho_s \int_0^{\varepsilon_{sf}} f_{sh}\, d\varepsilon_{sh} = \left(A_{cc} \int_0^{\varepsilon_{cu}} f_{cc}\, d\varepsilon_c - A_{cc} \int_0^{\varepsilon_{sp}} f_{co}\, d\varepsilon_c \right) + A_{cc}\rho_{cc} \int_0^{\varepsilon_{cu}} f_{sl}\, d\varepsilon_c \qquad \text{.....} \qquad (6.6)$$

where A_{cc} = sectional area of concrete core measured to centre of peripheral spiral or hoop

f_{cc} = compressive stress in confined concrete

f_{co} = compressive stress in unconfined concrete

f_{sh} = tensile stress in hoop reinforcement

f_{sl} = compressive stress in longitudinal reinforcement

ε_c = compressive strain in confined and unconfined concrete

ε_{cu} = longitudinal compressive strain in core concrete at first hoop fracture

ε_{sh} = tensile strain in hoop reinforcement

ε_{sf} = tensile fracture strain of hoop steel

ε_{sp} = compressive strain at which unconfined concrete is assumed to have completely spalled

ρ_{cc} = sectional area ratio of compression reinforcement to concrete core

ρ_s = volumetric ratio of hoop reinforcement to concrete core

In Eq. 6.5, the left hand term is the total area under the transverse steel stress-strain curve up to fracture strain ε_{sf}. Based on the results from tests on Grade 275 and Grade 380 reinforcement of various bar diameters, Mander et al [6.3] found that the total area under the transverse steel stress-strain curve up to fracture strain (denoted by U_{sh}) was effectively independent of bar size or yield strength and could be taken as 110 MJ/m^3. That is,

$$\int_0^{\varepsilon_{sf}} f_{sh}\, d\varepsilon_{sh} = 110\ MJ/m^3 \qquad \text{.....} \qquad (6.7)$$

For the estimation of U_{co} for per unit volume of concrete core, the following empirical equation [6.3] was used.

$$\int_0^{\varepsilon_{sp}} f_{co} d\varepsilon_c = 0.017 \sqrt{f'_{co}} \text{ kJ / m} \quad \text{.....} \quad (6.8)$$

Thus Eq. 6.5 simplifies to

$$110\,\rho_s = \int_0^{\varepsilon_{cu}} f_{cc}\, d\varepsilon_c + \rho_{cc} \int_0^{\varepsilon_{cu}} f_{sl}\, d\varepsilon_c - 0.017 \sqrt{f'_{co}} \text{ MJ / m}^3 \quad \text{.....} \quad (6.9)$$

With a knowledge of f_{cc} and f_{sl} as functions of longitudinal strain, Eq. 6.9 can be solved for ε_{cu} by numerical trial and error methods. Using Eq. 6.9 and the proposed stress-strain models [6.3] for confined concrete and longitudinal reinforcement, Mander et al demonstrated that the ultimate compressive strains of concrete at hoop fracture predicted by Eq. 6.9 agreed well with the values obtained from the accompanied column tests [6.3, 6.11].

6.3 PREDICTION OF THE ULTIMATE LONGITUDINAL COMPRESSIVE CONCRETE STRAIN AT FIRST HOOP FRACTURE USING THE ENERGY CONSIDERATIONS

6.3.1 Introduction

Mander et al [6.3, 6.7, 6.10] have proposed a theory for the prediction of the ultimate longitudinal compressive concrete strain at the stage of first hoop fracture referred to as the "Energy Balance Theory". The ultimate longitudinal compressive concrete strain at first hoop fracture predicted by this theory agreed well with most of the accompanied test results [6.3, 6.11]. However, the theory as presented by Mander et al is simplified and may not always give an adequate estimation of the ultimate concrete strain at first hoop fracture for the following two reasons.

Firstly, in the main energy equation used in the theory, the relation between the strain energy stored or dissipated in the core and cover concrete, longitudinal bars and hoops was simplified by neglecting several

energy factors which might not be negligible. For example, the treatment of the strain energy absorbed in the longitudinal bars seems to be inadequate, especially when buckling of the longitudinal bars commences at large axial strain.

Secondly, the strain energy stored in the hoops prior to first hoop fracture could be overestimated by about 20 to 40 % or more if the value proposed, based on tensile tests on steel bars, was used. The value proposed for the strain energy stored in the hoops prior to first hoop fracture was determined by assuming that all region of the hoop (that is, the whole length of hoop) reached the fracture strain at the same time. It is more reasonable to consider that at first hoop fracture the strains in the all parts of the hoop bar except the small length which necks and fractures will be same or less than the strain at ultimate strength of the hoop bar which is usually 20 to 40 % less than the fracture strain of the hoop bar.

This probable overestimation of the strain energy stored in the hoops prior to first hoop fracture appears to have compensated for the omission of the absorbed energy in the longitudinal bars when the theory was applied by Mander et al to test results. However, a significant error in the estimation of the ultimate longitudinal compressive concrete strain at first hoop fracture can possibly be made in the case of a column with a combination of a large amount of longitudinal bars and a small amount of hoop reinforcement or in case of a column which has a large strain gradient in the section by bending.

In the following sections, after discussing in more detail the problems in the energy balance theory proposed by Mander et al, a modified theory for the prediction of the ultimate longitudinal compressive concrete strain at which first hoop fracture occurs is proposed using a simple failure model of a reinforced concrete column under axial compression load.

6.3.2 The Theoretical Defects in the Energy Balance Theory Proposed by Mander et al

In the energy balance theory proposed by Mander et al [6.3, 6.7, 6.10], it was assumed that the ultimate strain energy capacity of the transverse confining reinforcement per unit volume of core concrete core (U_{sh}) could be equated to the difference in area between the confined (U_{cc}) and

unconfined (U_{co}) stress-strain curves plus the stored strain energy in the compressed longitudinal reinforcement per unit volume of concrete core (U_{sc}), as expressed by Eq. 6.4. It is evident that the assumption of the energy balance theory expressed in the form of Eq. 6.4 is not always adequate. For example, the use of Eq.6.4 can result in a large error in case of a column which has a large amount of longitudinal bars compared with the amount of transverse confining reinforcement as can be demonstrated by the following check. In the limit, if transverse confining reinforcement is not provided, then $U_{sh} = 0$ which from Eq.6.4 means that

$$U_{sc} = U_{co} - U_{cc} \quad \text{.....} \quad (6.10)$$

But for this case $U_{co} - U_{cc}$ is equal to zero if there is no confinement, or $U_{co} - U_{cc}$ is less than zero if some confining effect by the longitudinal reinforcement can be expected, and hence $U_{sc} \leq 0$. However, U_{sc} can be neither zero nor negative since the longitudinal reinforcement is acting as compression reinforcement. Hence, Eq.6.4 yield a contradiction in this case.

A further check for Eq. 6.4 can be conducted as follows. The energy balance theory indicates that Eq. 6.4 can be rewritten in terms of strains and stresses as expressed by Eqs. 6.5 or 6.6. Note that for the calculation of U_{sc} in the last term in Eqs. 6.5 and 6.6, $d\varepsilon_c$ was used in stead of $d\varepsilon_s$ where ε_s = axial compressive strain in the longitudinal bars. However the axial strain of the concrete core will only be equal to the axial strain in the longitudinal bars before buckling of the longitudinal bars occurs and provided that there is no bond slip of the longitudinal bars. Once buckling of the longitudinal bars has commenced the strain ε_c should be expressed as the sum of the axial compressive strain of the longitudinal bars ε_s and an apparent strain due to the axial shortening of the longitudinal bars induced by the bar buckling ε_s'. This can be expressed in the form

$$\varepsilon_c = \varepsilon_s + \varepsilon'_s \quad \text{.....} \quad (6.11)$$

The buckled condition of a longitudinal bar may be modelled as shown in Fig. 6.2. The total displacement ΔT can be separated into the displacement due to the axial compression ΔA and the displacement due to the buckling ΔB. ε_c, ε_s and ε'_s in Eq. 6.11 correspond to $\Delta T/l$, $\Delta A/l$ and $\Delta B/l$, respectively. The energy relation between the external work done by

the force P_{sl} and the corresponding strain energy in the longitudinal bar and the hoop reinforcement can be written in the form

$$P_{sl}\,\Delta T = P_{sl}\,\Delta A + P_{sl}\,\Delta B$$

$$= A_s\, l \int_0^{\varepsilon_s} f_{sl}\, d\varepsilon_s + \left[\int_0^{l} \frac{E_b I_b}{2}\left(\frac{d^2 y}{d x^2}\right)^2 dx + \int_0^{\delta} T_h\, d\delta \right] \quad \ldots\ldots\ldots \quad (6.12)$$

where A_s = sectional area of a longitudinal bar

l = initial length of a longitudinal bar before loading

E_b = tangent modulus of a longitudinal bar in the inelastic range

I_b = moment of inertia of longitudinal bar cross section

T_h = lateral restraining force due to hoop reinforcement

δ = lateral deflection of a longitudinal bar at hoop position

d^2y/dx^2 = curvature of a longitudinal bar

ε_s = axial strain due to stress $f_{sl} = P_{sl} / A_s$

Only inelastic buckling of a longitudinal bar is considered here because the spacing of the hoop sets is normally close enough to prevent elastic buckling as specified in the New Zealand design code for reinforced concrete structures [6.12]. Hence, in Eq. 6.12, the first term in the square parentheses expresses the strain energy stored in a longitudinal bar due to bending during inelastic buckling using tangent modulus theory [6.13], while other theories of inelastic buckling [6.14, 6.15, 6.16] might give more accurate estimation. However, which theory is the most suitable is not so important here because the magnitude of the strain energy of that term will be considerably smaller than of the other terms in Eq. 6.12 due to small bending stiffness of the longitudinal bar in the inelastic range and thus that term may be neglected.

Now, reconsider the meaning of Eq. 6.6 here. Rearranging Eq. 6.6,

$$A_{cc}\int_0^{\varepsilon_{cu}} f_{cc}\, d\varepsilon_c + A_{cc}\,\rho_{cc}\int_0^{\varepsilon_{cu}} f_{sl}\, d\varepsilon_c = A_{cc}\,\rho_s \int_0^{\varepsilon_{sf}} f_{sh}\, d\varepsilon_{sh} + A_{cc}\int_0^{\varepsilon_{sp}} f_{co}\, d\varepsilon_c \quad \ldots\ldots \quad (6.13)$$

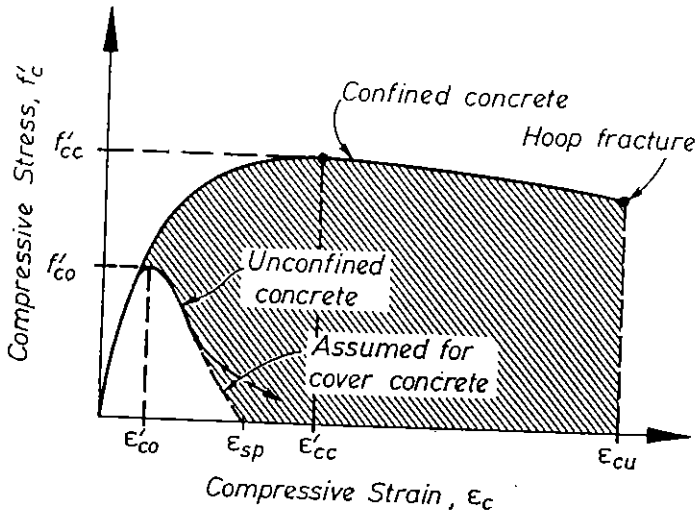

Fig. 6.1 Stress-Strain Model for Confined and Unconfined Concrete [6.3, 6.7, 6.10].

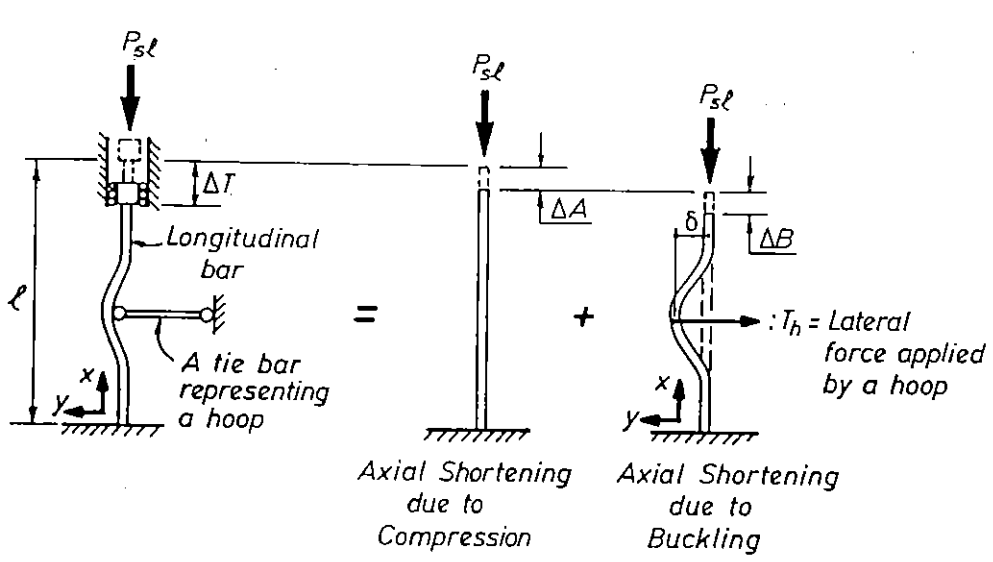

Fig. 6.2 Buckling Model for a Longitudinal Bar.

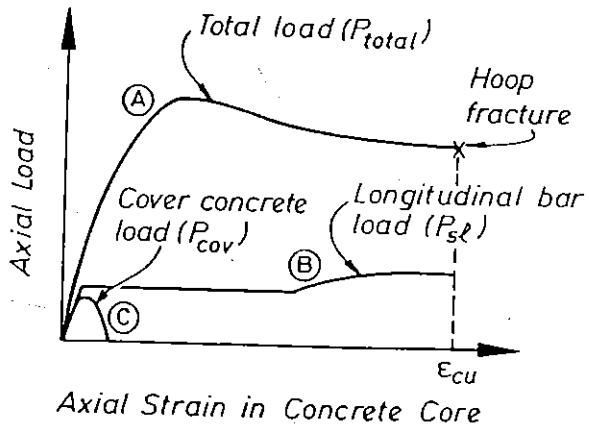

Fig. 6.3 Axial Load Components versus Axial Strain Relation in a Reinforced Concrete Column.

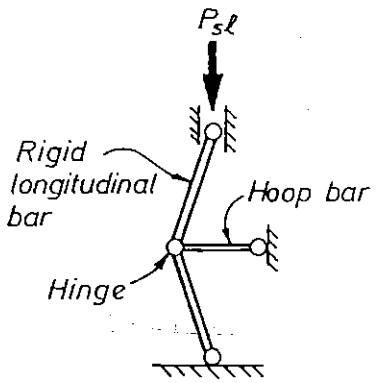

Fig. 6.4 Buckling Model for a Longitudinal Bar with Frictionless Hinges.

The left hand side of the equation is almost equivalent to the external work done on an axially loaded column per unit length (U_g). To be more precise, the external work per unit length of the column U_g can be expressed in the form

$$U_g = U_{cc} + U_{sc} + U_{cov}$$

$$= A_{cc}\int_0^{\varepsilon_{cu}} f_{cc}\, d\varepsilon_c + A_{cc}\rho_{cc}\int_0^{\varepsilon_{cu}} f_{sl}\, d\varepsilon_c + A_{cov}\int_0^{\varepsilon_{sp}} f_{co}\, d\varepsilon_c \quad \ldots\ldots\ldots \quad (6.14)$$

where U_{cov} = strain energy absorbed in cover concrete prior to complete spalling

A_{cov} = sectional area of concrete cover

Note that all the integrations are against $d\varepsilon_c$.

The energy absorbed by the cover concrete U_{cov} is usually only a small fraction of U_g because cover concrete area is usually much smaller than the core concrete area and the strain at spalling is also smaller than the ultimate concrete core strain (See U_{cov} in Table 6.2). Therefore, U_g can be approximated by the terms on the left hand side of Eq. 6.13. The meaning of Eq. 6.14 can be reconfirmed by recalling the typical procedure used to determine the stress-strain relation of confined concrete from a concentric loading test on a reinforced concrete column. As the first step, a total load versus axial strain relation, Curve (A) in Fig. 6.3, is obtained from the measurement of the machine load and corresponding axial displacement within the gauge length. Secondly, the axial load sustained by the longitudinal bars at each corresponding axial strain is estimated using a stress-strain relation obtained from tensile or compression tests on the identical bars. The curve (B) in Fig. 6.3 indicates the case where the reduction of the axial stress in the longitudinal bars due to buckling is negligible. Thirdly, the axial load sustained by the cover concrete, curve (C) , is estimated from the stress-strain relation obtained from compression tests on plain concrete specimens or control cylinders. Finally, the axial load sustained by the core concrete (P_{cc}) can be determined by subtracting the loads sustained by the longitudinal bars (P_{sl}) and the cover concrete (P_{cov}) from the total load (P_{total}). The stress in the confined concrete can be found by dividing P_{cc} by A_{cc} and then the stress-strain curve of confined

concrete can be drawn as shown in Fig. 6.1. Therefore, the external work done by the loading machine for a unit length of the column can be expressed in the form

$$U_g = \int_0^{\varepsilon_{cu}} P_{total}\, d\varepsilon_c = \int_0^{\varepsilon_{cu}} P_{cc}\, d\varepsilon_c + \int_0^{\varepsilon_{cu}} P_{sl}\, d\varepsilon_c + \int_0^{\varepsilon_{sp}} P_{cov}\, d\varepsilon_c \quad \text{..... (6.15)}$$

Eq. 6.15 is identical with Eq. 6.14.

Hence, it can be considered that the left hand side in Eq. 6.13 is almost equivalent to the external work done on the column. Now some part of the external work done on the column by the loading machine should be transferred to the longitudinal bars. However, a term with the strain energy directly related to the longitudinal bars can not be found in the right hand side of the Eq. 6.13. Therefore, in order to ensure that the terms on the right hand side of Eq. 6.13 are adequate, all of the external works done on the longitudinal bars needs to be transferred to the hoop reinforcement. In this case, in Eq. 6.12, this requires that

$$A_{sl}\, l \int_0^{\varepsilon_s} f_{sl}\, d\varepsilon_s = 0 \text{ and } \int_0^{l} \frac{E_b\, I_b}{2}\left(\frac{d^2y}{dx^2}\right)^2 dx=0$$

To satisfy the above conditions, it would be necessary to assume that the buckling of the longitudinal bar occurs from the beginning of the loading, that the axial stiffness of the longitudinal bars is infinitively large and that the longitudinal bars have hinges free to rotate. This assumption can be modelled as shown in Fig. 6.4. However, it is unrealistic to apply this model to the column reinforcement from the early stage of loading where the longitudinal bars are neither yielded nor buckled. As a matter of course, this model can be adequate from a certain stage of loading where the longitudinal bars have been compressed far into the inelastic range and their bending stiffness has become negligibly small due to axial yielding.

On the other hand, if the axial force P_{sl} reduces to zero due to serious buckling, the elastic energy released from the longitudinal bars U_{sb} (which is represented by the shaded area in Fig. 6.5) might be transferred to the hoop reinforcement. However, this elastic energy U_{sb} may be negligibly small compared with the total strain energy absorbed in the longitudinal bars in the case where the hoop spacing and the amount of hoop are adequate to achieve sufficient ductility for a column during severe earthquake loading. For example, such serious buckling can be expected only at very high axial compressive strain in the case of a column designed by the New Zealand concrete code [6.12] which is based on ductile design philosophy. Hence, it might be unnecessary to take into account this factor in Eq. 6.12 for a ductile column.

From the considerations described above, it can be predicted that Eq. 6.4 may not be adequate except for a concrete column in which the strain energy stored in the longitudinal bars is quite small compared with the strain energy stored in the core concrete and in the hoop reinforcement.

6.3.3 The Strain Energy Capacity of the Transverse Reinforcement

To estimate the strain energy capacity of the hoop reinforcement (U_{sh}) in Eq. 6.4, in the theory proposed by Mander et al it was recommended to use Eq. 6.7. This value of U_{sh} was based on several tensile tests on reinforcing steel bars [6.3]. Note that the integration range in Eq. 6.7 is from zero to the hoop fracture strain ε_{sf}. Eq.6.7 may be inadequate to estimate the value of U_{sh} at hoop fracture for the following reason. Usually, the measurement of fracture strain of a steel bar ε_{sf} is significantly affected by the gauge length used in the tensile test. The strain distribution along the bar axis at the bar fracture can be represented as in Fig. 6.6. It is evident that large strains concentrate over a small length of necked bar at the fracture. The fracture strain calculated from the elongation between points A and B, which includes the necking part of the bar, is the average strain between those points. The corresponding stress-strain curves can be expressed as shown in Fig. 6.7. The curves (1) and (2) are the stress-strain relations with a small and a large gauge length AB, respectively. If the necking part is not in the gauge length, that is for example the strain is measured between points B and C, the stress-strain relation will follow curve(3) after reaching the ultimate stress f_{su}. Hence, the calculated strain energy capacity of the

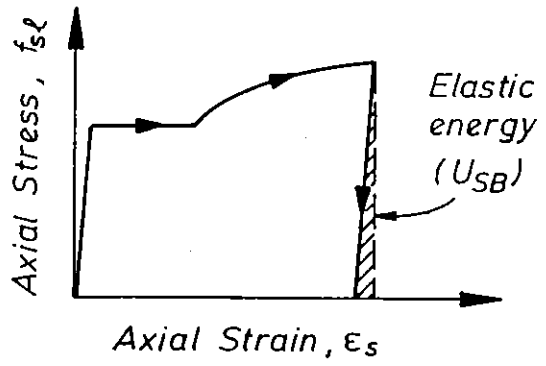

Fig. 6.5 Stress-Strain Curves for Steel with Unloading Part.

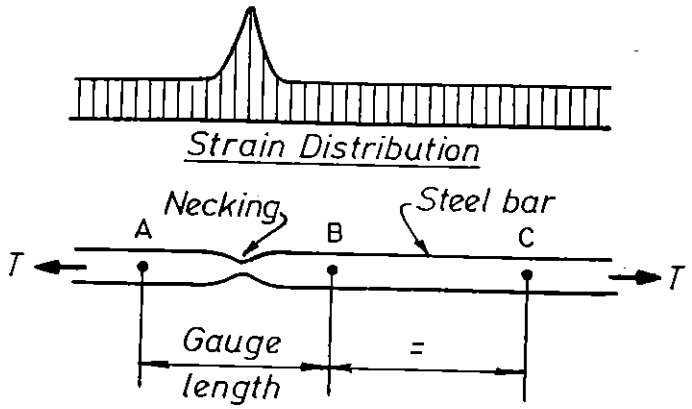

Fig. 6.6 Strain Distribution in a Steel Bar with Necking.

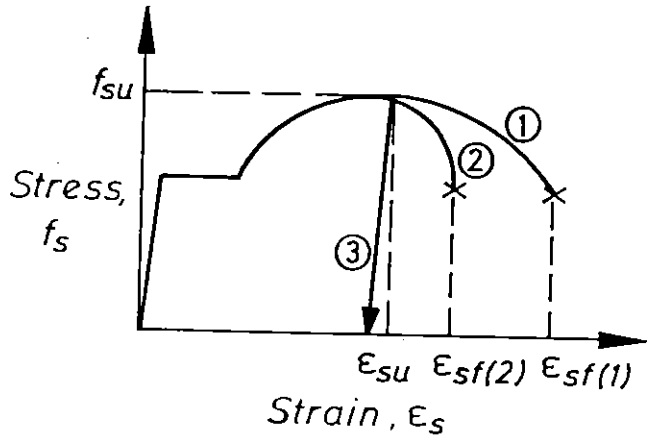

Fig. 6.7 Stress-Strain Curves for Steel with Different Gauge Length.

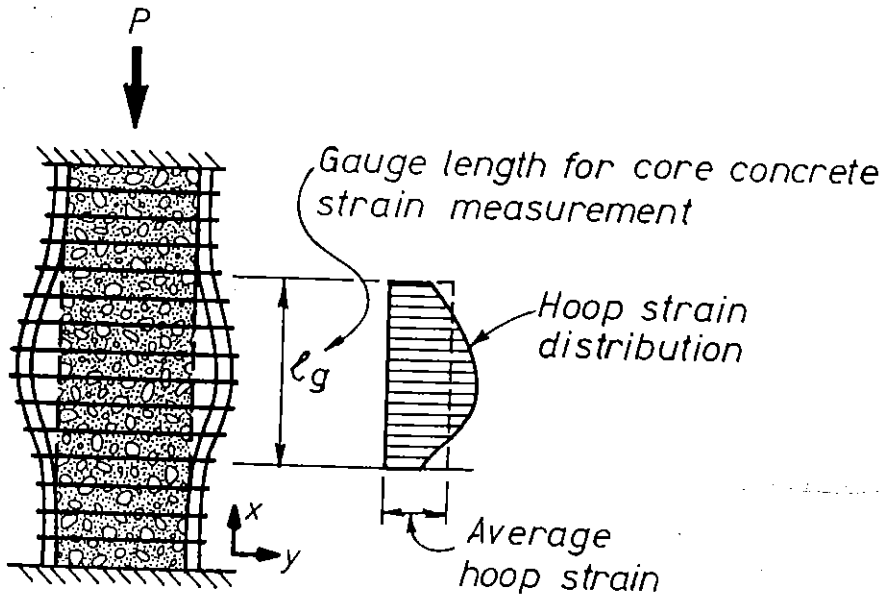

Fig. 6.8 Hoop Strain Distribution Along Column Axis with Longitudinal Bar Buckling.

steel bar up to the hoop fracture, which corresponds to the area between the stress-strain curve and the strain axis, depends on the gauge length. In the tests conducted for this thesis (see Table 6.1), the calculated value of U_{sh} was found to vary from about 150 MJ/ m^3 with gauge length of 5 d_b (where d_b= bar diameter) to 110 MJ/ m^3 with gauge length of 20 d_b and to 100 MJ/ m^3 to 70 MJ/ m^3 for larger gauge length. The last values of 100 MJ/ m^3 to 70 MJ/ m^3 were estimated using the relation,

$$U'_{sh} = \int_0^{\varepsilon_{su}} f_{sh}\, d\varepsilon_{sh} \qquad \text{..... (6.16)}$$

where ε_{su} = strain at the ultimate tensile strength of steel (See Fig. 6.7),

instead of Eq. 6.7. The details of these tests are described in the following section. Hence, the gauge length needs to be properly chosen for the estimation of the strain energy capacity of the hoop reinforcement U_{sh}. For example, if circular spirals with 16 mm bar diameter are provided in a column with a concrete core diameter of 1m, the total length of the spiral in one turn of the spiral is about 200 times the spiral bar diameter. In this case, for the strain energy capacity of the spiral at first spiral fracture, U'_{sh} = 70 to 100 MJ/ m^3 calculated from Eq. 6.16 will give a better estimation than U_{sh} = 110 to 150 MJ/ m^3 from Eq. 6.7.

Moreover, the strain distribution for the spirals or hoops along the column axis also needs to be taken into account for the estimation of the U_{sh}. This is because the corresponding strain energy stored in the core concrete has to be calculated from a theoretical or a measured stress-strain relation of confined concrete over a defined gauge length. That is, the longitudinal concrete strain is an average strain within the gauge length used for the concrete strain definition or measurement. Hence, the calculated strain energy of the concrete core does not usually just correspond to the strain energy stored in the damaged region concentrated within one hoop spacing at which the first hoop fracture occurs. The longitudinal concrete strain used in the stress-strain relation might mean an average strain within a plastic hinge region of the column with a length of one-third to a full section depth of the column. Therefore, if the buckled shape of the longitudinal bar is represented as in Fig. 6.8, the average strain of the hoops within the above mentioned length of the column needs to be used for the

estimation of the strain energy stored in the hoops. As a result, the value of U_{sh} needs to be modified again based on the buckled shape expected.

If buckling over more than two hoop spacing is not expected prior to the hoop fracture, the value of U_{sh} obtained from Eq.6.16 can be used without further modification because the hoop strains distributed along the column axis may be almost constant. However, if buckling is limited within one hoop spacing, the external work done on the longitudinal bars may hardly be transferred to the hoop reinforcement because such buckling condition corresponds to the case without a tie bar representing hoops in Fig. 6.4 and thus the last term in Eq. 6.12 must be eliminated. In this case, the proposed equations (Eqs. 6.4 to 6.6) lose their validity because those equations are based on the assumption that the external work done on the longitudinal bars is all transferred to the hoop reinforcement.

Table 6.1 Measured Strain Energy Capacity of Reinforcing Bars.

Study	Reinforcing Bar	Yield Strength in MPa	Ultimate Strength in MPa	Strain at Ultimate Strength GL = 5 d_b	Fracture Strength in MPa	Fracture Strain		Strain Energy Calculated by Eq.6.7 in MJ/m^3		Strain Energy Calculated by Eq.6.16 in MJ/m^3
						GL = 5d_b	GL = 20d_b	GL = 5d_b	GL = 20d_b	GL = 5d_b
Tanaka (*1)	HD24	432	588	0.169	415	0.289	0.199	151	107	91
	HD20	485	644	0.148	475	0.265	0.177	152	104	87
	Φ12	305	446	0.246	298	0.415	0.288	163	117	100
	Φ10	308	431	0.250	288	0.420	0.293	161	117	100
	Average							157	111	95
Mander et al [6.3](*2)	Φ16	295	433	0.19	-	-	0.25	-	98	74
	HD16	360	567	0.15	-	-	0.24	-	121	77
	D20	286	429	0.18	-	-	0.28	-	111	69
	D24	260	567	0.18	-	-	0.29	-	111	70
	Average								110	73
Zahn et al [6.22](*3)	Φ12	328	492	-	-	-	0.24	-	110	-
	HΦ10	466	688	-	-	-	0.175	-	110	-
	Average								110	

(*1) The values for each bar are average values from 5 test pieces
(*2) Gauge length = 203 mm (= 8 ~ 13d_b)
(*3) Gauge length = 203 mm (= 17 ~ 20d_b)

As a corollary, it can be considered that the stored energy in the hoop reinforcement at first hoop fracture could be overestimated by 20 to 40 % or more if Eq. 6.7 is used. In Eqs. 6.4 to 6.6, this overestimation may successfully compensate for the neglect of the absorbed energy in the longitudinal bars due to axial yielding in some cases but not always. Therefore, it can be considered that the equations in the energy balance theory proposed by Mander et al need to be modified or to be limited in their use.

6.3.4 A Proposed Energy Principle Model for a Reinforced Concrete Column Subject to Axial Compression

6.3.4.1 Observed Failure Mechanism for Concrete in Compression

In a conservative system of energy, such as the elastic behaviour of a member, the work performed by both internal and external forces is independent of the path travelled by these forces and hence the work can be determined only from the initial and the final positions of these forces. However, in the case of inelastic behaviour of a reinforced concrete member, the system is usually non-conservative because there exists internal frictions due to inelastic deformation of each constituent which includes cracking. Therefore the failure mechanism of the member, determined by the path of internal forces, becomes the key to estimate the

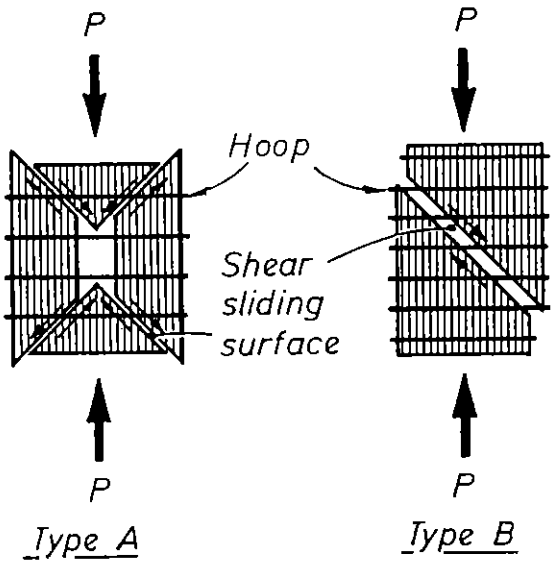

Fig. 6.9 Formation of Shear Sliding Surfaces in Core Concrete.

internal work performed. In this study, the following failure mechanism is assumed for a reinforced concrete column under axial compression.

When a reinforced concrete column is compressed far into the plastic range by an axial load, it can be assumed that shear sliding surfaces are formed inside the core concrete with the propagation of micro cracks [6.17], as illustrated in Fig. 6.9. The shear sliding surfaces are either of a type A or a type B. Shear sliding surfaces of type A separate the concrete core into top and bottom cones (in case of a circular column) or pyramids (in case of a square column) and side shells. Shear sliding surfaces of type B separate the concrete core into two wedge shaped parts. This assumption is based on the failure modes usually observed in compression tests on circular or square columns. Figs. 6.10 and 6.11 show typical examples of the failure modes observed in such column tests [6.18]. In Fig. 6.11, the two protruding bars which were provided to mount potentiometers passed through the concrete core and were originally straight bars. During testing the top and bottom bars began to bend upward and downward, respectively, as the axial compressive displacement of the square concrete column increased. This phenomenon would be the result of wedging action of the top and bottom concrete pyramids as illustrated in Fig. 6.9 , type A.

6.3.4.2 Proposed Failure Mechanism Model

Based on the observed failure mechanism mentioned in Section 6.3.4.1, the assumed role and behaviour of each concrete and steel constituent can be described and a failure mechanism model for a reinforced concrete column subjected to axial loading shown in Fig.6.12 can be proposed.

The assumed role and behaviour of each constituent, with reference to Fig. 6.12, are as follows:

(1) Cover concrete: Works as a compression strut (spring k_{cov}) against the axial load until spalling is completed and thereafter vanishes.

(2) Core concrete : In the initial stage, works as a compression strut (spring k_{cc}) in the same manner as the cover concrete until the complete formation of the shear sliding surfaces but some percentage of the external work is

Fig. 6.10 Typical Failure Mode of a Circular Column.

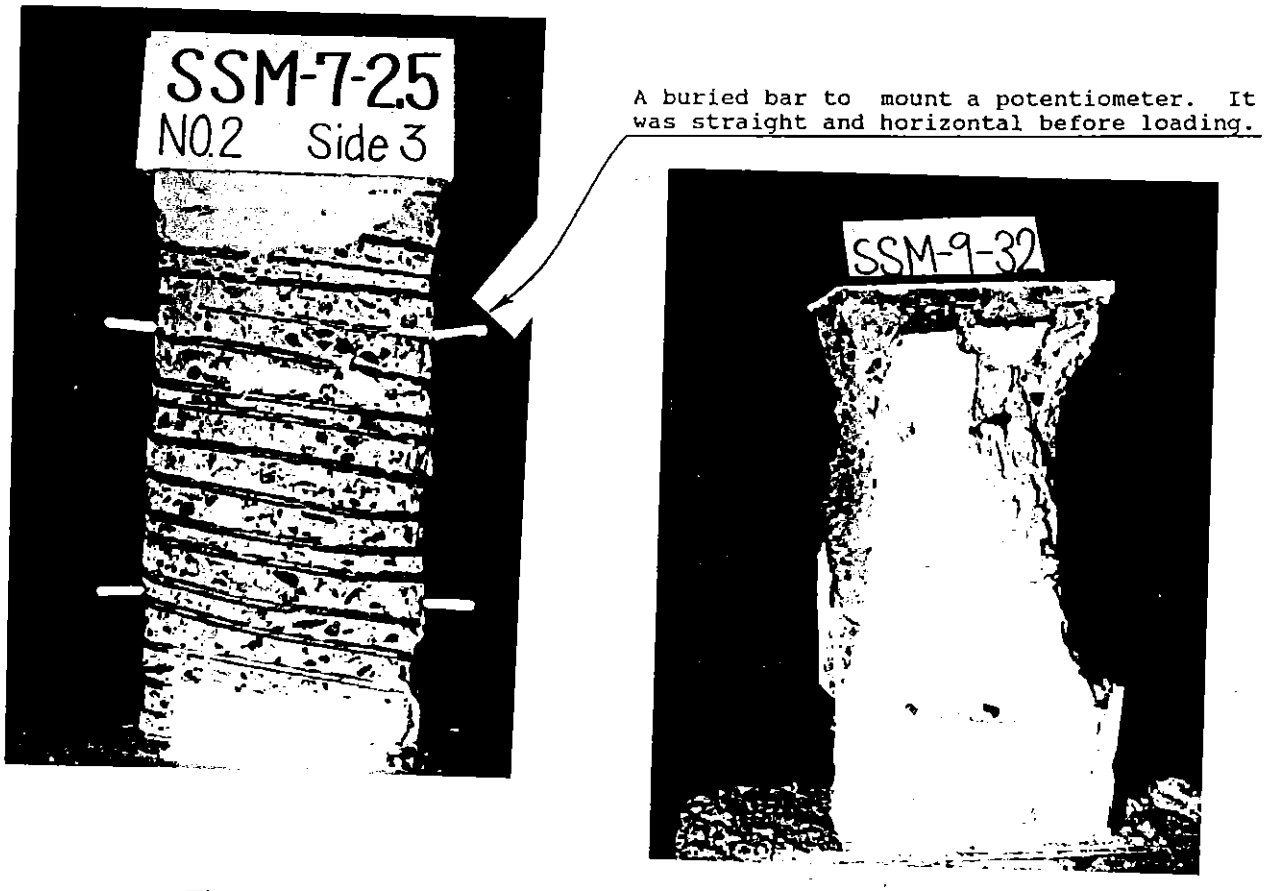

Fig. 6.11 Typical Failure Mode of Square Columns.

transferred to hoops by Poisson's effect as represented by a pantograph in Fig. 6.12 (a). The angle θ in the pantograph corresponds to the Poisson's ratio of the concrete treated as a unit solid material. It is assumed that the second stage commences with the complete formation of the shear sliding surfaces which is simultaneous with the complete spalling of cover concrete. After formation, the shear sliding surfaces act as a transformer which changes the axial load into lateral load by the wedging effect of the top and bottom cones in the case of type A or wedge shaped lumps in the case of type B (see Fig. 6.9). Hence, the angle θ' of the pantograph in Fig. 6.12 (b) can be determined from the inclination of the shear sliding surface. The friction between the shear sliding surfaces (spring k_{ccf}) also provides resistance against the axial load.

(3) Longitudinal Reinforcement : In the initial stage, works as a compression strut (spring k_{sc}) against the axial load. In the final stage, after the onset of buckling, works as a pantograph which can transfer the axial load work to the hoop reinforcement by changing the load direction from axial direction to lateral direction. The angle θ'' in Fig. 6.12 (c) can be determined from the buckling mode of the longitudinal bars.

(4) Hoop Reinforcement : In the initial stage, works as lateral confinement which provides quasi-fluid pressure to the core concrete. In the second stage, after the formation of the shear sliding surfaces in the core concrete, works as hoops to prevent sliding of the top and bottom cones or the wedge shaped lumps until the buckling of the longitudinal bars commence. In the final stage, works as anti-buckling support until the hoop fracture.

In the proposed failure model mechanism of Fig. 6.12, in the initial stage where the core concrete can be treated as a unit solid body the improvement of the load carrying capacity of the confined concrete is attributed to the lateral pressure from the hoop reinforcement as a result of lateral expansion of the core concrete due to the Poisson's effect. On the other hand, in the high strain region in the second stage after the formation of the shear sliding surfaces, the improvement of the load carrying capacity is attributed to the restraint against the shear sliding along the surfaces between the core concrete parts separated by cracks shown in Fig. 6.9.

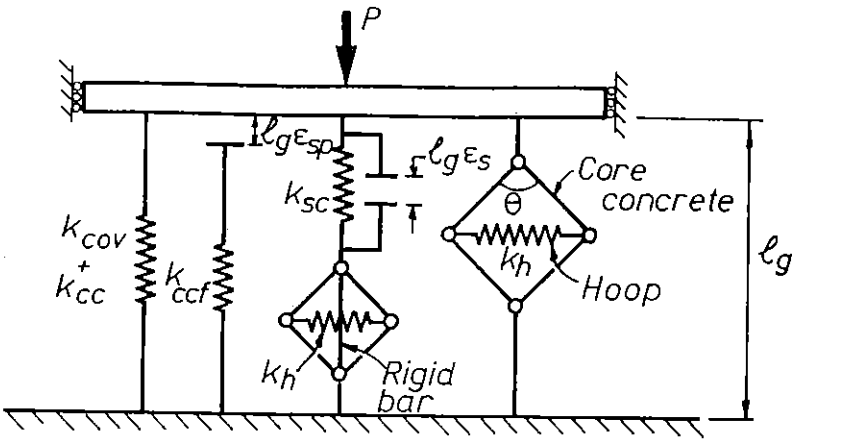

(a) Initial Stage

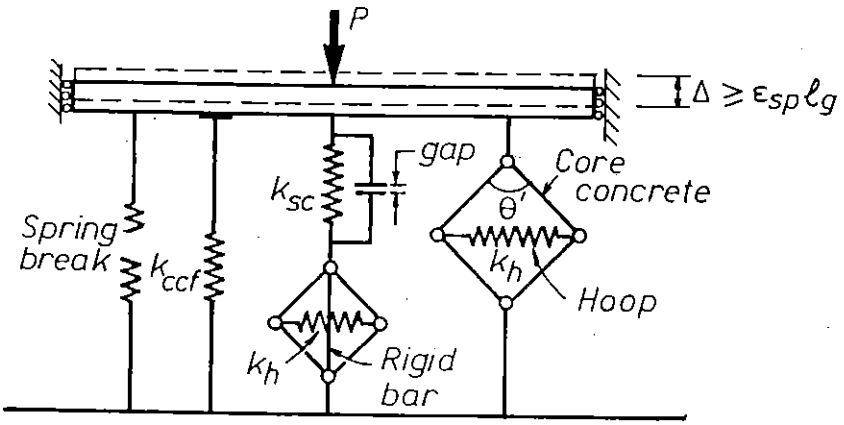

(b) Second Stage (After formation of shear sliding surfaces but without buckling of longitudinal bar.)

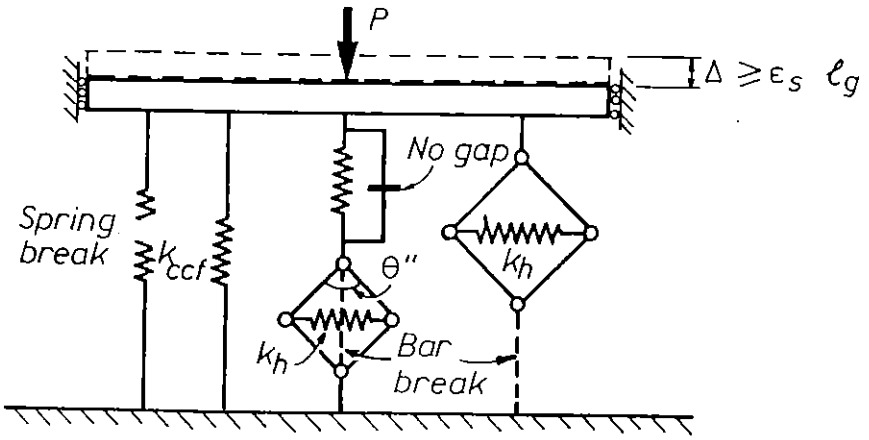

(c) Final Stage (After onset of longitudinal bar buckling)

Fig. 6.12 Proposed Failure Mechanism Model for a Reinforced Concrete Column Subjected to Axial Loading.

It is of interest that the angles θ, θ' and θ'' in Fig. 6.12 need not be determined in order to calculate the longitudinal concrete strain at first hoop fracture. This is because only the strain energy capacity of the hoop reinforcement up to its fracture is required to be determined for this case. Only when the stress-strain relation of the confined concrete needs to be computed step by step, it is necessary to determine the angles θ, θ' and θ''.

In Fig. 6.12, the initial gap $l_g \varepsilon_{sp}$ between the spring k_{ccf} and the loading plate corresponds to the axial displacement to complete the spalling of cover concrete and the formation of the shear sliding surfaces. At the initial stage of loading , the rigid bar connector beside the spring k_{sc} has a gap of $l_g \varepsilon_s$ and the pantograph below the spring k_{sc} can not be deformed due to the restraint by the inserted rigid bar. This model for the longitudinal bars represents the situation expressed in Eqs. 6.11 and 6.12 but neglecting the bending resistance of the longitudinal bars.

6.3.4.3 Energy Equation for the Proposed Failure Mechanism Model

Based on the above failure mechanism model, the external work done on the column per unit length U_g can be equated to the following internal work.

$$U_g = U_{cov} + U_{co} + U_{ccf} + U_{scr} + \alpha U'_{sh} \quad \text{.....} \quad (6.17)$$

where U_{cov} = strain energy absorbed in cover concrete prior to complete spalling.

U_{co} = strain energy absorbed in core concrete prior to complete formation of shear sliding surfaces.

U_{ccf} = dissipated energy by friction between shear sliding surfaces in concrete core prior to first hoop fracture.

U_{scr} = strain energy absorbed in compression reinforcement due to axial yielding.

U'_{sh}= strain energy stored in hoop reinforcement at first hoop fracture in the case where the longitudinal bars are not buckled or are buckled within one hoop spacing.

α = reduction factor for U'_{sh} determined from the hoop strain distribution along the column axis.

Eq. 6.17 can be equated to the external work expressed by Eq. 6.14 and hence,

$$U_{cc} + U_{sc} + U_{cov} = U_{cov} + U_{co} + U_{ccf} + U_{scr} + \alpha\, U'_{sh} \quad \ldots\ldots\ldots \quad (6.18)$$

Rearranging this equation,

$$U_{cc} - U_{co} = U_{ccf} + \alpha\, U'_{sh} - (\, U_{sc} - U_{scr}\,) \quad \ldots\ldots\ldots\ldots\ldots \quad (6.19)$$

U_{scr} may be expressed in the form of

$$U_{scr} = \beta\, U_{sc}$$

where β = ratio of strain energy absorbed in the longitudinal bars by axial yielding to the external work done on the longitudinal bars.

Substituting it into Eq.6.19,

$$U_{cc} - U_{co} = U_{ccf} + \alpha\, U'_{sh} - (1 - \beta)\, U_{sc} \quad \ldots\ldots\ldots\ldots\ldots \quad (6.20)$$

Eq.6.20 can be rewritten for a unit length of the column in the form of stresses and strains as

$$A_{cc}\int_0^{\varepsilon_{cu}} f_{cc}\, d\varepsilon_c - A_{cc}\int_0^{\varepsilon_{sp}} f_{co}\, d\varepsilon_c = A_{cc}\int_{\varepsilon_{sp}}^{\varepsilon_{cu}} f_{ccf}\, d\varepsilon_c + \alpha\, \rho_s A_{cc}\int_0^{\varepsilon_{su}} f_{sh}\, d\varepsilon_{sh} - (1-\beta)\rho_{cc} A_{cc}\int_0^{\varepsilon_{cu}} f_{sl}\, d\varepsilon_c$$

$\ldots\ldots\ldots\ldots$ (6.21)

or for unit volume of the column,

$$\int_0^{\varepsilon_{cu}} f_{cc}\, d\varepsilon_c - \int_0^{\varepsilon_{sp}} f_{co}\, d\varepsilon_c = \int_{\varepsilon_{sp}}^{\varepsilon_{cu}} f_{ccf}\, d\varepsilon_c + \alpha\, \rho_s \int_0^{\varepsilon_{su}} f_{sh}\, d\varepsilon_{sh} - (1-\beta)\rho_{cc}\int_0^{\varepsilon_{cu}} f_{sl}\, d\varepsilon_c$$

$\ldots\ldots$ (6.22)

where f_{ccf} : axial stress component in core concrete due to friction between shear sliding surfaces.

Using theoretical relations for f_{cc}, f_{co}, f_{ccf} and f_{sl} as functions of the longitudinal strain of the concrete core , and with adequate values of ε_{sp}, α, β and U'_{sh}, Eq.6.22 can be solved for ε_{cu} by numerical trial and error methods.

6.3.4.4 Values of the Terms in the Proposed Energy Equation

Many theoretical curves for f_{cc}, f_{co} and f_{sl} have already been established for example see Ref . 6.19. Concerning f_{ccf} , the following relation can be assumed:

$$f_{ccf} = \gamma f'_{co} \quad \text{..... (6.23)}$$

where γ : constant determined by magnitude of friction between shear sliding surfaces in the concrete core.

f'_{co} : compressive strength of plain concrete assumed to be 85% of the control cylinder strength.

Eq. 6.23 is derived from the observation of compression tests on plain concrete cylinders or prisms. In the tests, the stress reduction in the strain softening region becomes gradual after reaching a longitudinal strain of 0.004 to 0.006 and thereafter a stress level of 0.1 to 0.2 f'_{co} is maintained [6.17, 6.19]. This stress level can be considered to indicate the potential magnitude of the friction between the shear sliding surfaces formed in the confined concrete core.

As a value of ε_{sp} , 0.004 to 0.008 may be adequate. The actual value will depend on the strain gradient of the column section and on the quantity of transverse reinforcement. If there exists a large strain gradient (that is, a small neutral axis depth) the complete spalling of cover concrete is usually delayed due to a restraint by the neighbouring concrete layers which stay at a smaller strain [6.19, 6.20] . It has also been observed that a high quantity of transverse reinforcement results in a plane of weakness between core and cover concretes which results in a lower ε_{sp} [6.19]. For reinforced concrete columns subjected to concentric axial compression, a value for ε_{sp} of 0.004 may be assumed because of absence of the strain gradient in the column section. For the reinforced concrete columns subjected to combined axial

load and bending moment, a value for ε_{sp} of 0.006 or more may be adequate if the transverse reinforcement provided in the columns is not extremely congested, as has been found appropriate in a previous study [6.21].

The value of α varies with the expected buckling mode of the longitudinal bars. The buckling mode can be expressed as a combination of the modes of a gross buckling and a local buckling as shown in Fig. 6.13. If the expected local buckling is limited to within one hoop spacing without occurrence of the gross buckling, $\alpha = 1$ may be adopted because the hoop strain distribution along the column length will be approximately constant. In the case of a column with the gross buckling of longitudinal reinforcement as shown in Fig. 6.8, α can be calculated as follows. If the core diameter of column is d_c, the total height of column is $3d_c$ and the gauge length of the concrete core strain measurement is d_c, the gross buckled shape of the longitudinal bars may be approximated by the following equation.

$$y = \frac{a}{2}\left(1 - \cos\frac{2\pi x}{3 d_c}\right) \qquad \text{.....} \qquad (6.24)$$

where a = the maximum lateral displacement of the longitudinal bar at the mid- height of the column

$3 d_c$ = the height of the column (see Fig.6.13 (a))

In Eq. 6.24 it is assumed that the lateral expansion of the column at each end is negligible because even a spalling of cover concrete cannot usually be observed in the end portion of the column, due to the effects of friction between the loading plate and the contact surface of the concrete at the end of the column. The average lateral displacement within the gauge length l_g of d_c in the middle third of the column can be expressed in the form

$$y_{ave} = \frac{1}{d_c}\int_{d_c}^{2d_c} \frac{a}{2}\left(1 - \cos\frac{2\pi x}{3 d_c}\right)dx = 0.91a \qquad \text{.....} \qquad (6.25)$$

Hence, in this case $\alpha = 0.9$ might be an adequate value. If the local buckling occurs over several hoop spacings in addition to the above gross buckling, the value of α needs to be reduced to a value which is less than 0.9 . If the

local buckling in addition to the above gross buckling does not occur or is limited within one hoop spacing , the value of α needs not to be reduced from 0.9.

The value of β which expresses the ratio of strain energy absorbed in the compression reinforcement by axial yielding to external work done on the compression reinforcement is not so simple to calculate theoretically, because it depends on several factors such as the hoop spacing, the stiffness of the hoop reinforcement against the longitudinal bar buckling, the bending stiffness of the longitudinal bar in inelastic buckling, and so on. However, the value of β could be approximated using Fig. 6.14 from Ref. 6.22, which shows the theoretical buckling strain of a longitudinal bar, ε_s^T , in relation to the hoop spacing assuming that the buckling occurs only within one hoop spacing . It is evident that Fig. 6.14 gives an upper bound for the compression strain at buckling because of the buckling mode assumed. Using this ε_s^T value, β may be approximated in the form

$$\beta = \frac{\varepsilon_s^T}{\varepsilon_{cu}} \qquad \text{.....} \qquad (6.26)$$

If Eq. 6.26 is used with value of ε_s^T from Fig. 6.14, a check might be necessary to determine whether the error in β due to overestimation of ε_s^T is negligible or not taking into account the expected buckling mode of the longitudinal reinforcement. However, the error in the value of β usually does not affect the accuracy of the prediction of ε_{cu} greatly because the total energy stored in the longitudinal bars is less than a half of the strain energy stored in a well confined core concrete even for high compression reinforcement ratios of about 3% (see U_{cc} and U_{sc} in Table 6.2).

Several tensile tests on reinforcing steel bars were conducted with strain measurements using various gauge lengths in order to estimate the values of Eqs. 6.7 and 6.16 which could be used to calculate U_{sh} in the energy balance theory and U'_{sh} in the proposed theory. The test results are listed with the results of other researchers [6.3, 6.22] in Table 6.1. As mentioned in the previous section, the calculated values of U_{sh} depend significantly on the gauge length adopted in the particular test. Moreover, the values obtained by the three sets of tests are also different. However, the values of

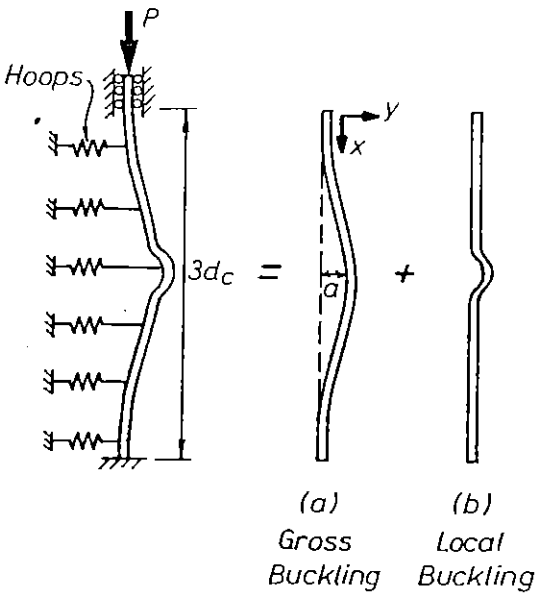

Fig. 6.13 Buckling Modes of a Compressed Longitudinal Bar in a Reinforced Concrete Column.

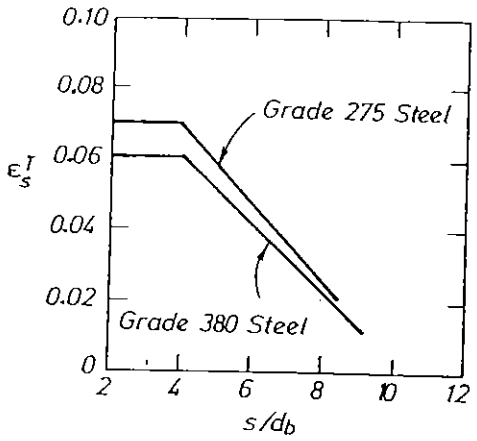

Fig. 6.14 Buckling Strain of a Longitudinal Bar and the Corresponding Hoop Spacing [6.22].

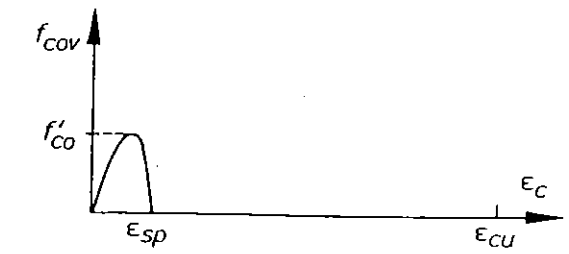

(a) Cover and Core Concrete Before Formation of Shear Sliding Surface (Spring $k_{cov} + k_{cc}$)

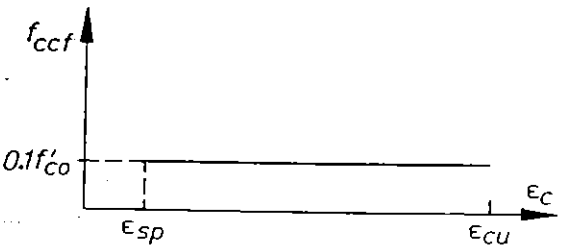

(b) Core Concrete After Complete Formation of Shear Sliding Surface (Spring k_{ccf})

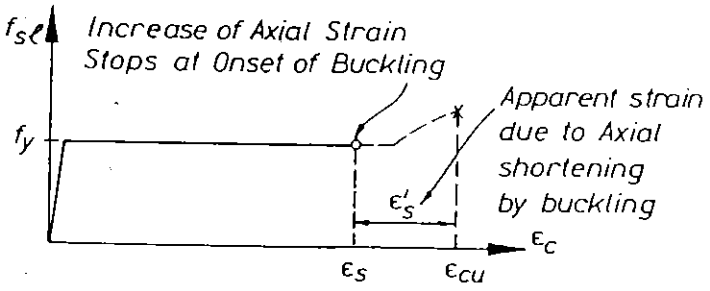

(c) Longitudinal Bars (Spring k_{sc})

Fig. 6.15 Stress-Strain Behaviour of Concrete and Steel Constituents.

U_{sh} with gauge length of 20 d_b obtained from the author's tests are very close to the values obtained by Zahn et al [6.22]. For the value of Eq. 6.16 which is used to calculate U'_{sh}, it is suggested that the average of values obtained by author's test and by Mander et al [6.3] which are given in Table 6.1 could be used. That is, in this case, the strain energy stored at ultimate strength of steel per unit volume of reinforcement is

$$U'_{sh} = 84 \text{ MJ} / \text{m}^3 \qquad \text{.....} \qquad (6.27)$$

6.3.4.5 Comparison of the Predictions of the Proposed Theory and the Results of Tests

In order to assess the accuracy of the theory proposed here, the predictions of the theory were compared with the test results obtained from the monotonic axial compression tests on circular columns with core diameter of 450 mm and octagonal columns with core diameter of 384 mm conducted by Mander et al [6.3] and Zahn et al [6.22], respectively. In those tests, the concrete strengths measured on control cylinders varied from 28 to 33 MPa. For the spirals, as hoop reinforcement, 10 to 12 mm diameter plain bars from both 275 and 380 Grade steel were used. For the longitudinal reinforcement, 16 to 24 mm diameter deformed bars from Grade 275 steel were used except for one column (C.12 in Table 6.2) in which Grade 380 longitudinal bars were used.

The stress-strain relations for the cover and core concrete and the longitudinal reinforcement assumed in the proposed failure mechanism model are shown in Fig. 6.15. For the estimation of U_{co}, Eq. 6.8 was used. For the value of ε_{sp}, because no serious strain gradient was present in the section due to the concentric loading , ε_{sp} =0.004 was assumed. A value of α = 0.9 was used because all of the tests columns had similar ratios of the column diameter, height and gauge length as that assumed in the derivation of Eq. 6.25. A value of β = 0.9 was estimated, because the ratios of hoop spacing to the longitudinal bar diameter (s/d_b) were less than 4 in most test columns and hence ε_s^T obtained from Fig. 6.14 is close to or greater than ε_{cu} measured in those tests. For U_{cc} and U_{sc}, the values directly obtained from the measured load-axial strain relations were used. U_{ccf} was calculated assuming that γ =0.1 in Eq. 6.23. U'_{sh} was calculated taking the

value of Eq. 6.16 as 84 MJ/m^3. The properties of eighteen concrete columns tested at the University of Canterbury [6.3, 6.22] and the calculated results are listed in Table 6.2.

In order to check the agreement of the theoretical value with the experimental value , the ratios of

$$I_{ag}^{T} = \frac{\{\alpha\, U'_{sh} + U_{ccf} - (1-\beta)U_{sc}\}}{(U_{cc}-U_{co})} \qquad \text{.....} \qquad (6.28)$$

for the theory proposed in this study and

$$I_{ag}^{M} = \frac{(U_{sh} - U_{sc})}{(U_{cc} - U_{co})} \qquad \text{.....} \qquad (6.29)$$

for the energy balance theory proposed by Mander et al are also listed in Table 6.2. In Eq. 6.29, U_{sh} was calculated using Eq. 6.7. The average percentage error given by I^{T}_{ag} is 12 % with a maximum percentage error of 33 %, while those percentage errors for I^{M}_{ag} are 17 % and 77 %, respectively. As predicted, in case of the energy balance theory which neglects the strain energy absorbed by the axial yielding of longitudinal bars, the largest error is found for test column U.2 which has a small amount of hoop reinforcement and large amount of longitudinal reinforcement.

The calculated results for the ultimate concrete strain, defined as that longitudinal compressive strain of concrete where the hoops first fracture, using the modified theory are also listed in Table 6.2. In the calculation, a bilinear stress-strain relation determined by the measured yield strength of steel was used for the longitudinal reinforcement. For the confined core concrete, the stress-strain model due to Mander et al [6.3, 6.7, 6.10] was used. The calculated ultimate concrete strains compare quite well with the measured values in most cases. However, it should be noted that any stress-strain model for confined concrete does not perfectly predict the experimental stress-strain behaviour and hence these calculated ultimate concrete strains include the error due to any inaccuracy in the stress-strain model used. It is evident from the comparison in Table 6.2 that the ultimate concrete compressive strain at first hoop fracture can be well predicted using the theory proposed in this study.

Table 6.2 Properties of Axially Loaded Reinforced Concrete Columns, Strain Energy Stored in Each Component Per Unit Length and Longitudinal Concrete Strain at First Spiral Fracture.

	Test Unit	Concrete Cylinder Strength f'_c in MPa	Longitudinal Reinforcement: Number of Bar	Longitudinal Reinforcement: f_y in MPa	Transverse Reinforcement: Bar and Spacing in mm	Transverse Reinforcement: f_y in MPa	ρ_s in %	S/d_b	ε_{sm}^T in %	U_{cc} in KJ/m	U_{co} in KJ/m	U_{cov} in KJ/m	U_{sc} in KJ/m	U_{sh} in KJ/m	U_{ccf} in KJ/m	$\alpha U'_{sh}$ in KJ/m	$(1-\beta)U_{sc}$ in KJ/m	U_{sb} in KJ/m	I_{ag}^M	I_{ag}^T	ε_{cu} by Theory in %	ε_{cu} Measured in tests in %
Spiral Columns Tested by Mander et al [6.3]	C.a	30	12-D16	290	R12-52	310	2.00	3.25	7	287	15	2	48	350	23	242	5	1	1.11	0.96	5.3	6.0
	C.b	31	12-D16	310	R12-52	340	2.00	3.25	7	205	15	3	31	350	14	242	3	1	1.68	1.33	5.0	3.9
	C.1	28	12-D16	310	R12-41	340	2.50	2.56	7	342	14	3	47	437	20	302	5	1	1.19	0.97	5.8	5.8
	C.2	28	12-D16	310	R12-69	340	1.50	4.31	6.5	221	14	3	46	262	20	181	5	1	1.04	0.95	4.8	5.6
	C.3	28	12-D16	310	R12-103	340	1.00	6.81	4	142	14	3	45	175	20	121	5	1	1.02	1.06	4.3	5.5
	C.4	28	12-D16	310	R12-119	320	0.60	7.43	3.5	91	14	3	26	105	12	72	3	1	1.03	1.05	3.9	3.5
	C.5	28	12-D16	310	R10-36	320	2.00	2.25	7	303	14	3	48	350	20	242	5	1	1.04	0.89	5.5	5.8
	C.6	28	12-D16	310	R16-93	307	2.00	5.81	5	272	14	3	47	350	20	242	5	1	1.17	1.00	5.8	5.7
	C.7	31	8-D28	300	R12-52	340	2.00	1.86	7	298	15	3	120	350	24	242	12	3	0.81	0.90	4.9	6.0
	C.8	27	11-D24	750	R12-52	340	2.00	2.17	7	281	14	3	96	350	20	242	10	2	0.95	0.94	5.1	5.7
	C.9	31	16-D20	260	R12-52	340	2.00	2.60	7	293	15	3	97	350	24	242	10	2	0.91	0.92	4.8	6.0
	C.10	27	24-D16	310	R12-52	340	2.00	3.25	7	346	14	4	93	350	20	242	9	2	0.77	0.76	5.3	5.8
	C.12	31	24-HD16	380	R12-52	340	2.00	3.25	6	238	15	3	89	350	16	242	9	3	1.17	1.12	5.3	4.3
Spiral Columns Tested by Zahn et al [6.22]	U.1	31	16-D16	300	R12-135	328	0.91	8.43	2	72	10	3	49	110	12	76	7	1	0.98	1.31	4.0	5.1
	U.2	31	16-D16	300	HR10-135	466	1.63	8.43	2	93	10	3	56	75	16	52	9	1	0.23	0.71	3.0	5.9
	U.3	33	16-D16	300	R12-75	328	1.63	4.69	6	129	11	3	58	196	14	135	6	1	1.17	1.21	4.6	5.2
	U.4	33	16-D16	300	HR10-75	466	1.13	4.69	6	119	11	3	42	137	10	95	4	1	0.88	0.94	3.4	3.8
	U.6	29	16-D16	300	HR10-40	466	2.12	2.50	7	200	10	2	65	256	14	177	7	1	1.01	0.98	4.5	5.2
																		Error Average	17%	12%		
																		Maximum Error	77%	33%		

Notes: $\alpha = 0.9$, $\beta = 0.9$, $U_{sh} = A_{cc}\ \rho_s\ 110\ MJ/m^3$, $U'_{sh} = A_{cc}\ \rho_s\ 84\ MJ/m^3$

6.3.4.6 Application of the Proposed Theory to Flexural Members

The proposed method, which has been established based on the assumed failure mechanisms for a column loaded to failure by axial load only, will need to be modified when it is applied to a member subjected to bending mainly for the following two reasons:

(1) The energy stored in the core concrete in compression zone of a flexural member becomes smaller as the strain gradient along the transverse section of the member increases, when the comparison is made for a particular value of extreme concrete compression fibre strain. This will mean to that, in a column subjected to bending, the extreme concrete compression fiber strain at first hoop fracture becomes larger as the imposed axial load becomes smaller, since the strain energy stored in the hoop reinforcement at fracture is mainly balanced by the stored energy in the core concrete in compression zone. This may be the main reason for the fact that the measured extreme compressive fibre strain of concrete at first spiral fracture in Unit 12 with an axial load level of $0.5\ f'_cA_g$ was much smaller than that in Unit 10 with axial load level of $0.1\ f'_cA_g$. It is noted that Units 10 and 12 had the same longitudinal reinforcing arrangement and almost the same amount of spiral reinforcement, and hence the theoretical ultimate compressive strains at first hoop fracture for those units, described in the following poaragraphs, are almost the same as listed in Table 6.3 .

(2) The strain distribution along hoop bars also changes depending on both the degree of the strain gradient and the bond condition of the hoop bars. It is notable that the spiral or hoop bar strain measured near the neutral axis depth becomes much smaller than that measured in the extreme compression fibre region of column, as shown in Chapter four (see Figs. 4.68 to 4.71). This means that the strain energy stored in hoop reinforcement at fracture is affected by the strain gradient along transverse section of column and the bond condition of the hoop bars.

In the case of a column subjected only to axial load, the basic energy equation could be reduced to a comparatively simple form as the form for per unit volume of concrete core (see Eq. 6.22). For the case that a reinforced concrete member is subjected to bending with or without axial

load, the energy relations need to be established considering the energy system along both the longitudinal and transverse axes of the member because of the two reasons mentioned above, and hence the equation may not be able to be reduced to a simple form. The establishment of such energy relations will require a great effort due to the large number of factors involved, and it needs to be a topic of future research. However, an approximation for the ultimate concrete compressive strain at first hoop fracture in a flexural member can be made by applying the method proposed below to the compression zone of the member section.

For Units 10 to 12 described in Chapter four, the double spirals interlocked at the mid depth of colum were used as transverse reinforcement. Those test units were subjected to cyclic horizontal loading under a constant axial load from 0.1 to 0.5 $f'_c A_g$. In those test units, the stress condition in the compression zone at the critical section may be considered to be comparatively close to that of a circular column with single spiral reinforcement subjected to axial loading. Hence, the proposed method was applied to Units 10 to 12, assuming that the half of the column section in compression side can be represented by a circular column section with single spiral reinforcement. That is, the theoretical ultimate compressive strain of concrete at first spiral fracture for each test unit was calculated by assuming that each represented circular column (column diameter = 400 mm, longitudinal reinforcement = eight 20 mm diameter deformed bars of Grade 380 steel, single spiral reinforcement = 10 mm diameter plain bar of Grade 275 steel, using the same spacing as for the interlocking spirals) is subjected to axial loading. In the calculation, a bilinear stress-strain relation determined from the measured yield strength of steel was used for the longitudinal reinforcement. For the confined concrete, the stress-strain model due to Mander et al [6.3, 6.10] was used. The calculated results for variously assumed α, β, γ are listed in Table 6.3.

When $\alpha = 0.9$, $\beta = 0.9$ and $\gamma = 0.1$ were assumed as in the calculations to obtain Table 6.2, the predicted ultimate compressive strains of concrete at first hoop fracture were all larger than the measured values as can be seen from Table 6.3. The value of γ, which is determined from the behaviour of the shear sliding surfaces formed in the compressed concrete core region, may need to be increased as the strain gradient along the column transverse section becomes large, because the core concrete in small axial compression

or in tension will disturb the shear sliding. Actually, when the assumed value of γ was increased to 0.12, the predicted ultimate compressive strains for Units 10 and 11 agreed well with the test results.

It is noted that $\alpha = 0.9$ was determined by Eq. 6.25 assuming that the buckled shape of longitudinal reinforcement can be represented by a sinusoidal curve over three times column diameter (see Fig. 6.8). Judging from the visual damage in the compression failure zone of Units 10 to 12 (see Figs. 4.47 to 4.50), α which is determined from the average strain in spirals along the column axis in that zone may need to be smaller than the value estimated by Eq. 6.25, especially in the case of Units 10 and 11. Hence, as a reference, the calulation was conducted by reducing the value of α to 0.7. As listed in Table 6.3, the assumed values, $\alpha = 0.7$, $\beta = 0.9$ and $\gamma = 0.12$, gave conservative estimates of the ultimate compressive strain of concrete at first spiral fracture for Units 10 and 11 but still gave a non-conservative estimate for Unit 12. However, it may be said that those assumed values gave acceptable estimates of the ultimate compressive strain of concrete at first spiral fracture, on average.

The influence of the assumed value of β (= ratio of strain energy absorbed in compression reinforcement by axial yielding to external work done on compression reinforcement) was also examined by reducing its value to 0.7. As can be seen from Table 6.3, the change of the assumed value of β affects the estimate of the ultimate compressive strain of concrete at first spiral fracture in the same order as that of α.

Table 6.3 Comparison between Measured and Theoretical Ultimate Concrete Compressive Strains at First Hoop Fracture for Units 10 to 12

Column Unit	Extreme Compressive Fibre Strain of Concrete Measured at Core Surface, at First Hoop Fracture	Ultimate Compressive Strain of Concrete by Theory			
		α =0.9 β = 0.9 γ = 0.1	α =0.9 β = 0.9 γ = 0.12	α =0.7 β = 0.9 γ = 0.12	α =0.9 β = 0.7 γ = 0.12
U10	5.7%	6.4%	6.0%	5.1%	5.0%
U11	5.4%	5.7%	5.5%	4.6%	4.5%
U12	4.1%	6.1%	5.7%	4.8%	4.8%

Since the data employed in the above study are only from three tested columns at this stage, it cannot be suggested how to determine adequate values of α, β and γ in accordance with the change of axial load level imposed on a flexural member. However, it has been shown that the proposed method can lead to an approximate estimate of the ultimate compressive strain of concrete at first hoop fracture not only for axial compression members but for flexural members by modifying $\alpha = 0.7$ to 0.9, $\beta = 0.7$ to 0.9 and $\gamma = 0.1$ to 0.12 as far as the employed data is concerned.

6.4 CONCLUSIONS

To estimate the ultimate concrete compressive strain, defined as that strain where first hoop fracture occurs, a theoretical method using an energy principle model was established in this study. The basic idea of this method originated from the theory referred to as the energy balance theory by Mander et al. The following modifications to the energy balance theory were carried out in the method presented here:

(1) In the energy balance theory, the relationship between external work done on a reinforced concrete column and the corresponding internal work performed was not completely stated. In the proposed method, the above relationship is clarified by introducing a failure model for a reinforced concrete column subject to axial compression load.

(2) The strain energy absorbed in the longitudinal reinforcement due to axial compressive yielding is taken into account in the proposed method. It was neglected in the energy balance theory.

(3) The energy dissipated by friction between shear sliding surfaces formed in the concrete core is considered on the basis of a proposed failure model in this method. This energy factor was not included in the energy balance theory.

(4) One of the key aspects in the prediction of the occurrence of the hoop fracture is a proper estimate of the strain energy stored in the hoop reinforcement at the stage of hoop fracture. In the energy balance theory it was assumed that all part of the hoop reinforcement

simultaneously reached fracture strain when the first hoop fracture occurred. In the proposed method the strain energy stored in the hoop reinforcement is estimated using an assumed strain distribution in the hoop reinforcement where only the necking part of the hoop bar reaches the fracture strain and the strains in the remaining parts of the hoop bar are equal to or less than the strain at the ultimate strength of the steel.

The proposed method was applied to the results of concentric loading tests on 18 reinforced concrete columns conducted at the university of Canterbury. The theoretical values calculated by the proposed method agreed well with the test results. It is considered that the proposed method can be used to estimate with reasonable accuracy the ultimate longitudinal compressive concrete strain defined as the strain at first hoop fracture.

The proposed method was also applied to the three columns subjected to cyclic horizontal loading under a constant axial load level of 0.1 to 0.5 $f'_c A_g$ (that is, Units 10 to 12 described in Chapter four). It was found that the proposed method can give an approximate estimate of the ultimate compressive strain of concrete at first hoop fracture not only for axial compression members but for flexural members by changing α from 0.7 to 0.9, β from 0.7 to 0.9 and γ = from 0.1 to 0.12 as far as the employed data is concerned. Further study is recommended to rationally determine the values of α, β and γ in accordance with the change of axial load level imposed on the flexural member.

CHAPTER SEVEN

CONCLUSIONS AND RECOMMENDATIONS

7.1 CONCLUSIONS

The conclusions reached as a result of the experimental and theoretical work carried out for each chapter in this thesis are listed below:

Chapter 2

In Chapter Two, several notable stress-strain models previously proposed for confined concrete were reviewed and compared with experimental observations. The conclusions reached in Chapter Two are as follows.

(1) For concrete confined by circular hoops or spirals, the stress-strain model proposed by Mander et al [2.6] gives the largest estimate of the strength and ductility enhancement due to lateral confinement when compared with the models proposed by Desayi et al [2.15], Park and Leslie [2.16] and Watanabe et al [2.17]. For concrete confined by rectangular hoops with or without cross ties, the Mander et al model [2.6] also gives the largest estimate of the strength and ductility enhancement when compared with the models proposed by Scott et al (the modified Kent and Park model [2.29]) and Sheikh et al [2.13]. Since the stress-strain model proposed by Mander et al has been calibrated by tests on realistically sized columns with realistic reinforcing arrangement, for design purposes this model might be more reliable than the other models which were calibrated using comparatively small sized columns, sometimes without longitudinal reinforcement, provided that the strengths of the plain concrete and the transverse reinforcement are within the range ordinarily used. For example, when those stress-strain models for confined concrete were applied to the moment-curvature analyses of four realistically sized test columns (=Units 9 to 12 described in Chapter 4), the analytical results obtained using stress-strain model proposed by Mander et al showed the best fit with the test results.

The main variables used to determine the above stress-strain models for confined concrete are: (a) the configuration of transverse reinforcement, (b) the volumetric ratio of transverse reinforcement, (c) the yield strength of the transverse steel, (d) the spacing of the transverse reinforcement, (e) the compressive strength of plain concrete, (f) the spacing between the longitudinal reinforcing bars, (g) the content of longitudinal reinforcement and (h) the rate of loading.

(2) In order to investigate the influence of the strain gradient in member section on the confining stress condition and the corresponding stress-strain relationships of the confined core concrete, eccentric loading tests and, for comparison, concentric loading tests were conducted on eight concrete columns by the author et al [2.8]. Those columns had 200 mm square section and no longitudinal reinforcement was provided. Four of them were laterally confined by square spirals and the other four had no confining reinforcement.

The magnitude of the tensile strains observed in the hoop reinforcement in extreme compression fibre region of the concrete in eccentrically loaded columns was significantly smaller than that attained in the columns subjected to axial compression, when the extreme compression fibre strain in the eccentrically loaded columns was the same as the compression strain in the axially loaded columns. Hence, when the improvement in the strength and ductility of confined concrete is evaluated in terms of the lateral pressure provided by the transverse reinforcement, the effectiveness of the transverse reinforcement may be significantly reduced by the presence of a strain gradient in the section. In effect, the calculated stress-strain curves of the confined concrete indicated that the increase in the strength and ductility of the confined concrete attained in the eccentric loading tests was less than that in axial loading tests, where the stress-strain relationships of the confined concrete subjected to eccentric loading were calculated using the same numerical differential procedure adopted in the study by Soliman and Yu [2.14].

(3) The influence of variations in the compressive strength of the plain concrete, f'_{co}, on the increase in the strength and ductility of the confined concrete was investigated using the data obtained from axial loading tests

on 29 spirally reinforced concrete cylinders (15 cm in diameter by 30 cm in height) conducted by the author et al [2.8, 2.36, 2.37, 2.46]. In these tests, f'_{co} was varied from 16.5 to 55.9 MPa.

A statistical analysis on those test results indicated that the influence of variations in the compressive strength of the plain concrete on the strength increase of the confined concrete is not significant for f'_{co} up to about 60 MPa, when the strength increase of the confined concrete is expressed in terms of the lateral pressure as in Eq. 2.1" in Section 2.3.3.1.

In the above tests, the influence of variations in the compressive strength of the plain concrete on the ductile behaviour of columns was quite significant as already found in other previous studies. Hence, it is of necessity to take this factor into account when estimating the ductility improvement of confined concrete. All stress-strain models introduced in this thesis involve this factor. However, those models may need to be modified when applied to cases when f'_{co} is more than 80 MPa, as shown by the study by Muguruma et al [2.47].

(4) The evaluation of the confining effect of longitudinal reinforcement by various researchers is not consistent. However, even if the effect of the longitudinal reinforcement is appreciable, it is not significant when compared with the other factors. This is because the bending stiffness of longitudinal reinforcement, which determines its efficiency as confinement, is rapidly lost from a comparatively small compressive strain such as 0.2 % due to its yielding in axial compression. A further reason is that when the bending stiffness of longitudinal reinforcement is maintained, under small axial strains less than 0.2 %, the confining effects of the longitudinal reinforcement as well as of lateral reinforcement do not appear explicitly since they apply passive confinement.

(5) In axial loading tests on concrete cylinders (15 cm in diameter by 30 cm in height) confined by spirals with yield strength of from 161 MPa to 1352 MPa, which were conducted by the author et al [2.8, 2.36, 2.37, 2.46], the strength and ductility of the confined concrete were remarkably enhanced as the yield strength of the spiral steel was increased.

The observed strength increase of the confined concrete was found to be proportional to the square root of the yield strength of the spiral steel, although most of the stress-strain models [eg. 2.6, 2. 16, 2.18] assume that it is proportional to the yield strength of the spiral steel. The following three reasons for this observation can be considered. Firstly, in the case of spirals with yield strength of more than 1000 MPa, the passive confinement from the lateral pressure of the spirals is gradually increased, as the damage of concrete core progresses, and the maximum lateral pressure which is attained by yielding of the spirals can only be reached at a comparatively large compressive strain of concrete of about 2 to 3 %. Secondly, when high strength steel spirals were used, bearing failure of the core concrete may occur beneath the spiral bars due to the high local pressure before the maximum possible load carrying capacity of the core concrete is reached. Thirdly, at the ultimate condition, the area of critical section of the concrete core after spalling of the concrete in the ineffectively confined region between spiral bars is significantly smaller in the case of high strength spirals than in the case of ordinary strength spirals. This third reason may be eliminated when the area of the critical section is rigorously evaluated to estimate the real stress condition in the section.

It is noted that the failure of concrete cylinders confined by steel spirals with yield strength more than 1000 MPa was sudden and explosive due to crushing of the core concrete between the spiral bars or to the bearing failure beneath the spiral bar, whereas the failure observed for the concrete cylinders with ordinary strength steel spirals was normally gradual and gentle.

When cyclic loading was applied to cylinders confined by steel spirals with yield strength less than 400 MPa, the envelope stress-strain curves normally coincided with the stress-strain curves obtained from monotonic loading tests, regardless of the strain accumulated prior to a particular cycle. Hence, for concrete confined by ordinary strength spirals, it can be assumed that the monotonic loading curve represents the skeleton curve of the stress-strain curves under cyclic loading, as is normally assumed for modelling of cyclic loading curves. On the contrary, when cyclic loading with constant maximum load is applied to the cylinders confined by spirals with yield strength of more than 1000

MPa, fatigue failure of the concrete occurred before the cyclic loading curves reached the monotonic loading curves. Moreover, when cyclic loading was applied so as to follow the monotonic loading curve, the cyclic loading curves rapidly degraded when a certain compressive strain of concrete was reached and deviated from the monotonic loading curve. Thus, when concrete confined by high strength spirals is subjected to cyclic loading, the compressive strain at failure significantly decreases as the strain accumulated prior to the failure cycle increases.

Chapter 3

In Chapter Three, the effectiveness of various anchorage details for transverse reinforcement was studied. Eight reinforced concrete columns, with either 400 mm or 550 mm square cross sections, were tested subjected to axial compression loading and cyclic lateral loading which simulated a severe earthquake. The major variable examined was the type of anchorage used for the transverse reinforcement. The transverse reinforcement consisted of arrangements of square perimeter hoops with 135° end hooks, crossties with 90° and 135° or 180° end hooks, and 'U' and 'J' shaped cross ties and perimeter hoops with tension splices. The following conclusions with regards to the anchorage of the ends of transverse reinforcement, formed from deformed Grade 275 steel bar of diameter d_b, in plastic hinge regions of reinforced concrete columns subjected to severe earthquake loading, were reached based on the test results:

(1) Satisfactory behaviour was observed for: (a) perimeter hoops with 135° end hooks with an 8 d_b extension into the core concrete, (b) interior cross ties formed from 'J' bars in which one end was anchored by a tension splice of 24 d_b in the core concrete and the other end by 180° end hook with a 5 d_b extension, (c) interior cross ties formed from 'U' bars in which the ends were anchored by tension splices of 24 d_b in the core concrete. In the columns tested inclined flexure-shear cracks were predominant and hence the bond conditions along the tension splices of the 'J' and 'U' bars were not affected by cracking although some cracks did run along the splices.

(2) The interior cross ties with a 90° end hook and 6 d_b extension at one end and a 180° end hook and a 5 d_b extension at the other end, alternating end for end along longitudinal reinforcement, behaved satisfactorily in columns, at least up to a displacement ductility factor of 8. Beyond that displacement level the 90° end hooks commenced to open and the effectiveness of those end hooks was reduced gradually. The same conclusion is reached for when the interior cross ties with a 90° end hook and 6 d_b extension at one end and a 135° end hook and 8 d_b extension at the other end were used.

(3) The effectiveness of perimeter hoops formed from 'U' bars lapped in the cover concrete with a 17 d_b tension splice degraded rapidly when loss of the cover concrete occurred after the loading cycles to nominal displacement ductility factors of 4. This transverse reinforcement detail is to be discouraged. A similar conclusion can be reached about rectangular perimeter hoops which are anchored by 90° end hooks, since they were observed to perform poorly in the 1968 Tokachi-oki earthquake and the 1985 Mexican earthquake, although not tested in this study. This is because perimeter hoops anchored by 90° end hooks are not held against the longitudinal bars at the 90° end hooks after spalling of the cover concrete has occurred.

(4) The effect of the magnitude of the axial load level of the column on the effectiveness of tie bars anchored by tension splices was not found to be a significant variable within the tested range of axial load levels between 0.1 and 0.3 $f'_c A_g$.

(5) The equivalent plastic hinge lengths estimated for the tested columns at the nominal displacement ductility factor of 6 were from 0.46 to 0.75 of the overall depth of the column section. The larger equivalent plastic hinge lengths occurred at the larger imposed axial load levels. Those equivalent plastic hinge lengths are in the range normally evaluated for columns with conventional hoops and cross ties anchored by 135° end hooks. This also supports the conclusion that the 'J' or 'U' bar cross ties with tension splices and the cross ties with 90° end hooks at one end and 135°end hooks at the other end are as effective as conventional cross ties with 135° end hooks at least up to the nominal displacement ductility factor of 6.

Based on the theoretical considerations, the following conclusions were reached:

(1) With regard to the flexural strength reached by the columns; (a) The maximum measured flexural strength exceeded theoretical flexural strength calculated using the ACI concrete compressive stress block and the measured material strengths by 11 to 31 %. The strength enhancement above the moment estimated by the ACI method was well predicted by the empirical equations proposed by Ang [3.23, 3.25] which takes into account the effect of concrete confinement and of the axial load imposed. (b) A theoretical moment obtained using the modified Kent and Park stress-strain curve for confined concrete gave more realistic estimate of the ultimate strength of column. This is because the modified Kent and Park models take into account the enhancement of concrete strength and ductility due to the confinement by transverse reinforcement. Also, it was evident that additional confinement of the critical section of the test units was caused by the presence of the adjacent stub or base block which simulated an adjoining beam or other member.

(2) For all test units, except for one unit in which perimeter hoops formed from 'U' bars lapped in the cover concrete were used (= Unit 3), the envelope curves of the measured moment-curvature responses agreed well with or indicated higher load carrying capacities than the theoretical monotonic moment-curvature relationships obtained using the modified Kent and Park stress-strain curves for concrete, at least up to the ductility displacement ductility factor of 6. These results confirmed that the 'J' or 'U' bar cross ties with tension splices and the cross ties with 90° end hooks at one end and 135°end hooks at the other end were as effective as the conventional cross ties with 135° end hooks, since the modified Kent and Park stress-strain curves for concrete have been calibrated by tests on reinforced concrete columns with conventional hoops and cross ties having 135° end hooks. In case of the test unit in which perimeter hoops formed from 'U' bars lapped in the cover concrete were used (= Unit 3), the envelope curve, which degraded severely after opening of the 90° bends of the lapped 'U' bars making up the perimeter hoops, agreed well with the theoretical monotonic moment-curvature relationship obtained by assuming that the confinement from the lapped 'U' bars was totally

lost. Thus the ineffectiveness of the lapped 'U' bars making up the perimeter hoops was also confirmed.

(3) For the test units with the ratio of the shear span length to the column depth of 4 (= Units 1 to 4), the first yield displacement of column was well predicted by the theoretical method introduced in this study. In this method the first yield displacement of column was calculated as the sum of : (a) The flexural deformation calculated by integrating the theoretical curvature distribution determined by section analysis of the cracked region of the column, (b) The elastic flexural deformation of the uncracked region of the column, (c) The shear deformation of the cracked region of the column, (d) The shear deformation of the uncracked region of the column. For the test units with the ratio of the shear span length to the column depth of 3 (= Units 5 to 8), the first yield displacement of column was underestimated by that method for two reasons. One reason is that the concrete near the bottom of those test units (Units 5 to 8) was apparently not fully compacted at the time of concrete placing. The other reason is that shear deformations of those test units would be significantly larger than those estimated by the method used in this study due to the comparatively small aspect ratio of column.

Chapter 4

In Chapter Four, general aspects and related problems associated with determining appropriate reinforcing details using interlocking spirals as transverse reinforcement were first discussed. Then, the effectiveness of interlocking spirals was studied experimentally by tests on four columns Three columns with interlocking spirals and, for comparison, one column with rectangular hoops and cross ties were tested under cyclic horizontal loading which simulated severe seismic loading. Each column with overlapping spirals contained two spirals. The size of the columns tested was approximately one third of that expected to be used in practical design situations for bridge piers. From these theoretical studies and experimental observations following conclusions were reached:

(1) The amount of transverse reinforcement required for the confinement of core concrete in the potential plastic hinge region of a column can be considerably reduced by using interlocking spirals instead of rectangular

hoops and cross-ties, when the amount of transverse reinforcement is determined by NZS 3101 .

(2) The local volumetric ratio of interlocking spirals in the extreme compression region of column section, ρ_{se}, can become significantly less than the volumetric ratio ρ_s required for the case of single spirals, when it is determined following the normal code, where ρ_{se} = ratio of volume of spirals ouside the area of interlock to the corresponding concrete core (see notation in Fig. 4.5) and ρ_s = ratio of volume of spiral or circular hoop reinforcement to total volume of concrete core (out-to-out of spirals or hoops). This result affects the stress-strain relationship for confined core concrete. A proposal is made for an appropriate definition of the volumetric ratio of interlocking spirals for use in codes.

(3) The shear carried by interlocking spirals can be estimated by a proposed method which considers the equivalent transverse reinforcement.

(4) When the interlocking of spirals is weak, due to a small overlap distance between adjacent spirals, the load carrying capacity of the column can be estimated by the combined beam-arch action theory proposed in this study. However, the overlap distance between adjacent spirals should not be made inadequately small because the load carrying capacity and stiffness of the column under cyclic loading can rapidly decrease as a result. If an inadequately small overlap distance needs to be adopted because of some architectural requirement, it is recommended that a proposed reinforcing detail, in which ties are provided in addition to the interlocking spirals, be used.

(5) In order to determine an adequate overlap distance for the adjacent interlocking spirals an approach is proposed. This approach is based on the concept that the initial stiffness of interlocking must be secured by the concrete core in the interlocking area, since dowel action of the longitudinal bars to interlock the spirals can only be expected after cracking of the concrete. In the proposed approach, the interlocking concrete core is modelled by a concrete corbel under a particular loading condition and the sectional area of the corbel is determined to resist direct shear from spirals.

(6) The amount of longitudinal bars required to interlock the spirals can be determined by using a proposed method based on the shear friction method introduced in ACI 318-89. However, it must be emphasized that the longitudinal bars become largely ineffective for such purpose when they yield due to column bending.

(7) At least four longitudinal bars should be provided inside the interlocking area of the spirals in order to achieve the suspension mode of resistance of the spirals suggested in this study. This is because the anchorage of the spirals can only be achieved by a suspension mode when local fracture of core concrete occurs.

(8) The three columns tested with interlocking spirals in this study satisfied all of the above requirements and checks. The behaviour of those columns under simulated severe earthquake loading was very satisfactory. That is, all the measured hysteresis loops displayed good energy dissipation and limited reduction in strength up to the end of the test at a displacement ductility factor μ of more than 10. Hence, it can be said that all the above requirements and the checks were adequate as far as the columns tested are concerned.

(9) For all columns tested, the longitudinal bar strains measured by electric resistance wire strain gauges indicated rapid deterioration of bond between longitudinal reinforcement and concrete in the plastic hinge region from an early stage of inelastic loading. Hence, it was considered that those tested columns were subject to combined beam-arch action rather than to the perfect beam action in the inelastic range of loading. In effect, when both the perfect beam action theory and the combined beam-arch action theory were applied to the columns with interlocking spirals, the behaviour predicted by the latter theory showed better agreement with the test results.

(10) In those columns tested, inclined flexural shear cracks were predominant due to the comparatively small aspect ratio of those columns. Based on the crack pattern observed, a shear deformation model was proposed and could satisfactorily interpret the deformation mechanism that actually occurred in the tested columns.

(11) For the columns tested, the shear deformation defined in this study reached 10 to 30 % of the column deflection and this ratio was almost constant from displacement ductility factor μ = 0.75 to the final stage of loading where μ of more than 8 was applied. This indicates that the deflection of a column cannot always be predicted by a curvature distribution found assuming that plane sections remain plane within acceptable error. It is suggested that for a column with aspect ratio of 3 similar to those columns tested, when the theoretical column deflection is calculated based on curvature distribution, the calculated column deflection needs to be increased by about 20 % or more to take shear deformations into account.

Chapter 5

In Chapter Five, a buckling model for an intermediate longitudinal bar restrained by cross ties with a 90° end hook at one end and a 135° or 180° end hook at the other end, alternating end for end along the longitudinal reinforcement, was proposed. Using this model, an analytical study to assess the effectiveness of the cross ties with 90° and 135° end hooks was conducted and the following conclusions were reached:

(1) The initial bending stiffness of a 90° hook at the end of a bar of diameter of 10 to 12 mm is normally large enough to prevent buckling of an intermediate longitudinal bar with bar diameter of 20 to 25 mm, provided that the intermediate longitudinal bar is perfectly straight before loading. However, the maximum elastic deflection of the 90° end hook at the contact point with the longitudinal bar is in the order of only 0.01 to 0.1 mm, in practice. Hence, the initial deflection of the longitudinal reinforcement due to imperfection must be considered in practical design.

(2) An equation (Eq. 5.55) was proposed to estimate the maximum allowable initial deflection of the longitudinal bar due to imperfection δ_o^c . If the calculated value of δ_o^c is impractically small, lateral restraint by the 90° end hook against longitudinal bar buckling should not be expected. In such case, the end of cross ties with a 90° hook should not be included in the evaluation of the transverse reinforcement required to prevent bar buckiling.

(3) The initial stiffness of a peripheral hoop, with regard to the restraint of an intermediate longitudinal bar, is negligibly small compared with that of a cross tie with a 90° end hook. Hence, it is not necessary to take the restraint of peripheral hoops into account in the early stage of loading of the column.

(4) If the amount of transverse reinforcement is large enough to delay tensile yielding of the transverse reinforcement until the column reaches a large displacement ductility factor (e.g. more than 6), buckling of the longitudinal bar may be adequately delayed by the restraint of 90° end hooks and the peripheral hoop. This can be explained as follows. When a displacement ductility factor of about more than 6 is reached, the longitudinal reinforcement has already been loaded far into the inelastic range. As a result, the bending stiffness of the longitudinal bar degrades rapidly as its compression strain increases. Under such condition, the lateral pressure from the core concrete concentrates at the positions of the 135° or 180° end hooks of the transverse bars. As a consequence, the deflection of the longitudinal bar due to lateral pressure can remain small in magnitude, which results in a moment due to deflection that can be balanced by a small sustaining force from the 90° end hook and the peripheral hoop. However, such a state of stable equilibrium in the longitudinal bar may be only temporary. That is, buckling of the longitudinal bar can eventually occur at a large displacement ductility factor of more than 6, as the lateral pressure distribution along the longitudinal bar changes.

(5) In a numerical example it was found that a 90° end hook on a cross tie could only sustain about 12 % of the yield force of the cross tie. The ratio of the force sustained by a 90° end hook on a cross tie to the yield force of the cross tie depends on the bar diameter, the diameter of the bend of the 90° hook and the yield strength of the tie bar steel and that ratio will become 10% or so for a normal case.

(6) The transition of loading conditions on the longitudinal bar, which includes the lateral pressure from the core concrete, is well predicted for stages of loading on the column using the model proposed in this study .

(7) In the inelastic range of behaviour of the column, the effective confinement of the core concrete may be a more critical requirement than the prevention of buckling of the longitudinal reinforcement, except for the case when the column has an extremely large amount of longitudinal reinforcement. If the buckling of the intermediate longitudinal reinforcement restrained by a 90° end hook results in a rapid decrease in the load carrying capacity of the column, it may be mainly because the effective confinement of the core concrete is lost due to large lateral deflection of the longitudinal reinforcement. That is, decrease in the load carrying capacity of of the column caused by buckling of an intermediate longitudinal bar can be insignificant providing that the core concrete is adequately confined. Hence, it is recommended that an adequate margin for the amount of transverse reinforcement be provided if cross ties with 90° and 135° or 180° end hooks are used.

(8) In order to reduce the ratio of the area of compression reinforcement restrained by 90° end hooks to the area of compression reinforcement more securely restrained by 135° or 180° end hooks, a preferable transverse reinforcement detail (see Fig.3.11(b)) is suggested.

(9) In the previous column tests with axial load level of up to 0.3 $f'_c A_g$, which are reported in references [5.14, 5.18, 5.19,5.20, 5.21], the effectiveness of the cross ties with 90° end hook at one end and 135° or 180° end hook at the other end alternating along longitudinal reinforcement was generally as satisfactory as that of conventional cross ties with 135° or 180° end hooks. The analytical study developed in this chapter also indicates the possibility of such a result, since bond between the tie leg and the confined concrete aids the anchorage of the cross tie. However, it should be noted that deformed bars were used for the cross ties in those previous column tests and hence the tie legs might have confined the core concrete by bond without relying significantly on the end hooks for anchorage.

(10) It should be noted that only cross ties with 90° end anchorages are considered here. That is, cross ties which pass through the core concrete. Peripheral hoops with 90° end hooks are definitely inadequate as transverse reinforcement since once the cover concrete spalls such

perimeter hoops can move away (outwards) from the longitudinal bars and render the anchorage useless.

Chapter 6

To estimate the ultimate concrete compressive strain, defined as that strain where first hoop fracture occurs, a theoretical method using an energy principle model was established in Chapter Six. The basic idea of this method originated from the theory referred to as the energy balance theory by Mander et al [6.3, 6.11]. The following modifications to the energy balance theory were carried out in the method presented in this chapter:

(1) In the energy balance theory, the relationship between external work done on a reinforced concrete column and the corresponding internal work performed was not completely stated. In the proposed method, the above relationship is clarified by introducing a failure model for a reinforced concrete column subject to axial compression load.

(2) The strain energy absorbed in the longitudinal reinforcement due to axial compressive yielding is taken into account in the proposed method. It was neglected in the energy balance theory proposed by Mander et al.

(3) The energy dissipated by friction between shear sliding surfaces formed in the concrete core is considered in the proposed failure model in this method. This energy factor was not included in the energy balance theory.

(4) One of the key aspects in the prediction of the occurrence of hoop fracture is a proper estimate of the strain energy stored in the hoop reinforcement at the stage of hoop fracture. In the energy balance theory it was assumed that all parts of the hoop reinforcement simultaneously reached the fracture strain when the first hoop fracture occurred. In the proposed method the strain energy stored in the hoop reinforcement is estimated using an assumed strain distribution in the hoop reinforcement where only the necking part of the hoop bar reaches the fracture strain and the strains in the remaining parts of the hoop bar are equal to or less than the strain at the ultimate strength of the steel.

The proposed method was applied to the results of concentric loading tests conducted on 18 reinforced concrete columns conducted at the University of Canterbury. The theoretical values calculated by the proposed method agreed well with the test results. It is considered that the proposed method can be used to estimate with reasonable accuracy the ultimate longitudinal compressive concrete strain defined as the strain at first hoop fracture.

The proposed method was also applied to the three columns subjected to cyclic horizontal loading under a constant axial load level of 0.1 to 0.5 $f'_c A_g$ (that is, Units 10 to 12 described in Chapter Four). It was found that the proposed method can be used to estimate of the ultimate compressive strain of concrete at first hoop fracture not only for concentrically loaded compression members but also for flexural members by modifying the values of the several constants used in the proposed equations.

7.2 RECOMMENDATIONS FOR FUTURE RESEARCH

Several additional problems encountered during the research work conducted for this thesis could not be investigated in detail due to lack of time. The following research topics are suggested to obtain a better understanding of the characteristics of confined concrete and to improve transverse reinforcing details for reinforced concrete structures subjected to severe seismic loading.

1. In axial loading tests on reinforced concrete columns, the gauge length used for the longitudinal strain measurement of concrete significantly affects the slope of the falling branch of the stress-strain curves of confined concrete. This is because, when diagonal failure planes (= diagonal shear sliding planes) are formed after peak load, the strain in the falling branch region is the apparent strain calculated by dividing the gauge length into the relative displacement between the parts separated by those planes. It was found that the difference between the slopes of the falling branches in the stress-strain models proposed by various researchers can be attributed to the difference of the gauge lengths used in their tests.

The most appropriate gauge length to be adopted in column tests, for application to the analyses of columns under combined bending and axial load, cannot be simply suggested. This is because the length of the compression failure zone along the column axis varies depending on the axial load level and moment gradient imposed. In axial compression tests on columns, when a gauge length shorter than the least section dimension is used, the measured strain values normally show a wide scatter, depending on the location of the gauge with respect to the diagonal shear sliding planes formed in the concrete core. This feature limits the gauge length to be adopted in axial compression tests on concrete columns. Hence, a future study should establish a method which can appropriately modify the strains measured in axial compression tests using a certain gauge length, for application to flexural members with various levels of axial load and moment gradient.

2. From the eccentric loading tests on columns conducted for this thesis, it was clarified that the magnitude of the hoop tensile strains observed in the region of the extreme compression fibre in eccentrically loaded columns was significantly smaller than that attained in columns subjected to axial compression, when the extreme compression fibre strain in the eccentrically loaded columns was the same as the compression strain in the axially loaded columns. A similar phenomenon was also found in the flexural shear tests on the columns described in Chapters Three and Four. Hence, the derived conclusion was that the effectiveness of transverse reinforcement is significantly reduced by the presence of a strain gradient in the section, when the improvement in the strength and ductility of confined concrete is evaluated in terms of the lateral pressure provided by the transverse reinforcement.

If the used stress-strain models for confined concrete based on concentric loading tests do not result in any overestimation of the strength and ductility of a member subjected to flexure with shear, the increase of strength and ductility of the confined concrete may need to be attributed not only to the lateral pressure provided by the lateral confining reinforcement but also to other factors such as the restraint against damage progress in extreme compression fibre region due to the flexural strain gradient in section, and due to the longitudinal stress gradient, suggested by Uppal and Kemp [2.38].

As a future research, the effects of the strain gradient in member section and the stress gradient along the member axis on the stress-strain behaviour of the confined concrete should be quantitatively estimated.

3. When transverse reinforcement formed from ordinary strength steel bars is used as lateral confining reinforcement for the core concrete, the ultimate available compressive strain of the core concrete could be determined from the stage of first fracture of the transverse reinforcement as described in Chapter Six. When circular spirals formed from high strength steel bars with yield strength of more than 1000 MPa were used, the strength and ductility of the confined core concrete were remarkably enhanced without spiral fracture (see Chapter Two). However, in this case the core concrete suddenly crushed in the effectively confined region between the spiral bars or immediately beneath the spiral bars when axial compressive strain reached 2% or more. Thus crushing of the core concrete limits the ultimate compressive strain of the confined core concrete when high strength steel bars are used for the transverse reinforcement.

In Chapter Two, the ultimate compressive strain due to crushing of the core concrete, for when high strength steel bars with yield strength of more than 1000 MPa are used for the transverse reinforcement, could not be clearly established, although the relationships between the fatigue cycles to the applied stress level were evaluated statistically.

As a future research project, the ultimate compressive strain of confined core concrete determined at the stage of crushing of concrete in the effectively confined region between the spiral bars or immediately beneath the spiral bars, needs to be quantitatively evaluated for the case when transverse reinforcement of high strength steel is used. When sudden crushing of concrete occurs immediately beneath the high strength steel spirals, the ultimate compressive strain of the confined core concrete may be determined in terms of the bearing strength of the core concrete. This future research project is of particular importance since a number of high rise reinforced concrete buildings are being constructed using high strength concrete and high strength transverse reinforcement in countries where the land price is extremely expensive like Japan.

4. In the study described in Chapter Three, the effect of the magnitude of the axial load level of the column on the effectiveness of cross tie bars anchored by tension splices was not found to be a significant variable within the tested range of axial load levels between 0.1 and 0.3 $f'_c A_g$. As a future research project, the effectiveness of cross tie bars anchored by tension splices needs to be examined for the case of exterior columns of a tall building which are often subjected to both cyclic tension and compression axial load under severe earthquake loading. This is because tension splices are likely to become ineffective when the columns are subjected to tension axial load, due to cracking along the splices, although effective confinement by the cross ties may not be required when the columns are under tension axial load.

5. The previous column tests [5.14, 5.18, 5.19,5.20, 5.21] described in Chapter Three and the analytical study developed in Chapter Five indicated that effectiveness of cross ties with a 90° end hook at one end and a 135° or 180° end hook at the other end could be as satisfactory as that of conventional cross ties with 135° or 180° end hooks. However, it should be noted that deformed bars were used for the cross ties in those studies and hence the tie legs could confine the core concrete partly by bond without relying significantly on the end hooks for anchorage. Further research on the effectiveness of cross ties with a 90° end hook at one end and a 135° or 180° end hook at the other end is recommended for the case when plain bar is used, since in NZS 3101 and other codes plain bar is allowed to use for transverse reinforcement.

6. In Chapter Six, a method for the prediction of the ultimate compressive strain of the confined core concrete based on the occurrence of first hoop fracture was proposed based on energy considerations. It was shown that the proposed method could predict that strain with reasonable accuracy for columns subjected to axial loading. It was also shown that the proposed method could be applied to columns subjected to combined axial load and bending by modifying the values of three constants, determined for columns subjected to axial loading, in the proposed equations. However, since the modified values of those constants for the case of columns subjected to bending and axial load were calibrated using the data from only the three column tests described in Chapter Four, generally reliable values

for those constants could not be suggested in terms of the axial load level imposed on a column. A further study is recommended to rationally determine the values of those constants for the general case, taking into account the change of axial load level and the moment gradient imposed on the flexural member.

References - Chapter 1

[1.1] "Basic Concepts for Seismic Codes," International Association of Earthquake Engineering, Comite Euro-International du Beton, Bulletin D'Information N°149 Part I, 1982 ,p.30

[1.2] "Commentary on the Fourth Edition of the Recommended Lateral Force Requirements", Seismology Committee, Structural Engineers Association of California, 1975,pp.84

[1.3] Freeman,S.A., Nicoletti,J.P. and Matsumura,G.,"Seismic Design Guidelines for Essential Buildings",Proceedings of The Eighth World Conference on Earthquake Engineering, San Francisco, July 1984,Vol.1,pp.715-722.

[1.4] Hutchison,D.L., Andrews,A.L., Butcher,G.W. and Kolston,D. "Draft Revision of NZS 4203:1984: Seismic Provisions", Bulletin of the New Zealand National Society for Earthquake Engineering, Vol.19, No3, September 1986,pp.158-166

[1.5] "Code of Practice for General Structural Design and Design Loadings for Buildings-NZS 4203:1984," Standards Association of New Zealand,Wellington

[1.6] The Ministry of Construction, Housing Bureau and Building Research Institute, "Commentary on the Structural Calculation based on the Revised Enforcement Order ,the Building Standard Law(in Japanese)", Building Center of Japan, November 1980, p.173

[1.7] Umemura,H.(coordinating editor), "New Earthquake Resistant Design (in Japanese) ", Building Centre of Japan, May 1979

[1.8] Aoyama,H.,"Outline of Earthquake provisions in the Recently Revised Japanese Building Code", Bulletin of The New Zealand National Society for Earthquake Engineering,Vol.14,No2,June 1981, pp.63-80

[1.9] Xiaowang,G. and Aibin, B.,"Determination of Moderate and Major Earthquakes for Aseismic Design by Probabilistic Method", Proceedings of Pacific Conference on Earthquake Engineering, Vol. 3, New Zealand, August 1987, pp.231-236.

[1.10] Otsuki,Y.,"Development of Earthquake Building Construction in Japan," Proceedings of the World Conference on Earthquake Engineering , Berkeley, California, June 1956, pp.16-1 to 16-17

[1.11] Kanai,K., Kobori T. and Hiruta S.,"Kenchikugaku Taikei- 11, Jishin Shindogaku, "Shokokusha, Tokyo,1974 ,p.516

[1.12] Wiegel,R.L.(coordinating editor),"Earthquake Engineering," Prentice-Hall, Inc. Englewood Cliffs,N.J.,U.S.A.,1970, p.518

[1.13] Skinner,R.I., Stephenson,W.R. and Hefford, R.T.,"Strong Motion Earthquake Recording in New Zealand,"Bulletin of the New Zealand Society for Earthquake Engineering, Vol.4,No1, March 1971, pp.31-42

[1.14] Moss,P.J.,"Review of Current Earthquake Engineering Research in New Zealand," Bulletin of the New Zealand Society for Earthquake Engineering,Vol.20,No.2,June 1987,pp.91-98.

[1.15]Pender,M.J. and Robertson,T.W.,"Edgecumbe Earthquake:Reconnaissance Report," Bulletin of the New Zealand National Society for Earthquake Engineering, Vol.20,No.3,September 1987, pp.201-249

[1.16]Tomisawa,M."Jitsuyo Doteki Taishin Sekkeiho", Omusha, Tokyo, 1983, p.287

[1.17]Esteva,l.,"Earthquake Engineering Research and Practice in Mexico after the 1985 Earthquake,"Bulletin of the New Zealand National Society for Earthquake Engineering, Vol.20,No3,September 1987,pp.159-200

[1.18] Stephenson, W.R.,"Seismic Microzoning in New Zealand",Bulletin of the New Zealand Society for Earthquake Engineering, Vol.14,No1, March 1971, pp.43-50.

[1.19] Tanaka,T., Yoshizawa,S., Sakue,M. and Osawa,Y.," Estimation of Acceleration Characteristics of Strong Earthquake Ground Motions by a Simple Method of Synthesis", Proceedings of the Eighth World Conference on Earthquake Engineering, Vol.II, July 1984, SanFrancisco, California U.S.A. pp.441-448.

[1.20] Irikura,K." Prediction of Strong Ground Motions Using Observed Seismograms from Small Events", Proceedings of the Eighth World Conference on Earthquake Engineering, Vol.II, July 1984, SanFrancisco, California U.S.A. pp.465-472.

[1.21]Mitchell,D., Adams,J., DeVall,R.H., Lo,R.C. and Weichert,D.,"Lessons from the 1985 Mexican Earthquake", Canadian Journal of Civil Engineering, Vol. 13 No.5., 1986,pp.535-557.

[1.22] Suzuki,S. (Chief Editor), "General Report on The Tokachi-oki Earthquake of 1968", Keigaku Publishing Co., Ltd. Tokyo, Japan,1971, p.754.

[1.23]"Code of Practice for the Design of Concrete Structures(NZS 3101,Part 1:1982" and "Commentary on the Design of Concrete Structures(NZS 3101, Part 2:1982)", Standard Association of New Zealand, Wellington.

[1.24]"Notes on Earthquake Insurance in California and New Zealand", Bulletin of the New Zealand National Society for Earthquake Engineering, Vol.19, No4, December 1986,pp.251-254

[1.25] Park, R., et al(a study group for structures of limited ductility),"Structures of Limited Ductility", Bulletin of the New Zealand Society for Earthquake Engineering, Vol.19,No4, December 1986, pp.285-336.

[1.26] Saida,T.,"Jishin Katsudo to Bunka," Jishin 8-kan 6-go,1936,pp.271-283

[1.27] "Seismic Design of Concrete Structures, Second Draft of an Appendix to the CEB-FIP Model Code," Bulletin D'Information N°149-Part 2, Comité Euro International du Beton, Paris, March 1982.

[1.28]"Japanese Architectural Standard Specification-5, Reinforced Concrete Construction", Architectural Institute of Japan, Tokyo, 1979.

[1.29]"Standard Specifications for Highway Bridges, Relating to Seismic Design", adopted by The American Association of State Highway and Transportation Officials, Twelfth Edition 1977 with Revisions by Caltrans Office of Structures Design, 1983, Washington,D.C. 20001

[1.30] Mander, J. B., Priestley, M. J. N. and Park, R., "Seismic Design of Bridge Piers", Research Report 84-2, Department of Civil Engineering, University of Canterbury, February 1984, 483 pp.

References - Chapter 2

[2.1] Sheikh, S.M., "Effectiveness of Rectangular Ties as Confinement Steel in Reinforced Concrete Columns", Ph.D Thesis, Department of Civil Engineering, University of Tronto, Canada, 1978, pp.256.

[2.2] Park, R. and Paulay,T.," Reinforced Concrete Structures", Jhon Wiley and Sons, New York, 1975, pp.769.

[2.3] Richart, F.E., Brandzaeg, A. and Brown, R.L., "A study of the Failure of Concrete under Combined Compressive Stresses", University of Illinois Engineering Experimental Station, Bulletin No. 185, 1928, 104 pp.

[2.4] Balmer, G. G., "Shearing Strength of Concrete under High Triaxial Stress - Computation of Mohr's Envelope as a Curve", Structural Research Laboratory Report No. SP-23, U.S. Bureau of Reclamation, 1943, 13 pp. plus tables and figures.

[2.5] Richart, F.E., Brandzaeg, A. and Brown, R.L., " The Failure of Plain and Spirally Reinforced Concrete in Compression", University of Illinois Engineering Experimental Station, Bulletin No. 190, 1929, 74 pp.

[2.6] Mander, J.B., Priestley, M.J.N. and Park, R.,"Theoretical Stress-Strain Model for Confined Concrete", Journal of Structural Engineering, American Society of Civil Engineers, Vol. 114, No. 8 August 1988, pp. 1804-1826.

[2.7] Timoshenko, S.P. and Goodier, J.N., "Theory of Elasticity", third edition, McGraw-Hill International Book Company, Auckland, London, Tokyo, Paris and so on, 1970, 567 pp.

[2.8] Muguruma, H., Watanabe, F., Tanaka, H., Sakurai, K. and Nakamura, E., "Effect of Confinement by High Yield Strength Hoop Reinforcement upon the Compressive Ductility of Concrete", Proceedings of the Twenty-Second Japan Congress on Materials Research, The Society of Materials Science, Japan, 1979, pp.377-382

[2.9] Bertero, V.V. and Felippa, C., " Discussion of " Ductility of Concrete", by Roy, H.E.H. and Sozen, M.A., Proceedings of the International Symposium on Flexurala Mechanics of Reinforced Concrete, ASCE-ACI, Miami, November 1964, pp.227-234

[2.10] Roy, H.E.H. and Sozen, M.A., " Ductility of Concrete", Proceedings of the International Symposium on Flexural Mechanics of Reinforced Concrete, ASCE-ACI, Miami, November 1964, pp.213-224

[2.11] "Code of Practice for the Design of Concrete Structures (NZS 3101, Part 1:1982" and "Commentary on the Design of Concrete Structures (NZS 3101, Part 2:1982)",Standards Association of New Zealand, Wellington.

[2.12] "Building Code Requirements for Reinforced Concrete (ACI 318-89)" and "Commentary on Building Code Requiremens for Reinforced Concrete (ACI 318R-89)", American Concrete Institute, Detroit, 1989.

[2.13] Sheikh, S.A. and Uzumeri, S.M., "Analytical Model for Concrete Confinement in Tied Columns", The Journal of the Structural Division, Proceedings of the Americal Society of Civil Engineers, Vol. 108, No. ST.12, December, 1982, PP 2703- 2722.

[2.14] Soliman, M.T.M. and Yu, C.H., "The Flexural Stress-Strain Relationship of Concrete Confined by Rectangular Transverse Reinforcement", Magazine of Concrete Research: Vol. 19, No. 61: December 1967, pp.223-238

[2.15] Parakash Desayi, Sundara Raja Iyengar, K.T. and Sanjeeva Reddy, T., "Equation for Stress-Strain Curve of Concrete Confined in Circular Steel Spiral", Matériau et Constructions, Vol.11- N° 65, Sept/October 1978, pp. 339-345

[2.16] Park, R. and Leslie, P.D., " Curvature Ductility of Circular Reinforced Concrete Columns Confined by the ACI Spiral", 6th Australasian Conference on the Mechanics of Structures and Materials, Vol. 1: Technical Papers, Christchurch, New Zealand, August 1977, pp. 342-349.

[2.17] Watanabe,F., Muguruma,H., Tanaka, H. and Katsuda,S.,"Improving the Flexural Ductility of Prestressed Concrete Beam by Using the High Yield Strength Lateral Hoop Reinforcement", FIP, Symposia on Partial Prestressing and Practical Construction in Prestressed and Reinforced Concrete, Proceedings: Part 2, Sept. 1980, Bucuresti-România, pp.398-406.

[2.18] Sundara Raja Iyengar, K.T., Parakash Desayi and Nagi Reddy, K., " Stress-Strain Characteristics of Concrete Confined in Steel Binders", Magazine of Concrete Research, Vol. 22, No72: September 1970, pp.173-184

[2.19] Muguruma, H., Watanabe, F., Tanaka, H., Sakurai, K. and Nakamura, E.,"Study on Improving the Deformation Capacity of Concrete by Lateral Confinement (in Japanese) ", The 24-th Kozokogaku (Structural Engineering) Symposium, Kozo no Hisenkei Mondai (The problems related to non-linear behaviour of structures), Nihon-Gakujutsu Kaigi, Doboku Gakkai (Japan Society of Civil Engineers), Kenchiku Gakkai (Architectural Institute of Japan), Japan, February 1978 , pp.109-116

[2.20] Muguruma, H., Watanabe, F., Tanaka, H., Sakurai, K. and Nakamura, E., " Study on Improving the Flexural and Shear Deformation Capacity of Concrete Member by Using Lateral Confining Reinforcement with High Yield Strength", Comité Euro-International du Béton, BULLETIN D'INFORMATION N° 132, Volume 2 - Technical Papers, AICAP-CEB Symposium, Rome, May 1979, pp.37-44

[2.21] Muguruma, H. and Nagai, E., " On the Ultimate Flexural Compressive Strain of Concrete (in Japanese) ", Proc. of the 30th General Meeting of the Cement Association of Japan, 1976, pp.362-365

[2.22] Kosaka,Y. and Morita,S.,"Reinforced Concrete Structures (written in Japanese)", Maruzen, Tokyo, Japan ,1975, pp.385

[2.23]"Code of Practice for General Structural Design and Design Loadings for Buildings (NZS 4203:1984) ", Standards Association of New Zealand, Wellington.

[2.24] Mander, J. B., Priestley, M.J.N., and Park, R.,"Observed Stress-Strain Behaviour of Confined Concrete", Journal of Structural Engineering, Americal Society of Civil Engineers, Vol. 114, No.8, August 1988, pp. 1827-1849.

[2.25] Popovics, S., " A Numerical Approach to the Complete Stress-Strain Curves of Concrete", Cement and Concrete Research,Vol. 3, No. 5,September 1973, pp.583- 599.

[2.26] Pam, H.J.,"Ductility of Prestressed Concrete Piles Subjected ot Simulated Seismic Loading", Master of Engineering Report, Department of Civil Engineering, University of Canterbury, 1984, pp.169.

[2.27]"Reinforced Concrete Structures. Design Code and Interpretation (Commentary)", Architectural Institute of Japan, Tokyo, 1982.

[2.28] Burdette, E.G. and Hilsdorf, H.K.,"Behavior of Laterally Reinforced Concrete Columns", Journal of the Structural Division, Proceedings of the ASCE, Vol. 97, No.ST2, February 1971, pp. 587-602

[2.29] Scott, B.D., Park, R. and Priestley, M.J.N.,"Stress-Strain Behavior of Concrete Confined by Overlapping Hoops at Low and High Strain Rates", ACI Journal, Title no. 79-2, January-February 1982, pp. 13-27

[2.30] Park, R., Priestley, M.J.N. and, W.D. Gill,"Ductility of Square Confined Concrete Columns", Proceedings ASCE, Vol. 108, ST4, April 1982, pp. 929-950

[2.31] Kent, D. C. and Park, R.,"Flexural Members with Confined Concrete", Proceedings ASCE, Vol. 97, No. ST 7, July 1971, pp. 1969-1990.

[2.32] Bertero, V.V. and Felippa, C., Discussion of reference [2.10], pp.227-234

[2.33] Soliman, M.T.M. and Yu, C.W., "The Flexural Stress-Strain Relationship of Concrete Confined by Rectangular Transverse Reinforcement", Magazine of Concrete Research, Vol. 19, No. 61, December 1967, London, pp.223-238

[2.34] Sheikh, S. A. and Uzumeri, S.M.,"Properties of Concrete Confined by Rectangular Ties", AICAP-CEB Symposium on Structural Concrete under Seismic Actions (Rome, May 1979), Bulletin d'Information No. 132, Comité Euro-International du Beton, Paris, 1979, pp. 53-60

[2.35] William, K.J. and Warnke, E.P., "Constitutive model for the Triaxial Behaviour of of Concrete", International Association for Gridge and Structural Engineering, Proceedings, Vol. 19, 1975

[2.36]Muguruma, H., Watanabe, F. and Tanaka, H., "Improving the Flexural Ductility of Prestressed Concrete by Using the High Yield Strength Lateral Hoop Reinforcement", Journal of Japan Prestressed Concrete Engineering Association, Vol.24, Extra Number, Special Issue for The Ninth International Congress of the FIP (Stockholm June 1982), September 1982, Japan, pp.109-123

[2.37] Muguruma,H., Watanabe,F., Tanaka, H. and Katsuta,S.," Fatigue Failure Behaviour of Concrete Confined by High Yield Strength Hoop Reinforcement", Proceedings of the Twenty-third Japan Congress on Materials Research, The Society of Materials Science, Japan, 1980, pp.249-254.

[2.38] Uppal, J. Y. and Kemp, K. O., "The Effect of Longitudinal Gradients of Compressive Stress upon the Failure of Concrete", Magazine of Concrete Research, Vol. 23, No.74, March 1971, pp.11-22, with 'Discussion' in pp.46-47.

[2.39] Hognestad, E., Hanson, N.W. and McHenry, D., "Concrete Stress Distribution in Ultimate Strength", Title No. 52-28, Journal of the American Concrete Institute, V.27, No. 4, Dec. 1955

[2.40] Sturman, G.M., Shah, S.P. and Winter, G., "Effects of Flexural Strain Gradients on Microcracking and Stress-Strain Behavior of Concrete", Title No. 62-50 Journal of the American Concrete Institute, July 1965, pp.805-822

[2.41] Karsan, I.D. and Jirsa J.O., "Behavior of Concrete under Varying Strain Gradients", Journal of the Structural Division, Proceedings of the American Society of Civil Engineers, ST 8, August 1970, pp. 1675-1696

[2.42] Morita. S. and Adachi, N., "The Stress-Strain Behaviour of Concrete in the Compression Zone of Flexural Members", Mechanical Behaviour of Materials, Proceedings of the International Conference on Mechanical Behaviour of Materials, Kyoto, August 1971, Vol. 4, The Society of Materials Science, Japan, 1972, pp.162-171.

[2.43] Tanaka, H., Park, R. and McNamee, B., "Anchorage of Transverse Reinforcement in Rectangular Reinforced Concrete Columns in Seismic Design", Bulletin of theNew Zealand National Society for Earthquake Engineering, Vol.18 No.2 June 1985, New Zealand, pp. 165-190

[2.44] Tanaka, H. and Park, R., "Effectiveness of Transverse Reinforcement with Alternative Anchorage Details in Reinforced Concrete Columns", Pacific Conference on Earthquake Engineering, Proceedings Vol. 1, New Zealand National Society for Earthquake Engineering, August 1987, pp.225-235

[2.45] Ben-Zvi, E., Muller, G. and Rosenthal, I.,"Effect of Active Triaxial Stress on the Strength of Concrete Elements", Paper No.9, Active Triaxial Stress, Reinforced Concrete Column, ACI-SP, pp.193-233

[2.46] Tanaka, H. and Sakomizu, K.,"Study on Improving the Deformation Capacity of Concrete by Using the High Yield Strength Lateral Hoop Reinforcement (in Japanese)", Memoirs of the Akashi Technological College, Vol. 24, January 1982, Akashi, Japan, pp.71-90

[2.47] Muguruma, H., Watanabe, F. and Komuro, T., "Application of High Strength Concrete to Ductile Reinforced Concrete Columns (in Japanese)", Proceedings of JCI (Japan Concrete Institute) 11th Conference, 1989 (to be published)

[2.48] Tanaka, H. and Park, R., "Prediction of the Ultimate Longitudinal Compressive Concrete Strain at Hoop Fracture Using Energy Considerations", Bulletin of the New Zealand National Society for Earthquake Engineering, Vol. 20, No. 4, December 1987, pp. 290-305.

[2.49] Watanabe, F., "Complete Stress-Strain Curve for Concrete in Concentric Compression", Mecahnical Behaviour of Materials, Proceedings of the 1971 International Conference on Mechanical Behaviour of Materials, Vol. 4, Kyoto, Japan, pp. 153-161.

[2.50] Kotsovos, M.D., "A Mathematical Description of the Strength Properties of Concrete under Generalized Stress", Magazine of Concrete Research, Vol. 31, No. 108, September 1979, pp.151-157.

[2.51] Hannant, D.J.,"Nomograms for the Failure of Plain Concrete subjected to Short Term Multi-Axial Stresses", The structural Engineer, Vol. 52, No. 5, May 1974, pp.151-159.

[2.52] Gerstle, K. H. et al. , "Strength of Concrete under multiaxial Stress States", Douglas McHenry International Symposium on Concrete and Concrete Structures (Mexico City, October 1976), Detroit American Concrete Institute, 1978, ACI Publication SP-55, pp. 103-131.

[2.53] Karsan, I. D. and Jirsa, J.O., "Behaviour of Concrete under Compressive Loading", Journal of the Structural Division, Proceedings of the American Society of Civil Engineers, December 1969, pp.2543-2563.

[2.54] Blume, J.A., Newmark, N.M. and Corning, L.H., " Reinforced Concrete Buildings for Earthquake Motions", Portland Cement Association, Illnois, 1961, 318 pp.

[2.55] Park, K., Kent, D.C. and Sampson, R.A.,"Reinforced Concrete Members with Cyclic Loading", The Journal of the Structural Division, Proceedings of the Americal Society of Civil Engineers, Vol. 98, No. ST.7, July 1987

[2.56] Tanigawa,Y., and Kosaka, Y, "Stress-Strain Relationship of Confined Concrete under Cyclic Loading (in Japanese)", Sement Gijutsu Nenpo 33 (Review of the 33rd General Meeting, Technical Session), The Cement Association of Japan, Tokyo, 1979, pp.456-459

[2.57] Tanaka, H., Muguruma, H. and Watanabe, F., "Improvement of the Cofining Effects of Rectangular Hoops by Wave Shaped Supplementary Ties (written in Japanese)", Transactions of the Japan Concrete Institute, Volume 6, 1984, pp. 561- 564.

[2.58] Willam, K.J. and Warnke, E.P., "Constitutive Model for the Triaxial Behaviour of Concrete", International Association for Bridge and Structural Engineering, Proceedings, Vol. 19, 1975.

[2.59] Schickert, G. and Winkler, H., "Results of Tests Concerning Strength and Strain of Concrete Subjected to Multiaxial Compressive Stresses", Deutscher Ausschuss für Stahlbeton, Heft 277, Berlin, West Germany, 1977.

[2.60] Sinha, B.P., K.H. Gerstle and Tulin, L.G., " Stress-Strain Relations for Concrete under Cyclic Loading", Journal of the ACI, Proceedings, Vol. 61 No. 2, 1964, pp. 195-211

[2.61] Tanaka, H. and Sakomizu, K, "Study on Improving the Deformation Capacity of Concrete by Using the High Yield Strength Lateral Hoop Reinforcement", Memoirs of the Akashi Technological College, Japan, Vol. 24, January 1982, pp.71-90.

References - Chapter 3

[3.1] Jennings, P.C., Editor, "Engineering Features of the San Fernando Earthquake February 9, 1971", Earthquake Engineering Research Laboratory, California Institute of Technology, Pasadena, 1971, p.512.

[3.2] "Reinforced Concrete Structures. Design Code and Interpretation (written in Japanese)", Architectural Institute of Japan, Tokyo, 1982.

[3.3] Suzuki, Z., Chief Editor, "General Report on the Tokachi-oki Earthquake of 1968", Keigaku Publishing Co. Ltd, Tokyo, 1971, p. 754.

[3.4] "Code of Practice for the Design of Concrete Structures (NZS 3101,Part 1:1982)" and "Commentary on the Design of Concrete Structures (NZS 3101,Part 2 :1982)," Standards Associations of New Zealand.

[3.5] "Seismic Design of Concrete Structures, Second Draft of an Appendix to the CEB-FIP Model Code," Bulletin D'Information N°149-Part 2, Comité Euro International du Beton, Paris, March 1982.

[3.6]"Japanese Architectural Standard Specification-5, Reinforced Concrete Construction", Architectural Institute of Japan, Tokyo, 1979.

[3.7]"Building Code Requirements for Reinforced Concrete (ACI318-83)" and "Commentary on Building Code Requirements for Reinforced Concrete (ACI318-83)", American Concrete Institute, Detroit, 1989.

[3.8] "Excerpts from the Standard Specifications for Highway Bridges Relating to Seismic Design Adopted by the American Association of State Highway and Transportation Officials, Twelfth Edition 1977, with Revisions by Caltrans Office of Structures Design", The Association General Offices, Washington, 1983.

[3.9] "Recommended Lateral Force Requirements and Commentary", Seismology Committee, Structural Engineers Association of California, 1975, San Francisco.

[3.10] Priestley, M.J.N. and Park, R., "Strength and Ductility of Bridge Substructures", Research Report No. 84-20, Department of Civil Engineering, University of Canterbury, December 1984, p. 120.

[3.11] Tanaka, H. and Park, R.,"Anchorage of Transverse Reinforcement in Rectangular Reinforced Concrete Columns in Seismic Design", Bulletin of The New Zealand National Society for Earthquake Engineering, Vol. 18, No. 2, June 1985, pp. 165 - 190.

[3.12] Tanaka, H. and Park, R.,"Effectiveness of Transverse Reinforcement with Alternative Anchorage Details in Reinforced Concrete Columns," Pacific Conference on Earthquake Engineering, Proceedings Vol.1, New Zealand, August,1987,pp.225-235

[3.13] Moehle,J.P.and Cavanagh,T.,"Confinement Effectiveness of Cross Ties in RC", Journal of Structural Engineering, Vol.111, No.10, October, 1985, pp.2105-2120.

[3.14] Oesterle, R. G., Fiorato, A. E. and Corley, W.G., "Reinforcement Details for Earthquake Resistant Structural Walls", Research and Development Bulletin RD073.01D, Portland Cement Association,1981, Reprinted from Concrete International, December 1980, pp.1-12.

[3.15] Hanson, N. W. and Rabbat, B. G., "Tests of Ductile Behaviour of Lightweight Concrete Columns for Seismic Design",Eighth World Conference on Earthquake Engineering, Proceedings Vol.6, San Francisco, California, July 21-28, 1984,pp.545- 552.

[3.16] Ozcebe, G. and Saatcioglu, M.,"Confinement of Concrete Columns for Seismic Loading," A Journal of the American Concrete Institute, Vol. 84 No.4, Detroit, July-August 1987,pp.308-315.

[3.17] Sheikh, S. A., Yeh, C. C.and Menzies,D., "Confined Concrete Columns,"Pacific Conference on Earthquake Engineering, Proceedings Vol.1, New Zealand, August,1987,pp.177-188.

[3.18] Park, R., Priestley, M. J. N. and Gill, W.D., " Ductility of Square Confined Concrete Columns", Journal of Structural Division, Proceedings of American Society of Civil Engineers, Vol. 108, No. ST4, April 1982, pp. 929-950.

[3.19] Park, R. and Paulay,T.,"Reinforced Concrete Structures," John Wiley & Sons, 1975, p.769.

[3.20] Zahn, F.A., Park, R. and Priestley, M. J. N., "Design of Reinforced Concrete Bridge Columns For Strength and Ductility", Research Report 86-7, Department of Civil Engineering, University of Canterbury, Christchurch New Zealand, March 1986, p. 330.

[3.21] Baker, A. L. L. and Amarakone, A. M. N., "Inelastic Hyperstatic Frames Analysis", Proceeedings of the International Symposium on the Flexural Mechanics of Reinfroced Concrete, ASCE-ACI, Miami, November 1964, pp. 85-142.

[3.22] Mander, J. B., Priestley, M. J. N. and Park, R., "Seismic Design of Bridge Piers", Research Report 84-2, Department of Civil Engineering, University of Canterbury, Christchurch, New Zealand, February 1984, p.442.

[3.23] Priestley, M.J.N. and Park, R., "Strength and Ductility of Bridge Substructures", Road Research Unit Bulletin 71, National roads Board, Wellington, 1984, p.120.

[3.24] Priestley, M. J. N., Park, R. and Potangaroa, R. T., "Ductility of Spirally-Confined Concrete Columns", Journal of Structural Division, Proceedings of

American Society of Civil Engineers, Vol. 107, No. ST1, January 1981, pp. 181-202.

[3.25] Ang, B. G.,"Dynamic Shear Strength of Concrete Piers", Ph.D. Thesis, University of Canterbury, New Zealand, 1987

References - Chapter 4

[4.1]"Standard Specifications for Highway Bridges, Relating to Seismic Design" adopted by The American Association of State Highway and Transportation Officials, Twelfth Edition 1977 with Revisions by Caltrans Office of Structures Design, 1983, Washington,D.C. 20001

[4.2] "Code of Practice for the Design of Concrete Structures (NZS 3101, Part 1:1982" and "Commentary on the Design of Concrete Structures (NZS 3101, Part 2:1982)",Standards Association of New Zealand, Wellington.

[4.3] Priestley,M. J. N. and Park, R.,"Strength and Ductility of Bridge Substructures", Road Research Unit Bulletin 71, Bridge Design and Research Seminar, Auckland 1984, National Roads Board, Wellington, New Zealand, pp.120

[4.4] Zahn, F. A., Park, R. and Priestley, M. J. N.,"Design of Reinforced Concrete Bridge Columns fro Strength and Ductility", Research Report, March 1986, Department of Civil Engineering, University of Canterbury, pp.330.

[4.5] Soesienawati M. T., Park, R. and Priestley,M. J. N, "Flexural Ductility of Reinforced Concrete Columns with Low Axial Load and Limited Transverse Reinforcement", Pacific Conference on Earthquake Engineering, Proceedings Volume 1, New Zealand National Society for Earthquake Engineering , August 1987, pp201-212

[4.6] "Building Code Requirements for Reinforced Concrete (ACI 318-89)" and "Commentary on Building Code Requiremens for Reinforced Concrete (ACI 318R-89)", American Concrete Institute, Detroit, 1989.

[4.7] Muguruma, H., Watanabe, F., Tanaka, H. and Katsuta, S.," Fatigue Failure Behaviour of Concrete Confined by High Yield Strength Hoop Reinforcement", Proceedings of the Twenty-third Japan Congress on Materials Research, The Society of Materials Science, Japan, 1980, pp.249-254.

[4.8] Kani, G. N. J.,"The riddle of Shear Failur and It's Solution", Journal of the ACI, April,1964,pp.441-467.

[4.9] Blume, J. A., Newmark, N. M. and Corning,. L. H.," Design of Multistory Reinforced Concrete Buildings for Earthquake Motions", Portland Cement Association, Chicago,1961, 318pp.

[4.10] Alexander, M.," Plasticity: Theory and Application", The Macmillian Company, New York, 1968, pp.353

[4.11] Johnston, D. W. and Zia, P.,"Analysis of Dowel Action", Journal of the Structural Division, ASCE, ST 5, May 1971,pp1611-1630

[4.12] Jimenez, R., White, R. N. and Gergely, P.,"Bond and Dowel Capacities of Reinforced Concrete", ACI Journal, Symposium Paper, Title no. 76-4, January 1979,pp.73-93

[4.13] Mattock, A. H. and Hawkins, N. M., " Shear Transfer in Reinforced Concrete Recent Research", PCI Journal Vol.17, Number 2, March-April 1972 pp.55-75.

[4.14] Dulácska, H., " Dowel Action of Reinforced Crossing Cracks in Concrete", ACI Journal, No.69-70, December 1972, pp.754-757.

[4.15] Krefeld, W. J. and Thurston, C. W., "Contribution of Longitudinal Steel to Shear Resistance of Reinforced Concrete Beams," ACI Journal, Proc. V. 63, March 1966.

[4.16] Gergely, P., "Splitting Cracks Along the Main Reinforcement in Concrete Members", Dept. of Structural Engineering, Report Cornell University, 1969

[4.17] Paulay, T., Park, R., and Philips, M. H.,"Horizontal Construction Joints in Cast-In-Place Reinforced Concrete", Shear in Reinforced Concrete, ACI Special Publication 42, Vol.2, Detroit 1974, pp.599-616.

[4.18] Park, R. and Paulay, T.," Reinforced Concrete Structures", Jhon Wiley and Sons, New York, 1975, pp.769.

[4.19] Kosaka, Y. and Morita, S.,"Reinforced Concrete Structures (written in Japanese)", Maruzen, Tokyo, Japan ,1975, pp.385

[4.20]"Code of Practice for General Structural Design and Design Loadings for Buildings (NZS 4203:1984) ", Standards Association of New Zealand, Wellington.

[4.21] Park, R.,"Ductile Design Approach for Moment Resisting Reinforced Concrete Frames", Proceedings of the Japan Concrete Institute, Vol. 10, No.1, Japan, 1988, pp.1-21.

[4.22] Mander, J. B., Priestley, M. J. N. and Park, R.," Seismic Design of Bridge Piers", Research Report, Department of Civil Engineering, University of Canterbury, New Zealand, February 1984, pp.442.

[4.23]Leslie, P. D., " Ductility of Reinforced Concrete Bridge Piers", M.E. Report, University of Canterbury, New Zealand, 1982.

[4.24]Muguruma, H., Watanabe, F. , Tanaka, H. and Katsuta, S.,"Fatigue Failure of Concrete Confined by High Yield Strength Hoop Reinforcement", Proceedings of the twenty-third Japan Congress on Marterials Research, the Society of MaterialsScience, Kyoto, Japan, 1980, pp.249-254.

[4.25] Priestley, M. J. N., Park, R. and Potangaroa, R. T., " Ductility of Spirally-Confined Concrete Columns", Journal of Structural Division, Proceedings of American Society of Civil Engineers, Vol. 107, No. ST1, January 1981, pp.181-202.

[4.26] Tanaka, H., Park, R. and McNamee, B., "Anchorage of Transverse Reinforcement in Rectangular Reinforced Concrete Columns in Seismic Design", Bulletin of the New Zealand National Society for Earthquake Engineering, Vol.18 No.2 June 1985, New Zealand, pp. 165-190

[4.27] "Recommended Lateral Force Requirements and Commentary", Seismology Structural Engineers Association of California San Francisco, 1975

[4.28] Muguruma, H., Watanabe, F. and Tanaka, H., "Improving the Flexural Ductility of Prestressed Concrete by Using the High Yield Strength Lateral Hoop Reinforcement", Journal of Japan Prestressed Concrete Engineering Association,Vol.24, Extra Number, Special Issue for The Ninth International Congress of the FIP (Stockholm June 1982), September 1982, Japan, pp.109-123

References - Chpater 5

[5.1] "Code of Practice for the Design of Concrete Structures (NZS 3101,Part 1:1982)" and "Commentary on the Design of Concrete Structures (NZS 3101,Part 2 :1982)," Standards Associations of New Zealand.

[5.2]"Building Code Requirements for Reinforced Concrete(ACI318-89) " and "Commentary on Building Code Requirements for Reinforced Concrete (ACI318-89)", American Concrete Institute, Detroit, 1989.

[5.3] "Excerpts from the Standard Specifications for Highway Bridges Relating to Seismic Design Adopted by the American Association of State Highway and Transportation Officials, Twelfth Edition 1977, with Revisions by Caltrans Office of Structures Design", The Association General Offices,Washington,1983.

[5.4] Euler, L.,"Sur la Forces des Colonnes", Acad. Roy. Sci. Belles Lett. Berlin, Mém., Vol. 13, 1759, p. 252. English Translation by J. A. Van den Broek, Am. J. Phys., Vol. 15, 1947, p.309.

[5.5] Engesser, F., "Ueber die Knickfestigkeit gerader Stäbe", Z. Architekt. Ing. Vol. 35, 1889, p 455.

[5.6] Engesser, F., "Knickfragen", Schweiz. Bauztg. Vol. 25, No. 13, March 30, 1895, p. 88.

[5.7] von Kármán, T., "Untersuchungen über knickfestigkeit," Mitteilungen über Forschungsarbeiten auf dem Gebiete des Ingenieurwesens, Berlin, No.81,1910.

[5.8] Shanley, F. R., "Inelastic Column Theory", J. Aeron, Sci., Vol. 14, No. 5, May 1947, p. 261.

[5.9] Johnston, B. G., editor," Guide to Stability Design Criteria for MetAL Sructures", Structural Stability Research Council, Third Edition, A Wiley-Interscience Publication, John Wiley & Sons, New York, 1976, p.616.

[5.10] Mander,J.B., Priestley,M.J.N. and Park,R., "Seismic Design of Bridge Piers", Research Report 84-2, Department of Civil Engineering, University of Canterbury, Christchurch, New Zealand, February 1984, p.442.

[5.11] Zahn, F. A., Park, R. and Priestley, M. J. N., "Design of Reinforced Concrete Bridge Columns for Strength and Ductility", Research Report 86-7, Department of Civil Engineering, University of Canterbury, Christchurch, New Zealand, March 1986, p.330.

[5.12] Scribner, C. F., "Reinforcement Buckling in Reinforced Concrete Flexural Members", ACI Journal, Technical Paper, Title No. 83-85, November-December 1986, pp. 966-973.

[5.13] Chajes, A.,"Principles of Structural Stability Theory,"Prentice-Hall, Inc., Englewood Cliffs, New Jersey,1974, p.336

[5.14] Tanaka, H. and Park, R.,"Effectiveness of Transverse Reinforcement with Alternative Anchorage Details in Reinforced Concrete Columns," Pacific Conference on Earthquake Engineering, Proceedings Vol.1, New Zealand, August,1987, pp.225-235

[5.15] Park, R.,Paulay,T.,"Reinforced Concrete Structures," John Wiley & Sons, 1975, p.769.

[5.16] Priestley, M. J. N. and Park, R. ,"Strength and Ductility of Bridge Substructures", Research report No. 84-20, Department of Civil Engineering, University of Canterbury, December 1984, p.120.

[5.17] Yashiro,H., Hanai,S. and Takahashi,K., " Effect of Transverse Reinforcement on Strength and Ductility of Tied Columns", Transactions of the Japan Concrete Institute, Vol. 6, 1984, pp. 703-710.

[5.18] Oesterle,R.G.,Fiorato A.E.,and Corley, W.G.,"Reinforcement Details for Earthquake Resistant Structural Walls", Research and Development Bulletin RD073.01D, Portland Cement Association,1981, Reprinted from Concrete International, December 1980, pp.1-12.

[5.19] Hanson, N. W. and Rabbat, B. G., "Tests of Ductile Behaviour of Lightweight Concrete Columns for Seismic Design",Eighth World Conference on Earthquake Engineering, Proceedings Vol.6, San Francisco, California, July 21-28, 1984,pp.545- 552.

[5.20] Moehle,J.P.and Cavanagh,T.,"Confinement Effectiveness of Cross Ties in RC", Journal of Structural Engineering, Vol.111,No.10, October,1985,pp.2105-2120.

[5.21] Ozcebe,G. and Saatcioglu,M.,"Confinement of Concrete Columns for Seismic Loading," A Journal of the American Concrete Institute, Vol. 84 No.4, Detroit, July-August 1987,pp.308-315.

[5.22] Sheikh, S.A.,Yeh, C.C.and Menzies,D.,"Confined Concrete Columns,"Pacific Conference on Earthquake Engineering, Proceedings Vol.1, New Zealand, August,1987,pp.177-188.

[5.23] "Erläuterungen zur Verwendung von Rippen-Torstahl", 2nd Edition, Istegstahl Gesellschaft, Köln,November,1961.

References - Chapter 6

[6.1] "Code of Practice for General Structural Design and Design Loadings for Buildings (NZS 4203:1984)", Standards Association of New Zealand, 1984.

[6.2] Paulay, T., "Capacity Design of Earthquake resisting Ductile Multistorey Reinforced Concrete Frames", Third Canadian Conference on Earthquake Engineering, June, 1979, Montréal, Canada, pp. 917-947

[6.3] Mander, J. B., Priestley, M. J. N. and Park, R., " Seismic Design of Bridge Piers," Research Report 84-2, Department of Civil Engineering, University of Canterbury, February 1984, 483 pp.

[6.4] Baker, A. L. L. and Amarakone, A. M. N., " Inelastic Hyperstatic Frame Analysis", Flexural Mechanics of Reinforced Concrete, SP-12, American Concrete Institute/American Society of Civil Engineers, Detroit, 1965, pp.85-142.

[6.5] Corley, W. G., "Rotational Capacity of Reinforced Concrete Beams", Proceedings ASCE, Vol. 92, ST5, October 1966, pp. 121-146.

[6.6] Scott, B. D., Park, R. and Priestley, M. J. N., "Stress-Strain Behaviour of Concrete Confined by Overlapping Hoops at Low and High Strain Rates", ACI Journal, January-February 1982, pp.13-27.

[6.7] Priestley, M.J.N. and Park, R., "Strength and Ductility of Bridge Substructures," Road Research Unit Bulletin 71, National Road Board, Wellington , New Zealand, 1984, p120.

[6.8] Muguruma, H., Watanabe, F., Tanaka, H., Sakurai, K. and Nakamura, E., "Study on Improving the Flexural and Shear Deformation Capacity of Concrete Member by Using Lateral Reinforcement with High Yield Strength", BULLETIN D'INFORMATION N° 132, Structural Concrete under Seismic Actions, Volume 2-Technical Papers, AICAP-CEB Symposium, Rome, May 1979, pp.37-44

[6.9] Watanabe, F., Muguruma, H., Tanaka, H. and Katsuda, S., "Improving the Flexural Ductility of Prestressed Concrete Beam by Using the High Yield Strength Lateral Hoop Reinforcement", Symposia on Partial Prestressing and Practical Construction in Prestressed and Reinforced Concrete, Proceedings: Part 2, FIP, Bucuresti-România, September 1980, pp. 398-406.

[6.10] Mander, J.B., Priestley, M.J.N. and Park, R., "Theoretical Stress-Strain Model for Confined Concrete," Journal of Structural Engineering, American Society of Civil Engineers, vol. 114, No.8, August 1988, pp.1827-1849.

[6.11] Mander, J.B., Priestley, M.J.N. and Park, R., "Observed Stress-Strain Behaviour of Confined Concrete," Journal of Structural Engineering, American Society of Civil Engineers, vol. 114, No.8, August 1988, pp.1804-1826.

[6.12] "Code of Practice for the Design of Concrete Structures (NZS 3101, Part 1:1982)" and" Commentary on the Design of Concrete Structures (NZS 3101, Part 2: 1982)," Standard Association of New Zealand, Wellington.

[6.13] Engesser, F., "Ueber die Knickfestigkeit gerader Stäbe," Zeitschrift für Architektur und Ingenieurwesen, Vol. 35, 1889.

[6.14] Engesser, F., "Knickfragen," Schweizerische Bauzeitung, Vol.26,1895.

[6.15] von Kármán, T., "Untersuchungen über knickfestigkeit," Mitteilungen über Forschungsarbeiten auf dem Gebiete des Ingenieurwesens, Berlin, No.81, 1910.

[6.16] Shanley, F.R., "Inelastic Column Theory", Journal of the Aeronautical Sciences, Vol. 14, No. 5, 1947.

[6.17] Watanabe, F., "Complete Stress-Strain Curve for Concrete in Concentric Compression," Mechanical Behaviour of Materials, Proceedings of the 1971 International Conference on Mechanical Behaviour of Materials, Volume 4, pp. 153-161.

[6.18] Muguruma, H., Watanabe, F., Tanaka, H., Sakurai, K., and Nakamura, E., "Effect of Confinement by High Yield Strength Hoop Reinforcement upon the Compressive Ductility of Concrete," Proceedings of the Twenty-Second Japan Congress on Material Research, The Society of Materials Science, Japan, 1979, pp.377-382.

[6.19] Park, R. and Paulay,T., "Reinforced Concrete Structures," John Wiley and Sons, New York, 1975 , p.769.

[6.20] Sturman, G.M., Shah, S.P. and Winter, G., " Effects of Flexural Strain Gradients on Microcracking and Stress-Strain Behaviour of Concrete," ACI Journal, 62, 1965, pp.805-822

[6.21] Tanaka, H., Park, R. and McNamee, B., "Anchorage of Transverse Reinforcement in Rectangular Reinforced Concrete Columns in Seismic Design," Bulletin of the New Zealand National Society for Earthquake Engineering, Vol.18 No.2, June 1985, pp.165-190.

[6.22] Zahn, F.A. , Park, R. and Priestley, M.J.N., " Design of Reinforced Concrete Bridge Columns for Strength and Ductility," Research Report 86-7, Department of Civil Engineering , University of Canterbury, March 1986, p.380.